Advances in Civil Engineering

Advances in Life Cycle Environmental Sustainability of Civil Infrastructure Systems

Lead Guest Editor: Endong Wang
Guest Editors: Haimin Yao, Mbakisya A. Onyango, Jingfeng Yuan, and Xiaodong Zhang

Advances in Life Cycle Environmental Sustainability of Civil Infrastructure Systems

Advances in Civil Engineering

Advances in Life Cycle Environmental Sustainability of Civil Infrastructure Systems

Lead Guest Editor: Endong Wang
Guest Editors: Haimin Yao, Mbakisya A. Onyango, Jingfeng Yuan, and Xiaodong Zhang

Contents

Hindawi
Advances in Civil Engineering
Volume 2021, Article ID 8756569, 8 pages
https://doi.org/10.1155/2021/8756569

Research Article

Evaluation of Reclaimed Hydrated Fly Ash as an Aggregate for Sustainable Roadway Base Material

Mark H. Wayne,[1] David J. White,[2] Jayhyun Kwon,[3] and Jacek Kawalec[4]

[1]*Tensar International Corporation, Alpharetta, GA 30009, USA*
[2]*Department of Civil Construction and Environmental Engineering, Iowa State University, Ames, IA, USA*
[3]*Kennesaw State University, Marietta, GA 30060, USA*
[4]*Tensar International Limited, Blackburn, UK*

Correspondence should be addressed to Jacek Kawalec; kawalec@tensar.pl

Received 29 May 2019; Revised 7 December 2020; Accepted 23 December 2020; Published 7 January 2021

Academic Editor: Jingfeng Yuan

This paper summarizes the findings from laboratory and field performance testing of reclaimed hydrated class C fly ash (HFA) stabilized with a triangular aperture geogrid. This phase of testing was performed on HFA laboratory specimens and field test sections. The laboratory test results provided estimates for design input values, while the field testing assessed performance characteristics including the as-constructed modulus of the subgrade reaction, the in situ resilient modulus, and permanent deformation. For the laboratory portion, all results were derived from tests conducted on specimens immediately after sample preparation and after a 7-day cure. The compressive strength of reclaimed hydrated class C fly ash increases with curing. The strength of the HFA material can be further increased when mixed with a chemical stabilizer. For this project, chemical stabilization with lime was not viable because the lime supplier was too far from both HFA source and project site. Based on cyclic plate load tests, the in situ resilient modulus of the HFA and geogrid-stabilized HFA layers were determined on site. This paper reports the findings from the laboratory and field plate load test and highlights the potential use of geogrids in the stabilization of HFA.

1. Introduction

In many locations across the globe, subgrade soils are, in general, not suitable for use as a pavement foundation, and a suitable fill is difficult to find in many instances. So, depending on regions, anthropogenic materials like blast furnace slags and burnt and unburnt mining wastes (clay shales) are more often used for construction as reported by Haibin and Zhenling [1], Ebrahimi, et al. [2], Rafalski and Wilczek [3], Akbarnejad, et al. [4], and Hainin, et al. [5]. The key to success is the long-term stability of such materials due to possible mineralogical changes reported by Adamczyk et al. [6]. Also, reclaimed hydrated class C fly ash (HFA and market name C-stone), which is produced by Headwaters Resources, Inc. [7], has been used as a road base material or as a select fill for rigid and flexible pavements. Reclaimed hydrated class C fly ash has pozzolanic properties and therefore is able to gain strength over time when moistened and compacted. The use of reclaimed hydrated fly ash provides environmental benefits by reuse of waste products, as reported by Zabielska-Adamska [8].

Research done by Bergeson and Barnes [9] demonstrated that the compressive strength of the reclaimed hydrated class C fly ash base can increase from zero to as much as 50 psi within 7 days of curing. Furthermore, research by Bergeson and Barnes [9] and White [10] documents strength increases and improved long-term durability of reclaimed hydrated fly ash when mixed with chemical stabilizers such as raw fly ash and hydrated lime. Compressive strength test results show that the addition of 10% raw fly ash could increase the compressive strength by 80% compared to the untreated reclaimed ash, while the addition of 2.5% hydrated lime could increase the strength of the reclaimed ash by 8 times. Based on the laboratory test results, Bergeson and Barnes [9]

determined layer coefficients for reclaimed hydrated class C fly ash base for use in AASHTO flexible pavement design as a function of layer thickness.

Senadheera et al. [11] investigated strength characteristics and microstructure of hydrated fly ash to evaluate the suitability of the material as a flexible base material. The study found that the reclaimed fly ash was crushed during compaction, but it gained strength after placement due to the hydration and formed a stiff layer. To prevent moisture loss during hydration, the researchers recommended the application of asphalt emulsion after compaction as the curing moisture is crucial to the microstructure formation of hydrated fly ash.

As a lime supplier was located too far from the project site, mechanical stabilization of the HFA using geogrid was proposed as opposed to traditional chemical stabilization. The inclusion of geogrid in pavement structures has long been accepted to improve the performance of aggregate base course. A hypothesis employed in this trial is that the geogrid synergistically interacts with the HFA during construction in such a way that the HFA obtains its optimal engineering properties so that the performance of the HFA is maximized. When the HFA layer is in service, the composite consisting of HFA and geogrid has enhanced properties over those of the original host material.

The objective of this study was to evaluate the performance of the mechanically stabilized HFA and provide design related input properties, such as the strength or modulus of mechanically stabilized HFA. Resilient modulus of the HFA is not performed as the untreated HFA has not been considered as a suitable alternative to the crushed rock base materials. Pavement design guide with reclaimed HFA is based on the 28-day compressive strength of HFA stabilized with fly ash or hydrated lime. Typical resilient modulus of crushed rock aggregate base course ranges from 100 to 200 MPa. In order to use the untreated HFA as an aggregate, the mechanically stabilized HFA should achieve resilient modulus values higher than 100 MPa.

A series of laboratory testing was conducted on both untreated and mechanically stabilized HFA specimen. Further, field test sections were constructed containing three different test items. The field test program included two untreated control test items and one mechanically stabilized HFA for performance comparison. Field plate load tests confirmed that the construction of an HFA mechanically stabilized layer resulted in a composite that exhibited increased strength development in a shorter period of time.

2. Laboratory Test Program

A total of four triaxial test specimens were tested using an HFA marketed material known as C-stone and produced by Headwaters Resources, Inc. Material composition is provided on the manufacturer's website and is not discussed in detail within this paper apart from basic chemical composition and engineering properties as shown in Table 1. It is noted that tests were conducted in series - resilient modulus and quick shear strength tests followed by permanent deformation testing. The former tests were conducted in accordance with AASHTO T307 protocol [12] and the latter using procedures found in NCHRP 598. Permanent deformation tests were conducted on an independently remolded test specimen in order to assess the materials resistance to long-term rutting behavior.

To investigate the effect of geogrid on modulus and permanent deformation behavior of C-stone, two samples were prepared with geogrid placed at mid-depth of the sample. One control and one geogrid-stabilized sample were tested without curing and the other two samples (one control and one geogrid-stabilized sample) were cured for 7 days to investigate the curing effect on strength. Mechanical properties of the geogrid used in this study are summarized in Table 2.

Grain-size distribution curve (Figure 1), Standard Proctor, and laboratory California bearing ratio (CBR) values (Figure 2) were established for the C-stone used in this study. Based on the conceptualized construction specification, a pretest target of 98 percent Maximum Dry Density (MDD) at the optimum moisture content (OMC), as determined by ASTM D698, was established for remolding specimens in the laboratory for characterization testing and evaluation. The source material contained in excess of 25% fines. Triaxial specimens were remolded in a 150-millimeter diameter split mold using a manual Modified Proctor hammer. Once testing was initiated, the lab reported that the intended 98% MDD value could not be achieved due to the fact that the full aggregate sample was tested in a large-scale test and only the 19.05 millimeter minus material was used for the development of the proctor curve. As such, a maximum effort yielded a compacted dry density of 96% MDD, and this density value was targeted for all testing in order to provide useful comparisons between tests and treatments.

2.1. Resilient Modulus (AASHTO T307). The resilient modulus test was conducted in accordance with procedures contained within the referenced test standard. The specimen was subjected to a series of load pulses at a variety of axial stresses and confining pressures (15 specific combinations of stress levels), and recoverable deformation resulting from these load pulses were recorded. The data is used to fit a constitutive model, where resilient modulus can be predicted for any level of stress the pavement designer wishes to consider in his/her design. The predictive moduli are plotted in Figure 3 to compare values associated with specimen prepared using differing curing and reinforcement conditions. The data graphically depicted in Figure 3 are generated based on the universal model.

The 0-day cure results demonstrated that the geogrid had a minimal influence on stiffness properties. This is most likely due to the fact that the C-stone did not begin to engage with the geogrid. In contrast, Figure 3(b) indicates that curing time does tend to have an effect. The time allowed for curing (7 days) produces a material approximately 10–25% stiffer (with no grid reinforcement) and 25–60% stiffer (with the geogrid). These relative improvements indicate that the C-stone material possesses cementitious bonding behavior

Table 1: Chemical constituent and engineering properties of the HFA [7].

Chemical composition	Mass percentage (%)
Silicon dioxide (SiO_2)	26.81
Aluminum oxide (Al_2O_3)	15.94
Ferric oxide (Fe_2O_3)	5.21
Calcium oxide (CaO)	22.45
LOI (loss on ignition) 950°C	18.96
Engineering properties	
Bulk specific gravity	1.5
Dry unit weight (kN/m^3)	1440
Los Angeles abrasion (AASHTO T96), grading B, loss %	<55

Table 2: Summary of geogrid material mechanical properties.

Property	Test method	Units	Minimum value
Aperture shape	Observation		Triangular
Aperture size (longitudinal × diagonal direction)	Direct measurement	mm	40 × 40
Radial stiffness at 0.5% strain, min.	ASTM D6637-11	kN (m)	300
Junction efficiency	ASTM D7737	%	93

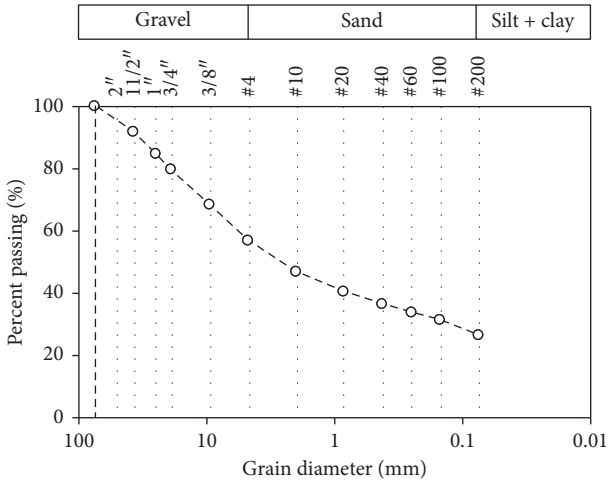

Figure 1: Hydrated class C fly ash (C-stone) grain-size distribution curve.

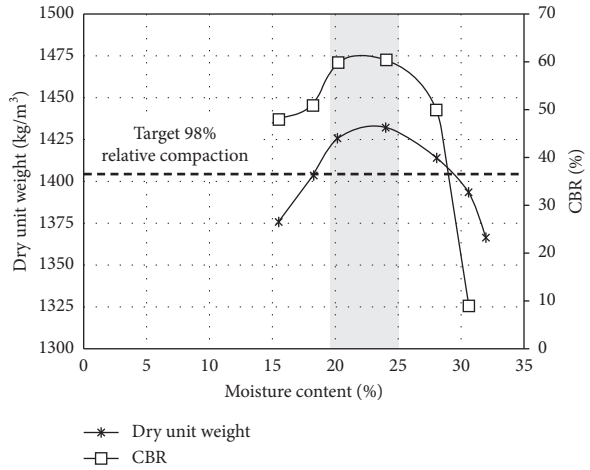

Figure 2: Standard Proctor and California bearing ratio results.

which is enhanced by the inclusion of the geogrid. It is postulated that this is due to a higher level of locked-in lateral stress that is generated as a result of the inclusion of the geogrid. This residual stress allows the particles to remain in contact with one another, allowing stronger bonds to be established during the pozzolanic reaction. The generation of locked-in lateral stresses was initially reported by White et al. [13] and substantiated by the work of Wayne et al.[14].

Bergeson and Barnes [9] provided HFA structural layer coefficients (a_i) for use in the design of flexible pavement. A structural layer coefficient is an abstract number that represents the relative strength of the construction materials in the 1993 AASTHO procedure [12]. In pavement design, the design strength of the self-cementitious and pozzolanic materials increased with an increase in thickness. In general, semirigid or rigid layers have California bearing ratio (CBR) values greater than 100%. Therefore, the layer coefficient of the semirigid or rigid layer can be estimated using the correlation of unconfined compressive strength and layer coefficient. The suggested layer coefficients for untreated HFA ranged from 0.12 to 0.19, depending upon the layer thickness. For 150 millimeters of untreated HFA base, the layer coefficients ranged from 0.13 to 0.13, while layer coefficients for 300-millimeter thick untreated HFA ranged from 0.18 to 0.19.

In this study, the resilient modulus values obtained from the triaxial test are used to estimate the structural layer coefficients by using the formula provided in the 1993 AASHTO Guide for Design of Pavement Structures [12] for granular base layers, a_2. The predicted structural layer coefficients for the untreated 7-day cured HFA specimen ranged from 0.08 to 0.16. The predicted structural layer coefficient values of geogrid-stabilized 7-day cured HFA specimen ranged from 0.09 to 0.19. It is important to note that the specimens in this study were not cured for 28 days. It is believed that the low structural layer coefficients of the specimens result from the early stages of the pozzolanic reaction.

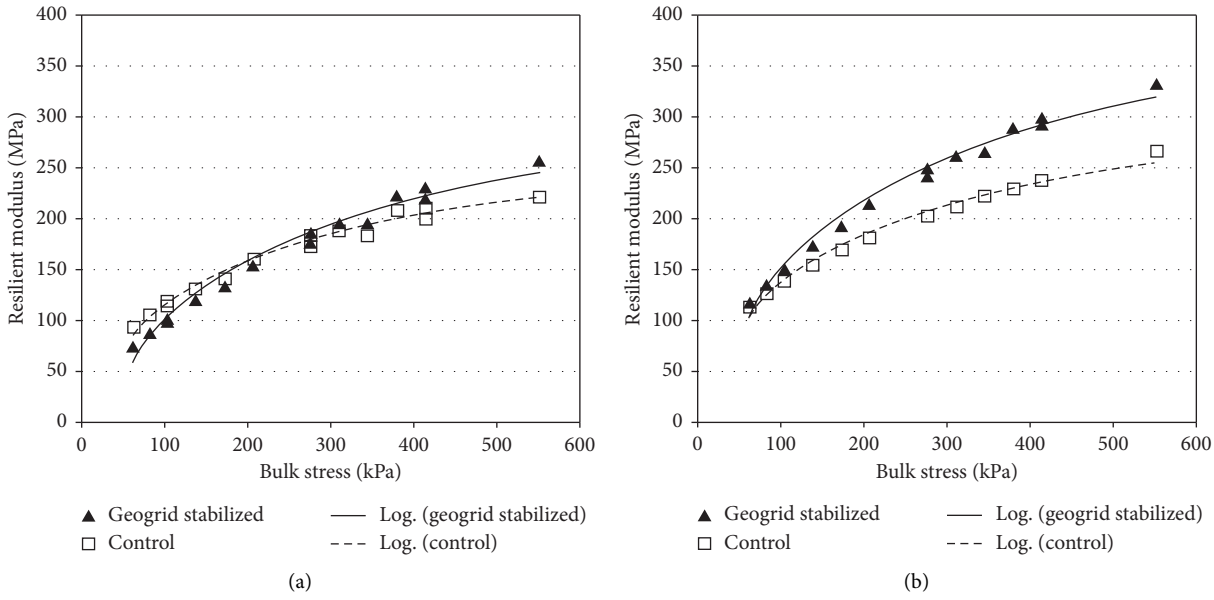

Figure 3: Resilient modulus from AASHTO T307 test. (a) Results of 0-day cured samples. (b) Results of 7-day cured samples.

2.2. Quick Shear Test. An interesting behavior can readily be seen when looking at the results of the quick shear test. The quick shear test is prescribed in AASHTO T307 as a simple shear controlled by the rate of axial deformation (1% per minute up to 5% strain) following the 15 stress sequences of the repeated load testing. The test is performed at a confining pressure of 34.47 kPa. Figure 4 graphically depicts the results of this test and demonstrates the positive influence of the geogrid. The geogrid increased the strength by 23% (730 kPa vs. 592 kPa). Also noteworthy is the fact that the geogrid extends the strain-carrying capability by 25 percent or better. The curing time has little effect on the results, although in both cases (stabilized and unstabilized), the result of the 7-day cure specimen was a slightly higher maximum stress at a slightly lower failure strain (thus, moderately stiffer).

2.3. Repeated Load Permanent Deformation (NCHRP 598). The permanent deformation test was conducted in accordance with procedures documented in NCHRP Report no. 598. The results of the NCHRP 598 testing are graphically depicted in Figure 5. The NCHRP 598 test specifies 1,000 cycles of the axial load be applied in a step-sequence of axial stress (69, 138, 276, 413, 551, 689, 827, 965, 1100, and 1240 kPa), all at a constant confining pressure of 103 kPa. This translates into 10,000 cycles of loading to complete the test. The axial strain is monitored throughout each test. If an axial strain of 10 percent is reached prior to completion of the regimen of 10,000 cycles, the specimen is considered to have failed, and the test is halted. This test is intended to serve as a "torture" test for aggregate base layers.

Because of the moisture-density profile of the aggregate material, the Control nearly withstood the tortures of the test, crumbling almost instantaneously as the axial stress approached 1240 kPa. The geogrid-stabilized specimen exceeded 10% strain during the test. As such, the testing continued at the highest axial stress (1240 kPa) until 10% strain was reached, or an additional 10,000 cycles, whichever came first.

As shown in Figure 5, the untreated specimen exhibits a quick sudden failure after the specimen reached 2% axial strain, whereas geogrid stabilization prevents brittle failure. The result indicates the cementitious bonds of HFA were broken as strain levels increased. The benefit is the resistance to long-term permanent deformation or rutting. The stabilized specimen withstood an additional 7,140 cycles of load at this highest axial stress level, indicating a positive influence of the geogrid.

2.4. Discussion of Laboratory Tests. These results highlight the fact that resilient modulus testing can be used to characterize HFA for use as artificial base course aggregates. Although resilient modulus curves for mechanically stabilized and unbound crushed limestone specimen were similar, repeated load permanent deformation tests show that the inclusion of a triangular aperture geogrid has a positive effect on permanent deformation behavior. Laboratory tests confirmed that there is no direct correlation between AASHTO layer coefficients for HFA and the structural layer coefficient that needs to be adjusted to account for long-term performance using field performance testing.

3. Field Performance Testing

The field performance testing program involved static and cyclic plate load tests. Figure 6 illustrates the field conditions and material for the test sections at the project site located in Iowa.

The static plate load test is utilized to determine the as-constructed unit load deflection relationship, while the cyclic plate load test is used to determine field strength values. The static plate load tests were conducted in general accordance with AASHTO T-222. The groundwater surface was

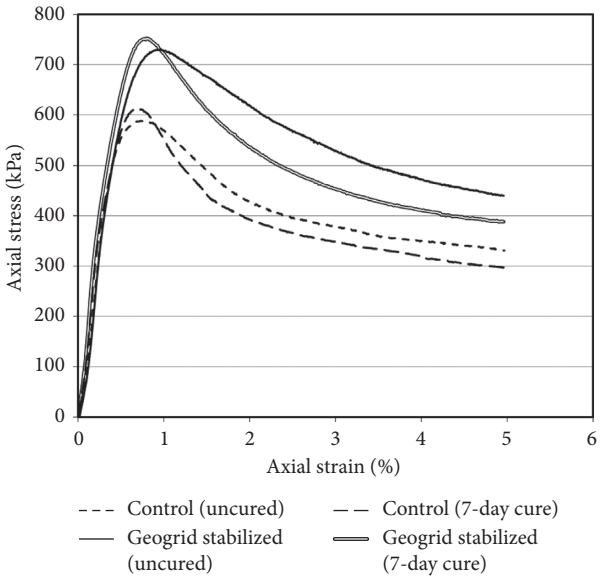

Figure 4: Quick shear results from the AASHTO T307 test.

reportedly 6 to 7 feet below the existing ground surface. The native subgrade material at the surface was sandy silt based on visual classification. The CBR values for the 7-day cured HFA sections were about 24%, while the 4- to 6-hour cured HFA CBR values were 7 to 16%. Compared to the laboratory CBR values (Figure 2), the field CBR values are about 50% lower, which is not uncommon when relating the laboratory to the field.

For this study, a 300-millimeter diameter flat plate was selected as the basis of performance verification. Based on heavy equipment loading over some portions of the site, the cyclic loading regime was selected to be between 0 and 689 kPa. The plate footprint and stress regime simulate construction equipment loading. This loading regime was selected to help demonstrate the ability of the geogrid to minimize dynamic deflection. Laboratory testing demonstrated that these loading conditions result in particle breakdown and premature shear failure of unstabilized HFA C-stone. Results from the field performance tests were more distinguishing than the performance differences identified from laboratory tests presented earlier.

Three different sections were tested on the project including the following:

Test item 1: 200 millimeters of HFA over the native subgrade placed 4–6 hours prior to testing

Test item 2: 200 millimeters of HFA stabilized with a triangular aperture geogrid placed about 7 days prior to testing

Test item 3: 200 millimeters of HFA over native subgrade placed 28 days prior to testing

3.1. Cyclic Plate Load Test. In addition to the static plate load tests, cyclic tests were performed on all sections. The cyclic tests were set up to simulate 40 or 100 passes of a loaded truck with 689 kPa tire pressures. Results show the relationship between the cycle number and permanent and recoverable deflection at the surface. Key parameters derived from this testing include the overall permanent deflection after 40 or 100 cycles and the in situ resilient modulus. In situ resilient modulus was calculated using the following:

$$M_{Rin-\text{situ}@689\text{kPa}} = \frac{\left(1-\nu^2\right)\sigma_o a}{\Delta \text{d}} f, \quad (1)$$

where ν is Poisson's ratio (assumed to be 0.3), σ_o is the cyclic stress, a is the plate radius, f is the plate rigidity factor (assumed to be 2 for uniform stress distribution), and Δd is the resilient deformation (during unloading).

Figure 7 compares the cyclic plate load test results of each item. It should be noted that item 2 was cured for 7 days but was stabilized with geogrid and item 3 was cured for 28 days. The result shows that item 1 has an initial average displacement of 17 mm after 10 load cycles, whereas 28-day cured item 3 has only 7.2 mm of an initial displacement at the same load cycles. The result shows the effect of the curing period on the stiffness of HFA C-stone.

The results of item 2 and item 3 show 7-day cured geogrid-stabilized item 2 has greater strength than that of 28-day cured item 3. The cyclic deflection (deformation that would occur as a wheel passes over the section) of item 2 after 100 load cycles is about 6 millimeter, while item 3 exhibited 9 millimeters of deflection at 40 load cycles. This demonstrated that the use of the geogrid would permit faster construction while achieving higher stiffness over the 28-day cured HFA.

3.2. Static Plate Load Test. Static plate load tests were performed on test item 1 and item 2 to determine the in situ modulus of subgrade reaction (also known as "spring" constant or k value) in the unit load range of 0 to 689 kPa. The k values reported herein are not adjusted for plate size corrections or bending. These corrections can be determined with additional testing on site but are generally only needed for applications involving pavements. The stress-deflection response in Figure 8 shows that the control section produced about 6 times more permanent deflection than the C-stone + TX160 section.

It is important to note that test item 2 has been cured for 7 days, whereas item 1 was not cured at the time of testing.

The in situ resilient modulus values are determined based on the cyclic plate load test, and the results are summarized in Table 3 with k values obtained from the static plate load test. Results show that the resilient modulus is highest for the 7-day cured geogrid section and lowest for the zero-day cure with no geogrid. This field performance testing conclusively demonstrates that for the selected loading sequence, the geogrid-stabilized HFA will perform well and is significantly better than the control section both in metrics of resilient behavior and permanent deflection.

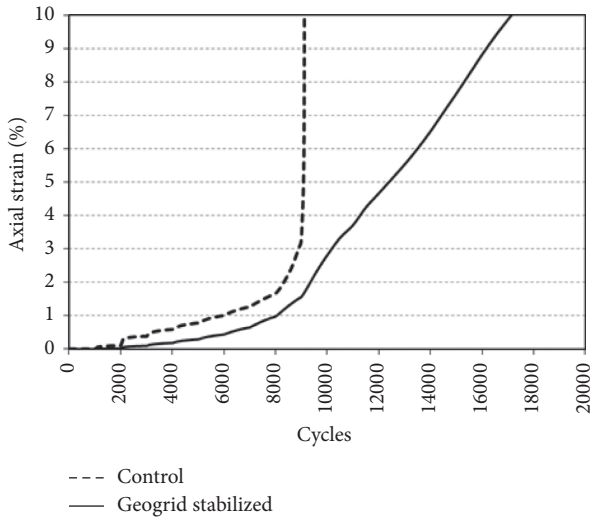

Figure 5: Repeated load permanent deformation from NCHRP 598 test (uncured samples).

Figure 6: (a) C-stone and geogrid and (b) C-stone unstabilized test sections.

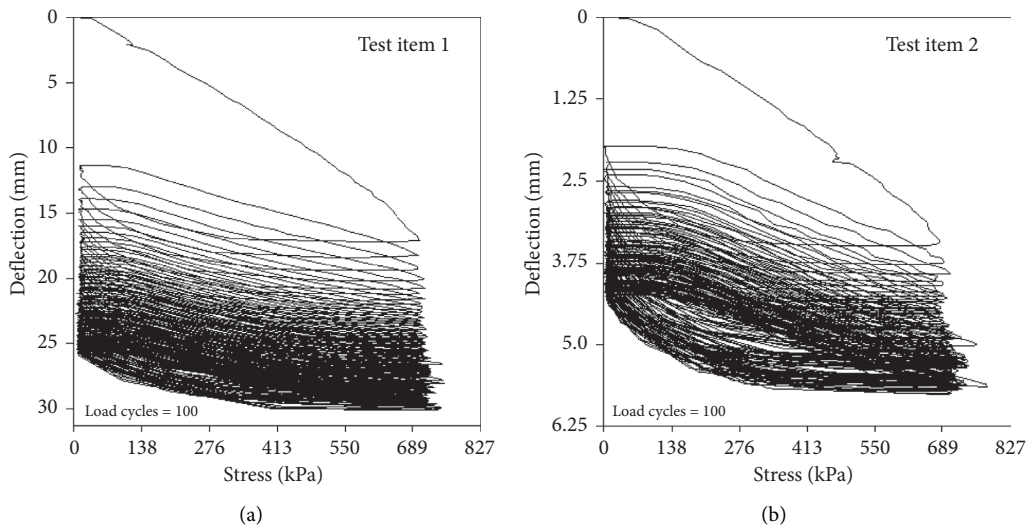

Figure 7: Continued.

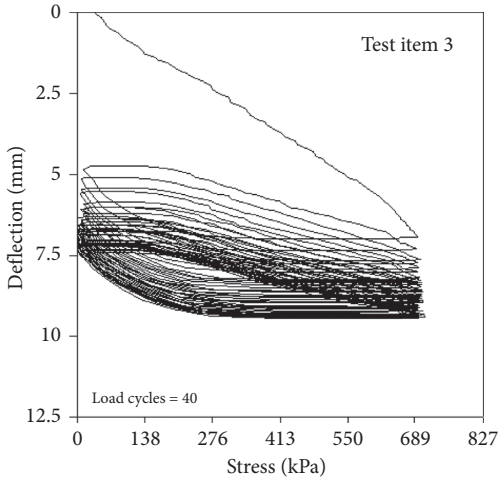

(c)

Figure 7: Cyclic plate load test results. (a) Test item 1: 200 mm of HFA. (b) Test item 2: 200 mm of HFA stabilized with the geogrid (7-day cure). (c) Test item 3: 200 mm of HFA (28-day cure).

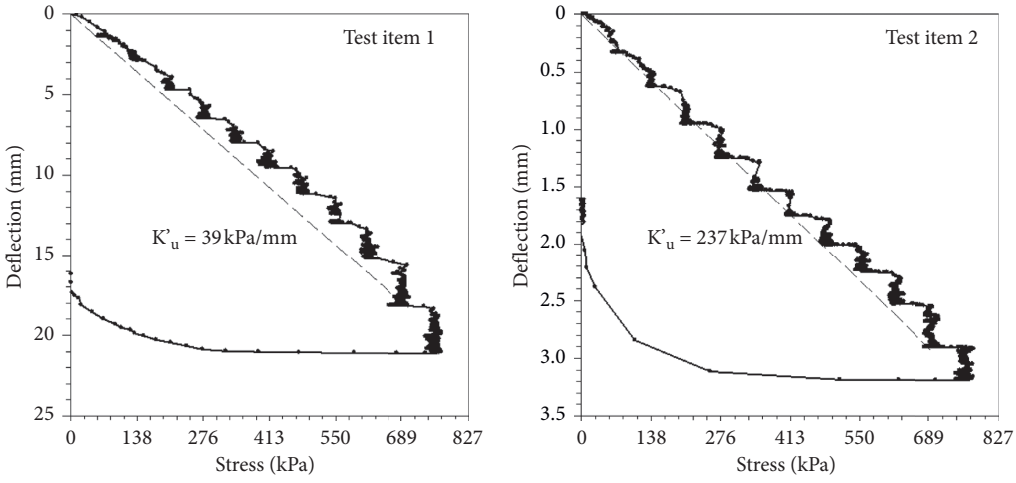

(a) (b)

Figure 8: Static plate load test results of test item 1 and item 2. (a) Test item 1: 200 mm of HFA. (b) Test item 2: 200 mm of HFA stabilized with the geogrid (7-day cure).

Table 3: In situ resilient modulus and modulus of the subgrade reaction for HFA C-stone.

Test item	Cure # days	Geogrid	Modulus of the subgrade reaction (kPa mm)	Resilient modulus (MPa)	Permanent deflection-cyclic plate load test (mm)*	Number of 690 kPa stress cycles
1	0.5	No	39	42	11	100
2	7	Yes	237	122	2	100
3	28	No	— **	83	3	40

*Total deflection minus seating deflection (cycle = 1). **Not tested due to weather delay.

4. Conclusions

A series of laboratory and field plate load tests were conducted to characterize HFA and evaluate the in situ performance of the HFA. Laboratory tests were used as an initial assessment of the performance of nontraditional pavement material and then used to predict how this material is expected to perform over time. The laboratory test results provide a fundamental understanding of the behavior of HFA C-stone. Tests currently used for characterizing unbound aggregate material can be used to characterize HFA C-stone. These tests can also be used to evaluate the

influence of geogrid in HFA C-stone performance. Evaluation of nontraditional base materials may be made through laboratory and field plate load tests as presented in this paper.

The conclusions of the laboratory and field plate load tests described in this paper are as follows:

Long-term strength gain due to the pozzolanic reaction was demonstrated in the laboratory and field plate load tests.

The use of a triangular aperture geogrid was demonstrated as a suitable alternative to the use of chemical stabilization. The in situ resilient modulus value can be increased by more than 30%.

Care should be taken for the use of untreated HFA C-stone as it could exhibit a brittle failure at low strain levels.

Untreated HFA C-stone may not be appropriate as a surface layer for unpaved gravel road as untreated HFA exhibits a brittle failure mode at small axial strain levels. As a result, a crushed quartzite aggregate wearing surface was used in the field prior to the use of this system for a parking lot and construction laydown yard.

Additional testing should be performed to better illustrate the interaction between the geogrid and pozzolanic reaction of HFA. Furthermore, the long-term strength gain effects and conditions during spring thaw should be evaluated. The field testing can also be targeted for other selected stress levels to simulate various equipment loading conditions and the number of loading events.

Data Availability

The laboratory and field data used to support the findings of this study are included within the article.

Conflicts of Interest

The authors declare that they have no conflicts of interest.

References

[1] L. Haibin and L. Zhenling, "Recycling utilization patterns of coal mining waste in China," *Resources, Conservation and Recycling*, vol. 54, no. 2, pp. 1331–1340, 2010.

[2] A. Ebrahimi, B. R. Kootstra, T. B. Edil, and C. H. Benson, "Practical approach for designing flexible pavements using recycled roadway materials as base course," *Road Materials and Pavement Design*, vol. 13, no. 4, pp. 731–748, 2012.

[3] L. Rafalski and J. Wilczek, "Polish experience with testing of selected shales as material for road base courses," *Multiphysical Testing of Soils and Shales*, vol. 295, 2012.

[4] S. Akbarnejad, L. J. M. Houben, and A. A. A. Molenaar, "Application of aging methods to evaluate the long-term performance of road bases containing blast furnace slag materials," *Road Materials and Pavement Design*, vol. 15, no. 3, pp. 488–506, 2014.

[5] M. R. Hainin, Md. M. Aziz, Z. Ali, R. P. Jaya, M. M. El-Sergany, and H. Yaacob, "Steel Slag as A Road Construction Material," *Jurnal Teknologi*, vol. 73, no. 4, 2015.

[6] Z. Adamczyk, M. Grygierek, M. Lupiezowiec, J. Nowak, and E. Strzalkowska, "The effects of mineralogical changes that occur in artificial aggregates," *Gospodarka Surowcami Mineralnymi-Mineral Resources Management*, vol. 34, no. 2, pp. 37–54, 2018.

[7] Headwater Resources Inc, "(2019) C-Stone technical information," 2019, http://www.flyash.com.

[8] K. Zabielska-Adamska, "Laboratory compaction of fly ash and fly ash with cement additions," *Journal of Hazardous Materials*, vol. 151, no. 2-3, pp. 481–489, 2008.

[9] K. L. Bergeson and A. G. Barnes, *Iowa Thickness Design Guide for Low Volume Roads Using Reclaimed Hydrated Class C Fly Ash Bases*, Iowa State University, Ames, Iowa, 1999.

[10] D. J. White, "Reclaimed hydrated fly ash as a geomaterial," *Journal of Materials in Civil Engineering*, vol. 18, no. 2, pp. 206–213, 2006.

[11] S. P. Senadheera, P. W. Jayawickrama, and A. S. M. A. Rana, "Use of hydrated fly ash as a flexible base material," *Transportation Research Record: Journal of the Transportation Research Board*, vol. 1546, no. 1, pp. 53–61, 1996.

[12] American Association of State Highway and Transportation Officials, *AASHTO Guide for Design of Pavement Structures*, American Association of State Highway and Transportation Officials, Washington, D.C., 1993.

[13] D. J. White, P. K. R. Vennapusa, H. H. Gieselman, S. C. Douglas, J. Zhang, and M. H. Wayne, "In-ground dynamic stress measurements for geosynthetic reinforced subgrade/subbase," in *Advances In Geotechnical Engineering, Geotechnical Special Publication No. 211, Proceedings of GeoFrontiers 2011*, J. Han and D. E. Alzamora, Eds., pp. 4663–4672, 2011.

[14] M. H. Wayne, I. Fraser, B. Reall, and J. Kwon, "Performance verification of a geogrid mechanically stabilized layer," in *Proceedings of the 18th International Conference on Soil Mechanics and Geotechnical Engineering*, pp. 1381–1384, Paris, France, September 2013.

Hindawi
Advances in Civil Engineering
Volume 2020, Article ID 7247134, 10 pages
https://doi.org/10.1155/2020/7247134

Research Article

Mechanical Properties of Tunnel Muck with Fly-Ash Geopolymer

Dong Yang,[1] **Zhiqin Xi**,[1] **Qiang Chen**,[2] **and Shuisheng Li**[1]

[1]*China Construction Fifth Engineering Division Co., Ltd., Changsha, Hunan 410004, China*
[2]*East China University of Technology, Nanchang, Jiangxi 330013, China*

Correspondence should be addressed to Dong Yang; ydcscec@hotmail.com

Received 26 July 2019; Revised 29 October 2019; Accepted 9 December 2019; Published 12 February 2020

Guest Editor: Mbakisya A. Onyango

The tunnel muck has a great potential to be used as a recyclable engineering material in transit and other civil work projects instead of being deposited as construction waste. In this work, the geopolymer is generated by alkali-activated fly ashes, which act as cementitious materials to strengthen the tunnel muck. The tunnel muck has to be dehydrated, grinded, and screened before being treated by alkali-activated fly ash. The effect of the mass ratio between fly ash and tunnel muck (M_{fa}/M_{tm}), the mass ratio between Na_2SiO_3 solution and NaOH solution ($M_{Na_2SiO_3}/M_{NaOH}$), the ratio between liquid and solid (M_{liquid}/M_{solid}), and molarity of NaOH on the strength of geopolymer were systematically studied by conducting the uniaxial compression experiments. The experimental results indicate that the liquid-to-solid ratio is the most important parameter to the geopolymer strength after the alkali-activated fly ash treatment. On the contrary, molarity of NaOH is less effective on the geopolymer strength. Moreover, the optimum scheme is concluded according to the experimental results as follows: the mass ratio between tunnel muck and fly ash, the mass ratio between Na_2SiO_3 solution and NaOH solution, the ratio between liquid and solid, and molarity of NaOH are 1 : 2, 1.8, 0.18, and 10 mol/L, respectively. Meanwhile, the SEM images indicate that flocculence from the active substance in fly ash is a crucial component as the cementing material.

1. Introduction

Tunneling structures have been well applied in urban subway construction and traffic tunnel as one of the most effective ways to enhance the urban land utilization efficiency [1, 2]. People are even proposing to apply the tunneling structures into the Lunar exploration [3–5]. Meanwhile, a big amount of excavated materials/tunnel muck has been removed from tunnel, which has been considered to be waste material of little or no value for a long time [6, 7]. The main contents of the tunnel muck are gravel, sand, and clay with different amount of water. The instability of these geomaterials might trigger dreadful disasters [4, 8–12]. Hence, an efficient way to deposit or even to recycle the tunnel muck is of great significance to the environment.

The gravel and sand are typical geogranular materials [13–16], whose mechanical properties have been systemically reported by using the photoelastic experimental method since the 1990s [17–21], and they can be very easily used as building materials after being filtered out from the tunnel muck. However, the clay content in the tunnel muck is always one of the trickiest parts to deal with, which is usually mixed with ameliorants like bentonite, frothier, resin, tackifier, and so forth. Efforts have been made to recycle the clay content into geopolymer as a green material all the time [22–24]. Davidovits [25] presented a new type of material called geopolymers as a possible solution to this problem, since their physical properties make them a viable alternative for many conventional cements and plastics. Compared to conventional cements, geopolymers are powerful with high chemical resistance, fire resistance, temperature resistance, and so forth [26]. In view of these superior properties, generating geopolymers by using alkali-activated fly ash to improve the bearing capacity of foundation soil has been reported recently [27, 28]. Moreover, geopolymers combined with loess and fully weathered granite were developed as useful building materials [29–31]. However, little literatures can be found on the alkali-activated fly ash as cementing material for tunnel muck.

In this work, the geopolymer that is generated by alkali-activated fly ash for reusing the high clay content tunnel muck is studied. For making the geopolymer samples, the advantages and disadvantages between casting method and pressing mold method are discussed. In order to understand the strength of the geopolymer sample, the orthogonal analysis is conducted based on the compression experiments by varying four different parameters. The optimum scheme to make the geopolymer sample from the high clay content is proposed eventually, which could be a valuable reference for the tunnel muck reutilization.

2. Experimental Materials and Protocol

2.1. Experimental Materials. The tunnel muck excavated from subway tunnel in Changsha is used to make the geopolymer. The main content of the tunnel muck here is completely weathered conglomerate with approximately 26.9% moisture content, 26.9% silt content, and 18.4% clay content. The particle size distribution of the tunnel muck is shown in Figure 1. The measured plastic limit and liquid limit of the excavated tunnel muck are 13.3% and 29.0%, respectively.

Before fabricating the geopolymer, the excavated tunnel muck is dried and smashed. The fine grain muck with less than 2 mm diameter is picked by sieve. The X-ray fluorescence (XRF) results of a typical fine grain muck after filtering by 2 mm diameter sieve are shown in Table 1. Most of the elements are SiO_2 and Al_2O_3 of the fine grain muck. There is approximately 1 percent of MgO and very few CaO in the fine grain muck. The fly ash with 450 m^2/kg specific surface area is applied into the tunnel muck in this work. The alkali-activator is a mixture of NaOH solution and $Na_2O{\cdot}nSiO_2$ in this work, where the NaOH solution is made by dissolving the industrial grade tablet alkali into water. The freshly prepared NaOH solution has to be cooled down to the room temperature before being used to make the geopolymer. In order to ensure equilibrium state in the mixture, the mixed solutions need to be stored for a minimum of 24 hours prior to use as suggested by Duxson et al. [29, 32, 33].

2.2. Experimental Protocol to Mode the Geopolymer Sample. Four different methods were tried to make the raw materials mixtures. The one that can have the highest strength sample is applied in this work. The details of the applied method include the following: (1) add a certain amount of muck in the container; (2) according to the scheme, the fly ash is well mixed with muck; and (3) the solution is poured into the muck and fly ash mixture, and well mix them. The details of the other three methods will not be introduced here, since these methods are not applied in the present work. Two prevailing procedures can be applied to make the geopolymers: casting and mold pressing (semidry pressing) [34]. By using casting method, the raw material mixtures with alkali-activated fly ash are made as flexible slurry is poured into sample mold. The geopolymers will form after a certain time. The casting method is a relatively easy method, which can even make complicated geometry geopolymer samples. Different amount of water is added into the sample to get the optimal amount of water that can make the raw material flexible. In order to pour the raw materials into the mold, a mass percentage of approximately 20%~40% of water has to be added, which is too much. Moreover, there will always be cracks forming on the surface of geopolymer sample due to the high clay content as shown in Figure 2(a), [35, 36]. For the mold pressing method, the raw materials mixtures with alkali-activated fly ash are made as colloidal solution to be compressed to solid sample in the mold, which requires much less water than casting method. The force applied here is 19.625 kN with a 10 MPa corresponding pressure. Moreover, the same pressure (10 MPa) is used to make the samples with pressing method in this work. The geopolymer sample made by mold pressing method has relatively smooth surface as shown in Figure 2(b). Hence, the mold pressing method is applied in this work to make the geopolymers.

2.3. Uniaxial Compression Protocol. Comprehensive experiments are conducted to systemically study the effect of each parameter on the strength of geopolymers. Orthogonal experimental design is applied to schematize the uniaxial compression protocol. Four different parameters are considered as orthogonal factors, and three factor levels are involved in total. The details of the experimental protocol are shown in Table 2. The parameters include the mass ratio between fly ash and tunnel muck (M_{fa}/M_{tm}), the mass ratio between Na_2SiO_3 solution and NaOH solution ($M_{Na_2SiO_3}/M_{NaOH}$), the mass ratio between liquid and solid (M_{liquid}/M_{solid}), and molarity of NaOH, where the mass ratio between fly ash and tunnel muck means the mass of fly ash versus the mass of dry tunnel muck here.

The geopolymer sample is pressed in a cylinder mold with a diameter of 50 mm and a height of 100 mm under 10 MPa compression pressure. The samples are cured for 28 days before being placed on the uniaxial compression apparatus (Instron 1346). The experiments are conducted by combining stress control method and displacement control method. At the initial state, the stress control method is applied with 10 kN/min loading speed, and the 0.2 mm/min displacement control method is applied at 80% of the estimated peak strength until complete failure stage.

3. Experimental Results

3.1. Stress-Strain Curve of the Geopolymers. The stress-strain curves of all 9×3 uniaxial compression experimental results are shown in Figure 3. In general, four stages can be observed in the stress-strain curves; the region of each stage on a typical stress-train curve is shown in the inset of Figure 3. The four stages include the following. (1) The first is strain hardening stage, which happens right after the initial compression. The slope of the curve tends to increase as the compression strain increases, which indicates the vertical stiffness is increasing in this stage. (2) The second is linear elastic deformation stage, at which the stress increases linearly as the strain increases. The deformation of the

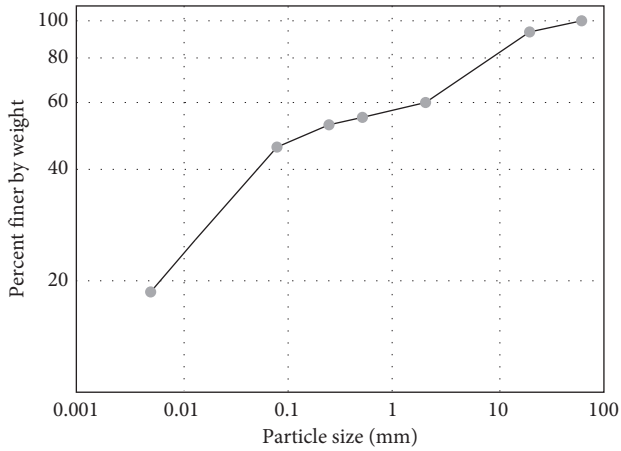

Figure 1: Particle size distribution of the tunnel muck.

Table 1: XRF results of a typical fine muck sample with the particles size less than 2 mm.

Element	SiO_2	Al_2O_3	Fe_2O_3	K_2O	MgO	Ti_2O	CaO
Percentage by weight (wt%)	72.7	18.10	3.29	3.51	1.08	1.03	0.13

(a) (b)

Figure 2: The typical geopolymer sample made by two methods. The same percentage of material in proportions is used for these two methods, except that 18% more water is added for casting method in order to make the raw materials able to be poured into the mold: (a) made by casting method; (b) made by pressing mold method.

Table 2: The details of uniaxial protocol for orthogonal experimental design.

No.	M_{fa}/M_{tm}	$M_{Na_2SiO_3}/M_{NaOH}$	M_{liquid}/M_{solid}	NaOH (mol/L)
1	1 : 3	1.8	0.14	8
2	1 : 3	2.0	0.16	10
3	1 : 3	2.2	0.18	12
4	1 : 2	1.8	0.16	12
5	1 : 2	2.0	0.18	8
6	1 : 2	2.2	0.14	10
7	2 : 3	1.8	0.18	10
8	2 : 3	2.0	0.14	12
9	2 : 3	2.2	0.16	8

geopolymer sample is recoverable after unloading in this stage. No or only a few local rearrangements happen in the sample. The maximum stress in the linear elastic deformation stage is approximately 50% of the peak stress. (3) The third is strain softening stage, where the slope of the stress-strain curve decreases as the strain increases. Cracks start to form in the sample and eventually percolate through the sample. Meanwhile, the stress is corresponding to the peak stress. (4) The fourth is post-peak-deformation stage, where the stress decreases as the strain increases. Several vertical cracks along the compression direction would be generated with the increase of strain.

3.2. Mechanical Properties of the Geopolymer Samples. Several mechanical parameters of the geopolymer samples can be extracted from the stress-strain curves, including strength, elasticity modulus, residual strength, peak strain, and tenacity. The elasticity modulus is calculated by fitting the stress-strain curves in the range from 25% to 50% of the compression strength. For the definition of residual strength, the strain at peak stress, γ_p, is obtained from the

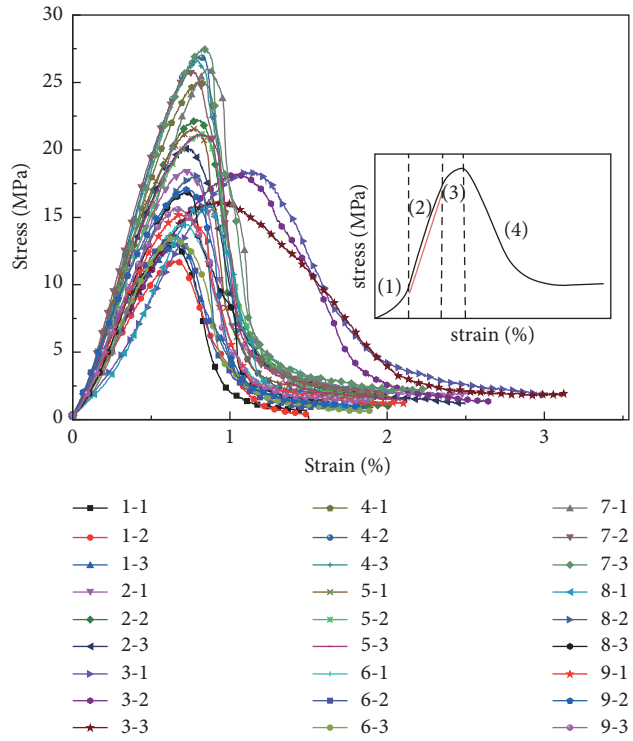

Figure 3: The stress-strain curves of the uniaxial experimental results. Inset: a schematic to show the four stages of a typical stress-strain curve. The red line is a reference line to indicate a linear relationship of stage 2.

Table 3: Mechanical properties of the geopolymer samples from uniaxial compression experimental results.

No.	M_{fa}/M_{tm}	$M_{Na_2SiO_3}/M_{NaOH}$	M_{liquid}/M_{solid}	NaOH (mol/L)	Strength (MPa)	Elasticity modulus (GPa)	Residual strength (MPa)	Peak strain ($\times 10^{-3}$)	Tenacity (J/m^3)
1	1 : 3	1.8	0.14	8	12.61	2.44	1.22	6.31	83.02
2	1 : 3	2.0	0.16	10	20.27	3.50	2.81	7.08	163.22
3	1 : 3	2.2	0.18	12	17.54	2.28	3.88	9.82	229.41
4	1 : 2	1.8	0.16	12	26.18	4.40	2.52	7.41	186.26
5	1 : 2	2.0	0.18	8	21.29	3.80	2.08	7.55	161.52
6	1 : 2	2.2	0.14	10	13.87	2.60	1.56	6.35	96.73
7	2 : 3	1.8	0.18	10	26.41	4.31	2.82	7.27	190.91
8	2 : 3	2.0	0.14	12	16.93	2.79	1.31	7.30	112.47
9	2 : 3	2.2	0.16	8	15.98	3.11	1.91	6.56	118.35

stress-strain curve first, and then the stress at the strain equaling $2\gamma_p$ is defined as residual strength. The stress usually reaches a stable state after the strain becomes twice bigger than that at the peak stress. Hence, the stress at the strain twice bigger than that at the peak stress is defined as the residual strength. The tenacity is defined as the area under the stress-strain curve. The mechanical properties of the geopolymer samples from uniaxial compression experimental results are shown in Table 3, where all the mechanical parameters are averaged over three experiments with the same initial condition.

4. Discussions

As shown in Table 3, group 7 sample has the maximum strength, which is 26.41 MPa. Group 4 has the highest elasticity modulus of 4.40 GPa. The maximum residual strength is 3.88 MPa, which is exhibited by group 3. The peak strain of the tested geopolymer samples is located in $6.31 \times 10^{-3} \sim 9.82 \times 10^{-3}$, which is several times bigger than the peak strain of concrete [37]. The average residual strength is approximately 11.9% of the peak strength.

The orthogonal analysis is applied to understand the importance of each parameter to the strength and tenacity of the geopolymer sample [38, 39]. The details of orthogonal analysis are shown in Table 4. The results indicate that the liquid/solid ratio is the most important parameter to the geopolymer strength after the alkali-activated fly ash treatment. On the contrary, the geopolymer strength is less sensitive to molarity of NaOH. Meanwhile, the optimum scheme is concluded according to the experimental results as follows: the mass ration between fly ash and tunnel muck,

Table 4: Details of orthogonal analysis.

	Index	M_{fa}/M_{tm}	$M_{Na_2SiO_3}/M_{NaOH}$	M_{liquid}/M_{solid}	NaOH (mol/L)
Strength (MPa)	K1	50.42	65.20	43.41	49.88
	K2	61.34	58.49	62.43	60.55
	K3	59.32	47.39	65.24	60.65
	k1	16.81	21.73	14.47	16.63
	k2	20.45	19.50	20.81	20.18
	k3	19.77	15.80	21.75	20.22
	R	3.64	5.93	7.28	3.59
	Weight of influence factors	$M_{liquid}/M_{solid} > M_{Na_2SiO_3}/M_{NaOH} > M_{fa}/M_{tm} >$ NaOH			
	Optimal solution	2132			
Tenacity (J/m^3)	K1	475.65	460.19	292.22	362.89
	K2	444.51	437.21	467.83	450.86
	K3	421.73	444.49	581.84	528.14
	k1	158.55	153.40	97.41	120.96
	k2	148.17	145.74	155.94	150.29
	k3	140.58	148.16	193.95	176.05
	R	17.97	7.66	96.54	55.08
	Weight of influence factors	$M_{liquid}/M_{solid} >$ NaOH $> M_{fa}/M_{tm} > M_{Na_2SiO_3}/M_{NaOH}$			
	Optimal solution	1133			

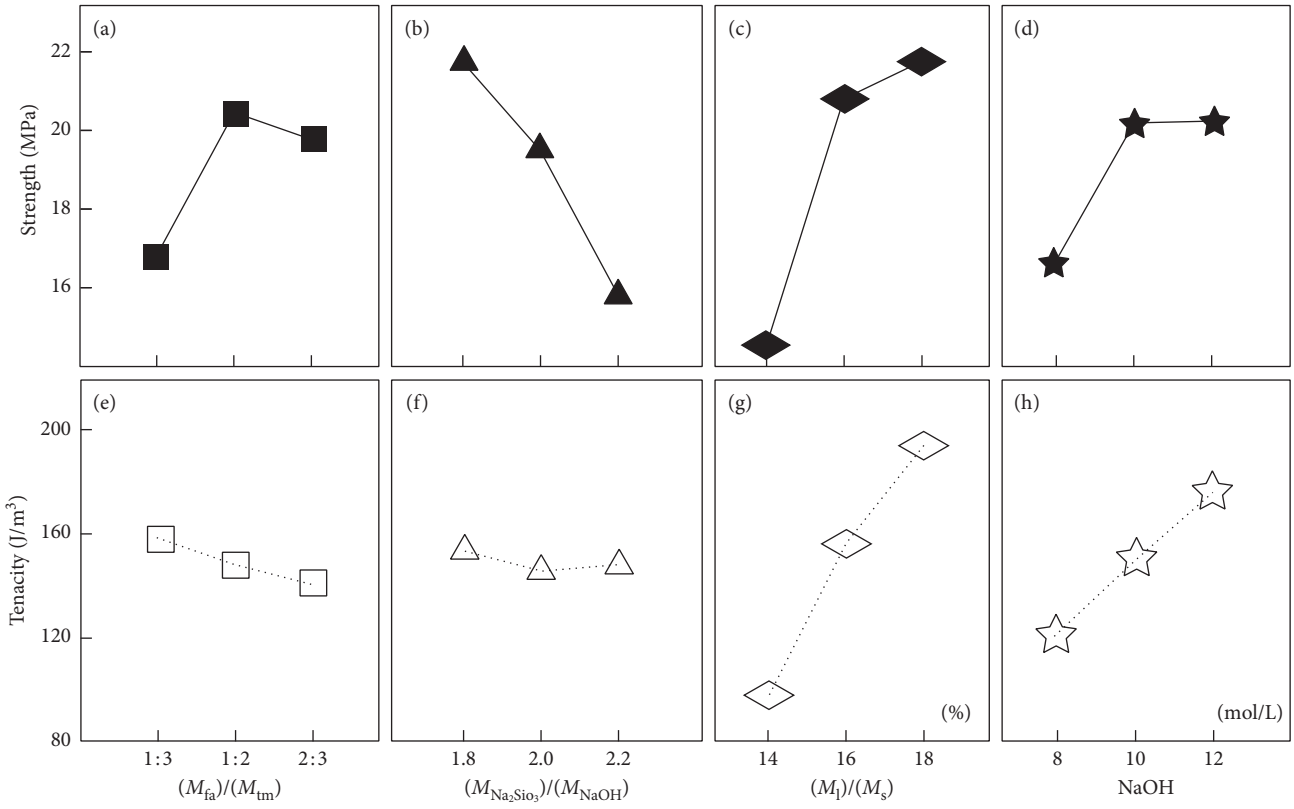

Figure 4: The strength and tenacity affected by each parameter.

the mass ratio between Na_2SiO_3 solution and NaOH solution, the ratio between liquid and solid, and molarity of NaOH are 1 : 2, 1.8, 0.18, and 10 mol/L, respectively.

The effects of the mass ratio between fly ash and tunnel muck (M_{fa}/M_{tm}), the mass ratio between Na_2SiO_3 solution and NaOH solution ($M_{Na_2SiO_3}/M_{NaOH}$), the ratio between liquid and solid (M_{liquid}/M_{solid}), and molarity of NaOH on the strength of geopolymer are shown in Figures 4(a)–4(d). The strength approaches the highest value when M_{fa} : $M_{tm} = 1 : 2$ and molarity of NaOH is 10 mol/L. The strength increases as the M_{liquid}/M_{solid} increases, which is one of the most important control factors to the geopolymer strength. However, it is hard to make the geopolymer sample with $M_{liquid}/M_{solid} > 0.2$ as the mixture would be squeezing out

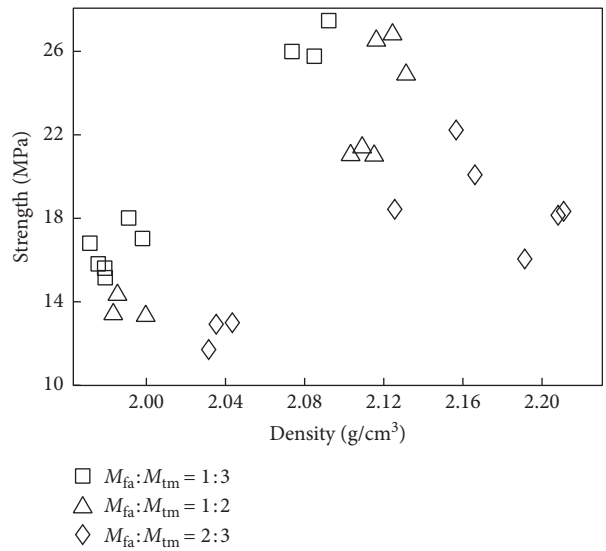

Figure 5: The density of geopolymer sample versus strength for different $M_{fa}:M_{tm}$.

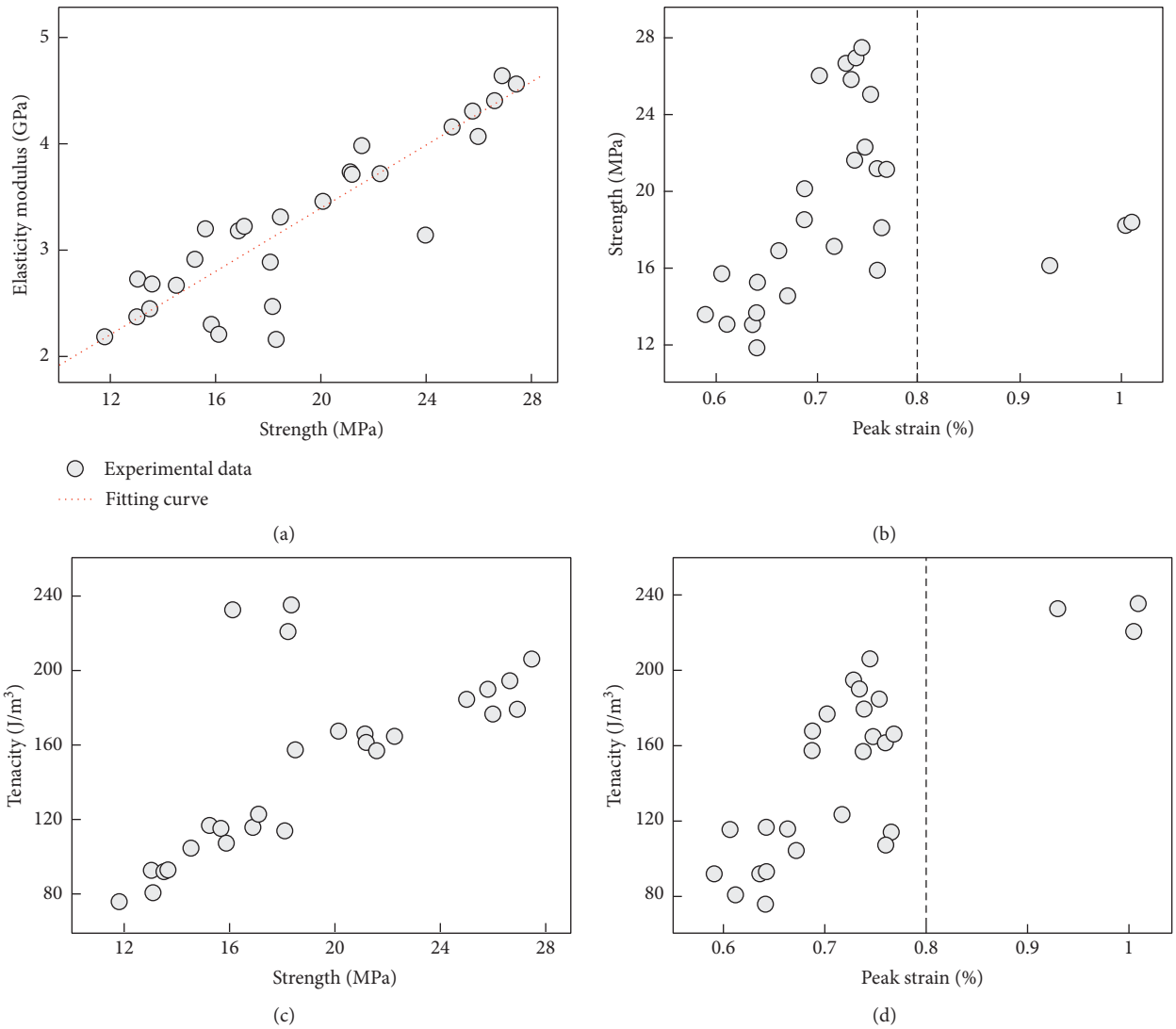

Figure 6: The strength and corresponding peak strain as a function of tenacity, elasticity modulus, and so forth.

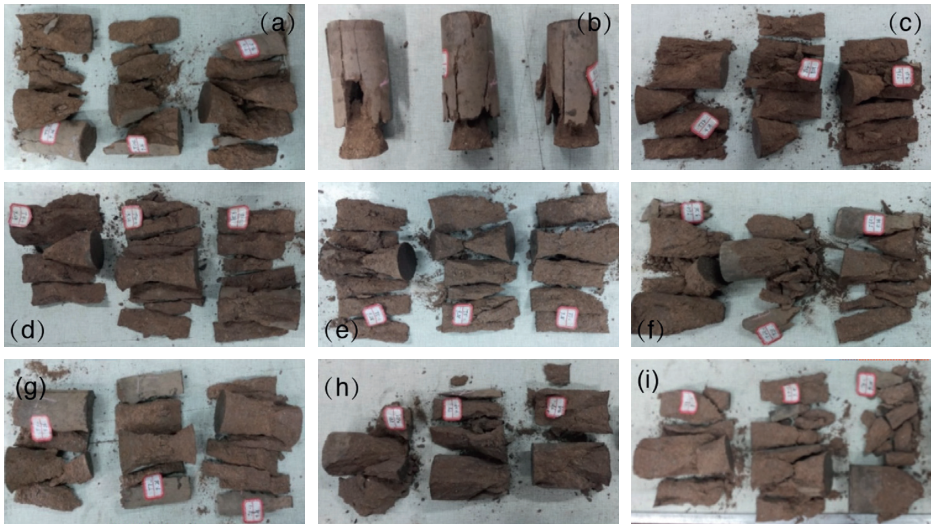

Figure 7: Pictures of geopolymer samples after uniaxial compression tests. Each row has the same M_{fa}/M_{tm} values, which are 1 : 3, 1 : 2, and 2 : 3 from the first to the third row, respectively. Each column has the same $M_{Na_2SiO_3}/M_{NaOH}$ values, which are 1 : 8, 2.0, and 2.2 from the first column to the third column, respectively. M_{liquid}/M_{solid} ratios of each raw vary among 0.14, 0.16, and 0.18. The NaOH concentrations of each row vary among 8, 10, and 12. The details of the M_{liquid}/M_{solid} ratios and NaOH concentration can refer to Table 2.

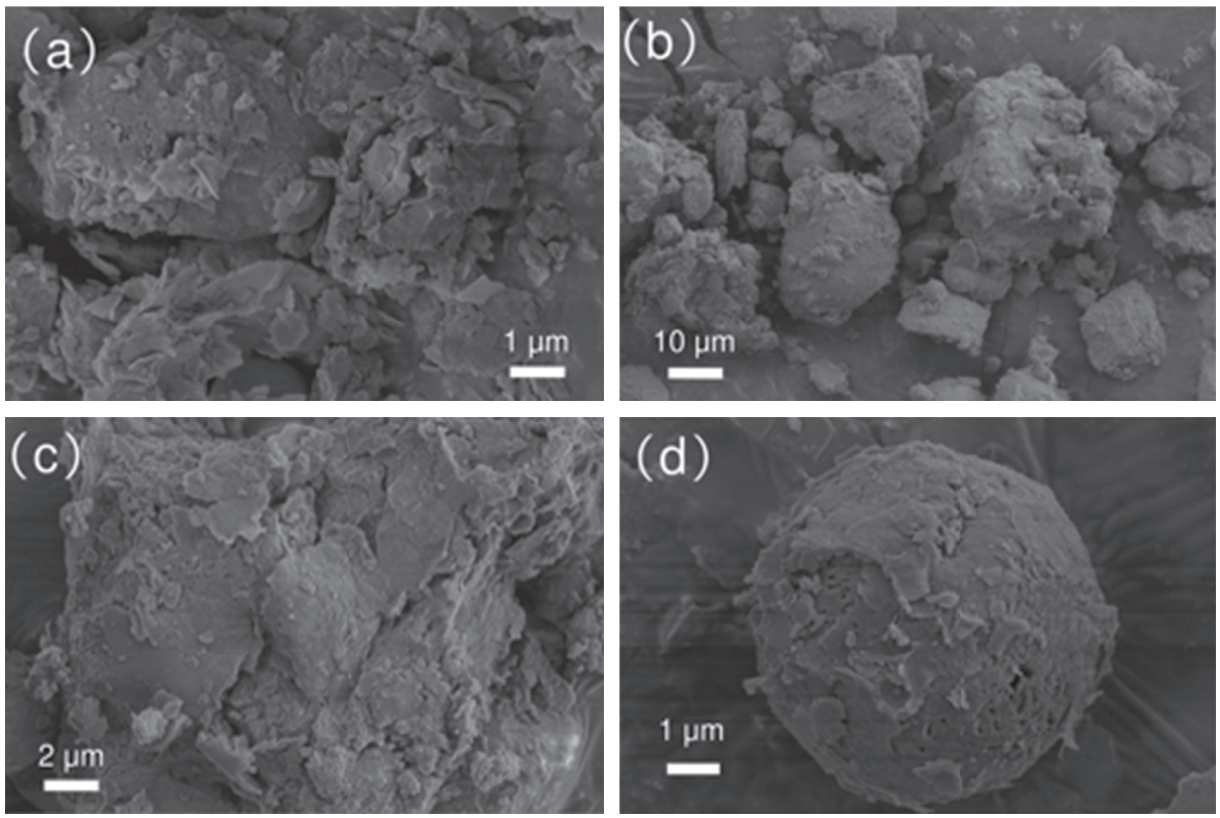

Figure 8: Different scale of SEM images of geopolymer sample: (a) the soil particle and fly ashes are strengthened by flocculence; (b) 10-time zoomed out view of (a); (c) the materials that were not involved in the chemical reaction, which are filler and skeleton of geopolymer sample; (d) typical fly ash particle after the reaction with structural holes on the surface.

from the mold. The ratio $M_{liquid}/M_{solid} = 0.18$ is set to make the geopolymer in this work. $M_{Na_2SiO_3}/M_{NaOH}$ is another important factor to the geopolymer strength, which has a negative correlation with the geopolymer strength. The tenacity of the geopolymer sample affected by these four influence factors is shown in Figures 4(e)–4(h). According to

the orthogonal analysis results in Table 4, the geopolymer sample has the highest tenacity at $M_{fa}:M_{tm}=1:3$, $M_{Na_2SiO_3}/M_{NaOH}=1.8$, $M_{liquid}/M_{solid}=0.8$, and molarity of NaOH is 12 mol/L.

Microscale pore filled by the agglutination aggregates is another important factor that can influence the strength of geopolymer sample. The filling degree can be estimated by the density of geopolymer sample, which has positive correlation with the density. Figure 5 shows the strength of the geopolymer sample as a function of density for different mass ratio between fly ash and tunnel muck. The strength increases as the density increases when $M_{fa}:M_{tm}=1:2$ and $2:3$. However, when M_{fa}: $M_{tm}=1:3$, the strength increases to approximately 20 MPa as the density increases and then decreases.

The scatter of strength and tenacity versus elasticity modulus and peak strain is shown in Figure 6. The peak strain seems to have an asymptotic value of 8×10^{-3}, which is indicated by the dashed lines in Figures 6(c) and 6(d). Both of elastic modulus and tenacity show positive correlation with strength, while the strength (σ_0) and elasticity modulus (E) can be fitted by a linear equation as

$$E=0.148\sigma_0+0.428. \quad (1)$$

The pictures of failure geopolymer sample are shown in Figure 7. A cone geometry part can be found for almost every failure sample, which might be due to the basal friction between the machine and sample. Meanwhile, an "X" shape shear band geometry can also be found in the failure sample as shown in Figure 7(g) [16, 40]. There is another uncommon failure as shown in Figure 7, where the top of the sample is relatively complete, while the bottom of the sample is broken into pieces. This might be caused by the inhomogeneous density distribution in the sample, which results from the high friction between the sample and the mode stopping the sample from sliding down under compression applied from the top [41]. A much dense top and less dense bottom would form in this case.

Different microscopic levels of scanning electron microscope (SEM) tests were conducted to understand the microscope structure of the geopolymer. The SEM images are shown in Figure 8, the flocculence is geopolymers, spheres are fly ashes, and bulks are soil particles. The fly ashes and soil particles are wrapped by flocculence (Figures 8(a) and 8(b)) to strengthen the sample. The flocculence is mainly from the chemical reaction of active substance in fly ashes. The left materials without chemical reaction became filler and skeleton of geopolymer sample, as shown in Figure 8(c). The corrosion on the surface of fly ash particle can be seen after the chemical reaction; several structural holes are visible as shown in Figure 8(d).

5. Conclusions

The mechanical properties of the geopolymer made by different recipes are reported. The strength, tenacity, and residual strength are analyzed systematically. The orthogonal analysis is applied to understand the effects of the mass ratio between fly ash and tunnel muck (M_{fa}/M_{tm}), the mass ratio between Na_2SiO_3 solution and NaOH solution ($M_{Na_2SiO_3}/M_{NaOH}$), the ratio between liquid and solid (M_{liquid}/M_{solid}), and molarity of NaOH on the strength of geopolymer. Our experimental study has made the following findings:

(1) The pressing mold method is better than casting method for the tunnel muck with high clay content. In order to make high-strength geopolymer sample, the dry soil and fly ash should be mixed homogeneously together first and then mixed with alkali-activator.

(2) The orthogonal analyses conclude that the optimum scheme for making geopolymer sample is to set the mass ration between fly ash and tunnel muck, the mass ratio between Na_2SiO_3 solution and NaOH solution, the ratio between liquid and solid, and molarity of NaOH to be 1 : 2, 1.8, 0.18, and 10 mol/L, respectively.

(3) The failure of geopolymer sample shows cone geometry part and "X" shape shear failure. The SEM images show that the flocculence from the active substance in fly ash is a crucial component as the cementing material.

Data Availability

The data used to support the findings of this study are included within the article.

Conflicts of Interest

The authors declare that there are no conflicts of interest regarding the publication of this paper.

Acknowledgments

This work was supported by the China State Construction Engineering Corporation Limited Funded Project (Grant no. CSCEC-2018-Z-1), Natural Science Foundation of Hunan Province, China (Grant no. 2018JJ3578), and China Construction Fifth Engineering Division Group., LTD, Funded Project (Grant no. CSCEC5b-2017-03).

References

[1] W. Liu, T. Zhao, W. Zhou, and J. Tang, "Safety risk factors of metro tunnel construction in China: an integrated study with EFA and SEM," *Safety Science*, vol. 105, pp. 98–113, 2018.

[2] P. Li, Y.-w. Zhang, F.-y. Jiang, and H. Zheng, "Comprehensive health assessment of shield tunnel structure based on prototype experiment," *Journal of Central South University*, vol. 25, no. 3, pp. 681–689, 2018.

[3] J. Rostami, C. Dreyer, and B. Blair, "Lunar tunnel boring machines," in *Proceedings of the 16th Biennial International Conference on Engineering, Science, Construction, and Operations in Challenging Environments*, pp. 240–252, American Society of Civil Engineers, Cleveland, OH, USA, April 2018.

[4] H. Zheng and Y. Huang, "Model tests on flow slide of lunar regolith simulant," *Environmental Earth Sciences*, vol. 73, no. 8, pp. 4853–4859, 2015.
[5] Y. Huang and H. Zheng, "Mechanical characteristics of a lunar regolith simulant at low confining pressure," *Environmental Earth Sciences*, vol. 71, no. 8, pp. 3697–3703, 2014.
[6] R. Bellopede, M. Francini, P. Marini, A. Migheli, E. Moretti, and P. Oreste, "Alkali aggregate reaction for concrete made with tunnel muck: experimental investigations," in *Engineering Geology for Society and Territory-Volume 5: Urban Geology, Sustainable Planning and Landscape Exploitation*, pp. 81–84, Springer, Berlin, Germany, 2015.
[7] R. Bellopede, D. Colaiacomo, P. Marini, P. Oreste, and O. Radis, "The aggregates from tunnel muck and their use as secondary raw material: the case study of turin underground," in *Engineering Geology for Society and Territory-Volume 5: Urban Geology, Sustainable Planning and Landscape Exploitation*, pp. 75–79, Springer, Berlin, Germany, 2015.
[8] W. Zhang, H. Zheng, F. Jiang, Z. Wang, and Y. Gao, "Stability analysis of soil slope based on a water-soil-coupled and parallelized Smoothed Particle Hydrodynamics model," *Computers and Geotechnics*, vol. 108, pp. 212–225, 2019.
[9] Y. Huang, H. Zheng, W. Mao, G. Li, and B. Ye, "Numerical simulation of air-soil two-phase flow based on turbulence modeling," *Natural Hazards*, vol. 58, no. 1, pp. 311–323, 2011.
[10] Y. Huang, H. Zheng, W. Mao, M. Huang, and G. Li, "Triaxial tests on the fluidic behavior of post-liquefaction sand," *Environmental Earth Sciences*, vol. 67, no. 8, pp. 2325–2330, 2012.
[11] Y. Huang, H. Zheng, and Z. Zhuang, "Seismic liquefaction analysis of a reservoir dam foundation in the South–North Water Diversion Project in China. Part I: liquefaction potential assessment," *Natural Hazards*, vol. 60, no. 3, pp. 1299–1311, 2012.
[12] Y. Huang, H. Zheng, and Z. Zhuang, "Seismic liquefaction analysis of a reservoir dam foundation in the South–North Water Diversion Project in China. Part II: seismic response simulation," *Natural Hazards*, vol. 60, no. 3, pp. 1313–1324, 2012.
[13] H. M. B. Al-Hashemi and O. S. B. Al-Amoudi, "A review on the angle of repose of granular materials," *Powder Technology*, vol. 330, pp. 397–417, 2018.
[14] A. D. Burnett and P. G. D. Whiteside, "Dredged sand and gravel for construction purposes: an assessment procedure and Hong-Kong case-study," *Journal of Coastal Research*, vol. 8, no. 1, pp. 105–124, 1992.
[15] D. Penumadu and R. Zhao, "Triaxial compression behavior of sand and gravel using artificial neural networks (ANN)," *Computers and Geotechnics*, vol. 24, no. 3, pp. 207–230, 1999.
[16] H. Zheng, D. Wang, and R. P. Behringer, "Experimental study on granular biaxial test based on photoelastic technique," *Engineering Geology*, vol. 260, Article ID 105208, 2019.
[17] Y. Zhao, H. Zheng, D. Wang, M. Wang, and R. P. Behringer, "Particle scale force sensor based on intensity gradient method in granular photoelastic experiments," *New Journal of Physics*, vol. 21, no. 2, Article ID 023009, 2019.
[18] H. Zheng, D. Wang, D. Z. Chen, M. Wang, and R. P. Behringer, "Intruder friction effects on granular impact dynamics," *Physical Review E*, vol. 98, no. 3, 2018.
[19] H. Zheng, D. Wang, J. Bares, and R. P. Behringer, "Sinking in a bed of grains activated by shearing," *Physical Review E*, vol. 98, no. 1, Article ID 010901, 2018.
[20] D. Wang, J. Ren, J. A. Dijksman, H. Zheng, and R. P. Behringer, "Microscopic origins of shear jamming for 2D frictional grains," *Physical Review Letters*, vol. 120, no. 20, Article ID 208004, 2018.
[21] H. Zheng, J. A. Dijksman, and R. P. Behringer, "Shear jamming in granular experiments without basal friction," *EPL (Europhysics Letters)*, vol. 107, no. 3, p. 34005, 2014.
[22] L. Yun-Ming, H. Cheng-Yong, M. M. Al Bakri, and K. Hussin, "Structure and properties of clay-based geopolymer cements: a review," *Progress in Materials Science*, vol. 83, pp. 595–629, 2016.
[23] B. Singh, G. Ishwarya, M. Gupta, and S. K. Bhattacharyya, "Geopolymer concrete: a review of some recent developments," *Construction and Building Materials*, vol. 85, pp. 78–90, 2015.
[24] X. Y. Zhuang, L. Chen, S. Komarneni et al., "Fly ash-based geopolymer: clean production, properties and applications," *Journal of Cleaner Production*, vol. 125, pp. 253–267, 2016.
[25] J. Davidovits, "Man-made rock geosynthesis and the resulting development of very early high strength cement," *Journal of Materials Education*, vol. 16, no. 2, pp. 91–139, 1994.
[26] K. Komnitsas and D. Zaharaki, "Geopolymerisation: a review and prospects for the minerals industry," *Minerals Engineering*, vol. 20, no. 14, pp. 1261–1277, 2007.
[27] N. Cristelo, S. Glendinning, T. Miranda, D. Oliveira, and R. Silva, "Soil stabilisation using alkaline activation of fly ash for self compacting rammed earth construction," *Construction and Building Materials*, vol. 36, pp. 727–735, 2012.
[28] C. Suksiripattanapong, S. Horpibulsuk, P. Chanprasert, P. Sukmak, and A. Arulrajah, "Compressive strength development in fly ash geopolymer masonry units manufactured from water treatment sludge," *Construction and Building Materials*, vol. 82, pp. 20–30, 2015.
[29] P. Duxson, J. L. Provis, G. C. Lukey, S. W. Mallicoat, W. M. Kriven, and J. S. J. van Deventer, "Understanding the relationship between geopolymer composition, microstructure and mechanical properties," *Colloids and Surfaces A: Physicochemical and Engineering Aspects*, vol. 269, no. 1–3, pp. 47–58, 2005.
[30] J.-B. M. Dassekpo, X. Zha, and J. Zhan, "Compressive strength performance of geopolymer paste derived from completely decomposed granite (CDG) and partial fly ash replacement," *Construction and Building Materials*, vol. 138, pp. 195–203, 2017.
[31] J.-B. M. Dassekpo, X. Zha, and J. Zhan, "Synthesis reaction and compressive strength behavior of loess-fly ash based geopolymers for the development of sustainable green materials," *Construction and Building Materials*, vol. 141, pp. 491–500, 2017.
[32] P. Duxson, A. Fernández-Jiménez, J. L. Provis, G. C. Lukey, A. Palomo, and J. S. J. van Deventer, "Geopolymer technology: the current state of the art," *Journal of Materials Science*, vol. 42, no. 9, pp. 2917–2933, 2007.
[33] P. Duxson, G. C. Lukey, F. Separovic, and J. S. J. van Deventer, "Effect of alkali cations on aluminum incorporation in geopolymeric gels," *Industrial & Engineering Chemistry Research*, vol. 44, no. 4, pp. 832–839, 2005.
[34] H. Y. Leong, D. E. L. Ong, J. G. Sanjayan, and A. Nazari, "Strength development of soil-fly ash geopolymer: assessment of soil, fly ash, alkali activators, and water," *Journal of Materials in Civil Engineering*, vol. 30, no. 8, Article ID 04018171, 2018.
[35] P. Boivin, P. Garnier, and D. Tessier, "Relationship between clay content, clay type, and shrinkage properties of soil samples," *Soil Science Society of America Journal*, vol. 68, no. 4, pp. 1145–1153, 2004.

[36] J. M. Kanema, "The influence of soil content on the mechanical properties, drying shrinkage and autogenous shrinkage of earth concrete," *Journal of Building Engineering*, vol. 13, pp. 68–76, 2017.
[37] M. M. Attard and S. Setunge, "Stress-strain relationship of confined and unconfined concrete," *ACI Materials Journal*, vol. 93, no. 5, pp. 432–442, 1996.
[38] T. Mizuno, S. Kinoshita, T. Ito, S. Maedera, and H. Kusuhara, "Development of orthogonal linear separation analysis (OLSA) to decompose drug effects into basic components," *Scientific Reports*, vol. 9, no. 1, 2019.
[39] Z. Wu, W. Wang, D. Wang, K. Zhao, and W. Zhang, "Global sensitivity analysis using orthogonal augmented radial basis function," *Reliability Engineering & System Safety*, vol. 185, pp. 291–302, 2019.
[40] H. Zheng, D. Wang, X. Tong, L. Li, and R. P. Behringer, "Granular scale responses in the shear band region," *Granular Matter*, vol. 21, no. 4, p. 107, 2019.
[41] D. E. M. Gooding, "Improved processes for the production of soil-cement building blocks," Ph. D. thesis, Department of Philosophy in the Faculty of Engineering, The University of Warwick, Coventry, UK, 1994.

Hindawi
Advances in Civil Engineering
Volume 2020, Article ID 1097696, 10 pages
https://doi.org/10.1155/2020/1097696

Research Article

A Study on the Sloshing Problem of Vertical Storage Tanks under the Action of Near-Fault Earthquakes

Lijian Zhou,[1] Tian Xu,[1] Zhaohong Lu,[1,2] and Dong Zhang[2]

[1]*Northeast Petroleum University, Daqing, China*
[2]*CNPC Key Laboratory of Oil & Gas Storage and Transportation, PetroChina Pipeline R&D Center, Langfang, China*

Correspondence should be addressed to Zhaohong Lu; luzh2008@126.com

Received 30 July 2019; Revised 4 December 2019; Accepted 2 January 2020; Published 22 January 2020

Guest Editor: Jingfeng Yuan

In this study, through a vibration table test, finite element simulation, and research on the rationality of the wave-height fortification of national storage tank specifications, the sloshing response of vertical storage tanks under the action of near-fault ground motion was analyzed. The test results showed that the sloshing wave height of a vertical storage tank was larger under near-fault or long-period ground motions, and the relationship between the sloshing wave height and the peak acceleration of input ground motions was approximately linear. The numerical simulations of the model tank showed that the simulation wave height and the test wave-height data were well fitted. Therefore, it was feasible to simulate the sloshing of large vertical storage tanks using ADINA software. In addition, a large number of sloshing simulations of near-fault ground motions on 10,000 m^3 vertical storage tanks were performed. The simulated wave height had a high correlation with the predominant period or pulse period of near-fault ground motions. Under the calculation with similar parameters, the wave height of the tank standard in several countries had a lower fortification of the near-fault excitation wave height. Through the root mean-square method using a small sample size, a wave-height correction under a near-fault effect was applied to the wave-height formula for the Chinese tank seismic specification. Finally, the problem of a double-damping correction was addressed by adjusting China's GB50341 wave-height formula. This work provides a reference value for practical engineering applications.

1. Introduction

Large vertical storage tanks have thin tank walls and hold a large volume, and the basic self-vibration period of the liquid storage is long. Under the action of long-period ground motion, liquid storage produces a large nonlinear sway, and the huge force easily causes damage to the filling roof and buckling of the tank wall [1, 2]. For example, in the 1980s, the earthquake in the middle of the Sea of Japan caused damage to oil tanks with a shaking period of about 10 s in the nearby city of Niigata and caused a fire [3]. Then in 1991, the 6.9 magnitude earthquake in Costa Rica caused overturning and instability of storage tanks in local steel plants, which caused huge losses [4].

With the increasing demand for large vertical tanks in various countries of the world, their role in the development of the economy and petrochemical industry is becoming increasingly important. Many scholars have conducted research on tank sloshing. Yan [3] conducted three-dimensional shaking table tests on a vertical open tank and a floating roof tank. Through the input of different amplitudes and frequency of ground motion, the data of tank sloshing wave height and displacement were obtained. Wang et al. [5] simulated three kinds of tanks with different liquid levels under earthquake conditions using ADINA software and analyzed the wave height of liquid sloshing, peak acceleration of the tank wall, and hydrodynamic pressure. Cheng et al. [6] studied the sloshing response of liquid in a rigid cylindrical tank with a rigid annual baffle uncle. The problem of a shaking response under near-fault ground motion, however, was not involved. Near-fault ground motions have large velocity pulses and abundant long-period waveforms, which are liable for producing double resonance with storage tanks, resulting in large-scale sloshing of storage

fluid and potential hazards to storage tanks and the surrounding environment [7]. Moreover, because China is located between the Pacific Rim Seismic Zone and the Himalayan Seismic Zone, near-fault earthquakes often occur in China. Therefore, this article studied the sloshing effect of near-fault ground motions with different spectral characteristics under excitation. On the basis of a comparison of the shaking table test, numerical simulation, and the wave-height formula of the national tank standard, we corrected the Chinese version of the wave height under near-fault ground motion to study the sloshing effect. This study provides a reference for the wave-height design of vertical storage tanks under the action of near-fault ground motion.

2. Shaking Table Test of Vertical Storage Tank

Seismic waves are not only complex in the frequency domain but also complex in the time domain. Therefore, it is not enough to rely solely on national codes and simulation calculations to fully reflect the response of structures to real earthquakes over time. The shaking table test is the most effective method to verify theoretical calculations and simulation calculations at present, so the engineering community often uses the shaking table test to examine the response superposition problem of a structure under the action of ground motion [8]. We selected a 1000 m^3 vertical storage tank and subjected the prototype can to quarter-scale processing. According to the similarity relationship, we designed the model tank and adjusted the input ground motion parameters [1]. To study the relationship between the sloshing wave height and the seismic spectrum characteristics and the acceleration peak, we extracted the wave-height data by unidirectional seismic loading. Finally, we verified the sway simulation using the finite element software ADINA.

2.1. Test Layout and Seismic Wave Input. The geometric dimensions of the test model tank were as follows: the tank height was 2.65 m, the tank diameter was 2.9 m, and the liquid storage height was 2.38 m. The arrangement of the experimental wave-height displacement meter was 0 mm, 560 mm, and 1300 mm from the center of the liquid surface, and the table-top output acceleration collector was arranged on the table below the ring beam. The tank layout is shown in Figure 1.

In this test, we selected EL-Centro wave, TCU089 wave, JM wave, and Pasadena for the input of the shaking table because of the limitation of the displacement of the table. These four waves are commonly used in the world, among which TCU089 is used for near-fault ground motion. We assigned each displacement wave a corresponding 0.05 g, 0.1 g, 0.15 g, 0.2 g, 0.25 g, 0.3 g, 0.35 g, and 0.4 g peak acceleration and derived the time similarity ratio based on the model's similarity ratio. We finally determined the time interval of each seismic wave to be 0.024 s. Figure 2 shows the displacement time history curve of each seismic wave of 0.4 g.

2.2. Test Data Analysis. By extracting the maximum acceleration recorded by the acceleration collector installed on the platform and comparing it with the peak acceleration of each input seismic wave, the acceleration transmitted from the vibration table to the foundation can be truly and accurately reflected. The comparison data are shown in Figure 3.

As shown in Figure 3, the difference between the output acceleration extremum and the peak value of the input acceleration is not exactly the same because the slight deviations between the input and output acceleration of seismic wave are inevitable in engineering tests. Thus, the test output data are reasonable.

We extracted the wave height corresponding to each seismic wave at different acceleration peaks, as shown in Table 1, and made a trend relationship diagram between the wave height and the corresponding acceleration peak, as shown in Figure 4.

Using Fourier transform for each of acceleration waves collected on the platform, we obtained the predominant periods of the EL-Centro wave, TCU wave, Jinmen seismic wave, and Pasadena wave, which were 0.163 s, 0.204 s, 0.28 s, and 0.463 s, respectively. As shown in Table 1, there were differences in the excitation wave heights of different ground motions. The excitation wave height of the excellent period was short, and the excitation wave height of the EL-Centro wave and the Golden Gate wave, whose long-period waveforms were lower, was relatively low. Conversely, the long-period waveform was rich, and the period of the near-fault ground motion TCU and Pasadena waves was relatively large. Therefore, the sloshing wave height of the vertical storage tank under the earthquake had a significant correlation with the spectral characteristics of ground motion, in particular, because the wave-height sloshing under the action of long-period ground motion cannot be ignored. It is evident from Figure 4 that as the input ground motion peak increased, the excitation wave height and the input acceleration peak increased linearly. Notably, the linear relationship between the near-fault TCU wave and the Pasadena wave with more long-term characteristics was more obvious. The ratio of any two wave heights was approximately equal to the ratio of the two acceleration peaks.

2.3. Numerical Simulation Analysis of Model Cans. We numerically simulated the model cans using the ADINA software. The purpose of the numerical simulation was to verify each simulation with the test and to verify the reliability of the finite element sloshing analysis while also comparing the differences. We based the physical properties of the numerical simulation materials on experimental measurements. The tank-sloshing simulation used the potential flow module, the tank foundation used the solid unit, and the base and tank contact surfaces adopted the contact unit. The tank model and the contact model are shown in Figure 5. The vertical tank wall and tank bottom plate selected the four-node shell unit, the foundation adopted an eight-node solid unit (3-dsold) for simulation, the liquid storage adopted an eight-node three-dimensional fluid unit,

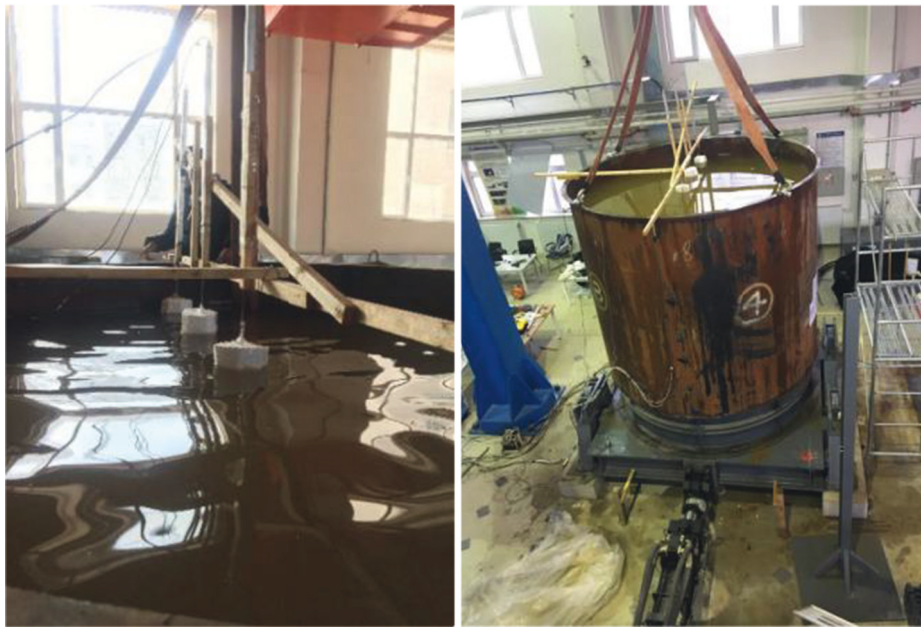

Figure 1: Test layout.

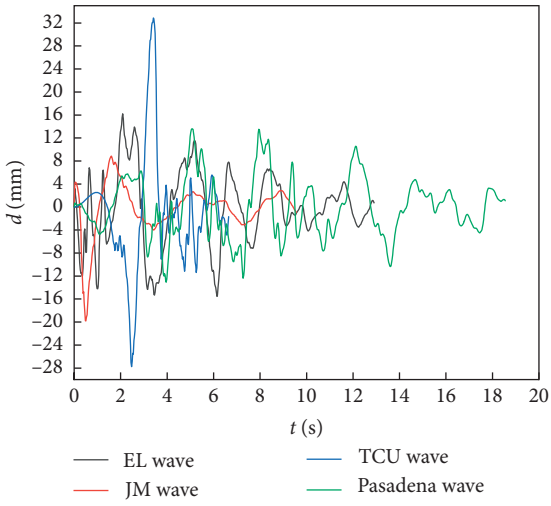

Figure 2: Seismic wave displacement time history diagram.

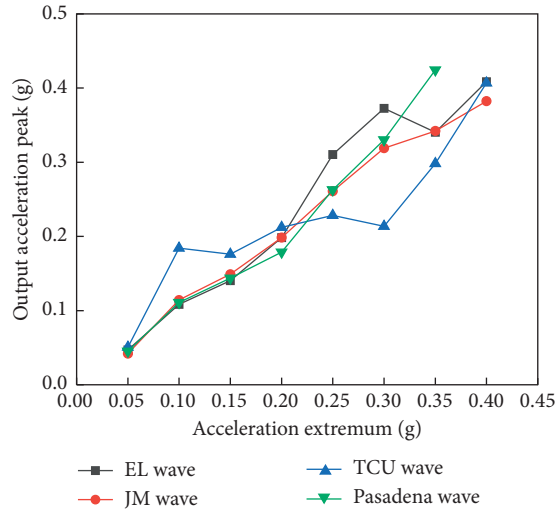

Figure 3: Table-top output acceleration peak. *Note*. Pasadena wave with an extremum acceleration of 0.4 g exceeds the mesa displacement.

the upper surface of the liquid storage was set as the free liquid level, and the other surface was the fluid unit. ADINA automatically identified the coupling contact surface when potential flow theory was adopted, thus greatly improving the calculation speed.

The finite element model ground motion input used the accelerometer wave collected by the test bench accelerometer with a 0.3 g peak. We conducted a dynamic time history analysis for each seismic wave of the model. The collected sloshing wave height and the extreme value of the test wave height are shown in Table 2. Figure 6 compares the real time history curve and the test time history curve of the wave-height extreme point.

Table 2 shows that the simulated wave height and the test wave-height sway extreme values are similar. The average difference rate was 12.7%, and the simulated wave height was slightly larger than the test wave height, which also was related to the wave-height acquisition device. Because the elastic displacement meter had a suppression effect on the sloshing wave height, the test wave height was slightly smaller than the simulated wave height. Figure 6 shows that the simulation and experimental extreme wave-height time history curves were basically the same—only the wave-height value was slightly different. From the four wave-height time history comparison curves, the simulation and test data were basically the same, and both were mutually verified. Thus, it was feasible to use the finite element software ADINA to simulate vertical tank sloshing.

Table 1: Test sloshing wave height (in millimeters).

Seismic wave	0.05 g	0.1 g	0.15 g	0.2 g	0.25 g	0.3 g	0.35 g	0.4 g
EL-Centro wave	11.167	25.813	34.787	47.076	57.967	53.161	68.742	88.73
JM wave	14.064	14.59	20.36	27.25	37.35	43.26	53.52	61.1
TCU wave	15.9	31.46	50.11	64.506	79.92	92.49	115.6	120.2
Pasadena wave	11.4	18.62	33.54	59.17	101.6	126.3	149.26	

Note. Pasadena wave with an extremum acceleration of 0.4 g exceeds the mesa displacement.

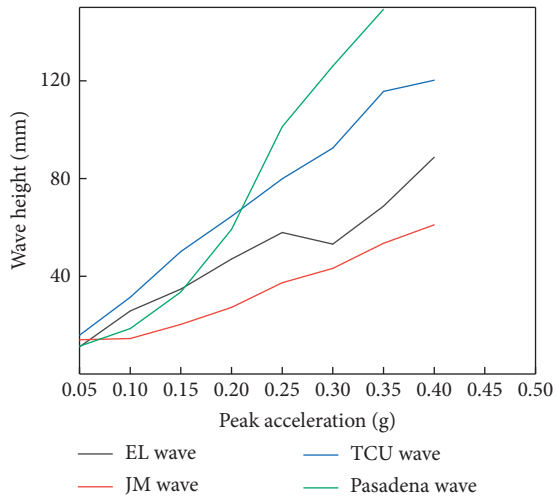

Figure 4: Wave height and peak acceleration trend graph.

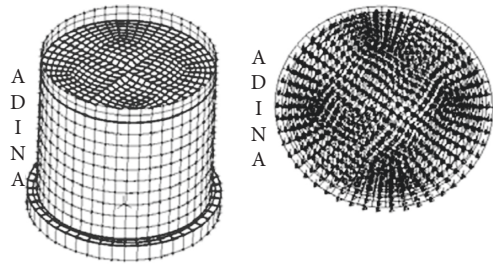

Figure 5: Finite element model of storage tank. (a) Tank model. (b) Contact model.

Table 2: Simulation and test wave heights (in millmeters).

Seismic wave	EI-Centro wave		JM wave		TCU wave		Pasadena wave	
	"−"	"+"	"−"	"+"	"−"	"+"	"−"	"+"
Simulation wave height	39	51	32	28	59.6	50.5	76.1	76.3
Test wave height	46.9	47.1	27	27.3	38.8	59.17	50.6	64.5
Difference rate (%)	16.8	8.2	18.5	2.5	54	14.6	50.3	18.3

Note. "+" and "−" correspond to the extreme peak and trough of wave height, respectively.

3. Finite Element Analysis of Vertical Storage Tanks and Correction of Chinese Standard Wave-Height Formula

From the analysis of the test results, we determined that the sloshing wave height of the vertical storage tank was related to the spectral characteristics of the ground motion. The richer the long-period waveform, the higher the excitation wave height. This was especially true for the near-fault ground motion, which often contained a large number of long-period seismic waveforms, and the excitation wave height was large. Because of the large-scale pulse of near-fault ground motion, the excitation displacement of the structure was large, and the ultimate displacement of the vibration table was small. This

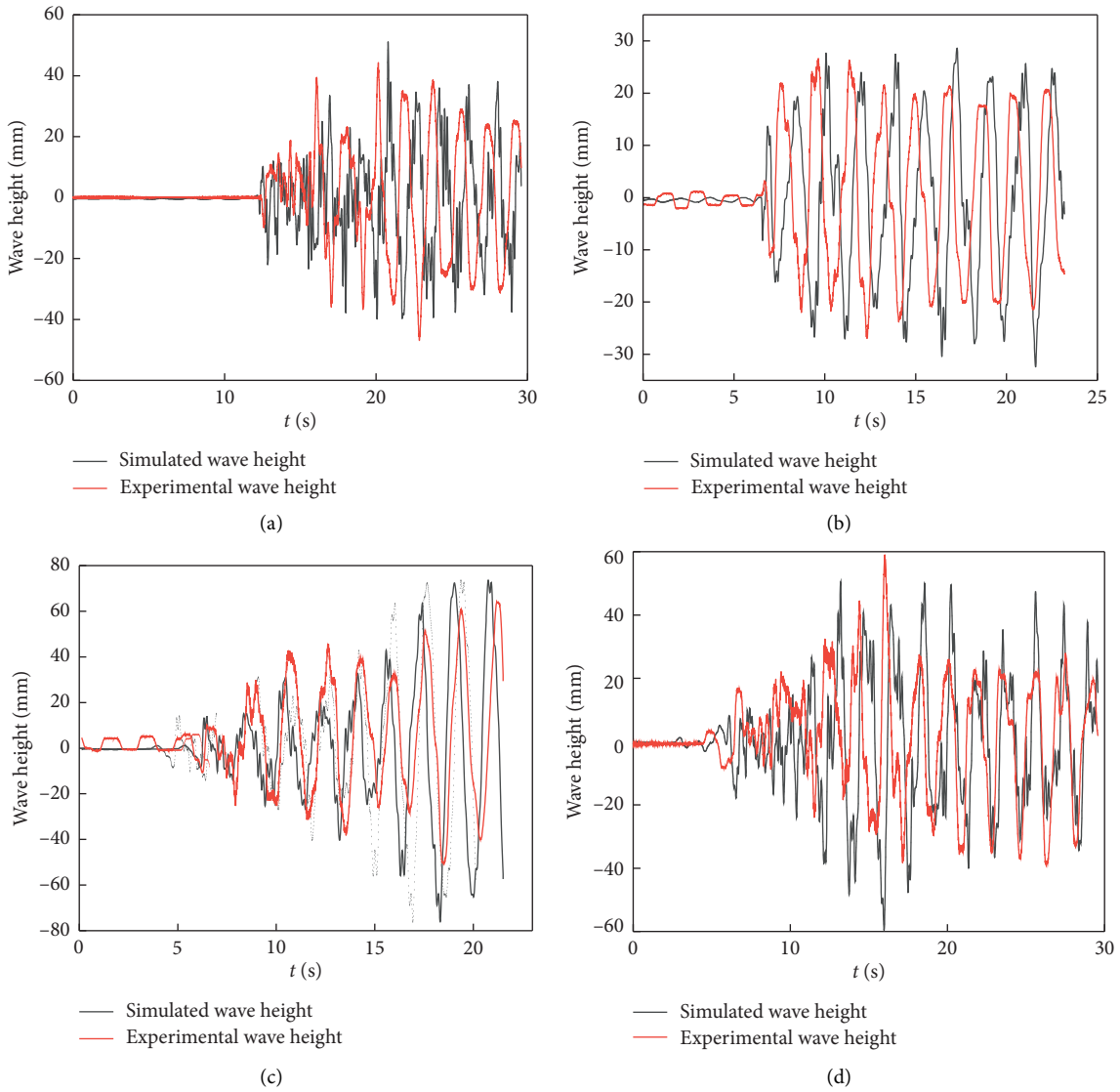

Figure 6: Comparison of simulated wave-height and test wave-height time history curves. (a) EL-Centro time history curve of the wave. (b) JM time history curve of the wave. (c) Taft time history curve of the wave. (d) Pasadena time history curve of the wave. *Note*. When the duration time of ground motion stopped, the storage fluid will turn into free vibration. The damping ratio of the storage fluid is 0.005. So there will be a attenuation trend after the shaking wave height of the storage fluid in the figure.

limited the output of the near-fault ground motion to the structural displacement. The engineering community often uses numerical analysis because this method can be used to explore the sloshing effect of large vertical storage tanks under near-fault ground motion. Therefore, in this part of the test, we selected a 10,000 m^3 vertical storage tank for numerical simulation under near-fault ground motion to explore the correlation between excitation wave height and the predominant period and pulse period. We also examined the high envelope of the excitation wave of the near-fault ground motion. We corrected the wave-height formula of the seismic specification of the Chinese tank for near-fault ground motion.

3.1. Numerical Simulation of 10,000 m^3 Vertical Tank Sloshing. The basic dimensions of the 10,000 m^3 vertical storage tank were as follows: tank height was 17.5 m, diameter was 28.3 m, and liquid storage height was 14 m. The finite element model and the first-order mode with a period of 5.42 s are shown in Figure 7. The selection of seismic waves was based on three elements of ground motion, namely, ground motion duration, spectral characteristics, and effective peaks. From the Pacific Earthquake Engineering Research Center (PEER), we selected 38 near-fault ground motions recorded worldwide. Using the potential flow theory of the finite element software ADINA, we input the 0.2 g near-fault ground motion into the storage tank and used the dynamic time-integration method to calculate the sloshing wave height of the storage tank. Table 3 gives the excitation wave height and period parameters of the 38 near-fault ground motions.

As can be seen in Table 3, different seismic waves have different wave heights. Because different ground motions have different frequency characteristics, the wave heights are

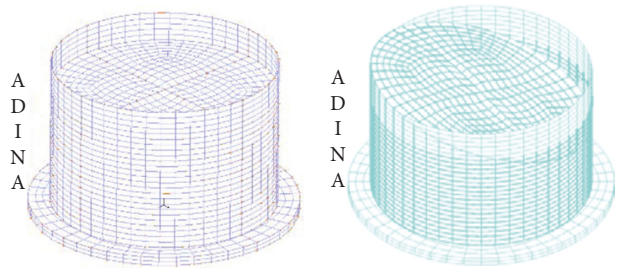

(a) (b)

Figure 7: 10,000 m^3 finite element model and first-order model. (a) Finite element model. (b) First-order mode.

Table 3: Spectrum parameters and excitation wave heights of near-fault ground motions.

Seismic wave	Wave height (mm)	Seismic wave	Wave height (mm)	Seismic wave	Wave height (mm)	Seismic wave	Wave height (mm)	Seismic wave	Wave height (mm)
RSN1496	1880	RSN180	558	RSN1244	1409	RSN1511	1445	RSN176	870
RSN147	173	RSN182	776	RSN1475	1854	RSN1519	1581	RSN6911	1448
RSN159	499	RSN285	1028	RSN1476	240	RSN1528	1752	RSN6927	1926
RSN170	1449	RSN900	1507	RSN1478	3410	RSN1531	4548	RSN185	1383
RSN171	661	RSN1085	448	RSN1486	1789	RSN6887	1859	RSN8119	843.3
RSN173	2300	RSN1161	1116	RSN1503	1837	RSN6897	1823	RSN8606	3090
RSN1165	888	RSN1505	1724	RSN6906	1483	RSN6942	1510	RSN6962	2797
RSN6959	1734	RSN6969	4626	RSN1489	970				

Note. RSN is coded by Pacific Seismic Engineering Research Center (PEER).

different. The experiments showed that the excitation wave height had a certain correlation with the spectral characteristics of ground motion. Therefore, we studied the near-fault ground motion predominant period and the trend of pulse period and wave height to explore the correlation between wave height and ground motion period parameters. The trend chart is shown in Figure 8.

As shown in Figure 8, the use of the near-fault predominant cycle and pulse period to characterize wave height contributed to certain tendencies. Large wave-height values were concentrated mainly near the first-order sloshing cycle, and the larger the waveform period, the larger the excitation wave height. We used the Pearson correlation coefficient to measure the correlation between the predominant period and the pulse period and excitation wave height, and the calculated correlation coefficients were 0.495 and 0.458, respectively. Both exhibited a moderate degree of correlation. The predominant period was slightly higher than the correlation of the pulse period and wave height. Therefore, it was reasonable to use the predominant period and pulse period of the near-fault ground motion to characterize the excitation wave height.

3.2. Comparative Analysis of Incentive Wave Height of Near-Fault Ground Motion and Wave Height of Storage Tanks in Different Countries. Although the seismic specifications of the Sino-U.S. European and Japanese storage tanks differed in terms of seismic concept, design level, and definition of ground motion parameters, the design of the sloshing was similar. The sloshing cycle of the four countries' specifications was a first-order sloshing cycle that was quoted from the Housner [9] rigid tank wall. The sloshing wave-height formula was also based on the rigid tank wall to consider the two-point or three-mass theoretical model of the elastic tank wall [10], and we applied this formula to the sloshing formula of each country's response spectrum. National normative sloshing wave heights and period formula are shown in Table 4. We used 8 degrees 0.2 g ground basic acceleration, class III site, and seismic grouping for the first group of seismic design parameters for China's 10,000 m^3 standard wave-height formula. Finally, according to the research results of Hui, Li, Zhinan, and others [11–13], and through a comparison and analysis of national norms, we selected the seismic design parameters with similar specifications in foreign countries to calculate the sloshing period and wave height. The calculated results are compared with the simulated wave height of near-fault ground motion. The distribution diagram of simulated wave height of near-fault ground motion is shown in Figure 9.

The calculated wave heights in China, United States, Europe, and Japan are basically within 1500 mm. Among them, Chinese code GB50761 is 1067 mm, American code API650 is 1465 mm, European code BS EN8-4 is 426 mm, and Japanese code JIS B850 is 1372 mm. From the simulated wave height distribution of near-fault ground motion in Figure 9, it can be seen that the specifications cannot fully envelop the excitation wave height of the near-fault ground motion. The European standard calculation wave height was lower than most of the excitation wave heights and was 10 times smaller than the individual seismic excitation wave. From the mean effect, we determined that the average wave height of 38 ground motions was 1611 mm, which was 1.51

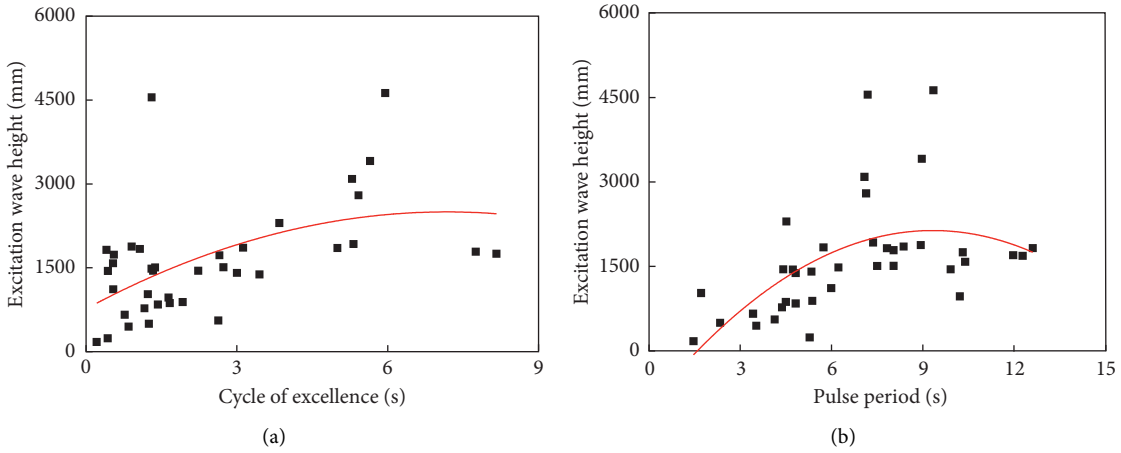

FIGURE 8: Spectrum parameters of near-fault ground motion and wave height scatter plot. (a) Trend map of predominant period and wave height. (b) Trend chart of pulse period and wave height.

times that of the calculated wave height of China's standard GB50761, 1.1 times that of the US standard, 3.78 times that of the European standard, and 1.21 times that of the Japanese standard wave height. From this, we also concluded that it is unreasonable for countries to standardize the fortification of high-period waveforms with near-fault ground motion excitation wave heights, and it was necessary to correct the wave height of near-fault ground motion for normal waves.

3.3. Wave-Height Correction of China's Tank Specification. Excessive wave height under the action of ground motion will cause the "stuck" of the floating roof or the buckling of the dome. In the norm of API 650, GB 50341, or GB 50761, the calculation of the base shear force, base bending moment, and the stress of the tank wall of each layer did not consider the influence of the sloshing wave height. They only specify the reserved height from the liquid storage surface to the tank top. So it is necessary for designers to consider the effect of shaking wave height on the tank under the seismic action with large excitation wave height. In order to reasonably set up defenses of the wave height of near-fault ground motions, this article will propose a long-period correction of the Chinese standard wave height formula using the root-mean-square method.

The root mean square (RMS) represented the effective value of a set of discrete data (formula (1)). Compared with the mean value of data, RMS better represented the confidence value of discrete data. We took 38 near-fault ground motion excitation wave heights, used RMS to calculate the effective value of this set of discrete data, and corrected the wave height according to the ratio of the effective value and the normative wave-height value. We processed the mean square root and mean values of the excitation wave heights of 38 near-fault seismic waves for 10,000-m^3 vertical storage tanks. The calculated data are shown in Table 5:

$$X_{\text{rms}} = \sqrt{\frac{\sum_{i=1}^{N} X_i^2}{N}} = \sqrt{\frac{X_1^2 + X_2^2 + \cdots + X_N^2}{N}}, \quad (1)$$

where X_i denotes the value of elements in the sample and N denotes the total amount of samples.

Table 5 shows that the RMD value was larger than the average value because the RMS value had a larger confidence interval for a group of data than the average value, which was more representative of the effective value of a set of discrete data. The RMS value was larger than the normative wave-height value of the weak site calculated using China's two norms. Because GB50341 repeatedly considered the damping correction, its calculated wave height was larger, but it was still less than the effective value of the sample wave height.

We applied the formula $h_v = 0.837\,\text{Ra}$ to the sloshing wave height of GB50341, which was derived from the potential flow theory and considered the fluid viscosity. We referred to the 0.005 damping ratio correction for such countries as Japan and the United States, which was multiplied by a factor of 1.79. When the earthquake impact coefficient a was calculated, the relevant parameters were still calculated using the damping ratio of 0.005, so we considered the double-damping correction. The wave-height formula of GB50761, however, considered the single-damping correction. Therefore, when we calculated the wave-height correction of GB50341 by statistical RMS value, we performed a single-damping correction and considered only the damping correction when calculating the seismic influence coefficient. We simulated wave height by ground shaking with a small sample size of a specific tank type and used the ratio of effective value to normal value to correct the wave height under near-fault ground motion. This value can be used for practical engineering. For other types of tanks, this method can also be used to make small sample capacity comparison, get the RMS value for correction, and calculate the conservative wave height for design. The correction formula is as follows:

GB50341-2014, Code for Design of Vertical Cylindrical Steel Welded Tank:

$$h_v = 1.67\eta aR. \quad (2)$$

Table 4: Standard wave-height formula and periodic formula of various countries.

Country	Wave-height formula		Sloshing period formula
China GB50341 [14]	$h_v = 1.5\eta aR$		$T_w = K_s\sqrt{D}$
China GB50761 [15]	$h_v = \eta K_V a_v R$ $K_V = 3.03629 - 0.67886 \times T_w + 0.06602 \times T_w^2 - 0.00197 \times T_w^3$		$T_w = 2\pi\sqrt{(D/3680g)\coth(3.68H_w/D)}$
America	For functional groups I and II	For class III use function groups	
API650 [16]	$T_c \le 4$ $h_V = KS_{D1}I(1/T_c) = 1.05\,DK\,QF_aS_oI(T_s/T_c)$ $T_c > 4$ $h_V = KS_{D1}I(4/T_c^2) = 1.05\,DK\,QF_aS_oI(4T_s/T_c^2)$ $T_s = F_vS_1/F_aS_s$	$T_c \le T_L$ $h_V = KS_{D1}I(1/T_c) = 1.05\,DK\,QF_aS_oI(T_s/T_c)$ $T_c > T_L$ $h_V = KS_{D1}(T_L/T_c^2) = 1.05\,DK\,QF_aS_o(T_sT_L/T_c^2)$ $T_s = F_vS_1/F_aS_s$	$Tc = 1.8K_s\sqrt{D}$ $K_s = 0.578/\sqrt{\tanh(3.68H/D)}$
Europe EC-8 [17]	$d = 0.84R(S_e(T_{\text{con}}))/g$		$T_{\text{con}} = C_c\sqrt{R}$
Japan JIS B8501 [18]	$h_v = 0.00268\,DS_{vo}V_1/T$		$\mathrm{T} = 2\pi\sqrt{D}/\sqrt{3.68g\tanh(3.68H_w/D)}$

Note. h_v, d is the height of the shaking wave; η is the tank type coefficient; K_v is the long-period response spectrum adjustment coefficient; K is the spectrum acceleration adjustment coefficient, generally $K = 1.5$; Q is the design liquid level spectrum acceleration scaling factor, generally taking $Q = 1.0$; T_L is the long-term excessive period; S_o is the response spectrum response instantaneous acceleration parameter, generally $S_o = 0.4S_s$; S_{vo} is the velocity elastic spectrum value, generally taking $S_{vo} = 1$; and V_1 is the regional correction coefficient.

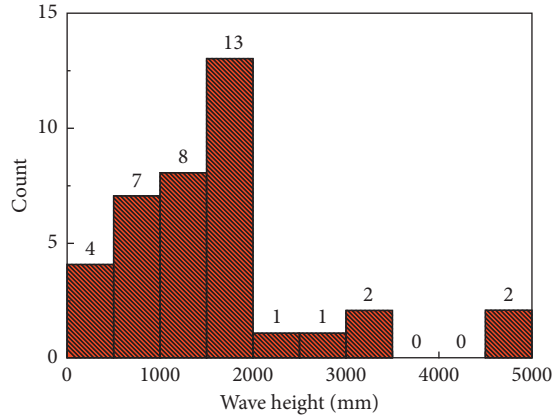

Figure 9: Simulated wave height distribution of near-fault ground motion.

Table 5: RMS and gauge wave heights of excitation wave heights for near-fault ground motions.

Vertical storage tank	Root mean square value	Mean value	GB50341 computed wave height	GB50761 computed wave height
10,000 m^3	1893	1611	1680	1067

GB50761-2018, Code for Seismic Design of Petrochemical Steel Equipment:

$$h_v = \eta K_V a R,$$
$$K_V = 5.3868 - 1.2043 \times T_w + 0.11712 \times T_w^2 - 0.003495 \times T_w^3, \quad (3)$$

where η is the tank type coefficient; the floating roof tank is taken as 0.85, the fixed top tank is taken as 1; a is the seismic influence coefficient of damping of 0.005; K_v is the long-period adjustment coefficient; and the adjustment factor of this section is included.

4. Conclusion

On the basis of this study, we drew two main conclusions. First, it was evident from the shaking table test of the vertical storage tank that the wave height of long-period ground motion and near-fault ground motion excitation with rich long-period waveforms was larger. This wave-height value had a certain linear relationship with the peak acceleration of ground motion, and the ratio of two wave heights was approximately equal to the ratio of two accelerations. In addition, the finite element simulation of the model tank under the same ground motion action showed that the simulation wave height and the test wave height had a good fit, and the two could be mutually verified.

Second, it was possible to simulate the shaking of a 10,000 m^3 large vertical storage tank under the action of a near-fault earthquake. We used the pulse period or predominant period as the ground motion parameter to characterize the wave height. Through comparison, we found that the envelope ratio of the wave height calculated according to tank specifications in China, the United States, Europe, Japan, and other countries to the near-fault ground motion excitation wave height was not high. Therefore, to achieve the near-fault ground motion, it was necessary to modify the wave-height formula. In addition, we proposed the RMS method to modify the wave-height formula of the Chinese code for long-period waveforms. We also adjusted the double-damping correction of the Chinese tank code GB 50341, which provides a reference method for the scientific design of near-fault ground motion in the engineering of wave-height design.

Data Availability

The data used to support the findings of this study are included within the article. The data used to support the findings of this study are available from the corresponding author upon request.

Conflicts of Interest

The authors declare that they have no conflicts of interest.

References

[1] S. J. Gang, *Isolation of Large Vertical Storage Tank—Theory, Method, Test*, Science Press, Beijing, China, 2009.

[2] C. L. Fu, *Base Isolation and Sloshing Control of Large-scale LNG Storage Tanks*, Dalian Maritime University, Dalian, China, 2012.

[3] S. J. Yan, *Experimental Study about Dynamic Response of Unanchored Model Tank with Floating Roof under Lateral Earthquake Excitation*, Zhejiang University, Hangzhou, China, 2012.

[4] Z. L. Jian, "Research and optimization of 15 km^3 gas spherical tank design," *World Earthquake Engineering*, vol. 34, no. 2, pp. 190–199, 2018.

[5] J. D. Wang, D. Zhou, and W. Q. Liu, "Response of liquid in cylindrical tank with rigid annual baffle considering damping effect," *Advances in Civil Engineering*, vol. 255–260, pp. 3687–3691, 2011.

[6] X. D. Cheng, J. J. Hu, and L. M. Zhao, "Dynamic response analysis of vertical cylindrical storage tanks based on ADINA," *Advances in Civil Engineering*, vol. 90–93, pp. 1482–1485, 2011.
[7] Z. L. Jian, "Study on sloshing wave height of large vertical storage tanks under long period earthquake," *Journal of Natural Disasters*, vol. 28, no. 3, pp. 87–95, 2019.
[8] Z. L. Jian, "Study on shock absorption performance of spherical tank with viscous damper," *World Earthquake Engineering*, vol. 35, no. 2, pp. 57–67, 2019.
[9] G. W. Housner, "Dynamic pressure on accelerated fluid containers," *Bulletin of Seismological Society of America*, vol. 47, no. 1, pp. 15–35, 1957.
[10] M. A. Haroun and G. W. Housner, *Dyamic Interaction of Liquid Storage Tanks and Foundation Soil*, Atlanta, Georgia, 1981.
[11] L. Hui, *The Seismic Action Comparison Between Chinese, American, European and Japanese Seismic Design Codes for Buildings*, Harbin Institute of Technology, Harbin, China, 2011.
[12] F. Li, "Comparison of seismic fortification aims and earthquake actions between eurocode 8 and Chinese seismic design code for buildings," *Structural Engineers*, vol. 12, pp. 22–26, 2006.
[13] J. Zhinan, *The Evolution of Some Provisions in Chinese Seismic Code of Buildings and Comparison of these Provisions between Chinese and European Codes*, Institute of Engineering Mechanics, China Seismological Bureau, Harbin, China, 2010.
[14] GB 50341-2014, *Code for Design of Vertical Cylindrical Welded Steel Oil Tanks*, Planning Publishing House, Beijing, China, 2014.
[15] GB 50761-2018, *Standard for Seismic Design of Petrochemical Steel Equipment*, Planning Publishing House, Beijing, China, 2018.
[16] American Petroleum Institute, *API 650-2013 Welded Tanks for Oil Storage*, AP Institute, Washington, DC, USA, 2013.
[17] Structural seismic design—silos, tanks and pipes, Eurocode 8-4, 2006.
[18] JIS B 8501-1995, *Structure of Steel Welded Tank*, JISC, Tokyo, Japan, 1997.

Hindawi
Advances in Civil Engineering
Volume 2020, Article ID 9128704, 11 pages
https://doi.org/10.1155/2020/9128704

Research Article

Study on Underground Utility Tunnel Fire Characteristics under Sealing and Ventilation Conditions

Hongtao Zhang[1] **and Yufei Zhao**[2]

[1]*College of Civil Engineering, North China University of Technology, Beijing 100144, China*
[2]*Institute of Water Hydropower and Resource, Beijing 100041, China*

Correspondence should be addressed to Yufei Zhao; zhaoyf@iwhr.com

Received 11 July 2019; Revised 15 October 2019; Accepted 20 December 2019; Published 9 January 2020

Guest Editor: Endong Wang

With the development of the underground utility tunnel in China, the safety evaluation during facility operation inside tunnels is increasingly important after construction. In contrast to fixed fire source in the traffic tunnel, the fire characteristics of the electric cable compartment of the utility tunnel with different ventilation modes are studied. Firstly, the thermal physical parameters of cable material are determined by experiment and numerical simulation. Different fire sealing and ventilation conditions are established according to the practical utility tunnel engineering in FDS. The maximum temperature and smoke gas concentrations are obtained, as well as the heat release rate. The results show that the utility tunnel fire has obvious differences compared with road tunnel fire, where the maximum ceiling temperature and the distributions of smoke is related to fire sealing and ventilation mode. Some suggestions related to evaluation and firefighting are provided for practical purposes.

1. Introduction

With the development of the underground utility tunnel in China, the safety evaluation during facility operation inside the tunnel is increasingly important after construction, especially the electric power cable compartment is threatened by fire catastrophes. Fire sealing doors should be used every 200 m in underground utility tunnel because fire of a piece of cable will cause the whole cable compartment fire.

Study of fire characters are similar between road traffic tunnel and utility tunnel, and existing researches on the former are more widely carried out in many fields [1]. Researches on road tunnel fire are firstly reviewed and compared with utility tunnel fire.

1.1. Maximum Gas Temperature Related to the Heat Release Rate and Ventilation. Kurioka et al. [2] proposed an empirical formula for predicting fire phenomena. Ingason and Li [3] carried out model scale tunnel fire tests with longitudinal ventilation. Heat release rate, maximum gas temperature, temperature distribution, and backlayering length were investigated. Li et al. [4] proposed maximum gas temperature beneath the ceiling was related to the heat release rate and the longitudinal ventilation velocity. Khattri [5] studied the influence of ventilation velocity and developed an analytical expression for predicting the maximum ceiling temperature, the maximum ceiling flux, and the maximum flux on the tunnel floor during a heavy goods vehicle fire. Zhang and Gao [6] analyzed the CO concentration and temperature related to fire heat release rates and ventilation velocities and fire source locations using the support vector machine (SVM) regression method. In contrast with the road tunnel fire, the fire heat release rate of utility tunnel fire can be predicted with fire source and ventilation mode, also the maximum ceiling temperature.

1.2. Special Issues Such as Different Fire Locations or Sidewall Confined Condition. Gao et al. [7] studied the transverse ceiling flame length and the temperature distribution of a

sidewall confined tunnel fire with experiments. Based on the proportional relation between the flame volume and HRR, the effective HRR at the ceiling is determined. Tang et al. [8] studied ceiling maximum temperature and longitudinal decay along the centerline of the tunnel with different transverse fire source locations. Yao et al. [9] proposed an improved model to predict the maximum smoke temperature in an enclosed channel applying it to different boundary conditions. The fire source location in the utility tunnel is confined and spread, different from road tunnel fire.

1.3. Firefighting Such as Water Mist Screens or Sealing Entrance. Chen et al. [10] studied the ceiling temperature inside tunnel varies versus sealing ratio, which is primarily due to the comprehensive effect between the heat loss by the hot smoke flowing out of tunnel entrance and the heat produced by combustion significantly related to ventilation, and both the above factors are related to the open area of tunnel entrance. Huang et al. [11] proposed ceiling temperature increases with sealing ratio due to the heat accumulation inside the tunnel when the heat release rate is relatively small. Moreover, the longitudinal ceiling temperature decreases with the increase of the tunnel entrance sealing ratio at the initial stage and then tends to stability due to less oxygen supply when the heat release rate is relatively large. The maximum temperature along the tunnel ceiling decays exponentially. Liang et al. [12] proposed a new system with simultaneous water mist screen and transverse ventilation system (WMSTV system). The effects of natural and transverse ventilation systems without water mist are also investigated for comparison. Zhou et al. [13] conducted tests and simulations with varying transverse fire locations in a full-scale tunnel to investigate the constraint effect of sidewall on the maximum smoke temperature distribution. The maximum temperature with different sealing ratio and heat release rate has been studied in road tunnel fire, while it is important in utility tunnel fire as well.

1.4. New Ventilation Mode as Ceiling Jet or Moving Fan. A. Król and M. Król [14] compared the jet fan modeling with experimental data. Oka and Imazeki [15] proposed a new correlation for representing the temperature distribution, which takes the tunnel inclination into account and consists of an exponential function and a cubic function with a coordinated transformation. Tang et al. [16] studied the maximum temperature of a ceiling jet induced by rectangular-source fires with different burner aspect ratios (ranging from 1 to 8.2) in a tunnel, using a ceiling smoke extraction. Zhou et al. [17] found that the distance between the movable fan and the fire source has a critical range, where the effects of smoke exhaust on reducing the maximum temperature under the ceiling and preventing the backlayering were more significant when the fan was placed in this distance range. Tang et al. [18] put forward a modified model to predict the maximum temperature of smoke flow beneath the ceiling with combined effect of ceiling single point extraction and longitudinal ventilation in tunnel fires. Tang et al. [19] proposed a new nondimensional factor to predict the thermal smoke backlayering flow length. Mei et al. [20] conducted experiments in a model-scale mechanical ventilation tunnel to study the characteristics of smoke layer thickness and plug-holing with multiple-point extraction system. These researches showed that the maximum temperature can be predicted under new ventilation mode so as in the utility tunnel fire.

1.5. Special Structure Construction Such as Tilted or Sloped Tunnel and Node Area. Chow et al. [21] discussed a tilted tunnel fire under natural ventilation. Empirical expressions of smoke temperature and velocity decays along the longitudinal axis were derived. Liu et al. [22] investigated ceiling temperature in the common node area of tunnels. Normalized expression of longitudinal temperature decay coefficients were correlated as well by taking the heat release rate and transverse fire locations under the elliptic ceiling into account. Weng et al. [23] deduced the dimensionless expression of backlayering length and critical velocity of smoke in tunnel fires using the dimensional analysis method. Zhong et al. [24] conducted a full-scale experiment to research the smoke development of a sloped long and large curved tunnel in the natural ventilated underground space under three different fire powers. Some new expression of smoke temperature and ventilation velocity are proposed based on traditional expression for special structures, and maybe also applicable for utility tunnel.

Although many researches on the traffic tunnel fire are carried out, the tunnel is relatively spacious, air supply is sufficient, and fire source location is generally fixed, just as compared with utility tunnel above all. Compared with road tunnel fire, the underground utility tunnel is connected with other utility tunnels on both ends of the partition and the tunnel space is long and narrow. Only air vents are used to exhaust the smoke, and fire is flowing with cable in electric power compartments. These are the differences from the road tunnel fire. A few researches are carried out on utility tunnel fire. Li et al. [25] studied the resistance characteristics of the ventilation system of a utility tunnel under different pipeline layouts. A multiscale analysis of the fire problems in an urban utility tunnel was studied [26]. A multivariate cubic function that considers the global effects of relative width, height, and distance was further proposed to estimate the enhancement coefficient. If the fire happens in the practical utility tunnel, the frequently used firefighting method now is to close the fire sealing door and switch the water mist on. But if there is some person in tunnel or firefighting equipment failure, how to evaluate the fire risk, as well as the fire heat release rate, and smoke and temperature under combination of fire sealing and ventilation need to be further studied.

This paper is based on the most dangerous fire case in utility tunnel fire, where the whole cabin is fully occupied by the electrical cable. Fire spreads from the middle to both sides, and fire control facilities do not work. Under such condition, the temperature and smoke movement with ventilation and fire sealing door are studied. The experiment

and numerical simulation is used to determine the cable material thermal parameters. Different fire sealing and ventilation conditions are established according to the practical utility tunnel engineering in FDS. The maximum temperature and smoke gas concentrations are obtained, as well as the heat release rate. Temperature and smoke gas concentration are obtained, and the relation between them is proposed.

2. Thermal Parameters Determination

In this paper, the combustion parameters of PVC cable sheath material used in the electrical cable utility tunnel are studied by the burning test and verified by numerical analysis in FDS (Version 5). Experiment is carried out in a combustion furnace shown in Figure 1. The external dimensions of the furnace are 1.2 m × 1.3 m × 1.4 m with wall thickness 0.2 m, and the platform of firebrick masonry is in the center. There are two air inlets on the right side of the furnace and an exhaust outlet on the left side. The detailed location is shown in the FDS model in Figure 2.

The amount of 500 g combustion material is burned, and alcohol is used to ignite. The residual slag in the burning plate is 280 g weight after fire extinguished. CO and CO_2 concentration detectors are arranged shown as "Gas DT" in Figure 2. A smoke exhaust fan is installed at the outlet. In order to avoid a large amount of toxic gas produced by the combustion, the exhaust fan is running during test and the exhaust velocity is measured. There are two thermocouples for temperature measurement in the combustion furnace on 0.8 m height (0.2 m from the furnace wall) shown as "THCP1" and "THCP2" in Figure 2.

Then FDS is used to simulate the experiment; due to the combustion time is short, heat exchange with outside is ignored. The unsteady ignition source is adopted, and mass of combustion material is 220 g. According to cable material thermal parameters [26], heat release rate 80 kW is chosen to simulate and verified by experiment. The air density is 1.205 kg/m^3, and specific heat is 1.005 kJ/(kg·K). The ambient temperature is 273 K, and the gravity acceleration value is 9.81 m/s^2.

Based on the theoretical heat release of PVC material burning with unit oxygen, the fire heat release is $h_r = E_0 n_{O2} M_{O2} / (n_F \cdot M_F) = 16.7$ kJ/g, where $E_0 = 13.1$ kJ/g, n_{O2} is the amount of oxygen (unit: mol), M_{O2} is the molar mass of oxygen (unit: g/mol), n_F the amount of fire source (unit: mol), and M_F is the molar mass of fire source (unit: g/mol). And different grid size in FDS is used to check the grid sensitivity. The results with different grid sizes are listed in Table 1, and the burning rate and fire heat release rate are shown in Figures 3(a) and 3(b), respectively. From the results, grid size (0.05 m × 0.05 m × 0.05 m) of fire source is used. The results of temperature and CO and CO_2 concentration in FDS and in experiment are shown in Figures 4–6.

Figure 4 shows temperatures of two monitoring points. In test, the highest temperature is 135°C, and 25°C is lower in FDS. This is because in test, the heat transfer happens due to the unsealing of the combustion furnace, and in FDS, only the heat absorption of fireproof bricks is considered and no heat exchange with outside. The moment reaching the highest temperature is 200 s, which is 110 s later in FDS. This is caused by the instantaneous combustion of the FDS ignition mode, while it does not happen in test. After 400 s, the temperature is decreased in experiment, while it happens 200 s earlier in FDS. This is due to the cable material's self-extinguishing character. In FDS, the temperature is reduced sharply after 800 s, while the fire naturally burns out in experiment. Concentrations of CO and CO_2 in FDS are relatively fitted well with experimental results shown in Figure 5 and 6. Only during 600 s to 900 s the differences happen due to the material self-extinguishing, which will continue to produce CO and CO_2 in test while not in FDS. Through the comparisons between the experimental and numerical simulation, it is shown that the selected parameters can be used to simulate the combustion characteristics of the cable in the utility tunnel.

3. Numerical Simulation of Utility Tunnel Fire

In this paper, according to the practical utility tunnel engineering, the general cross-sectional size is 2.2~3 m width and 2.6~3.2 m height. So cross section 2.6 m width and 2.9 m height with 300 mm thickness concrete wall and 0.5 m width cable block is studied. 10 kv, 110 kv, and 220 kv cables lay on both sides of the cable block, and the layer interspace is 0.25 m, 0.4 m, and 0.55 m separately. Figures 7(a) and 7(b) are the cross section and simulation model in FDS. Monitoring points are shown in Figure 7(c)

Longitudinal ventilation is used in the utility tunnel, and the shaft is located at both ends of the fire partition as in Figure 8. The fire protection zone is 200 m long, and three fire zones have been set up to simulate. The fire is supposed to ignite initially in the middle. Due to the long and narrow space of the tunnel, the fire will be under restricted combustion. The wall surface is not considered for heat exchange with outside and selected as heat absorption. The ambient temperature is 20°C, and the external wind speed is 0 m/s.

In order to determine the effects in combination with fire sealing door and smoke ventilation mode, this paper studies the fire and smoke movement under different fire scenes with sealing door opened or closed and natural ventilation (ventilation velocity is zero) or mechanical ventilation (ventilation velocity is 3 m/s) mode. The fire scenarios (FS1-6) are listed in Table 1, here NN represents natural ventilation inlet and natural ventilation outlet, NM represents natural ventilation inlet and mechanical ventilation outlet, MM represents mechanical ventilation inlet and mechanical ventilation outlet.

4. Results and Discussion

4.1. Maximum Ceiling Temperature. The heat release rate (HRR) in middle of the tunnel with time is shown in Figure 9 and the ceiling maximum temperature is listed in Table 2. The highest temperature is FS1, and the lowest is FS3. The largest HRR is FS6, and the smallest is FS3.

(a) (b)

Figure 1: Combustion furnace and test process.

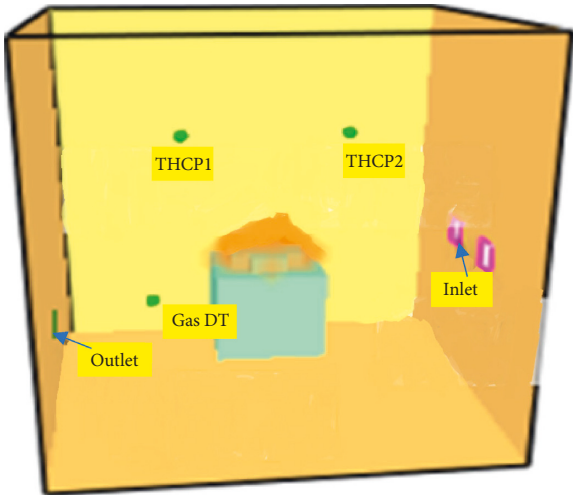

Figure 2: FDS model.

Table 1: Heat release and mass source with different sizes.

Grid size (m)	Mass of fire source (g)	Theoretical heat release (kJ)	Numerical heat release (kJ)	Error (%)
$0.04 \times 0.04 \times 0.04$	244	4122	4340	5.3
$0.05 \times 0.05 \times 0.05$	220	3730	3925	5.2
$0.06 \times 0.06 \times 0.06$	202	3388	3649	7.7

The most concerning factor is the maximum ceiling temperature in the tunnel. Some researchers have built relationships between ceiling temperature and HRR and longitudinal ventilation velocity. The empirical equation to predict the maximum excess gas temperature beneath the tunnel ceiling by Kurioka et al. [2] was widely used:

$$\frac{\Delta T_{\max}}{T_a} = \gamma \left(\frac{Q'^{2/3}}{\mathrm{Fr}^{1/3}} \right)^{\varepsilon}, \tag{1}$$

where the dimensionless heat release rate Q' is defined as

$$Q' = \frac{Q}{\rho_a C_p T_a g^{1/2} H_d^{5/2}}, \tag{2}$$

and the Froude number Fr is

$$\mathrm{Fr} = \frac{u^2}{g H_d},$$

$$\frac{Q'^{2/3}}{\mathrm{Fr}^{1/3}} < 1.35, \quad \gamma = 1.77, \quad \varepsilon = 1.2,$$

$$\frac{Q'^{2/3}}{\mathrm{Fr}^{1/3}} > 1.35, \quad \gamma = 2.54, \quad \varepsilon = 0. \tag{3}$$

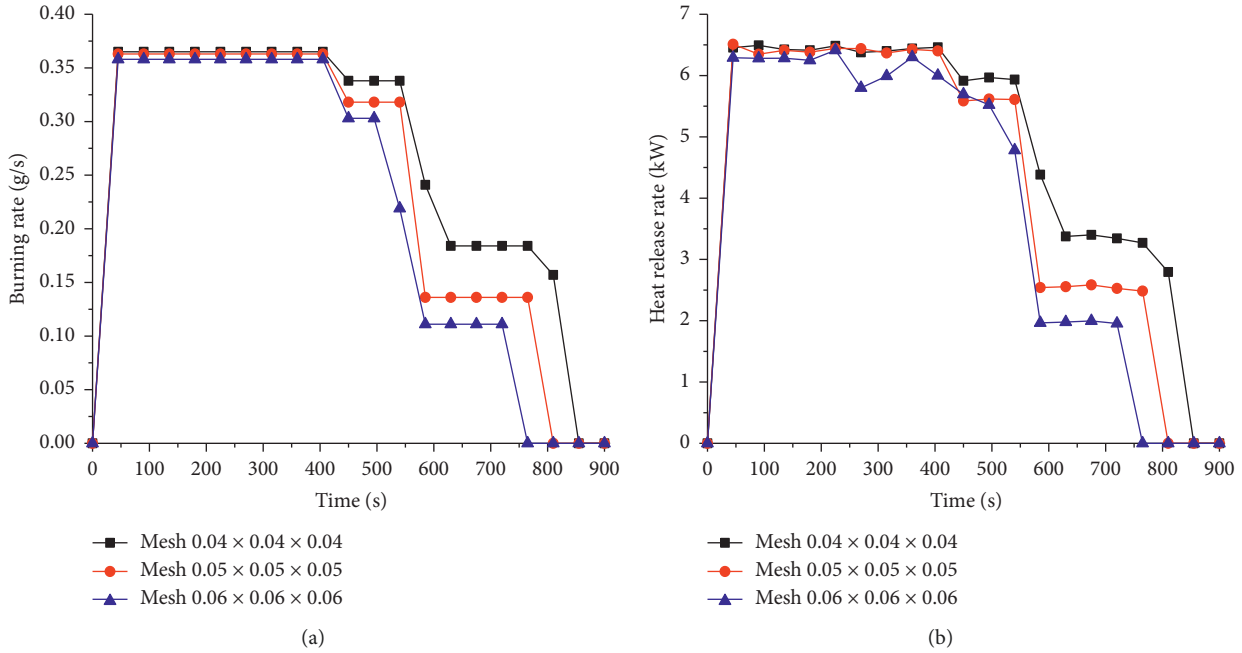

Figure 3: (a) The burning rate and (b) heat release rate with different grid size.

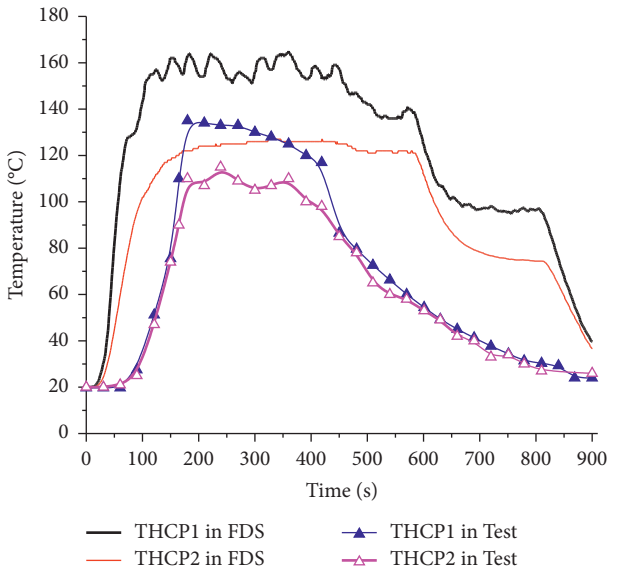

Figure 4: Temperature result in test and FDS.

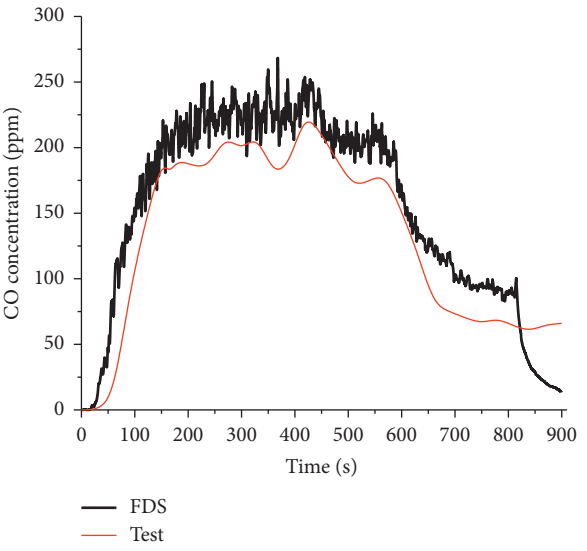

Figure 5: CO concentration in test and FDS.

As Ingason and Li [3] pointed out, equation (1) was available to predict the ceiling temperature when ventilation velocity was large. Here, equation (1) is used to predict the temperature in FS3 and FS6 with the coefficients $\gamma = 0.671$ and $\varepsilon = 1.467$.

Based on the maximum gas temperature beneath the ceiling under the small ventilation velocity in Ingason and Li [3],

$$\Delta T_{\max} = 17.5 \frac{Q^{2/3}}{H_d^{5/3}}, \tag{4}$$

and considering the fire sealing door and ventilation mode in FS1, FS2, FS4, and FS5, the maximum gas temperature beneath the ceiling is proposed as

$$\Delta T_{\max} = \alpha\beta\left(\frac{Q^{2/3}}{H_d^{5/3}}\right)^{\mu}, \tag{5}$$

with the coefficients $\alpha = 1$ (fire sealing door closed), $\alpha = 0.582$ (fire sealing door opened), $\beta = 1$ (NN mode), $\beta = 0.773$ (NM mode), $\mu = 1.481$.

From equations (1) and (5), compared with the road tunnel fire, the utility tunnel fire is different because of the fire sealing and the fire source. As the practical utility tunnel

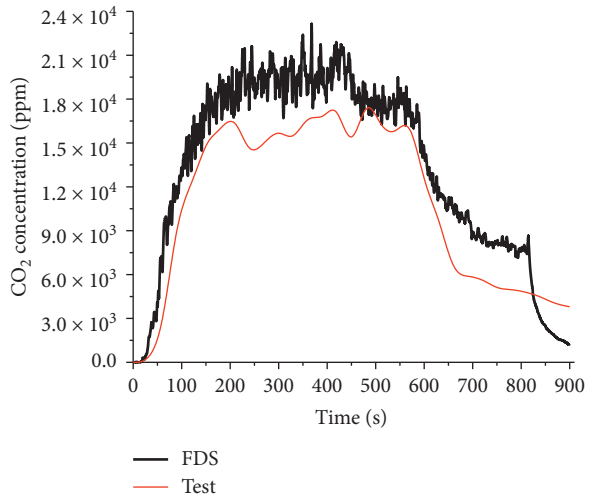

Figure 6: CO_2 concentration in test and FDS.

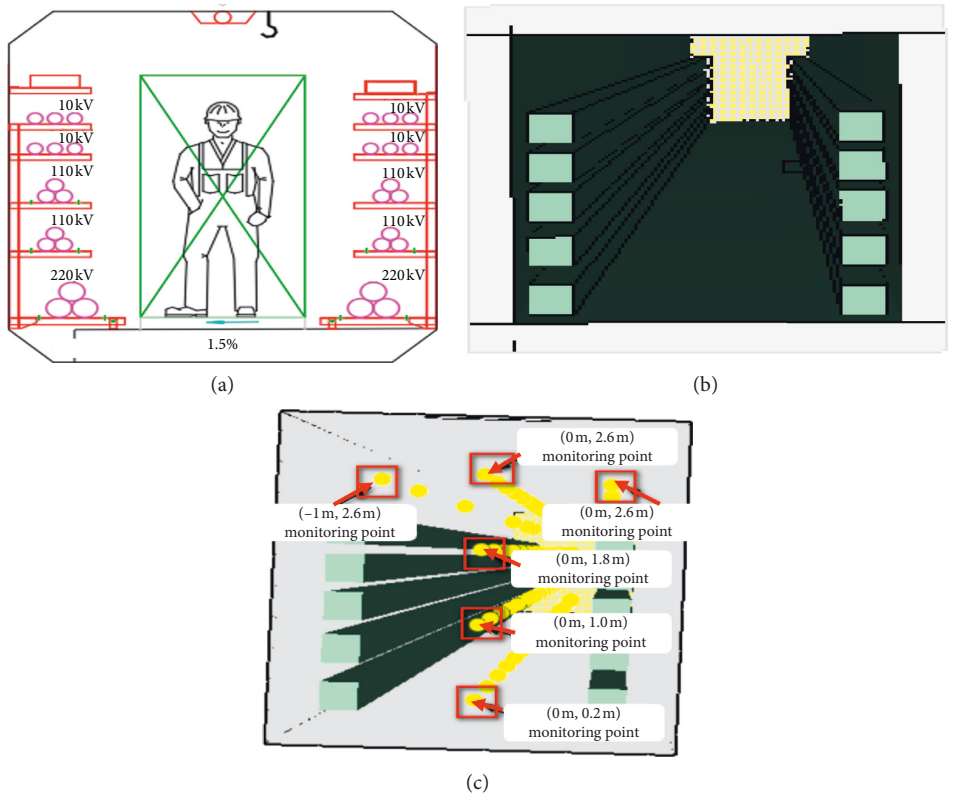

Figure 7: Cross section and simulation model monitoring point. (a) Practical tunnel. (b) Simulation model in FDS. (c) Monitoring points in FDS.

is constructed with the standard dimension, equations (1) and (5) can be used in normal tunnel fire.

4.2. Temperature Decay along Tunnel. In this paper, the fire source is the line. Fire is ignited in the middle tunnel and then spread to both sides. Temperature decay is different with fire sealing door close and open as shown in Figure 10.

In FS1, the temperature decay from the center is symmetric and quick. Because the fire door is closed, temperature is raised near the door.

In FS2, the temperature decay is different between upstream (air inlet) and downstream (air outlet). Temperature rises near the fire sealing door in upstream and fire spreads to the upstream.

In FS3, the temperature decay is more quick in upstream than downstream. Fire spreads to the downstream.

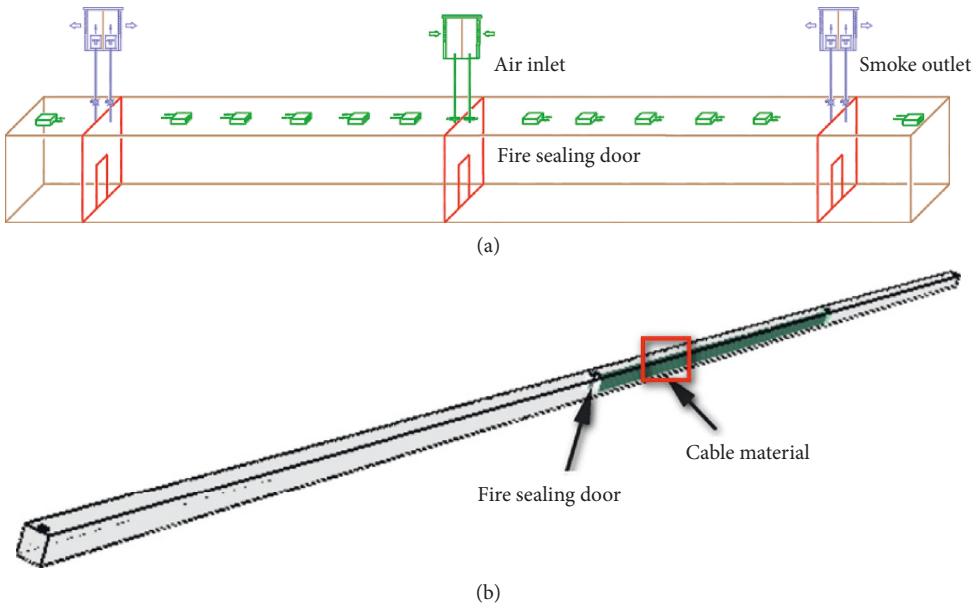

Figure 8: Utility tunnel ventilation mode. (a) Practical tunnel ventilation. (b) Simulation model in FDS.

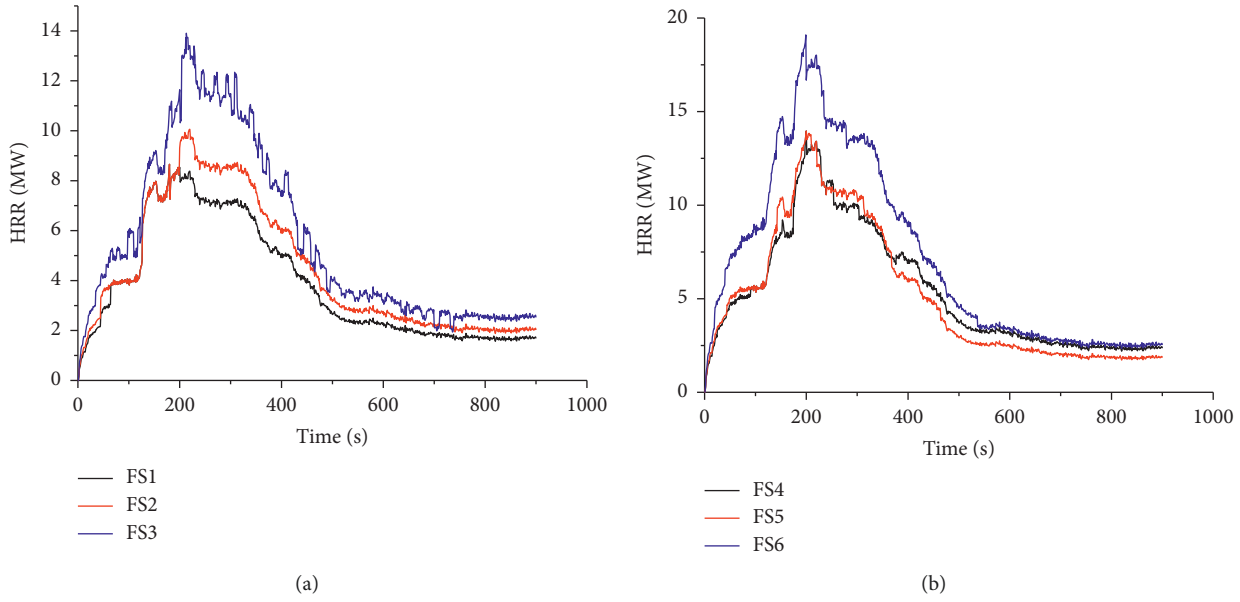

Figure 9: The heat release rate HRR. (a) HRR in FS1-3. (b) HRR in FS4-6.

Table 2: Fire scenarios with heat release rate and maximum ceiling temperature.

Fire scenario (FS)	Fire sealing door	Ventilation mode	Heat release rate (MW)	Maximum temperature ΔT_{max} (K)
FS1-3	Closed	NN, NM, MM	8, 9, 13	676, 575, 474
FS4-6	Opened	NN, NM, MM	13, 13, 17	637, 517, 611

In FS4, the temperature decay is not so quick as in FS1. The temperature arise near the fire sealing door is not very clear as in FS1.

In FS5, the temperature decay is more quick in downstream than upstream. Temperature decay is not very clear as in FS4.

In FS6, the temperature decay is not very quick and symmetric with center.

The former temperature distribution is confined to fixed asymmetric fire source in the road tunnel, without considering fire spreading and fire sealing door. Here the

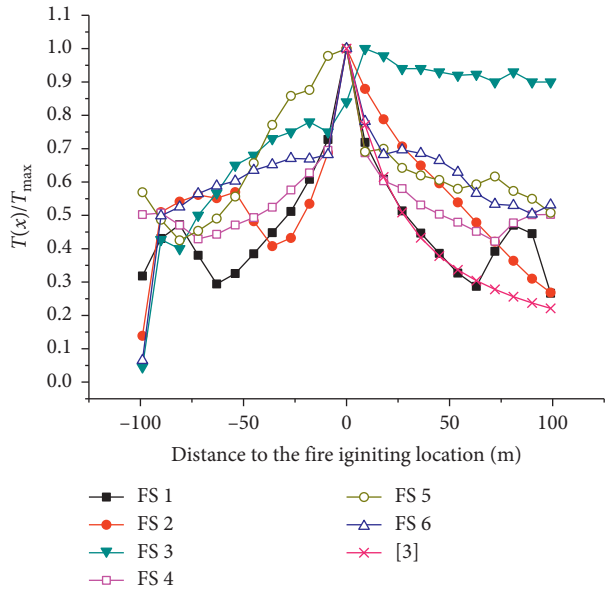

Figure 10: The maximum ceiling temperature along the tunnel.

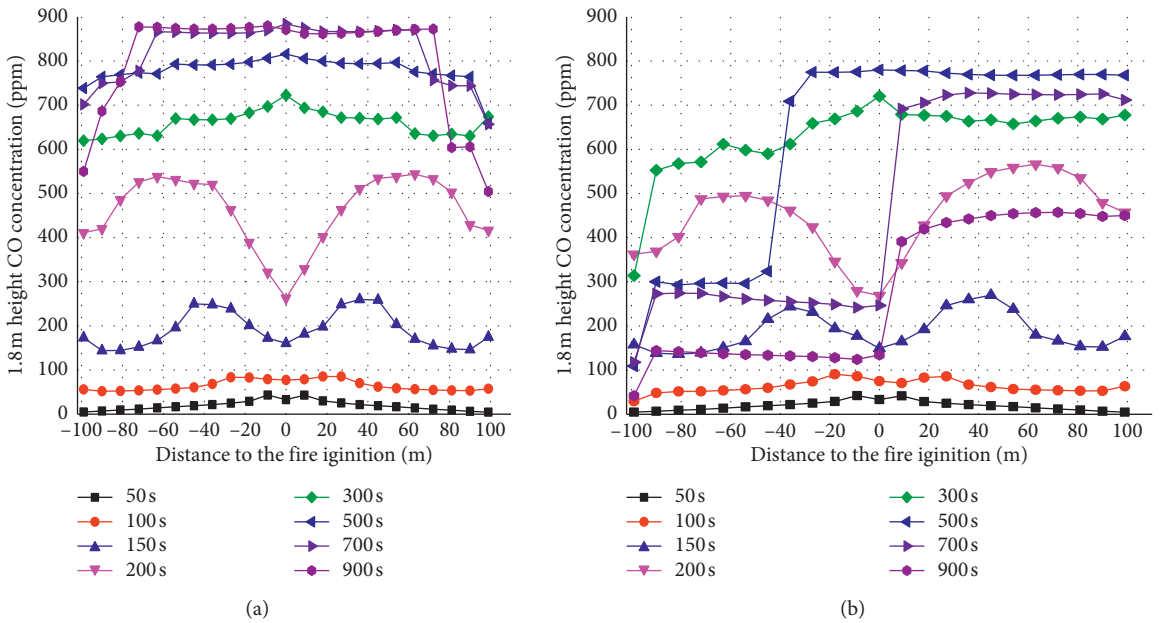

Figure 11: Continued.

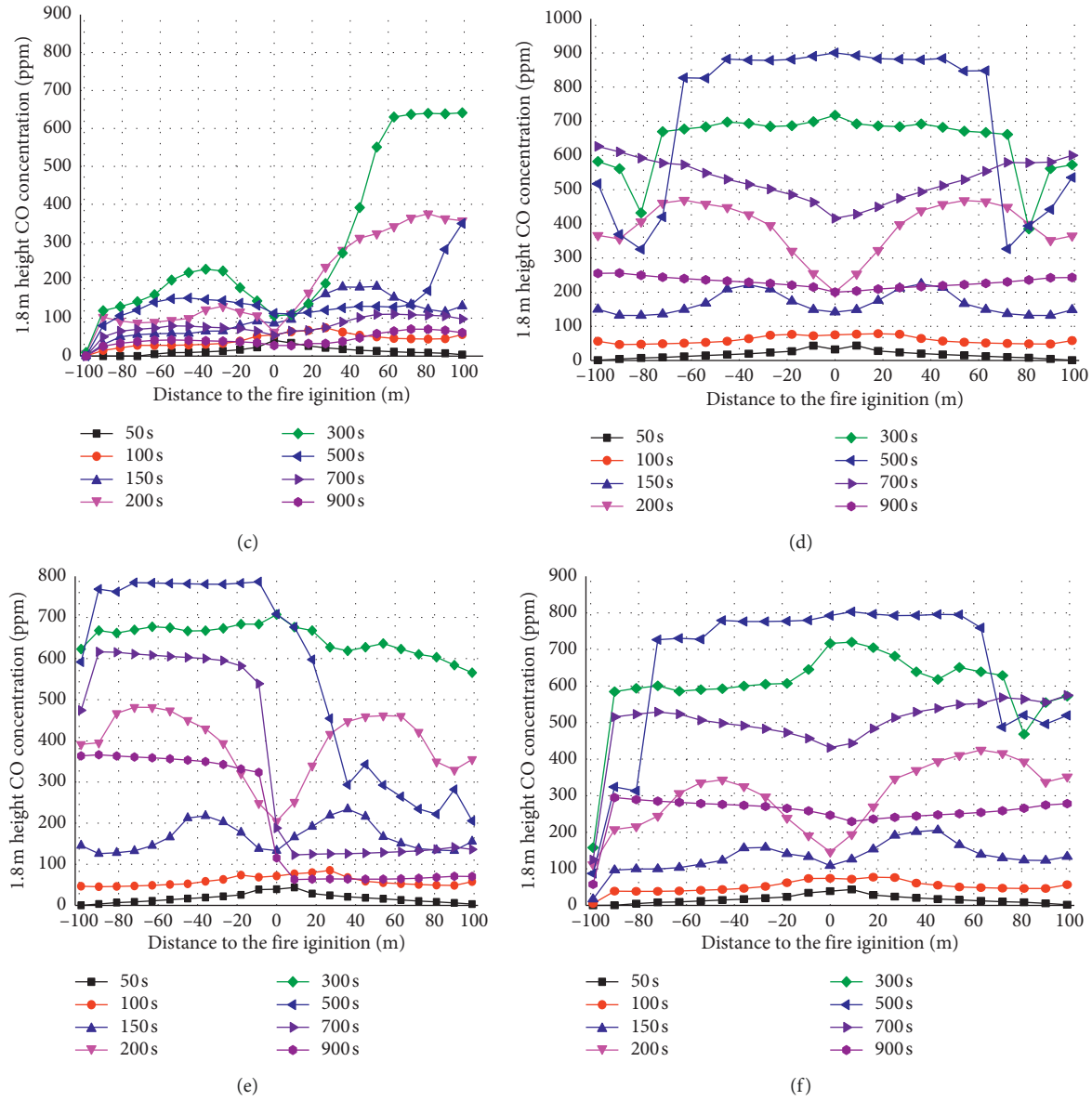

Figure 11: CO concentration at 1.8 m height along the tunnel with different time. (a) FS1. (b) FS2. (c) FS3. (d) FS4. (e) FS5. (f) FS6.

formula of temperature distribution in tunnel fire in the study of Ingason and Li [3] is compared and shown in Figure 10:

$$\frac{\Delta T(x)}{\Delta T_{\max}} = 0.57 \exp\left(-0.13 \frac{x}{H}\right) + 0.43 \exp\left(-0.021 \frac{x}{H}\right). \quad (6)$$

By comparing with the temperature distribution of utility tunnel fire in Figure 10, only the temperature in FS1 is coincident with equation (6). In addition, there is a temperature rise near the sealing door, which is due to the fact that the utility tunnel has a shaft open to cause smoke accumulation. This is similar to the sealing 75% ratio in tunnel fire in the study of Huang et al. [11].

The temperatures at the smoke outlet part of the rest scenes are higher than that in road tunnel fire because of the fire source and the section size of the tunnel.

In the NN mode (FS1 and FS4), the highest temperature is similar, but the temperature of FS1 is lower than FS4 at the same location, which means temperature decay is faster. This is because the fire sealing door in FS4 is open, and fire burns more fully, which can be indicated by the fire heat release rate of FS1 and FS4.

In the NM mode (FS2 and FS5), temperature decay is faster in FS2 in the natural ventilation part than that in FS5 because of the closed fire sealing door and insufficient air supply.

In the MM mode (FS3 and FS6), the temperature decay is slower in the smoke outlet part in FS3 than that in FS6 because the smoke gathered near the closed fire sealing door.

4.3. Smoke Gas Concentration along Tunnel. For the safety of fire fighters and operators to enter the utility tunnel during

fire, the CO concentrations at 1.8 m height along tunnel with different time are studied and shown in Figures 11(a)–11(f).

In FS1, CO concentration is highest with 900 ppm and spreads fully in the whole tunnel.

In FS2, CO spreads to the downstream after 200 s and reaches the peak at 500 s while CO concentration is lower in the upstream. Finally, CO concentration is half of the peak in the downstream.

In FS3, the CO concentration is lower in the upstream than in the downstream and reaches the peak 620 ppm at 300 s and then falls down quickly.

In FS4, CO concentration reaches the peak 900 ppm at 500 s and then falls down steadily.

In FS5, the CO concentration is higher in the upstream than in the downstream after 500 s in contrast with FS2.

In FS6, the smoke extraction is not very efficiently compared with FS3 before 500 s. The CO concentration reaches the peak 800 ppm and then falls down quickly.

In the NN mode (FS1 and FS4), CO concentration will decrease after 500 s in FS4, while increase constantly in FS1. In the NM mode (FS2 and FS5), CO concentration is different in the air inlet part and smoke outlet part. The CO concentration is higher in the smoke outlet part than in the air inlet part in FS2, while contrarily in FS5. The CO concentration will decrease after 500 s in FS2 and FS5. In the MM mode (FS3 and FS6), CO concentration is very lower in the air inlet part and will decrease quickly after 300 s in FS3. CO concentration is relatively higher and will decrease after 500 s in FS6.

From the smoke gas concentration and temperature decay, if the fire sealing door is closed, the MM mode is the best safe mode for evaluation and structure safety. If fire sealing door has to be opened, the NM mode is the best safe mode for evaluation and structure safety.

5. Conclusions

This paper studies the smoke characteristic of the cable compartment of utility tunnel fire with the experiment and numerical simulation method. The temperature distribution under different smoke exhaust modes which include the fire sealing door and ventilation mode is obtained. It is found that the utility tunnel fire has obvious differences compared with road tunnel fire. The relationship between maximum ceiling temperature and ventilation mode obtained and the smoke concentration is compared. The results show that after a fire occurs, it is best to close the fire sealing door and run the mechanical ventilation mode. This paper can provide some theoretical suggestions for other standard utility tunnel fire.

Nomenclature

Fr: Froude number defined in equation (1)
γ, ε: Coefficient in equation (1)
ΔV: Gas concentration in ppm
HRR: Heat release rate (kW)
$\Delta T(x)$: Smoke temperature rise at the fire distance of x relative to channel center (K)
$\Delta T_{\max}$: Maximum smoke temperature rise in the tunnel (K)
C_p: Thermal capacity of air (kJ/kg·K)
ρ_a: Ambient air density (kg/m^3)
T_a: Air temperature (K)
g: Gravity acceleration (m/s^2)
H_d: Tunnel height
u: Ventilation velocity (m/s)
h: Overall thermal conductance
P: Girth of tunnel cross section
$\dot{m}_a$: Total air mass flow.

Data Availability

The data used to support the findings of this study are available from the corresponding author upon request.

Conflicts of Interest

The authors declare that they have no conflicts of interest.

Acknowledgments

The authors are grateful to Beijing Municipal Education Commission Special Scientific Research "110052971921/063" and North China University of Technology "The Great Wall Scholar Reserve Force."

References

[1] L. Barbato, F. Cascetta, M. Musto, and G. Rotondo, "Fire safety investigation for road tunnel ventilation systems—an overview," *Tunnelling and Underground Space Technology*, vol. 43, pp. 253–265, 2014.

[2] H. Kurioka, Y. Oka, H. Satoh, and O. Sugawa, "Fire properties in near field of square fire source with longitudinal ventilation in tunnels," *Fire Safety Journal*, vol. 38, no. 4, pp. 319–340, 2003.

[3] H. Ingason and Y. Z. Li, "Model scale tunnel fire tests with longitudinal ventilation," *Fire Safety Journal*, vol. 45, no. 6–8, pp. 371–384, 2010.

[4] Y. Z. Li, B. Lei, and H. Ingason, "The maximum temperature of buoyancy-driven smoke flow beneath the ceiling in tunnel fires," *Fire Safety Journal*, vol. 46, no. 4, pp. 204–210, 2011.

[5] S. K. Khattri, "From small-scale tunnel fire simulations to predicting fire dynamics in realistic tunnels," *Tunnelling and Underground Space Technology*, vol. 61, pp. 198–204, 2017.

[6] H.-T. Zhang and M.-X. Gao, "The application of support vector machine (SVM) regression method in tunnel fires," *Procedia Engineering*, vol. 211, pp. 1004–1011, 2018.

[7] Z. Gao, J. Jie, H. Wan, J. Zhu, and J. Sun, "Experimental investigation on transverse ceiling flame length and temperature distribution of sidewall confined tunnel fire," *Fire Safety Journal*, vol. 91, no. S1, pp. 371–379, 2017.

[8] F. Tang, L. Li, W. Chen, C. Tao, and Z. Zhan, "Studies on ceiling maximum thermal smoke temperature and longitudinal decay in a tunnel fire with different transverse gas burner locations," *Applied Thermal Engineering*, vol. 110, pp. 1674–1681, 2017.

[9] Y. Yao, X. Cheng, S. Zhang, K. Zhu, H. Zhang, and L. Shi, "Maximum smoke temperature beneath the ceiling in an enclosed channel with different fire locations," *Applied Thermal Engineering*, vol. 111, pp. 30–38, 2017.

[10] C.-K. Chen, H. Xiao, N.-N. Wang, C.-L. Shi, C.-X. Zhu, and X.-Y. Liu, "Experimental investigation of pool fire behavior to

different tunnel-end ventilation opening areas by sealing," *Tunnelling and Underground Space Technology*, vol. 63, pp. 106–117, 2017.

[11] Y. Huang, Y. Li, B. Dong, J. Li, and Q. Liang, "Numerical investigation on the maximum ceiling temperature and longitudinal decay in a sealing tunnel fire," *Tunnelling and Underground Space Technology*, vol. 72, pp. 120–130, 2018.

[12] Q. Liang, Y. Li, J. Li, H. Xu, and K. Li, "Numerical studies on the smoke control by water mist screens with transverse ventilation in tunnel fires," *Tunnelling and Underground Space Technology*, vol. 64, pp. 177–183, 2017.

[13] T. Zhou, Y. He, X. Lin, X. Wang, and J. Wang, "Influence of constraint effect of sidewall on maximum smoke temperature distribution under a tunnel ceiling," *Applied Thermal Engineering*, vol. 112, pp. 932–941, 2017.

[14] A. Król and M. Król, "Study on numerical modeling of jet fans," *Tunnelling and Underground Space Technology*, vol. 73, pp. 222–235, 2018.

[15] Y. Oka and O. Imazeki, "Temperature distribution within a ceiling jet propagating in an inclined flat-ceilinged tunnel with natural ventilation," *Fire Safety Journal*, vol. 71, pp. 20–33, 2015.

[16] F. Tang, Z. Cao, A. Palacios, and Q. Wang, "A study on the maximum temperature of ceiling jet induced by rectangular-source fires in a tunnel using ceiling smoke extraction," *International Journal of Thermal Sciences*, vol. 127, pp. 329–334, 2018.

[17] T. Zhou, J. Liu, Q. Chen, X. Chen, and J. Wang, "Characteristics of smoke movement with forced ventilation by movable fan in a tunnel fire," *Tunnelling and Underground Space Technology*, vol. 64, pp. 95–102, 2017.

[18] F. Tang, F. Z. Mei, Q. Wang, Z. He, C. G. Fan, and C. F. Tao, "Maximum temperature beneath the ceiling in tunnel fires with combination of ceiling mechanical smoke extraction and longitudinal ventilation," *Tunnelling and Underground Space Technology*, vol. 68, pp. 231–237, 2017.

[19] F. Tang, L. J. Li, F. Z. Mei, and M. S. Dong, "Thermal smoke back-layering flow length with ceiling extraction at upstream side of fire source in a longitudinal ventilated tunnel," *Applied Thermal Engineering*, vol. 106, pp. 125–130, 2016.

[20] F. Mei, F. Tang, X. Ling, and J. Yu, "Evolution characteristics of fire smoke layer thickness in a mechanical ventilation tunnel with multiple point extraction," *Applied Thermal Engineering*, vol. 111, pp. 248–256, 2017.

[21] W. K. Chow, Y. Gao, J. H. Zhao, J. F. Dang, and N. C. L. Chow, "A study on tilted tunnel fire under natural ventilation," *Fire Safety Journal*, vol. 81, pp. 44–57, 2016.

[22] C. Liu, M. Zhong, C. Shi, P. Zhang, and X. Tian, "Temperature profile of fire-induced smoke in node area of a full-scale mine shaft tunnel under natural ventilation," *Applied Thermal Engineering*, vol. 110, pp. 382–389, 2017.

[23] M.-C. Weng, X.-L. Lu, F. Liu, and C.-X. Du, "Study on the critical velocity in a sloping tunnel fire under longitudinal ventilation," *Applied Thermal Engineering*, vol. 94, pp. 422–434, 2016.

[24] M. Zhong, C. Shi, L. He, J. Shi, C. Liu, and X. Tian, "Smoke development in full-scale sloped long and large curved tunnel fires under natural ventilation," *Applied Thermal Engineering*, vol. 108, pp. 857–865, 2016.

[25] S. Li, X. Liu, J. Wang, Y. Zheng, and S. Deng, "Experimental reduced-scale study on the resistance characteristics of the ventilation system of a utility tunnel under different pipeline layouts," *Tunnelling and Underground Space Technology*, vol. 90, pp. 131–143, 2019.

[26] K. Ye, X. Zhou, L. Yang et al., "A multi-scale Analysis of the fire problems in an urban utility tunnel," *Energies*, vol. 12, no. 10, p. 1976, 2019.

Hindawi
Advances in Civil Engineering
Volume 2020, Article ID 7525692, 18 pages
https://doi.org/10.1155/2020/7525692

Research Article

Application Research of New Cementitious Composite Materials in Saline Soil Subgrade Aseismic Strengthening

Shuai Huang, Yuejun Lyu, and Yanju Peng

Institute of Crustal Dynamics, China Earthquake Administration, Beijing 100085, China

Correspondence should be addressed to Shuai Huang; huangshuai3395@163.com

Received 5 August 2019; Revised 31 October 2019; Accepted 13 November 2019; Published 3 January 2020

Guest Editor: Endong Wang

Saline soil affected by earthquakes and groundwater can lead to subgrade subsidence and collapse in highway construction. Consequently, considering the potential activity of the waste slag and magnesia, new cementitious composite materials used in solid saline soil were developed in our study. The unconfined compressive strengths of the saline soil solidified by the new cementitious composite materials with a combination of magnesium oxide, calcium oxide, gypsum, and mineral powder and cement were investigated, and the optimum dosage proportion of the new cementitious composite material for solidifying saline soil was determined; then the SEM, EDS, and XRD of the saline soil solidified by the new cementitious composite materials and cement were analysed. The research result showed that the saline soil solidified by our newly developed cementitious composite material showed compact internal structure and uniformly distributed soil particles; moreover, the new cementitious composite material exhibited a favourable solidifying effect on harmful ions in saline soil, and the Cl^- trapping capacity of the new cementitious composite materials was stronger than that of cement. Finally, our developed cementitious composite material was applied to saline soil subgrade strengthening, and the displacement, acceleration, excess pore water pressure, and damage degree of the subgrade strengthening by our newly developed cementitious composite materials decreased remarkably; therefore, our newly developed cementitious composite material can improve the seismic behaviour of the saline soil subgrade and show potential future engineering application value.

1. Introduction

As a special rock and soil mass, saline soil shows a high structural strength in its natural state due to cementation caused by the salt. The soil structure is easily damaged when the saline soil is immersed in water, which can lead soluble salt to be dissolved and greatly decrease the bearing capacity and compression modulus of the saline soil. Compared with nonsaline soil, saline soil is a special kind of soil in engineering practice because it comprises a significant amount of soluble salt; as a result, the engineering properties of saline soil are complicated. Saline soil is widely distributed in Northwest China, where the areal distribution of saline soil reaches about 60% of saline-alkali land area of China [1]. The western region of China is prone to destructive earthquakes. If saline soil is used as subgrade filling, subgrade soil will be subjected to plastic deformation under the repeated effect of earthquake-induced dynamic loads, thus leading to cracking and failure of pavement structures (Figure 1); therefore, the purpose of this study is to develop new cementitious composite materials to solidify saline soil in a subgrade and improve the seismic behaviour of the saline soil subgrade.

Saline soil subgrades are likely to collapse such as differential settlement and cracking affected by various factors including groundwater and seismic load. At present, the methods for solidifying saline soil involve dynamic compaction, soil replacement, lowering groundwater level, and application of solidifying materials [2, 3]. Wen et al. [4] determined the key technical parameters for soil layer grading of saline soil subgrades, which provided a technical reference for solidifying saline soil subgrades. Song et al. [5] used the soil replacement method to solidify the saline soil subgrades, and it had a favourable strengthening effect. Zhang et al. [6] studied the influence of overburden load on the salt expansion of the saline soil subgrade with different salt contents, water contents, and initial dry density

(a) (b)

Figure 1: Saline soil-induced pavement cracking and settlement.

conditions, and they found that the salt expansion rate of the saline soil decreased significantly with the increase of the overburden pressure. Zhang et al. [7] used various measures to reinforce the stability of a saline soil subgrade and found that saline soil solidification is an economical method. Li et al. [8] used gravel to solidify the saline soil subgrade and found that the gravel plays an important role in improvement of the gradation of the saline soil. Qingfeng et al. [9] used a nuclear magnetic resonance (NMR) technique to test the microstructural characteristics of the saline soil solidified with different proportions of water glass, lime and fly ash, lime, fly ash, and water glass, respectively, and analysed the solidifying effect of the saline soil. Research showed that saline soil stabilised by solidifying materials exhibited a higher strength [10–12]; however, solidifying materials also suffer certain disadvantages. For example, saline soil solidified by utilising lime has poor water stability; the strength of saline soil solidified with fly ash is low; saline soils solidified by using cement and high-performance cementitious composite materials are expensive. From the perspective of effectively utilising resources, saving resources, and protecting the environment, the application of slag in industrial cementitious materials is of interest in many countries around the world. Slag has potential activity which is latent unless activated under certain conditions, such as the mechanical activation method, chemical activation method, and high-temperature activation method. Based on practical engineering experience, the chemical activation method is used in our study.

Magnesia (MgO) is often used to activate the potential activity of the cementitious composite materials. The dosage of MgO in clinker of the Portland slag cement cannot exceed 5.0%, which is stipulated in Chinese standard [13]. If the cement satisfies that standard after being subjected to a test of cement soundness using the autoclave method, the content of MgO in clinker is allowed to reach 6.0% at most. Light-burned MgO shows a series of advantages including small grains, significant lattice distortion, a comparatively looser structure, and high activity. Therefore, many scholars are studying the use of light-burned MgO. Jin and Wang [14] developed a new inorganic cementitious composite material using blast furnace slag, light-burned MgO, alkali-water glass, and potassium hydroxide, and the material showed favourable mechanical properties. Lou et al. [15] developed double-expansive cement by adding MgO into low-heat microexpansive cement, and the cement also exhibited synchronous expansion by virtue of aluminite and MgO. Harrison [16] developed new cementitious materials by adding a certain amount of active MgO into Portland cement, together with about 80% fly ash. Liska et al. [17] developed new cementitious materials by blending active MgO, volcanic ash, and hydraulic cement, which realised shrinkage compensation through hydration of active MgO with magnesium hydroxide. Inspired by the above studies, new cementitious composite materials were developed using mineral powder, magnesia, quicklime, and gypsum in our study, and compression strength tests, water stability tests, measurement of the soluble ion contents, SEM (scanning electron microscope) analysis, EDS (energy dispersive spectrometer) energy spectrum analysis, and XRD (X-ray diffractometer) analysis of the saline soil solidified by the new cementitious composite materials were investigated. Finally, the new cementitious composite material was applied to strengthen a saline soil subgrade located in a highly seismic region, and our study provides important technological guidance for seismic design of a saline soil subgrade.

2. Test Analysis

2.1. Specimen Preparation. The new cementitious composite materials were prepared using slag, building gypsum, quicklime, and magnesia, and the chemical activation method is used in our study. The samples of saline soil solidified by the new cementitious composite materials were made according to the standard [18] of TB10113-96 *Technical Code on Dry Jet Mixing Method to Stabilise Soft Foundations*, and the specific steps are as follows:

(1) The air-dried saline soil was crushed and screened through a 5 mm square aperture sieve, and water was added into the specimen configured as natural moisture gravimetric content 29.7%

(2) The solidified soil was uniformly packed into cubic testing moulds; then, the moulds were vibrated for 3 min on a shaking table at 3000 ± 200 cycles/min, and the vibration amplitude is 0.35 ± 0.05 mm

(3) The prepared samples of solidified soil are shown in Figure 2, and the samples are cured in a moist air

cabinet at the temperature of $(20 \pm 3)^{\circ}$C and a relative humidity of 75%

By analysing main chemical compositions of the blast furnace slag, the chemical compositions contents are shown in Table 1.

The new cementitious composite material was made by using slag, building gypsum, quicklime, and magnesia, and the key properties of the mineral powders are listed in Table 2.

The Portland slag cement (P·S·B32.5R) used in this study was purchased from Tangshan Jidong Cement Co., Ltd, Hebei Province, China, and its main performance indices are listed in Table 3.

The saline soil from Northwest China was used, and its key components of soluble salt were analysed, as shown in Table 4.

It can be seen in Table 2, $Cl^-/SO_4 > 2$. Therefore, the saline soil was classified as a chlorine saline soil. When the average salinity in soil was in the range of 1 to 5, saline soil was subordinated to an intermediate saline soil. According to the above analysis of soluble salt contents, the average salinity of the test soil was 1.39; thus, the saline soil in our study was classified as intermediate saline soil.

2.2. Test Methods

2.2.1. Compressive Strength Test. After the specimens of solidified saline soil were subjected to standard curing to certain curing age, the unconfined compressive strengths (UCSs) of the specimens were measured under the curing ages 7, 14, 28, 56, 90, 180, and 360 days, as shown in Table 5. The UCS was tested under the controlled stress. The pressure increased step by step, and the specimens were maintained at a stress level to measure the vertical deformation of the specimens. After deformation stabilised, next-level load was applied to specimens until the specimens were damaged. The specimens were regarded as stable when the vertical deformation rate was less than 0.5 mm/min, and the loading rate was set to 0.20 kN/s. The specimens were regarded as being damaged when the stress remained unchanged while deformation increased; moreover, cracks were found in specimens.

2.2.2. Water Stability Test. The specimens of solidified soil were subjected to standard curing for 6 d, and then their UCS (f_{u2}) was measured. On the seventh day, the specimens were immersed in fresh water for 24 h and then their UCS (f_{u1}) was measured. The softening coefficient K of solidified soil could be calculated, where $K = (f_{u1}/f_{u2}) \times 100\%$.

2.2.3. Soluble Ion Contents. In our study, the specimens of solidified soil being subjected to standard curing for 56 d and 360 d were milled to powder. Afterwards, according to NY/T112.16-2006 *Detection of Soil*, the contents of soluble ions (Cl^{-1} and SO_4^{2-}) in specimens were measured.

Figure 2: Solidified soil samples.

2.2.4. SEM Analysis. SEM observation was performed to analyse the hydration products of the specimens using a Zeiss SUPRATM55 scanning electron microscope. The magnification range is 12~1000000x, and the acceleration voltage range is 0.02~30 kV. By utilising the ISM-6480LV SEM, the microstructures of solidified soil undergoing standard curing for 28 d were observed.

2.2.5. EDS Analysis. By employing the Noran System Six EDS, EDS energy spectral analysis for standard curing age 28 d was conducted on hydration products of solidified soil, and the chemical compositions of the hydration products were calculated through the SEM.

2.2.6. XRD Analysis. XRD analysis was carried out on specimens of solidified soil for standard curing age 28 d by using the D8 Advance XRD. The X-ray diffraction (XRD) spectra of the specimens were observed using a D/Max-RC diffractometer (Japan) with Cu Kα radiation, voltage of 40 kV, current of 150 mA, and 2 h scanning ranging between 5 and 90. The samples were manually grounded.

3. Test Results and Analysis

3.1. Mix Design. Liu [19] used calcium oxide and gypsum as the activator to activate the activity of mineral powder. Inspired by Liu, we used MgO as the activator. $Mg(OH)_2$ in lime was dissociated into magnesium and hydroxide ions. The diffusion layer of clay particles in soil mostly contained ions, *i.e.*, K^+ and Na^+, and then Ca^{2+} and Mg^{2+} ions in lime underwent exchange interactions with K^+ and Na^+ in the soil. As a result, the diffusion layer of the colloid was thinned to reduce the potential, and particles became more tightly bound, which strengthened the condensed structure of this lime-stabilised soil and reduced the dispersion, shrinkage, and expansivity. In this way, engineering properties of soil were improved. A certain amount of active MgO was added into Portland cement to realise shrinkage compensation by hydration of active MgO to $Mg(OH)_2$. The addition of MgO to cementitious composite materials is mainly to take advantage of the activity of MgO and microexpansive properties of $Mg(OH)_2$, so adjusting the proportion of MgO can enhance the strength of the cementitious composite materials. The schematic diagram for the improvement mechanism is shown in Figure 3.

Table 1: Chemical composition of contents of blast furnace slag (w_t%).

Compositions	SiO_2	Al_2O_3	Fe_2O_3	MgO	CaO	MnO	TiO_2	Loss on ignition
Content	34.46	13.00	3.21	8.64	38.00	0.29	0.84	0.68

Table 2: Properties of mineral powders.

Specific surface area (m^2/kg)	Water content (%)	Fluidity (%)	Activity ratio (%)	Density g/cm^3	Fineness (%)	SO_3 (%)	Cl^-(%)
50	0.26	96	76.9	2.8	6.1	2.01	0.032

Table 3: Main performance indices of cement.

Cement grade	Setting time (min)	Fineness (%)	Fineness (%)	Water requirement of normal consistency (%)
P·S·B32.5R	Initial set 150	Final set 240	8.2	28.1

Table 4: Component analysis of soluble salt in saline soil.

Item	K^+ (mg/kg)	Na^+ (mg/kg)	Ca^{2+} (mg/kg)	Mg^{2+} (mg/kg)	HCO_3^- (mg/kg)	Cl^-(mg/kg)	SO_4^{2-} (mg/kg)	pH
Value	283	6000	785	812	128	10250	2575	7.5

Table 5: Details of specimens.

Curing ages		7 d	14 d	28 d	56 d	90 d	180 d	360 d
Serial number of the specimens	Specimens solidified by the new cementitious composite materials	A-1	A-2	A-3	A-4	A-5	A-6	A-7
	Specimens solidified by cement	B-1	B-2	B-3	B-4	B-5	B-6	B-7

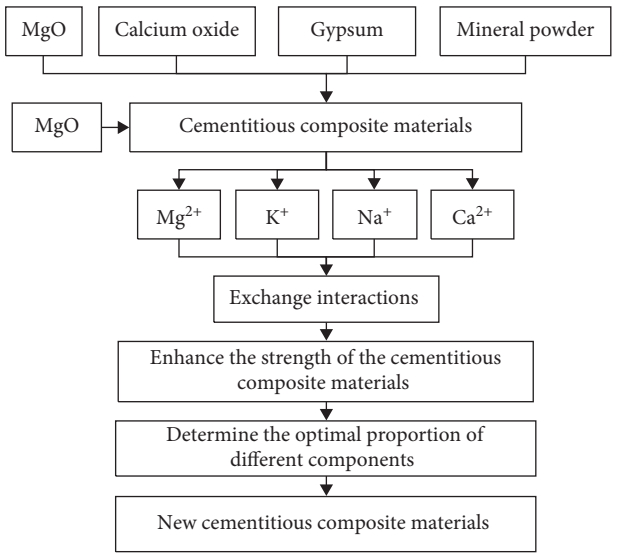

Figure 3: Schematic diagram for the improvement mechanism.

Owing to saline soil containing a high water content (30%) and there being no cement clinker used in the test, the activity of MgO and microexpansive properties of $Mg(OH)_2$ were fully employed. The proportions of MgO in the cementitious composite material were successively set to 4%, 5%, 6%, 7%, 8%, 9%, 10%, 11%, and 12%, respectively. By comparing strengths of the saline soil solidified by cementitious composite materials with different proportions of MgO, the optimal dose of MgO in the cementitious composite material was determined. The test blocks of the saline soil solidified by cementitious composite materials were cured for 7, 14, 28, 56, 90, 180, and 360 d, respectively. The proportions of the solidifying materials are listed in Table 6.

3.2. Determination of Optimal Proportions. In order to determine the optimal proportion of different components in the new cementitious composite materials, the influence of the different proportions of solidifying material on the strength of solidified saline soil was investigated, as shown in Table 6. Additionally, the amounts of the cementitious composite materials added in this solidified saline soil were separately set to 7%, 10%, 15%, and 20%, as shown in Figure 4.

It can be seen from Figure 4 that the UCS of the solidified saline soil all initially increased and then decreased at different curing ages with the increasing proportion of MgO. As the added amount of MgO was increased from 4% to 10%, the UCS of the solidified saline soil increased; as the added amount of MgO was increased from 10% to 12%, the UCS of the solidified saline soil decreased. Moreover, the growth in strength of solidified saline soil caused by increasing addition of MgO (from 4% to 10%) was more significant than the reduction of strength induced by decreasing addition of mineral powder. That is, the improvement of active and microexpansive effects of MgO mainly attributed to the growing addition amount of MgO. As the added amount of MgO was increased from 10% to

Table 6: Proportions of solidifying materials.

Serial number	MgO (%)	Calcium oxide (%)	Gypsum (%)	Mineral powder (%)
1	4	7.5	7.5	81
2	5	7.5	7.5	80
3	6	7.5	7.5	79
4	7	7.5	7.5	78
5	8	7.5	7.5	77
6	9	7.5	7.5	76
7	10	7.5	7.5	75
8	11	7.5	7.5	74
9	12	7.5	7.5	73
10			Cement	

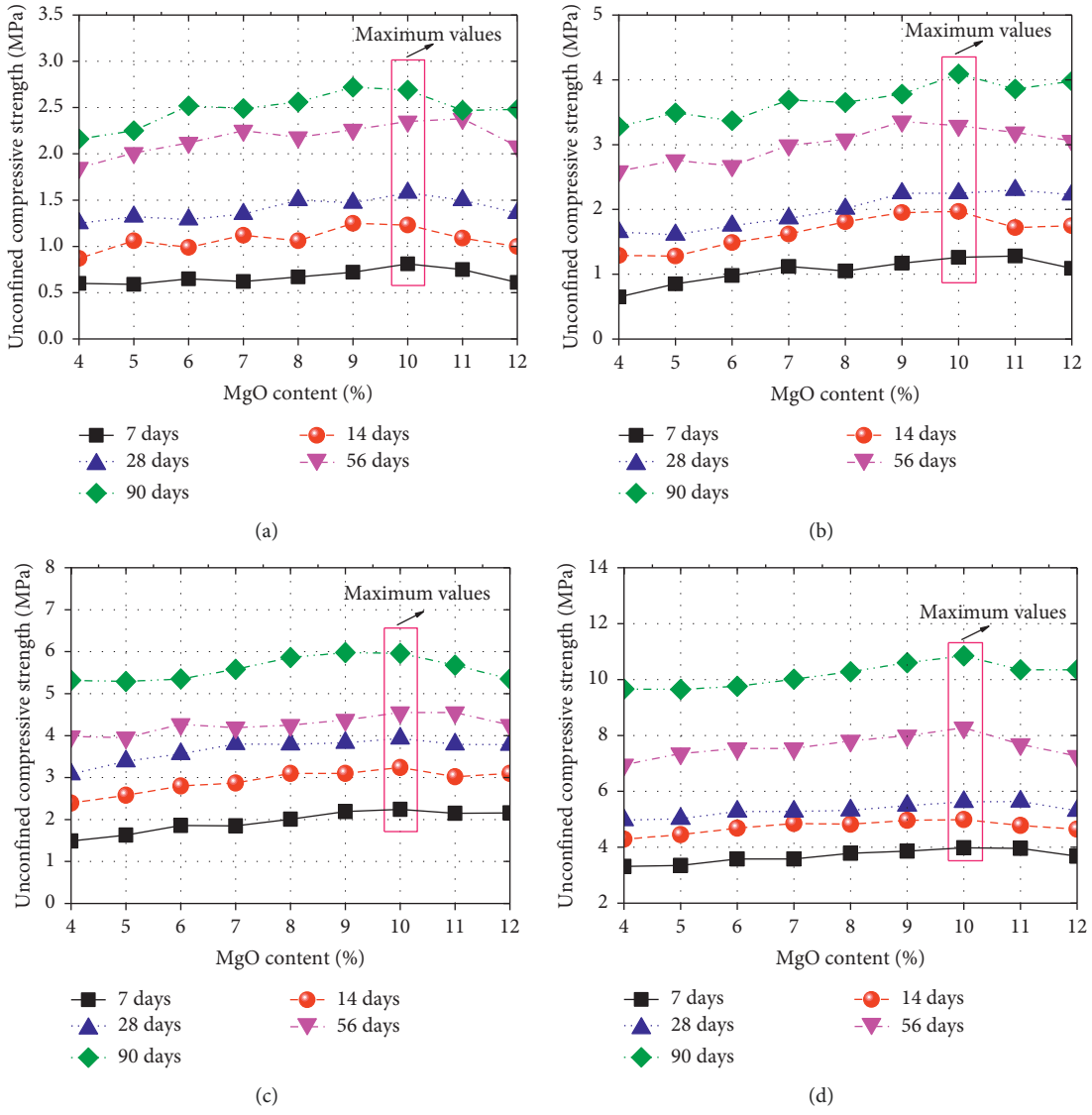

Figure 4: The influence of MgO content on the strength of solidified saline soil. (a) Adding 7% solidifying material. (b) Adding 10% solidifying material. (c) Adding 15% solidifying material. (d) Adding 20% solidifying material.

12%, the active effect of MgO increased while the active effect of mineral powders decreased. In this case, the large microexpansive effect of MgO caused the reduction of the solidified saline soil strength. With the addition of solidifying materials, the strength of solidified saline soil increased significantly. The optimal proportions of the

new cementitious composite materials were 75% mineral powders, 7.5% calcium oxide, 7.5% gypsum, and 10% active MgO.

3.3. Water Stability Test and Long-Term Strengths of the Solidified Saline Soil. According to the softening coefficient $K = (f_{u1}/f_{u2}) \times 100\%$, we can obtain the softening coefficients of the saline soil solidified by the new cementitious composite materials and cement (addition amounts 15%) at standard curing age 7 d, as shown in Table 7.

As shown in Table 7, the softening coefficient of the saline soil solidified by the new cementitious composite materials was greater than cement, which shows that the water stability of the saline soil solidified by the new cementitious composite materials is better than cement.

The use of the long-term UCS can save the engineering cost; thus, we investigated the UCS of the specimens at the curing ages 7, 14, 28, 56, 90, 180, and 360 d, and the specimens are cured through standard curing and immersion curing. The added amount of MgO in the cementitious composite materials was 10%, and the dosage of the new cementitious composite materials was 15%. The long-term UCS of the saline soil solidified by using the new cementitious composite materials and cement is shown in Figure 5.

It can be seen from Figure 5 that with the increase of the curing age from 7 d to 180 d, the growth rate of the strength of saline soil solidified by cements was greater than that solidified by the new cementitious composite material. When the curing age is 180 d, the UCS of the saline soil solidified by the new cementitious composite material began to be greater than that solidified by the cement through standard curing. When the curing age is 240 d, the UCS of the saline soil solidified by the new cementitious composite materials began to be greater than that solidified by the cement through immersion curing. Moreover, the test blocks of saline soil solidified by the new cementitious composite material were undamaged after being immersed in water. This indicated that the generated hydration products had coated the soil particles so that internal structure was compact, which allowed the solidified saline soil to resist damage. Therefore, with the increase of the curing ages, the strength of the saline soil solidified using two solidifying materials increased. However, when reaching certain curing age, the strength of the saline soil solidified by the cement increased very slowly, and the strength of the saline soil solidified by the new cementitious composite materials also increased fast. The long-term strength of saline soil solidified using the new cementitious composite material was greater than that of saline soil solidified using cement.

3.4. Analysis of Soluble Salts. The soluble salts in saline soil solidified using the cement and the new cementitious composite materials (added amount, 15%) were separately analysed. Table 8 listed the water-soluble ion contents and pH of the saline soil solidified using the two types of solidifying materials.

Table 7: Test result of the water stability of solidified soil.

Solidified material	f_{u1} (MPa)	f_{u2} (MPa)	K
New cementitious composite materials	5.12	5.45	0.94
Cement	5.20	5.74	0.91

It can be seen from Table 8 that saline soil approximated to neutral soil. After adding solidifying materials, cement was hydrated to generate $Ca(OH)_2$ while CaO in the added new cementitious composite materials reacted with H_2O to generate $Ca(OH)_2$, and the soil became alkaline. With the increase of the curing age, the soil pH decreased. Owing to active MgO being added to the new cementitious composite materials, the Mg^{2+} content in saline soil solidified using the new cementitious composite materials was always much greater than that in saline soil solidified using cement; however, the Mg^{2+} content in saline soil solidified using the new cementitious composite materials decreased with prolonged curing age. The main reason for this was that active MgO was subjected to a hydration reaction under the effect of soluble Mg^{2+} and Cl^-, and the hydration reaction generated $5Mg(OH)_2{\cdot}MgCl_2{\cdot}8H_2O$ and $Mg(OH)_2{\cdot}MgCl_2{\cdot}8H_2O$. On the other hand, active MgO reacted with H_2O to generate $Mg(OH)_2$. Owing to the solubility of $Mg(OH)_2$ being lower than that of $Ca(OH)_2$, Mg^{2+} preferentially reacted with OH^- to generate $Mg(OH)_2$, which replaced $Ca(OH)_2$ in mineral powders to react with active SiO_2 as follows: $Mg(OH)_2 + SiO_2 \longrightarrow$ M-S-H. The contents of soluble salt ions Na^+ and Cl^- in saline soil solidified using cement and the new cementitious composite materials both greatly decreased with the increase of curing age. This indicated that the two types of solidifying materials exhibited a favourable solidifying effect on harmful ions in saline soil. Moreover, the capacity of the new cementitious composite materials for solidifying Cl^- was stronger than that of cements as active MgO was subjected to a hydration reaction under the effect of soluble Mg^{2+} and Cl^- to generate $5Mg(OH)_2{\cdot}MgCl_2{\cdot}8H_2O$ and $3Mg(OH)_2{\cdot}MgCl_2{\cdot}8H_2O$. Thus, a certain amount of Cl^- was absorbed by active MgO added to the new cementitious composite material so that the capacity of the material for solidifying Cl^- was stronger than that of cement.

3.5. XRD Analysis. By conducting XRD analysis on hydration products of the new cementitious composite materials, the compositions of hydration products can be determined. Chemically pure NaCl was added into the new cementitious composite materials (taking up 2% of the material), and the test blocks composed entirely of the new cementitious composite materials cured for 28 d were prepared. In this way, the mechanism of the new cementitious composite materials cured for Cl^- was investigated. Figure 6 shows the test result obtained through XRD analysis.

As shown in Figure 6, A and B refer to the main diffraction peaks of SiO_2 and Friedel salts ($3CaO{\bullet}Al_2O_3{\bullet}CaCl_2{\bullet}10H_2O$), respectively; C denotes the main

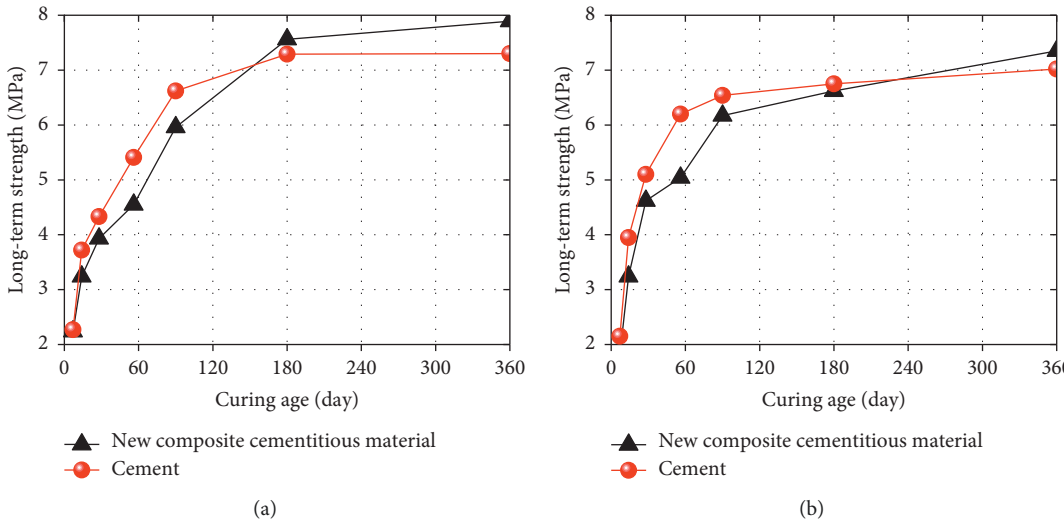

Figure 5: Long-term strengths of saline soil solidified by using the new cementitious composite materials and cement. (a) Standard curing. (b) Curing in fresh water.

Table 8: Water-soluble salt ion contents and pH.

Sample	pH	Na^+ (mg/kg)	Cl^- (mg/kg)	Ca^{2+} (mg/kg)	Mg^{2+} (mg/kg)	SO_4^{2-} (mg/kg)
Saline soil	7.6	4830	8830	1080	308	1765
Soil solidified using the cement for 56 d	10.7	3426	4152	385	51	416
Soil solidified using the cement for 360 d	9.6	727	1064	131	3	329
Soil solidified using the new cementitious composite material for 56 d	11.4	2900	3335	596	565	684
Soil solidified using the new cementitious composite material for 360 d	10.5	639	798	226	36	209

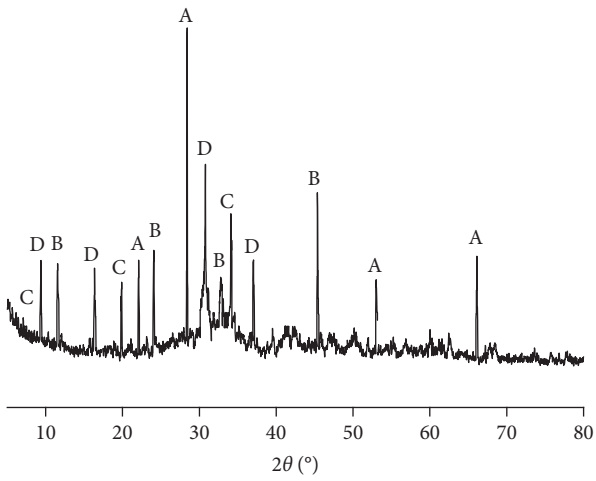

Figure 6: XRD result of the hydration product.

diffraction peak of AFm ($3CaO•Al_2O_3•CaSO_2•12H_2O$), and D represents the main diffraction peak of AFt ($3CaO•Al_2O_3•3CaCO_3•12H_2O$). According to XRD spectra, it can be found that AFt, AFm, and Friedel salts were generated in hydration products. Similarly, these compounds were also generated when solidifying saline soil using the new cementitious composite materials. This indicated that the use of the new cementitious composite materials not only solidified saline soil to endow the soil with certain strength but also absorbed Cl^- to reduce the harm.

3.6. SEM Analysis. The microstructures of the saline soil solidified using the cement and the new cementitious composite materials (added amount, 15%) after standard curing 28 d and 360 d were investigated, as shown in Figures 7 and 8.

As shown in Figures 7 and 8, the internal structure of saline soil solidified by applying the new cementitious composite materials for 28 d was compact: soil particles, the microstructure of the saline soil, were uniformly distributed, and they were surrounded by the cementitious materials, which are our newly developed cementitious composite materials. Although the water content in test blocks reached 30%, the internal structure of the test blocks did not show significant defects, *i.e.*, gaps, holes, and fractures. As a result, there was low possibility for the relative motion under the effect of external force, thus effectively improving the strength and stiffness of the solidified soil. By contrast, the internal structure of saline soil solidified by the cements for 28 d was loose: significant gaps and holes were found

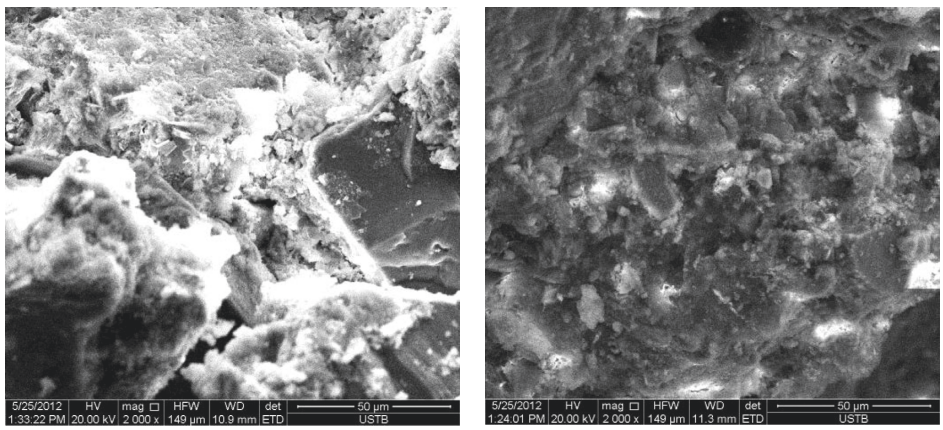

(a) (b)

Figure 7: SEM analysis of saline soil solidified using the two solidifying materials after standard curing 28 d. (a) Solidification using cement. (b) Solidification using our improved material.

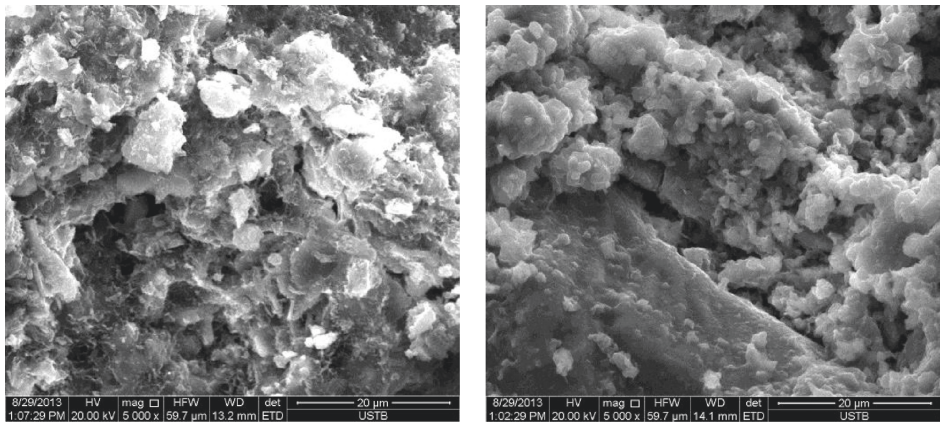

(a) (b)

Figure 8: SEM analysis of saline soil solidified by using cement and the cementitious composite material after standard curing 360 d. (a) Solidification using cement. (b) Solidification using our improved material.

between cementing agents and soil particles. After standard curing for 360 d, the saline soils solidified by using the two types of solidifying materials were both compact: soil particles were surrounded by hydration products and there were many clustered and petal-shaped C-S-H gels as well as flaky hydration products present. The main reason for this was that ettringite, Aft, and AFm were interactively crossed so that soil particles were less likely to be in relative motion, which was also the reason why the strength of the saline soil increased with prolonged curing time.

3.7. EDS Analysis. By conducting EDS, the chemical compositions of solidified saline soil can be determined. Therefore, when adding 15% of the new cementitious composite materials, the chemical compositions of the solidified saline soil for standard curing (28 d) were measured by SEM-EDS, as shown in Figure 9 and Table 9.

It can be seen from Figure 9 and Table 9 that Ca/Si in C-S-H gels was mostly between 0.8 and 2.0 at%. Therefore, it was supposed that Si was completely transformed into a C-S-H gel with Ca/Si = 1.5.

Then, subtracting atomic numbers of Si and Ca, the percentage contents of atomic numbers of the remaining elements (Al, Cl, and Ca) were calculated, as shown in Table 10.

As shown in Table 10, the ratios of Al : Cl : S : Ca at measurement points 1 and 2 were 1 : 0.57 : 0.09 : 1.77 and 1 : 0.54 : 0.13 : 1.80, respectively. The ratio (Al : Cl : Ca) of atomic numbers in Friedel salt ($3CaO{\bullet}Al_2O_3{\bullet}CaCl_2{\bullet}10H_2O$) was 1 : 1:2 while the ratio (Al : S : Ca) of atomic numbers in AFm ($3CaO{\bullet}Al_2O_3{\bullet}CaSO_4{\bullet}12H_2O$) was 1 : 0.5 : 2. Therefore, it can be determined that measurement points 1 and 2 separately denoted mixtures of AFm and Friedel salt. Chloroaluminate ($3CaO{\bullet}Al_2O_3{\bullet}CaCl_2{\bullet}10H_2O$) formed by using Cl^- and mineral admixture, also called Friedel salt, was a type of AFm series. The AFm series contained multiple compounds, and the typical compounds included $3CaO{\bullet}Al_2O_3{\bullet}CaCl_2{\bullet}nH_2O$, $3CaO{\bullet}Al_2O_3{\bullet}CaSO_4{\bullet}nH_2O$, and $3CaO{\bullet}Al_2O_3{\bullet}CaCO_3{\bullet}nH_2O$. In practical hydration

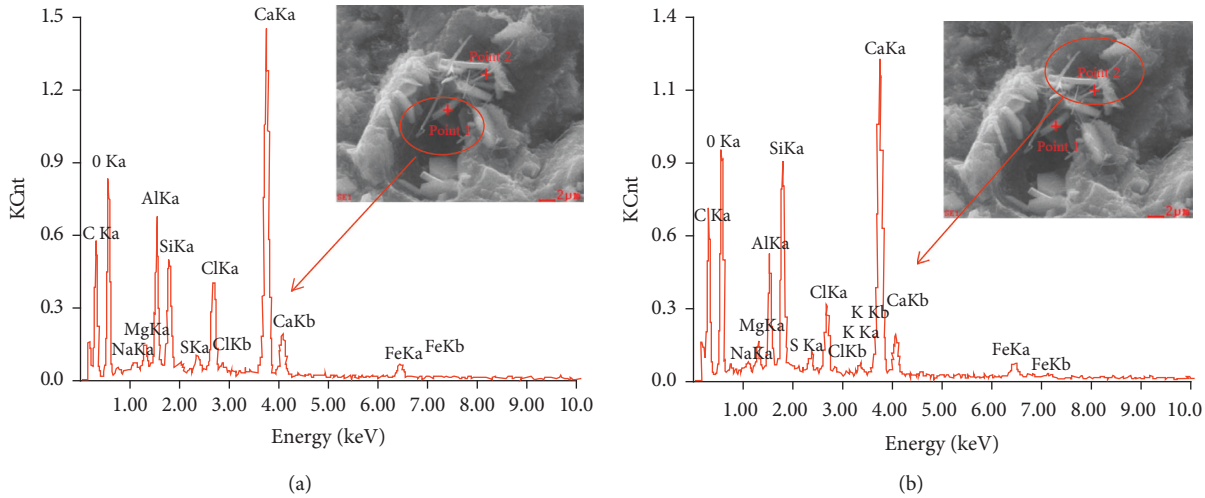

Figure 9: EDS analysis of the new cementitious composite material. (a) Point 1. (b) Point 2.

Table 9: EDS analysis result: points 1 and 2.

Element	O	Na	Mg	Al	Si	S	Cl	Ca	Fe
Point 1 (at%)	35.03	0.39	0.82	3.84	3.19	0.36	2.20	9.79	0.81
Point 2 (at%)	34.55	0.33	0.74	2.71	4.87	0.35	1.47	8.24	0.74

Table 10: Calculated chemical compositions: points 1 and 2.

Test point	Composition	O (%)	Na (%)	Mg (%)	Al (%)	Si (%)	S (%)	Cl (%)	Ca (%)	Fe (%)
Point 1	Percentage content of atomic number	35.03	0.39	0.82	3.84	3.19	0.36	2.2	11.58	0.81
	Si and Ca in C-S-H gel	—	—	—	—	3.19	—	—	4.79	—
	Percentage content of residual atomic number	35.03	0.39	0.82	3.84	0	0.36	2.2	6.80	0.81
	Percentage of atomic number	—	—	0.21	1.00	0.00	0.09	0.57	1.77	0.21
Point 2	Percentage content of atomic number	34.55	0.33	0.74	2.71	4.87	0.35	1.47	12.19	0.74
	Si and Ca in C-S-H gel	—	—	—	—	4.87	—	—	7.31	—
	Percentage content of residual atomic number	34.55	0.33	0.74	2.71	0.00	0.35	1.47	4.89	0.74
	Percentage of atomic number	—	—	0.27	1.00	0.00	0.13	0.54	1.80	0.27

processes, due to co-occurrence of multiple ions, several compounds which were likely to appear as synchronously or complex compounds containing multiple ions that can replace each other were generated; however, no matter which type of compounds was generated, the new cementitious composite material showed an excellent capacity for chemically bonding Cl^-. By analysing the molecular formula of the hydration products, it can be found that the Cl^- in saline soil can be eliminated through reaction with the material, which was the fundamental reason why the content of free Cl^- in saline soil declined with increase of the curing time. By calculating the volumes of various reactants and products before and after generation of $3CaO{\bullet}Al_2O_3{\bullet}CaCl_2{\bullet}10H_2O$, it was found that the volume of solid phase increased by about 76% during the generation of $3CaO{\bullet}Al_2O_3{\bullet}CaCl_2{\bullet}10H_2O$. It can also be seen that saline soil solidified using the new cementitious composite materials was more compact through SEM; therefore, the solid phase expanded when generating $3CaO{\bullet}Al_2O_3{\bullet}CaCl_2{\bullet}10H_2O$ to fill pores in the soil, which was also one of reasons why $CaO{\bullet}Al_2O_3{\bullet}CaCl_2{\bullet}10H_2O$ can increase the strength of the solidified soil.

4. Engineering Application in the Saline Soil Subgrade Strengthening

4.1. Finite Element Model of the Subgrade. In this section, we built the numerical simulation model to evaluate the seismic performance of the saline soil subgrade. The saline soil subgrade engineering of our study is located near the Sichuan-Tibet railway in China, which is under construction, as shown in Figure 10. Our research group drilled lots of boreholes in our survey region. The seismic activity around Sichuan-Tibet railway is relatively frequent. The groundwater level which changes with the season is commonly above 2.0 m.

In 2018, there have been more than eighty small earthquakes in Tibet Province while there were more than thirty small earthquakes in Sichuan Province. Soil salinization phenomenon is widespread in our survey region, and the saline soil often caused cracking and settlement of the subgrade under the

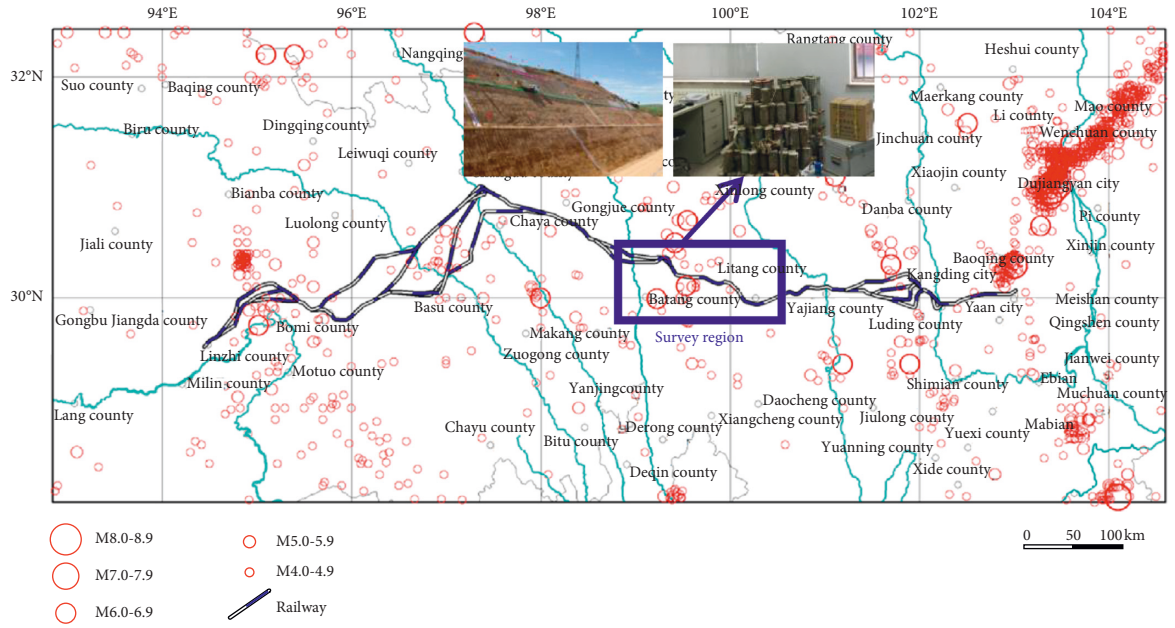

Figure 10: Geographic position of the survey region and seismic epicentral distribution map.

influence of the earthquake and rainfall. Consequently, a new composite cementing material for saline soil was developed by us to strengthen the subgrade, and a good effect of strengthening was achieved, as shown in Figure 11.

The slope models are established with finite element software MIDAS GTS NX, and we have simplified the slope models to some extent. The length of the model is 100 m, and the height of the model is 25 m. The subgrade width is 4.2 m, the right slope height of the subgrade is 6 m, and the left slope height is 20 m. In order to guarantee the accuracy of the calculation, the maximum size of the grid is less than 1/10~1/8 of the shortest wavelength of the input seismic waves. The Mohr–Coulomb elastic-plastic model is used to model the stress-strain behaviour of the soil. The grid size of the numerical simulation model is 0.5 m, and there are 5000 elements, as shown in Figure 12. Furthermore, the left, right, and bottom boundaries are set as viscoelastic artificial boundaries.

In the numerical simulation model, the quality damping coefficient α and the stiffness damping coefficient β are fixed as 0.2 and 0.0019, respectively. So, the damping coefficient of the numerical simulation model is calculated by the Rayleigh damping formula, as illustrated in the following equation:

$$[C] = \alpha[M] + \beta[K], \tag{1}$$

where α is the quality damping coefficient and β is the stiffness damping coefficient. Moreover, the quality damping coefficient and the stiffness damping coefficient are computed by the following equations:

$$\alpha = \frac{2\omega_i\omega_j\left(\xi_i\omega_j - \xi_j\omega_i\right)}{\omega_j^2 - \omega_i^2},$$
$$\beta = \frac{2\left(\xi_i\omega_j - \xi_j\omega_i\right)}{\omega_j^2 - \omega_i^2}, \tag{2}$$

where ω_i represents the natural frequency of the first model, ω_j corresponds to the natural frequency of the second model, and the range of the conventional damping ratios ξ_i and ξ_j are 2%~7%.

Based on the indoor experiment including the dynamic triaxial test and consolidation test, the physical parameters of the subgrade materials are shown in Table 11.

4.2. Selection of the Seismic Waves. The basic seismic intensity of the region of the subgrade is 7 degrees, and the site is II. According to *Code for Seismic Design of Railway Engineering (GB50111-2006)* [20] of China, the basic acceleration value of severe earthquake is 0.21 g, as shown in Table 12.

The El Centro earthquake, which happened in Imperial County, California, in the United States in 1940, is used in our study, as shown in Figure 13, and the peak accelerations of the seismic waves are adjusted for 0.21 g, as shown in Table 10. The acceleration time histories of the seismic wave are shown in Figure 9. Because the failure of the subgrade is mainly affected by the horizontal earthquake, only the influence of horizontal earthquake on the subgrade is considered.

4.3. Seismic Dynamic Response of Subgrade before and after Solidification. In order to determine the seismic dynamic response of the subgrade before and after strengthening using our newly developed cementitious composite material, we investigated the change laws of displacement, acceleration, and excess pore water pressure of the subgrade under the El Centro earthquake, which are the main index of reflecting the seismic resistant performance of the subgrade. The settlement and right slope stability of the subgrade are our main focus location in engineering, and we set the

(a) (b)

(c)

Figure 11: Solidification of the saline soil in the subgrade.

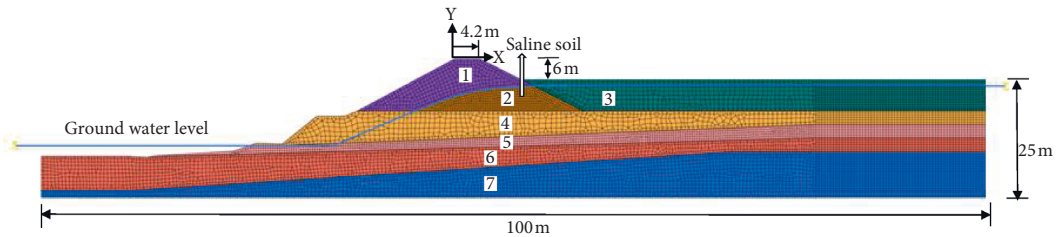

Figure 12: Calculation model of the subgrade. 1, subgrade filling; 2, saline soil; 3 and 5, silty soil; 4 and 6, silty clay soil; 7, weathered rock.

Table 11: Physical parameters of the subgrade.

Soil	Poisson's ratio	Elastic modulus (MPa)	Gravity ($kN \cdot m^{-3}$)	Cohesion (kPa)	Friction angle (°)	Initial void ratio	Coefficient of permeability ($cm \cdot s^{-1}$)
Material 1	0.38	100	15	32	24	0.85	$1e-5$
Material 2 (before solidification)	0.35	120	16	18	33	0.80	$1e-6$
Material 2 (after solidification)	0.27	320	19	50	38	0.40	$4e-9$
Material 3	0.32	129	17	35	26	0.78	$2e-6$
Material 4	0.3	185	16	35	34	0.75	$5e-7$
Material 5	0.28	274	18	45	35	0.65	$6e-7$
Material 6	0.25	756	20	65	30	0.50	$7e-9$
Material 7	0.21	975	21.2	80	32	0.40	$1e-10$

Table 12: Basic earthquake acceleration value in Chinese code.

Earthquake category	6 degrees	7 degrees	8 degrees	9 degrees
Frequent earthquake	0.02 g	0.04 g	0.07 g	0.14 g
Rare earthquake	0.11 g	0.21 g	0.38 g	0.64 g

subgrade top as the monitoring line 1 and the right slope of the subgrade as line 2. Also, the subgrade is often damaged by the excess pore water pressure during earthquake, and we set four monitoring points in different heights of the saline soil, as shown in Figure 14.

First, we compute the settlement displacement of the subgrade top and the horizontal displacement of the right slope of the subgrade before and after strengthening, as shown in Figure 15.

As shown in Figure 15, it can be found that the maximum settlement displacement is 0.095 m before strengthening while the maximum settlement displacement is 0.03 m after strengthening, and the settlement displacement of the subgrade after solidification is 3.2 times less than that before solidification. Consequently, our developed materials used in saline soil subgrade strengthening achieved good results.

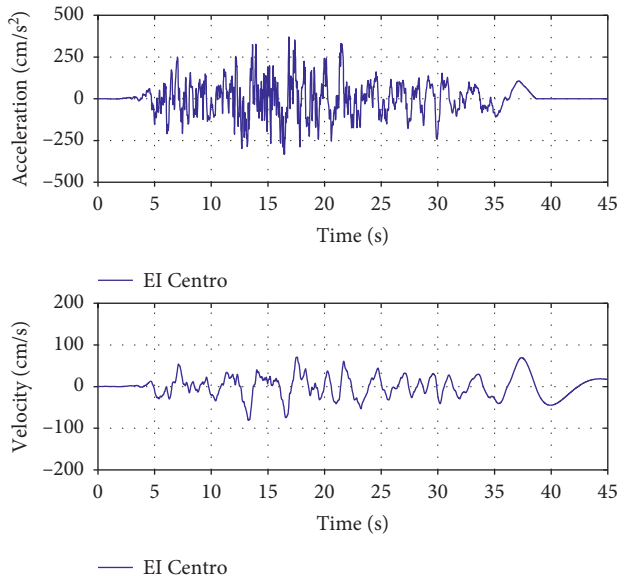

Figure 13: El Centro seismic wave.

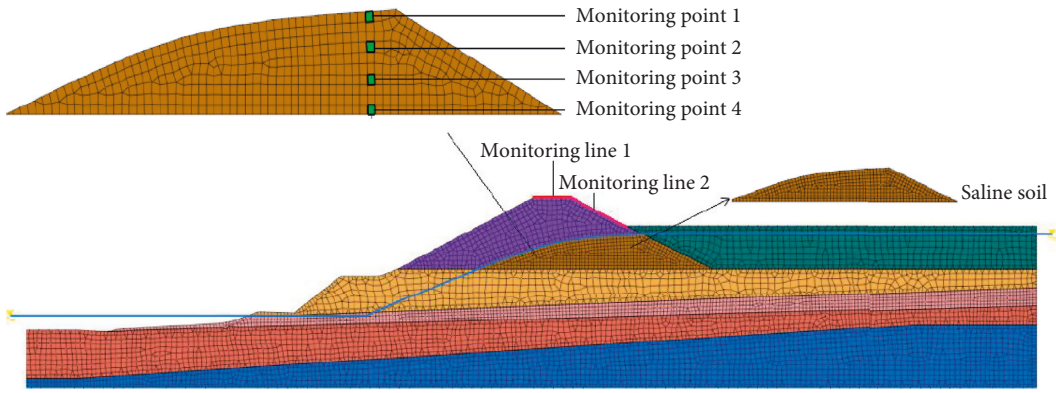

Figure 14: Monitoring lines and monitoring points of the model.

The horizontal displacement of the subgrade slope can determine whether the slope slides or not, and we found that the maximum horizontal displacement of the right slope after solidification is 1.7 times less than that before solidification, which shows that our developed materials can not only reduce the settlement deformation but also control the horizontal displacement of roadbed slope.

Since earthquake is dynamic load, the displacement is constantly changing under earthquake action, and the time at which the maximum deformation occurs can be quickly determined by observing the displacement time history; thus, the displacement time histories of the right slope top and slope toe are given as shown in Figure 16.

As shown in Figure 16, it can be seen that the displacement keeps fluctuating and accumulating under earthquake action, and the subgrade generated the permanent displacement, which shows that the subgrade produced the plastic deformation. The plastic deformation of the subgrade after solidification is less than that before solidification.

The contour of the maximum displacement is presented, and we can more intuitively observe the displacement changes of the subgrade before and after the strengthening, as shown in Figure 17.

As shown in Figure 17, we can see that the displacement of the subgrade top is the greatest under earthquake because of the dynamic amplification effect. However, the maximum displacement of the subgrade before strengthening is 5.09 cm while the maximum displacement of the subgrade before strengthening is 4.22 cm. The maximum displacement decreases 17%. Thus, our newly developed cementitious composite materials have good solidification effect on the subgrade deformation.

Through the above analysis, we can conclude that our developed materials have achieved good results in inhibiting the deformation of the saline soil subgrade under earthquake. Acceleration is another important index of the seismic performance of subgrade, and we also compute the horizontal accelerations of the subgrade top and the right slope of the subgrade before and after strengthening, as shown in Figure 18.

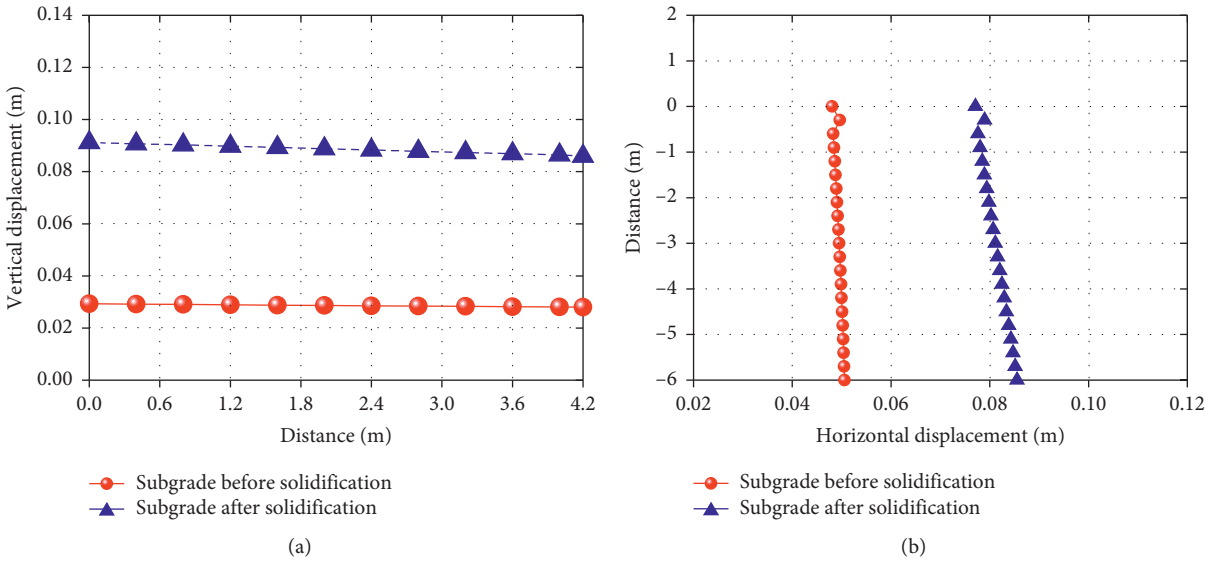

Figure 15: Settlement displacement of the subgrade top and the horizontal displacement of the right slope. (a) Subgrade top. (b) The right slope.

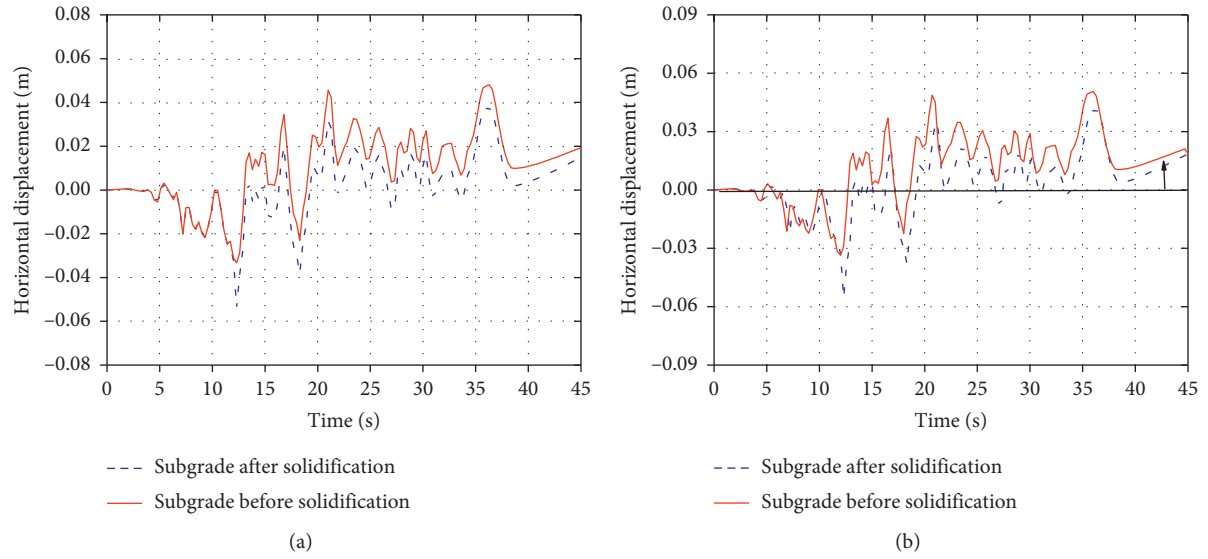

Figure 16: Displacement time histories of the right slope top and slope toe. (a) Slope top. (b) Slope toe.

As shown in Figure 18, we can see that the maximum accelerations of the subgrade top and the right slope after strengthening are less than those before strengthening, which shows that the solidification material can play a role in passive energy dissipation. The maximum acceleration of the subgrade top after strengthening decreases 1.1 times than that before solidification; while the maximum acceleration of the subgrade top after strengthening decreases 1.2 times than that before strengthening. Consequently, our newly developed cementitious composite materials not only have good solidification effect on the subgrade deformation but also have good solidification effect in passive energy dissipation control.

The acceleration is constantly changing under earthquake action, and the time at which the maximum acceleration occurs can be quickly determined by observing the acceleration time history; thus, the acceleration time histories of the right slope top and slope toe are given as shown in Figure 19.

As shown in Figure 19, we can see that the maximum acceleration of the right slope top is greater than that of the right slope toe under earthquake. The maximum accelerations are 2.92 m/s^2 and 2.34 m/s^2 of the right slope top before and after strengthening, respectively, while the maximum accelerations are 2.46 m/s^2 and 2.07 m/s^2 of the right slope toe before and after strengthening, respectively. Taking the right slope top as the example, the dynamic amplification factors are 1.47 and 1.2, which shows that the soil can amplify the seismic waves and the dynamic response of the subgrade is amplified by soil mass. In addition, our newly

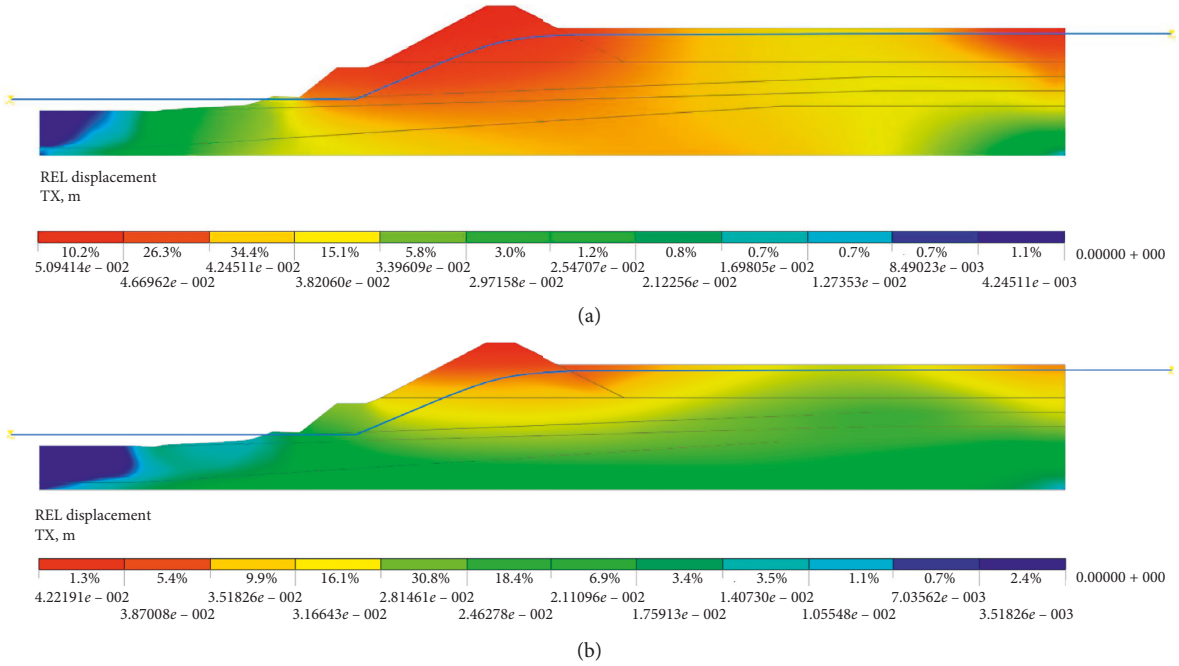

Figure 17: Displacement contour of the subgrade before and after strengthening. (a) Displacement contour of the subgrade before strengthening. (b) Displacement contour of the subgrade after strengthening.

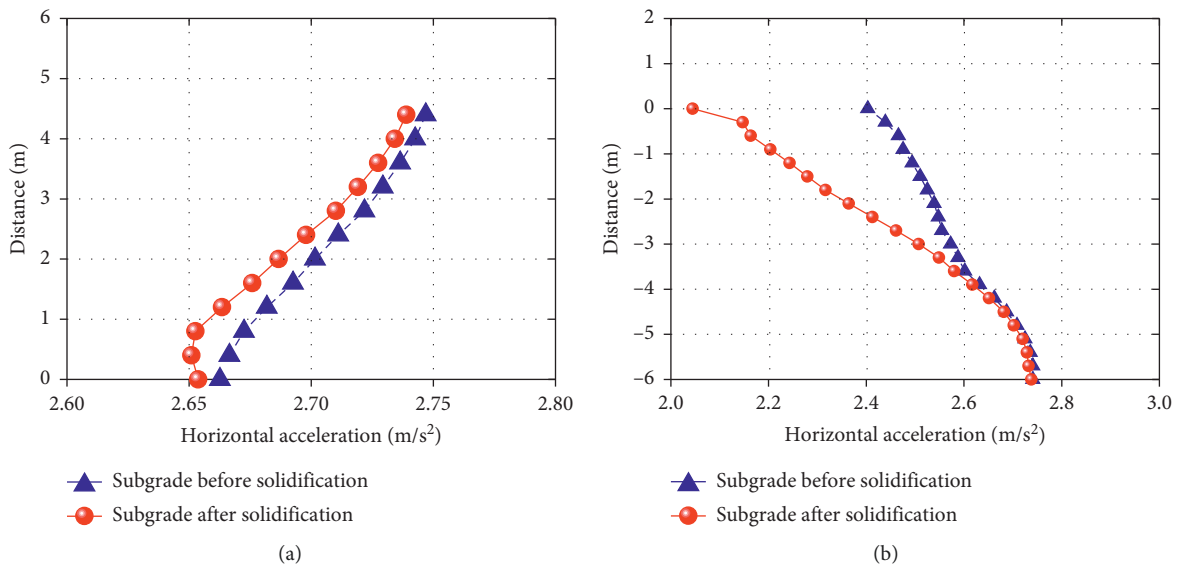

Figure 18: Horizontal accelerations of the subgrade top and the right slope of the subgrade before and after strengthening. (a) Subgrade top. (b) The right slope.

developed cementitious composite materials can not only strengthen the subgrade but also reduce the subgrade vibration under earthquake to ensure the traffic safety.

The main influencing factors of soil failure are the sharp increase of excess pore water pressure and the decrease of effective stress. Consequently, excess pore water pressure ratios of the saline soil before and after strengthening are investigated, as shown in Figure 20.

As shown in Figure 20, we can find that the excess pore water pressure ratio increases with the continuing effects of earthquakes. The excess pore water pressure ratios of the unstrengthened subgrade are greater than those of the strengthened subgrade. The maximum excess pore water pressure ratio of the unstrengthened subgrade is 0.82 while the maximum excess pore water pressure ratio of the strengthened subgrade is 0.65. Also, it can be seen that the excess pore water pressure of the unstrengthened subgrade continues to rise while the strengthened subgrade gradually dissipates, which shows that the excess pore water pressure dissipates fast.

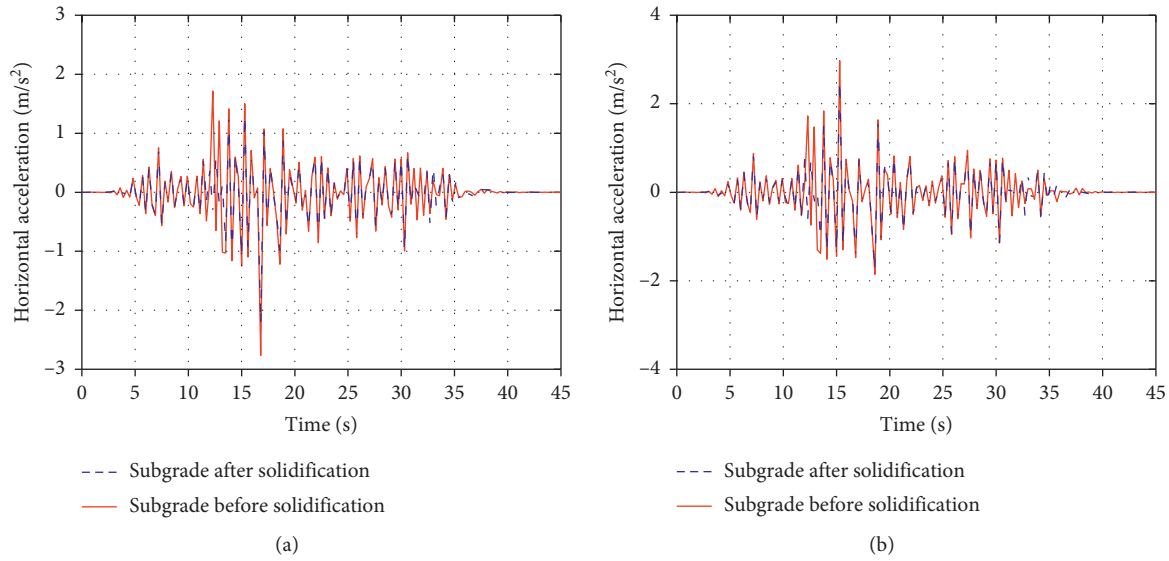

Figure 19: Horizontal acceleration time histories of the right slope top and slope toe. (a) Slope top. (b) Slope toe.

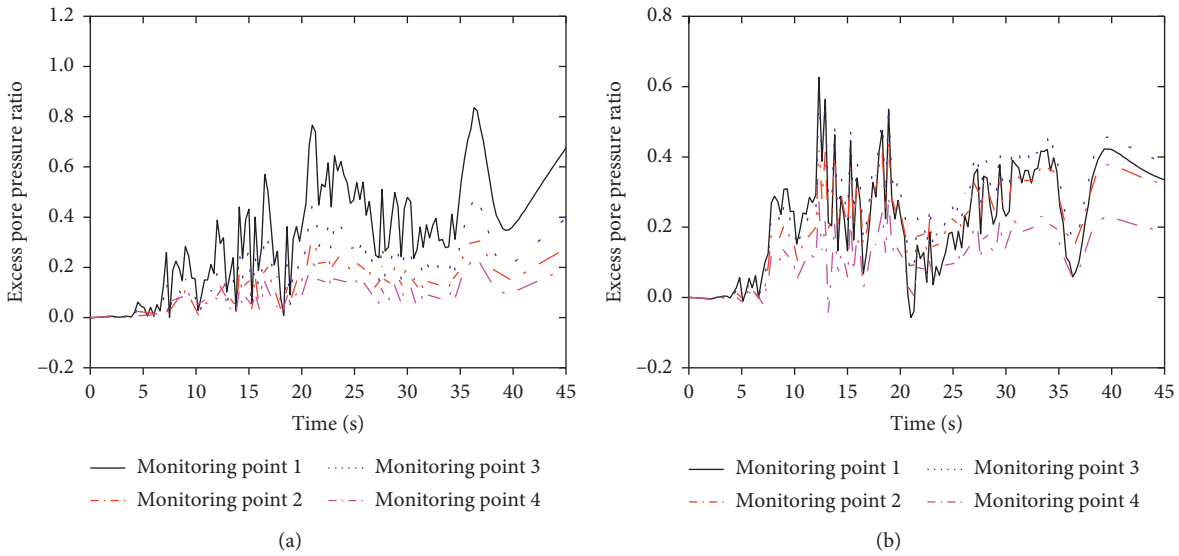

Figure 20: Excess pore water pressure ratios of the saline soil before and after strengthening. (a) Solidified subgrade. (b) Unsolidified subgrade.

4.4. Failure Modes of the Subgrade before and after Strengthening. We use the shaking table test which could reproduce the failure process of the subgrade under the real earthquakes to see the failure modes of the subgrade before and after strengthening. Figure 21 shows the shaking table test equipment to model the slope failure process under the seismic excitation.

As can be seen in Figure 21, the main technical indicators of the shaking table test equipment include rated working frequency (40 Hz), the maximum acceleration (20 m/s^2), the maximum test load (5000 kg), and dimensions of the shaking table (1.5 m × 1.5 m).

The size of the test model is 2 m × 1 m × 1.4 m. The slope rate of the subgrade is 1 : 1.5. To keep the soil uniform, the subgrade is repeatedly stirred. The sponge whose thickness is 20 m is to reduce the reflection of seismic waves at the border of the subgrade. The test model is shown in Figure 22.

The scaling law between our test model and the actual projects follow the Buckingham Pi theorem [21], and the proportional relation for the similarity ratio is developed by Jiang et al. [22]. Poisson's ratio μ of the soil in the test is 0.35, the coefficient $K = \mu/(1-\mu)$ of the lateral pressure is 0.54, and the dimensionless index $n = 2$. Other similarity coefficients based on similarity principle are shown in Table 13.where σ_v is the normal pressure stress (*i.e.*, the geostatic stress caused by burial depth); φ is the internal friction angle; c is cohesion; and k is the lateral pressure coefficient.

(a) (b) (c)

Figure 21: Shaking table test equipment. (a) Hydraulic system. (b) Shaking table. (c) Vibration controller.

(a) (b) (c)

Figure 22: Test model of the slope. (a) Geometric model. (b) Test model. (c) Rainer.

Table 13: Similarity coefficient between our test model and the actual projects.

Physical quantity	Similarity coefficient	Exegesis
Geometric dimensioning L	C_L	Control variable
Acceleration a	$C_a = C_{[\tau]}C_\rho^{-2/n}C_L^{-1}$	Control variable
Time T	$C_T = C_K^{-1/2}C_\rho^{1/2n}C_L^{2n-1/2n}$	Control variable
Density ρ	$C_\rho = 1$	
Strain level $\gamma/\overline{\gamma}$	$C_{(\gamma/\overline{\gamma})} = 1$	
Dynamic displacement u	$C_u = C_{[\tau]}C_K^{-1}C_\rho^{-1/n}C_L^{n-1/n}$	
Vibration velocity v	$C_v = C_u/C_T = C_{[\tau]}/C_K^{-1/2}C_\rho^{-(3/2n)}C_L^{-(1/2n)}$	
Vibration frequency w	$C_w = 1/C_T = C_K^{1/2}C_\rho^{-(1/2n)}C_L^{-(2n-1/2n)}$	
Damping ratio λ	$C_\lambda = 1$	
Dimensionless index n	$n = 2$	

$[\tau]$ is the horizontal shear strength and $[\tau]$ is computed by equation (3).

$$[\tau] = \sqrt{\left(\frac{1+k}{2}\sigma_v \sin\varphi + c\cos\varphi\right)^2 - \left(\frac{1-k}{2}\sigma_v\right)^2}, \quad (3)$$

In our experiment, similar material was developed based on the subgrade material. The similarity coefficients simulating the subgrade are shown in Table 14.

Next, we can more directly determine the failure degree of the subgrade before and after strengthening through the shaking table test, as shown in Figure 23.

As can be seen in Figure 23, through the shaking table test, we can more directly determine the failure degree of the subgrade before and after strengthening. Before strengthening, the destruction begins at the subgrade toe and the cracks in the subgrade spread gradually. Meanwhile, the position at the top of subgrade has obvious settlement phenomenon after earthquake. The sliding surface is approximately circular in shape. After strengthening, the destruction also begins at the subgrade toe, and the subgrade does not slip, while there are only a few cracks. Also, we found that the subgrade does not undergo subsidence deformation, which shows that our newly developed cementitious composite materials had a better strengthening effect.

Table 14: Similarity coefficients.

Physical quantity	Similarity constants
Dynamic shear strength (MPa)	4.85
Length (m)	6.00
Density (kg/m^3)	1.00
Acceleration (m/s^2)	0.81
Time (s)	2.72
Strain	1.00
Dynamic displacement (m)	51.56
Frequency (Hz)	0.19

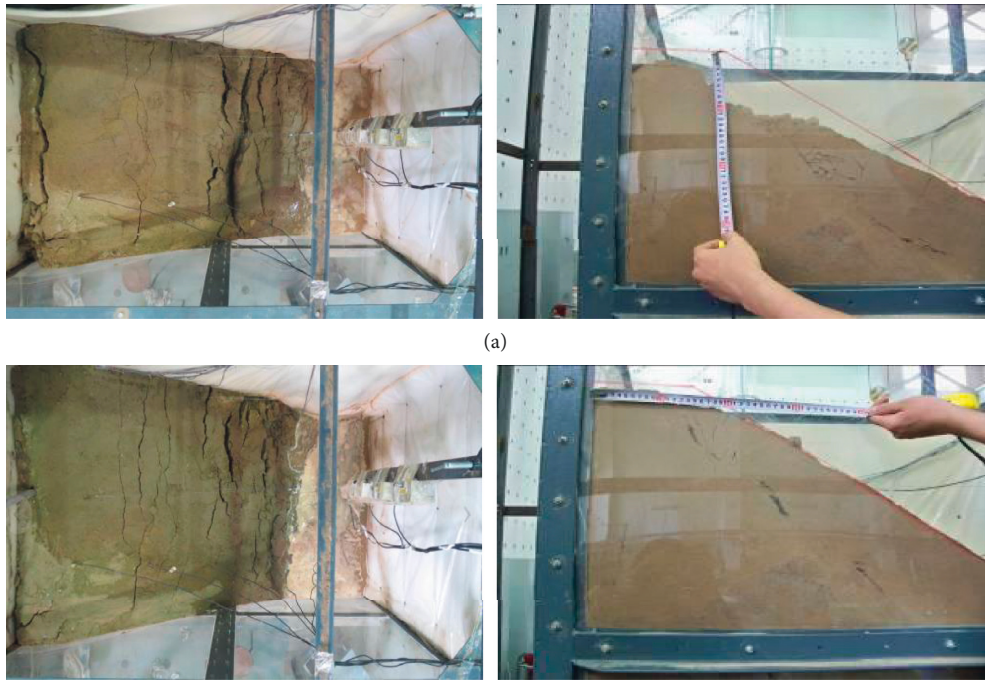

(a)

(b)

Figure 23: Plastic failure of the slope before and after strengthening. (a) Plastic failure of the slope before strengthening. (b) Plastic failure of the slope after strengthening.

5. Conclusions

(1) New cementitious composite materials were developed by using mineral powder, magnesia, quicklime, and gypsum. And the optimal proportion of different components in the new cementitious composite materials was determined through a series of tests and analyses.

(2) New cementitious composite materials were used to solidify saline soils, and the materials not only solidified saline soil to endow the soil with certain strength but also absorbed Cl^- to reduce the harm. The SEM analysis result showed that the saline soil solidified by the new cementitious composite materials had compact internal structure and uniformly distributed soil particles.

(3) New cementitious composite materials were applied to strengthen the saline soil subgrade in a highly seismic region. The results show that the newly developed cementitious composite materials have better aseismic behaviour, and the materials significantly reduced the seismic dynamic response and damage degree of the subgrade. This work provides important technological guidance for seismic design of saline soil subgrades.

Data Availability

The data used to support the findings of this study are available from the corresponding author upon request.

Conflicts of Interest

The authors declare that they have no conflicts of interest.

Acknowledgments

This study was financially supported by a research grant from the Institute of Crustal Dynamics, China Earthquake Administration (no. ZDJ2019-10), National Natural Science Foundation of China (grant no. 51708516), the Young Elite Scientists Sponsorship Program by CAST (2018QNRC001), Beijing Municipal Natural Science Foundation (8174078), National Key R&D Program of China (2017YFC1500404), and Natural Science Foundation of Hebei Province (E23019210126).

References

[1] T. Wen, *Study of Engineering Properties and Improvement of Loessial Sulfate Saline Soil in the Northwest area*, Lanzhou University of Technology, Lanzhou, China, 2012.

[2] X. Yang, Z. You, F. Niu et al., "Research progress in stabilizers and their effects in improving physical and mechanical properties of saline soil," *Journal of Glaciology and Geocryology*, vol. 36, no. 2, pp. 376–385, 2014.

[3] W. Li and S. Chai, "Evaluation of solidifying effect of SH agent on inshore saline soils," *Journal of Engineering Geology*, vol. 26, no. 2, pp. 407–415, 2018.

[4] Y. Wen, W. Zhang, Y. Luo, X. Liu, B. Li, and L. Wang, "Analysis of gradation characteristics and salt-resistance effect of subgrade layer in saline soil area," *Journal of Qinghai University*, vol. 36, no. 4, pp. 17–23, 2018.

[5] B. Song, L. Wang, and D. Zhu, "Subgrade design and construction technology in saline soil area," *Subgrade Engineering*, vol. 2, pp. 160–162, 2011.
[6] S. Zhang, Y. Wang, F. Xiao, and W. Chen, "Effect of overburden load on salt expansion of gravelly sand sulfate saline soil Subgrade," *China Railway Science*, vol. 40, no. 2, pp. 1–8, 2019.
[7] Y. Zhang, T. Zhang, R.-F. Zhang, and W. Yao, "Research on the selection of a railway subgrade filler in high saline soil region," *Journal of Railway Engineering Society*, vol. 33, no. 9, pp. 10–13, 2016.
[8] H. Li, R. Yin, and M. Zhang, "Study on use of gravel improved saline soil as subgrade fill," *Subgrade Engineering*, vol. 172, no. 1, pp. 53–57, 2014.
[9] L. Qingfeng, G. Zhou, S. Wang, Z. Huo, and B. Ma, "Microstructure characteristics of solidified saline soil based on nuclear magnetic resonance," *Rock and Soil Mechanics*, vol. 40, no. 1, pp. 245–249, 2019.
[10] F. Qi and W. Liu, "Subgrade design and construction technology in saline soil area," *Railway Construction Technology*, vol. 8, pp. 69–72, 2015.
[11] S. Zhang, S. Xie, X. Yang, and W. Chen, "Action mechanism of coarse particle sulfate soil subgrade modified by volcanic ash," *Chinese Journal of Geotechnical Engineering*, vol. 41, no. 3, pp. 588–594, 2019.
[12] Y. Cheng, H. Yu, B.-l. Zhu, and D.-X. Wei, "Laboratory investigation of the strength development of alkali-activated slag-stabilized chloride saline soil," *Journal of Zhejiang University-Science A*, vol. 17, no. 5, pp. 389–398, 2016.
[13] GB175-2007, Common portland cement, 2007.
[14] Z. Jin and P. Wang, "A laboratorial study of system"slag-light burnt magnesia-alkali"as cementitious material," *Material Applications*, vol. 33, no. 5, pp. 1–3, 2005.
[15] Z. Lou, Q. Ye, H. Chen, Y. Wang, and J. Shen, "Hydration of mgo in clinker and its expansion property," *Journal of the Chinese Ceramic Society*, vol. 4, pp. 430–436, 1998.
[16] J. Harrison, "New cements based on the addition of reactive magnesia to Portland cement with or without added pozzolan," in *Proceedings of the CIA Conference: Concrete in the Third Millenium*, pp. 24–35, CIA, Brisbane, Australia, 2003.
[17] M. Liska, L. J. Vandeperre, and A. Al-Tabbaa, "Influence of carbonation on the properties of reactive magnesia cement-based pressed masonry units," *Advances in Cement Research*, vol. 20, no. 2, pp. 1–12, 2008.
[18] China Railway Siyuan Survey and Design Group C, *Technical Code on Dry Jet Mixing Method to Stabilized Soft Foundation (TB 10113-96)*, Ministry of Railways, Beijing, China, 1996.
[19] C. Liu, *Study on Mechanism and Performance of the Coastal Saline Soil Cured by Slag Composite Curing agent*, University of Science and Technology Beijing, Beijing, China, 2015.
[20] Ministry of Railways of the People's Republic of China, *Code for Seismic Design of Railway Engineering (GB50112-2009)*, China Planning Press, Beijing, China, 2006.
[21] L. Brand, "The Pi theorem of dimensional analysis," *Archive for Rational Mechanics and Analysis*, vol. 1, no. 1, pp. 35–45, 1957.
[22] L. Jiang, L. Yao, and J. Wang, "Similitude for shaking table model test on side slope relating to dynamic characteristics and strength," *Journal of Transport Science and Engineering*, vol. 25, no. 2, pp. 1–7, 2009.

Hindawi
Advances in Civil Engineering
Volume 2019, Article ID 7450426, 10 pages
https://doi.org/10.1155/2019/7450426

Research Article

Research on Safety Management Application of Dangerous Sources in Engineering Construction Based on BIM Technology

Langni Deng,[1] Mengjun Zhong,[1] Ling Liao,[1] Lai Peng,[2] and Shijin Lai[1]

[1]*School of Civil Engineering and Architecture, Guangxi University of Science and Technology, Liuzhou 545006, China*
[2]*Department of Architectural Engineering, Guangxi Communications Vocational and Technical College, Nanning 530000, China*

Correspondence should be addressed to Mengjun Zhong; 1915461385@qq.com

Received 31 May 2019; Revised 9 August 2019; Accepted 5 September 2019; Published 11 December 2019

Guest Editor: Jingfeng Yuan

The construction industry is a high-risk industry, so many scholars have done research on how to reduce safety accidents at the construction site. However, due to the existence of hidden dangers in construction, accidents at the construction site still plague the development of the construction industry. Therefore, effective management of construction hazards is an important step to strengthen construction safety. At present, the technology of BIM has been gradually applied to various fields of construction projects, providing strong support for the smooth development of construction projects. Therefore, the purpose of this paper is to create a construction hazard source safety management module through secondary development of the Revit platform. At the same time, the Navisworks software is used to simulate the emergency rescue of construction safety accidents and formulate the corresponding emergency management plan. Finally, an engineering example is used to verify the performance of the development management module. The results show that (1) the security management module created in this paper is highly operational, easy to use, and real-time data update, which has important guiding significance for actual construction safety management; (2) simulation of construction safety accidents through Navisworks software can provide emergency management plans for engineering projects.

1. Introduction

The construction industry is one of the most dangerous industries in the world, and its work injury and death rate are extremely high [1]. As a high-risk industry, safety accidents in the construction industry will have a major impact on the social economy, people's lives, and natural environment [2]. Therefore, preventing the construction safety damage is essential to promote workers' safety and health, maintain the productivity level of construction projects, and reduce compensation for work-related injuries [3]. However, researchers and practitioners have been studying how to reduce the safety risks on the construction site and reduce the occurrence of safety accidents on the construction site. But it seems that no fundamental method has been found to solve this problem and the construction site safety accidents are still constantly plagued [4–7]. According to the theory of Heinrich's Law, construction hazard is one of the root causes of construction safety accidents. Hinze et al. [8] and Carter [4] have also pointed out that the important measures for building construction to prevent safety accidents are to effectively grasp the various hazards that cause safety accidents and pay attention to the real-time status of these hazards. Therefore, effectively identifying and managing various hazard sources will be one of the ways to fundamentally solve the frequent occurrence of safety accidents at construction sites. However, the current level of identification of safety hazards is far from ideal. It is necessary to propose an efficient method for the safe management of construction hazards.

As innovative technology has become a prominent topic in today's construction industry [9], the Building Information Model (BIM) has become the focus of attention in the latest developments in the construction industry [10]. In recent years, BIM technology has been gradually applied to various fields of construction projects [11], effectively

solving some problems that have long plagued the construction industry [12, 13]. Compared with the traditional working mode, the BIM method can help us to coordinate, cooperate, and integrate while improving and processing the information flow [14], which reflects the advantages of BIM technology in the field of construction engineering.

In the management of hazard sources, some scholars have begun to use BIM's own functions or functions based on the BIM platform to carry out secondary development around a specific project. For example, Gao et al. used BIM technology to carry out hazard source management for a large steel structure construction site [15]. Ding et al. carried out hazard source management of the steel structure construction process of a project based on the BIM and RFID technology [16]. Their research and application have achieved certain results for the management of dangerous sources in the construction process. However, there are some limitations in the function of BIM itself. Therefore, we need to carry out secondary development of its platform, further improve its functions, and improve the application value of BIM technology.

In view of the above advantages of BIM technology in the construction industry, this article will apply the technology of BIM to the safety management of engineering construction hazards, focus on the creation of safety management modules based on the secondary development of Revit platform, and establish a safety management system. Real-time monitoring and management of hazard sources such as safety signs, dangerous goods, and large machinery at the construction site use Navisworks software to simulate the rescue scene after the emergency of the construction site and respond to the emergency management rescue plan. Finally, the practicality of the research method proposed in this article is verified by combining specific engineering cases.

2. Creation of Secondary Management of Security Management Module Based on Revit Software

2.1. Design Ideas. In this paper, BIM technology is applied to the safety management of construction hazard sources. The BIM core software Revit is used as the development platform, and the C# language is used as the development language to build the RevitAPI secondary development environment. According to the secondary development process of Revit, the development and construction of dangerous source safety management module and its functions include the establishment of three types of construction hazard source management research on safety signs, dangerous goods, and large machinery. At the same time, the display class can be expressed in the solid modeling. The development technology implementation plan is shown in Figure 1.

2.2. Development Environment. Visual Studio is a software integration development environment developed by Microsoft, which encapsulates a large number of classes and methods that are frequently used in Microsoft development for developers to call. The C# language is an object-oriented, high-level programming language that runs on the NET Framework. The C# language is derived from the C language and the C++ language. It not only inherits the powerful functions of the C language and the C++ language but also removes some of their complex features, such as not allowing reinheritance and no macros and templates, and is simple, secure, and stable with other advantages. Winform forms have a rich set of controls to use and can connect to multiple databases. This article uses BIM core software Revit as the development platform, Visual Studio 2012 as the front-end development tool, C# as the programming language, and Winform form and uses the classes and methods encapsulated in Revit API to implement the security management module.

2.3. Revit Secondary Development Interface. In the Revit software provider, there is an open-source data interface. By inheriting the interface, the user can access the model data in the Revit software and can also recombine the new function module through the subfunction modules in the software. Revit API.dll and Revit APIUI.dll must be referenced in the integrated development environment for secondary development of Revit software. Revit API.dll mainly includes all data sets of Revit, currently open-model files, such as the application, document, element, and parameters of the model file. Revit APIUI.dll mainly includes external command-related interfaces, external application-related interfaces, user interaction selection, and task dialogs.

In the secondary development of Revit, there are two main methods: external application and external commands. The external application is a container for various external commands, mainly providing function-panel generation functions and implementing various specific function modules. External commands are used more frequently.

The interface of the external command must call the Execute function. The three parameters contained in the function are shown in Table 1. The CommandData parameter contains a reference to the application and view required by the external command to obtain the program object and document object of the current Revit model. ExternalCommandData contains some common view properties. The message represents the outgoing parameter. When the external command is executed, it will return a result. The message will pass the returned result as a string to the function panel. Elements, like the message, also represent outgoing parameters, but elements are mainly used to display the returned information in the model.

The interface of the external application is a container for external commands to run and can identify and load the addin file corresponding to the external command. Users can inherit the IExternalApplication interface and call the OnStartup and OnShutDown functions to achieve the required functionality. Its function parameters are shown in Table 2. The common functions for developing applications are shown in Table 3.

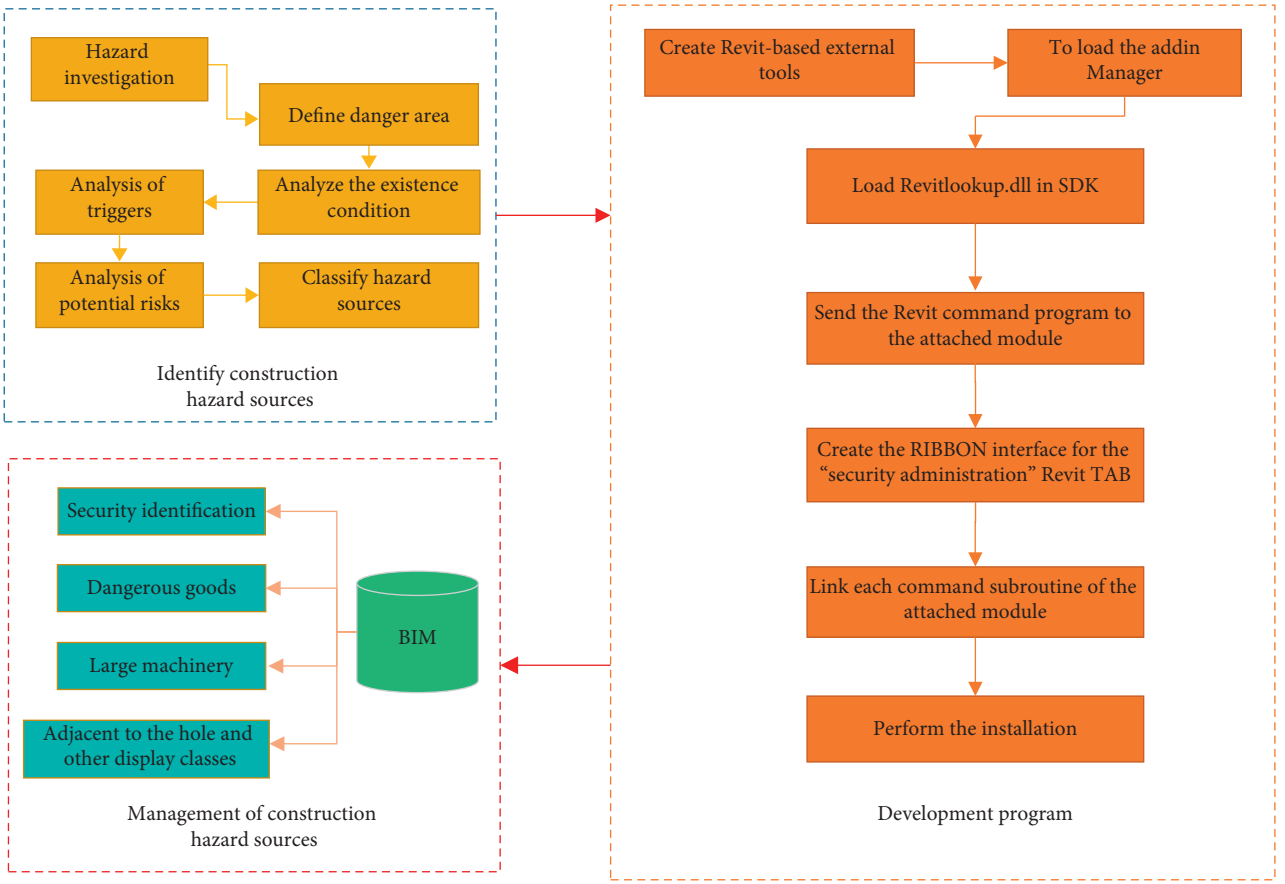

Figure 1: Development technology road map.

Table 1: Parameters of external command.

Development method	Method	Parameter
External commands	Execute	CommandData (ExternalCommandData), message (String), elements (ElementSet)

Table 2: Parameters of external application.

Development method	Method	Parameter
External application	OnStartup(), OnShutDown()	Application (UIControlledApplication)

Table 3: Function of external application.

Method	Features
Application.CreateRibbonTab()	Create a level one label
Application.CreateRibbonPanel()	Create a function panel
Panel.AddItem()	Add a function key to the function panel
BitmapImage()	Insert a picture for a function key

2.4. Revit Secondary Development Process. The process of Revit secondary development is shown in Figure 2. The specific steps are

(1) Create a class library project in Visual Studio 2012.

(2) Add two assemblies, Autodesk.RevitAPI.dll and Autodesk.RevitUI.dll, to the project. To reduce the system memory consumption of Revit runtime, change the "copy local" attribute of the above two assemblies to "False." A reference to the PresentationCore assembly is also required for external application development.

(3) Call the Execute method to automatically generate the corresponding interface and write the relevant function code.

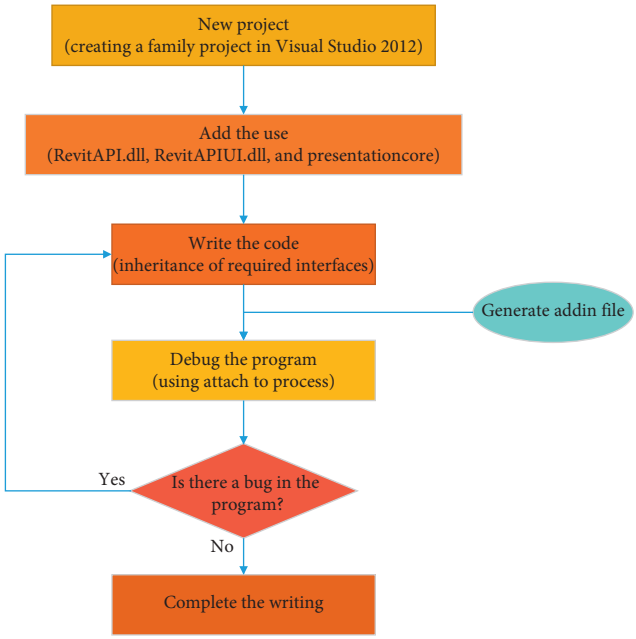

Figure 2: Revit secondary development process.

(4) Debug the program, use the method of attaching to Revit to debug the program in visual studio, and modify and adjust if there is any functional defect.

(5) Generate the addin file with the compiled code and register.

(6) Write external application function panel code.

(7) Register the addin file of the function panel.

2.5. Implementation of the Security Management Module. According to the above development process, the dangerous source safety management module is programmed and developed. Finally, the program is debugged to confirm that the program has no bugs and the construction danger source security management module is completed as shown in Figure 3. Then, according to the actual construction conditions of the construction project, the relevant hazard sources can be created in different ways (as shown in Table 4) in the BIM, and then, a series of work can be carried out on the safety management of the subsequent construction hazard sources based on the BIM. Construction safety risks are minimized to promote worker safety and health.

3. Case Study

3.1. Project Overview. The project is a public rental housing project in Liuzhou, with a total of 9 residential buildings. In this case, the 8# building is mainly used as a research application, which has 1 basement and 18 floors above ground. The total height of the building is 52.20 m; the building base area is 1127.27 m^2; the total construction area is 20474.6 m^2; the building structure is frame shear wall structure; the architectural structure category is C grade; the seismic fortification intensity is 6 degrees; the design life is 50 years. According to the design drawings, Revit's parametric modeling of the 8# building is shown in Figure 4.

3.2. Application Based on Revit Software Security Management Module. Using the already created BIM, combined with Navisworks software to simulate the construction plan of the project, according to the 3D visualization advantages of BIM, the hazard sources existing in the construction process are identified in advance and then various types of signs are loaded by adding new decal-type functions, as shown in Figure 5.

After identifying the existing hazard source in the BIM, the security mark is pasted in the form of a decal at the corresponding model position and the effect is shown in Figure 6. The placement of safety signs, dangerous goods, and large machinery in the BIM must be consistent with the actual construction site, and then, the actual process of the project is controlled in real time. The management personnel can effectively manage the hazard source through the developed construction safety management module, through the three-dimensional BIM. The model clearly controls the real-time information of the hazard source and can also count and manage the hazard source of the project through the development of the enhanced function list. Finally, the real-time construction safety management of the project is carried out through the mailbox in the construction safety management module. The mode is sent to the owner, supervisor, and other users to realize multiparty real-time monitoring and management to ensure the project is safe and efficient.

There are some high-risk parts during the construction process, such as stairs, elevator shafts, reserved openings, passage openings, balconies, picking platforms, elevators, scaffolding, cranes, and other parts. These parts are the focus of construction safety management, and protection measures must be taken in accordance with the requirements of the regulations. In order to effectively prevent the work, protective measures for these high-risk parts are created in the BIM (as shown in Figure 7) and the corresponding safety signs are attached to implement the interaction between the construction site and the BIM. The BIM can be used to control the management of multiple users, avoiding the individual factors of the manager to make incorrect decisions, and the installation and dismantling of protective measures are scientific and reasonable.

3.3. Application Based on BIM Technology Emergency Response Rescue Simulation. Once a construction safety accident occurs, timely and effective rescue work has become a crucial link. This link not only affects the cost of the project but also seriously affects people's life safety. Therefore, it is very necessary to draw up an emergency plan. The emergency plan is the basis for emergencies and the "bottom line" for emergency rescue [17]. Due to the unpredictability of construction projects, the formulation of emergency plans

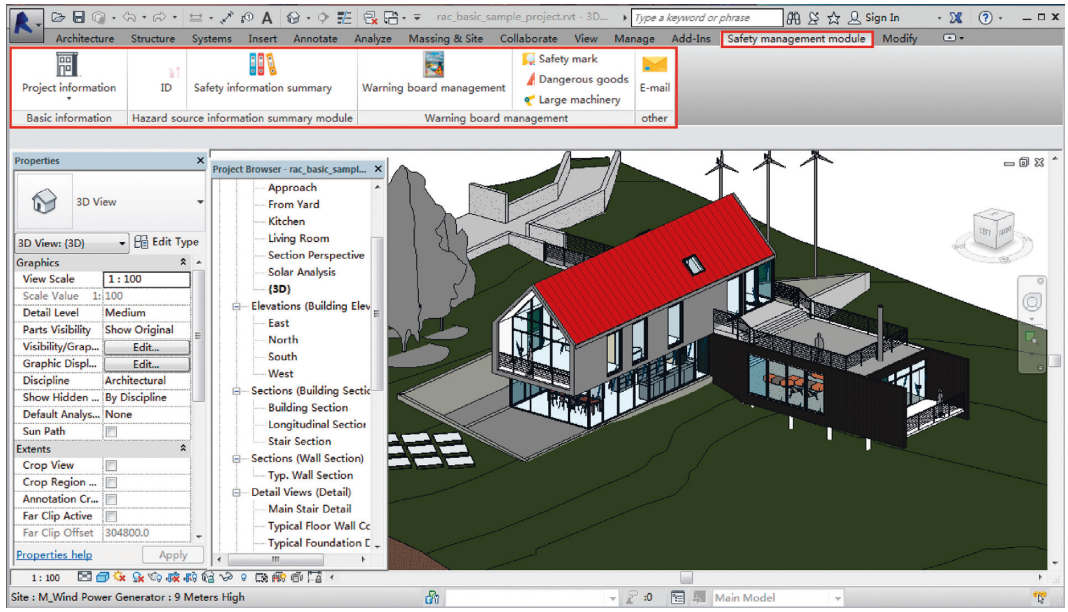

Figure 3: Construction danger source security management module based on Revit platform.

Table 4: Application name.

Security management name	Revit's own commands
Safety signs	Placing decals
Dangerous goods Large machinery	Placement component
Project parameters	Project parameters
Selection of the ID number	Select by ID
Warning sign management	Decal type
Summary of hazard information	List
Equipment item	Load family

using traditional thinking methods will be difficult to do. With the Animator animation tool, you can easily implement custom animations for each object in the model and you can create a simulation animation of a security incident emergency rescue [18]. Therefore, by using Navisworks software and Animator animation production tool, taking the 8# building as an example, according to the actual situation of the scene, the emergency rescue simulation of the construction workers of high-altitude falling objects is carried out. The animation is mainly divided into the following, according to the progress of the accident development section:

(1) Accident: the main body of a public rental project residential-area 8# building has been completed, the construction waste is being cleaned up, and a construction worker A does not even take a piece of discarded gypsum block out of the 4th floor balcony and is just walking in the middle of the building. Downstairs, there is a construction worker B wearing an uncovered helmet. B is smashed and he falls to the ground; a lot of blood is flowing, and he is in a coma. The whole simulation process of the high-altitude falling of the object on the construction worker B is shown in Figure 8.

(2) Accidents found: at this time, two scene management personnel pass by and find the accident. One of them immediately runs to the injured person to check the casualty situation. The other person immediately goes to the safety engineer to briefly report the accident location and personnel. Casualty: the safety engineer knowing the situation quickly reports the accident to the on-site commander, immediately dials the 120 emergency center to the scene to carry out the rescue, and then informs the project rescue team to handle the scene of the accident and the person in charge is asked to timely carry out rescue work, within the prescribed time. It is necessary to report to the director's office and relevant departments at the higher level. The entire accident simulation animation process is shown in Figure 9.

(3) Rescue: the engineering medical team rushes to the scene in time to immediately perform medical examinations and rescues, waiting for the ambulance to arrive. The safety and security team of the engineering department arrives at the scene, pulls up the cordon, blocks the scene. To ensure that the road is smooth and the ambulance reaches the accident site smoothly. Then, an employee is dispatched as a guide to convey the scene of the accident to the medical team, so that the medical team could prepare for the emergency rescue and at the same time guide the ambulance to the scene of the accident in the shortest path and the shortest time. The entire simulation process of the ambulance arriving at the accident site is shown in Figure 10.

(a) (b)

Figure 4: 8# floor renderings.

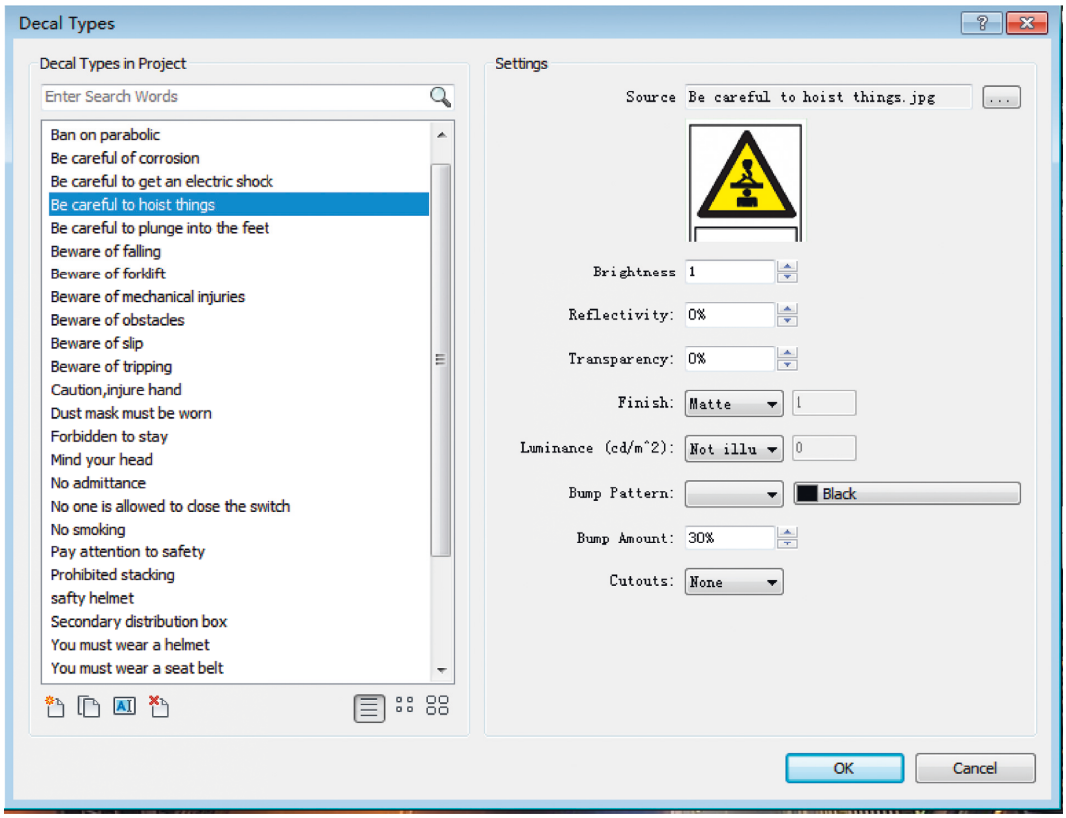

Figure 5: Schematic diagram of security ID loading.

(4) Based on the Revit software safety management module, the safety signs, dangerous goods, and other dangerous sources on the construction site are monitored and managed in real time, and the visual characteristics of BIM technology are used to manage the dangerous sources such as the border hole. At the same time, the Navisworks software was used to carry out emergency rescue simulation on the construction site emergency situation, and the emergency rescue site of the accident of high-altitude

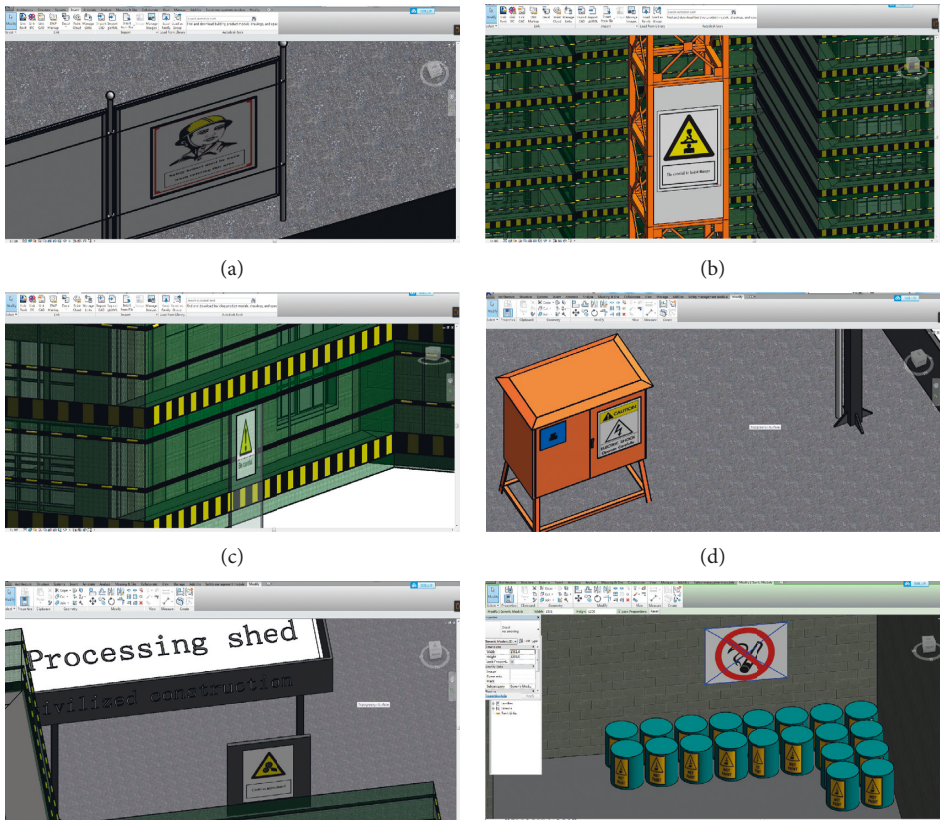

(a) (b) (c) (d) (e) (f)

Figure 6: Schematic diagram of hazard source identification.

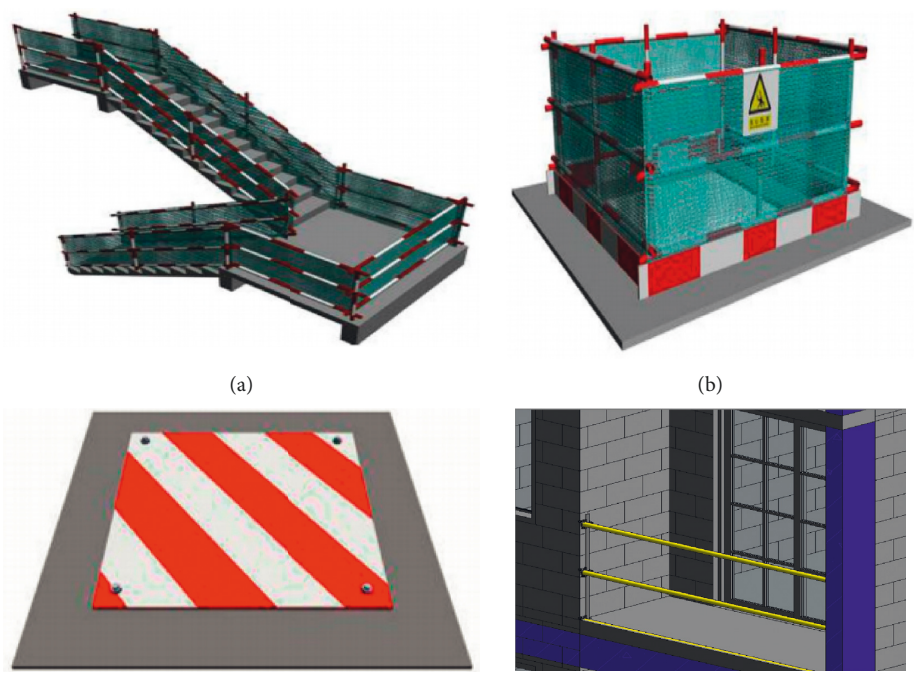

(a) (b) (c) (d)

Figure 7: Protection measures for the edge and the entrance.

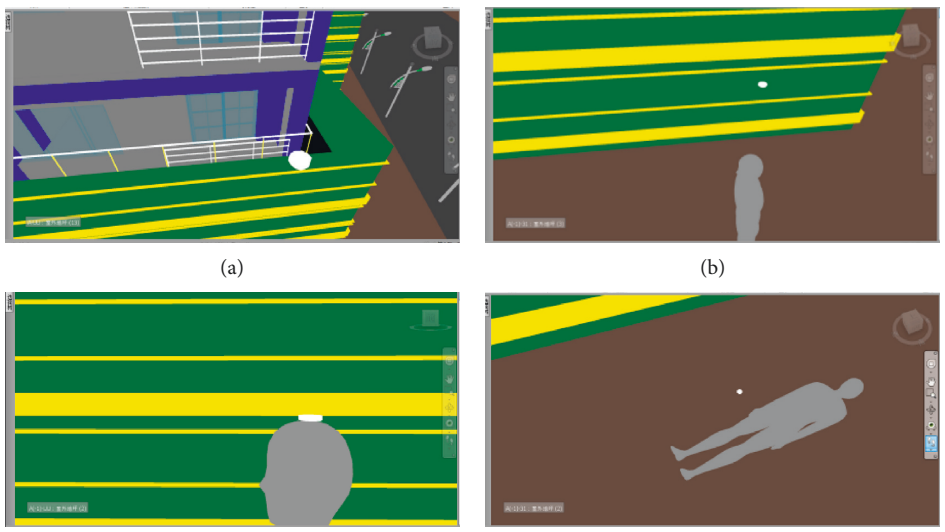

(a) (b)

(c) (d)

Figure 8: Schematic diagram of the animation of the accident.

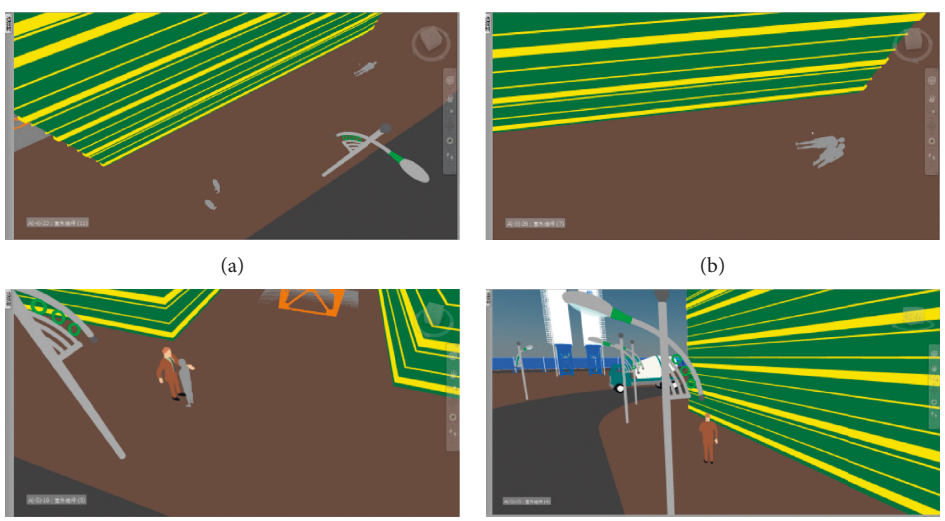

(a) (b)

(c) (d)

Figure 9: Schematic diagram of the accident animation simulation.

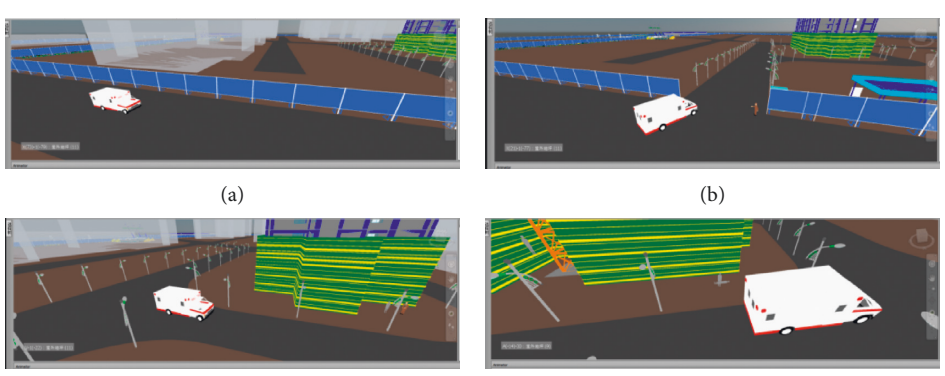

(a) (b)

(c) (d)

Figure 10: Schematic diagram of the animation simulation of the ambulance arrival accident scene.

falling of objects on the construction worker at the high altitude was displayed. Through the research and application of this case, we can know the following:

(i) The BIM information is comprehensive and interrelated. The function of "one modification, everywhere modification" greatly reduces the workload and time of information processing and improves work efficiency.

(ii) Based on the secondary development of Revit software security management module, we can realize the safety management of construction safety signs, dangerous goods, large machinery, and other construction hazards. The content is intuitive and clear, and the information parameters are easy to collect and manage. And it provides new technical means and management ideas for the safety management of dangerous sources in the construction site.

(iii) In the preconstruction preparation stage, the BIM can be used to rationally plan and arrange the construction site, master the direction and circulation of each road, eliminate the occurrence of fires and emergency roads, and clarify the safety management priorities and control measures during the construction process.

(iv) From the emergency rescue simulation based on BIM, the image is easy to understand, the response information is more intuitive, and the preparation of the emergency plan is optimized, which can impress the owner and the construction staff. At the same time, an important safety education and training can be conducted to guide the construction workers to safe construction to reduce accidents and reduce casualties and economic losses after the accident.

4. Conclusion

This paper studies the application of BIM technology in the construction process of safety management of construction projects. Based on the Revit platform, the C# language is used for secondary development and, together with the functionality of the Revit software itself, ultimately creates a hazard source security management module. Module features include project information, hazard source management, safety information digests, and other subfunctions. Through the actual construction project, the real-time monitoring and management of the safety signs, dangerous goods, large machinery, and other hazard sources on the construction site are carried out by using the Revit software safety management module, and the visual sources such as BIM technology are used to display the dangerous sources such as the edge of the tunnel. Visual port management was carried out, and the emergency rescue simulation of the construction site emergencies was carried out with Navisworks software to demonstrate the emergency rescue scene of the construction workers falling. The advantages and application effects of BIM technology for construction safety management can be summarized as follows:

(1) The BIM information is comprehensive and interrelated. The function of "one modification, everywhere modification" greatly reduces the workload and time of information processing and improves work efficiency;

(2) Based on the security management module developed by Revit platform, the content is intuitive and clear, and the information parameters are easy to collect and manage, providing new technical means and management ideas for the safety management of dangerous sources on the construction site;

(3) In the preconstruction preparation stage, the BIM can be used to rationally plan and layout the construction site, grasp the direction and circulation of each road, eliminate the occurrence of fire and emergency roads, and clarify the safety management priorities and control measures during construction;

(4) From the emergency rescue simulation based on BIM, the reaction information is more intuitive and can be used for safety education and training, guiding construction workers to safe construction, combined with the preparation of emergency plans to reduce accidents, casualties, and economic losses.

5. Discussion

BIM technology has good research value in the safety management of construction hazard source, but the research in this paper is only a preliminary exploration of BIM technology in the safety management of engineering construction hazard, only due to the unsafe state of the construction work. Safety signs, dangerous goods, and large mechanical equipment were considered, and other hidden hazard sources were not identified. The safety management module developed has not yet achieved safety warning.

Data Availability

The data used to support the findings of this study have not been made available because the plug-in development involves many Chinese places and the use of the plug-in address is also involved in the code, for some computers need to change part of the code.

Conflicts of Interest

The authors declare that they have no conflicts of interest.

Acknowledgments

The authors acknowledge the financial support provided by the National Natural Science Foundation of China (no. 51568008).

References

[1] M. Abbas, B. E. Mneymneh, and H. Khoury, "Assessing on-site construction personnel hazard perception in a Middle Eastern developing country: an interactive graphical approach," *Safety Science*, vol. 103, pp. 183–196, 2018.

[2] W. Wu, L. A. M. Patrick TI, Q. Li, C. H. Y. A. M. Michael, and A. S. C. H. E. W. David, "Research on real-time monitoring and safety risk prediction methods for safety hazard on construction site," *Chinese Engineering Science*, vol. 12, no. 3, pp. 68–72, 2010.

[3] K. Yang, C. R. Ahn, and H. Kim, "Validating ambulatory gait assessment technique for hazard sensing in construction environments," *Automation in Construction*, vol. 98, 2019.

[4] M. R. Hallowell and J. A. Gambatese, "Construction safety risk mitigation," *Journal of Construction Engineering and Management*, vol. 135, no. 12, pp. 1316–1323, 2009.

[5] J. Hinze, S. Thurman, and A. Wehle, "Leading indicators of construction safety performance," *Safety Science*, vol. 51, no. 1, 2013.

[6] G. Carter and S. D. Smith, "Safety hazard identification on construction projects," *Journal of Construction Engineering and Management*, vol. 132, no. 2, 2006.

[7] D. P. Fang, X. Y. Huang, and J. Hinze, "Bench marking studies on con-struction safety management in China," *Journal of Construction Engineering and Management*, vol. 130, pp. 424–431, 2004.

[8] J. Hinze, C. Pedersen, and J. Fredley, "Identifying root causes of construction injuries," *Journal of Construction Engineering and Management*, vol. 124, no. 1, pp. 67–71, 1998.

[9] D. W. M. Chan, T. O. Olawumi, and A. M. L. Ho, "Perceived benefits of and barriers to building information modelling (BIM) implementation in construction: the case of Hong Kong," *Journal of Building Engineering*, vol. 25, 2019.

[10] R. Takim, M. Harris, and A. H. Nawawi, "Building information modeling (BIM): a new paradigm for quality of life within architectural, engineering and construction (AEC) industry," *Procedia—Social and Behavioral Sciences*, vol. 101, pp. 23–32, 2013.

[11] J. Yang, D. Yu, T. Zhang, and C. Fu, "Study on construction simulation of deep foundation pit based on BIM technology," *Journal of Qingdao Technological University*, vol. 38, no. 3, pp. 114–118, 2017.

[12] D. Cao, G. Wang, H. Li, M. Skitmore, T. Huang, and W. Zhang, "Practices and effectiveness of building information modelling in construction projects in China," *Automation in Construction*, vol. 49, pp. 113–122, 2015.

[13] C. Eastman, P. Teicholz, R. Sacks, and K. Liston, *BIM Handbook: A Guide to Building Information Modeling for Owners, Managers, Designers, Engineers and Contractors*, Wiley Publishing, Hoboken, NJ, USA, 2008.

[14] B.-j. He, M. Ye, L. Yang, X.-P. Fu, B. Mou, and C. Griffy-Brown, "The combination of digital technology and architectural design to develop a process for enhancing energy-saving: the case of Maanshan China," *Technology in Society*, vol. 39, pp. 77–87, 2014.

[15] Y. Gao, Y. Wang, and N. Li, "Application of BIM technology in hazard source management of large steel structure construction," *Building Materials and Decoration*, vol. 51, pp. 141-142, 2018.

[16] W. Ding and B. Zhang, "Application of BIM technology in hazard source management of large steel structure construction," *Journal of Civil Engineering and Management*, vol. 34, no. 3, pp. 13–19, 2017.

[17] W. Chen, *Research on Emergency Management of Sudden Safety Incidents in Construction Enterprises*, Nanjing Forestry University, Nanjing, China, 2008.

[18] J. Zhou and Y. Hou, "Application of BIM technology in emergency rescue plan for safety accidents," *Civil Engineering and Information Technology*, vol. 06, no. 4, pp. 42–48, 2014.

Hindawi
Advances in Civil Engineering
Volume 2019, Article ID 3604369, 18 pages
https://doi.org/10.1155/2019/3604369

Research Article

Research on IFC- and FDS-Based Information Sharing for Building Fire Safety Analysis

Jianyong Shi, Jicao Dao, Liu Jiang, and Zeyu Pan

Department of Civil Engineering, School of Naval Architecture, Ocean and Civil Engineering, Shanghai Jiao Tong University, Shanghai 200240, China

Correspondence should be addressed to Jianyong Shi; shijy@sjtu.edu.cn

Received 30 July 2019; Revised 30 September 2019; Accepted 25 October 2019; Published 29 November 2019

Guest Editor: Endong Wang

With the development of computer processors, vast numerical simulation tools are widely used by fire engineers to determine the spread of fire and smoke. However, the fire modeling practices are often highly time-consuming and cost-intensive especially for building geometry information which does limit the further implementation of building fire safety analysis. Although nowadays building information modeling (BIM) has become a buzzword in the Architecture, Engineering, and Construction (AEC) field to facilitate information integration and interoperability, data sharing and exchange are still weak in the traditional interoperability between BIM applications and fire simulation software, since the data schema of them are totally different. In this paper, a quick and accurate approach for information sharing for building fire safety analysis between mainstream BIM applications and widely used fire simulation software has been successfully implemented, based on Industry Foundation Classes (IFC) and Fire Dynamics Simulator (FDS). And, both geometrical building information and sematic information can be shared by this approach through the transformation of coordinate systems, outer database, and IFC file extension. The BIM model restoring fire simulation results can support other performance-based design of building, such as structural fire-resistant design and evacuation design. And, all of the analysis results including building fire simulation, structure safety design, and evacuation simulation can be integrated in Autodesk Revit, establishing a framework of IFC- and FDS-based information sharing for building fire safety analysis successfully. A gymnasium has been taken as a case study to illustrate the capability of this framework.

1. Introduction

With the rapid development of urbanization, fire simulation study has great significance in safety design of large-scale public buildings. The information of fire simulation results can also support optimization of architectural design, structural safety analysis, and evacuation simulation. The first step of fire simulation is to obtain the geometry information to establish the building model. However, the current fire simulation modeling method requires remodeling instead of utilizing the existing building model because of differences in data format and interfaces. Consequently, it probably leads that the data exchange and information sharing in fire modeling practice are in a great difficulty. The data and information provided and resulted by fire simulation software can only support single disciplines or tasks for field-related experts or professionals (i.e., fire safety or structural analysis), rather than an integrated analysis environment.

Meanwhile, BIM (Building Information Modeling) attracts widespread attention and has become a buzzword in the Architecture, Engineering, and Construction (AEC) field, which is defined as a digital model containing all information created or gathered throughout building life cycle and a technology to achieve the information integration and interoperability, which is different from traditional drawing-based or CAD technologies-based design and construction methods [1]. In addition, comprehensive and standardized data format and integrated process of BIM technology play a significant role in the effective utilization of building information [2]. And, it can coordinate contradiction better, which results in smoothing communication in each aspect of such projects and orderly cooperation between the systems.

Thus, the Industry Foundation Classes (IFC) is developed as an open data model standard to serve the BIM interoperability needs of the industry [3, 4]. IFC supports multiple different geometric representations and contains rich semantic information. It is most widely used in BIM and has already become a formally registered international standard and as an international standard for 3D data exchange between different BIM software tools for many years.

However, the current fire simulation software and mainstream BIM applications are still locked into "information islands" which means it is inefficient for building model transmission, conversion, and model information storage, so that it does hinder the development of BIM technology in the research field of fire safety.

The main limitations of current data sharing between BIM applications and fire simulation software are mainly addressed in the difference of data schema, since the function of BIM applications and fire simulation software is totally different. For examples, Fire Dynamics Simulator (FDS), as one of fire simulation tools widely used by fire engineers, developed by the National Institute of Standards and Technology (NIST) can analyze smoke and heat transport process and describe the evolution of fire [5]. Nevertheless, the current building modeling practice of FDS often starts with manual gathering of basic building geometry information and semantic information required for performing fire simulations from either paper documents or electronic documents, such as electronic computer-aided design (CAD) drawing files. And then input all of the information into FDS input data files to support software simulation. Therefore, the current fire modeling practices based on FDS input data files are highly time-consuming, cost-intensive, and error prone, especially for large-scale building, which does limit the further application of FDS. Thus, the data sharing between BIM applications and fire simulation software can help fire engineers avoid manually reinserting data in fire modeling practices, since the BIM model contains a high level of detail, both geometric and semantic information, such as spatial layout, properties of the materials, and other data which are required for performing fire simulations. However, the data schema of mainstream BIM applications and FDS is totally different, and the current information sharing between them is inefficient and error prone.

Therefore, this paper proposes a comprehensive approach for information sharing for building fire safety analysis between mainstream BIM applications and widely used fire simulation software has been successfully implemented, based on IFC and FDS. For this purpose, the main objectives of fire simulation analysis based on BIM technology in this paper are to

(1) Develop a framework for direct translation of geometrical and semantic building information between BIM applications and fire simulation software to help fire engineers avoid manually reinserting data in fire modeling practices

(2) Store fire simulation results into building information model for further information exchanging and sharing to support performance-based design of buildings, including structural fire-resistant design and evacuation design

The rest of the paper is organized as follows: Section 2 reviews related works in terms of the information sharing between BIM applications and fire simulation software. Section 3 presents our proposed methodology framework utilized for the IFC- and FDS-based information sharing for building fire safety analysis. Sections 4 and 5 present the proposed IFC- and FDS-based information sharing for building fire safety analysis framework, the capability of which of is validated by a case scenario in Section 6. Conclusions and limitation in this paper are introduced in Section 7.

2. Related Works

2.1. Application of FDS for Building Fire Safety Analysis. The research on the use of mathematical fire modeling began in the early 1940's [6]. One of mathematical computer fire models is computational fluid dynamics (CFD), also known as field models [7]. FDS, as one of fire simulation tools widely used by fire engineers, developed by the National Institute of Standards and Technology (NIST) is a computational fluid dynamics model of fire-driven fluid flow which can analyze smoke and heat transport process and describe the evolution of fire [5]. The simulation accuracy of FDS has been verified by multiple experiments [8, 9]. The simulation output data of FDS can be displayed by the visualization program Smokeview (SMV) [10].

However, the fire modeling practices based on FDS input data files are inefficient and error prone. Then PyroSim [11], a preprocessor for FDS, was developed for engineers to create building geometry model and select the relevant parameters required for a fire simulation. It is a graphical user interface for the FDS and integrates the Smokeview visualization program [12], which can be used as a visual graphic form program for fire engineers to construct the 3D building model. However, the function of creating 3D building model in PyroSim is inefficient and unfriendly, because PyroSim only has two main modeling methods: one is importing FDS input files; the other is importing CAD file formats, including 3D or 2D DXF format to allow three-dimensional elements to be manually positioned by tracing DXF lines. Although we can use DXF format files exported from Revit, the building elements relations and the topology relation between points and lines will be damaged and lost. Thus, using the original FDS input files to establish the building model can guarantee the integrity of building component and avoid loss of topology relation. The commercial software PyroSim as the interface for inserting the FDS input file can only be used for the visualization of simulation result and the settings panel for fire scenario conditions.

2.2. Application of BIM for Building Fire Safety Analysis. Development of Building Information Modeling (BIM) started in the early 2000s [13], based on the early

computer-aided design (CAD) and 3D object-based parametric modeling, as a collaborative approach to design and construct buildings. BIM model contains a high level of detail, including both 3D geometric information and semantic information to support decision-making of a buildings' lifecycle. IFC, as an open international standard developed for BIMers, is an EXPRESS schema developed by the International Alliance of Interoperability (IAI), which has since changed its name to buildingSMART International. It is based on the EXPRESS language as a part of the Standard for the Exchange of Product model data (STEP) standard (ISO 103030), which facilitates the information interoperability and integration in the building industry.

Similar work investigating the use of BIM for building fire safety analysis has been conducted by several researchers. Zhang and Issa [14] have proposed a new method of BIM-based immersive serious gaming environment to provide an immersive emergency evacuation scenario for the evacuation performance evaluation of the building design, which extend the study of BIM in performance-based safety design. Cheng et al. [15] developed a BIM-based intelligent fire prevention and disaster relief system supporting the visualization of real-time and dynamic fire information in three dimensions to support the planning of fire safety and efficient evacuation. Mirahadi et al. [16] developed a framework, EvacuSafe, for evaluating the evacuation safety performance of buildings through the IFC-based integration of the BIM model and fire simulation tools. However, their research focuses on the path identification algorithm and egress routes related to building layout in BIM which only involves the coordinates of the x-axis and y-axis of components instead of the whole geometry information. Li et al. [17] proposed a BIM centered algorithm to achieve dual objectives of improving room-level localization accuracy, where BIM is used to provide the geometric information and a graphical interface for user interaction. As to the knowledge of the authors, the use of BIM for building fire safety analysis mainly focuses on the performance-based design of buildings combined with the power of immersive visualization of BIM, instead of data information sharing between BIM software and fire simulation packages, which reveals the importance and necessity of this study.

2.3. Building Fire Safety Analysis Based on the Integration of BIM and FDS. Data sharing and exchange are still weak in the traditional interoperability between BIM applications and fire simulation software. The data sharing between BIM and FDS need to be based on IFC format file and FDS input file. However, the data schema of them is totally different, since the two schemas are designed for different purposes. IFC, as a standardized data structure for the storage of building information, is also proposed to solve the problem of data exchange between varieties of professional engineering software, since EXPRESS modeling language capable of containing and representing product and process data fulfilling the requirements of an entire industry defines concepts and attributes considered relevant and creates semantic relationships between them [18].

Similar work investigating the integration of BIM and FDS has been conducted by several researchers. Dimyadi et al. [18] have proposed a practical method for querying spatial data from IFC file by using BIMRL (BIM Rule Language) which has an efficient IFC data querying capability. Then, the required geometric representation information from an IFC file can be mapped into the data specification of the FDS input file. However, in this approach, only geometrical data can be imported. Non-geometrical IFC data such as thermophysical properties of materials could not be present, although it is also required for performing fire simulations. Spearpoint et al. [16, 19, 20] developed a web-based FDS conversion tool and an IFC model parsing tool to convert building models created in Revit and ArchiCAD to FDS input data. However, this data mapping implementation is limited to basic building geometry and supports for neither complex building geometry, such as inclined and curved surfaces nor semantic information exchange, such as thermophysical properties of materials.

Overcoming the current limitations of IFC- and FDS-based information sharing for building fire safety analysis requires a more comprehensive framework for both geometric and semantic information sharing between them to support performance-based design of buildings, which will be described in this paper.

3. Methodology

Based on the study of background and related works, the proposed information sharing framework for building fire safety analysis based on IFC and FDS is as shown in Figure 1.

Firstly, the proposed framework can support direct translation of geometrical and semantic building information between BIM applications and fire simulation software. The data sharing between BIM and FDS needs to be based on IFC file and FDS input file, where major issues can be categorized as (1) geometrical building information sharing, including the translation of coordinate systems and geometry description information and (2) sematic information sharing, including material information, heat detectors, smoke detectors, ventilation system parameters, and simulation result data. Both geometrical building information and sematic information can be shared by this approach through the transformation of coordinate systems, outer database, and IFC file extension.

Secondly, the proposed framework can support fire simulation results storage based on building information model for further information exchanging and sharing to support performance-based design of building, including structural fire-resistant design and evacuation design, which is based on the Application Programming Interface (API) of Autodesk Revit.

4. Geometrical Information Sharing between BIM and FDS

The transformation of coordinate systems and geometry description method are two major issues in geometrical

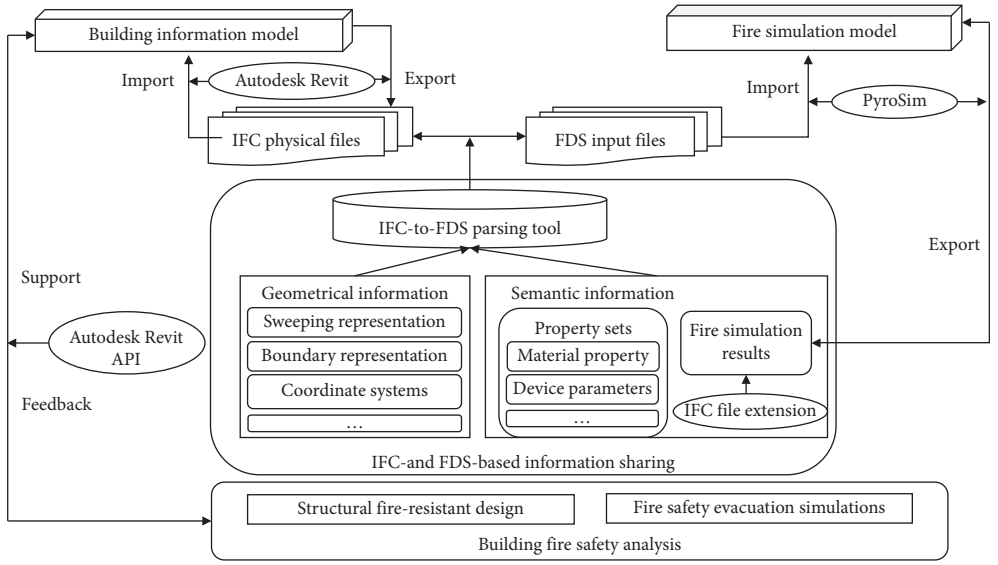

Figure 1: The framework of IFC and FDS-based information sharing for building fire safety analysis.

building information sharing between IFC and FDS. The FDS input files used in fire simulation containing parameters organized into name list groups provide all of the necessary information to describe the fire scenario and support fire simulation calculation, while BIM technology proposes Industry Foundation Classes (IFC) as an open and standardized data model to serve the BIM interoperability needs of the industry.

Parameters in FDS files are specified within the input file by using namelist formatted records [21], including input file header (HAED), simulation time (TIME), mesh parameters (MESH), miscellaneous (MISC), surface properties (SURF), material property (MATL), surface properties (SURF), obstruction (OBST), and device parameters (DEVC). Each fire scenario is defined within a three-dimensional computational domain consisting of rectilinear meshes. Since FDS approximates the governing equations on a rectilinear mesh, the geometry of the building is described by rectangular obstructions which are forced to conform to the underlying mesh. FDS input files use the name list group OBST to create obstructions mainly by defining the coordinates of the rectangular solid. The obstruction is defined by two points, which, respectively, are located at the end of the body diagonal of a rectangular solid, and each side of the obstruction must be parallel to coordinate axis. For example, "&OBST XB = 1.2, 1.2, 1.2, 1.5, 1.5, 1.5/" defines a rectangular solid with two diagonal points (1.2, 1.2, and 1.2) and (1.5, 1.5, and 1.5), as shown in Figure 2.

The entire geometry of the building model is made up of approximate rectangular solids, and the modeling method is primarily determined by the fire simulation algorithm. The simulated domain is divided into small three-dimensional rectangular control volumes or computational cells. Each computational cell with some calculation parameters, including density, speed, species concentrations, and temperature, is calculated based on the mass, energy, momentum equation, etc. Therefore, FDS can predict smoke, temperature,

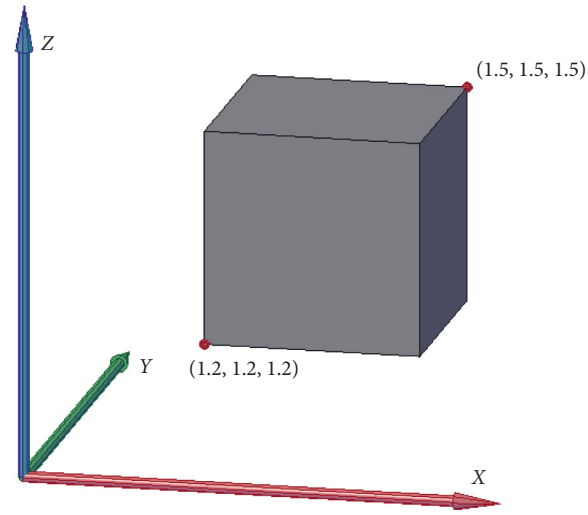

Figure 2: Obstruction positioned by two diagonal points.

carbon monoxide, and other substances during fires to solve practical fire problems and study fundamental fire dynamics and combustion.

The version of IFC used in this study is IFC2x3 which we observe most in use for current mainstream BIM applications now. The IFC files use the entity type *IfcSolidModel* to represent the 3D shape by different types of solid model representations [22]. Its subtypes are CSG representation, sweeping representation, boundary representation, and other solid representation schemes. The entity inheritance relationship is as shown in Figure 3.

Researchers have launched initiatives to establish an approach to convert IFC data to FDS input data, especially Dimyadi et al. from New Zealand, who have made great achievements in this field [23]. However, their current conversion tool has a number of limitations [1, 24]: first, it cannot support Boundary representation geometry; second,

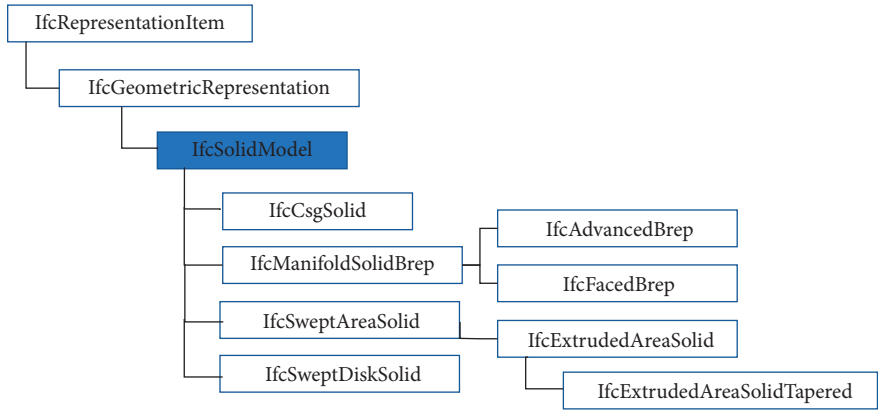

Figure 3: The IFC entity inheritance relationship.

only straight, orthogonal, and equal height building elements can be supported, and only single story buildings can be considered. In this paper, sweeping representation and boundary representation will be discussed more extensively to break those current limitations.

As shown in Figure 4, the two kinds of geometry modeling methods for a cone are greatly different. The cone entity represented by IFC data model uses the boundary representation model (Brep) in which closed surface is composed of several triangular patches. The cone expressed with FDS modeling method is divided into several small blocks. The size of those rectilinear blocks depends on the mesh configurations which have the significant influence on calculation accuracy and efficiency.

The IFC 3D shape representation, sweeping representation, and boundary representation are the common default geometry representation in IFC files. This section will describe the transformation of coordinate systems of these two geometry representation methods between IFC files and FDS files.

4.1. IFC Sweeping Representation Entity. Usually, building components are composed of regular geometrical objects, for example, the shape of beams, columns, slabs, and walls are cuboid. Therefore, the IFC data model often uses the sweeping representation entity, especially the *IfcExtrudedAreaSolid* entity allowing a two-dimensional planar cross section to sweep through space to generate these building components [25]. It has four attributes: *ExtrudedDirection* (determining the direction of the extrusion), *Depth* (defining the length of the extrusion), *Position* (determining the ordinate origin point of the extrusion), and *SweptArea* (defining swept area represented by a subtype *IfcProfileDef*).

This section will first solve the problem of geometry information transformation between FDS input file and IFC physical file which the building components are expressed by sweeping representation and swept area of the component is parallel to the *x*-*y* plane in the global coordinate system. For components with the unparalleled swept plane or special shape, the boundary representation will be provided to realize information conversion in the next section.

4.1.1. IFC Space Coordinate Transformation. Different with the only global coordinate system used in FDS modeling process, IFC uses the local coordinate system to express swept solid geometry model. Therefore, the basic and essential requirement for geometry information conversion from IFC to FDS is to get the global coordinate for every point in FDS files whose position is defined in local coordinate system in IFC files.

The IFC uses entity *IfcLocalPlacement* to define the relative placement of a building element. This entity has two attributes: *PlacementRelTo* and *RelativePlacement*.

The attribute *PlacementRelTo* provides object reference function to establish the relation of two local coordinate systems to determine the absolute placement of the element in global coordinate system. The attribute *RelativePlacement* defines the information about local coordinate origin, the *z*-axis and the *x*-axis. In the #168 statement, as shown in Figure 5, the origin of the coordinate system is at point (−999.6, −1352.4, 0) and the direction vectors of the *z*- and *x*-axes are both null values, which means the axes of this local coordinate system are parallel to the global coordinate system. Then, according to the other local coordinates referenced by the *PlacementRelTo* entity, the absolute placement origin or the positional coordinate of this column can be determined accurately.

As shown in Figure 6, the x'-y' coordinate is the local coordinate system and the *x*-*y* coordinate represents the global coordinate. The conversion of the coordinate system can be completed by the coordinate formulas for transforming.

4.1.2. IFC Shape Information Extraction. The shape information is stored in the *Representation Type*. Then *IfcShapeRepresentation* with the inherited attribute *Representation* Type is used to define all shape-relevant information. It has four attributes shown as follows in braces. The first attribute describes the environment. The second attribute is representation identifiers for shape representation [19], like "Body" type in this case. The third attribute is representation types, like "SweptSolid" in this case, which means it is a swept area solid built by extrusion and revolution. The fourth attribute describes the storage relationship with other descriptive statements:

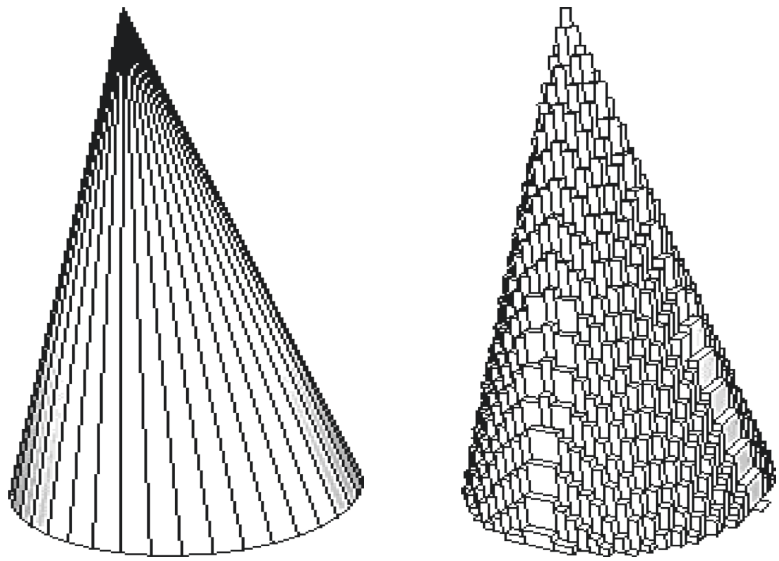

Figure 4: A cone expressed in the IFC data model and FDS model.

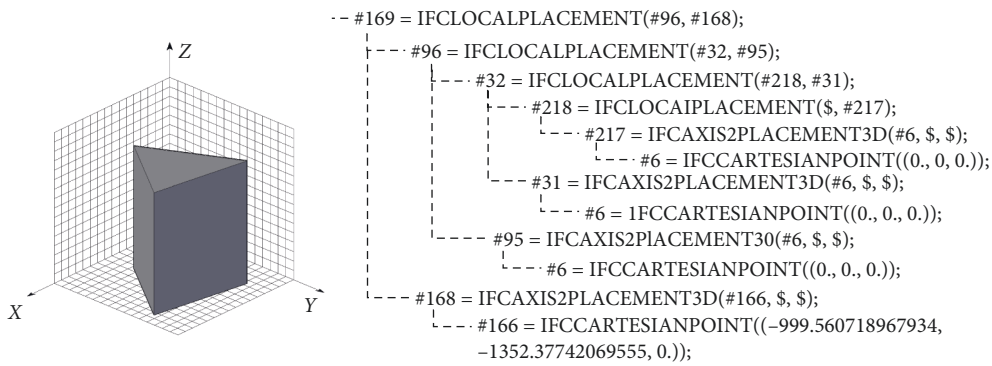

Figure 5: Swept solid geometry model.

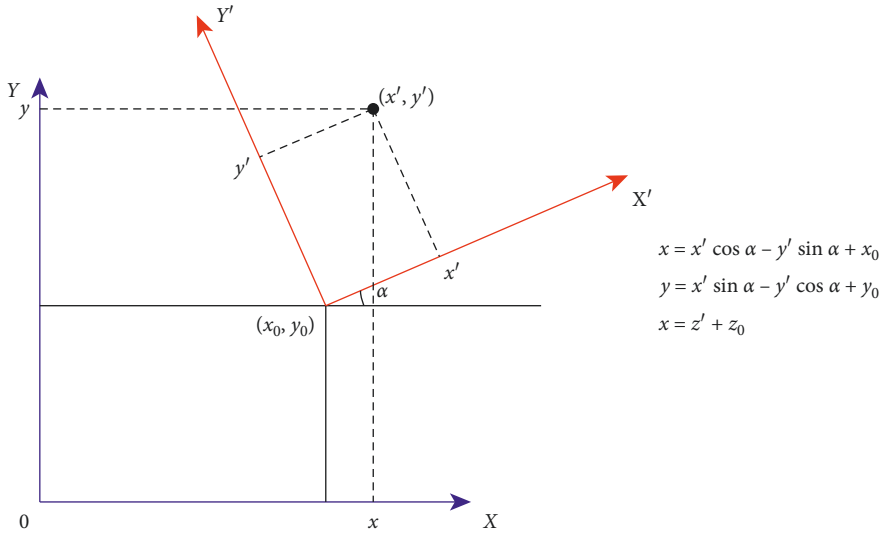

Figure 6: The transformation of coordinate systems.

#123 = IFCSHAPEREPRESENTATION(#73, "Body," "SweptSolid," (#122))

#73 = IFCGEOMETRICREPRESENTATIONSUBCONTEXT("Body," "Model," *, *, *, *, #68, $,.MODEL_VIEW., $)

#122 = IFCEXTRUDEDAREASOLID(#116, #121, #19, 2727.04444218262)

According to the above rule statement information, the detailed description of a swept solid can be found. As shown in the following IFC physical file, the records of an extruded area solid include its swept area, position, extrude direction, and depth. The swept area is closed by several polylines, which coordinate information is given by the *IFCPOLYLINE* entity:

#122 = IFCEXTRUDEDAREASOLID(#116, #121, #19, 2727.04444218262)

#116 = IFCARBITRARYCLOSEDPROFILEDEF(.AREA., "\X2\65CF\X0\2," #114)

#114 = IFCPOLYLINE((#108, #110, #112, #108))

#108 = IFCCARTESIANPOINT((−781.301086027169, −628.610820508116))

#110 = IFCCARTESIANPOINT((838.698913972831, −628.610820508116))

#112 = IFCCARTESIANPOINT((−57.3978279456615, 1257.22164101623))

#108 = IFCCARTESIANPOINT((−781.301086027169, −628.610820508116))

#121 = IFCAXIS2PLACEMENT3D(#117, #19, #119)

#117 = IFCCARTESIANPOINT((531.984645992552, −92.0883098110122, 3))

#19 = IFCDIRECTION((0., 0., 1.))

#119 = IFCDIRECTION((0.529919264233206, 0.848048096156425, 03))

#19 = IFCDIRECTION((0., 0., 1.))

Therefore, after extracting the shape information and transforming coordinate systems, all geometrical model information in the global coordinate system can be determined.

4.1.3. IFC Information Translation for FDS. A conversion tool primarily written in C# using the Microsoft. NET environment is developed to transfer building geometry information from IFC data model to FDS simulation model. The conversion process can be divided into three steps: firstly, mesh the contour of swept area, then describe the swept area with rectangular obstructions, and finally, convert the entire geometry of extruded solid into a series of orthogonal rectangular smaller solids.

The key requirement of the method to mesh the contour of swept area is to find the meshes which intersect the border line. The first step of algorithm is cutting the boundary line into several sections along the x-axis. The projection of each section along the x-axis is the side length of a single grid cell. Then, the grids where division points are located in are obtained as an intersecting grid. After the same operation takes place along the y-axis and the repeated part of the grid obtained in both X and Y directions removed, the remaining grids are obtained as the boundary grids, as shown in Figure 7.

After meshing the contour of swept area, the inner area also needs filling with grids, as shown in Figure 8. The lower and upper bounds of the inner area can be determined by the vertex coordinates of the boundary line.

Next, according to the extrude direction, the depth, and the center point of the swept surface obtained via the geometric shape extraction, the central axis of the extruded solid can be determined and divided into several sections along the z-axis. The length of each section projected along the z-axis is regarded as the cell height. As shown in Figure 9, the line AB is divided into 14 parts. The 13 division points are regarded as the center of each layer to copy the swept area and form the entire swept solid.

Base on the above steps, the entire geometry of extruded solid described in the IFC data model can be converted into FDS obstruction description. This kind of conversion process can support any form of geometry components expressed by the *IfcExtrudedAreaSolid* entity in the IFC data model, even for solids with arbitrary boundary shape or extrusion direction no-perpendicular to x-y plane as shown in Figure 10.

4.2. IFC Boundary Representation Entity. There are a number of challenges when creating building models which have a complicated architecture form, varied curvy shape, or special-shaped components in FDS because of the modeling rule of orthogonal rectangular obstructions. In the IFC data standard, the Boundary Representation (Brep) property is given as a description of special-shaped components.

Boundary Representation defines solids with complex surfaces by a limited number of bounding polygons, i.e., the complex surfaces are divided into a number of small patches to emulate the shape of the components and form a closed solid. Thus, the Boundary Representation type is a very common way to support description for any geometry. The specific information can be obtained from the attributes of the *IfcFacetedBrep* entity, which stores the data relative to bounding polygons.

For example, a triangular patch ABC in the IFC data is shown in Figure 11; the expression of this triangular segment in FDS model is using rectangular obstructions which are forced to conform to the underlying mesh. Thus, the smallest cuboid which can cover this triangular patch needs to be found firstly.

According to the vertexes of the triangle, the smallest cuboid can be determined, as shown in Figure 12.

After meshing the cuboid and forming the surfaces of the solid, there may be some inner cavities need to be filled with the obstruction blocks. A special curved roof is shown here as an illustration of the capability of this kind of conversion process [21], as shown in Figure 13.

However, it is obvious that, in large-span space structures, the expression of curved roof using IFC Boundary

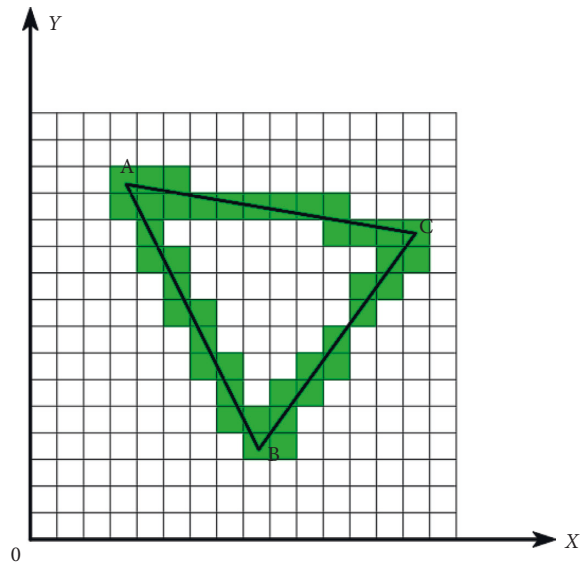

Figure 7: Meshing boundary lines.

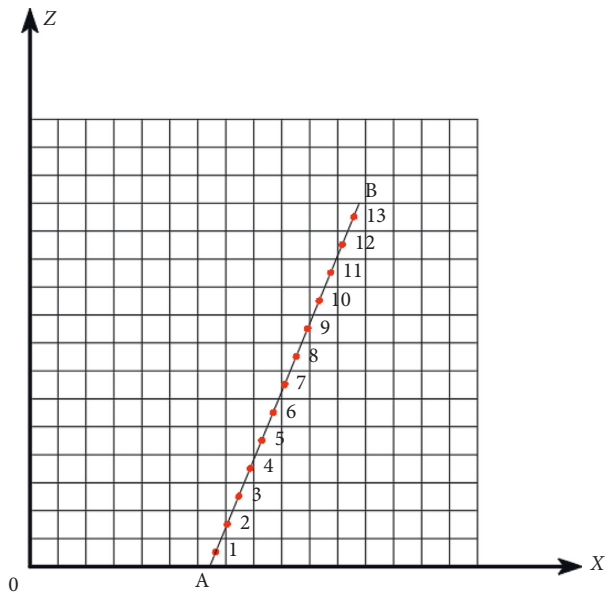

Figure 9: Divide the central axis.

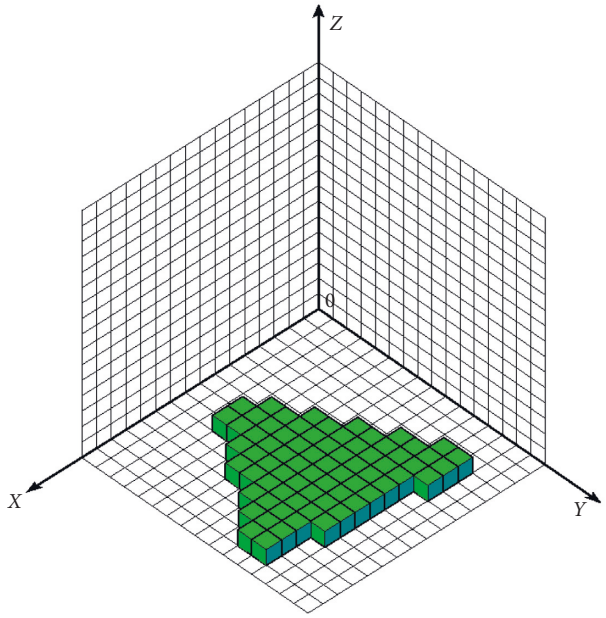

Figure 8: OBST representation for SweptArea.

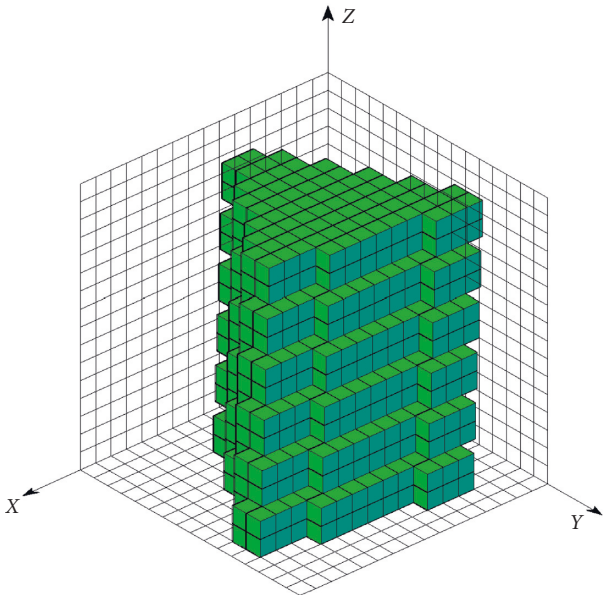

Figure 10: OBST representation for swept solid.

Representation is often composed of triangles with larger dimensions. Therefore, the geometry simulation accuracy will be greatly reduced in this situation. The improved approach is to divide the triangular facets into smaller triangular patches, i.e., proceed the second division, as shown in Figure 14. The triangle is divided into six smaller triangular patches via using the centroid of the triangle. Then, each triangular patch will be matched with its smallest cuboid, respectively.

After the second division, the curved roof mentioned above is shown as Figure 15, and it is much more accurate than the entity shown in Figure 13.

5. Semantic Information Sharing between BIM and FDS

The BIM model contains not only three-dimensional representations of buildings but also a high level of sematic information detail as well, such as fire properties of the materials and other data which must be required for performing fire simulations. The information sharing of this kind of properties can help fire engineers avoid manually reinserting data for setting an FDS input file.

However, recent data sharing implementation is limited to basic building geometry, which cannot support for

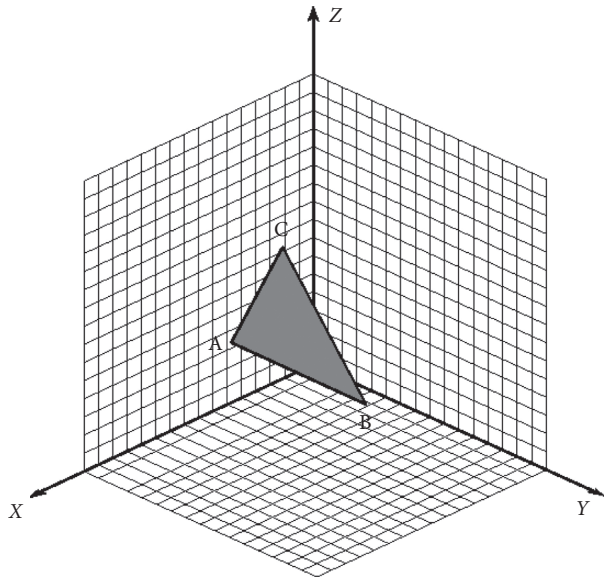

Figure 11: Triangular patch.

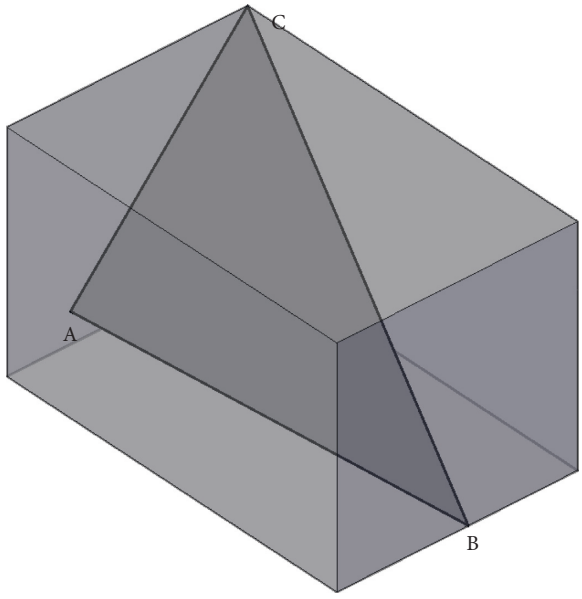

Figure 12: The smallest cube contained triangular patch.

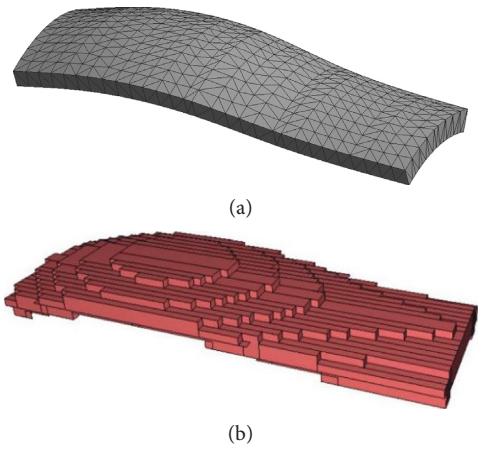

Figure 13: The curved roof models.

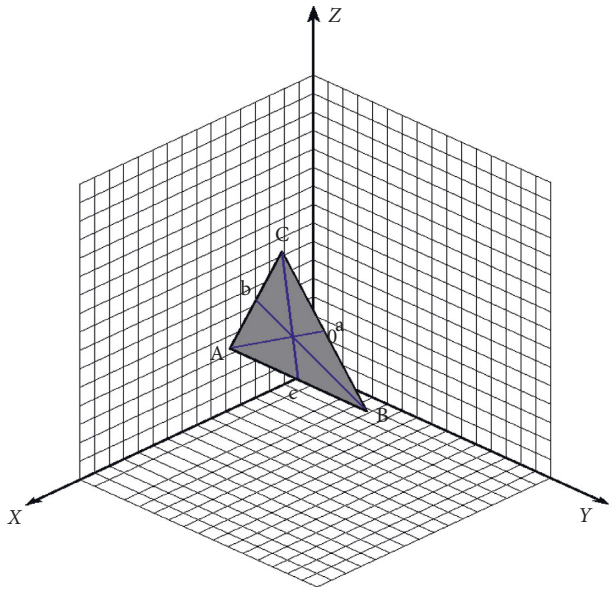

Figure 14: Subdivided triangular patch.

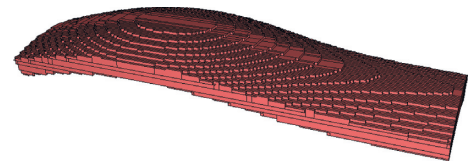

Figure 15: The optimized roof model.

semantic information exchange, including thermophysical properties of materials, heat detectors, smoke detectors, ventilation system parameters, and simulation result data. For example, since FDS input files use the outer material database to record basic description and combustion reaction of the material, the IFC data standard records the property of the material by some IFC material-related entities, which are totally different.

In this paper, the IFC data file and FDS input files are used to support direct and efficient information transformation between the BIM applications and the fire simulation software to break the barriers of "information islands." The content automatically written into FDS input files before fire simulation analysis and written into IFC files after fire simulation analysis by the conversion program includes both geometrical and sematic information, such as input file header, mesh parameters, surface properties, material property, obstruction, and mainly device parameters which are required in an FDS input file and fire simulation results which can be stored in IFC file by expanding the IFC types and entities.

5.1. From BIM to FDS. The issue of material information conversion is solved by using outer material database. The

outer material database referenced to FDS material library contains basic description and combustion reaction of the material. The IFC data standard records the property of the material by the *IfcMaterial* property. And every element uses the *IfcRelAssociatesMaterial* type to establish the contact with the IfcMaterial property and defines their material. The process is shown in Figure 16. First, obtain the *IfcMaterial* property from the *IfcBuildingElement* entity. Then, search the material in outer material database and write the information relevant to fire simulation into FDS files using the name list *SURF_ID*, *REAC FUEL*, and *MATL_ID*. Thus, material information sharing can be realized by using the outer material database. It will save the cost and time spent on assigning material to the components surfaces in the FDS modeling process.

The ability to create ventilation entities in the BIM model has potential downstream effects on the availability of those entities and their mapping to fire simulation model. The BIM model often has the entire HVAC system which is closely related to the fire simulation analysis. In IFC standard, the *IfcDistributionElement* entity is provided to descript all elements which participate in a distribution system, containing cooling system, heating system, ventilation system, and plumbing system. Therefore, the ventilation system can be read from IFC files and written into FDS files by using velocity boundary conditions.

For example, a supply or exhaust fan in a BIM model can be described in the FDS model as a VENT on a solid surface and designate a SURF_ID with specified velocity flow rate, as shown in Figure 17. In addition, our parsing tool can automatically identify some measurement point which needs recording some quantity of the simulated environment, like a thermocouple recording the change of temperature at one point. And, it can designate them into FDS files via the name list group DEVC.

After fire simulation in FDS, the key result data can be stored in IFC physical files by IFC expansion mechanism. And, it can be displayed in Revit by parsing tool developed by Revit API.

5.2. From FDS to BIM: IFC Expansion for Storing Fire Simulation Results. Most data are obtained from fire simulators or other simulators that cannot yet be contained in the IFC Data Model. But, the IFC data standard supports to add new object/attribute/relationship sets to the IFC data model to allow the inclusion of such data [25]. The approach of data storage and sharing about this information can be based on outer database and the IFC file extension.

The fire simulation information includes basic description of the fire scenario, temperature profile, heat flux and mass flow rate, particle output quantities, and other fire-related data. A specific example of a beam component will be used here to describe the method of expanding IFC entities relative to FDS simulation information.

The IFC data standard as an open data exchange format has a strict and clear organizational framework and data structure [26], as shown in Figure 18. Usually, the *IfcProperty* entity can be used to capture the properties defined by any users and associate them automatically with the related objects recorded in *IfcBuildingElement* entity by the IfcRelationship inverse attribute.

The *IfcProperty* entity has a subtype named *IfcPropertySingleValue* which can define the property with a single numeric or descriptive value. Take several fire simulation information as an example which is shown as follows:

#181 = IFCPROPERTYSINGLEVALUE ("FireScene," $, IFCTEXT ("(31, 46, 0); 3; 500; 0.04689; 179; t2"), $)

#182 = IFCPROPERTYSINGLEVALUE ("TimeInterval," $, IFCTEXT ("0.5; 0.5; 0.5; 0.5; . . .; 0.5"), $)

#183 = IFCPROPERTYSINGLEVALUE ("MeasuringPoint," $, IFCTEXT ("(10, 0, −1); (10, 1, −1); (10, 20, −1) (10, 40, −1) 2 $"))

#184 = IFCPROPERTYSINGLEVALUE ("TemperatureChange," $, IFCTEXT ("1; 20; 20; 21; 22; . . .; 450"), $)

The #181 statement describes the basic fire simulation information. The first value indicates that this command line records a fire scenario named as "FireScene." And, the fire source's position is at point (31, 46, 0). The second value points out that the fire area is 3 m^2. The third value is the heat release rates per unit area which is 500 kW/m^2. The other values are followed by fire growth coefficient (kW/s^2), fire growth time (s), and fire growth model.

The #182 and #183 statements define the time interval and location information related to devices, which record some quantity of the simulated environment, like a thermocouple or a smoke detector [21]. The #184 statement records the information of temperature variations which has a one-to-one correspondence with devices. And, these attribute sets can be expanded if there are new attributes needed to adding.

Then, the above properties will be grouped in the fire simulation attribute set, as shown in the #190 code. Finally, associate the attribute set with the relative component, as shown in Code #195. For example, in this case, they are associated with the #171 element:

#190 = IFCPROPERTYSET ("1M3DIiSTb9AucRq2_-VoiSr, #41," "\X2\ 9650523667614EF6\XO\," $, (#181, #182, #183, #184)")

#195 = IFCRELDEFINESBYPROPERTIES ("1hAXM-BYGT1Kw9_LNXJByBV, #41, $, $, (#171), #190")

In conclusion, it can complete the storage of the fire simulation information in the IFC data model by expanding the IFC types and entities. And, based on the Application Programming Interface (API) of Autodesk Revit, the visualization of fire simulation results in BIM applications by reading from IFC data files can be displayed in Autodesk Revit platform, which will be illustrated in the next section.

6. Case Scenario

6.1. IFC- and FDS-Based Information Sharing. In order to illustrate the capability of this transform mechanism and the feasibility of expansion of IFC model for fire simulation

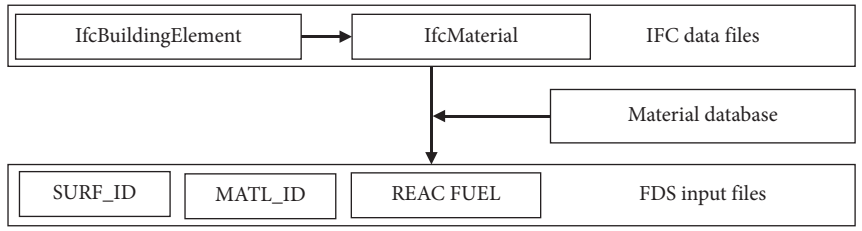

Figure 16: Material conversion method.

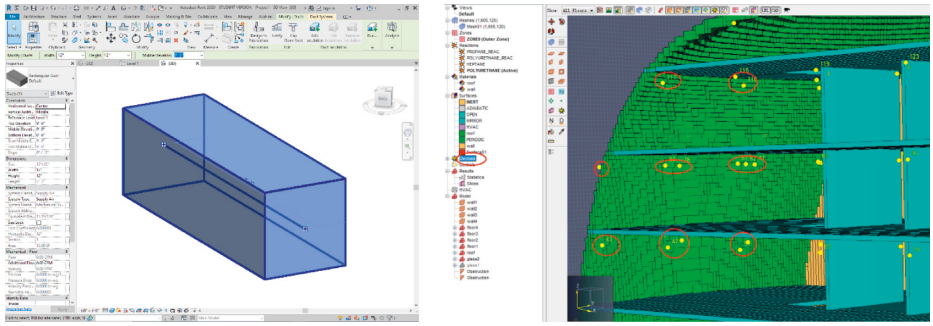

(a) (b)

Figure 17: (a) The ventilation in Revit building model. (b) The thermocouple in FDS model.

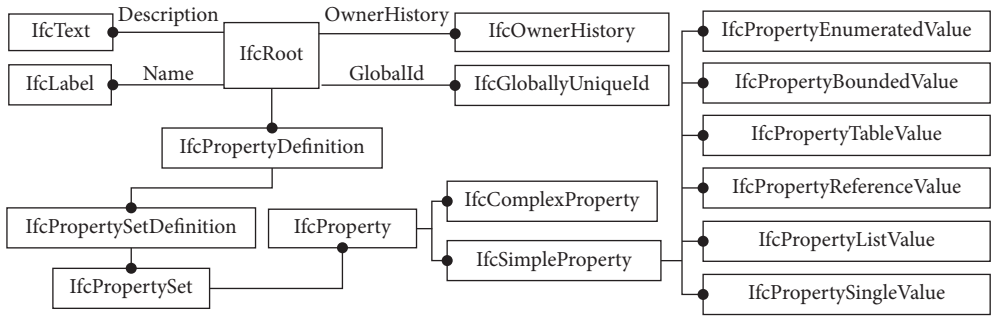

Figure 18: Inheritance definition of *IfcProperty*.

information, a gymnasium has been taken as a case study. Autodesk Revit 2014 is adopted as the virtualization platform for building information model and fire simulation results stored in IFC data files by the IFC file extension [27]. Autodesk Revit is one of the most popular BIM software, which includes three modules: Revit Architecture, Revit Structure, and Revit MEP, and together they form a complete design process based on the building information model. In addition, Autodesk Revit also offers an Application Programming Interface (API) designed to allow external application developers to integrate their applications with Autodesk Revit. Since Revit provides fully certified IFC import and export, model built in Revit can be stored as IFC data standard to support information storage for a building life circle. Therefore, in this case, both the data parsing tool and visualization function are developed by Autodesk Revit and its API.

The conversion process between BIM building model and FDS fire simulation model is as follows: first of all, the building information model of the gymnasium is established in a Revit template, which can provide a quicker and more convenient modeling scheme compared with FDS traditional modeling method. Then, output the IFC data file and convert it to the FDS input file via the conversion tool. Next, import this existing FDS input file into PyroSim to check the validity of each record and complete the FDS building model modeling process automatically and efficiently. From the comparison between Revit building model and FDS building model, as shown in Figure 19, it is obvious that geometry information can be converted successfully from IFC data model to FDS files by this way.

In this case, simulation results data are associated with its relative building components as a convenience to the users to search information by clicking the building components. As shown in Figures 20 and 21, there is relevant simulation data and diagrams of temperature change near a window and visibility near a door. Therefore, the BIM model containing fire simulation analysis results can be gained successfully.

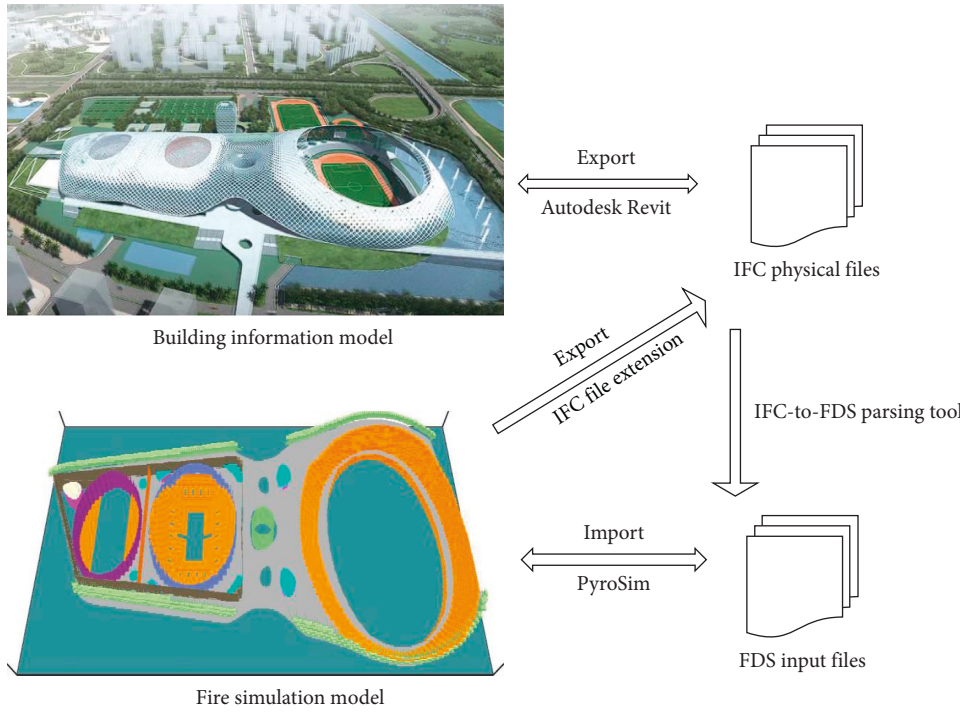

Figure 19: IFC- and FDS-based information sharing.

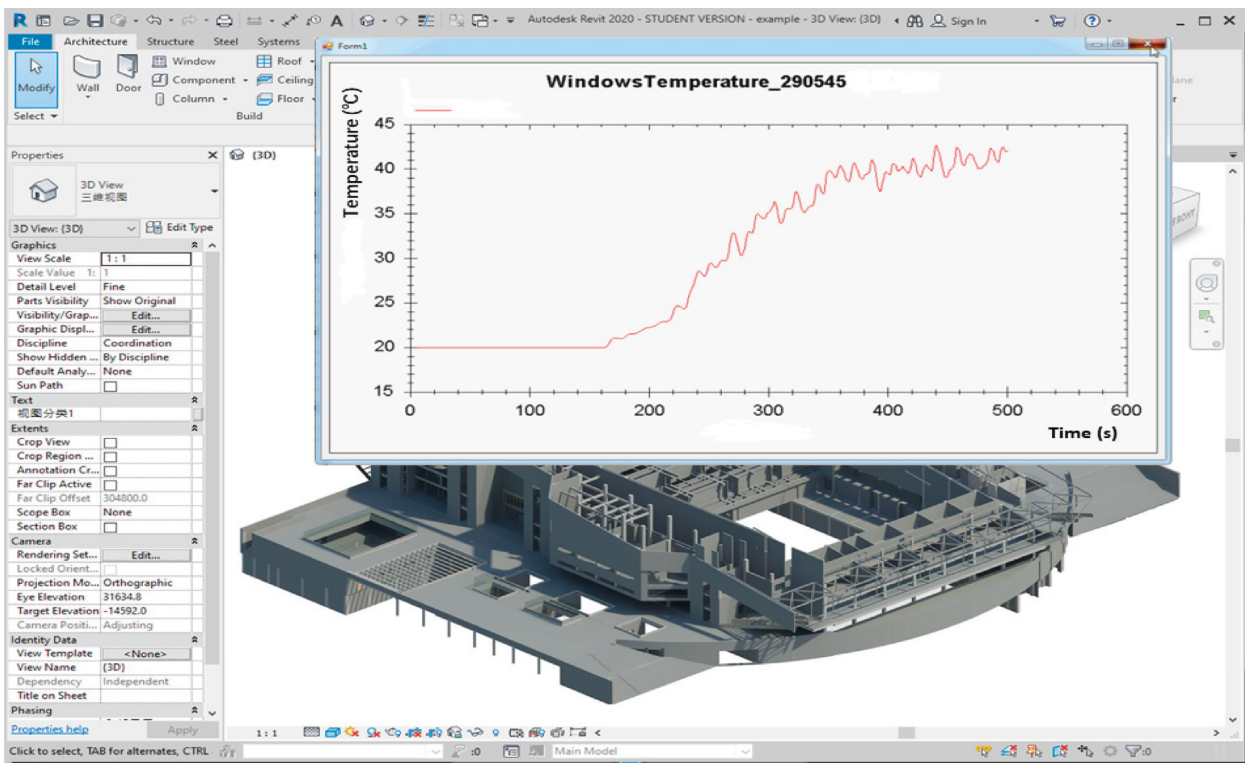

Figure 20: Data and diagrams of temperature change near a window.

6.2. Building Fire Safety Analysis Based on Unified BIM Model. It is a basic functional requirement that the structure remains stable to allow enough time for safe evacuation and rescue under real fire conditions. Therefore, structural fire-resistant design must integrate evacuation and fire interactions models. However, traditionally, fire safety design is still widely performed separately in specified individual study domains, such as fire engineering and structural

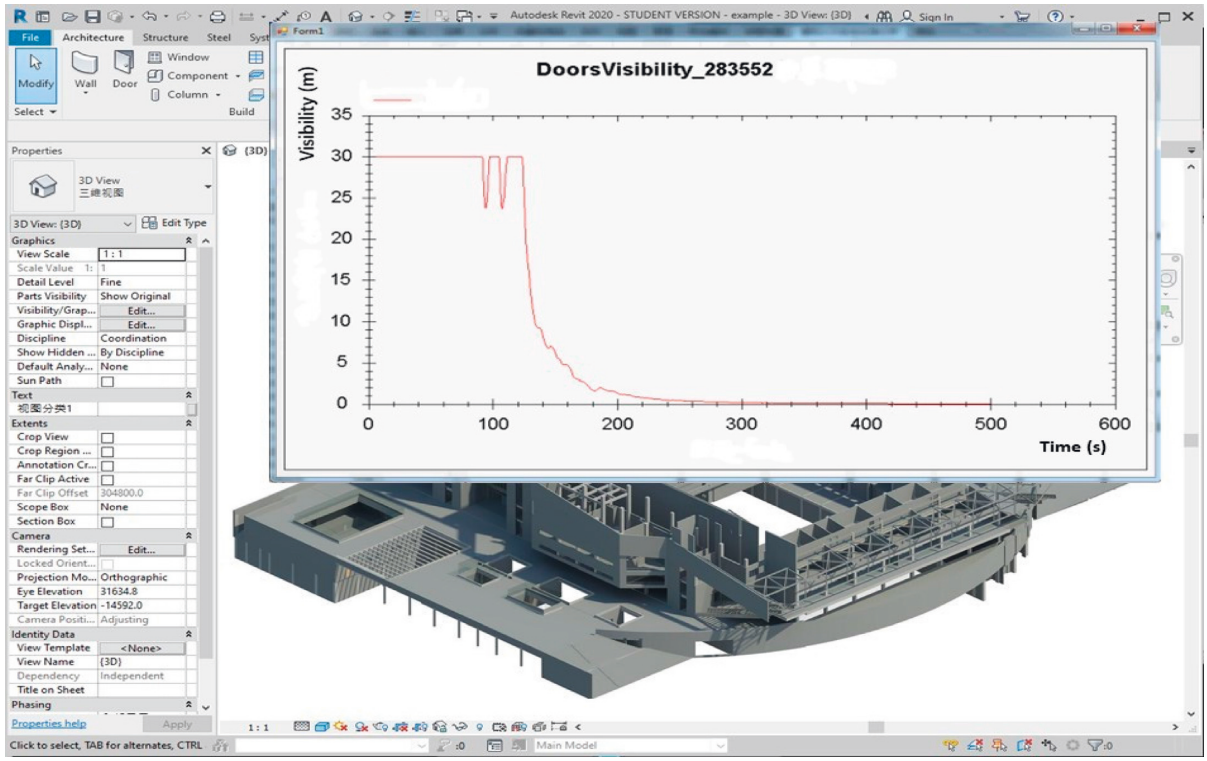

Figure 21: Data and diagrams of visibility near a door.

engineering. The impacts of a real fire have not been considered in structural fire-resistant design and in evacuation simulation.

In this paper, the BIM model containing fire simulation results can support optimization of the building performance-based design, including structural fire-resistant analysis and evacuation simulation of occupants under real fire condition [28, 29]. The effects of a natural fire on structures and evacuation can be simulated and analyzed through the unified BIM model, rather than using assumptive fire condition or ignoring fire as what previous works did. One part of the selected gymnasium has been taken as a case study of the application of the BIM model which stored the fire simulation information.

6.2.1. Structural Fire-Resistant Design. Structural fire-resistant design is a significant content of fire safety evaluation of buildings. It is extremely important to identify those members which may result in the collapse of the whole structure under fire conditions [30, 31].

The building studied is a circular gymnasium with a large-span covering an area of 12,000 sq·m^2 and an overall height of 36.5 m from the top to the ground (as shown in Figure 22). The roof structure of the gymnasium is supported by 288 radial prestressed steel cables with a diameter of 50 mm in two layers, namely, 144 cables in each layer. In the center of the roof, there exists a circular steel space truss structure that supports both the upper and lower sets of cables. The outer ends of all cables are anchored in concrete beams and columns around the building (as shown in Figure 23).

By running data conversion interface between BIM model and structural analysis model, the results of FDS simulation and structure analysis information in BIM model can be transformed and imported into ANSYS by Revit API. All structure analysis information in IFC files is represented by the IfcStructuralAnalysisModel entity, as shown in Figure 24. These fire simulation results were then taken as the boundary condition which is applied to the structural analysis model due to thermal transfer into the gymnasium structural members.

Based on finite-element analysis under thermal action, the temperature field history within the steel structure could be obtained. The thermal effects on the structural elements were treated by subdividing the steel structure into a number of uniaxial heat transfer elements. Heat conduction, nodal temperatures, and heat flow rate are calculated on the basis of the heat transfer elements.

The structural response analysis was then carried out using a 3D link finite-element to model the steel cable structure. The analysis was first carried out on the steel cable structure at ambient temperature. Under the service load of 7.5 kN/m^2, the center deflection was 27 mm, which is less than span/300. The maximum tensile force reached about 64% of the ultimate load carrying capacity. The structure was well designed to satisfy both the ultimate and serviceability limit states at ambient temperature.

By further coupled thermal-structural analysis, the safety status of the steel structure due to fire was evaluated. Figure 25 shows the displacements of the roof's steel structure under two different thermal loads at peak time. Figure 26 compares the stresses in the steel roof structure under

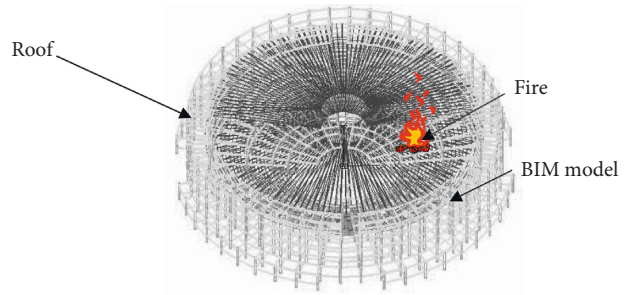

Figure 22: The building model and plan.

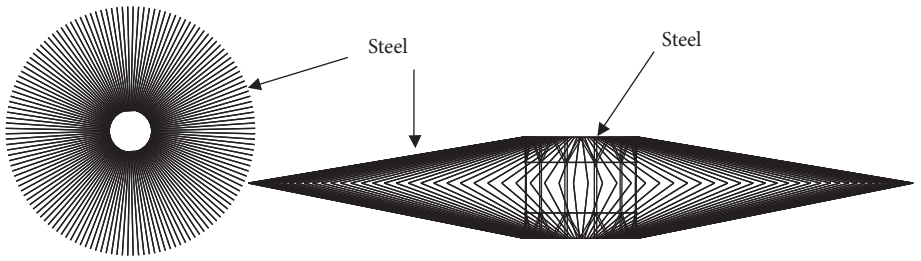

Figure 23: Roof structural view. (a) Top view. (b) Side elevation.

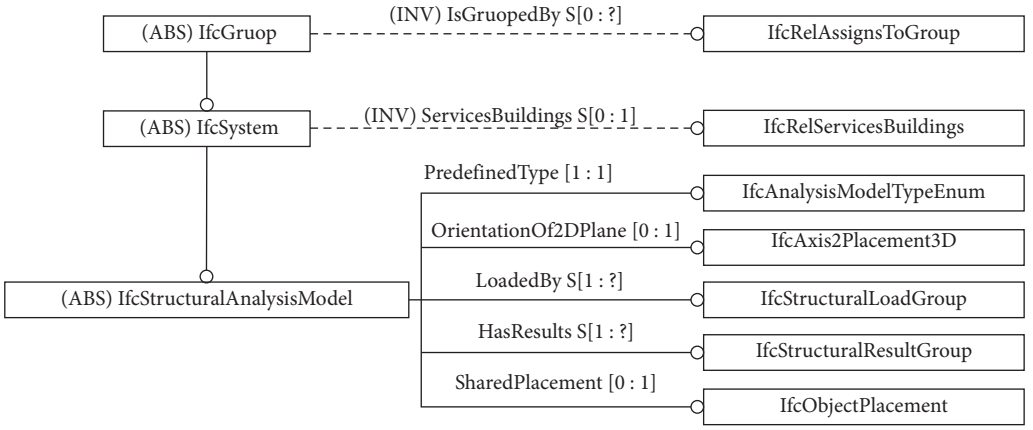

Figure 24: Properties of IfcStructuralAnalysisModel.

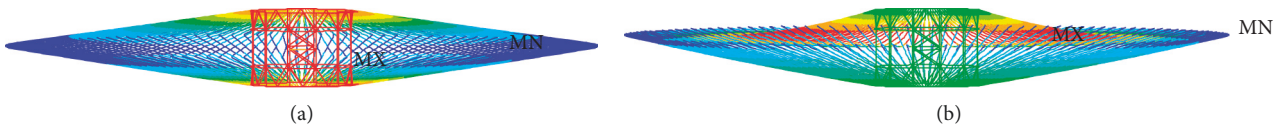

Figure 25: The final displacement of steel cable structure (a) under natural fire and (b) under standard ISO fire.

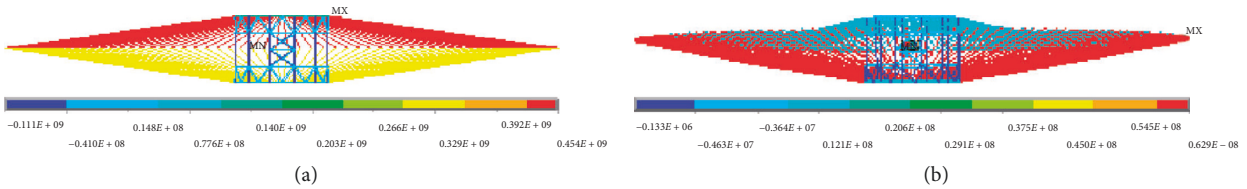

Figure 26: The stress of a steel cable structure (a) under natural fire and (b) under standard ISO fire.

different thermal loads at peak time. Figure 27 shows a comparison between two of the time-dependent predicted tension forces of a single steel cable with respect to the different temperature environments.

From the analysis results, we can observe the change of stress state in the steel structure under fire service loads. The prestress in the steel cables has been lost due to the increase of temperature. Meanwhile, the decrease of elastic modulus and yield strength has become more significant due to the increase of the steel temperature and the decrease of prestress in the cables. The loss of prestress in the upper cables is up to about 15% at the time of peak temperature but only about 2.7% in the lower cables. Stress redistribution occurred in the steel roof structural system due to the asymmetrical distribution of the temperature field. The maximum stress occurred in the central steel truss.

Finally, we also collect all the information about the structure analysis and feedback all the information to Revit building information model based on Revit API. Therefore, it presents a preliminary framework for the application of BIM model in structure analysis according to the information requirements at the fire safety designs.

6.2.2. Fire Safety Evacuation Simulations. The BIM model containing fire simulation analysis results can also support to simulate the emergency evacuation of this gymnasium. In this paper, a detailed analysis of emergency evacuation is completed with the egress and human movement simulator Pathfinder developed by Thunderhead Engineering. The FDS file outputted by parse tool in the last chapter can also be imported into Pathfinder. After importing the 3D data from FDS files, which provides the most helpful information for accurately extracting navigation area, we need to use the extract floors tool to extract navigation area on a room by room basis.

Evacuation paths can be confirmed as long as targets and directions are specified. In the model, the flow is regarded to circulate directionally within or among various types of architectural elements through "doors" [32]. The sequence during evacuation is established based on characteristics of the structure, as shown in Figure 28. Utilizing the geometry features of each element, this strategy fully reflects human experience and expands knowledge library of occupants. Thus, the behavior according to these rules will conform to practical situation.

It needs to be clarified that the above rules may not be applicable in some particular circumstances, such as congestion appears or smoke spreads within target enclosure. Then, adjustments must be made to the strategy. Occupants change current target for secondary one or select subordinate move direction for the balance of safety and efficiency.

Before running the evacuation simulation model, we also need to design evacuation scenario referring to the evacuation data at home and abroad in accordance with the principle of the unfavorable conservative. Then, we run the Pathfinder model and get the results including summary report file containing information about the simulation geometry, simulation performance, and usage information for each room, stairway, and door. And, Pathfinder 2015 provides the ability to view animation results from the Fire Dynamics Simulator (FDS) from NIST. Through a comparative analysis on fire simulation and personnel evacuation result, we can optimize the building model in order to achieve the safety requirements. Based on the fire scenario described above, an evacuation simulation was performed. The results of the temperature field and smoke distribution calculated by FDS were imported into the evacuation model.

Occupants were generated as randomly located before evacuation starts. Initial location and inherent qualities such as gender were randomly given to each individual. Some evacuation properties relevant to qualities were then assigned accordingly. Health and mobility statuses were assumed to be normal for occupants. The size of the space grid each occupant takes up was taken as $0.4\,\text{m} \times 0.4\,\text{m}$. Evacuation begins when a fire alarm detects smoke, i.e., when the gas volume fraction somewhere in the field exceeds 2%. Reaction time was assumed as 10 s for the occupants near the fire source, 20 s for others.

Figure 29 shows the profile of the evacuation process. The figure represents the evacuation state at a certain time after the fire occurred.

Some experimental data have indicated the relationship between the duration occupants is exposed to a certain volume of toxic substances and the corresponding hazard to the human body. Referring to this, it is possible to estimate the potential hazard due to toxic gases and the heat release to occupants in the fire field.

The critical fire danger condition could be determined by the following criteria:

(i) The critical temperature of the fumes layer could be set as 180°C.

(ii) The value of critical soot layer temperature in the model is determined to be 115°C.

(iii) When concentration of CO reaches 2500 ppm, serious hazard to health exists. The critical height of a man's eyes is normally 1.2~1.8 m, the model takes it as 1.6 m.

It can be seen from the simulation process that the speed changed as a result of obstacle avoidance in the evacuation routine and the influence of the evacuees. In the process of evacuation, due to the limited number of exits and aisles, congestion occurred. Thus, the number and width of the exits and aisles produce an important effect on safe evacuation. The evacuation time can be read from the output file. The total time of evacuation was 479 s. Compared with the potentially structural insecurity critical time and the direct hazards, occupants may suffer in fire, the evacuation will be safe, and the remainder of available safety time will be enough.

Finally, we also collect all the analysis result about the evacuation simulation and feedback all the information of evacuation simulation results to the BIM model.

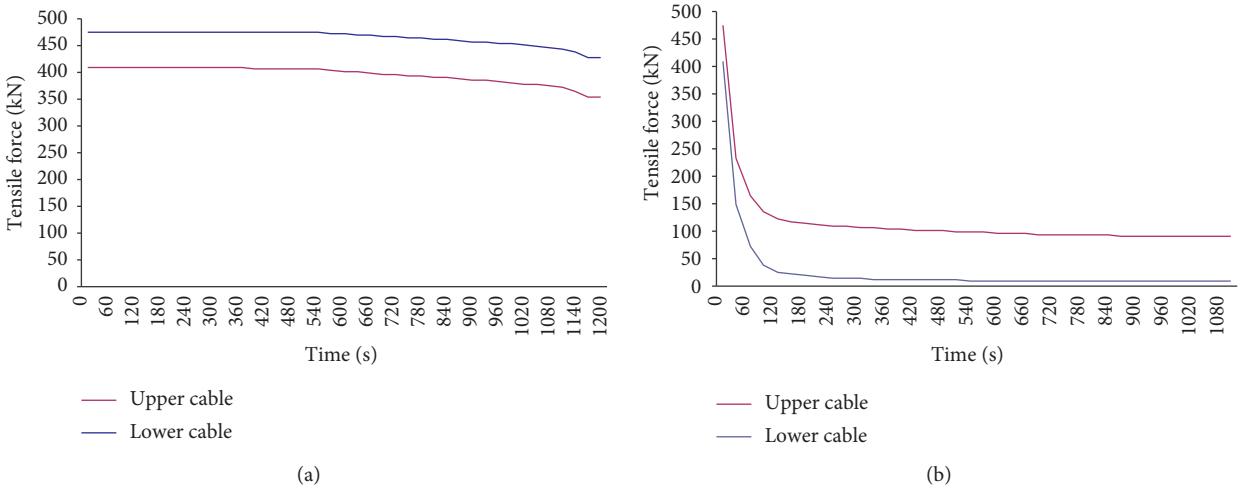

Figure 27: The tension force of central steel truss structure (a) under natural fire and (b) under standard ISO fire.

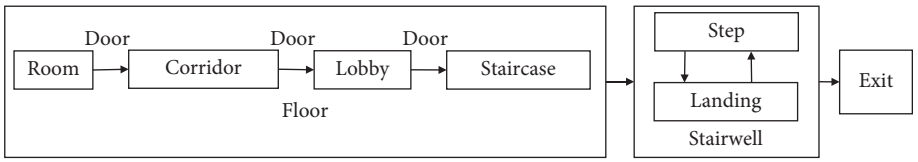

Figure 28: Evacuation sequence based on characteristics of structure.

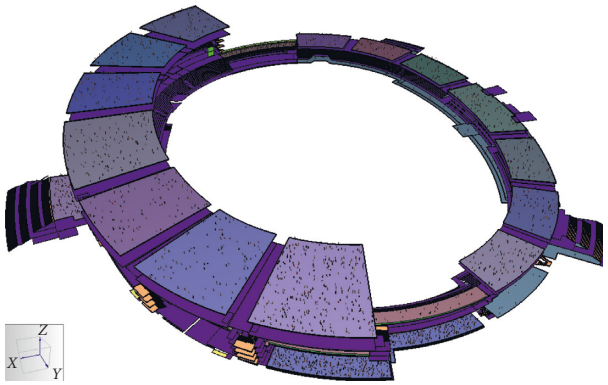

Figure 29: The scenario of evacuation.

7. Conclusions

The work in this study has successfully implemented a quick and accurate approach of IFC- and FDS-based information sharing for building fire safety analysis.

Through a series of theoretical study and practical exploration, the main achievements of the subject consist of the following: (1) according to comparison of modeling method in IFC physical files and FDS input files, the data parsing tool for direct information sharing and exchange between them are successfully developed. The coordinate systems of two common default geometry representation methods in IFC files, sweeping representation and boundary representation, which support both basic and complex building geometries can be transformed into FDS files quickly and accurately. (2) Semantic information sharing is also supported by this approach through outer database and the IFC file extension. The method of expanding IFC entities relevant to FDS simulation information is described, which can complete the storage of the fire simulation information in the IFC data model. The visualization of these data in BIM applications is based on the API of Autodesk Revit, which can read the fire simulation results from IFC data files and displayed in Revit platform. (3) The BIM model restoring fire simulation results can support other performance-based designs of the building, such as structural fire-resistant design and evacuation design. And, all of the analysis results including building fire simulation, structure safety design, and evacuation simulation can be feedback to BIM applications, of which the visualization was based on Autodesk Revit to establish a framework of IFC- and FDS-based information sharing for building fire safety analysis.

This study has several limitations that need further investigation. Firstly, given the complexity of data structure, especially IFC data standard, extension of IFC entity for fire simulation result storage in this paper only allows for the extension of generic level entities, mainly referring to some property sets, and geometric information sharing only supports for sweeping representation and boundary representation geometry, which are two of common default representations in IFC data standard. Secondly, the setup of the computational mesh has a significant impact on the accurateness of transformation of coordinate systems and geometry description between IFC physical files and FDS input files. The future direction and challenge are to support the automatic calculation and optimization of computational mesh for better

physical dimensions and resolution. In addition, in this paper, only IFC physical files and FDS input files are discussed as the information sharing foundation between mainstream BIM applications and fire simulation software. With a growing interest in the building fire safety analysis, other fire simulation software with different data schema and other IFC versions will be used in the IFC-based information integration. Therefore, both geometric and semantic information sharing between BIM applications and fire simulation software in this paper have specific limitations in data schema and data version. However, understanding all the limitations of this paper not only makes a significant opportunity for further research on information sharing between BIM applications and fire simulation software but also supports the further research relevant to IFC-based information integration for the development of the use of BIM models for the performance-based design of building as well.

Data Availability

The .fds data used to support the findings of this study are included within the supplementary information file.

Conflicts of Interest

The authors declare that they have no conflicts of interest.

References

[1] C. M. Eastman, *BIM Handbook: A Guide to Building Information Modeling for Owners, Managers, Designers, Engineers and Contractors*, Wiley, Hoboken, NJ, USA, 3rd edition, 2018.

[2] R. A. Kivits and C. Furneaux, "BIM: enabling sustainability and asset management through knowledge management," *The Scientific World Journal*, vol. 2013, Article ID 983721, 14 pages, 2013.

[3] M. Spearpoint and J. Dimyadi, "Sharing fire engineering simulation data using the IFC building information model," in *Proceedings of the 2007 International Congress on Modelling and Simulation*, Christchurch, New Zealand, December 2007.

[4] M. Laakso and A. Kiviniemi, "The IFC standard—a review of history, development, and standardization," *Electronic Journal of Information Technology in Construction*, vol. 17, pp. 134–161, 2012.

[5] K. McGrattan, S. Hostikka, R. McDermott, J. Floyd, C. Weinschenk, and K. J. N. s. p. Overholt, *Fire Dynamics Simulator Technical Reference Guide Volume 1: Mathematical Model*, Vol. 1019, National Institute of Standards and Technology, Gaithersburg, MD, USA, 2013.

[6] H. Nelson, "From phlogiston to computational fluid dynamics," *Fire Protection Engineering*, vol. 13, pp. 9–17, 2002.

[7] G. E. Gorbett, "Computer fire models for fire investigation and reconstruction," in *Proceedings of the 2008 International Symposium on Fire Investigation and Technology*, Cincinnati, OH, USA, May 2008.

[8] X. Yi, C. Lei, J. Deng et al., "Numerical simulation of fire smoke spread in a super high-rise building for different fire scenarios," *Advances in Civil Engineering*, vol. 2019, Article ID 1659325, 11 pages, 2019.

[9] J.-Y. Jung, S.-G. Kang, H.-J. Yoon, K.-B. Shin, and J.-K. Lee, "Analysis of heat and smoke flow according to platform screen door and fan conditions on fire in underground platform," *Advances in Civil Engineering*, vol. 2018, Article ID 4803058, 8 pages, 2018.

[10] Y. Xu, E. Kim, K. Lee, J. Ki, and B. Lee, "FDS simulation high rise building model for unity 3D game engine," *International Journal of Smart Home*, vol. 7, no. 5, pp. 263–274, 2013.

[11] J. Glasa, L. Valasek, P. Weisenpacher, and L. Halada, "Use of PyroSim for simulation of cinema fire," *International Journal on Recent Trends in Engineering & Technology*, vol. 7, no. 2, pp. 51–56, 2012.

[12] L. Valasek, "The use of PyroSim for creation of the input FDS geometry for cinema fire simulation," in *Proceedings of the 2012 European Conference of Systems*, Paris, France, December 2012.

[13] R. Volk, J. Stengel, and F. Schultmann, "Building information modeling (BIM) for existing buildings—literature review and future needs," *Automation in Construction*, vol. 38, pp. 109–127, 2014.

[14] J. Zhang and R. R. Issa, "Collecting fire evacuation performance data using BIM-based immersive serious games for performance-based fire safety design," in *Proceedings of the 2015 International Workshop on Computing in Civil Engineering*, pp. 612–619, Austin, TX, USA, June 2015.

[15] M.-Y. Cheng, K.-C. Chiu, Y.-M. Hsieh, I.-T. Yang, J.-S. Chou, and Y.-W. Wu, "BIM integrated smart monitoring technique for building fire prevention and disaster relief," *Automation in Construction*, vol. 84, pp. 14–30, 2017.

[16] F. Mirahadi, B. McCabe, and A. Shahi, "IFC-centric performance-based evaluation of building evacuations using fire dynamics simulation and agent-based modeling," *Automation in Construction*, vol. 101, pp. 1–16, 2019.

[17] N. Li, B. Becerik-Gerber, B. Krishnamachari, and L. Soibelman, "A BIM centered indoor localization algorithm to support building fire emergency response operations," *Automation in Construction*, vol. 42, pp. 78–89, 2014.

[18] J. Dimyadi, W. Solihin, and R. Amor, "Using IFC to support enclosure fire dynamics simulation," in *Advanced Computing Strategies for Engineering*, vol. 10864, pp. 339–360, 2018.

[19] M. Spearpoint, "Transfer of architectural data from the IFC building product model to a fire simulation software tool," *Journal of Fire Protection Engineering*, vol. 17, no. 4, pp. 271–292, 2007.

[20] M. Spearpoint, "Extracting fire engineering simulation data from the IFC building information model," in *Handbook of Research on Building Information Modeling and Construction Informatics: Concepts and Technologies*, pp. 212–238, IGI Global, Hershey, PA, USA, 2010.

[21] Y.-x. Chen, J.-y. Shi, and M. Chen, "Research on IFC-based BIM modelling for fire analysis," *Fire Science and Technology*, vol. 36, no. 10, pp. 1371–1373, 2017.

[22] T. Liebich, Y. Adachi, J. Forester, J. Hyvarinen, K. Karstila, and J. Wix, "International alliance for interoperability industry foundation classes IFC2x edition 3," 2006, https://standards.buildingsmart.org/IFC/RELEASE/IFC2x3/FINAL/HTML/.

[23] J. A. W. Dimyadi, M. Spearpoint, and R. Amor, "Generating fire dynamics simulator geometrical input using an IFC-based building information model," *Electronic Journal of Information Technology in Construction*, vol. 12, pp. 443–457, 2007.

[24] J. Dimyadi, M. Spearpoint, and R. Amor, "Sharing building information using the IFC data model for FDS fire simulation," *Fire Safety Science*, vol. 9, pp. 1329–1340, 2008.

[25] V. Bazjanac and D. B. Crawley, *The Implementation of Industry Foundation Classes in Simulation Tools for the Building Industry*, University of California, Berkeley, CA, USA, 1997.
[26] C. Clemen and L. Gründig, "The industry foundation classes (IFC)–ready for indoor cadastre?," in *Proceedings of 23rd International FIG Congress*, Munich, Germany, October 2006.
[27] J.-c. Dao and J. y. Shi, "Building fire safety analysis based on BIM," *Fire Science and Technology*, vol. 36, no. 3, pp. 391–394, 2017.
[28] U. Rüppel and K. Schatz, "Designing a BIM-based serious game for fire safety evacuation simulations," *Advanced Engineering Informatics*, vol. 25, no. 4, pp. 600–611, 2011.
[29] B. Liu, Z. Liu, D. Sun, and C. Bi, "An evacuation route model of crowd based on emotion and geodesic," *Mathematical Problems in Engineering*, vol. 2018, Article ID 5397071, 10 pages, 2018.
[30] J. Shi, W. Shi, and A. Ren, "An integrated model for the fire safety analysis of large space buildings," *Advances in Structural Engineering*, vol. 14, no. 5, pp. 763–775, 2011.
[31] A. Ren, J. Shi, and W. Shi, "Integration of fire simulation and structural analysis for safety evaluation of gymnasiums-with a case study of gymnasium for Olympic Games in 2008," *Automation in Construction*, vol. 16, no. 3, pp. 277–289, 2007.
[32] A. Ren, C. Chen, J. Shi, and L. Zou, "Application of virtual reality technology to evacuation simulation in fire disaster," in *Proceedings of the 2006 International Conference on Computer Graphics & Virtual Reality*, Las Vegas, NV, USA, June 2006.

Hindawi
Advances in Civil Engineering
Volume 2019, Article ID 6530626, 15 pages
https://doi.org/10.1155/2019/6530626

Research Article

A Data-Driven Framework for Smart Urban Domestic Wastewater: A Sustainability Perspective

Jing Du,[1] Biao Kuang,[1] and Yifan Yang[2]

[1]*Department of Construction and Real Estate, School of Civil Engineering, Southeast University, Nanjing 211189, China*
[2]*Department of Civil Engineering, The University of Hong Kong, Pokfulam 999077, Hong Kong*

Correspondence should be addressed to Biao Kuang; kuang_b@outlook.com

Received 24 July 2019; Revised 3 September 2019; Accepted 13 September 2019; Published 3 November 2019

Guest Editor: Endong Wang

With the continuous advancement of urbanization, the problem of urban domestic wastewater has become increasingly serious. Furthermore, information and communication technologies (ICTs) have flourished, providing smart ideas for the governance of urban problems, including smart urban domestic wastewater (SUDW), to improve efficiency and deliver smart cities. The framework of smart governance is vital for urban planning and development, but existing frameworks lack systematic characteristics. Therefore, this study aimed to systematically analyze the functions that SUDW can achieve from a sustainability perspective and to construct a framework of SUDW. This paper articulated the objectives of SUDW from the perspectives of service providers (mainly wastewater treatment plants, WWTPs), government, and public based on the goals of smart cities and sustainable development. Moreover, seven functions of SUDW were identified based on systematic literature analysis, such as the automation of WWTPs and operation and maintenance of sewer assets. Then, the information needed for the above functions was analyzed to clarify communication between the main stakeholders and functions, which were illustrated by an information chain model. The functions are interrelated and closely related to sustainable development, where information sharing is the foundation and key component. Based on the above analyses, a data-driven framework of SUDW consisting of five layers was proposed. The paper indicated that the core of SUDW is the perception, transmission, storage, analysis, and application of relevant data. The study not only contributes to the body of knowledge relating to smart cities but can also guide the planning of cities to realize SUDW, smart cities, and sustainable development.

1. Introduction

With the continuous development of the economy and the advancement of urbanization, the problem of urban domestic wastewater has become increasingly serious. In China (the latest Environmental Statistics Annual Report is the 2015-year version), the total discharge of wastewater was 73.53 billion tons in 2015, where urban domestic wastewater accounted for 53.52 billion tons (71.05% of the total) and increased annually, and chemical oxygen demand (COD) and ammonia-nitrogen (NH3-N) of urban domestic wastewater accounted for 38.09% and 58.33% of the corresponding volume of pollutants in wastewater, respectively [1]. Therefore, urban domestic wastewater has a considerable impact on the water environment. Faced with a large quantity of urban domestic wastewater, it has become important to govern domestic wastewater. In 2015, the urban domestic wastewater treatment rate reached 92%; however, problems remain in the field of domestic wastewater, such as the quality of the treated water and the sludge of disposal not meeting the corresponding standards, serious leakages of wastewater pipes, low rate of wastewater reuse, and large gap between the expectations of the public for improving the water environment and reality [2]. One of the sustainable development goals (SDGs) proposed by the United Nations is to ensure access to and sustainable management of water and sanitation for everyone. The specific targets include reducing pollution, increasing wastewater treatment rates, promoting waste recycling and safe reuse, and strengthening the involvement of local communities [3]. Thus, the

governance of domestic wastewater is closely linked to sustainable development.

Meanwhile, information communication technologies (ICTs), such as the Internet of Things (IoT) and big data, are booming [4]. In this context, to solve urban problems such as transportation, domestic wastewater, and pollution, relevant scholars and organizations have proposed the concept of smart city [5, 6]. The rapid development of smart cities has provided new ideas for the governance of urban problems as well as a new paradigm for urban development and sustainable social and economic growth [7]. Scholars have also proposed ways to achieve smart wastewater, such as managing the collection and treatment of wastewater and the final discharge of processed wastewater intelligently [8], warnings about floods, leakages of sewer networks and pollution [9], and reuse of wastewater [10]. However, most studies are fragmented. Besides, the lack of a systematic framework is one dilemma restricting the development of smart cities [11]. And most current architectures for smart cities are based on data [12], where we can extract useful information to support relevant decisions [13]. However, the water industry has lagged in utilizing the value of existing data [14]. Specifically, a large amount of data are collected and stored to meet operation and regulatory requirements; unfortunately, many of them are never accessed, and the potential capability of instruments is often unrealized [15], which goes against sustainable development.

Therefore, this study aimed to systematically construct the framework for smart urban domestic wastewater (SUDW) from a sustainability perspective to guide the planning and delivery of SUDW. This paper addresses the gap arising from the scattering of current research studies among different areas of smart wastewater and contributes to the body of knowledge relating to smart cities. Moreover, the proposed framework will help the government, urban developers, and service providers understand solutions for the development of SUDW and can be used to guide the planning of urban domestic wastewater to promote the realization of SUDW, eventually delivering smart cities and achieving sustainable development.

2. Literature Review

2.1. Sustainable Development and Smart City

2.1.1. Sustainable Development. The idea of sustainable development is originated from the World Commission on Environment and Development (WCED) and is defined as "*development that meets the needs of the present without compromising the ability of future generations to meet their own needs*" [16]. Then, development is divided into the social and economic aspects, and the environment, economy, and society are called the three pillars of sustainable development [17].

With the development of cities, problems such as social conflicts, natural corruption, and breakdown of essential services will gradually emerge. Basiago [18] maintained that the practices of economic, social, and environmental planning reflecting "urban sustainability" are the antidotes to these negative problems. Moreover, cities have become the main point of sustainable development due to the huge number of citizens in urban communities [19]. From the perspective of the city, considering the idea of sustainable development, the relevant sectors focus primarily on urban metabolic infrastructure, like water, energy, sewerage, and waste management [20]. Urban domestic wastewater belongs to this field.

2.1.2. Smart City. Various scholars have depicted the smart city from different perspectives. Based on applications of ICTs, Cretu [21] viewed the smart city as the collection of real-time data, sensors, intelligent devices, and other ICTs, which are integrated into all areas of our life. However, Xia and Wang [22] stated that to understand the smart city, we should focus on the city itself, rather than ICT, and smart cities aim to alleviate or resolve various problems to improve the performance and the quality of life. Molina-Giménez [10] also held that smart cities, with the assistant of new technologies, should solve their fundamental problems and their policies are supposed to concentrate on realizing economic productivity, social development, and environmental sustainability. The concept of the smart city is therefore argued to encapsulate user-centric considerations for improving quality of life, besides the ICT-driven development paradigm [23].

2.1.3. Relation between Sustainable Development and Smart City. Sustainable development is closely linked to smart city. Caragliu et al. [24] proposed that social and environmental sustainability are major strategic components of smart cities. Bătăgan [19] maintained that the goals of sustainable development are similar to those of smart cities and that smart systems support sustainable urban development. Analyzing eight smart cities and eight urban sustainability assessment frameworks, Ahvenniemi et al. [25] found that the frameworks of urban sustainability contained more environmental indicators than those of smart cities and emphasized the importance of the deployment of smart solutions towards economic, environmental, and social sustainability, where ICT plays a decisive role. In the context of smart cities, ICT assists to optimize production and consumption and has the potential to contribute to sustainability [26].

In summary, both sustainable development and smart city aim to improve the quality of life, of which ICT plays an important role in achieving smart cities and sustainability. From the perspective of the city, sustainable development focuses on the metabolism of cities, and smart cities are close to solving urban problems, including urban domestic wastewater. Therefore, in the context of smart cities, we can deploy ICTs to solve the problem of urban domestic wastewater to improve efficiency and thus deliver smart cities and achieve sustainability.

2.2. Smart Governance and Smart Urban Domestic Wastewater

2.2.1. Smart Governance and the Framework of Smart City. "*Governance is the sum of the many ways that individuals and institutions, both public and private, manage their*

common affairs" [27]. Giffinger and Gudrun [28] stated smart and transparent governance, including stakeholder participation in strategic decision-making and public and social services, as an essential part in the six divided dimensions of the smart city concept. Meijer and Bolívar [29] claimed that smart governance includes new types of collaboration by using ICTs to empower open governance processes and to acquire better results. Pereira et al. [30] also emphasized the role of ICT in smart governance to achieve collaboration among various stakeholders for better decisions. Therefore, ICT and stakeholder collaboration have been perceived as essential for smart governance.

In addition, to guide the realization of smart cities, some studies have examined frameworks of smart cities, including a general framework of smart cities [31]; different areas of smart cities, such as smart grids [32] and smart traffic [33]; and the specific application functions, like energy efficiency monitoring and short-term load forecasting [11] and water quality monitoring and management within smart drinking water and wastewater networks [9]. Specifically, Wenge et al. [31] presented a six-layer framework: data acquisition, data transmission, data storage and vitalization, support service, domain service, and event-driven application. Massana et al. [11] also proposed a six-layer framework, but the specific functions of each layer were acquisition, transmission, storage, preprocessing, service, and application. Ye et al. [34] built a three-layer framework with a sensing layer, network layer, and application layer. However, most current frameworks are limited to a single function or service and lack a systematic design and development for the field of SUDW. Although the number of layers and the function of each layer are not unified, the framework for smart cities is clearly data-oriented, and the collection, transmission, processing, and application of data are the basic components.

2.2.2. Smart Urban Domestic Wastewater. In the context of smart cities, some scholars have proposed applying the notion of smart governance to different infrastructures and public services, of which water and wastewater are important areas [35]. Currently, no uniform definition of smart water or smart wastewater exists, but researchers have realized the importance of ICTs in the water/wastewater sector. Perciavalle et al. [14] proposed an intelligent platform, deployed to collect real-time and other data from a multitude of source systems together, can produce significant results and improvements in digital water/wastewater, particularly in the fields of sewer, stormwater monitoring, and water production. Fattoruso et al. [9] also maintained that smart water network technology arms the operators with an exhaustive and effective set of capabilities of decision-making for sustainable water management.

In the field of SUDW, previous studies have explored different aspects of domestic wastewater. Edmondson et al. [36] proposed a smart sewer asset information model of sewerage networks that can provide real-time information and build towards the capacity to predict the performance of sewerage network with the help of real-time monitoring and reporting. Chow et al. [15] developed a web-based prototype portal for complex online data sets to provide real-time warnings to support treatment plant operation. Khatri et al. [37] considered the recycling of wastewater, and Saputra et al. [38] focused on the collaboration of stakeholders.

The value of relevant data on domestic wastewater has also received attention, and data-driven methods have been widely used in the wastewater and water industry. Specifically, Wei [39] proposed that traditional physics-based and mathematical models have limitations in predicting the behavior of wastewater processing and the optimization of wastewater plant operations, and deployed a data-driven approach to model and optimize the wastewater treatment process in a wastewater treatment plant (WWTP). Savic [40] studied data-driven methodologies to predict the failures of water and wastewater asset. Dürrenmatt and Gujer [41] also applied this method to process data from WWTPs to provide valuable information for optimal plant control. However, the potential value of wastewater-related data and the possible functions of SUDW are scattered in different areas of wastewater, which are fragmented and not systematic. In addition, less research has addressed the communication of related information between various fields, which is not conducive to the realization of smart governance.

Considering the above characteristics, the concept of smart governance, highlighting the deployment of ICTs and the involvement of stakeholders, has been applied to infrastructure and public utilities, such as urban domestic wastewater. SUDW has been studied, but the fields of most studies are scattered and lack systematic consideration. In addition, the existing frameworks are limited to a single function or service, which is not beneficial to the implementation of smart governance. Therefore, this study is based on a systematic literature analysis to identify the potential functions that can be realized by SUDW and analyzes the information needed by the corresponding functions, as well as the main stakeholders and information communication paths involved. Finally, based on the above analyses, a data-driven framework is proposed to facilitate the implementation of SUDW.

3. Methodology

The existing studies on SUDW are scattered and lack a systematic framework to guide practice. To compensate for this gap, this paper, based on the existing literature, identifies the achievable functions of SUDW by means of systematic literature analysis and then incorporates stakeholder involvement to analyze the information needed for each function. Finally, the information chain of SUDW is constructed, and the data-driven framework is proposed based on the above analysis. The process for developing the framework is shown in Figure 1.

A systematic literature review is *"a means of identifying, evaluating, and interpreting all available studies relevant to a particular research question, topic area, or phenomenon of interest to present a fair evaluation of a research topic by using a trustworthy, rigorous, and auditable methodology"* [42].

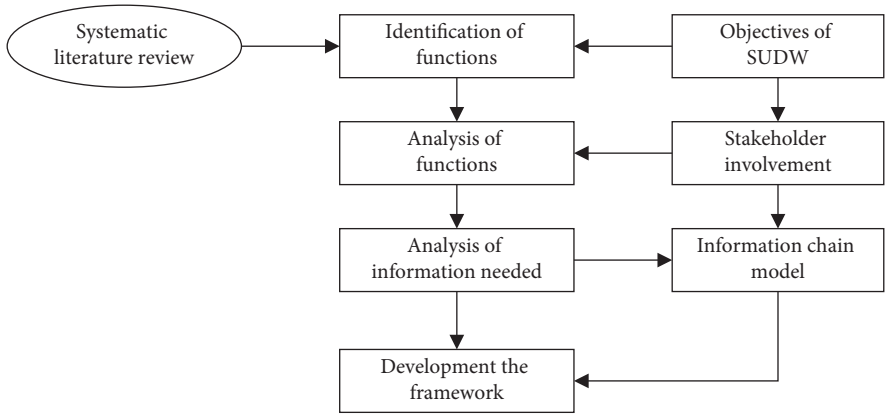

Figure 1: Process for developing the SUDW framework.

This method is a good approach to understand the diversity and complexity of smart cities [43]. Previous studies of smart wastewater provide a foundation for a systematic literature review. Some scholars have used this method to construct frameworks, like Chen et al. [44], who applied this method to build a conceptual framework for bridging BIM and building; Heaton and Parlikad [43] also applied this method to build a framework for the alignment of infrastructure assets to citizen requirements. As shown in Figure 2, this study identified the potential functions of SUDW through the following steps.

First, the study used the combination of "smart," "intelligent," "wastewater," and "sewerage" as keywords to search in SCOPUS, and the China Knowledge Network Index (CNKI) database was searched with "smart" and "wastewater" (in Chinese) as keywords. More than 1000 relevant Chinese and English studies were found covering many databases, such as the Science Citation Index and Social Science Citation Index. Then, after reading the abstract of each study to understand the core content, more than 100 Chinese and English studies closely related to the research topic were selected, and the rest of the literature with low relevance to the study was omitted. Next, 51 key articles were identified by reading and systematic analysis of the literature in order to refine the content and core viewpoints related to the tasks and functions of SUDW in combination with the objectives of SUDW to identify the potential application functions of SUDW. Finally, by screening and sorting the identified application functions, we obtained 7 application functions.

4. Identification and Analysis of Functions of SUDW from a Sustainability Perspective

4.1. Objectives of SUDW from a Sustainability Perspective. Urban domestic wastewater is an urban problem, and the governance of wastewater has a vital role in promoting sustainable development. Economic, environmental, and social sustainability are the three pillars of sustainable development [17], and both sustainable development and smart city aim to promote the quality of citizens' life. SUDW is an important part of smart cities that involves various stakeholders. The Organization for Economic Co-operation and Development (OECD) [45] noted that the core stakeholders in the water industry are the government, service providers, and public. The service providers include WWTPs and sewer asset O&M departments. Therefore, based on the goals of the smart city and sustainable development, this study analyzes the objectives of SUDW from the perspectives of the service providers, the government, and the public.

Service providers play an important role in domestic wastewater treatment. Taking WWTPs as an example, WWTPs shoulder the important task of mitigating the environmental impact caused by organizations and households at the end-of-pipe [46]. Ensuring that the effluent quality meets the standards, which is a vital part of the compliance objectives [14], is the main goal of the operation and management of the WWTP. In addition, the compliance objectives also include compliance with the production process and the quality of operation [47, 48]. Moreover, during the process, the WWTP consumes a large amount of energy and chemicals. Therefore, in the context of SUDW, the WWTP should optimize the process and improve the efficiency of wastewater treatment to reduce energy and chemical consumption without sacrificing the quality of effluent to reduce operation costs and the impact on the environment [49], which reflects the great economic value and environmental sustainability.

In China, the government has the responsibility for planning, supervision, financing, etc., in the supply of wastewater treatment services [50]. In the context of smart cities, the government and the relevant authorities are finding ways to reorient their information technology and policies to guide smart growth and address the needs of their citizens and businesses with the use of ICT and by incorporating more critical agents throughout the process [51]. Moreover, in the water sector, the smart city must equip itself with instruments to ensure universal, continuous, regular, and high-quality public services [10]. From the perspective of sustainability, the government optimizes resource allocation by implementing public policies to promote social, economic, and environmental sustainability. Therefore, in SUDW, the goal of the government is to

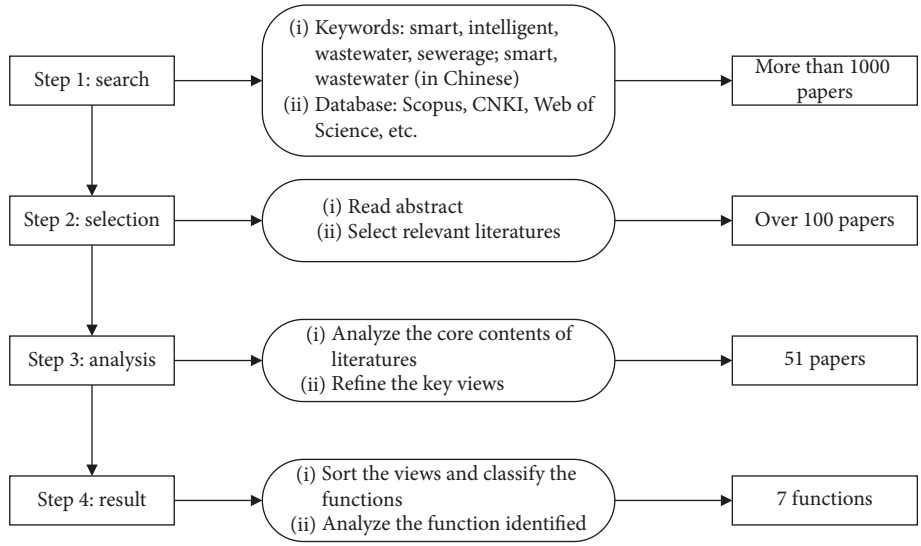

Figure 2: Process of systematic literature analysis.

improve the efficiency of public services, specifically improving the formulation of policies relating to domestic wastewater and achieving real-time and efficient supervision and performance evaluation.

The public is one of the most important subjects in smart cities [5]. Improving the quality of public life is a common goal of smart cities and sustainable development [19]. For SUDW, perception and participation platforms allow the public to obtain and understand information relating to domestic wastewater, provide feedback on their demands, or participate in SUDW decision-making; this can increase public participation and solve the problems of domestic wastewater in more satisfactory ways. In addition, the social and living environment can be improved by realizing SUDW, which can increase public satisfaction and improve their life as well. Therefore, the public's goal is to improve their quality of life.

In summary, the objectives of the SUDW are shown in Figure 3. Environmental, economic, and social sustainability are the three pillars of sustainable development. From a sustainability perspective, SUDW can not only improve the efficiency of wastewater treatment but also mitigate the pollution of domestic wastewater to the environment and reduce energy and chemical consumption, which would reduce the impact on the environment and promote economic sustainability. In addition, it can also improve the efficiency of public services and increase the quality of public life to promote sustainable social development. Therefore, the goals of SUDW are consistent with those of sustainable development.

4.2. Identification of the Functions of SUDW Based on a Systematic Literature Analysis. Through the systematic literature analysis, we identified seven functions: automation of WWTP, operation and maintenance (O&M) of sewer assets, alert and control of disasters, reuse of wastewater, public communication and participation, smart supervision and evaluation, and information sharing. The frequencies of the seven functions identified in the 51 studies are shown in Figure 4.

The results of the analysis show that among the 51 papers, the number of studies on the automation of WWTP is the highest, with 33 (65%), followed by alert and control of disasters and O&M of sewer assets, which are also important functions of SUDW, with 31 and 26 studies, respectively. In addition, public communication and participation and information sharing have also attracted the attention of some scholars, with 16 studies analyzing these two functions. Smart supervision and evaluation are considered in 12 papers. Some of the results of the systematic literature analysis are shown in Table 1.

4.3. Analysis of the Functions of SUDW from a Sustainability Perspective. This study analyzes the contents of the seven functions identified from a sustainability perspective.

4.3.1. Automation of WWTP. The WWTP deploys an automatic control system consisting of online detection and analysis instruments, monitoring systems, real-time transmission networks, etc. According to the characteristics of the influent water, such as the quality and quantity of domestic wastewater, and the standards of the treated effluent, the operating conditions of the key processes of wastewater treatment are analyzed and controlled intelligently to operate and manage in an automated and intelligent manner. Analysis of the collected data can help the WWTP to understand its operation conditions, support relevant decisions, and achieve real-time control of the operating parameters of critical equipment and the volume of chemicals, which can reduce reliance on engineers' experience [57]. These steps can not only ensure that the quality of the effluent water meets the standards but also save energy and chemical consumption, which can reduce operational costs. In addition, this function can also monitor the entire treatment process and detect

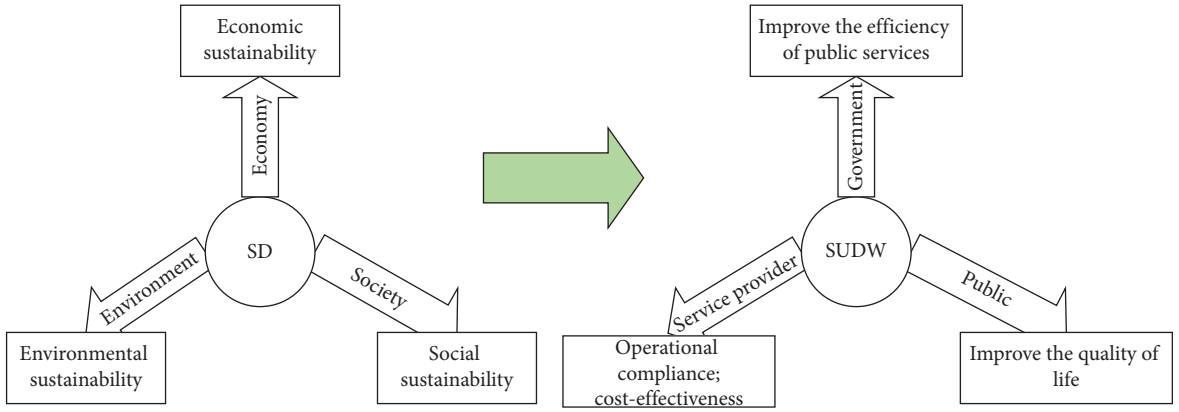

Figure 3: Objectives of SUDW (SD = sustainable development).

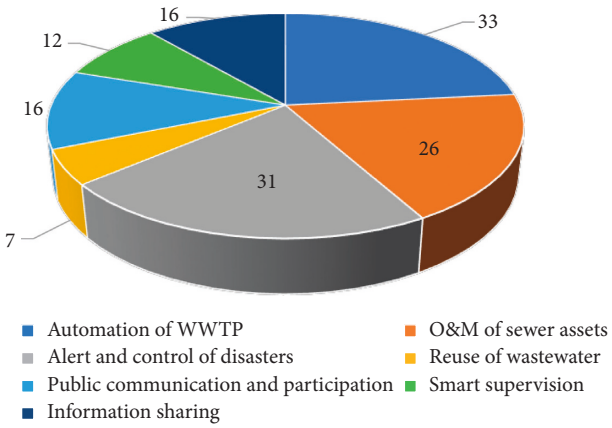

Figure 4: Frequencies of functions in 51 papers.

Table 1: Partial results of systematic literature analysis.

No.	References	Functions of SUDW						
		Automation of WWTP	O&M of sewer assets	Alert and control of disasters	Reuse of wastewater	Public communication and participation	Smart supervision and evaluation	Information sharing
1	[8]	√		√				√
2	[36]	√	√	√		√		
3	[52]		√	√		√	√	
4	[53]		√	√	√	√	√	
5	[14]	√	√	√		√	√	√
6	[10]			√	√	√		√
7	[9]		√	√				
8	[54]	√	√	√				
9	[55]	√			√			
10	[56]		√	√		√	√	√

anomalies to provide early alerts to ensure continuous and stable operation of the system.

4.3.2. O&M of Sewer Assets. Sewer assets comprise the physical infrastructure of pipes, manholes, pumps, and channels that convey wastewater to WWTPs for cleaning [36]. Inadequate upgrading, maintenance, and repairs over time will result in increased stress, decreased efficiency, and rapid deterioration and failure of infrastructure [52]. Therefore, the O&M of sewer assets is critical to the integrity and sustainability of the sewer system. The relevant O&M departments of sewer assets can deploy intelligent sensors, IoT, and other ICTs to monitor and report the performance of sewerage networks in real-time and present them in a visual form to assist operational decision-making, such as replacement and repair plans, monitoring and early alert of failures, and emergency plans for faults. In addition, the efficient O&M of

the key assets can maintain their service level with the lowest life cycle cost, and the saved funds can be reinvested in other infrastructure to help reduce gaps in infrastructure and promote economic and social sustainability [58].

4.3.3. Alert and Control of Disasters. Flooding and pollution are the main disasters related to wastewater [36]. The function, based on the integration and analysis of relevant historical data, combined with the perception of relevant real-time or near real-time data, such as water quality, water level, and precipitation, calculates and predicts disaster risks to support the disaster decision-making. This process enables early identification and warning of avoidable disasters and emergency response to unavoidable events, such as reminding the WWTPs and the public, and conceiving and evaluating reliable mitigation strategies. It can also improve the resilience of cities and thus reduce damage to urban wastewater treatment systems and the impact on the environment.

4.3.4. Reuse of Wastewater. Reclaimed water is highly treated wastewater that can be reused for other purposes, such as gardening, flushing toilets, watering plants and vegetables, washing cars, cleaning houses, and firefighting [55]. In smart cities, water governance should extend to the efficient management of wastewater, which reflects the circular economy [10] and reduces the impact on natural water sources. Smart cities can build reclaimed water networks and determine the overall status with the help of ICTs in real-time. Thus, the control center can make decisions, regulate the relationship between supply and demand, ensure the stable operation of the reclaimed water network system, and promote the recycling and reuse of wastewater, which is conducive to environmental and social sustainable development.

4.3.5. Public Communication and Participation. Public participation is an important feature of SUDW that embodies the notion of "bottom-up" and supports co-creation and social innovation [38]. Public participation can facilitate citizen involvement and support informed and sustainability-aware decisions based on an extended awareness of the environment and the consequences of human actions [59]. The government or enterprises disclose relevant information through the information channel, and the public can also use the information channel to express their own demands. This function can strengthen communication between different stakeholders, especially the public, and increase public participation. In addition, through propaganda and publicity of information related to reclaimed water, the public's acceptance of reclaimed water, as well as the awareness of water savings and the reuse of wastewater, can be enhanced to promote sustainable development.

4.3.6. Smart Supervision and Evaluation. An important function of SUDW is smart supervision and evaluation. Wastewater treatment, as necessary infrastructure, should assure reliability and compliance [14]. Moreover, most current wastewater treatment projects in China are public-private partnerships [50]. Therefore, the government bears the responsibility for operational supervision and performance evaluation. Corresponding government authorities obtain and analyze accurate monitoring data through ICT technologies and multiple intelligent detection methods to realize real-time supervision and evaluation of WWTPs and the departments of sewer assets operation, which can improve the accuracy of the evaluation results. In addition, smart supervision and evaluation are conducive to the effective allocation of resources, thereby improving the efficiency of public services and promoting sustainable development.

4.3.7. Information Sharing. Shared, timely, and actionable information is the kingpin of smart governance [60]. Planning and execution of the governance of wastewater involve coordinated efforts from different stakeholders and includes the collection of data, identification of appropriate authorities for their sources, and development of effective communication to these authorities [61]. The subjects of information sharing services and sources are diverse, and information sharing is the foundation for the realization of the above functions. In SUDW, data interaction and sharing among various stakeholders are realized by an information sharing platform, and the stakeholders can find potential value from a large amount of data to promote the realization of related functions. Data interaction and sharing can reduce the repeated collection of data and improve the utilization of data, which is favorable for sustainable development.

5. Development and Analysis of the Framework for SUDW Based on a Data-Driven Approach

Data-driven approaches can be used to extract valuable information and discover knowledge from static as well as operational data of infrastructure and public services and are suitable for real-time diagnosis and prediction [62]. Data-driven optimal techniques, without the need of skilled engineers and expensive instruments, are thus attractive in practice [57]. Besides, these strategies are widely used in areas where the speed of collection and recording of data exceed the ability of information processing [63]. In the wastewater sector, this strategy has been applied to process data from WWTPs to provide insightful information for optimal control [41]. SUDW utilizes data, namely, through data perception, transmission, and analysis, to support relevant decisions and achieve the corresponding functions. Based on the data-driven approach, this study analyzes the information needed for the above functions, the main stakeholders, and the information flows among different stakeholders and functions and builds a framework for SUDW.

5.1. Analysis of Information Demands for the Functions of SUDW

5.1.1. Information Needed for Automation of WWTP. The automation of WWTP is based on real-time monitoring and analysis of the quantity and quality of wastewater of the

inlet, outlet, and each reaction pool of WWTP, the operational status, and other parameters of the equipment combined with historical data to assist in the formulation of relevant decisions and to adjust the operational strategies of WWTP in real-time. This study considers the wastewater treatment process in the WWTP (as shown in Figure 5) to analyze the information needed for automation of the WWTP.

An online detector is installed at the inlet of the WWTP to monitor and analyze the data of influents in real-time, mainly the quantity and quality of wastewater, including COD, NH3-N, total nitrogen (TN), total phosphorus (TP), and other indicators. Then, the data are transmitted to the automation control system for analysis to facilitate control of the switches, running duration, rotation speed, and other parameters of the filtering grid, the lifting pump, the blower, and other relevant equipment to optimize equipment operation and achieve precise control. In terms of chemical management, real-time data, such as flow rate, phosphate concentration, volume of sludge, and moisture content, of each reaction tank are sent to the chemical management control system, and the number of chemicals, such as iron salt and aluminum salt, is calculated to adjust the dosing pump automatically to reduce the use of chemicals without affecting the quality of the WWTP effluent. In addition, by means of the fault diagnosis system and the analysis of historical data, potential faults or abnormalities can be identified. In the case of an adverse impact on the wastewater treatment system, an early alert is provided to prompt the relevant personnel to take corresponding measures to ensure the good operation of the WWTP.

5.1.2. Information Needed for O&M of Sewer Assets. Asset condition and real-time performance are important foundations for formulating decisions related to the O&M of sewer assets [36]. From the perspective of the information demand, the static project information of the sewer networks, such as the age of the sewerage pipelines and the locations of the control pump and the different diversion structures, are important foundations for O&M decision-making. In addition, the performance of the pipe networks must be monitored in real-time so that the departments can judge the damage degree of the networks and formulate short-term and long-term sewer asset replacement and maintenance plans, which can perform maintenance and improvement of the networks in stages and improve the performance of the sewerage network system. Based on various continuous and online sensors installed in sewage networks and historical data, such as the sewage network overflow duration, overflow probability, and overflow sequence, the network conditions, and weather data are collected and analyzed in real-time to predict sewerage overflow risk and provide early warning of failures in the network. This process can help managers address potential and real-time problems and ensure the smooth operation of the networks.

5.1.3. Information Needed for Alert and Control of Disasters. The alert and control of disasters is similar to the O&M of sewer assets. To achieve risk warning and emergency management for pollution and flooding, the real-time status of the networks must be monitored and meteorological data must be collected and analyzed in real-time to facilitate timely detection of pollution sources and predict flood risks to make corresponding control decisions to improve the resilience of the urban network system.

Continuous and real-time monitoring of various parameters of water quality along the sewerage network can be used to identify pollution caused by unregulated or abnormal, malicious discharge to the pipe network early, and warn pollution incidents to avoid serious pollution incidents and reduce the impact on the wastewater treatment system and the destruction of the environment. Real-time monitoring and analyses of the water level, volume, flow rate, etc., of sewerage networks are required for the early alert and control of floods and other disasters. Predicting and judging the volume of flow and the capacity of networks can provide decentralized and real-time control of the storage capacity of the combined sewerage system with the help of automatic smart valves, that is, controlling the amount of stormwater runoff in large reservoirs of wastewater networks to prevent the occurrence of sewage overflows.

5.1.4. Information Needed for Reuse of Wastewater. Improvement of the reuse of wastewater should be analyzed from the supply and demand sides [64]. On the supply side, through the deployment of ICTs, a smart network for urban reclaimed water reuse is constructed to perceive, analyze, and address the reclaimed water resources within the scope of the city and to determine the quality, quantity, and pressure of the reclaimed water in the network in real-time. Smart networks facilitate relevant decision-making and rational coordination of the supply-demand relationship to ensure the stable operation of the reclaimed water network system and the supply of the reclaimed water.

In terms of demand, the success of this practice depends on public acceptance and involvement [65], and water quality is an important concern for the utilization of reclaimed water [37]. Therefore, to promote the reuse of wastewater, WWTPs and the agency of reclaimed water should actively disclose information about reclaimed water. Meanwhile, the government plays a guiding and coordinating role, such as publicizing knowledge about reclaimed water, organizing convenient and comprehensive communications with users of reclaimed water, and coordinating the relationship between relevant departments and users, to increase public acceptance of reclaimed water and promote the reuse of wastewater.

5.1.5. Information Needed for Public Communication and Participation. Members of the public are both recipients and providers of information. The public can directly see the information disclosed by the government or relevant enterprises through information disclosure, such as disaster warning information, the water quality of reclaimed water and effluent of WWTP, to understand urban domestic wastewater. If the services provided by the government or relevant enterprises are not appropriate or cannot satisfy the

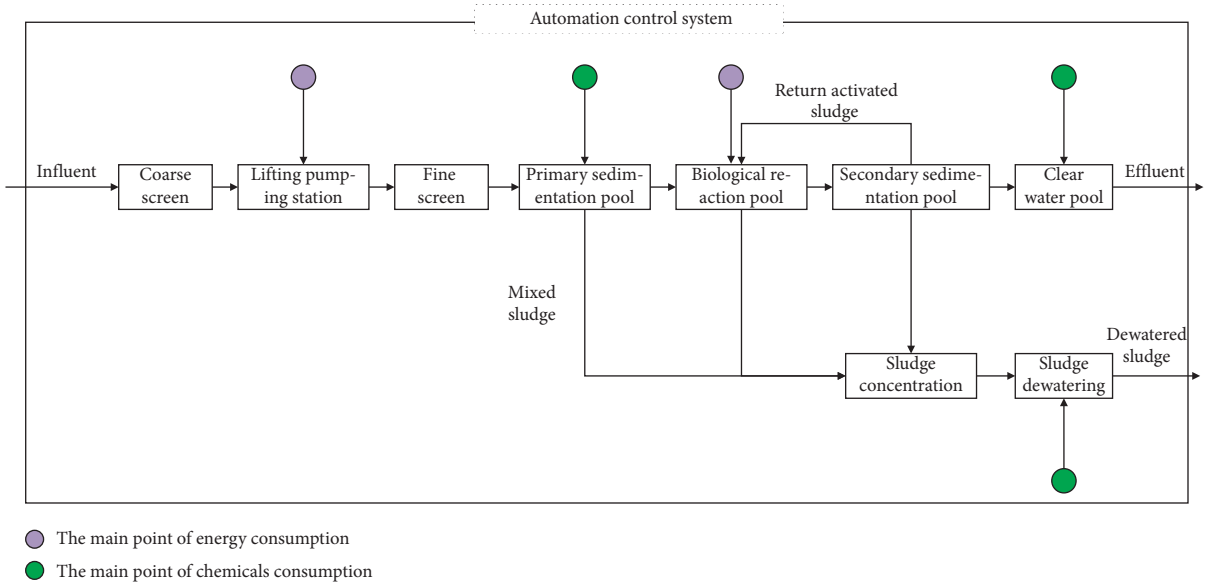

Figure 5: The process flow diagram of domestic wastewater treatment.

public's requirements, the public can express their claims through the online reporting system, including complaints about network leakage, water pollution reports, complaints about noise or odor of WWTPs, or request to disclose relevant information.

5.1.6. Information Needed for Smart Supervision and Evaluation. The government supervises and evaluates the processes and operation quality of wastewater treatment-related services offered by service providers, including the operation of WWTP, sludge disposal, management of malodors and environmental noise of the plant, consumption of energy and other materials, O&M of sewage networks, and reuse of reclaimed water [47, 48]. The WWTP uploads the quality and quantity of the influent and effluent of the plant and other information about its operation, through real-time online monitoring and transmission equipment, to report the operation status to the government. The government can supervise its operation management and pollutant discharge in a smart way. Moreover, the government can conduct performance evaluation, according to the water quality and quantity and other assessment information reported, to calculate pollutant reduction (COD, NH3-N, TN, TP, etc.) and other evaluation results to ensure that the load rate, quality of operation, and effluent water quality of the WWTP meet the standards and to improve the efficiency of public services. Similarly, sewer asset O&M departments upload water quality, water quantity, and other performance indicators of the sewage networks in real-time to report the real-time status of the networks, which can contribute to the regulation of sewer assets and improve the integrity of the sewerage network system. In terms of the reuse of wastewater, the government monitors the quality of reclaimed water in real-time and can combine the reported condition of the reuse of reclaimed water and other information to evaluate the status of wastewater reuse.

5.1.7. Information Needed for Information Sharing. Information sharing is the foundation for the realization of the above functions. Information sharing should determine the scope of information based on the source of information and the authorities who need it, as well as their confidentiality. According to the scope of shared information, information sharing includes intraorganizational and cross-organizational sharing. For example, in a WWTP, the biotechnology department and the laboratory department should share wastewater-related information, such as the water quality of the influent and effluent of the WWTP and each reaction pool, to improve operational management.

In terms of cross-organizational sharing, the operation status of the WWTP is supervised by the Ministry of Ecology and Environment, Ministry of Housing and Urban-Rural Development, etc.; therefore, information about the quality and quantity of wastewater, the process of treatment, etc., should be shared between the WWTP and the government. The O&M of sewer assets is closely related to weather-related data. Therefore, weather data, such as precipitation, are also an important source of cross-organizational sharing. Information sharing also includes the release of disaster alerts and the active disclosure of environmental regulatory data. In the release of disaster information, the real-time and continuous sensors of the sewage networks can quickly assess the occurrence of pollution or flooding to notify the WWTP and facilitate the development of an effective operation plan, which can ensure the stability of the wastewater treatment system. Potential areas affected by floods or overflows can also be notified by sharing disaster alert information to ensure the safety of the population, prevent loss of life, and reduce the social and environmental impacts.

5.2. Information Chain of SUDW. The functions of SUDW are interrelated. Specifically, the WWTP not only considers the water quality and condition of the equipment but also

accepts supervision and evaluation from the government and considers complaints of noise and odor of the WWTP from the surrounding residents or other citizens. In addition, when a network failure or disaster occurs, relevant information should be shared with the WWTPs so that the operators of plants can take relevant measures in advance to maintain the stability of the wastewater treatment system. The early alert and control of disasters require the O&M departments of sewer assets to provide information such as the real-time status of the pipeline networks, which is convenient for detecting pollution, floods, and other disasters. The alert is also based on weather-related information. The reuse of wastewater is closely related to other functions as well. The status of wastewater reuse is also a vital component of the evaluation by the government. Therefore, government departments must monitor the usage of reclaimed water, such as information about the quantity and quality. Moreover, the reuse of wastewater is an important issue in public communication.

The components of the smart city information chain model contain information, nodes, and paths, where the nodes are the senders and receivers of the information and the paths are the roads of the information flow [66]. The realization of each function of SUDW is based on the perception of data, through information transmission to the corresponding system or platform for analysis, and the output of relevant data to provide valuable operational information for the corresponding service providers. To clearly represent the information communication between the main stakeholders and functions, this study regards the above seven functions as corresponding functional platforms to complete information analysis and processing. By combining the analyses of the information needed for each function, this study constructs an information chain of SUDW, as shown in Figure 6.

This information chain model illustrates the information communication between the main stakeholders and the functions of SUDW and the information interaction among various functions. Taking the automation of WWTP as an example, the WWTP detects the quality and quantity and other useful data of domestic wastewater in real-time and transmits the data to the automation platform of the WWTP. Eventually, the operational control parameters of the equipment and the dosage of chemicals are the outputs of the functional platform. The public expresses complaints or other appeals to the WWTP or to the government, and the WWTP or the government receives the information and provides feedback on the implementation results to the public. In addition, by analyzing the real-time monitoring and uploaded evaluation information, the government can assess the WWTP and deliver feedback to the plant. In return, the plant can adjust its operational strategy based on complaints and feedback.

5.3. Data-Driven Framework of SUDW. The above analyses illustrated the functions of SUDW, the main stakeholders involved in each function, and the data required. The main stakeholders are service providers (including the WWTP, O&M departments of sewer assets, and the agency of reclaimed water), the government, and the public. The data required to realize the corresponding functions include wastewater-related data, such as wastewater quality, water quantity, water level, and flow rate; equipment-related data, such as the switch status of the equipment, running duration, current, energy consumption, noise, and other indicators; sewer assets-related data, such as the locations of facilities, age, and storage capacity of the pipeline network; real-time status of the networks, such as water level and quality of wastewater in the network; weather-related data, such as precipitation and temperature; and public feedback data, such as requests or complaints from the public and other descriptive data of life and activities recorded through social networks.

Different types of data are provided by different stakeholders, and they should be acquired by different technologies [67]. Water quality sensors, water level sensors, and water velocity sensors are used to collect real-time wastewater-related data and determine the real-time status of networks. Weather-related data are obtained by weather radar. Video surveillance is used to collect data about the equipment and pipeline network status. In addition, manual reporting, such as feedback from relevant departments in response to public demands, is an important source of data for SUDW.

Based on the above analyses, this study develops a data-driven framework for SUDW, as shown in Figure 7. With data as the core, the framework aims to explore the potential value and to support decision-making through the collection and the analysis of online and offline data to achieve the functions of SUDW. The framework consists of five layers, from bottom to top: data perception layer, data transmission layer, data storage layer, data analysis and application layer, and user interface layer.

The data perception layer collects relevant wastewater treatment data through sensing devices, such as precipitation gauges, sensors, and videos. Wired or wireless networks (such as TCP/IP, bluetooth, Zigbee, and other protocols) are used to transmit and exchange the perceived information and data in the data transmission layer. In the data storage layer, by means of data warehousing technology, databases are established to store structured, semistructured, and unstructured data [68], such as perceived wastewater-related data, equipment-related data, and sewer asset-related data. In the data analysis and application layer, the original data are denoised and cleaned via data processing and integration to obtain reliable data [69]. Then, artificial intelligence algorithms, such as neural networks and machine learning, are used to analyze and extract the potential value from the data to provide relevant information and support relevant decision-making to achieve the corresponding functions [67]. Finally, through the user interface layer, in the form of visualization, the relevant information is transmitted to stakeholders to strengthen the stakeholders' participation.

6. Discussion

From the perspective of the realizable functions of SUDW, this study proposed that SUDW is based on the application of ICT technologies; involves the collection and analysis of wastewater-related data, equipment-related data, sewer assets-related data, weather-related data, etc.; and helps

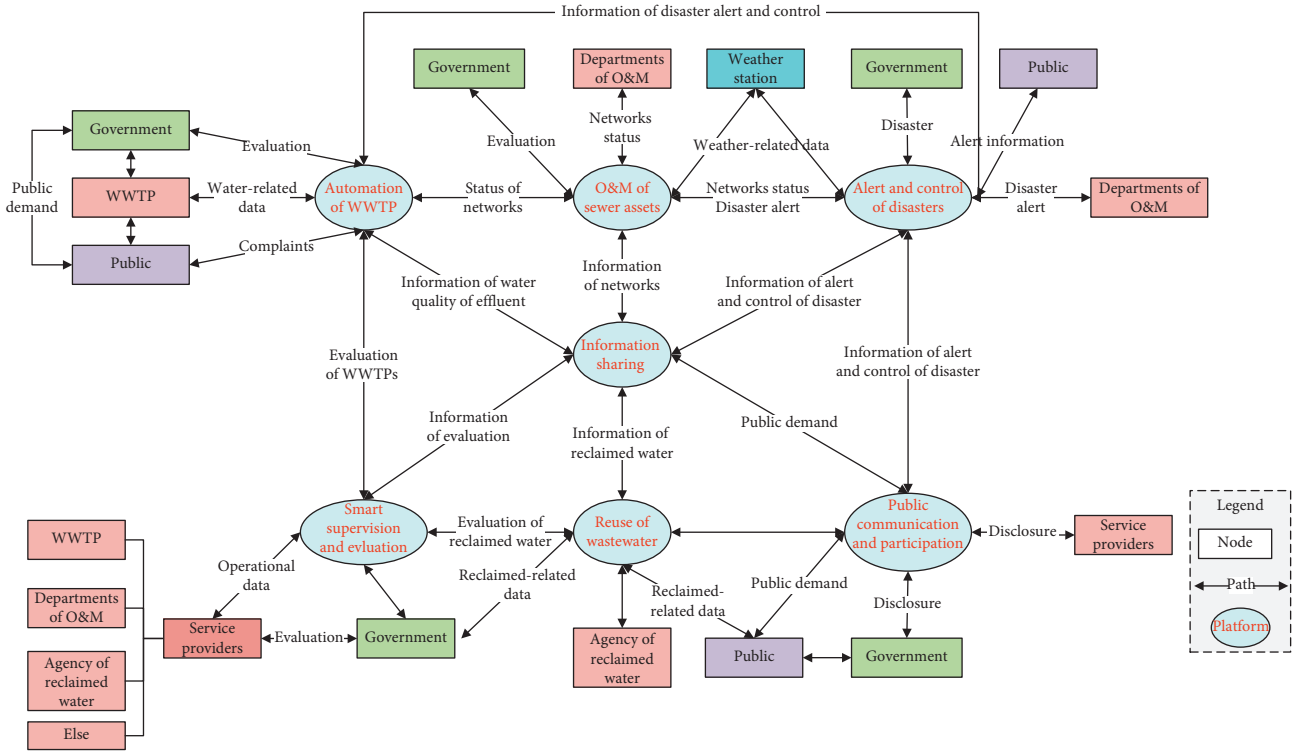

Figure 6: Information chain model of SUDW.

stakeholders obtain accurate information in real-time or near real-time to support relevant decision-making and realize relevant functions, thereby promoting the delivery of sustainable development and smart cities and improving the quality of public life.

This paper studied the framework for SUDW from the perspective of sustainability. A data-driven framework was constructed on the basis of the identification and analysis of the achievable functions, main stakeholders, information needed, and information transmission paths of SUDW. The proposed framework consists of five layers: data perception layer, data transmission layer, data storage layer, data analysis and application layer, and user interface layer. By means of perception, transmission, storage, analysis, and application of relevant data, the framework supports decision-making and helps achieve the corresponding functions. Finally, the relevant information is transmitted to the corresponding stakeholders in the user interface layer. The data are the core element of the framework. Therefore, the timeliness and validity of the data are important guarantees for the realization of SUDW [69, 70]. To ensure the timeliness and validity of the data throughout the process, in the data perception layer, the accuracy of the sensors should be guaranteed to ensure that the perceived data can be used to support decision-making [71]. Additionally, the timeliness of data collection, such as real-time monitoring of important water quality indicators, including BOD, PH, TN, and TP, and daily statistics of sludge quantity, should be ensured. In the data transmission layer, the perceived data should be transmitted securely through the transmission protocols to avoid data lag or data loss [72]. Therefore, a strong demand exists for related transmission technologies. Moreover, the storage of data should ensure the stability of the databases and facilitate the real-time read-in and accessing of data [70]. In addition, the database should be extensible to ensure the development of other functions. In the data analysis and application layer, data cleaning and preprocessing are important to ensure data validity, delete duplicate information, correct errors, and improve data reliability and effectiveness of the results [73]. The designed algorithm should be stable and applicable to the corresponding functions and provide correct and valuable information for decision-making to promote the realization of functions. Finally, the data are interpreted and visualized in the form of tables and images and transmitted to stakeholders to facilitate the understanding of relevant data.

In contrast to architectures built from a single service or function perspective, such as studies conducted by Fattoruso et al. [9] and Ye et al. [34], this paper proposed a comprehensive framework for SUDW that can facilitate an understanding of the achievable functions of SUDW systematically and noted the premise of achieving this goal, i.e., the perception, transmission, storage, and analysis of the corresponding data. Moreover, a holistic and comprehensive framework is conducive to clarifying and coordinating the relationships among stakeholders and between stakeholders and related functions, which can strengthen the utilization of existing resources and promote the planning and implementation of smart cities [74].

Under the guidance of this framework, the realization of SUDW can develop functions gradually and vertically and then realize information sharing among functions through

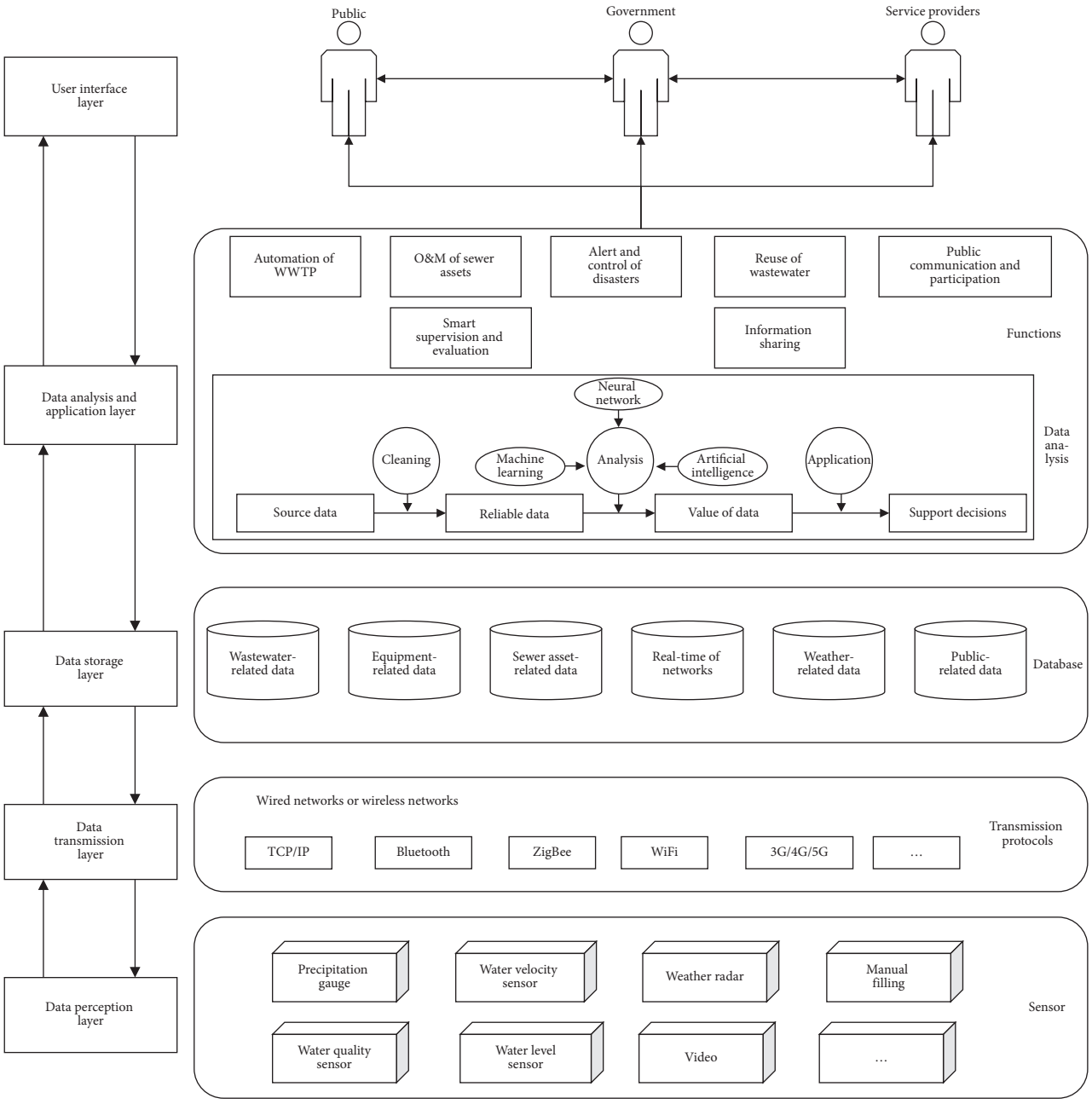

Figure 7: The data-driven framework of SUDW.

an information synthesis platform [74]. Alternatively, the planning of each function and their relationships can be achieved horizontally, gradually improving each function to ultimately realize SUDW.

After realization of SUDW, from the perspective of environmental benefits, the WWTP can improve the efficiency of wastewater treatment to ensure that the discharged treated wastewater meets the standards and can also reduce the consumption of energy and chemicals, eventually mitigating the impact on the environment [14, 75]. Early alert of sewage network overflows or disasters related to domestic wastewater reduces the impact on the public living environment as well [9]. Reuse of wastewater also reduces the use and destruction of water resources [10]. From an economic point of view, the use of ICTs and other technologies can improve the service efficiency of service providers and lead to greater cost-effectiveness [51]. Moreover, for the government and society, the improved infrastructure operation efficiency can more effectively realize the allocation of resources and facilitate economic sustainability. From the perspective of social benefits, the rational allocation of resources can also help narrow the gap between infrastructures and promote social equity and social sustainable development [58]. In addition, after the improvement of the living environment and promotion of public participation, it can improve the satisfaction of the public and eventually improve the quality of life [59]. Therefore, from the perspectives of the environment, economy, and

society, the objectives of SUDW are consistent with the goals of sustainable development. Guided by the goals of sustainable development, the framework for SUDW is designed to conduct the planning and development of SUDW, which in turn promotes sustainable development.

7. Conclusion

This research studied the framework for SUDW from the perspective of sustainability. Based on the goals of sustainable development, the objectives of SUDW, which are consistent with those of sustainable development, were assessed from the perspectives of service providers (mainly WWTPs), the government, and the public. Based on a systematic literature analysis, seven functions of SUDW were identified: (i) automation of WWTP, (ii) O&M of sewer assets, (iii) alert and control of disasters, (iv) reuse of wastewater, (v) public communication and participation, (vi) smart supervision and evaluation, and (vii) information sharing. These functions are interrelated and closely related to sustainable development, where information sharing is the foundation and key component. Then, an information chain model of SUDW was constructed to express the transmission paths of information between stakeholders and functions, which also highlighted the information interaction between functions and emphasized the importance of stakeholders. Finally, based on the above analyses, a data-driven framework for SUDW was developed systematically that consists of the following five layers, from bottom to top: (i) data perception layer, (ii) data transmission layer, (iii) data storage layer, (iv) data analysis and application layer, and (v) user interface layer. The premise of SUDW is defined as the perception, transmission, storage, analysis, and application of corresponding data. This paper also proposed data as the core element of the framework, and we should ensure the validity and timeliness of the data to provide valuable information for relevant decision-making.

Despite achieving the research objectives, some limitations remain. Because of different functions in different contexts or the use of different data analysis methods, the required data can vary. This paper did not define all the data required by SUDW, but the basic form of the indicators and the ways to obtain them were analyzed, thereby providing a reference for follow-up research and practice. Additionally, due to the complexity of the components of the framework, such as the transmission protocols and analysis algorithms, this study did not use actual cases to analyze the framework.

Nevertheless, this study, through the systematic analysis of the achievable functions of SUDW, compensates for the gap arising from the scattering of current research studies among different areas of smart wastewater and contributes to the body of knowledge relating to smart cities. In addition, the proposed smart framework can help the government, urban developers, and service providers understand solutions for the development of SUDW and can be used to guide the planning of urban domestic wastewater to promote the realization of SUDW, eventually delivering smart cities and achieving sustainable development.

Subsequent studies will consider specific cases to demonstrate and revise the framework. In future research, scholars can study the specific data indicators that must be obtained, the ICT technologies needed for the entire process, the data transmission protocols, and the data analysis algorithms to implement the application, which involve many disciplines and various fields.

Data Availability

The results of a systematic literature analysis used to support the findings of this study are included in the article.

Conflicts of Interest

The authors declare that there are no conflicts of interest regarding the publication of this paper.

Acknowledgments

This work was supported by the Ministry of Education of Humanities and Social Science Foundation (15YJZH012).

References

[1] Ministry of Ecology and Environment of People's Republic of China, *Environmental Statistics Annual Report of 2015*, Ministry of Ecology and Environment of People's Republic of China, 2015.

[2] National Development and Reform Commission, *National Plan for the Construction of Urban Wastewater Treatment and Recycling Facilities in the 13th Five-Year Plan*, National Development and Reform Commission, 2016.

[3] United Nations. https://www.un.org/sustainabledevelopment/zh/water-and-sanitation/.

[4] E. P. Trindade, M. P. F. Hinnig, E. Moreira da Costa, J. Marques, R. Bastos, and T. Yigitcanlar, "Sustainable development of smart cities: a systematic review of the literature," *Journal of Open Innovation: Technology, Market, and Complexity*, vol. 3, no. 1, p. 11, 2017.

[5] R. P. Dameri, "Searching for smart city definition: a comprehensive proposal," *International Journal of Computers & Technology*, vol. 11, no. 5, pp. 2544–2551, 2013.

[6] H. M. Kim and S. S. Han, "Seoul," *Cities*, vol. 29, no. 2, pp. 142–154, 2012.

[7] P. Neirotti, A. De Marco, A. C. Cagliano, G. Mangano, and F. Scorrano, "Current trends in smart city initiatives: some stylised facts," *Cities*, vol. 38, pp. 25–36, 2014.

[8] N.-B. Chang, C. Mostafiz, Z. Sun, W. Gao, and C.-F. Chen, "Developing a prototype satellite-based cyber-physical system for smart wastewater treatment," in *Proceedings of 2017 IEEE 14th International Conference on Networking, Sensing and Control (ICNSC)*, pp. 339–344, IEEE, Calabria, Italy, May 2017.

[9] G. Fattoruso, C. Tebano, A. Agresta et al., "A SWE architecture for real time water quality monitoring capabilities within smart drinking water and wastewater network solutions," in *Proceedings of International Conference on Computational Science and Its Applications*, vol. 9156, pp. 686–697, Banff, Canada, June 2015.

[10] A. Molina-Giménez, "Water governance in the smart city," in *Proceedings of Urban Growth and the Circular Economy*, vol. 179, pp. 13–22, Alicante, Spain, May 2018.

[11] J. Massana, C. Pous, L. Burgas, J. Melendez, and J. Colomer, "Identifying services for short-term load forecasting using data driven models in a smart city platform," *Sustainable Cities and Society*, vol. 28, pp. 108–117, 2017.

[12] B. N. Silva, M. Khan, and K. Han, "Towards sustainable smart cities: a review of trends, architectures, components, and open challenges in smart cities," *Sustainable Cities and Society*, vol. 38, pp. 697–713, 2018.

[13] K. Paskaleva, J. Evans, C. Martin, T. Linjordet, D. Yang, and A. Karvonen, "Data governance in the sustainable smart city," *Informatics*, vol. 4, no. 4, p. 41, 2017.

[14] P. Perciavalle, P. Woodall, J. Abrera, S. Vallabhaneni, and K. Johnson, "The digital water/wastewater utility of the future: case studies in leveraging smart utility technology and best management practices," *Proceedings of the Water Environment Federation*, vol. 2017, no. 15, pp. 548–554, 2017.

[15] C. W. K. Chow, J. Liu, J. Li, N. Swain, K. Reid, and C. P. Saint, "Development of smart data analytics tools to support wastewater treatment plant operation," *Chemometrics and Intelligent Laboratory Systems*, vol. 177, pp. 140–150, 2018.

[16] G. H. Brundtland, M. Khalid, S. Agnelli, and S. Al-Athel, *Our Common Future*, Oxford University Press, Oxford, UK, 1987.

[17] R. B. Gibson, *Specification of Sustainability-Based Environmental Assessment Decision Criteria and Implications for Determining "Significance" in Environmental Assessment*, Canadian Environmental Assessment Agency, Ottawa, Canada, 2001.

[18] A. D. Basiago, "Economic, social, and environmental sustainability in development theory and urban planning practice," *The Environmentalist*, vol. 19, no. 2, pp. 145–161, 1999.

[19] L. Bătăgan, "Smart cities and sustainability models," *Informatica Economică*, vol. 15, no. 3, pp. 80–87, 2011.

[20] M. Höjer and J. Wangel, "Smart sustainable cities: definition and challenges," in *ICT Innovations for Sustainability*, vol. 310, pp. 333–349, Springer, Berlin, Germany, 2015.

[21] L.-G. Cretu, "Smart cities design using event-driven paradigm and semantic web," *Informatica Economica*, vol. 16, no. 4, pp. 57–67, 2012.

[22] H. Xia and Z. Wang, "Systemic thinking on smart cities," *China Soft Science*, vol. 7, pp. 66–80, 2017, in Chinese.

[23] D. Schuurman, B. Baccarne, L. De Marez, and P. Mechant, "Smart ideas for smart cities: investigating crowdsourcing for generating and selecting ideas for ICT innovation in a city context," *Journal of Theoretical and Applied Electronic Commerce Research*, vol. 7, no. 3, pp. 49–62, 2012.

[24] A. Caragliu, C. Del Bo, and P. Nijkamp, "Smart cities in Europe," *Journal of Urban Technology*, vol. 18, no. 2, pp. 65–82, 2011.

[25] H. Ahvenniemi, A. Huovila, I. Pinto-Seppä, and M. Airaksinen, "What are the differences between sustainable and smart cities?," *Cities*, vol. 60, pp. 234–245, 2017.

[26] A. Kramers, M. Höjer, N. Lövehagen, J. Wangel, and E. Ab, "ICT for sustainable cities: how ICT can support an environmentally sustainable development in cities," in *Proceedings of ICT4S 2013: Proceedings of the 1st International Conference on Information and Communication Technologies for Sustainability*, pp. 183–188, ETH Zürich, Zürich, Switzerland, February 2013.

[27] Commission on Global Governance, *Our Global Neighbourhood: The Report of the Commission on Global Governance*, Oxford University Press, Oxford, UK, 1995.

[28] R. Giffinger and H. Gudrun, "Smart cities ranking: an effective instrument for the positioning of the cities?," *ACE: Architecture, City and Environment*, vol. 4, no. 12, pp. 7–26, 2010.

[29] A. Meijer and M. P. R. Bolívar, "Governing the smart city: a review of the literature on smart urban governance," *International Review of Administrative Sciences*, vol. 82, no. 2, pp. 392–408, 2016.

[30] G. V. Pereira, P. Parycek, E. Falco, and R. Kleinhans, "Smart governance in the context of smart cities: a literature review," *Information Polity*, vol. 23, no. 2, pp. 143–162, 2018.

[31] R. Wenge, X. Zhang, C. Dave, L. Chao, and S. Hao, "Smart city architecture: a technology guide for implementation and design challenges," *China Communications*, vol. 11, no. 3, pp. 56–69, 2014.

[32] J. Trefke, S. Rohjans, M. Uslar, S. Lehnhoff, L. Nordström, and A. Saleem, "Smart grid architecture model use case management in a large European smart grid project," in *Proceedings of IEEE PES ISGT Europe 2013*, pp. 1–5, IEEE, Lyngby, Denmark, October 2013.

[33] W. Q. Wang, X. Zhang, J. Zhang, and H. B. Lim, "Smart traffic cloud: an infrastructure for traffic applications," in *Proceedings of 2012 IEEE 18th International Conference on Parallel and Distributed Systems*, pp. 822–827, IEEE, Singapore, December 2012.

[34] Y. Ye, L. Liang, H. Zhao, and Y. Jiang, "The system architecture of smart water grid for water security," *Procedia Engineering*, vol. 154, pp. 361–368, 2016.

[35] R. A. Stewart, R. Willis, D. Giurco, K. Panuwatwanich, and G. Capati, "Web-based knowledge management system: linking smart metering to the future of urban water planning," *Australian Planner*, vol. 47, no. 2, pp. 66–74, 2010.

[36] V. Edmondson, M. Cerny, M. Lim, B. Gledson, S. Lockley, and J. Woodward, "A smart sewer asset information model to enable an "Internet of Things" for operational wastewater management," *Automation in Construction*, vol. 91, pp. 193–205, 2018.

[37] N. Khatri, A. Sharma, K. K. Khatri, and G. D. Sharma, "An IoT-based innovative real-time pH monitoring and control of municipal wastewater for agriculture and gardening," in *Proceedings of 1st International Conference on Smart System, Innovations and Computing*, vol. 79, pp. 353–362, Jaipur, India, January 2018.

[38] R. W. Saputra, S. H. Supangkat, and R. Iqbal, "Waste utilities development in industrial zone based on smart city concept and co creation: case study in Bekasi city," in *Proceedings of 2017 International Conference on ICT for Smart Society (ICISS)*, pp. 1–5, IEEE, Tangerang, Indonesia, September 2017.

[39] X. Wei, *Modeling and Optimization of Wastewater Treatment Process with a Data-Driven Approach*, University of Iowa, Iowa City, IA, USA, 2013.

[40] D. A. Savic, "The use of data-driven methodologies for prediction of water and wastewater asset failures," in *Proceedings of the Risk Management of Water Supply and Sanitation Systems*, pp. 181–190, Springer, Ohrid, Macedonia, October 2008.

[41] D. J. Dürrenmatt and W. Gujer, "Data-driven modeling approaches to support wastewater treatment plant operation," *Environmental Modelling & Software*, vol. 30, pp. 47–56, 2012.

[42] B. Kitchenham, "Procedure for undertaking systematic reviews," Joint Technical Report, Computer Science Department, Keele University (TRISE-0401) and National ICT Australia Ltd. (0400011T. 1), Keele, UK, 2004.

[43] J. Heaton and A. K. Parlikad, "A conceptual framework for the alignment of infrastructure assets to citizen requirements within a Smart Cities framework," *Cities*, vol. 90, pp. 32–41, 2019.

[44] K. Chen, W. Lu, Y. Peng, S. Rowlinson, and G. Q. Huang, "Bridging BIM and building: from a literature review to an integrated conceptual framework," *International Journal of Project Management*, vol. 33, no. 6, pp. 1405–1416, 2015.

[45] OECD, *Stakeholder Engagement for Inclusive Water Governance*, IWA Publishing, London, UK, 2015.

[46] C. Seifert, T. Krannich, and E. Guenther, "Gearing up sustainability thinking and reducing the bystander effect—a case study of wastewater treatment plants," *Journal of Environmental Management*, vol. 231, pp. 155–165, 2019.

[47] Ministry of Ecology and Environment of People's Republic of China, *Technical Specification for Management of Municipal Wastewater Treatment Plant Operation (HJ2038-2014)*, Ministry of Ecology and Environment, Beijing, China, 2014.

[48] Ministry of Housing and Urban-Rural Development, *Evaluation Criteria for Operation Quality of Municipal Wastewater Treatment Plants (CHHT 228-2014)*, Ministry of Housing and Urban-Rural Development, Beijing, China, 2014.

[49] A. Asadi, A. Verma, K. Yang, and B. Mejabi, "Wastewater treatment aeration process optimization: a data mining approach," *Journal of Environmental Management*, vol. 203, pp. 630–639, 2017.

[50] J. Wu and Z. Gao, "Thoughts on the government responsibility of sewage treatment industry under PPP upsurge," *Environmental Protection*, vol. 44, pp. 36–40, 2016.

[51] M. K. Mishra, "Role of technology in smart governance: "smart city, safe city"," *SSRN Electronic Journal*, 2013.

[52] P. F. Boulos and A. T. Walker, "Fixing the future of wastewater systems with smart water network modeling," *Journal—American Water Works Association*, vol. 107, no. 4, pp. 72–80, 2015.

[53] P. F. Boulos, "Smart water network modeling for sustainable and resilient infrastructure," *Water Resources Management*, vol. 31, no. 10, pp. 3177–3188, 2017.

[54] S. M. Abelin, "Intelligent future for wastewater pumping," *World Pumps*, vol. 2017, no. 3, pp. 34–37, 2017.

[55] D. Vakula and Y. K. Kolli, "Waste water management for smart cities," in *Proceedings of the International Conference on Intelligent Sustainable Systems, ICISS 2017*, pp. 275–279, IEEE, Palladam, India, December 2017.

[56] D. Granlund and R. Brannstrom, "Smart city: the smart sewerage," in *Proceedings of Conference on Local Computer Networks, LCN*, pp. 856–859, IEEE, Clearwater, FL, USA, October 2012.

[57] Y. Qiu, J. Li, X. Huang, and H. Shi, "A feasible data-driven mining system to optimize wastewater treatment process design and operation," *Water*, vol. 10, no. 10, p. 1342, 2018.

[58] P. F. Boulos, "Optimal scheduling of pipe replacement," *Journal—American Water Works Association*, vol. 109, pp. 42–46, 2017.

[59] C. Laspidou, "ICT and stakeholder participation for improved urban water management in the cities of the future," *Water Utility Journal*, vol. 8, pp. 79–85, 2014.

[60] H. J. Scholl and M. C. Scholl, "Smart governance: a roadmap for research and practice," in *Proceedings of the 2014 IConference*, London, UK, March 2014.

[61] R. K. Chowdhury and W. El-Shorbagy, *Informatics, Logistics and Governance in Water Treatment Processes*, InTechOpen, London, UK, 2013.

[62] Y. Yang, S. T. Ng, S. Zhou, F. J. Xu, and H. Li, "A physics-based framework for analyzing the resilience of interdependent civil infrastructure systems: a climatic extreme event case in Hong Kong," *Sustainable Cities and Society*, vol. 47, Article ID 101485, 2019.

[63] M. N. Karim, D. Hodge, and L. Simon, "Data-based modeling and analysis of bioprocesses: some real experiences," *Biotechnology Progress*, vol. 19, no. 5, pp. 1591–1605, 2003.

[64] M. A. Massoud, A. Kazarian, I. Alameddine, and M. Al-Hindi, "Factors influencing the reuse of reclaimed water as a management option to augment water supplies," *Environmental Monitoring and Assessment*, vol. 190, no. 9, p. 531, 2018.

[65] R. Saliba, R. Callieris, D. D'Agostino, R. Roma, and A. Scardigno, "Stakeholders' attitude towards the reuse of treated wastewater for irrigation in Mediterranean agriculture," *Agricultural Water Management*, vol. 204, pp. 60–68, 2018.

[66] J. Ma, M. Hu, and M. Lian, "Design of smart city information ecological chain based on multi-subject collaboration," *Information Science*, vol. 36, no. 12, pp. 70–74, 2016.

[67] A. M. S. Osman, "A novel big data analytics framework for smart cities," *Future Generation Computer Systems*, vol. 91, pp. 620–633, 2019.

[68] U. Aguilera, O. Peña, O. Belmonte, and D. López-de-Ipiña, "Citizen-centric data services for smarter cities," *Future Generation Computer Systems*, vol. 76, pp. 234–247, 2017.

[69] C. Lim, K.-J. Kim, and P. P. Maglio, "Smart cities with big data: reference models, challenges, and considerations," *Cities*, vol. 82, pp. 86–99, 2018.

[70] E. A. Nuaimi, H. A. Neyadi, N. Mohamed, and J. Al-Jaroodi, "Applications of big data to smart cities," *Journal of Internet Services & Applications*, vol. 6, p. 25, 2015.

[71] B. Jain, G. Brar, J. Malhotra, and S. Rani, "A novel approach for smart cities in convergence to wireless sensor networks," *Sustainable Cities and Society*, vol. 35, pp. 440–448, 2017.

[72] Z. Khan, Z. Pervez, and A. G. Abbasi, "Towards a secure service provisioning framework in a smart city environment," *Future Generation Computer Systems*, vol. 77, pp. 112–135, 2017.

[73] K. Zhou, C. Fu, and S. Yang, "Big data driven smart energy management: from big data to big insights," *Renewable and Sustainable Energy Reviews*, vol. 56, pp. 215–225, 2016.

[74] H. Kumar, M. K. Singh, M. P. Gupta, and J. Madaan, "Moving towards smart cities: solutions that lead to the smart city transformation framework," *Technological Forecasting and Social Change*, 2018, in Press.

[75] W. H. Biehl and J. A. Inman, "Energy optimization for water systems," *Journal—American Water Works Association*, vol. 102, no. 6, pp. 50–55, 2010.

Hindawi
Advances in Civil Engineering
Volume 2019, Article ID 9454929, 13 pages
https://doi.org/10.1155/2019/9454929

Research Article

Comparison of Environmental Impacts of Two Alternative Stabilization Techniques on Expansive Soil Slopes

Rui Zhang,[1,2] **Mingxu Long**,[2] **and Jianlong Zheng**[1,2]

[1]*National Engineering Laboratory of Highway Maintenance Technology, Changsha University of Science & Technology, Changsha, Hunan 410114, China*
[2]*School of Traffic and Transport Engineering, Changsha University of Science & Technology, Changsha, Hunan 410114, China*

Correspondence should be addressed to Rui Zhang; zr@csust.edu.cn

Received 1 August 2019; Revised 29 September 2019; Accepted 15 October 2019; Published 31 October 2019

Guest Editor: Endong Wang

Two alternative techniques, the lime stabilization technique (LST) and the geogrid reinforcement technique (GRT), are both useful to stabilize expansive soil slopes, but their impacts on the environment need be further evaluated. Based on a case study, two techniques as well as their construction processes were introduced. The energy consumption and carbon dioxide (CO_2) emissions were investigated by the life cycle assessment (LCA). The sensitivity analyses were carried out, including the lime content for LST, the reinforcement spacing for GRT, the embankment height, delivery distance, and treatment width for both techniques. From the LCA results, with the GRT, the energy consumption and CO_2 emissions can be reduced by 7.52% and 57.09%, respectively. The main sources of two techniques are raw material production, soil transportation, and paving stage while the CO_2 emissions of lime production are about 11.68 times of those of geogrid production. From the sensitivity analysis results, as the lime content of LST increases by 1%, the total energy consumption and CO_2 emissions increase by 8.27% and 13.16%, respectively; as the reinforcement spacing of GRT increases by 0.05 m, the total energy consumption and CO_2 emissions increase by 1.63% and 0.69%, respectively; as the embankment height increases by 1 m, the increase rates of energy consumption and CO_2 emissions of LST are 1.68 and 1.61 times of those of GRT, respectively. In this project, when the embankment height is less than 10 m, the geogrid technique has the advantages of energy-saving and emission-reduction. It was found that the GRT is not sensitive to the change of delivery distance and treatment width and significantly reduces the environmental impacts, especially in reducing the impact of global warming.

1. Introduction

Expansive soils are widely distributed in more than 60 countries and regions [1]. They are classified as high plasticity soils that typically contain hydrophilic clay minerals such as montmorillonite and illite. These kinds of clays are characterized by significant swelling and shrinkage properties in the wetting and drying cycles. The deformation and damage of geotechnical infrastructures occur due to the variation in volume and strength of expansive soils with moisture content fluctuation [2–4].

Due to the extensive distribution of expansive soils and the high demand for infrastructure construction in China, it is inevitable to fill and cut the slope in expansive soil regions. In general, the surficial expansive soil on the slope is replaced by plenty of nonexpansive soil to inhibit their significant swelling and shrinkage properties. However, unreasonable treatment method results in significant economic loss and environmental risk due to the disposal of expansive soil and massive consumption of natural material. In order to minimize energy consumption and greenhouse gas emissions in the process of extraction, processing, and transportation, it is important to make full use of expansive soils instead of discarding them [5].

Two types of techniques, chemical treatment and physical treatment, are used for stabilizing surficial layer of expansive soil slope. In the chemical treatment, different additives, including lime or cement, are mixed into expansive soil to improve the physical and mechanical properties (strength, stiffness, California bearing ratio (CBR), durability, etc.) [6, 7].

The sustainable and relatively slow pozzolanic reaction between lime and expansive soils in a high pH environment is the key to the effective and durable stability of lime-soil mixture [8]. Chen et al. [9] used the expansive soil with medium swelling force to construct an embankment slope with a total length of 80 m stabilized by the lime. It is shown that the lime stabilization technique (LST) can ensure the stability of embankment slope, and the combination of LST and edge covering technique can greatly reduce the consumption of lime, which has been popularized and applied in Xiangyang to Jingzhou (Xiangjing) Highway. Li et al. [10] conducted repeated shear tests before and after drying-wetting cycles. It is theoretically proved that the LST combined with the edge covering technique has a good performance. In the physical treatment, the geogrid reinforcement is widely used to stabilize the expansive soil slope, which reduces the soil swelling by tension grids [11]. Several test sections reinforced by different techniques were constructed in Nanning to Youyiguan (Nanyou) Highway. From the results of monitoring and investigation for several years, it is shown that these techniques can significantly reduce the damage of slope [1]. Because of its advantages of good maneuverability, shortening the construction period, and reducing construction cost, the geogrid reinforcement technique (GRT) has been popularized in expansive soil section of highway.

After the stabilization mechanisms of the above two techniques were studied, the economic benefits of them were also analyzed. However, most studies in this field have focused on the reduction of costs and execution time of the project rather than the environmental impacts [12, 13]. In order to reduce the environmental impacts of engineering construction, life cycle assessment (LCA) is often used for the ecological assessment of environmental impacts of pavement materials, lime, cement, concrete, and geosynthetic materials. In addition, it is also a powerful environmental management tool used for quantifying the use of energy and materials and the waste emissions of products [14, 15] and guiding the in situ sustainable alternative plans [16–20]. In pavement projects, environmental impacts of different materials (warm mix asphalt, hot mix asphalt, steel slag, or natural aggregate) or techniques (asphalt rehabilitation technique or reclaimed asphalt pavement application technique) applied in the projects were analyzed and evaluated by the LCA to determine the optimum material or technique. Therefore, engineers can conduct a sustainable construction plan in the field [21–25]. In addition, the LCA was utilized to assess the environmental impacts of various production processes of building materials, such as lime or cement. Based on the results analyzed by LCA, the emission-reduction effects in the recovery process of cement production and the calcination process in lime production were further evaluated [26–29]. In slope project, compared with the concrete, geosynthetic materials, such as geogrid, are alternative building materials due to their high efficiency in construction. The energy consumption and carbon emission of rigid concrete retaining wall were compared with the geogrid-reinforced retaining wall through the LCA method. It is indicated that the geogrid is far superior to the concrete in terms of economic benefits and environmental protection [30, 31].

In this study, two techniques of lime stabilization and geogrid reinforcement for the expansive soil slope were analyzed by LCA, including the production, transportation, and construction stages of raw materials. The energy consumption and greenhouse gas emissions of different slope reinforcement techniques were determined. Environmental impacts were compared by changing the lime content, reinforcement spacing, and delivery distance. Moreover, based on the above results, the sensitivity analysis of relevant factors was carried out.

2. Materials and Methods

The lime and geogrid are often used to reinforce the expansive soil slope. In order to facilitate the comparison of these two techniques, the expansive soil embankment with the same length of 100 m was selected, and the lime stabilization and geogrid reinforcement techniques were adopted to reinforce the embankment slope.

2.1. Lime Stabilization Technique (LST). The structures of embankment stabilized by the lime are shown in Figure 1. The width and height of embankment are 24 m and 8 m, respectively. The slope ratio is 1 : 1.5, that is, 1.5 m in length and 1 m in height. The slope angle is 33.7°.

The embankment was divided into three layers. The first part is the bottom layer. It is built with gravel and 0.5 m in height, and 2,362.5 m^3 gravels were used as the rising barrier of capillary water.

The second part is the lower embankment. The central part of the embankment was filled with expansive soil for directly reducing the material waste. According to the wet compaction standard, the maximum dry density and the optimum moisture content of lime-soil determined are 1.74 g/cm^3 and 16.8%, respectively [10]. And the degree of compaction should reach 90% according to the specification. A total of 18,900 m^3 of expansive soils has been utilized. The lime was used to stabilize the edge of expansive soil embankment. Two key design parameters, including treatment width and lime content, need to be determined.

The strength decline of expansive soil embankment is mainly controlled by the repeated changes in temperature and humidity of the natural environment. To ensure higher initial strength and avoid the influence of seasonal wetting-drying cycle and rainfall on the embankment, it is necessary to determine the treatment depth of expansive soil by the edge covering technique [32]. The treatment width can be calculated by combining the depth of active zone with the slope ratio. The depth of active zone or atmosphere refers to the effective depth of the earth's deformation caused by the precipitation, evaporation, and ground temperature under the action of natural climate. Its value should be determined by observation data of deep deformation or water content and temperature of the soil in each climatic region. If there are no data, it can also be selected according to the relevant regulations. Based on the available data on the depth of the active zone in the Jingmen area [9], considering the vegetation protection and drainage systems, the treatment width was set at 3 m and a total of 3,600 m^3 of lime-soil was used.

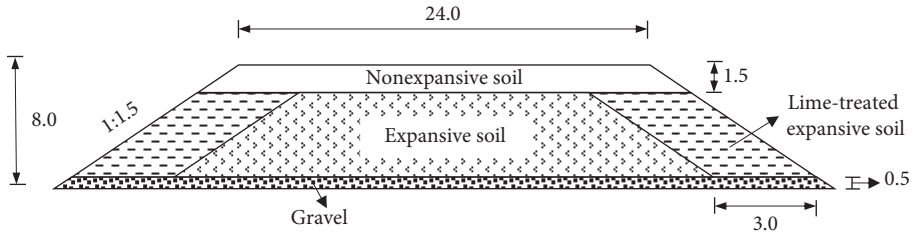

Figure 1: Structure of lime-stabilized embankment (unit: m).

The lime content refers to the ratio of quicklime mass to dry soil mass. The main purpose of lime stabilization method is to improve the swelling and shrinkage properties and mechanical properties of expansive soil. The optimum lime content should also be determined by laboratory tests, including CBR test, swelling test under the pressure of 50 kPa, and shrinkage test. According to the requirement of *Specifications for Design of Highway Subgrades (JTG D30-2015)* [33] in China, the CBR value of roadbed filler must be more than 3% before it can be used for the embankment filling. The natural expansive soil often cannot meet this requirement. The expansive soil was taken to test and control the dry bulk density of 18 KN/m^3. As shown in Figure 2, when the lime content is more than 3%, the CBR value of lime-soil will be obtained, which is far greater than that of normative requirements. The total rate of swelling-shrinkage (e_{ps}) is the sum of the expansion rate and shrinkage rate of soil under the pressure of 50 kPa; when the weak and medium expansive soils are used as fillers, the total rate of swelling-shrinkage should not exceed 0.7% after treatment with an inorganic binder. According to the formula of *Specifications for Design of Highway Subgrades (JTG D30-1995)* [34] in China, when the lime content is 4%, the total rate of swelling-shrinkage is negative, which meets the requirements. Based on the above analysis, it is determined that the best effect can be achieved by adding 3% lime to the expansive soil. However, considering the effect of climate, crushing degree of soil particles, amount, and homogeneity of lime in construction, the actual amount of lime should be increased by 1~2% appropriately. Therefore, the lime content is determined to be 5%. In order to ensure the construction quality, the lime must meet the requirements of Grade III; that is, the effective content of CaO and MgO in calcareous quicklime should not be less than 70%. In this study, the contents of CaO and MgO in tested lime are 73.28% and 3.87%, respectively [10].

The third part is the roadbed (0~0.8 m) and the upper embankment (0.8~1.5 m), commonly known as the working zone. In order to prevent the effect of weathering and drying-wetting cycle on the expansive soil, 3,937.5 m^3 of nonexpansive soil with high water stability was used. The construction steps are shown in Figure 3.

2.2. Geogrid Reinforcement Technique (GRT). The structure of embankment reinforced by geogrid is shown in Figure 4(a). The size and material of the first and third parts of this embankment are the same as those of lime-stabilized

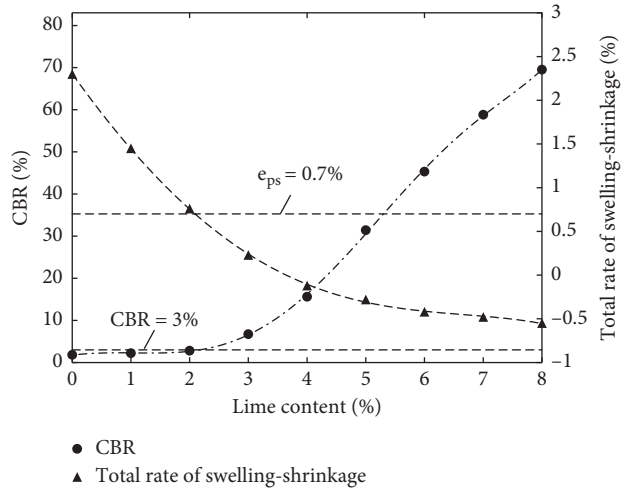

Figure 2: Relationship between the lime content and CBR, and total rate of swelling-shrinkage.

embankment. The roadbed and the upper embankment were also covered by nonexpansive soil with a height of 1.5 m. The gravel was used as the bottom layer with a height of 0.5 m. The difference is that the second part uses geogrid to reinforce the edges. The central part of embankment and the reinforced area of geogrid were directly filled with 22,500 m^3 expansive soil. Compared with the LST, it is also necessary to determine the reinforcement length and spacing.

The detailed layout of the geogrid reinforcement is shown in Figure 4(b). The reinforcement length can be calculated by combining the depth of active zone with the slope ratio. According to the data of depth of the active zone in the Ningming area, the length of reinforcement was determined to be 3 m [1]. To avoid the failure of geogrid caused by the softening of soil material in the fixed part of the geogrid and wetting-drying cycle, a 0.5 m anchorage section was set up with a total reinforcement length of 3.5 m.

Some researchers have deduced the load-deformation relationship of geotextiles and substituted the reinforcement width and the allowable tensile strength of geogrid, thus directly calculating the reinforcement spacing. This method can ensure that the tensile strength mobilized in the reinforcement is consistent with the mobilized deformation [35]. In addition, the friction between soil and geogrid improves the strength and stability of reinforced soil. The spacing of reinforcement is closely related to the stability of slope. The reasonable thickness of each layer can be assumed based on experience, and the spacing can be determined by

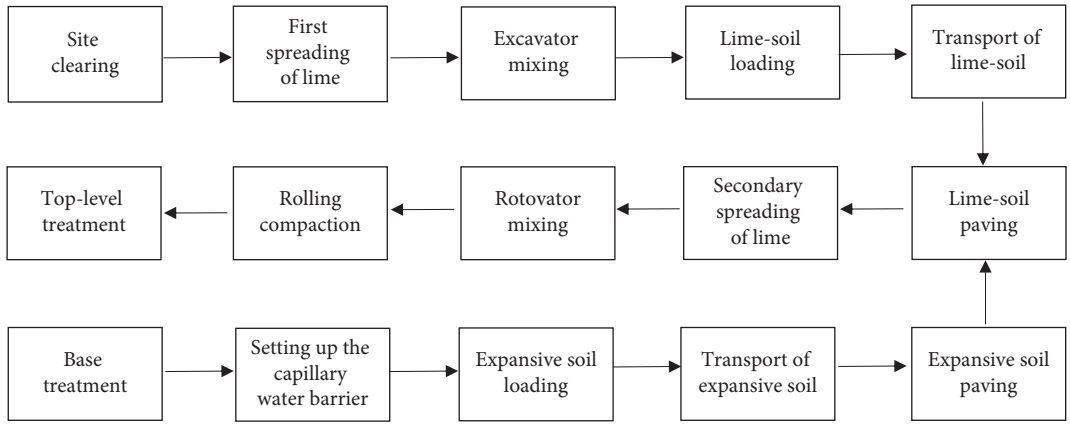

Figure 3: Construction process of embankment stabilized by lime.

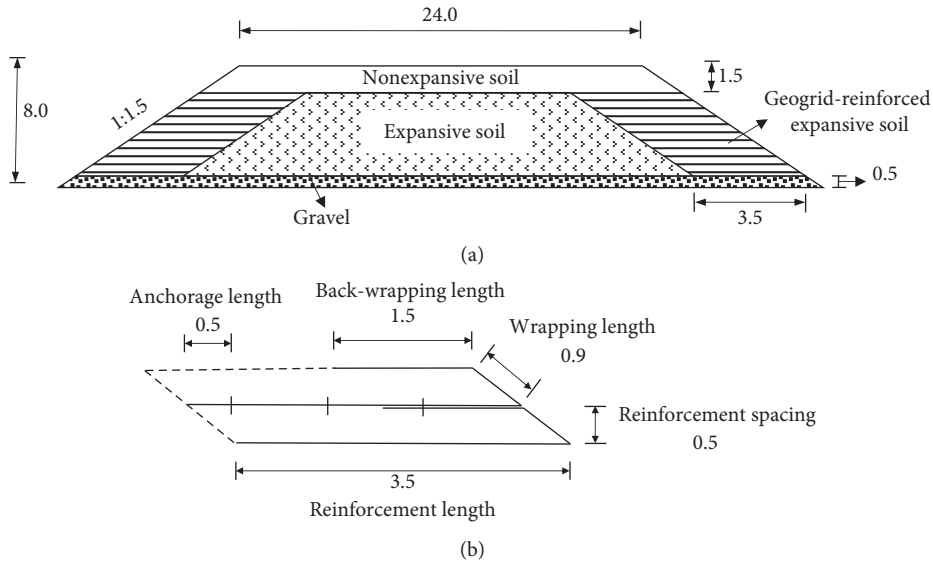

Figure 4: Structure of geogrid-reinforced embankment. (a) Cross section of geogrid-reinforced embankment and (b) design parameters of geogrid-reinforced embankment (unit: m).

the minimum safety factor provided. If the reinforcement spacing is too large to provide sufficient tensile strength, it will still lead to the failure of reinforcement. The slope failure and too small spacing can cause waste of materials. Based on the Bishop method, the slope stability was analyzed in this study. The swelling effect of expansive soil after rainfall infiltration and the interaction between soil and geogrid were considered. Due to the establishment of the capillary water barrier, the calculation of soil includes two layers of nonexpansive and expansive soils without considering the effect of groundwater rise. The basic physical properties and shear strength of expansive and nonexpansive soils in the Ningming area of Nanyou Road are shown in Table 1. The tensile strength of geogrid is 35 KN/m. The safety factor (Fs) corresponding to different reinforcement spacing is shown in Figure 5.

As shown in Figure 5, when the reinforcement spacing is less than 1 m, the safety factor of slope meets the specification of greater than 1.2. To facilitate the layered filling of expansive soil, the reinforcement spacing was determined to be 0.5 m, and 12 layers of geogrid were laid. Each layer of geogrid was filled with two layers of soil. The compaction thickness of each layer is 25 cm. The geogrid was connected by a rod, and the length of back-wrapping is 1.5 m. The construction steps are shown in Figure 6.

Table 1: Physical parameters of expansive soils.

Properties	Expansive soils	Nonexpansive soil
Specific gravity	2.75	2.72
Liquid limit (%)	71.2	52.0
Plastic limit (%)	31.5	22.0
Natural moisture content (%)	31.6	30.0
Optimum moisture content (%)	16.3	16.0
Maximum dry density (g/cm^3)	1.74	1.70
Free swelling index, FSI (%)	57.5	10.0
Natural unit weight (KN/m^3)	19.0	18.0
Cohesion (kPa)	33.3	38.0
Friction angle (°)	15.6	24.0

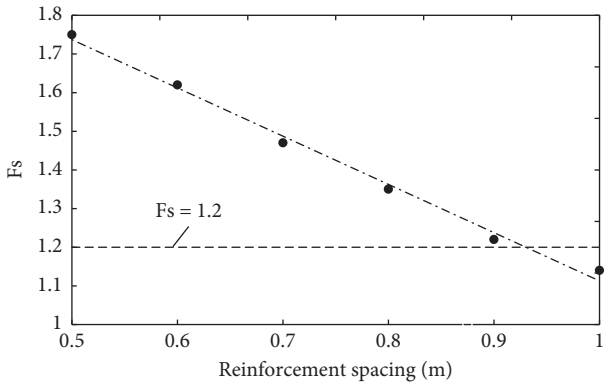

Figure 5: Analysis results of slope stability with different reinforcement spacing.

3. Life Cycle Assessment (LCA)

The LCA is a tool for systematically analyzing the environmental performance of a product or process during its life cycle, from the cradle to the grave. It includes the whole life cycle of a product or process, including the extraction and processing of raw materials, manufacturing, transportation and distribution, use, reuse, maintenance, recycling, and final disposal [36]. Based on ISO 14040, its methodology consists of four steps: goal and scope definition, inventory analysis, life cycle impact assessment, and interpretation. As shown in Figure 7, the goal and scope definition include system functions, functional units, system boundaries, environmental impact types, and quality criteria for inventory data. The life cycle inventory analysis is defined as a phase of life cycle assessment involved in the compilation and quantification of inputs and outputs for a product throughout its life cycle. In the life cycle impact assessment, these environmental impacts of various flows of material and energy are assigned to different environmental impact categories. The characterization factor is used to calculate the contribution of each component for different environmental impact categories (climate change, ozone depletion, ecotoxicity, human toxicity, photochemical ozone formation, acidification, eutrophication, resource depletion, and land use). For example, the environmental impact of all greenhouse gases is expressed in terms of carbon dioxide (CO_2) equivalent. The life cycle interpretation deals with the interpretation of results from both the life cycle inventory analysis and life cycle impact assessment [14].

3.1. System Boundaries. A section of the embankment with length, height, and width of 100 m, 8 m, and 24 m, respectively, was considered as the functional unit. The pavement construction, operation, and abandonment of embankments are not considered in this study because these activities are common for two techniques. In the material acquisition stage, only high energy consumption materials, such as lime, geogrid, and soil, were considered. The amount of wood, steel bar, and other materials is not significant, and the corresponding energy consumption is relatively low. The source of natural gravel is similar to that of nonexpansive soil. Hence, to simplify the calculation, the gravel is considered as nonexpansive soil. The dimensions of the first part of gravel and the third part of nonexpansive soil are the same in the two techniques, which has little influence on the research objectives. The same transport standard (i.e., vehicle and fuel types) was used to calculate the environmental impacts during material transportation stage, and the effect of the delivery distance was also taken into account. The energy consumption and emission of construction machinery were mainly considered during the construction stage. For the manual operation, the energy consumption was calculated while the CO_2 emission was neglected. The activities, including the preparations of embankment foundation, construction of drainage facilities, and cultivation layer on the surface of the slope, were not considered by the life cycle analysis.

The lime and geogrid manufacturers are 50 km away from the project site. The nonexpansive soil pit is 20 km away from the project site. The natural bulk density of nonexpansive soil is 18 KN/m^3. The effect of delivery distance was taken into account when energy consumption was calculated.

In LST, 5% lime was added. The maximum dry density of lime-soil is 1.80 g/cm^3. Then, 324 t of quicklime was used. The expansive soil was premixed with 2% (129.60 t) quicklime in the excavation site, and the remaining 3% (194.40 t) quicklime was mixed with the previous lime-soil mixture before the final compaction in the worksite. After the mixing, bulldozers and graders were used to pave the soil.

In GRT, the width of geogrid is 5.9 m in total, including the reinforcement width of 3.5 m, wrapping length of 0.9 m (calculated from the reinforcement spacing of 0.5 m and slope ratio), and back-wrapping length of 1.5 m. 12-layer grids were used on each side of the slope. Each grid is 4.5 m in length, and the overlapping area between the two grids is about 10 cm. The overlapping area of this part is omitted. The lime, geogrid, and nonexpansive soil were transported by the dump truck with the same transport standard (vehicle and distance). The expansive soil was transported by the dump truck. The bulldozer and grader were used to level the mound. Rolling steps and precautions are the same.

3.2. Data Inventory. Assuming that the production process of China's lime rotary kiln is used, 153.00 kg standard coal and 42.97 kW·h power are consumed per ton of lime. According to the National Bureau of Statistics' *China Energy Statistical Yearbook 2013*, the average calorific value of the raw coal is 20,908 kJ/kg and that of the standard coal is 29,271 kJ/kg. The standard coal consumption rate for thermal power generation is 321 g/kW·h, which is converted to 9,396 KJ/kW·h. It is obtained that the energy consumption per ton of lime is 4,882.50 MJ/t. The emission in the lime reaction process is 0.683 t/t. The emission of fossil fuel combustion is 1.85 t/t, and the indirect emission of power consumption is 0.9402 t/t [37]. It is obtained that the CO_2 equivalent emission per ton of lime is 1,006.49 kg/t. Assuming that the production process of German geogrids is

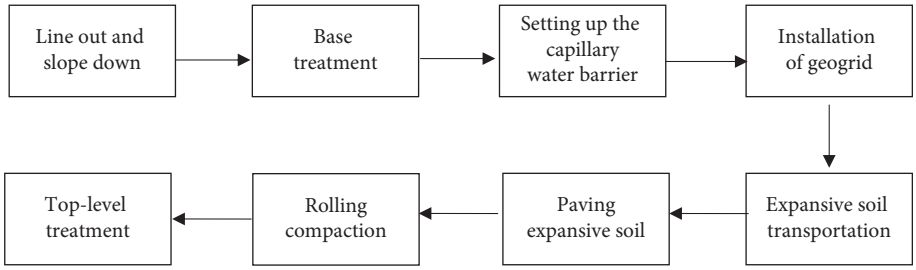

Figure 6: Construction process of embankment reinforced by geogrid.

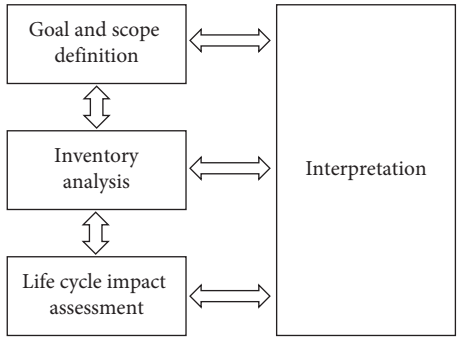

Figure 7: Life cycle assessment framework based on ISO 14040.

adopted [31], the mass of grids per square meter is 0.58 kg/m^2. The production energy consumption of grids per square meter is 78.70 MJ/m^2 and the CO_2 equivalent emission of grids per kilogram is 3.4 kg/kg [30].

Due to the constraints of construction level, both techniques need to adopt artificial cooperation to calculate the total working hours. 170 calories are consumed for moderate labor per hour, and each calorie is equivalent to the energy of 4.186 kJ for calculating the artificial energy consumption. 270 h and 210 h are consumed by the lime-stabilized soil per 1000 m^3 and laying artificial geogrid per 1000 m^2, respectively.

2.423 MJ is consumed by highway transportation per t·km [38]. The energy consumption can be obtained from the total amount and distance of transportation of lime, geogrid, and soil. The default value of diesel emission factor is shown in Table 2. Diesel fuel trucks can calculate various greenhouse gas emissions according to the total energy consumption and then be expressed by the CO_2 equivalent. For a given greenhouse gas, the impacts on the environment can be measured over a period of time (usually 100 years), the environmental impacts of these gases vary, and the mass of other greenhouse gases is converted to the CO_2 equivalent by the global warming potential (GWP). The global warming potential of various greenhouse gases is shown in Table 3.

The type of energy was determined by the type of construction machinery. According to the *Highway Construction Quota* and *Highway Construction Machinery Cost Quota (JTG/TB06-03-2007)* [39] in China, the number of shifts of excavators, bulldozers, rollers, and dump trucks per 100 m^3 and their diesel consumption per shift were counted, as shown in Table 4. The net calorific value of diesel is 43 MJ/kg, as shown in Table 2. The energy consumption and

Table 2: Carbon emission factor of diesel.

Fuel type	Net calorific value (MJ/kg)	Default emission factor (kg/TJ)		
		CO_2	CH_4	N_2O
Diesel	43	74100	3	0.6

equivalent emissions of CO_2 were calculated by the diesel combustion.

4. Results and Discussion

4.1. Comparison of Two Alternative Stabilization Techniques

4.1.1. Energy Consumption. The specific energy consumptions of LST and GRT are shown in Tables 5 and 6, respectively. Among them, the energy consumptions of lime production and geogrid production are 1,581,930.00 MJ and 1,114,392.00 MJ, respectively. The calculation results show that these two materials in the production process with the same order of magnitude of energy consumption are the main sources of energy consumption in the whole LCA analysis process. The energy consumption of material production accounts for a large proportion in both techniques. The lime production process includes quarrying, crushing and screening, calcination, hydration and classification, packaging, and other steps. The geogrid production process includes plastic sheet extrusion, hole-making, heating, horizontal and vertical tension, directional cutting, and other steps. Both of them have the heating process. However, due to the lime production process, the specific heat capacity of stone is much higher than that of plastics, and the energy consumption of decomposition of calcium carbonate is much more than that of melting of plastics. Therefore, the energy consumption of lime production is higher than that of geogrid production.

In LST, the lime production (40.34%), expansive soil transportation (17.34%), nonexpansive soil transportation (14.30%), and expansive soil paving (9.41%) are the major energy-consuming processes. In GRT, the geogrid production (30.73%), expansive soil transportation (22.32%), nonexpansive soil transportation (15.46%), and expansive soil paving (12.11%) are the major energy-consuming processes. Because of the same amount, transportation standard, and paving technique of expansive soil and nonexpansive soil, the main source of energy consumption of the two techniques are also the same. Considering the balance of filling and excavation, the source of

Table 3: Global warming potentials of various greenhouse gases.

Impact category	Impact factor	Unit	Characteristic factor
Energy consumption	Diesel	MJ	1
Greenhouse gas	CO_2	kg (equivalent of CO_2)	1
	CH_4		25
	N_2O		298

Table 4: Mechanical construction and shift quota.

Machinery	Diesel (kg/shift)	Mechanical quota
Excavator	92.12	100 m^3/0.105 shift
Bulldozer	120.35	100 m^3/0.312 shift
Rotovator	115.15	100 m^3/0.124 shift
Grader	134.2	100 m^3/0.0585 shift
Roller	105.6	100 m^3/0.143 shift
Dump truck	67.89	100 m^3/1.232 shift

Table 5: Energy consumption of the lime-stabilized expansive soil technique.

Construction process	Energy consumption (MJ)	Proportion (%)
Lime production	1581930.00	40.34
Transport of lime	39252.60	1.00
Lime paving	691.69	0.02
First mixing	53047.85	1.35
Transport of lime-soil	129475.46	3.30
Lime-soil paving	70279.05	1.79
Secondary mixing	22103.27	0.56
Lime-soil compaction	23376.04	0.60
Expansive soil loading	78609.22	2.00
Transport of expansive soil	679746.18	17.34
Expansive soil paving	368964.99	9.41
Expansive soil compaction	122724.20	3.13
Nonexpansive soil loading	26203.07	0.67
Transport of nonexpansive soil	560751.43	14.30
Nonexpansive soil paving	122988.33	3.14
Nonexpansive soil compaction	40908.07	1.04
Total	3921051.46	100

Table 6: Energy consumption of the geogrid-reinforced expansive soil technique.

Construction process	Energy consumption (MJ)	Proportion (%)
Geogrid production	1114392.00	30.73
Transport of geogrid	994.98	0.03
Geogrid laying	2116.07	0.06
Expansive soil loading	363288.51	10.02
Transport of expansive soil	809221.64	22.32
Expansive soil paving	439244.03	12.11
Expansive soil compaction	146100.24	4.03
Nonexpansive soil loading	26203.07	0.72
Transport of nonexpansive soil	560751.43	15.46
Nonexpansive soil paving	122988.33	3.39
Nonexpansive soil compaction	40908.07	1.13
Total	3626208.38	100

expansive soil is relatively close, but the amount of expansive soil is relatively large. Due to the heavy workload of the dump truck, the transportation energy consumption of expansive soil is higher. Nonexpansive soil needs to be transported for a long distance. The long-distance road transportation increases fuel consumption and energy consumption. Expansive soil paving requires bulldozers and graders to work successively, which also causes more fuel consumption.

The total energy consumptions of the two techniques are shown in Tables 5 and 6. The total energy consumptions of

LST and GRT are 3,921,051.46 MJ and 3,626,208.38 MJ, respectively. The energy consumption of LST is about 1.08 times of that of GRT. Compared with the energy consumption of LST, the energy consumption of GRT is reduced by 7.52%. There is no obvious energy-saving advantage. Through comparison, it can be found that the total energy consumption of LST is higher than that of GRT because of the higher energy consumption of lime production and the increase of process steps of lime-stabilized expansive soil. The energy consumption of geogrid per unit mass is obviously less than that of lime, but the total content of geogrid used as the main material is larger than that of lime. In the case of large contents of geogrids, the GRT has no obvious energy-saving advantages.

4.1.2. Carbon Dioxide Emissions. The specific CO_2 emissions of LST and GRT are shown in Tables 7 and 8, respectively. Among them, the emissions of lime production and geogrid production are 326,102.76 kg and 27,923.52 kg, respectively. The results show that the energy consumption of the two materials in the production process is not the same order of magnitude. Lime production process is the main source of carbon emissions in the whole life cycle analysis process, while the carbon emissions in the grille production process account for a small proportion in the whole life cycle analysis process. The CO_2 emission of lime production is about 11.68 times of that of geogrid production. A large number of CO_2 emissions were produced by the decomposition of calcium carbonate in the lime production process. It is the main source of production emissions. However, no corresponding chemical reaction occurs in the geogrid production process. The CO_2 emissions mostly are produced from other energy consumptions. Therefore, the CO_2 emissions of geogrid production are far lower than those of lime production.

The major processes of CO_2 emissions in LST are the lime production (65.22%), expansive soil transportation (10.11%), nonexpansive soil transportation (8.34%), and expansive soil paving (5.49%). The major processes of CO_2 emissions in GRT are the geogrid production (14.34%), expansive soil transportation (30.90%), nonexpansive soil transportation (21.41%), and expansive soil paving (16.77%). The main sources of CO_2 emissions and energy consumption of the two techniques are the same. The proportion of lime production in LST is much higher than that of other sources while the CO_2 emissions of geogrid production in GRT are less and even much lower than those of fuel combustion in soil transportation and paving process.

The total CO_2 emissions of the two techniques are shown in Tables 7 and 8. The total emissions of LST and GRT are 499,973.90 kg and 214,529.27 kg, respectively. The emissions of LST are about 2.33 times of those of GRT. Compared with the CO_2 emissions of LST, the CO_2 emissions of GRT are reduced by 57.09%. It can be seen that GRT has obvious emission-reduction advantages. From the above analysis, it can be seen that the emission-reduction mainly results from the low emission of geogrid production and the simplification of construction steps. The carbon emission of geogrid per unit mass is much lower than that of lime. Although the total content of geogrid used as the main material is larger than that of lime, the GRT still has obvious emission-reduction advantages.

Table 7: Carbon dioxide emissions of the lime stabilization technique.

Construction process	CO_{2-eq} (kg)	Proportion (%)
Lime production	326102.76	65.22
Transport of lime	2918.58	0.58
First mixing	3944.31	0.79
Transport of lime-soil	9626.99	1.93
Lime-soil paving	5225.51	1.05
Secondary mixing	1643.46	0.33
Mixing lime-soil compaction	1738.10	0.35
Expansive soil loading	5844.89	1.17
Transport of expansive soil	50541.71	10.11
Expansive soil paving	27433.95	5.49
Expansive soil compaction	9125.01	1.83
Nonexpansive soil loading	1948.30	0.39
Transport of nonexpansive soil	41694.00	8.34
Nonexpansive soil paving	9144.65	1.83
Nonexpansive soil compaction	3041.67	0.61
Total	499973.90	100

Table 8: Carbon emission of the geogrid reinforcement technique.

Construction process	CO_{2-eq} (kg)	Proportion (%)
Geogrid production	27923.52	13.02
Transport of geogrid	73.98	0.03
Geogrid laying	27011.88	12.59
Expansive soil loading	60168.70	28.05
Transport of expansive soil	32659.46	15.22
Expansive soil paving	10863.11	5.06
Expansive soil compaction	1948.30	0.91
Nonexpansive soil loading	41694.00	19.44
Transport of nonexpansive soil	9144.65	4.26
Nonexpansive soil paving	3041.67	1.42
Total	214529.27	100

4.2. Sensitivity Analysis. The LCA results of the two techniques vary with some parameters. If the material is determined, the analysis results depend on the amount of material and the delivery distance. For the LST, the lime consumption is directly determined by the lime content. For the GRT, the geogrid consumption is directly determined by the reinforcement spacing. The treatment scope of the slope is directly determined by the height of embankment and the width of overlapping, which indirectly determine the amount of lime and geogrid. Also, the results of the two techniques are also affected by the distance between the manufacturers of lime and geogrid.

4.2.1. Sensitivity to Lime Content of LST. From the previous analysis, when the lime content is more than 3%, it has better treatment effect on expansive soil roadbed. According to the construction conditions, the lime content should increase appropriately. The current lime content is 4%, 5%, 6%, 7%, and 8%, respectively. Energy consumption and CO_2 emissions were calculated. Other conditions remained unchanged, and the calculation results are shown in Figure 8.

As shown in Figure 8, as the lime content increases by 1%, the total energy consumption increases by 324,236.52 MJ and the effect on the resource consumption increases by 8.27%; the total emissions increase by 65,804.27 kg and the effect on the global warming increases by 13.16%. It can be seen that as the lime content increases, the energy consumption and emissions of the production process also increase. As shown in Tables 5 and 7, the CO_2 emissions and energy consumption in the production process accounted for 65.22% and 40.34%, respectively, in the whole LCA process. As a result, for every 1% increase in lime content, the growth rate of total emissions is greater than that of total energy consumption. Therefore, the global warming is more sensitive to the change of lime content.

4.2.2. Sensitivity to Reinforcement Spacing of GRT. The dimension of reinforcement includes the reinforcement length, reinforcement spacing, and back-wrapping length. For ensuring the slope stability, the reinforcement width is 3.5 m and the back-wrapping length is 1.5 m. The energy consumption and CO_2 emission were calculated when the reinforcement spacing was 0.5, 0.55, 0.6, 0.65, 0.7, 0.75, and 0.8 m, respectively. The calculation results are shown in Figure 9.

As the reinforcement spacing increases by 0.05 m, the total energy consumption decreases by 59,094.96 MJ, and the effect on energy consumption decreases by 1.63%. The total emission decreases by 1,480.54 kg and the effect on global warming decreases by 0.69%. When the embankment height is constant, the increase of reinforcement spacing will change the number of wrapping layers of geogrid, thus reducing the consumption of geogrid materials. However, it is shown from the data that the environmental impact is not sensitive to the change of reinforcement spacing, mainly due to the low energy consumption and emission of production and transportation of geogrid, and its low proportion in the whole LCA process.

4.2.3. Sensitivity to Embankment Height of Two Techniques. The original embankment height is 8 m. The energy consumption and CO_2 emission of the two techniques were calculated when the embankment height is 10 m, 12 m, 14 m, and 16 m, respectively. The heights of bottom and top (0.5 m and 1.5 m, respectively) remained unchanged; that is, the height of the treated slope increased from 6 m to 8 m, 10 m, 12 m, and 14 m, respectively. Other conditions remained unchanged, and the calculation results are shown in Figures 10 and 11.

As shown in Figure 10, the total energy consumptions of LST and GRT increase by 389,675.46 MJ and 655,011.69 MJ, respectively. The increase rate of energy consumption of GRT is about 1.68 times of that of LST's. As the embankment height increases by 1 m from 8 m, the energy consumptions of both techniques increase with the increase of subgrade workload. The increase rate of energy consumption of LST is slower than that of GRT's. There is an intersection point where energy consumption is equal. It is shown that the GRT is more sensitive to the change of embankment height.

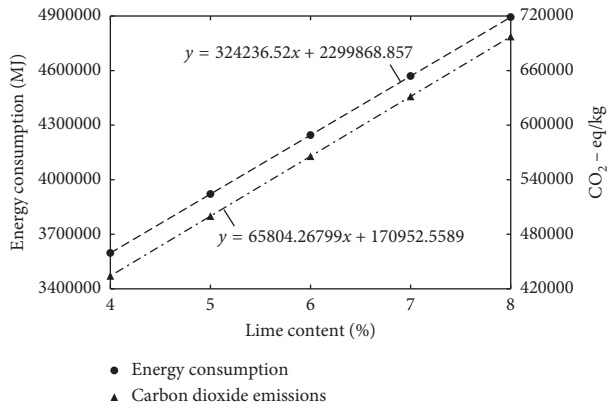

Figure 8: Sensitivity analysis of lime content of the lime stabilization technique.

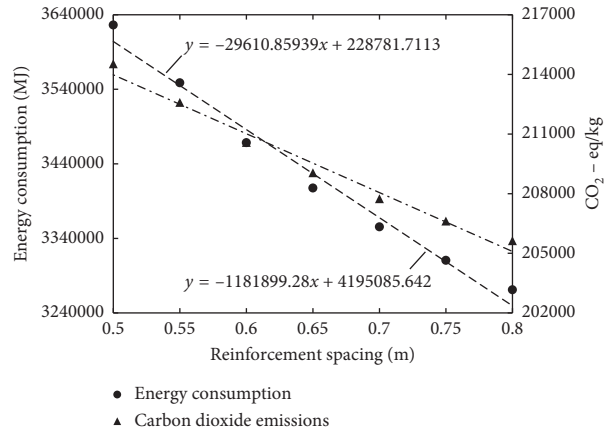

Figure 9: Sensitivity analysis of reinforcement spacing of the geogrid reinforcement technique.

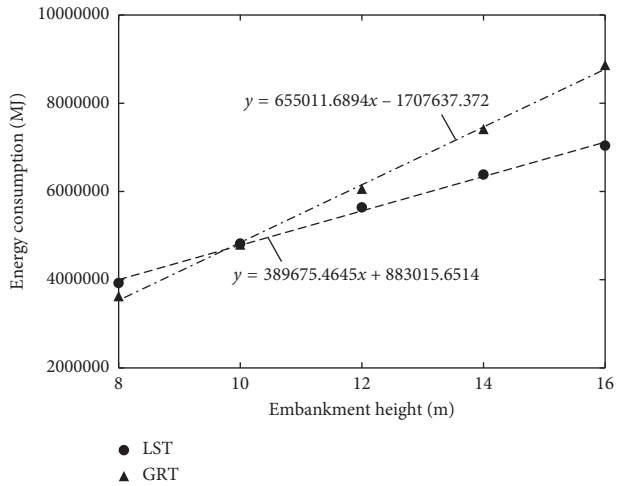

Figure 10: Sensitivity analysis of embankment height to energy consumption.

When the embankment height exceeds 10 m, the LST is more sensitive to the change of embankment height and has more energy-saving advantages.

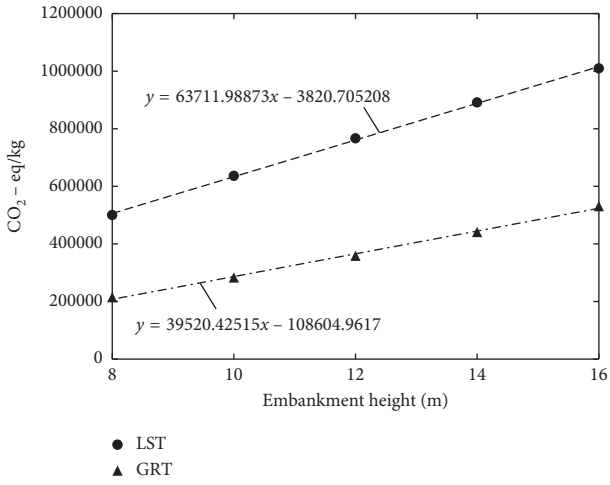

Figure 11: Sensitivity analysis of embankment height to carbon dioxide emissions.

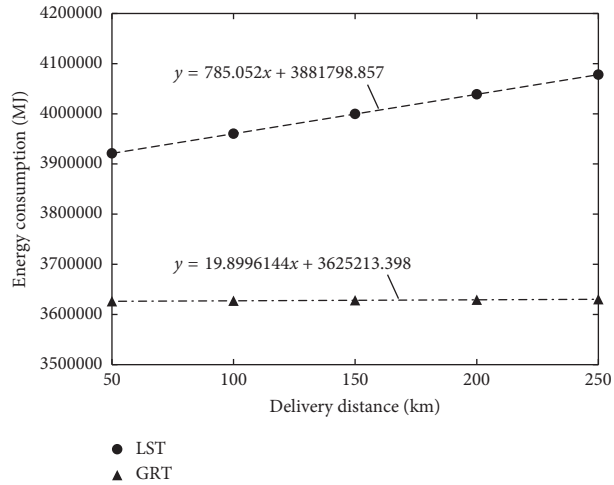

Figure 12: Sensitivity analysis of delivery distance to energy consumption.

As shown in Figure 11, as the embankment height increases by 1 m from 8 m, the total CO_2 emissions of LST and GRT increase by 63,711.99 MJ and 39,520.43 MJ, respectively. The increase rate of CO_2 emissions of LST is 1.61 times of that of GRT's. The LST has an energy-saving advantage when the embankment height is greater than 10 m. However, because of a large number of emissions in the lime production process, with the increase of embankment height, the emissions of LST are still far higher than those of GRT, and there is no emission-reduction advantage.

4.2.4. Sensitivity Analysis to Delivery Distance between the Manufacturer and the Worksite of Two Techniques. The delivery distance between the lime and geogrid manufacturers is 50 km. Assuming that the delivery distance between the manufacturer and the worksite is 100, 150, 200, and 250 km, respectively, other conditions remained unchanged, and the energy consumption and CO_2 emissions of the two techniques were calculated. The calculation results are shown in Figures 12 and 13.

As shown in Figure 12, as the delivery distance between the lime or geogrid manufacturer and the worksite increases by 1 km, the energy consumptions of LST and GRT increase by 785.05 MJ and 19.90 MJ, respectively. The increase rate of energy consumption of LST is about 39.45 times of that of GRT's. In treating the expansive soil slope with the same size, the mass of lime required is much higher than that of geogrid. With the same delivery distance, transportation volume and fuel consumption increase significantly. With the increase of delivery distance between the manufacturer and the worksite, the energy consumption of geogrid does not increase significantly.

As shown in Figure 13, as the delivery distance between the lime or geogrid manufacturer and the worksite increases by 1 km, the CO_2 emission of LST increases by 58.37 MJ and the energy consumption of GRT increases by 1.48 MJ. The increase rate of energy consumption of LST is about 39.44 times of that of GRT's. With the increase of lime delivery

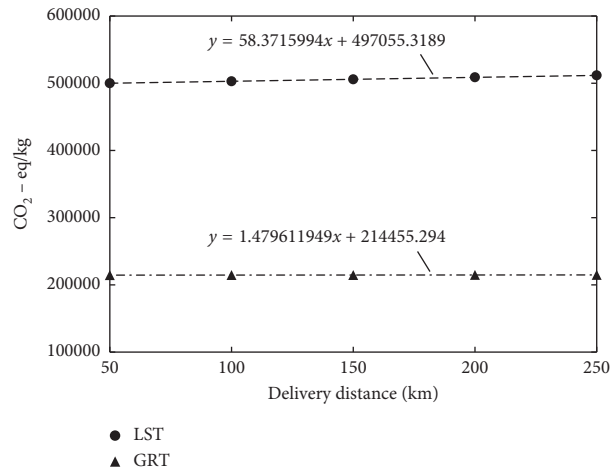

Figure 13: Sensitivity analysis of delivery distance to carbon dioxide emissions.

distance, the energy consumption increases significantly, but transportation emission accounts for a small proportion in the whole LCA process. Therefore, the CO_2 emissions of the two techniques do not show a significant increasing trend.

4.2.5. Sensitivity Analysis to Treatment Width of Two Techniques. The original treatment widths of LST and GRT are 3 m and 3.5 m, respectively. For ensuring the stability of the slope and not wasting materials, the treatment width increases from 3 m to 5 m, and it increases by 0.5 m each time. The energy consumption and CO_2 emissions of two techniques were calculated, respectively, as shown in Figures 14 and 15.

As shown in Figure 14, as the embankment treatment width increases by 0.1 m, the energy consumptions of LST and GRT increase by 56,068.41 MJ and 198.99 MJ, respectively. The increase rate of energy consumption of LST is 281.76 times of that of GRT's. With the increase of embankment treatment width, the volume of treated expansive

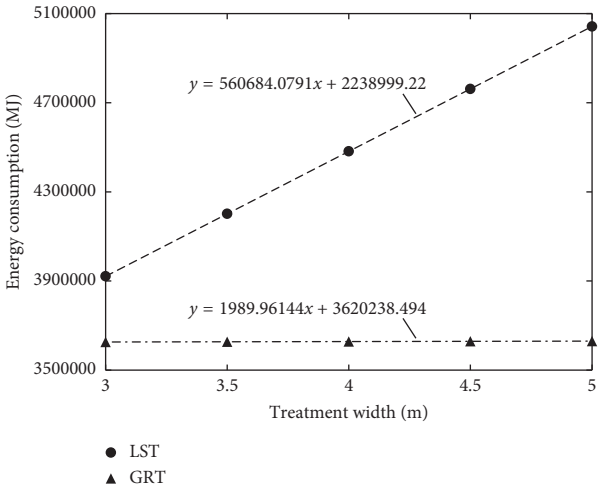

Figure 14: Sensitivity analysis of treatment width to energy consumption.

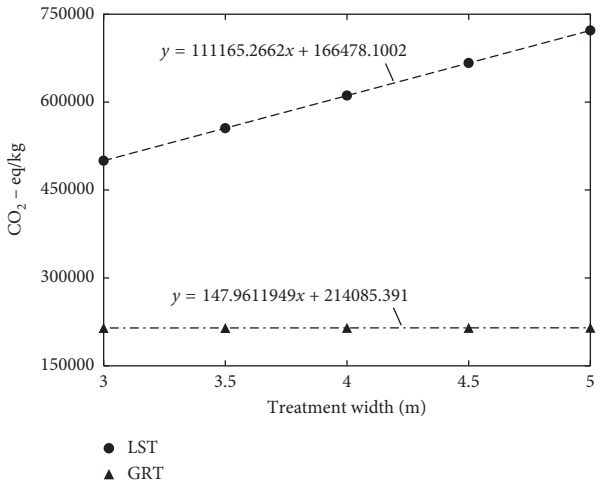

Figure 15: Sensitivity analysis of treatment width to carbon dioxide emissions.

soil increases, and the amount of lime and geogrid increases accordingly. On the one hand, because the lime needs to be evenly mixed in expansive soil, the amount of lime will be significantly increased while the geogrid is wrapped around expansive soil and the increased reinforcing area is limited. On the other hand, because of lime with the secondary mixing process, the volume of lime-stabilized soil will increase and cause additional workload of construction machinery. Therefore, the energy consumption of LST is more sensitive to the treatment width.

As shown in Figure 15, as the embankment treatment width increases by 0.1 m, the CO_2 emissions of LST and GRT increase by 11,116.53 MJ and 14.80 MJ, respectively. The increase rate of CO_2 emissions of LST is 751.12 times of that of GRT's. With the increase of embankment treatment width, the energy consumption of LST increases significantly due to the increase of lime consumption and extra workload, and the CO_2 emissions of lime production are much higher than those of geogrid production, resulting in a significant increase of CO_2 emission. However, the production emission caused by the increase of geogrid consumption is relatively low. Therefore, CO_2 emissions of LST are more sensitive to the treatment width.

5. Conclusions

Based on the LCA results and sensitivity analyses of two techniques, the conclusions are summarized as follows:

(1) The case study on an expansive soil embankment of 8 m high and 24 m wide shows that compared with the LST, the GRT can reduce the energy consumption by 7.52% and CO_2 emissions by 57.09%.

(2) The main sources are raw material production, soil transportation, and paving stage. Because much energy (1,581,930 MJ) is consumed in the lime production process, which is 1.42 times that of the geogrid production process (1,114,392 MJ), a large amount of CO_2 (326,102.76 kg) is released during the reaction process, which is 11.68 times that of the geogrid production process (27,923.52 kg). Therefore, in this study, under the same other conditions, the selection of geogrid materials for the slope reinforcement can significantly reduce the environmental impacts, especially in reducing the impact of global warming. In addition, there is no potential of groundwater pollution in the GRT.

(3) For the LST, as the lime content of LST increases by 1%, the total energy consumption and CO_2 emissions increase by 8.27% and 13.16%, respectively; as the reinforcement spacing of GRT increases by 0.05 m, the total energy consumption and CO_2 emissions increase by 1.63% and 0.69%, respectively. When the geogrid reinforcement spacing decreases, more materials will be consumed, but the environment impact is not obvious.

(4) As the embankment height increases by 1 m, the increase rates of energy consumption and CO_2 emissions of LST are 1.68 and 1.61 times of those of GRT, respectively. The energy consumption of two techniques intersects. When the embankment height is less than 10 m, the GRT has the advantages of energy-saving and emission-reduction.

(5) With the increase of delivery distance between the manufacturer and the worksite, the energy consumption of LST increases obviously in transportation, but the increase of CO_2 emissions is not obvious in transportation. The GRT is not sensitive to the change of delivery distance between the manufacturer and the worksite.

(6) Increasing the width of embankment treatment will increase the amount of lime and geogrid. The LST with larger increase of lime and the additional consumption caused by construction technique is more sensitive to the change of treatment width while the GRT with smaller increase of geogrid and lower production is insensitive to it.

Data Availability

The data used to support the findings of this study are available from the corresponding author upon request.

Conflicts of Interest

The authors declare that there are no conflicts of interest regarding the publication of this paper.

Acknowledgments

This research was funded by China Scholarship Council, the National Natural Science Foundation of China (grant no. 51978085), Highway Industry Standard Compilation Project of Ministry of Transportation (grant no. JTG-201507), and Open Fund of National Engineering Laboratory of Highway Maintenance Technology (Changsha University of Science & Technology) (grant no. kfj180102).

References

[1] J.-L. Zheng, R. Zhang, and H.-P. Yang, "Highway subgrade construction in expansive soil areas," *Journal of Materials in Civil Engineering*, vol. 21, no. 4, pp. 154–162, 2009.

[2] M. Sánchez, D. Wang, J.-L. Briaud, and C. Douglas, "Typical geomechanical problems associated with railroads on shrink-swell soils," *Transportation Geotechnics*, vol. 1, no. 4, pp. 257–274, 2014.

[3] B. Shi, H. Jiang, Z. Liu, and H. Y. Fang, "Engineering geological characteristics of expansive soils in China," *Engineering Geology*, vol. 67, no. 1-2, pp. 63–71, 2002.

[4] J. Jin, Y. Q. Tan, R. H. Liu, J. Zheng, and J. Zhang, "Synergy effect of attapulgite, rubber, and diatomite on organic montmorillonite-modified asphalt," *Journal of Materials in Civil Engineering*, vol. 31, no. 2, Article ID 04018388, 2019.

[5] A. G. Correia, M. G. Winter, and A. J. Puppala, "A review of sustainable approaches in transport infrastructure geotechnics," *Transportation Geotechnics*, vol. 7, pp. 21–28, 2016.

[6] A. A. Ashango and N. R. Patra, "Behavior of expansive soil treated with steel slag, rice husk ash, and lime," *Journal of Materials in Civil Engineering*, vol. 28, no. 7, Article ID 06016008, 2016.

[7] Y. Liu, Y. Su, A. Namdar, G. Zhou, Y. She, and Q. Yang, "Utilization of cementitious material from residual rice husk ash and lime in stabilization of expansive soil," *Advances in Civil Engineering*, vol. 2019, Article ID 5205276, 17 pages, 2019.

[8] T. M. Petry and D. N. Little, "Review of stabilization of clays and expansive soils in pavements and lightly loaded structures-history, practice, and future," *Journal of Materials in Civil Engineering*, vol. 14, no. 6, pp. 447–460, 2002.

[9] S. Chen, S. Yu, L. Kong et al., "Wrapping method for middle expansive soil embankment and its experimental verification," *Chinese Journal of Rock Mechanical Engineering*, vol. 25, no. 9, pp. 1777–1783, 2006.

[10] X. M. Li, L. W. Kong, A. G. Guo et al., "Experimental research on shear strength of expansive soil under wetting-drying cycles based on wrapping method," *Rock Soil Mechanics*, vol. 35, no. 3, pp. 675–682, 2014.

[11] R. R. Al-Omari and F. J. Hamodi, "Swelling resistant geogrid-A new approach for the treatment of expansive soils," *Geotextiles and Geomembranes*, vol. 10, no. 4, pp. 295–317, 1991.

[12] R. Kenley and T. Harfield, "Greening procurement of infrastructure construction: optimizing mass haul operation to reduce greenhouse gas emissions," in *Proceeding of the CIB W78-W102 International Conference*, Sophia Antipolis, France, October 2011.

[13] M. Gangolells, M. Casals, S. Gassó, N. Forcada, X. Roca, and A. Fuertes, "A methodology for predicting the severity of environmental impacts related to the construction process of residential buildings," *Building and Environment*, vol. 44, no. 3, pp. 558–571, 2009.

[14] L. F. Cabeza, L. Rincón, V. Vilariño, G. Pérez, and A. Castell, "Life cycle assessment (LCA) and life cycle energy analysis (LCEA) of buildings and the building sector: a review," *Renewable and Sustainable Energy Reviews*, vol. 29, pp. 394–416, 2014.

[15] M.-L. Pannier, P. Schalbart, and B. Peuportier, "Comprehensive assessment of sensitivity analysis methods for the identification of influential factors in building life cycle assessment," *Journal of Cleaner Production*, vol. 199, pp. 466–480, 2018.

[16] I.-F. Häfliger, V. John, A. Passer et al., "Buildings environmental impacts' sensitivity related to LCA modelling choices of construction materials," *Journal of Cleaner Production*, vol. 156, pp. 805–816, 2017.

[17] E. Hoxha, G. Habert, J. Chevalier, M. Bazzana, and R. Le Roy, "Method to analyse the contribution of material's sensitivity in buildings' environmental impact," *Journal of Cleaner Production*, vol. 66, pp. 54–64, 2014.

[18] B. K. Oh, S. W. Choi, and H. S. Park, "Influence of variations in CO 2 emission data upon environmental impact of building construction," *Journal of Cleaner Production*, vol. 140, pp. 1194–1203, 2017.

[19] A. P. Gursel and C. Ostertag, "Life-cycle assessment of high-strength concrete mixtures with copper slag as sand replacement," *Advances in Civil Engineering*, vol. 2019, Article ID 6815348, 13 pages, 2019.

[20] T. Blankendaal, P. Schuur, and H. Voordijk, "Reducing the environmental impact of concrete and asphalt: a scenario approach," *Journal of Cleaner Production*, vol. 66, pp. 27–36, 2014.

[21] R. Cao, Z. Leng, and S.-C. Hsu, "Comparative eco-efficiency analysis on asphalt pavement rehabilitation alternatives: hot in-place recycling and milling-and-filling," *Journal of Cleaner Production*, vol. 210, pp. 1385–1395, 2019.

[22] J. Turk, A. Mauko Pranjić, A. Mladenovič, Z. Cotič, and P. Jurjavčič, "Environmental comparison of two alternative road pavement rehabilitation techniques: cold-in-place-recycling versus traditional reconstruction," *Journal of Cleaner Production*, vol. 121, pp. 45–55, 2016.

[23] X. Chen and H. Wang, "Life cycle assessment of asphalt pavement recycling for greenhouse gas emission with temporal aspect," *Journal of Cleaner Production*, vol. 187, pp. 148–157, 2018.

[24] A. Mladenovič, J. Turk, J. Kovač, A. Mauko, and Z. Cotič, "Environmental evaluation of two scenarios for the selection of materials for asphalt wearing courses," *Journal of Clean and Production*, vol. 87, pp. 683–691, 2015.

[25] X. Shi, A. Mukhopadhyay, and D. Zollinger, "Sustainability assessment for portland cement concrete pavement containing reclaimed asphalt pavement aggregates," *Journal of Cleaner Production*, vol. 192, pp. 569–581, 2018.

[26] D. N. Huntzinger and T. D. Eatmon, "A life-cycle assessment of portland cement manufacturing: comparing the traditional

process with alternative technologies," *Journal of Cleaner Production*, vol. 17, no. 7, pp. 668–675, 2009.

[27] A. S. Gutiérrez, J. Van Caneghem, J. B. Cogollos Martínez, and C. Vandecasteele, "Evaluation of the environmental performance of lime production in Cuba," *Journal of Clean and Production*, vol. 31, pp. 126–136, 2012.

[28] A. S. Gutiérrez, J. B. Cogollos Martínez, and C. Vandecasteele, "Energy and exergy assessments of a lime shaft kiln," *Applied Thermal Engineering*, vol. 51, no. 1-2, pp. 273–280, 2013.

[29] P. A. Ochoa George, A. S. Gutiérrez, J. B. Cogollos Martínez, and C. Vandecasteele, "Cleaner production in a small lime factory by means of process control," *Journal of Cleaner Production*, vol. 18, no. 12, pp. 1171–1176, 2010.

[30] R. Frischknecht, S. Büsser-Knöpfel, R. Itten et al., "Comparative life cycle assessment of geosynthetics versus concrete retaining wall," in *Proceedings of the 18th International Conference on Soil Mechanics and Geotechnical Engineering: Challenges and Innovations in Geotechnics*, vol. 3, Paris, France, 2013.

[31] G. Heerten, "Reduction of climate-damaging gases in geotechnical engineering practice using geosynthetics," *Geotextiles and Geomembranes*, vol. 30, pp. 43–49, 2012.

[32] F. Yu and S. X. Chen, "Study on determination of treatment depth for expansive soil subgrade in Hefei," *Rock Soil Mechanics*, vol. 27, no. 11, pp. 1963–1967, 2006.

[33] Ministry of Transport of the People's Republic of China, *JTG D30 Specifications for Design of Highway Subgrades*, China Communications Press, Beijing, China, 2015.

[34] Ministry of Transport of the People's Republic of China, *JTG D30 Specifications for Design of Highway Subgrades*, China Communications Press, Beijing, China, 1995.

[35] H. R. Schneider and R. D. Holtz, "Design of slopes reinforced with geotextiles and geogrids," *Geotextiles and Geomembranes*, vol. 3, no. 1, pp. 29–51, 1986.

[36] W. Klöpffer, "The role of SETAC in the development of LCA," *International Journal of Life Cycle Assessment*, vol. 11, no. 1, pp. 116–122, 2006.

[37] Y. Shan, Z. Liu, and D. Guan, "CO2 emissions from China's lime industry," *Applied Energy*, vol. 166, pp. 245–252, 2016.

[38] M. P. Pan, "Research and application of LCA-based calculation method for expressway energy consumption and carbon emissions," *Doctoral dissertation*, South China University of Technology, Guangzhou, China, 2011.

[39] Ministry of Transport of the People's Republic of China, *JTG/T B06-03 Highway Construction Machinery Cost Quota*, Ministry of Transport of the People's Republic of China, Beijing, China, 2007.

Hindawi
Advances in Civil Engineering
Volume 2019, Article ID 1576292, 12 pages
https://doi.org/10.1155/2019/1576292

Research Article

Evaluation of Coupling Coordination among the Urban Physical Environment, Economy, and Population: A Case Study of 36 Main Cities in China

Min Chen, Zhihao Sun, Yuanjie Wang, and Shuaifeng Guo

School of Transportation and Civil Engineering, Nantong University, Nantong, Jiangsu 226019, China

Correspondence should be addressed to Zhihao Sun; 524439668@qq.com

Received 31 May 2019; Accepted 26 August 2019; Published 29 October 2019

Guest Editor: Mbakisya A. Onyango

In the past three decades, about 0.93% of people moved from rural areas to cities per year in China. Therefore, understanding of the relationships among urban physical environment (UPE), economic development, and population growth are significant for China to realize sustainable urban development. Based on the concept and connotation of UPE and ecocity, the UPE evaluation system was constructed containing 6 first-level of indicators (i.e., climate, quality of ambient air and atmosphere, freshwater, wastewater, built environment, and noise pollution) and 13 second-level indicators. An entropy weight-TOPSIS model was developed in order to evaluate the UPE system, using the data of China's 36 main cities from 2003 to 2016. The coupling coordination degree (CCD) among the UPE, economy, and population was measured by a ternary CCD model. The results showed that (1) the UPE of 36 main cities showed periodic fluctuations throughout the 14 years, and the coastal cities and southern cities had superior UPE than the inland cities and northern cities, respectively; (2) the vast majority of cities' CCD had experienced steady upward trends. UPE, economy, and population promoted mutually in most of the cities, but in a few super cities, the economic development and population growth exceeded the capacity of UPE. Meanwhile, the CCD gaps between the northern and southern cities were significantly widened.

1. Introduction

At present, more than 50% of the world's population lives in cities, and the urbanization rate is expected to reach 60% by 2030 [1]. The modern society develops surrounding cities. In China, with the rapid urbanization, the urban population is expected to reach 80% in the next 20 years [2], and 13~15 million peasants will migrate to cities in the following each year [1]. China's urbanization rate is 59.58% in 2018, in an accelerated developing state [3]. As the carrier of human survival and development, UPE bears tremendous pressure from rapid economic development and continuous population growth. Meanwhile, the quality of UPE affects people's migration decision [4, 5], and migration (immigration or emigration) successively affects the city's economic development (growth or and decline). The UPE, economy, and population system of the city constitute a complex social ecosystem, interacting with each other. Examining the relationships among the three systems are crucial for cities to achieve sustainable and healthy development. 36 main cities of China were taken as the study objectives which are of great regional influence, including 4 municipalities, 26 provincial capital cities, and 5 planned cities and Suzhou. It should be noted that Lhasa and Suzhou were two exceptions. Lhasa was excluded from the study cities because of the missing data in most years. In addition, Suzhou was selected because Suzhou is known as for "the most developed prefecture-level city in China," whose GDP is perennially in the top ten among all cities, surpassing most provincial capitals [6].

This research aims to fulfill three primary objectives. Firstly, we intend to construct the UPE indicator system basing on the concept of sustainable development. Secondly, we plan to develop a dynamic entropy weight-TOPSIS

method to evaluate the UPE system of the cities being researched, revealing their dynamic trends and spatial distribution in the period of 2003–2016. Thirdly, this study aims to expound those cities' dynamic trend and spatial distribution of CCD among UPE, economy, and population basing on a ternary coupling model. The rest of the research was organized as follows: Data and methodology are focused on in Section 2 with data sources and preprocessing description, an improved TOPSIS method, and a triple CCD model. An evaluation index system of the UPE, population, and economy is constructed in Section 3. Evaluation results of both the UPE system and the CCD among three systems are given in Section 4. The conclusions and policy implications in this study are summarized in Section 5.

2. Data and Methods

2.1. Data Sources and Preprocessing. The required data of this study were collected from the China Statistical Yearbook, China Environmental Statistics Yearbook, China City Statistical Yearbook, China Agriculture Yearbook, and China Urban Construction Statistical Yearbook, and so on. The missing data were substituted by moving averages. In particular, due to the revision of the Ambient Air Quality Standard (GB3095-2012) by the Chinese Ministry of Environmental Protection in 2012, the monitoring method of pollutants has been changed, two indicators "Air quality" and "Airborne hazardous substances" being involved (Table 1). In order to maintain the comparability of the data before and after 2012, the two indicators were proceeded as follows: with regarding to the indicator "Air quality," we predicted the days of reaching secondary ambient air quality standard in 2012 basing on the data from 2003 to 2011, using the gray prediction method. The difference between the predicted value and the actual value was accepted as an adjustment value to adjust the data after 2012. As for the indicator "Airborne hazardous substances," the content value of PM10 with the changed monitoring method of 2012 has increased about 7% according to relevant research [9], so the values of PM10 content from 2012 to 2016 were subtracted by 7% to ensure the comparability of the data.

2.2. Research Method

2.2.1. Dynamic Entropy Weight-TOPSIS Method. The steps are as follows, using the entropy weight method [10] to determine the weight of the indicators.

Firstly, normalize the indicators:

$$\text{positive indicator, } r_{ij}^{+} = \frac{\left(x_{ij} - \min\left\{x_j\right\}\right)}{\left(\max\left\{x_j\right\} - \min\left\{x_j\right\}\right)},$$
$$\text{negative indicator, } r_{ij}^{-} = \frac{\left(\max\left\{x_j\right\} - x_{ij}\right)}{\left(\max\left\{x_j\right\} - \min\left\{x_j\right\}\right)}, \tag{1}$$

where i is the evaluation object $(i = 1, 2, \ldots, m)$, j is the indicator $(j = 1, 2, \ldots, n)$, and r_{ij} is the normalized value. x_{ij} is the original value and $\max\left\{x_j\right\}$ and $\min\left\{x_j\right\}$ are the maximum and minimum values of the indicator j of all evaluation objects.

Secondly, calculate the weights of indicators:

$$\text{entropy value of indicator, } H_j = -\frac{\sum_{i=1}^{m}\left(r_{ij}/\sum_{i=1}^{m} r_{ij}\right)\ln\left(r_{ij}/\sum_{i=1}^{m} r_{ij}\right)}{\ln(n)},$$
$$\text{weight of indicator, } w_j = \frac{\left(1 - H_j\right)}{\left(n - \sum_{j=1}^{n} H_j\right)}. \tag{2}$$

After using the entropy method to determine the weight, the technique for order preference by similarity to the ideal solution (TOPSIS) will be applied to evaluate the relative merits of the evaluation objects. The traditional TOPSIS method orders the objects by ordering the distance between the evaluation object and the ideal solution (negative-ideal solution). The evaluation object will perform best while it has both the shortest distance from the ideal solution and the farthest distance from the negative-ideal solution, otherwise, perform worst. The distance between the evaluation object and the ideal solution (negative-ideal solution) is given as

$$d_i^{\pm} = \sqrt{\sum_{j=1}^{n}\left(f_{ij} - f_j^{\pm}\right)^2}, \tag{3}$$

where f_{ij} is equal to the normalized value of the indicator multiplied w_j and $f_j^{\pm}$ is the ideal solution (negative-ideal solution).

The relative closeness rc_i is taken as the basis of the TOPSIS ordering and calculated as follows:

$$rc_i = \frac{d_i^{-}}{\left(d_i^{-} + d_i^{+}\right)}. \tag{4}$$

Using the traditional TOPSIS method, the ideal solution and negative-ideal solution at different time points varied; therefore, it is only applicable to order the evaluation object at a certain time point, failing to reflect the time trend of the evaluation objects. So the TOPSIS method was improved by fixing the ideal solutions and negative-ideal solutions, respectively. Specifically, to a certain indicator, the arithmetic means of the maximum value (minimum value) during the study period is taken as the ideal solution (negative-ideal solution).

Then, the ideal solution can be calculated as

$$b_{kj}^{+} = \begin{cases} \max \\ \min \end{cases}\left(f_{1j}(k), f_{2j}(k), \ldots, f_{mj}(k)\right). \tag{5}$$

If the indicator is positive, $b_{kj}^{+} = \max_i f_{ij}(k)$, otherwise, $b_{kj}^{+} = \min_i f_{ij}(k)$.

The negative-ideal solution is calculated as

$$b_{kj}^{-} = \begin{cases} \min \\ \max \end{cases}\left(f_{1j}(k), f_{2j}(k), \ldots, f_{mj}(k)\right). \tag{6}$$

If the indicator is positive, $b_{kj}^{-} = \min_i f_{ij}(k)$, otherwise, $b_{kj}^{-} = \max_i f_{ij}(k)$, where $f_{ij}(k)$ represents the normalized

Table 1: The UPE indicator system.

First-level	Second-level	Description	Properties
Climate	Temperature	Consistency with the optimal temperature range	Positive
	Humidity	Deviation from the optimum humidity range interval	Negative
	Precipitation	Deviation from the equilibrium dryness index	Negative
	Sunshine condition	Annual sunshine hours	Positive
Quality of ambient air and atmosphere	Air quality	Days of reaching secondary ambient air quality standard	Positive
	Airborne hazardous substances	Content of PM10	Negative
Freshwater	Water resource	Water resources per capita	Positive
Wastewater	Sewage treatment rate	Actual volume of sewage treatment (i.e., industrial wastewater and municipal wastewater)	Positive
Built environment [7, 8]	Road	Urban road area per capita	Positive
	Public transport	Number of buses per 10,000 people	Positive
	Urban green level	Green coverage rate in built-up areas	Positive
	Urban construction level	Proportion of built-up areas in urban areas	Positive
Noise pollution	Noise	Equivalent sound level	Negative

value of the indicator and k represents the year ($k = 1, 2, \ldots, N$).

The new distance of the ideal solution (negative-ideal solution) $\overline{d}_i^{\pm}(k)$ is defined as

$$\overline{d}_i^{\pm}(k) = \sqrt{\sum_{j=1}^{n} \left(f_{ij}(k) - \overline{f}_j^{\pm}\right)^2}, \tag{7}$$

where $\overline{f}_j^{\pm} = \sum_{k=1}^{N} b_{kj}^{\pm}/N$ is the new ideal solution (negative-ideal solution).

Lastly, the new relative closeness is calculated as

$$\overline{rc}_i(k) = \frac{\overline{d}_i^{-}(k)}{\overline{d}_i^{-}(k) + \overline{d}_i^{+}(k)}, \tag{8}$$

where $\overline{rc}_i(k)$ is taken as the comprehensive score of the object i in k year.

2.2.2. CCD Model. The concept of "coupling" originated from physics, a process in which two or more elements mutually affect each other [11]. The CCD model is now widely used to measure the relationship between urbanization and eco-environment [12]. This study constructed a ternary CCD model to calculate the coordination degree among the UPE, economy, and population of 36 main cities.

Firstly, the coupling degree is denoted as

$$C_i = \frac{(U_i \times V_i \times Z_i)}{\left((U_i + V_i + Z_i)/3\right)^3}, \tag{9}$$

where U_i, V_i, and Z_i are the comprehensive scores of the three subsystems.

Lastly, CCD score D_i can be calculated as follows:

$$\begin{aligned} D_i &= \sqrt{C_i \times E_i}, \\ E_i &= \alpha \times U_i + \beta \times V_i + \gamma \times Z_i, \end{aligned} \tag{10}$$

where E_i represents the level of effect of three subsystems and α, β, γ are the weights of the subsystems and $\alpha = \beta = \gamma = 1/3$.

According to the scores of CCD, the degree of the coupling coordination among UPE, economy, and population can be divided into six development stages [13] as follows: $0.8 < D \leq 1$, superiorly balanced development; $0.6 < D \leq 0.8$, favorably balanced development; $0.5 < D \leq 0.6$, barely balanced development; $0.4 < D \leq 0.5$, slightly unbalanced development; $0.2 < D \leq 0.4$, moderately unbalanced development; and $0 \leq D \leq 0.2$, seriously unbalanced development.

3. The Indicator System of UPE, Economy, and Population

3.1. The Indicator System of UPE. Quinn et al. [14] concluded that the UPE contained the physical structure and infrastructure of the city, including roads, buildings, parks, and so on. Diez Roux and Mair [15] pointed out that the UPE included not only traditional environmental exposures, such as air pollution but also various aspects of the man-made environment (e.g., land use and transportation, street design, urban design, and public space). Handy et al. [7] deemed that built environment comprises urban design, land use, transportation systems, and people's activities in these physical environments. The Bulletin of American Meteorological Society and the US Department of Agriculture believed that exploring the UPE contribute to improving people's living facilities with the use of vegetation, space, and structure [16]. Therefore, this study defines the UPE as the necessary material environment for urban residents to survive and develop, including the natural physical environment and artificial physical environment.

China's rapid urbanization in the past three decades has aggravated the conflict between environment and economy, population growth [17]. Therefore, the first-level indicator of UPE should be developed basing on the concept of sustainable development, covering the main aspects of the urban material

environment which is essential to human activities. Firstly, four indicators (i.e., quality of ambient air and atmosphere, freshwater, wastewater, and noise pollution) were selected as the first-level indicators, referring to the categories of the environment index in International Urban Sustainability Indicators List (IUSIL) [18]. In addition, focusing on the material environment, some management indicators of the IUSIL were abandoned such as "Waste generation and management" and "Mechanisms to prepare and implement environmental plans." Secondly, climate and built environment were added as the first-level indicators. The reasons are as follows: climate reflects the physical characteristics of the atmosphere, affecting human activities. Climate change can indeed affect human migration, with which even the international mobility of the population changes [19]. Lu et al. [20] found that temperature changes had a significant positive impact on population migration in China. In summary, climate is an indispensable indicator of UPE. Finally, human activities in cities mainly occur in the man-made environment. Hence, the built environment should also be added to first-level indicators. In conclusion, the UPE indicator system was constructed with the six first-level indicators (i.e., climate, quality of ambient air and atmosphere, freshwater, wastewater, built environment, and noise pollution) (shown in Table 1).

The second-level indicators should be both representative and operative. Take the added indicators "Climate" as an example. Although most climate researches focus on temperature and precipitation [21], humidity and sunshine also affect human activities [22]. So the climate indicator in this study includes four second-level indicators, namely, temperature, humidity, precipitation, and sunshine. Firstly, the indicator of temperature should reflect the optimal temperature; we defined the degree of temperature coincidence γ to evaluate the temperature and $\gamma = h/(h - H)$, where h is the difference between the annual maximum temperature and the annual minimum temperature of every city; H is the most comfortable temperature range referring to the China Ambient Air Quality Standards (GB3095-2012). Because the urban temperature ranges of all studied cities are large enough to cover the most comfortable temperature ranges, γ can be set to a positive indicator. Secondly, since the optimal humidity varies from person to person, the optimal relative humidity of the human body should also be a range rather than a certain value. Peteris [23] claimed that the optimum humidity range of human perception is from 45% to 55%; consequently, the offset value of humidity L was defined to measure the humidity indicator, and $L = \sqrt{(x-a)^2 + (x-b)^2}$, where x is the annual average humidity and $[a, b]$ is the optimum humidity range for the human body. The greater the value of L, the greater the distance between the humidity of the city and the optimal humidity range; thus, L is a negative indicator. Thirdly, we use the dryness index to measure whether a city's precipitation is suitable, for the suitable range of precipitation is difficult to be defined directly. When the amount of precipitation is greater than the amount of evaporation, the area is wet; otherwise, the area is dry. The balance of the precipitation and evaporation is accepted as the best dryness, and the value of the dryness will be 1 [24]. The dryness K can be estimated by the formula $K = 58.93 \times \sum(T/12)/P$ [25, 26], where P is the precipitation and T is the biological temperature and $T \in (0, 30)$. We finally use the deviation between a city's dryness index and value 1 to evaluate the precipitation indicator, which is a negative indicator. At last, the indicator of sunshine condition is represented by the annual sunshine index. Considering that the longer the sunshine time, the better for plant growth and solar energy utilization, the indicator is set to be positive.

3.2. The Economic Indicator System and Population Indicator System. The economic indicator system and the population indicator system used in this study refer to the previous study [27, 28]. The economic indicator system contains 4 first-level indicators being divided into 10 second-level indicators (i.e., GDP, fixed asset investment, total retail sales of consumer goods, per capita GDP, percentage of secondary industry in GDP, actual utilization of foreign capital, percentage of tertiary industry in GDP, GDP growth rate, productivity of total industry employed persons, and per capital value-added of tertiary industry) (See Table 2). The population indicator system consists of total population and number of employees (See Table 2).

4. Results and Interpretations

4.1. Evaluate Results of UPE

4.1.1. Time Trends of UPE. The weights of the indicators were calculated by the entropy weight method (see Supplementary Materials (available here)). The first-level indicators were sorted according to the weights with the following results: climate (27.0%), built environment (25.8%), freshwater (16.6%), quality of ambient air and atmosphere (14.6%), noise pollution (8.8%), and wastewater (7.3%). Climate had the highest weight and was the most influential factor at the first level. The second influential factor was the built environment. These two factors occupied 52.8% of the total impact. The entropy weight-TOPSIS method was used to calculate the evaluation scores of the UPE system (see Figure 1 and Supplementary Materials). Kunming had the highest average score of 0.607 among all cities from 2003 to 2016, and Lanzhou had the lowest average score of 0.328. The five cities with the most superior UPE were ranked by the average score: Kunming, Haikou, Shenzhen, Xiamen, and Nanning, meanwhile, with the worst UPE five cities Lanzhou, Zhengzhou, Xi'an, Taiyuan, and Harbin in turn. Figure 1 showed that the evaluation scores of 36 main cities generally revealed upward trends in the long term but fluctuations in the short term during the study period. Further comparison of the values of indicators showed that the rising trends of UPE were mainly caused by the improvement of the built environment and air quality. With regard to the built environment, the value of "The proportion of built-up areas in urban areas" and "per capita urban road area" was growing rapidly from 2003 to 2016. These results can be considered as the consequence of rapid

Table 2: Economic indicator system and population indicator system.

Subsystem	First-level	Second-level	Description	Properties
Economy	Economic aggregates	GDP	The total market value of all final products and services produced within one year	Positive
		Fixed asset investment	The accumulation of physical assets such as machinery	Positive
		Total retail sales of consumer goods	The volume of physical transaction and the service revenue	Positive
		Per capita GDP	GDP divided by the household registered population	Positive
	Economic structure	Percentage of secondary industry in GDP	The added value of the secondary industry divided by GDP	Positive
		Actual utilization of foreign capital	The actually received foreign capital within one year	Positive
		Percentage of tertiary industry in GDP	The added value of the tertiary industry divided by GDP	Positive
	Economic growth	GDP growth rate	Annual growth rate of GDP calculated at comparable prices	Positive
	Economic benefit	Productivity of total industry employed persons	GDP divided by the number of total employees	Positive
		Per capital value-added of tertiary industry	The added value of the tertiary industry divided by the total population	Positive
Population		Total population	Household registered population	Positive
		Number of employees	The number of the population participating in economic activity	Positive

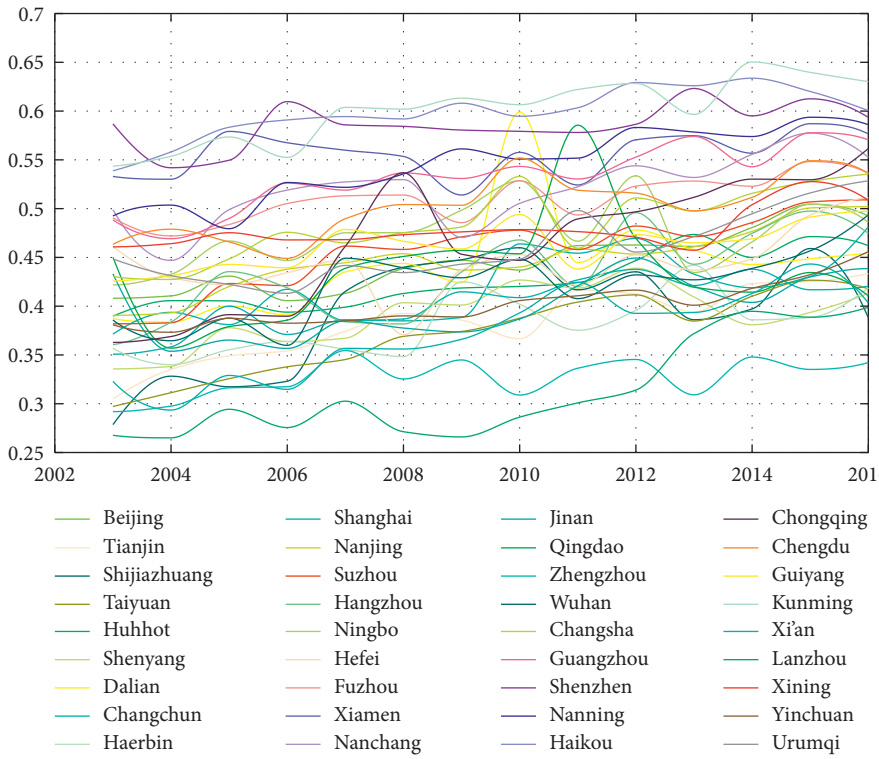

Figure 1: Trends of comprehensive levels of 36 main cities' UPE system.

urbanization and industrialization in China. In fact, most of the cities have experienced unprecedented expansion, and the total urban built-up land area expanded by about 7 times in the past three decades [29]. As for the air quality, China issued the Environmental Air quality Standard (GB3095-2012) in 2012 and the Action Plan for Air pollution Prevention and Control in 2013, recommending to strengthen the monitoring of urban air quality and to significantly reduce the number of inhalable particles. Therefore, after 2013, the air quality improved significantly, presented as the increasing of the reaching secondary ambient air quality standard days and the decreasing of the

PM10 content. In addition, the periodic fluctuation of the UPE primarily attributes to the instability of the climate, with the humidity, precipitation, sunshine, temperature all in fluctuating states. Although the causes of climate instability are still unclear, it is prone to be related to climate warming [30].

The UPE of 36 main cities generally improved rapidly, but a few cities had relatively large fluctuations such as Dalian, Qingdao, and Hefei. Firstly, the UPE score of Dalian increased sharply in 2010 primarily because the average precipitation in Dalian increased by 23.9%, as water resources per capita increased nearly four times in 2009 compared to the previous year. Meanwhile, the appropriate humidity index rose from the 10th place in 2009 to the 1st place in 2010. Secondly, the UPE score of Qingdao also increased sharply in 2011, while the reasons were different. The UPE improvement of Qingdao, mostly due to several much-improved indicators, for example, temperature and humidity of Qingdao, tended to be optimal, the number of per capita buses increased, and the content of PM10 decreased. All these phenomena occurred simultaneously in 2011, leading to a duplicate effect. Finally, the UPE of Hefei undoubtedly showed a downward trend in 2008. The cause may be that the Hefei government committed to building a strong industrial city in 2007. Thus, the number of industrial enterprises increased by more than 500 in 2008 [31], leading to the deterioration of some indicators in the year of 2008. For example, the days of reaching the secondary ambient air quality standard dropped sharply with the ranking dropping from the second to the last, and the ranking of the harmful substance content fell to the fourth from bottom.

In order to deeply compare the improvement of the 36 cities' UPE during the study period, the rankings of 36 main cities' UPE scores in both 2003 and 2016 are plotted in Figure 2. The cities with greater improvement were Chongqing and Suzhou, while Qingdao had the largest decline. From 2003 to 2016, Chongqing's UPE score had the largest amplitude, jumping from the 25th place to 7th. The indicators of "Urban construction level," "Urban green level," and "Air quality" played key roles in the ranking change. During the study period, Chongqing's urban built-up area increased by 906 square kilometers, the green space coverage rate increased by 22.9%, and the days of reaching the secondary ambient air quality standard reached 195 days. As one of the four municipalities directly under the central government, Chongqing has developed rapidly in the past 20 years after the direct administration. The city scale was keeping expanding, with the rapid growth of the built-up area and the increase of urban green coverage. Suzhou was the second-biggest riser, moving up 9 places to 15th mainly due to the decline of airborne hazardous substances. Suzhou issued a document in 2006, announcing the phasing out of backward production capacities, mainly relating to those industries which exert greater pressure on the environment, such as coal, petrochemical, and building materials industries. Thereafter, the emission of waste gas and discharge of industrial wastewater were reduced, and the air quality and water environment quality were obviously improved consequently. Qingdao was the city with the biggest drop in the ranking of UPE and dropped from 20th place in 2003 to 32nd in 2016. This result may be explained by the fact that noise pollution of Qingdao increased by 6.76 decibels in 14 years, much higher than other study cities. Compared with other cities, Qingdao urgently needs to strengthen the noise pollution control.

4.1.2. Spatial Distribution of UPE. To reveal the geographical distribution of UPE, the spatial distribution maps of the 36 main cities' UPE in 2003 and 2016 are shown in Figure 3 and 4. In general, the coastal or riverside cities had higher UPE scores than those cities of inland. This means that the cities located in the coastal areas (e.g., Guangzhou, Shenzhen, Fuzhou, Xiamen, and Haikou) and the cities along the Yangtze river (e.g., Nanchang, Wuhan, Changsha, and Chengdu) have more superior UPE. Secondly, there were notable differences between the northern and southern urban agglomerations, and the UPE scores of the southern cities were higher than northern cities in general. Moreover, the high-scoring urban agglomerations were more concentrated in the south in 2016 than in 2003, while a small number of northern cities' UPE scores even declined, such as Jinan, Qingdao, Xining, and Yinchuan.

There are several possible explanations for this result. Firstly, the winter weather is cold in northern China, accompanied by the dry climate and big temperature gap, resulting in the low scores of the climate indicator. Secondly, the air quality of northern China is poor. On the one hand, sandstorms occur frequently because of the low coverage of surface vegetation and grassland desertification; comparatively, coal-fired heating and thermal power generation were widely used in northern cities which exacerbate air pollution [32]. In contrast to the northern cities, southern cities' UPE were relatively better. The results may be explained by the following facts. Most of the southern cities are located in the frontier area of reforming and opening-up and experienced the rapid expansion of the built environment; simultaneously, the climate condition of southern cities are better than the northern cities with warm and humid climate and rich precipitation as well. Furthermore, because of the high precipitation, suspended particles are not easy to float in the air, leaving the air quality generally better than that of the north.

4.2. CCD among UPE, Economy, and Population

4.2.1. Time Trends of the CCD. The results of CCD among UPE, economy, and population of 36 main cities are shown in Figure 5. During the study periods, the CCD of 36 main cities demonstrated overall increasing trends, and the average CCD score of each city was 0.467. The evolution of the CCD system appeared to have two distinct time periods. Before 2009, most of the cities conformed to the "unbalanced development" stage. Afterward, most of the cities moved to the "balanced development" stage. From 2003 to 2008, only five cities achieved the "favorable balanced development" stage. Most of the other cities' CCD scores were between 0.4 and 0.6; in other words, they were in the phase of "barely

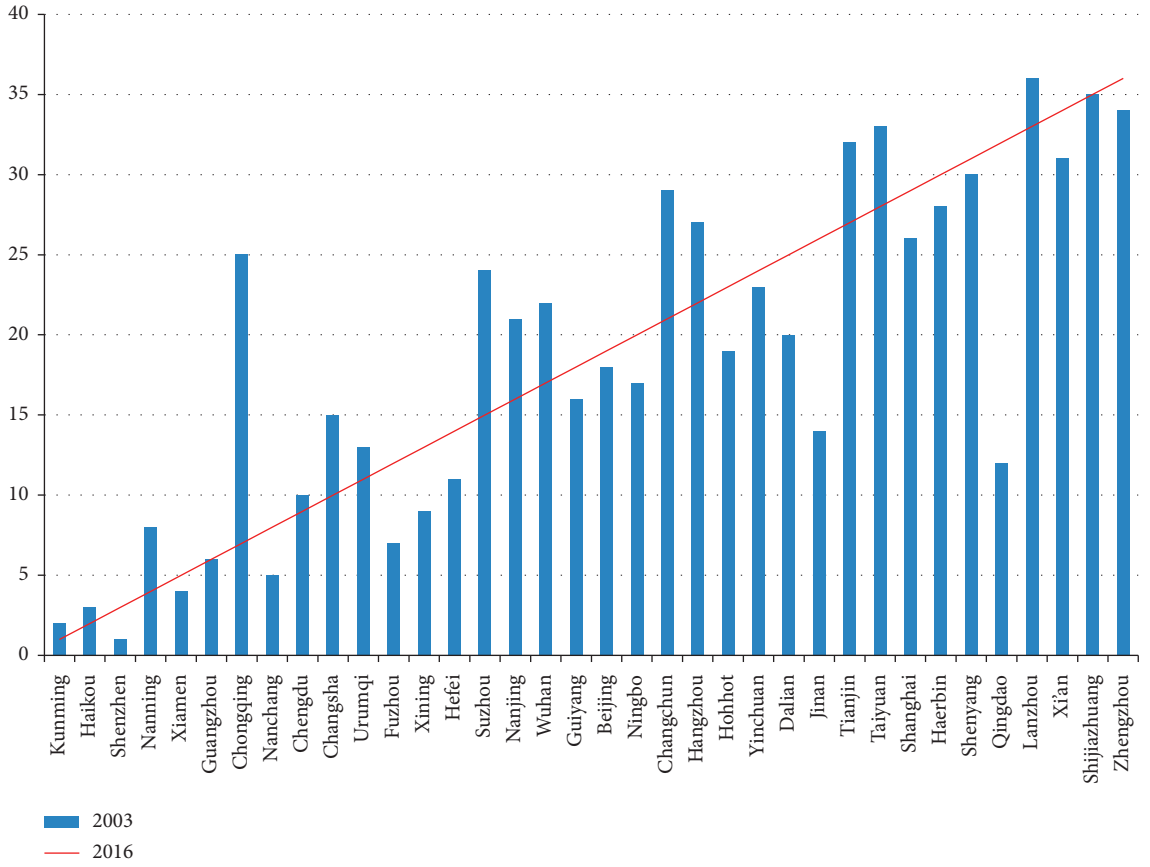

Figure 2: Ranking changes of 36 main cities' UPE scores in 2003 and 2016.

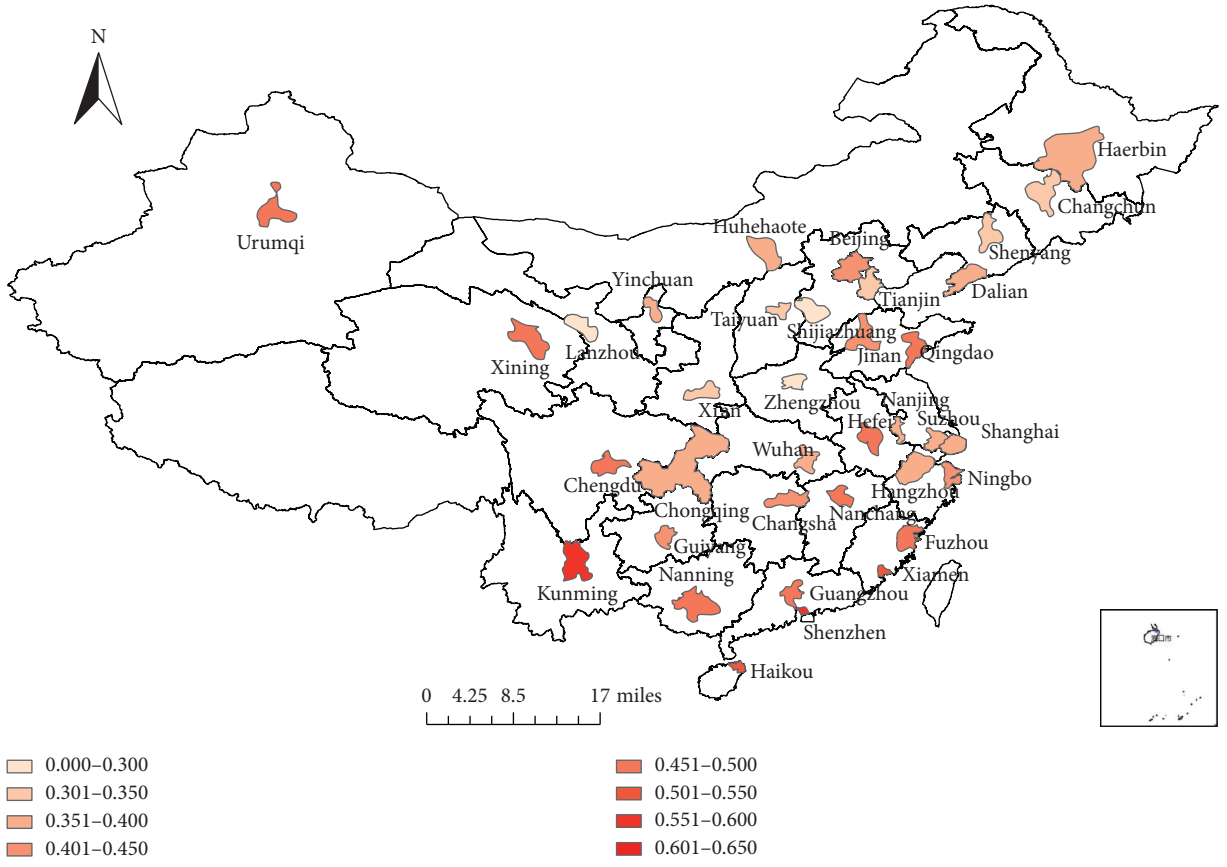

Figure 3: Spatial distribution of 36 main cities' UPE scores in 2003.

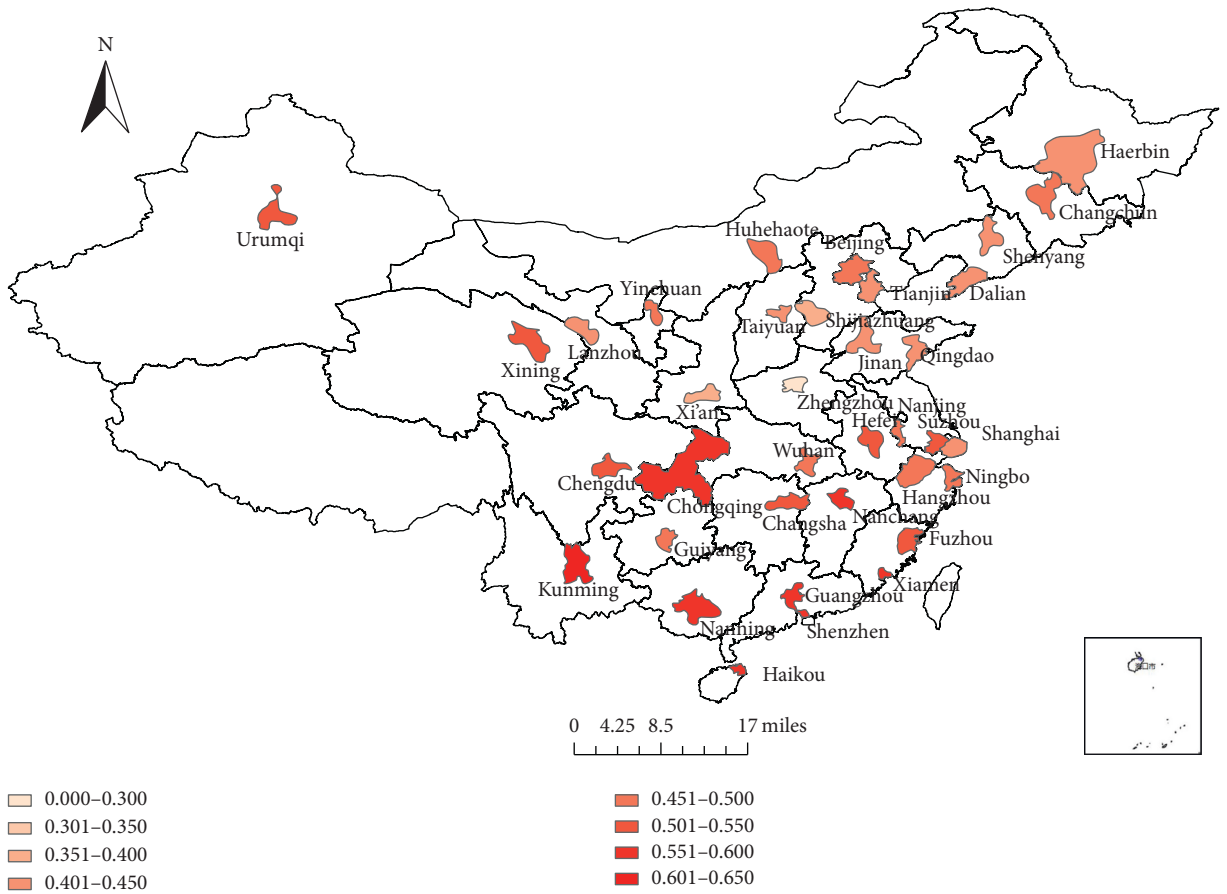

Figure 4: Spatial distribution of 36 main cities' UPE scores in 2016.

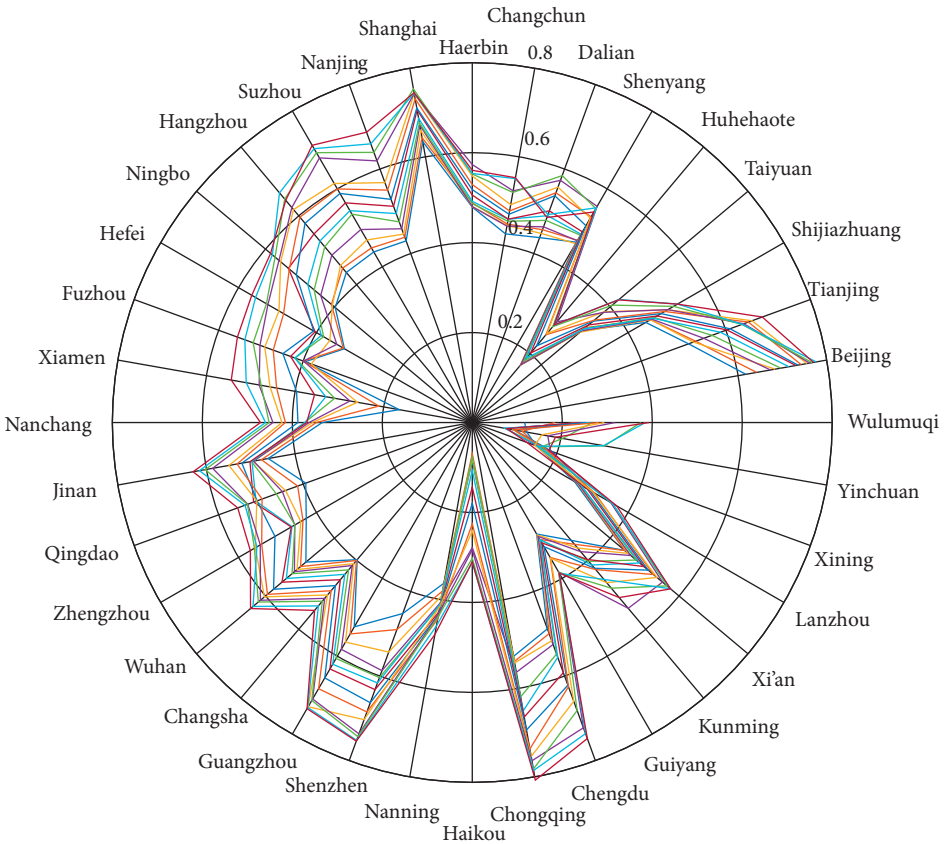

Figure 5: Radar diagram of CCD among UPE, economy, and population.

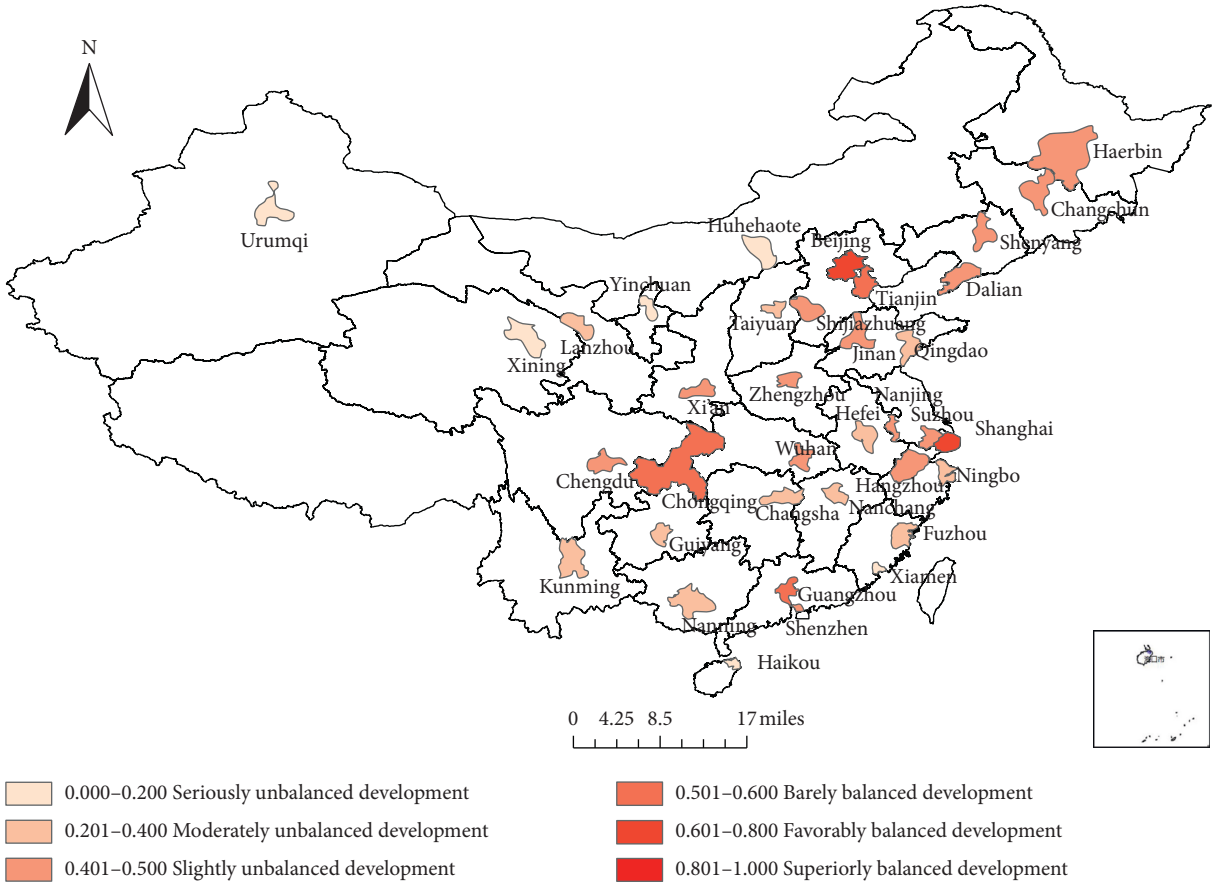

Figure 6: Spatial distribution of CCD in UPE, economy, and population in 2003.

unbalanced development" or "slightly unbalanced development." From 2009 to 2016, the CCD score of most cities had reached above 0.5, and twelve cities reached the stage of "favorable balanced development."

During the 14 years, the CCD scores of the super cities (i.e., Beijing, Shanghai, Shenzhen, and Guangzhou) were in the "favorably balanced development" stage, but the scores of Beijing and Shanghai had little increase after 2011. The specific scores of the three systems revealed that the economic development level and population growth level both exceeded the comprehensive UPE level in those two cities. Chongqing's CCD is of the fastest growing. In 2016, Chongqing became the only city that reached the "superiorly balanced development" phase. A possible explanation for this may be Chongqing has the absolute advantage of attracting immigration as the only municipality directly under the central government in the vast western region of China. Chongqing exhibited a development mode that population gathered, with the UPE improving and economic growth followed by. It should be pointed out that Dalian's CCD score plummeted in 2015; the main cause may be that the Liaoning Provincial Government began to strictly examine and verify the official statistics since 2015, leading to the shrink of Dalian's GDP and population data [33]. Comparing the specific scores of the three subsystems (see Supplementary Materials), the UPE scores of the majority study cities were higher than the scores of economy and population, which illustrated that the main development mode in China was the government invested the infrastructure first, and then introduced industries and attracted population. However, the rapid development of the economy and the continuous accumulation of population placed increasing pressure on the UPE. When the UPE capacity was exceeded, the CCD would stop growing or fall back, just as Beijing and Shanghai.

4.2.2. Spatial Distribution of CCD. The spatial distribution maps of CCD in 2003 and 2016 are shown in Figure 6 and 7. The CCD presented a diversified distribution pattern among different urban agglomerations. For a certain urban agglomeration, the core city takes the high CCD score as the leader. For example, Beijing, Shanghai, Shenzhen, and Chongqing had the highest CCD scores in the four urban agglomerations of Beijing-Tianjin-Hebei, the Yangtze River Delta, the Pearl River Delta, and the Chengdu-Chongqing, respectively. The CCD scores of the cities in the northwest (Yinchuan, Xining, and Urumqi) and northeast (Shenyang, Changchun, Harbin, and Dalian) were generally at a lower level. With the comparison of Figures 6 and 7, the growth rates of CCD in those two regions were much lower than the cities in the south during the 14 years, and the gap was widening. However, the reasons for the poor CCD of the two regions may be slightly different. The comprehensive UPE

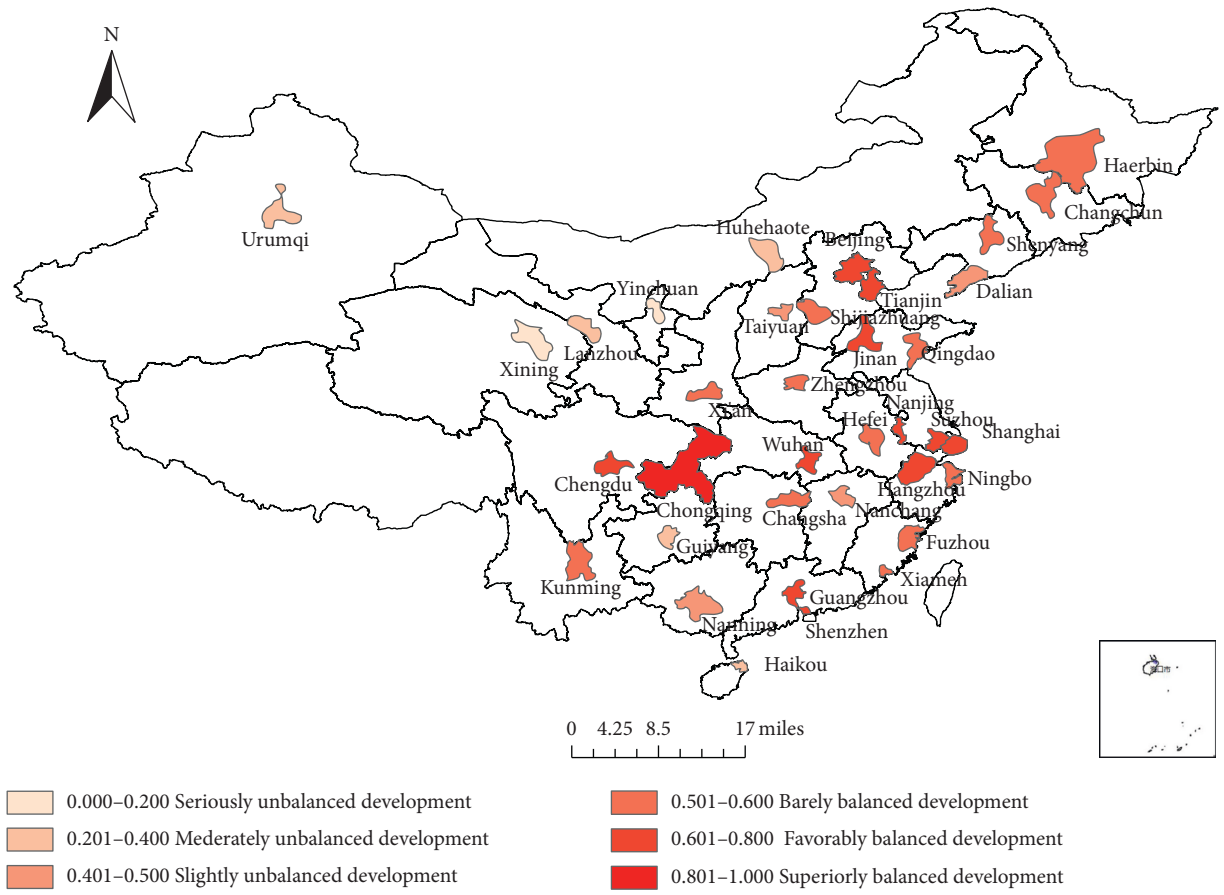

Figure 7: Spatial distribution of CCD in UPE, economy, and population in 2016.

scores of the cities in northeast China (Shenyang, Changchun, and Harbin) were at a medium level, but their climate scores were at the lowest level among all study cities because of the extremely cold climate, which probably results in the large population migration; for example, Harbin had experienced population loss, which was rare in all the study cities. The reason for the poor CCD in the northwestern region (Yinchuan, Xining, and Urumqi) should attribute to the joint action of the poor economic foundation and weak centripetal force of population gathering. The CCD of Xining, Hohhot, and Yinchuan had not made significant progress, especially Xining, which was always in the "seriously unbalanced development" stage during the study period.

5. Conclusions and Discussion

During the last two decades, most of the Chinese cities have experienced a rapid development process. The economic development, population growth placed increasing pressure on the urban environment. Under the background of rapid urbanization, the UPE index system and the triple CCD model developed in this study make it possible to further study the relationship between UPE, economy, and population. Such empirical work can provide an evidence base for future attempts to achieve more sustainable city development.

The results of this research suggest that the indicator of climate (27.0%) made the greatest contribution to the UPE level. The fluctuation of the UPE level mainly attributed to the cyclical changes of climate. The indicator of the built environment weighted the second largest (25.8%) in the UPE system. The overall UPE level of the study cities had slightly improved during 14 years, which were mainly resulted from the continuous improvement of the built environment, the improved water quality after 2008, and the improved air quality after 2013. These results revealed that the changeable climate made the UPE system fragile. Those cities with insufficient natural endowment must pay more attention to the adverse impacts of industrial development and the population expansion on the UPE and adhere to the new road of industrialization to achieve the coordinated development among UPE, economy, and population.

The CCD of 36 cities had generally increased steadily, most of which presented a path of city development, the improvement of UPE drive the industry, and the industry attract the population. However, in certain super cities (i.e., Beijing and Shanghai), the economy and population development exceeded the carrying capacity of the UPE. This result suggests that most of China's main cities still have a considerable room of the UPE system, but the government should recognize the capacity limitation of the UPE and strive to reduce the environmental impact of the population agglomeration and economic growth by enforcing reduction

pollution. Meanwhile, some measures must be taken to increase the capacity of the UPE, such as increasing housing supply, improving public transportation systems, and so on.

The CCD of the study cities showed obvious regional differences. In general, the southern cities were of better coupling coordination than the northern cities. Due to the relatively backward economy and slowly growing population, the coupling coordination of both northwest and northeast regions improved slowly. Our findings implicated these cities should seize the opportunity of the national strategy to promote balanced development. As the node cities of the new Silk Road, the northwest cities including Xi'an, Lanzhou, Xining, and Urumqi should take full advantage of the One Belt One Road strategy to develop the economy. The cities located in the northeast region should fully utilize the preferential policies of Northeast Revitalization to promote the reflow of high-quality population.

Data Availability

The raw data used to support the findings of this study are available from the corresponding author upon request.

Conflicts of Interest

The authors declare that they have no conflicts of interest.

Acknowledgments

This work was supported by the Ministry of Housing Urban-Rural Development of China (2018R2024) and the Practice and Innovation Fund for University Students of Jiangsu Province (201910304039Z).

Supplementary Materials

Table 1: weights of the UPE system; Table 2: weights of economic and population system; Table 3: comprehensive scores of the UPE system; Table 4: comprehensive scores of the economic system; Table 5: comprehensive score of the population system; and Table 6: the scores of CCD among UPE, economy, and population. (*Supplementary Materials*)

References

[1] J. Luo, X. Zhang, Y. Wu, J. Shen, L. Shen, and X. Xing, "Urban land expansion and the floating population in China: for production or for living?," *Cities*, vol. 74, pp. 219–228, 2018.

[2] G.-Y. Cao, G. Chen, L.-H. Pang, X.-Y. Zheng, and S. Nilsson, "Urban growth in China: past, prospect, and its impacts," *Population and Environment*, vol. 33, no. 2-3, pp. 137–160, 2012.

[3] J. Shang, P. Li, L. Li, and Y. Chen, "The relationship between population growth and capital allocation in urbanization," *Technological Forecasting and Social Change*, vol. 135, pp. 249–256, 2018.

[4] R. Black, W. N. Adger, N. W. Arnell, S. Dercon, A. Geddes, and D. Thomas, "The effect of environmental change on human migration," *Global Environmental Change*, vol. 21, pp. S3–S11, 2011.

[5] B. Cao, K. Fu, J. Tao, and S. Wang, "GMM-based research on environmental pollution and population migration in Anhui province, China," *Ecological Indicators*, vol. 51, pp. 159–164, 2015.

[6] L. Wang, J. Shen, and C. K. L. Chung, "City profile: Suzhou—a Chinese city under transformation," *Cities*, vol. 44, pp. 60–72, 2015.

[7] S. L. Handy, M. G. Boarnet, R. Ewing, and R. E. Killingsworth, "How the built environment affects physical activity," *American Journal of Preventive Medicine*, vol. 23, no. 2, pp. 64–73, 2002.

[8] R. Ewing, "Can the physical environment determine physical activity levels?," *Exercise and Sport Sciences Reviews*, vol. 33, no. 2, pp. 69–75, 2005.

[9] J. Xu, H. Fan, D. Li, J. Deyu, and W. Linlin, "On analysis of the increased reasons and control measure on the PM10 pollution in Dalian city," *Environment and Sustainable Development*, vol. 40, no. 3, pp. 129–131, 2015, in Chinese.

[10] B. M. dos Santos, L. P. Godoy, and L. M. S. Campos, "Performance evaluation of green suppliers using entropy-TOPSIS-F," *Journal of Cleaner Production*, vol. 207, pp. 498–509, 2019.

[11] Y. Li, Y. Li, Y. Zhou, Y. Shi, and X. Zhu, "Investigation of a coupling model of coordination between urbanization and the environment," *Journal of Environmental Management*, vol. 98, pp. 127–133, 2012.

[12] J. Lu, H. Chang, S. Zhao, and C. Xu, "The evolution of coupling relationship among energy, economy and environment in Shandong province," *Economic Geography*, vol. 36, pp. 42–48, 2016, in Chinese.

[13] Z. Tang, "An integrated approach to evaluating the coupling coordination between tourism and the environment," *Tourism Management*, vol. 46, pp. 11–19, 2015.

[14] A. Quinn, D. Vlahov, D. Ompad, and S. Galea, "Physical urban environment," in *Encyclopedia of Environmental Health*, J. O. Nriagu, Ed., pp. 526–535, Elsevier, Burlington, NJ, USA, 2011.

[15] A. V. Diez Roux and C. Mair, "Neighborhoods and health," *Annals of the New York Academy of Sciences*, vol. 1186, no. 1, pp. 125–145, 2010.

[16] C. J. Shultz, L. D. Garey, E. V. Schultz, G. T. Stano, R. J. Blakeslee, and S. J. Goodman, "Integration of the total lightning jump algorithm into current operational warning environment conceptual models," in *Proceedings of the AMS Annual Meeting*, American Meteorological Society, Atlanta, Georgia, February 2014.

[17] Z. Pingyu, S. Fei, L. He, and S. Qiu, "Coordination degree of urban population, economy, space, and environment in shenyang since 1990," *China Population, Resources and Environment*, vol. 18, no. 2, pp. 115–119, 2008.

[18] L.-Y. Shen, J. Jorge Ochoa, M. N. Shah, and X. Zhang, "The application of urban sustainability indicators—a comparison between various practices," *Habitat International*, vol. 35, no. 1, pp. 17–29, 2011.

[19] R. McLeman, "Developments in modelling of climate change-related migration," *Climatic Change*, vol. 117, no. 3, pp. 599–611, 2012.

[20] H. Lu, J. Wen, and W. Xu, *Research on the Effects of Climate Change on Population Mobility in China*, pp. 77–84, China Academic Journal Electronic Publishing House, Beijing, China, 2017, in Chinese.

[21] M. Chang, C. Dereczynski, M. A. V. Freitas, and S. C. Chou, "Climate change index: a proposed methodology for assessing susceptibility to future climatic extremes," *American Journal of Climate Change*, vol. 3, no. 3, pp. 326–337, 2014.

[22] P. Zhang, J. Zhang, and M. Chen, "Economic impacts of climate change on agriculture: the importance of additional climatic variables other than temperature and precipitation," *Journal of Environmental Economics and Management*, vol. 83, pp. 8–31, 2017.

[23] S. Peteris, S. Andrejs, K. Galina, and S. Janis, "Potential of solar cooling in Latvian conditions," *Energy Procedia*, vol. 57, pp. 2629–2635, 2014.

[24] J. T. Houghton, L. G. Meiro Filho, B. A. Callander, N. Harris, A. Kattenburg, and K. Maskell, *Climate Change 1995: The Science Of Climate Change*, pp. 367-368, Cambridge University Press, Cambridge, UK, 1996.

[25] M. Meng, J. Ni, and Z. Zhang, "Aridity index and its applications in geo-ecological study," *Chinese Journal of Plant Ecology*, vol. 28, no. 6, pp. 853–861, 2004, in Chinese.

[26] X. Zhang, D. Yang, and W. Ni, "The potential evapotranspiration (PE) index for vegetation and vegetation-climatic classification (III): an introduction of main methods and PEP program," *Chinese Journal of Plant Ecology*, vol. 17, pp. 97–109, 1993, in Chinese.

[27] Y. Liu, C. Yao, G. Wang, and S. Bao, "An integrated sustainable development approach to modeling the eco-environmental effects from urbanization," *Ecological Indicators*, vol. 11, no. 6, pp. 1599–1608, 2011.

[28] Q. Han, X. Xu, and W. Chang, "Study on city's ecological environment and assessment index system of sustainable development," *Environmental Protection Science*, vol. 31, pp. 52–55, 2005, in Chinese.

[29] Z. Zhang, J. Liu, and X. Gu, "Reduction of industrial land beyond Urban Development Boundary in Shanghai: differences in policy responses and impact on towns and villages," *Land Use Policy*, vol. 82, pp. 620–630, 2019.

[30] X. Wang, D. Jiang, and X. Lang, "Future extreme climate changes linked to global warming intensity," *Science Bulletin*, vol. 62, no. 24, pp. 1673–1680, 2017.

[31] National Bureau of Statistics of China, "China Statistical Yearbook 2008," National Bureau of Statistics of China, Beijing, China, 2008.

[32] X. Wang, Z. Dong, J. Zhang, and L. Liu, "Modern dust storms in China: an overview," *Journal of Arid Environments*, vol. 58, no. 4, pp. 559–574, 2004.

[33] The release of GDP data for 31 provinces: Liaoning shrank bymore than 600 billion yuan, 2017, in Chinese, https://www.yicai.com/video/5232162.html.

Hindawi
Advances in Civil Engineering
Volume 2019, Article ID 4956067, 14 pages
https://doi.org/10.1155/2019/4956067

Research Article

Behavior Selection of Stakeholders toward Megaproject Social Responsibility: Perspective from Social Action Theory

Linlin Xie,[1] **Ting Han**,[1] **Haitao Chu**,[2] **and Bo Xia**[3]

[1]*South China University of Technology, School of Civil Engineering & Transportation, Guangzhou 510000, China*
[2]*Tongji University, School of Economics and Management, Shanghai 200000, China*
[3]*Queensland University of Technology, School of Civil Engineering and Built Environment, Brisbane 4001, Australia*

Correspondence should be addressed to Haitao Chu; huddechu@tongji.edu.cn

Received 17 February 2019; Accepted 23 August 2019; Published 24 October 2019

Guest Editor: Endong Wang

The importance of social responsibility strategy for the sustainable development of megaprojects has been widely concerned, while types and motivations of social responsibility behavior have also been analyzed and examined in the corporate management literature. However, the typical social responsibility behaviors in megaprojects and the various motivations and factors that influence stakeholders' selection of social responsibility behavior have not been fully considered and confirmed. In this study, camouflage behavior and collaborative behavior are taken as representative social responsibility behaviors. Based on the social action theory, the impact of relevant influencing factors is empirically examined and stakeholder's selection of these two behaviors toward megaproject social responsibility (MSR) is explored. Results from the sample data of 127 management staff with megaproject experience from the participating parties revealed that synergistic behavior is driven mainly by relationship quality (RQ), whereas hypocritical behavior is affected by RQ, institutional pressure, and external appeals. In addition, the mutual feedback mechanism significantly improves the RQ of participating parties, which indirectly affects both behaviors. These findings bear implications in realizing the management of social responsibility behavior in megaprojects and guiding the participating parties to coordinate and implement social responsibility.

1. Introduction

Megaproject social responsibility (MSR) refers to the obligation of megaproject participating parties on the social and environmental impacts of their decisions and activities through transparent and ethical behavior during the project life cycle [1, 3]. Under the current emphasis on green development and social stability, megaprojects are increasingly prioritizing cross-integration with society [4], economy [5], culture [6], and ecology [7]. MSR is undoubtedly an important "value" element in measuring the success of engineering projects.

MSR is closely related to the behavior of stakeholders. Unlike the corporate social responsibility (CSR) of a single organization, MSR involves multiple participating parties, and the fulfillment of their social responsibilities requires engagement from a large number of other participating parties [8–10]. The lack, improperness, or alienation of any party's behavior toward responsibility may damage the investment efficiency and break the social image of the project and even lead to its termination [11, 12]. Construction accidents and casualties in many megaprojects are caused by the contractor's low safety cognition [13]. Moreover, the role of the stakeholders' social responsibility in many megaprojects is often vague, thus inducing negativity toward social behavior, such as violating social responsibility for personal gain, evading one's social responsibility, or exhibiting hypocritical behavior (HB) [14]. Successful implementation of MSR requires close cooperation among all parties during the entire project life cycle. However, the motivations and factors that influence the social responsibility behavior of each stakeholder vary, thus leading to different MSR behaviors (MSRBs). Their behavior exhibits remarkable multiheterogeneity, complex

situational dependence, and dynamic evolution [14]. As the project phase advances, various factors, such as construction environment, project system, and public appeals, affect the behavior selection of social responsibility.

In-depth exploration of the underlying mechanism of stakeholders' MSRB selection is necessary to achieve effective social responsibility behavior management and ensure the synergy of the social responsibility behavior at all stages of the project life cycle. Parsons' social action theory holds that social action includes four main elements, namely, actor, behavioral purpose, condition and means, and normative orientation. Purpose is the future state of affairs expected by the subject; conditions and means clarify the situation that the subject can and cannot control, respectively; and normative orientation indicates the subject's preference of means. Based on this theory, previous studies summarize the correspondence among the elements of behavioral systems, such as MSR subjects, behavior, and situations. Key actors, such as construction units and governments, are identified, and unilateral and interactive behaviors are classified. In addition, situation is introduced to construct a MSRB selection model, which emphasizes that the stakeholders' selection of social responsibility behavior is under the combined effect of the internal characteristics of the organization, interorganizational relations, and external scenarios in megaprojects [14].

However, the effect of these aspects (i.e., internal characteristics, interorganizational relations, and external scenarios) on the actors' behavior selection in megaprojects and the degree of impact remain unclear. This study aims to empirically test the impact of relevant influencing factors on MSRB. First, HB and synergistic behavior (SB) are selected as endogenous variables. HB symbolizes the phenomenon in which the subject's behavior is exaggerated and falsified when performing social responsibility [15]. SB is characterized by the multisubject and synergistic implementation of MSR and improvement of social welfare [16]. Second, the influencing factors of the three levels (i.e., the institutional pressure (IP) and mutual feedback mechanism (MFM) at the external scenarios level, relationship quality (RQ) and external appeal (EA) at the interorganizational relationship level, and the social responsibility cognition (SRC) at the internal level of the organization) are identified as exogenous variables. The influence path model between endogenous and exogenous variables is constructed. This study explored the behavior selection mechanism of stakeholders toward MSR through survey questionnaires. Finally, the core viewpoints are summarized, and the guiding suggestions for carrying out major engineering social responsibility behaviors are given on the basis of the empirical results combined with the actual social responsibility of major projects.

2. Theoretical Background and Research Hypothesis

2.1. Social Responsibility Behavior in Megaprojects. MSRB means that under the combined effect of institutional environment and social pressure, the stakeholder attempts to cope with MSR issues related to the organization and the corresponding actions taken for this purpose, whether positive or negative, because of the social responsibility consciousness of the organization [14]. The stakeholders' choice of social responsibility behavior in specific projects not only depends on their own traits [17] but also on the project characteristics and other participants because different stakeholders have distinct social responsibilities in various project stages.

Research on social responsibility of construction projects is in its primary exploration stage. In the existing literature, the mechanism of social responsibility is discussed mainly around a single subject [18]. Moreover, as a contractor bears the MSR for construction, the social responsibility behavior of the contractor has become the focus of attention from all walks of life. For example, Qi et al. [19] proposed the green construction driving mechanism and action path of construction enterprises. Liu and Liang [20] started from the road construction stage to explore the cultivation path of the social responsibility behavior of the contractor. Basing on a stakeholder perspective, Liao et al. [21] identified seven stakeholders in the construction industry and constructed a social responsibility behavior framework that involves various stakeholders to guide the construction company to implement social responsibility behavior at the project level. However, MSR involves multiple stakeholders and complex project construction backgrounds. Existing social responsibility behavior analysis, situational research, and driving mechanisms from the perspective of single corporation are not fully compatible with MSR [14]. The objective laws of social responsibility behavior in the selection and evolution of major projects must be explored.

Xie et al. [14] emphasized that MSRBs include unilateral and interactive behaviors. In unilateral behavior, disguise behavior is negative based on the perspective of social responsibility performance. This behavior is similar to greenwashing, which means that the enterprise intentionally uses symbolic rather than substantive behavior [22]. In contrast with the lack of social responsibility, this behavior implies that the actors are aware and have made a commitment or propaganda but have not practiced their social responsibility [23]. Such fraudulent behavior should be avoided in megaprojects because it not only does not improve social welfare but also wastes valuable social public resources. In megaprojects, the ability of social responsibility behavior subjects cannot be limited to a large number of social responsibilities. In the face of pressure from the public media and supervision by various stakeholders, they may opt to pretend to win by word-of-mouth and establish a good image. This study defines this hypocritical social responsibility behavior as disguise, which is a false fraudulent behavior in which the subject pretends to perform social responsibility to maintain its own image or under external pressure.

In interactive behavior, SB is a positive social behavior that is conducive to improve social well-being. This behavior is in line with the concept of collaborative governance called for in today's megaproject construction [16]. The complexity

of megaprojects and the variability of risks strengthen the dependence of subjects on one another and require close and deep synergy to better address social responsibility issues [24]. Ma et al. constructed a governance of MSR framework for "government-business-society" [16]. The SB has strengthened the overall awareness and cohesiveness of megaproject organizations, enhanced the ability and efficiency of response to engineering risks, and enabled social responsibility issues in megaprojects to be resolved timely and effectively. Cooperative implementation is a behavior of planning, decision-making, and implementation with other subjects in the form of communication, negotiation, and cooperation when the subject is faced with megaproject social responsibilities with multidimensional behavioral interaction and dynamic characteristics. This behavior is defined as synergistic.

In view of the importance and representativeness of both behaviors, this study selects HB and SB as the endogenous variables.

2.2. IP and MSRB. Considering the project and social attributes of megaprojects, the external context is extensive, involving many influencing factors, including constraints of macro systems (e.g., laws and regulations, contract documents) and impacts of project characteristics (e.g., major project types and construction environmental conditions) [14, 25]. Scholars discussed the application value of institutional theory in major projects [26], and the role of institutional norms has gradually attracted the attention of scholars in the field of construction engineering. IP is an obvious external influence factor, but its influence is inconsistent due to differences in research perspectives. For example, the government punishment mechanism stimulates the environmental behavior of enterprises, but the illegal cost and profit-seeking nature of the enterprise limit the incentive effect of the regulation [27]. Nevertheless, in the field of construction engineering, Qi and other scholars found that government environmental regulations are significantly related to contractors' green construction [19].

In organization field theory, the field institution guides the behavior of the subject, limiting the scope of the action plan. Social responsibility behavior, as a kind of collective behavior in the field, should also meet the "legality" requirement of the institution [28, 29]. The IP dimension in this study includes mandatory institution, such as construction laws, contracts, industry, and norms. These mandatory institutions have a clear reward and punishment nature. The behavior subject of social responsibility must pay attention to the terms of the contract and the requirements of social responsibility in the law. If they are violated, then the subject will be punished. Relevant empirical research demonstrates that a reasonable and clear punishment mechanism effectively controls a company's environmental compliance with regulations [27]. Ge et al. also confirmed that mandatory IP significantly promotes social responsibility behavior in megaproject environments [30].

From the perspective of rational people, the actors must weigh the cost of action to implement social responsibility and the penalty cost caused by the nonfulfillment of social responsibility. They must also pretend to perform but not to pay the cost of their corresponding action to obtain the maximum benefit. HB can win the greatest benefit at the lowest cost, but this behavior is contrary to institutional requirements. The lack of the normative nature of the institution place the behavior subject at risk, that is, the behavior subject will suffer substantial losses after the behavior is exposed. The contract and project management system in megaprojects not only constitute the reference standard for the actions of various actors but also form the relationship of interests, powers, and responsibilities among the actors. These factors are the normative basis for joint actions, such as communication, negotiation, and decision-making, when the behavior subject deals with MSR issues. In addition, contracts and regulations are often inescapable. Under the pressure of having to fulfill the responsibility and the difficulty of achieving it alone, the behavior subjects will actively seek help and support from others.

Hypothesis 1a. IP positively affects SB.

Hypothesis 1b. IP negatively affects HB.

2.3. MFM and MSRB. The MFM, which includes information disclosure and communication mechanism, is the key system to improve project transparency, ensure the collaborative analysis of subjects, and make decisions on MSR issues [31]. Communication is an important means for the construction project team to know and cooperate with one another. A good communication mechanism provides a way for the actor to communicate; standardizes the communication process, methods, and requirements; and helps eliminate understanding bias and avoid information silos. Previous research on organizational transparency confirms that transparency plays a positive role in increasing members' trust in the organization [32], and this trust lays the foundation for MSR actors to coordinate social responsibility. Wang [31] emphasized that the information sharing mechanism directly affects the evolution of stakeholders to cope with the social responsibility crisis in major engineering projects. Information technology and strategy have created possibilities for collaboratively solving social responsibility crisis. Ma et al. [16] believed that transparency plays a role in MSR governance, such as preventing and combating corruption and power abuse. An effective MFM helps subjects pay attention to the interests of stakeholders, thereby gaining the support and collaboration of megaproject teams and reducing the loss of social responsibility crisis. By contrast, in the study of hypocritical social responsibility behavior, the reasons for that are also closely related to exposure difficulties. However, in the case of effective information disclosure system, the hidden behavior of the subject is exposed, and the participating parties realize that the information of the social responsibility behavior of the party will be disclosed. Under such psychological pressure, the actor reduces speculative behavior with a lucky attitude. Frequent communication also increases the exposure of the social responsibility behavior of the subject, thereby causing difficulty in concealing and falsely performing social responsibility and raising the

possibility that inconsistent words and deeds are perceived by the subject.

Hypothesis 2a. MFM positively affects SB.

Hypothesis 2b. MFM negatively affects HB.

2.4. RQ and MSRB. Stakeholders always affect the decision-making of the actors [21], and the actors must consider the interests and attitudes of stakeholders during behavior selection. Therefore, the relationship of organizations affects the selection of actors' social responsibility behavior [14]. Interorganizational relationships can be divided into two types: participating and nonparticipating parties in construction. This study opts to use RQ as a variable to measure the interaction among participants to determine the influence of the relationship between the participants. RQ is related to the project performance and satisfaction of the participants, such as the owner [33]. A harmonious working atmosphere is conducive to synergy and other social responsibility interactions.

RQ is a variable that measures the degree of interaction among various subjects in a project. RQ includes commitment [34], communication, coordination, trust [35], and fairness [36]. Black et al. [37] used trust, confidence, and communication to investigate the relationships in engineering projects. The subdimensions of these relationships are closely related to interaction behavior. Communication and commitment shape the impression of the actor on the other side of the project. Trust allows the behavior subject to have the willingness to contact and cooperate. Therefore, good RQ is achieved when many parties are willing to coordinate social responsibility and reduce the occurrence of negative behavior, such as hypocrisy. Scholars, including Lu and Wang [38] and Wu et al. [39], found that the relationship between RQ and engineering project cooperation and coordination behavior is significantly correlated. SB also emphasizes that multiparty subjects rely on collective power to fulfill social responsibilities on the basis of trust and communication. RQ determines the frequency and implementation effect of collaborative behavior.

Hypothesis 3a. RQ positively affects SB.

Hypothesis 3b. RQ negatively affects HB.

As a variable for the participants to perceive and evaluate each other's interaction behavior, RQ includes subelements such as trust, commitment, communication, cooperation, and reciprocity. Trust and fulfillment of commitments are prerequisites for establishing cooperative relationships. Communication promotes information transmission, so that all parties can resolve disputes through joint efforts, achieve reasonable and fair benefits, and form a win–win situation. The subdimension of RQ indicates that the communication and information feedback between the parties can enhance RQ [24]; efficient communication and transparent information disclosure mechanisms in megaprojects have laid a solid foundation for the mutual exchange of participants. Efficient information communication strengthens the mutual understanding between the parties and is conducive to the formation of good partnerships. Moreover, the quality of communication is an evaluation criterion for RQ. Therefore, RQ can be regarded as a mediator variable, which plays a mediating role in the impact of MFM on MSRB.

Hypothesis 3c. MFM indirectly affects MSRB through RQ.

2.5. EAs and MSRB. EAs for MSR resulted from nonparticipating parties [3, 16]. Among the influences of nonparticipating parties, many scholars investigated social responsibility and proposed that social pressures, such as government regulation and public participation, remarkably affect social responsibility behavior [19]. With the aforementioned conclusions from the existing literature as basis, this study uses EAs as research variables and selects nonparticipating parties, including public media, local community residents, government regulatory agencies, and NGOs, for discussion. The requirements and supervision of such organizations for megaprojects reflect the social expectations of major social responsibility behavior from outside the project.

Projects carry considerable social responsibility expectations when the public and local communities are highly concerned about them, and the negative effects of failing to fulfill social responsibilities are high [4]. At the same time, government regulators and NGOs have constrained the social responsibility of the participants [19, 30]. Judging from the characteristics of megaprojects, large investment and long construction period greatly affect the social economy and ecology. The social attributes of major projects have been repeatedly emphasized in academic circles and engineering practice [11, 16, 40]. In this context, MSRB subjects have to pay attention to the demands of major social projects and prevent social conflicts. The demand for social responsibility in the outside world is related to the project as a whole, requiring the government to perform the top-level command and construction unit to coordinate the implementation of multiple designers, contractors, and supervisors to maximize social satisfaction [41]. However, excessive EAs correspond to high manpower and resource investment, and the increase in the cost of social responsibility behavior make the subjects inclined to pretend to fulfill their social responsibility for maintaining a good image [42, 43]. That is, EAs lead to the emergence of false social responsibility behavior.

Hypothesis 4a. External claims positively affect SB.

Hypothesis 4b. External claims negatively affect HB.

2.6. SRC and MSRB. The earliest theory of action and the far-reaching theory of rational behavior demonstrate a direct relationship between cognition and behavior [44, 45]. Scholars who study CSR empirically showed that SRC is positively correlated with social responsibility behavior [46, 47].

Managers' cognitive attitudes toward social responsibility directly affect organizational behavioral decision-making [46]. Research confirms that managers' perceptions of social responsibility directly affect organizational social responsibility behavior or indirectly influence the social responsibility behaviors of actors. In megaprojects, the subjects' understanding of the social responsibility of megaprojects determines their attitude toward social responsibility behavior, which in turn affects actual behavior selection.

In the current situation, the management personnel in the participating organizations remain vague about the concept of MSR, thus requiring increased attention to the three traditional construction goals and ignoring social expectations. However, failure to properly consider social responsibility issues may not be due to negative values of engineering managers but because of their insufficient understanding of the major engineering social responsibilities. From a social person perspective, the profound and clear understanding of the actor toward social responsibility of megaprojects indicates that he is inclined to select positive social responsibility behavior, such as synergy, while reducing negative social responsibility behavior, such as hypocrisy against values.

Hypothesis 5a. SRC positively affects SB.

Hypothesis 5b. SRC negatively affects HB.

Figure 1 depicts the conceptual model of this study based on the hypotheses.

3. Methodology

3.1. Measurement. Combining the identified influencing factors, the exogenous variables investigated in this study include five potential variables according to the classification of variables in the structural equation model. These variables are IP, MFM, RQ, EA, and SRC. Endogenous variables include two potential variables, namely, camouflage and cooperative behavior. The scale uses a 7-point Likert scale that ranges from 1 (strongly disagree) to 7 (strongly agree) to ensure measurement accuracy. The scale items draw on existing research, and on this basis, the situation of major projects is combined to modify the design. Table 1 lists the variable measurement items and reference sources ("R" means reverse item).

3.2. Sample and Data Collection. Considering that the managers of the participating organizations in megaprojects have a clear understanding of the implementation of megaproject social responsibilities, the questionnaire was distributed to the management staff of the participating parties. Before the formal investigation, a preset questionnaire survey was conducted on 32 on-the-job masters of engineering management to test the validity of the questionnaire. According to the respondent's answer and feedback, combined with the research group's discussion results, the structure and expression of the item were modified to form a formally issued questionnaire.

After revising the questionnaire according to the trial situation, 195 questionnaires were distributed to the management personnel of the participating parties who had remarkable engineering experience in the form of online publication and mailing, and 145 were recovered, with a recovery rate of 74.4%. A total of 127 valid questionnaires were screened on the basis of the time of answering the questionnaire, the years of participating in megaproject, and whether the answer was neutral, with an effective rate of 87.6%. The following megaprojects were selected from the questionnaire: the main bridge and Zhuhai port of Hong Kong–Zhuhai–Macao Bridge and the infrastructure project of Nanning East Railway Station in Guangxi Province, Zhuhai Hengqin New Area Project of Guangdong Pilot Free Trade Zone, Shanghai World Expo Project, and Shenzhen Qianhai City New Center Construction Project. The sample source covers developed areas in southern China and has certain representativeness.

Table 2 provides the descriptive statistics of the respondents. The respondents were mainly the owner and the government (43.3%), followed by the contractor (22.8%). Differences are observed in the megaproject social responsibilities of various participating parties. In contrast with other units, such as survey and design, the MSR issues faced by owners, governments, and contractors are becoming complicated. This study used one-way analysis of variance (ANOVA) to test the two variables of HB and SB among different participating organizations to test the problem considering that differences in the choice of social responsibility behaviors for project roles may be observed [47]. The results indicate no significant difference (P value is 0.203 and 0.571, both values are greater than 0.05).

3.3. Selection of Research Tools. The reliability of the latent variable scale in the context of MSR needs to be tested because the development stage of the scale is based on the measurement scale of existing measurement-related research. This study used exploratory and confirmatory factor analysis methods to correct and detect the scale. An empirical study was conducted using the PLS-SEM method in the hypothesis testing phase. In the structural equation model test, the study tested the results of AMOS and SmartPLS software, and PLS-SEM was used as the data analysis tool according to the conclusions of existing research. PLS-SEM is suitable for early exploratory research [24, 47]. The potential variables of this study, such as IP, MFM, and cooperative behavior, are newly proposed. The impact path is an extension of existing research results or theoretical frameworks, but, overall, it is still in the preliminary exploration stage. PLS-SEM is also suitable for studies with small sample [55]. AMOS, LISREL, and Mplus are the mainstream software for today's structural equation model research. The sample size must be larger than the sample size, and the boundary should be 200. The number of samples in this study (127) was applied by PLS-SEM.

4. Data Analysis

4.1. Factor Analysis. Exploratory factor analysis was first performed to test the validity of the MSRB measurement

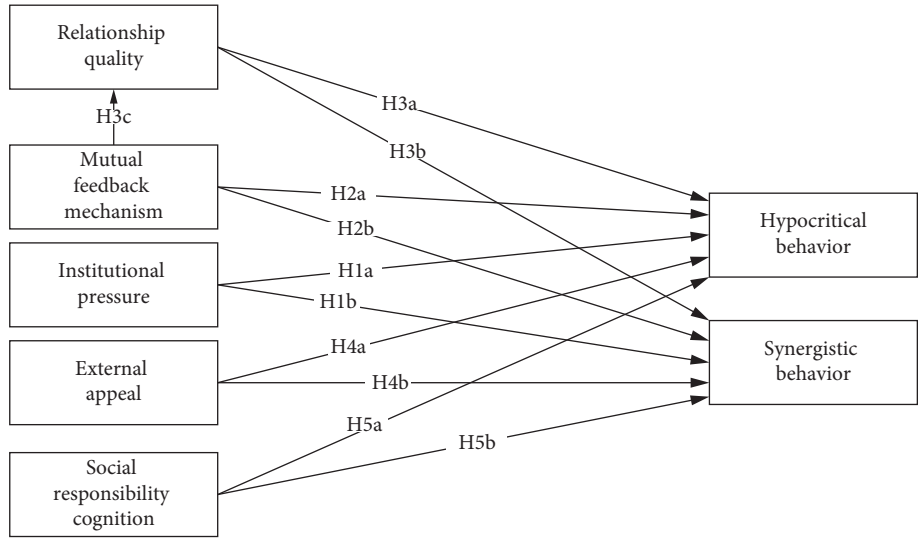

Figure 1: MSRB selection concept model.

Table 1: Development and design of the scale items.

Construct	Items	Reference source
Institutional pressure	PRES2: contract documents contain clear requirements for project quality and safety, handling public social events, and ecological environmental protection PRES3: contents of construction standard specification regarding quality and safety of megaprojects, environmental protection, occupational health, green construction, etc. are specific PRES4: project culture advocates the importance of engineering quality and safety, social impact, and ecological environmental protection PRES5: project has strict supervision and information feedback on engineering quality and safety, occupational health, social impact, and ecological environment	Wang et al. [30]; Zheng [48]
Mutual feedback mechanism	MFM1: project has adopted effective communication methods such as charts, tables, etc. MFM2: through regular meetings, information sharing between project parties is very accurate MFM3: it is very timely to communicate with other participants through documents MFM4: project team hopes that the participants know what the project is doing and why	Wu et al. [39]; Holland et al. [32]
Relationship quality	REQUA1: other project participants always abide by our commitment to us REQUA2: we can trust that the project participants are sincere REQUA3: when making important decisions, the project participants will consider our interests. REQUA5: we are satisfied with the project participants in terms of technology and management. REQUA6: considering the overall performance of the project participants, it can be said that they have reached our expectations	Lu and Wang [38]; Xu et al. [49]

Table 1: Continued.

Construct	Items	Reference source
External appeal	EXAPPE2: relevant government regulatory authorities require attention to social responsibility issues EXAPPE3: the public is highly concerned about megaprojects, and the media frequently reports on project social responsibility. EXAPPE5: relevant NGOs require projects to pay attention to social responsibility issues	Wang et al. [30]; Zhao [50]
Social responsibility cognition	SCAW3R: the society's expectation for megaprojects is only to complete the construction task (R) SCAW4R: we must pay attention to the construction of megaprojects and should not assume social responsibility (*R*). SCAW5R: taking social responsibility consumes our extra resources and deviates from the main project objectives (R)	Xu and Liang [51]; Zheng [48]
Hypocritical behavior	HYBE1R: when we fulfill our social responsibilities, we can fully do what we say and do (R) HYBE2R: we never make an empty social responsibility commitment® HYBE3R: we will not pretend to perform social responsibility at any time (R)	Wagner et al. [52]; Xiao et al. [53]
Synergistic behavior	SYBE1: other participants can provide support to help us solve social responsibility problems SYBE2: we can provide support to help other participants solve social responsibility issues. SYBE3: when there is a social responsibility problem in the implementation of the project, there is no shirking responsibility. SYBE4: participants actively and continuously consider social responsibility issues. SYBE6: in the implementation of social responsibility behavior, the participants have maintained a good cooperative relationship	Yan et al. [54]

Table 2: Descriptive statistics of respondents.

Item	Category	Number	(%)
Organizational nature	Government, construction unit	55	43.30
	Survey and design unit	24	18.90
	Contractor	29	22.80
	Supervision, consulting, operating units, etc.	19	15.00
Working years in engineering	Less than 5 years	38	29.90
	6–10 years	41	32.30
	11–20 years	32	25.20
	More than 20 years	16	12.60
Working years in megaproject	Less than 5 years	68	53.50
	6–10 years	37	29.10
	More than 10 years	22	17.30
Project type	Skyscraper	35	27.60
	Large-scale event exhibition facilities	19	15.00
	Energy base, power station, airport	8	6.30
	High-speed rail, highway, etc.	25	19.70
	Long bridge, mountain tunnel	13	10.20
	Port engineering, airport	10	7.90
	Subway	17	13.40

scale item, which was evaluated by KMO value and Bartlett spherical detection. Empirically, when the KMO value is higher than 0.6 and the Bartlett test reaches a significant level ($P < 0.001$), the measurement items have strong correlation and are suitable for factor analysis. In the exploratory factor analysis, the items with low factor load or cross-load condition in the measurement item were deleted. After factor analysis of measured items, five factor dimensions were extracted, which correspond to five endogenous latent variables: IP, MFM, RQ, EA, and SRC. Table 3 shows that the factor loading of the measurement items generally exceeds 0.7 (above the limit of 0.5). In the same way, two factors were extracted from the endogenous variables, corresponding to SB and HB. The KMO value and the Bartlett test significance of the two exploratory factor analyses met the requirements.

4.2. Scale Validity Analysis. The structural validity analysis show discriminant and aggregation validity, which are tested by SmartPLS 3.0. Table 4 lists the results of the discriminant validity test. The factor load of each item in the construct of the influencing factors and MSRB is significantly higher than the load value of other constructs. Furthermore, the minimum value of the AVE square root value of each construct is 0.862, which is higher than the maximum correlation coefficient of other constructs by 0.832, indicating that the scale has satisfactory discriminant validity.

Table 5 lists the results of the polymerization validity test, which is evaluated by Cronbach's α value, mean variation extract (AVE) value, and combination reliability (CR). Empirically, a CR of 0.7 or more is considered relatively stable, and the AVE criterion is 0.50. When it is greater than this value, the latent variable has an ideal polymerization validity [51]. The Cronbach's α value of each potential variable obtained before is above 0.85, which is greater than 0.7, followed by the CR value of the latent variable, which is almost above 0.9, and the AVE value is approximately 0.80, and both are above 0.74. The three indicators show that the scale has satisfactory structural validity. In summary, the measurement items represent the measurement of the influencing factors and MSRB.

4.3. PLS-SEM Analysis. The hypothesis test of the previous behavior selection was carried out by using SmartPLS 3.0 software. According to the theoretical hypothesis, the influence paths of the five influencing factors on the endogenous variables of the two behavioral modes were drawn. After the questionnaire data were imported, the model was run, and the results are illustrated in Figure 2. As an influential factor, the R-party interpretation level of HB and SB reached 0.510 and 0.723, indicating that the model explained the two behaviors to a high degree, respectively. The path coefficient of the relationship between the MFM and the RQ is 0.592, and the P value is <0.001, indicating that the impact is very significant. In addition, the R-square value is 0.351, indicating that the MFM has a high degree of interpretation of the RQ. The path hypothesis of the influence of RQ on HB and SB is supported and reached the level of $P < 0.001$. The direct influence of MFM on SB is insignificant ($P > 0.05$). Thus, feed mechanism indirectly affects HB and SB through RQ. The influence of IP and EA on HB passed the hypothesis test at the significance level of 0.05. The influence path of SRC variables on the two social responsibility behavior did not reach the significant level (P value >0.05). Table 6 summarizes the results of the hypothesis test.

5. Discussion and Implication

As an exploratory study, this paper attempts to use social action theory, through social responsibility cognition at the level of internal characteristics, relationship quality and external appeals at the level of interorganizational relations, and mutual feedback mechanism and institutional pressure at the level of external scenarios to explore the decision-making of stakeholders on hypocritical behavior and synergistic behavior in megaproject social responsibility. The empirical results show that the theoretical framework of megaproject social responsibility behavior choice proposed by previous research has certain explanatory power for the behavior selection of participating parties. In addition, there may be differences in the influencing factors and influence paths of different behaviors. Specifically, for the hypocritical behavior and synergistic behavior in this study, the relationship quality has a direct impact on both behaviors, which means that relationship quality not only effectively promotes the cooperation and mutual assistance of the participants in the implementation of social responsibility, but also plays an effective role in reducing disguised social responsibility behavior. The mutual feedback mechanism indirectly affects these two behaviors selection through the relationship quality as mediator variable. For hypocritical behaviors, in addition to the influence path of the above variables, institutional pressure and external appeals can directly effectively inhibit the false social responsibility behavior of the participating parties. However, for the synergistic behavior, among the variables selected in this paper, except for the mutual feedback mechanism and the relationship quality, the residual exogenous variables are not statistically significant. In addition, it is surprising that the impact of social responsibility cognition on both behaviors is not significant. This means that the level of social responsibility is not effective in reducing the performance of the participating parties in making false social responsibility and promoting the assistance for other participants in fulfilling their social responsibilities.

5.1. Influential Path of IP. The institution in this study is the regulatory requirement for MSR in industry norms, contract terms, and project culture. According to the empirical results of two statistical methods, IP has an inhibitory effect on HB but does not significantly affect SB. The results confirm that IP affects the choice of social responsibility behavior of the subjects in megaprojects. However, the degree of impact is not very high and only passes the significant level of 0.05, indicating that simply pursuing institutional constraints to promote the fulfillment of megaproject social responsibilities

Table 3: Exploratory factor analysis of endogenous variables.

Item	Ingredient1	Ingredient2	Ingredient3	Ingredient4	Ingredient5
IP2	**0.816**	0.315	0.105	0.069	0.056
IP3	**0.832**	0.226	0.096	0.131	0.082
IP4	**0.695**	0.381	–0.006	0.305	–0.006
IP5	**0.706**	0.236	0.311	0.167	0.143
MFM1	0.287	**0.732**	–0.048	0.241	0.09
MFM2	0.206	**0.845**	0.113	0.197	0.149
MFM3	0.301	**0.799**	0.286	0.082	0.136
MFM4	0.294	**0.78**	0.042	0.053	0.165
RQ1	0.263	–0.058	**0.838**	0.044	–0.172
RQ2	0.267	0.006	**0.858**	0.203	–0.094
RQ3	–0.011	0.13	**0.861**	0.189	–0.151
RQ5	0.043	0.119	**0.881**	0.139	0.035
RQ6	–0.012	0.122	**0.816**	0.204	–0.069
EA2	0.324	0.3	0.254	**0.675**	0.067
EA3	0.096	0.216	0.277	**0.839**	0.098
EA5	0.29	0.072	0.413	**0.651**	0.094
SCA3R	–0.005	0.371	–0.105	–0.294	**0.695**
SCA4R	0.055	0.134	–0.205	0.165	**0.864**
SCA5R	0.16	0.063	–0.056	0.203	**0.879**
Factor extraction	Institutional pressure	Mutual feedback mechanism	Relationship quality	External appeal	Social responsibility cognition
Variance interpretation ratio (%)	22.128	16.836	15.856	11.565	11.191
Cumulative variance interpretation ratio (%)	77.576				

Table 4: Discriminant validity analysis of measurement scale.

Constructive	Mutual feedback mechanism	Hypocritical behavior	Relationship quality	Institutional pressure	Synergistic behavior	External appeal	Social responsibility cognition
Mutual feedback mechanism	**0.907**						
Hypocritical behavior	–0.492	**0.895**					
Relationship quality	0.59	–0.659	**0.914**				
Institutional pressure	0.774	–0.574	0.591	**0.901**			
Synergistic behavior	0.576	–0.79	0.832	0.616	**0.89**		
External appeal	0.7	–0.624	0.688	0.724	0.685	**0.913**	
Social responsibility cognition	–0.001	0.122	–0.264	–0.068	–0.218	–0.157	**0.862**

Note: The bold is the square root of the potential variable AVE value. Here, in order to compare with the correlation coefficient matrix, the original autocorrelation coefficient (1.000) is replaced.

is insufficient. For example, the Hong Kong-Zhuhai-Macao Bridge under the common constraints of different construction institution of Guangdong, Hong Kong and Macao, while participating in the construction standards according to different systems, the participating parties also need to resolve the differences between the system norms to solve the lack of social responsibility.

Although the effectiveness of the system is not the most effective, it cannot be ignored. The empirical analysis of Wang Ge and other scholars emphasized that the imitation and normative pressures under institutional theory are more effective than those in mandatory institutions [30]. Therefore, the selection of "standards engineering" to create a typical model of social responsibility behavior, give play to the influence of experts and scholars, speed up the formulation of megaproject social responsibility industry norms and assessment mechanisms, and create a good learning atmosphere for social responsibility practices and other practices will greatly benefit the entire society and megaprojects. In addition, the application of institutional theory in megaproject, which has a positive effect on social stability and regulation of megaproject construction behavior, should be continuously explored by scholars [26].

5.2. Influence Path of MFM and RQ. According to the empirical results, the MFM is based on the RQ variable, which indirectly affects the MSRB selection. As a technology platform and management model to strengthen trust, communication, and collaboration among participants, MFM has remarkable effects on megaproject organization integration, information sharing, and decision-making negotiation [31], which are

Table 5: Analysis of the polymerization validity of the measurement scale.

Latent variable	Measurement item	Factor load	Measurement error variance	P value	Cronbach's α	AVE	CR
Institutional pressure	PRES2	0.918	0.157	***	0.923	0.813	0.945
	PRES3	0.917	0.159	***			
	PRES4	0.882	0.222	***			
	PRES5	0.888	0.211	***			
Mutual feedback mechanism	MFM1	0.9	0.19	***	0.928	0.822	0.949
	MFM2	0.918	0.157	***			
	MFM3	0.931	0.133	***			
	MFM4	0.876	0.232	***			
Relationship quality	REQUA1	0.91	0.171	***	0.951	0.836	0.962
	REQUA2	0.938	0.12	***			
	REQUA3	0.923	0.149	***			
	REQUA5	0.914	0.165	***			
	REQUA6	0.887	0.214	***			
External appeal	EXAPPE2	0.914	0.164	***	0.9	0.833	0.937
	EXAPPE3	0.921	0.152	***			
	EXAPPE5	0.903	0.185	***			
Social responsibility cognition	SCAW3R	0.931	0.133	0.001	0.865	0.743	0.895
	SCAW4R	0.904	0.183	***			
	SCAW5R	0.738	0.456	0.002			
Hypocritical behavior	HYBE1R	0.862	0.257	***	0.876	0.801	0.924
	HYBE2R	0.905	0.182	***			
	HYBE3R	0.918	0.157	***			
Synergistic behavior	SYBE1	0.863	0.255	***	0.934	0.792	0.95
	SYBE2	0.907	0.177	***			
	SYBE3	0.88	0.225	***			
	SYBE4	0.914	0.165	***			
	SYBE6	0.883	0.22	***			

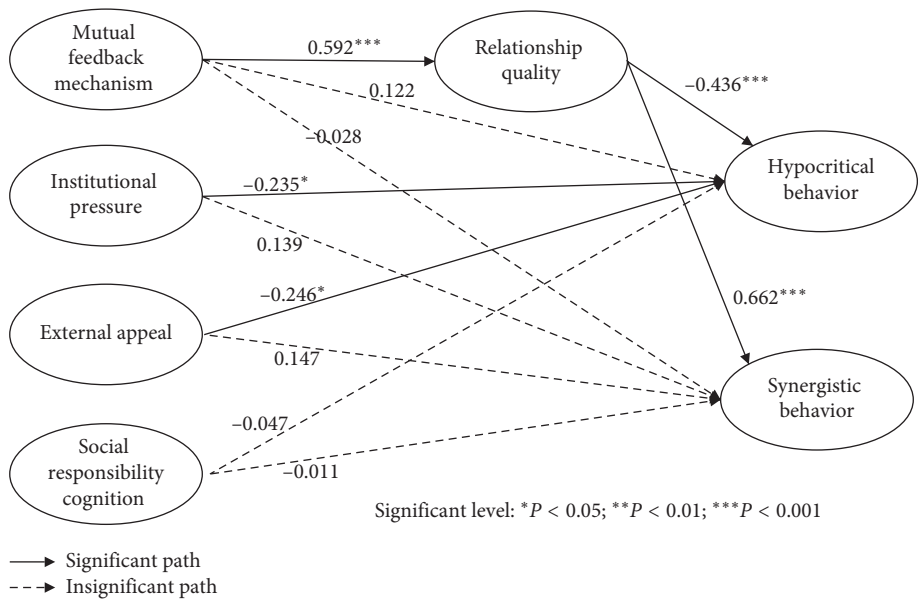

Figure 2: PLS-SEM analysis results.

beneficial in improving the relationship performance between subjects [24] and RQ. In the analysis results of this study, the path coefficient of the relationship between the MFM is high (0.592), and the significance level (P value) is below 0.001. MFM plays a key role in the interaction behavior of mega-projects. The impact of the path indicates that the RQ has great impetus in the MSRB. The impact path assumed in this study is the RQ composed of elements, such as trust and communication, which help enhance the SB in MSR. On a recently research of Zheng [48], the relationship behavior in megaproject construction greatly contributes to the improvement of RQ [24]. Although the starting point of study is

Table 6: Hypothesis test results.

	Path coefficient	T value	P value	Test result
MFM ⟶ RQ	0.592	5.793	<0.001	Accept
MFM ⟶ HB	0.122	0.862	0.389	Not accepted
RQ ⟶ HB	−0.436	3.990	<0.001	Accept
IP ⟶ HB	−0.235	2.127	0.034	Accept
EA ⟶ HB	−0.246	2.081	0.038	Accept
SRC ⟶ HB	−0.047	0.446	0.656	Not accepted
MFM ⟶ SB	−0.028	0.287	0.774	Not accepted
RQ ⟶ SB	0.662	8.063	<0.001	Accept
IP ⟶ SB	0.139	1.415	0.158	Not accepted
EA ⟶ SB	0.147	1.461	0.145	Not accepted
SRC ⟶ SB	−0.011	0.225	0.822	Not accepted

different, the consensus is that information sharing and open communication significantly affect the achievement of a high-level RQ.

The complexity of megaprojects, whose social responsibility involves multiple subjects, requires participants work together to maximize the benefits of the project to fulfill social responsibility at the lowest cost and eliminate the risk of crisis caused by lack of social responsibility in real rather than in falsehood. Therefore, timely and accurate information services in today's major projects and the resource integration of participating parties to coordinate and effectively deal with social responsibility issues, BIM technology, cloud computing, and grid technology can create a megaproject construction atmosphere with open communication and information sharing [31]; especially for project group with hundreds of participating parties, such as Shenzhen Qianhai City New Center Construction Project or Zhuhai Hengqin New Area Project of Guangdong Pilot Free Trade Zone, these information communication technologies have a positive effect on synergistically improving project quality, progress, reducing risk and other social responsibilities, and reducing negative hypocritical performance.

5.3. Influence Path of EA. According to the empirical results, the assumption of the influence of EA on HB is accepted, but the impact on the cooperative behavior is not remarkable. EAs come from government regulators, the general public, the media, and relevant NGOs. The results show that the pressure of these supervisory forces on the behavior subjects of megaproject is obvious, and their demands require substantial social responsibility actions and effects, which will reduce the intentional tendency of the actors to take pretense. The act of exposure after false performance results in considerable negative effects to megaprojects.

However, for the influence of EA on camouflage behavior, Zhao et al. [50] held different views and believed that this external pressure violated the organization's interests. Thus, the organization is likely to take false actions. However, this study believes that EAs positively affect the HB of megaprojects. The main reason is that megaprojects are highly concerned and are key projects at the national and regional levels, such as high-speed rail and nuclear power plants. Construction units and other participants have been pressured by the public and the community at the beginning. Thus, when the appeal is strong, the risk of hypocrisy is great, and hypocrisy will be rejected by the behavior subject. The government, as the most powerful force in EA, should enhance its regulatory capabilities and increase information disclosure on megaprojects [16] to guide the improvement of megaproject.

5.4. Influence Path of SRC. During hypothesis testing, the SRC variable has no significant impact on the HB and SB. However, this finding does not mean that SRC has nothing to do with MSRB. However, the influence of other factors in HB and SB is dominant, and the SRC affects the performance of major engineering social responsibility behavior [47], and perhaps the impact of SRC on the purpose and lofty behavior is evident [57, 58]. In the field research and interviews with project leaders and experts, although the current MSR is still a concept of academia, practitioners in the construction engineering community do not have a clear and accurate understanding of it. Nevertheless, almost everyone agrees that the responsibility of megaprojects is far more than the three major construction goals. The impact of megaprojects, like the South-to-North Water Transfer, the Three Gorges Dam and other livelihood projects, on society, economy, politics, and ecology has been deeply rooted in the hearts of the people.

6. Limits and Prospect

This article has limits in four areas.

First, this study attempts to demonstrate the MSRB mechanism from a systematic and global perspective. However, in the identification of influencing factors, the influencing factors with frequent occurrences and are closely related to MSRB in literature retrieval are selected. The role of the project's transparency and other factors that are not involved in this study are ignored. In addition, in endogenous variables, HB and SB are selected as representatives to study. In the previously investigated MSRB system, socially responsible behaviors, such as profit-making behavior, compliance behavior, imitative behavior, and escape behavior, were reported [14]. The selection mechanism of these behaviors needs to be developed further.

Second, MSRB has interaction and dynamic evolution problems. This study explores the influence path relationship among subjects, MSRB, and situation. However, under the perspective of social responsibility behavior network, the interaction rules between behaviors have not been discussed in depth. For example, whether SB will promote imitative behavior and suppress HB is worthwhile to continue for in-depth study and test. In addition, the issue of MSRB evolution under each phase of the project life cycle has yet to be resolved.

Third, the results of the study still require further empirical testing. This study adopts the exploratory PLS-SEM analysis method. After the later MSRB theory is gradually improved, sample size should be further expanded for

confirmatory empirical research, and megaprojects under different types, management modes, and cultural and social environments need to be examined separately in accordance with their social responsibility characteristics. For instance, the research in this study is carried out in China, and its suitability is yet to be tested for the selection of MSRB in Western countries.

Finally, after determining the selection mechanism of the MSRB, the researchers can further develop MSRB method, behavioral performance measurement, MSRB performance-driven mechanism, explore the relationship between MSRB and megaproject project performance, and the differences in MSRB and different project types.

7. Conclusion

Good performance of MSR plays an active role in promoting economic development (for example, the Anglo-French tunnel promotes the integration process in Europe), eliminating social conflicts (for example, the Cologne Cathedral reduces religious conflicts), establishing a harmonious relationship between human and environmental ecology (for example, the Qinghai-Tibet Railway takes measures to protect wild animals), and implementing the concept of sustainable development (for example, the Moses Mabhida Stadium in South Africa considering the sustainability of urban regeneration) [3, 7]. Analyzing the social responsibility behavior selection mechanism of megaproject subjects provides theoretical guidance for various megaproject participants to fulfill their social responsibilities and helps behavior subjects make sound choices when encountering social responsibility issues in megaproject [14].

The selection of stakeholders toward MSRB is the decision and adjustment of how to fulfill their social responsibilities under the joint effect of internal characteristics of organization, interorganizational relationship, and external scenarios. In the megaproject, the behavioral subject in the face of social responsibility is the object of this study. On the basis of selection model of MSRB, this study verifies the impact of five influencing factors on the two types of social responsibility behaviors from three levels: intra-organization, interorganization, and situation. The empirical results reveal that under the background of major engineering social responsibility, not all choices of social responsibility behavior result from the combination of multiple factors but may also be the result of a specific factor of "catalysis." Hypocrisy is a form of alienated social responsibility behavior. This inconsistent behavior not only fails to achieve the goal of improving social welfare [53] but also creates the illusion of deceiving the public. SB is an interactive social responsibility behavior manifested by mutual support. This study considers these two typical social responsibility behaviors as an example to analyze the selection mechanism of MSRB. The results show that RQ has a significant driving effect on HB and has a significant inhibitory effect on HB. Effective MFM indirectly affects hypocritical behavior and coordinated behavior through the mediation variable RQ. This result confirms that ensuring the correct implementation of megaproject social responsibility requires the establishment of an effective MFM to enhance the quality of participant relationships. HB is affected by the constraints of the institutional norms and the influence of the supervision and appeal of the external public media. Therefore, advocating for the comprehensive management of behavioral subjects in megaprojects is necessary to actively respond to social responsibility behaviors from various aspects, such as institutions and relationships.

The empirical research on megaproject social responsibility in the past only focused on the behavioral performance and did not try to explore how the participating parties fulfill their social responsibility behaviors, that is, the way they behave. Although this study only examines the factors that influence the selection of two types of social responsibility behaviors, it illustrates the possibility of exploring the influencing factors of more social responsibility behavior selection from the perspective of social action theory. In addition, selection mechanisms of other different MSRB, interactions between different MSRB, and the dynamic evolution during the project life cycle have the value of being further explored. It is also worthwhile to verify the interpretation of MSRB selection by other behavior theories.

Data Availability

All data generated or used during the study are available in the supplementary materials.

Disclosure

The authors are solely responsible for the content.

Conflicts of Interest

The authors declare that they have no conflicts of interest.

Acknowledgments

The authors gratefully acknowledge the funding and support provided by the National Natural Science Foundation of China (NSFC) (Grant no. 71871096) and 2016 College International Research Cooperation "Seed Fund" from School of Civil Engineering and Transportation, South China University of Technology.

Supplementary Materials

The first file, titled "smartpls original data," is the original statistical data file for subsequent data analysis, obtained from the recycled questionnaires; and the another one, titled "megaproject social responsibility behavior Smartpls report," is the report exported by the statistical software "smartpls," used to analyze the hypothesis test results in the article. (*Supplementary Materials*)

References

[1] Z. Liu, Y. Sui, Z. Jin, and X. Yanf, "Evolution of major infrastructure project's social responsibility: from a global

perspective," *Journal of Systems and Management*, vol. 27, no. 1, pp. 101–108, 2018, in Chinese.

[2] International Organization for Standardization, *Guidance on Social Responsibility*, International Organization for Standardization, Geneva, Switzerland, 2006.

[3] S. X. Zeng, H. Y. Ma, H. Lin, R. C. Zeng, and V. W. Y. Tam, "Social responsibility of major infrastructure projects in China," *International Journal of Project Management*, vol. 33, no. 3, pp. 537–548, 2015.

[4] L. Strauch, G. Takano, and M. Hordijk, "Mixed-use spaces and mixed social responses: popular resistance to a megaproject in Central Lima, Peru," *Habitat International*, vol. 45, pp. 177–184, 2015.

[5] J. Korytarova, V. Hromadka, M. Radujković, M. Vukomanović, and R. Wagner, "The economic evaluation of megaprojects—social and economic impacts," *Procedia—Social and Behavioral Sciences*, vol. 119, pp. 495–502, 2014.

[6] R. Dyer, "Cultural sense-making integration into risk mitigation strategies towards megaproject success," *International Journal of Project Management*, vol. 35, no. 7, pp. 1338–1349, 2017.

[7] Z. Liu, L. Wang, Z. Sheng, and X. Gao, "Social responsibility in infrastructure mega-projects: a case study of ecological compensation for Sousa chinensis during the construction of the Hong Kong-Zhuhai-Macao Bridge," *Frontiers of Engineering Management*, vol. 5, 2018.

[8] H. Lin, S. Zeng, H. Ma, R. Zeng, and V. W. Y. Tam, "An indicator system for evaluating megaproject social responsibility," *International Journal of Project Management*, vol. 35, no. 7, pp. 1415–1426, 2017.

[9] X. Lin, C. M. F. Ho, and G. Q. P. Shen, "Who should take the responsibility? Stakeholders' power over social responsibility issues in construction projects," *Journal of Cleaner Production*, vol. 154, pp. 318–329, 2017.

[10] Z. Zhou and C. Mi, "Social responsibility research within the context of megaproject management: trends, gaps and opportunities," *International Journal of Project Management*, vol. 35, no. 7, pp. 1378–1390, 2017.

[11] G. Jia, F. Yang, G. Wang, B. Hong, and R. You, "A study of mega project from a perspective of social conflict theory," *International Journal of Project Management*, vol. 29, no. 7, pp. 817–827, 2011.

[12] C. Lee, W. W. Jin, W. Jang, W. Jung, S. H. Han, and Y. H. Kwak, "Social conflict management framework for project viability: case studies from Korean megaprojects," *International Journal of Project Management*, vol. 35, no. 8, pp. 1683–1696, 2017.

[13] X. Xue, R. Zhang, X. Zhang, R. J. Yang, and H. Li, "Environmental and social challenges for urban subway construction: an empirical study in China," *International Journal of Project Management*, vol. 33, no. 3, pp. 576–588, 2015.

[14] L. Xie, H. Chu, T. Han, and Y. Le, "Selection of megaproject social responsibility behavior based on social action theory," *Journal of Civil Engineering and Management*, vol. 35, no. 6, pp. 57–64, 2018, in Chinese.

[15] H. Kim, W. M. Hur, and J. Yeo, "Corporate brand trust as a mediator in the relationship between consumer perception of CSR, corporate hypocrisy, and corporate reputation," *Sustainability-Basel*, vol. 7, no. 4, pp. 3683–3694, 2015.

[16] H. Ma, S. Zeng, H. Lin, H. Chen, and J. J. Shi, "The societal governance of megaproject social responsibility," *International Journal of Project Management*, vol. 35, no. 7, pp. 1365–1377, 2017.

[17] P. A. Stanwick and S. D. Stanwick, *The Relationship between Corporate Social Performance, and Organizational Size, Financial Performance, and Environmental Performance: An Empirical Examination*, Springer, Netherlands, 2013.

[18] S. J. Yun, "Experts' social responsibility in the process of large-scale nature-transforming national projects," *Development and Society*, vol. 43, no. 1, pp. 109–141, 2014.

[19] G. Y. Qi, L. Y. Shen, S. X. Zeng, and O. J. Jorge, "The drivers for contractors' green innovation: an industry perspective," *Journal of Cleaner Production*, vol. 18, no. 14, pp. 1358–1365, 2010.

[20] L. Liu and Z. F. Liang, *The Study of Social Responsibility for Construction of Highway Engineering*, in *Proceedings of the 2008 Third International Conference on Convergence and Hybrid Information Technology*, pp. 1031–1036, Busan, South Korea, November 2008.

[21] P. C. Liao, G. Tsenguun, and L. W. Liang, "Development of social responsibility evaluation framework of construction projects: a multi-stakeholders perspective," *Procedia Engineering*, vol. 145, pp. 234–241, 2016.

[22] T. P. Lyon and J. W. Maxwell, "Greenwash: corporate environmental disclosure under threat of audit," *Journal of Economics & Management Strategy*, vol. 20, no. 1, pp. 3–41, 2011.

[23] A. La Cour and J. Kromann, "Euphemisms and hypocrisy in corporate philanthropy," *Business Ethics: A European Review*, vol. 20, no. 3, pp. 267–279, 2011.

[24] Z. Xian, Y. Lu, L. Yun, Y. Li, and J. Fang, "Formation of interorganizational relational behavior in megaprojects: perspective of the extended theory of planned behavior," *Journal of Management in Engineering*, vol. 34, no. 1, Article ID 4017052, 2018.

[25] D. Matten and J. Moon, ""Implicit" and "explicit" CSR: a conceptual framework for a comparative understanding of corporate social responsibility," *Academy of Management Review*, vol. 33, no. 2, pp. 404–424, 2008.

[26] C. Biesenthal, S. Clegg, A. Mahalingam, and S. Sankaran, "Applying institutional theories to managing megaprojects," *International Journal of Project Management*, vol. 36, no. 1, pp. 43–54, 2017.

[27] S. Jin, Z. Yang, and M. Qingfeng, "Evolutionary dynamics of firm's environmental compliance behavior under dynamic punishment," *Journal of Systems and Management*, vol. 26, no. 6, pp. 1122–1130, 2017, in Chinese.

[28] J. A. C. Baum and F. Dobbin, "The iron cage revisited: institutional isomorphism and collective rationality in organizational fields," *American Sociological Review*, vol. 48, no. 2, pp. 147–160, 1983.

[29] W. R. Scott, *Institutions and Organizations: Ideas and Interests*, Sage Publications, Los Angeles, CA, USA, 3rd edition, 2008.

[30] G. Wang, Q. He, Y. Delei, X. Yan, and T. Yu, "Institutional pressures, organizational citizenship behaviors for the environment and environmental management performance: evidences from China's megaproject," *Journal of Systems and Management*, vol. 27, no. 1, pp. 118–128, 2018, in Chinese.

[31] A. Wang, "Information strategy for synergic megaproject social responsibility fulfillment and crisis management," *Science and Technology Management Research*, vol. 23, pp. 21–24, 2014.

[32] D. Holland, A. Krause, J. Provencher, and T. Seltzer, "Transparency tested: the influence of message features on public perceptions of organizational transparency," *Public Relations Review*, vol. 44, no. 2, pp. 256–264, 2017.

[33] P. Williams, N. J. Ashill, E. Naumann, and E. Jackson, "Relationship quality and satisfaction: customer-perceived success factors for on-time projects," *International Journal of Project Management*, vol. 33, no. 8, pp. 1836–1850, 2015.

[34] H. L. Angle and J. L. Perry, "An empirical assessment of organizational commitment and organizational effectiveness," *Administrative Science Quarterly*, vol. 26, no. 1, pp. 1–14, 1981.

[35] A. Kadefors, "Trust in project relationships—inside the black box," *International Journal of Project Management*, vol. 22, no. 3, pp. 175–182, 2004.

[36] P. Naude and F. Buttle, "Assessing relationship quality," *Industrial Marketing Management*, vol. 29, no. 4, pp. 351–361, 2000.

[37] C. Black, A. Akintoye, and E. Fitzgerald, "An analysis of success factors and benefits of partnering in construction," *International Journal of Project Management*, vol. 18, no. 6, pp. 423–434, 2000.

[38] W. Lu and J. Wang, "The influence of conflict management styles on relationship quality: the moderating effect of the level of task conflict," *International Journal of Project Management*, vol. 35, no. 8, pp. 1483–1494, 2017.

[39] G. Wu, C. Liu, X. Zhao, and J. Zuo, "Investigating the relationship between communication-conflict interaction and project success among construction project teams," *International Journal of Project Management*, vol. 35, no. 8, pp. 1466–1482, 2017.

[40] B. Flyvbjerg, "What you should know about megaprojects and why: an overview," *Project Management Journal*, vol. 45, no. 2, pp. 6–19, 2014.

[41] Y. Hu, Y. Le, X. Gao, Y. Li, and M. Liu, "Grasping institutional complexity in infrastructure mega-projects through the multi-level governance system: a case study of the Hong Kong-Zhuhai-Macao bridge construction," *Frontiers of Engineering Management*, vol. 5, no. 1, pp. 52–63, 2018.

[42] Y. Fassin, "The reasons behind non-ethical behaviour in business and entrepreneurship," *Journal of Business Ethics*, vol. 60, no. 3, pp. 265–279, 2005.

[43] M. Orlitzky and D. L. Swanson, "Corporate social and financial performance: an integrative review," *Organization Studies*, vol. 24, pp. 403–441, 2008.

[44] M. Fishbein and S. Middlestadt, "Noncognitive effects on attitude formation and change: fact or artifact?," *Journal of Consumer Psychology*, vol. 4, no. 2, pp. 181–202, 1995.

[45] T. Parsons, *The Structure of Social Action*, Free Press, New York, USA, 1980.

[46] H. Lin, Y. Sui, H. Ma, L. Wang, and S. Zeng, "CEO narcissism, public concern, and megaproject social responsibility: moderated mediating examination," *Journal of Management in Engineering*, vol. 34, no. 4, Article ID 04018018, 2018.

[47] G. Wang, Q. He, X. Meng, G. Locatelli, T. Yu, and X. Yan, "Exploring the impact of megaproject environmental responsibility on organizational citizenship behaviors for the environment: a social identity perspective," *International Journal of Project Management*, vol. 35, no. 7, pp. 1402–1414, 2017.

[48] H. Zheng, *On the Behavior of Corporate Social Responsibility: Dimensions, Determinants, and Impact on Business Performance*, Zhejiang University, Hangzhou, China, 2007, in Chinese.

[49] J. Xu and Y. Ren, "An empirical study on project relationship quality, project performance and their impact relationship," *Forecasting*, vol. 29, no. 1, pp. 71–75, 2010, in Chinese.

[50] H. Zhao, "A study of the driving factors of enterprises' pseudo-social responsibility behaviors," *Contemporary Finance and Economics*, vol. 35, no. 12, pp. 77–86, 2014, in Chinese.

[51] Y. Hua, J. Tao, and J. Yang, "The impact of corporate social responsibility performance on employee loyalty," *Enterprise Economy*, vol. 34, no. 5, pp. 51–55, 2014, in Chinese.

[52] T. Wagner, R. J. Lutz, and B. A. Weitz, "Corporate hypocrisy: overcoming the threat of inconsistent corporate social responsibility perceptions," *Journal of Marketing*, vol. 73, no. 6, pp. 77–91, 2009.

[53] H. Xiao, J. Zhang, and W. Li, "Research on the behaviors of pseudo-CSR," *China Industrial Economics*, vol. 27, no. 6, pp. 109–121, 2013, in Chinese.

[54] M. Yan, L. Yan, and J. Deng, "Industry practice, relational norms and cooperative behavior: a study based on construction project organizations," *East China Economic Management*, vol. 29, no. 8, pp. 165–174, 2015, in Chinese.

[55] J. F. Hair, W. C. Black, B. J. Babin, and R. E. Anderson, *Multivariate Data Analysis: A Global Perspective*, Pearson Education, London, UK, 2010.

[56] J. F. Hair, C. M. Ringle, and M. Sarstedt, "PLS-SEM: indeed a silver bullet," *Journal of Marketing Theory and Practice*, vol. 19, no. 2, pp. 139–152, 2011.

[57] M. E. Drumwright, "Socially responsible organizational buying: environmental concern as a noneconomic buying criterion," *Journal of Marketing*, vol. 58, no. 3, pp. 1–19, 1994.

[58] L. Zu and L. Song, "Determinants of managerial values on corporate social responsibility: evidence from China," *Journal of Business Ethics*, vol. 88, no. S1, pp. 105–117, 2009.

Hindawi
Advances in Civil Engineering
Volume 2019, Article ID 5650463, 20 pages
https://doi.org/10.1155/2019/5650463

Research Article

Study on the Evaluation Method of Green Construction Based on Ontology and BIM

Zhao Xu,[1] **Xuerong Wang**,[2] **Wentao Zhou**,[1] **and Jingfeng Yuan**[1]

[1]*Department of Civil Engineering, Southeast University, Nanjing 210096, China*
[2]*Department of Engineering Management, Nanjing Audit University, Nanjing 210096, China*

Correspondence should be addressed to Zhao Xu; bernardos@163.com

Received 26 April 2019; Revised 15 July 2019; Accepted 28 August 2019; Published 1 October 2019

Guest Editor: Endong Wang

Many problems and issues affect the green construction process. Inaccurate assessment is one of the important factors for green construction. The objective of this study is to propose a BIM and ontology-based approach that enables the evaluation information of green construction to be inferred from a knowledge base in order to achieve scheme optimization. To automate the inference, this study established the BIM ontology that consists of BIM shared ontology and BIM construction ontology. First, IFC extension is adopted in green construction assessment system to generate attribute sets. IFC-based parameters stored in BIM models are mapped to OWL and will be used as the data source of the evaluation indicators. Then, BIM-shared ontology and BIM construction ontology are defined. Protégé is employed to simulate the evaluation indicator system. Last, utilizing BIM knowledge base, through the construction of SWRL rule language and the Drools inference, the scores of evaluation indicators could be obtained. The experimental results demonstrated that BIM knowledge base for the evaluation of green construction could realize the sharing, maintenance, and acquisition of knowledge among different participants of the project and improve the management of green construction. The proposed ontological inference of evaluation item enables an automated search of the aspects needing improvements in green construction and assist project managers in using BIM data more easily and effectively.

1. Introduction

Sustainability in the AEC (architecture, engineering, and construction) industry has gained popular momentum over the past decades to enable all people to meet their basic needs and improve their quality of life while saving our natural resources and diversity [1]. By virtue of its size, the construction industry is one of the largest users of energy, material resources, and water, and it is a formidable polluter [2]. Construction and the environment are inextricably linked. Energy, materials, water, and land are all consumed in the construction stage of buildings and infrastructure.

Green construction is defined to ensure quality, safety, and other basic requirements and adopt scientific management and technological progress in the process to maximize the conservation of resources and reduce the construction activities which will bring negative impacts on the environment [3]. Green construction is the application of sustainable development idea in the AEC industry. The traditional construction method is to achieve the project quality, schedule, and cost as the basic goal [4]. The resource conservation and the environmental protection get less focus in the construction stage, while green construction emphasizes the efficient use of resources as the core and the environmental conservation as the priority principle in order to pursue the integrated construction method with the high efficiency, low consumption, and environmental protection [5]. Practitioners in construction industry have begun to pay attention to evaluating and controlling the environmental impacts due to their activities. Architects, designers, engineers, and others involved in the construction process have their opportunities to reduce environmental impacts through the implementation of sustainability objectives.

Over the last couple of years, BIM (Building Information Modeling) adoption has seen quite a significant growth in

the AEC industry, and it has been impacting design and construction practices at the fundamental level. Seeing the value of BIM, more and more firms are migrating their practices to the BIM process. This approach enables stakeholders to participate in the construction process and maximizes the use of prefabrication, thereby optimizing the construction phase while staying within budget restraints. Through the digitalization of construction information, the BIM process gives us a great control in the construction stage. Having the data about all the construction products gives the possibility to check the impacts of construction activities on the environment.

As the green construction phenomenon continues to grow and gain popularity, many problems and issues cast doubts on the development of green construction. In one respect, green construction implementation on an integrated and comprehensive scale to satisfy the holistic perspective and collaboration has encountered many challenges [6]. The challenges need robust methods to tackle the complexity of green construction management and environmental treatments which involve better energy efficiency, improved environmental quality, and the minimization of resource usage in construction phase [1, 7, 8]. On the other hand, the inaccurate assessment of the green construction is a major obstacle to overcome [9, 10]. There is a need to better understand the pivotal attributes that participants should possess to manage green construction. Previous evaluation studies related to green construction are dependent on the subjective feedback from construction technicians, which are thought to be inefficient and unreliable. So as to make one step forward towards the development of green construction assisted by the improvements of information technologies, there is the need to integrate the process of green construction evaluation with BIM technology [11].

The challenge that this incorporation faces is the parameterized expression of the evaluation knowledge and BIM-related information synthesis of all the available elements in purpose of achieving optimized measurements. In recent years, information synthesis has turned out to be more complicated with the increased use of data mining and decision-making support [12]. It is noticed that semantic-based approaches using domain ontologies have been adapted for data modeling and information integration [13, 14]. In general, an ontology represents a shared, agreed, and detailed model (or set of concepts) of a certain problem domain [15]. Ontology-based information synthesis in evaluation process mainly aims at improving the interface between feature attributes and evaluation requests in order to bring the result sets closer to the users' requirements in practices.

The objective of this study is to propose a BIM and ontology-based approach that enables the evaluation information of green construction to be inferred from a knowledge base in order to achieve scheme optimization. To automate this inference, this study established the BIM ontology that consists of BIM-shared ontology and construction ontology. The basic attributes contained in the established BIM-shared ontology are identity, size, space, and material. BIM construction ontology is created to include principles of the green construction and evaluation indicators. According to the definition of ontological meanings based on the BIM data, specific evaluation results can be acquired. Also, the proposed ontological inference of evaluation items enables an automated search of the aspects needing improvements in green construction and assists project managers in using BIM data more easily and effectively.

In this paper, Section 2 briefly discusses the trends of research and system developed for green construction and BIM technology. Section 3 introduces the methodology suggested in this paper. Sections 4 and 5, in order to build BIM knowledge base, IFC (Industrial Foundation Classes) expression, and data mapping are presented to confirm that the proposed ontology can fully represent the content of green construction. Finally, the paper concludes by offering some final remarks in Section 6.

2. Related Works

Green construction aims to eliminate or reduce negative environmental effects on the construction phase. It is also known as sustainable construction. Construction is one of the largest contributors to greenhouse gas emissions. With the development of society, new requirements such as saving labor resources, selecting machinery, and building information platform are put forward and green construction emerges [16].

2.1. Green Construction. The adoption of green construction strategies is mainly driven by concerns about climate change and nonrenewable energy use and also economic and ergonomic reasons like to increase efficiency and improve the construction performance. Previous studies about green construction evaluation mainly focus on the indicator selection and the quantitative methods. Li et al. [17] developed a green construction evaluation system of mountain highway projects using gene analysis and fuzzy matter element method. Zhang and He [18] adopted fuzzy integrated method and AHP (Analytic Hierarchy Process) to set indicator in all levels for the evaluation system of green construction. Then, the weight of each indicator was calculated, and the evaluation model was established. In order to refine the quality management and evaluation, Gu and Li [19] discussed the common knowledge connotation on the compliance evaluation system of complex quality and proposed an ontology model of it with generic knowledge modeling method. Passornpakorn and Kamolphiwong [20] raised an ontology-based framework based on REST principles and SPARQL (SPARQL Protocol and RDF Query Language) rules to interactively self-assess e-health services. They also demonstrated its capability to maintain new data schema during run-time and support of IoT (Internet of Things). By analyzing semantic web technologies and the IFC standard, Pauwels and Terkaj [21] connected them with an agreed Web Ontology Language (OWL) ontology for IFC (termed ifcOWL) in order to support data interoperability, flexible data exchange, distributed data management, and

the development of reusable tools. Yang et al. [22] applied the theory of the knowledge base and ontology to describe the four aspects of the telecommunications fraud cases and build a scalable case model. Through one example, the validity of the model in the analysis of telecommunications fraud cases is verified.

Internationally, many governments also make the efforts to develop different approaches in order to evaluate green construction. The first sustainability assessment method called BREEAM was developed in England in 1990. Besides, in America, LEED (Leadership in Energy and Environmental Design) raised the Green Building Rating System in 1995. In the same year, another green building assessment tool (GBtool) managed by the International Initiative for a Sustainable Built Environment (iiSBE) of Canada was released. Although their evaluation indicators vary from one standard to another, their goals are consistent to reduce the use of resources, protect the environment, and conform to the idea of sustainable development while meeting the standards in quality and safety. In China, according to the green construction guideline released by the Ministry of Housing and Urban-Rural Development, the aim of green construction is to conserve water, energy, land, material, and protect the environment through project management and advanced construction technology. With reference to these evaluation standards and their indicators, the Evaluation Standard for Green Building (ESGB) is developed by the China Academy of Building Research. The level of interior environment, operation management, and water, energy, land, material conservation are the main evaluation criteria of ESGB.

2.2. BIM and Green Construction Evaluation. It is indicated that the manual evaluation method, widely adopted now, relies on the experiences of the evaluators and is less efficient [23]. This complexity and need for reliable results claim for assistance of more integrated and intelligent tools, like BIM. BIM is an object-oriented, intelligent, and parameterized digital representation of building with rich semantic information. In order to manage the tremendous amount of information created in BIM and realize data exchange between different sectors, the information standards like IFC standard and its relevant EXPRESS language are developed. As a common adopted standard format for BIM data exchange and collaboration, IFC (Industry Foundation Classes), in which categories are called entities, is presented by object-oriented method. The architecture of IFC consists of four layers: resource layer, core layer, interoperability layer, and domain layer [24]. The information description module of each layer contains the definition of entities, types, and attribute sets, which can be modified by users to extend green construction information. The data modeling language of IFC schema is called EXPRESS, which is an international standard data modeling language for product data [25]. One of the advantages of using EXPRESS is its sufficient capability of describing data type, entity, algorithm, rules, etc. Through the definition of entities, physical, or conceptual objects in the real world, which share common characteristics, can be categorized and grouped together. Besides, the data content in these objects can be expressed by attributes in IFC and the behavior of these objects is represented by static constraints.

With the help of IFC schema and EXPRESS language, the green construction information can be connected to the BIM model. However, because the rich information from the real world is often implicit and do not have very logical schema, it is complicated for the computers to understand and digitalize it. To conquer the problem of relating target objects to the computer, the standardization would help a lot and facilitate model-based problem solving.

2.3. Ontology Method. Ontology method is introduced into the computation field from the 1980s to provide a basis of building models of all things in which computer science is interested; thus, it is intelligible both to computers and humans. Ontology is a domain and application-oriented method to assist in extracting knowledge that is specific to a particular domain and/or application [26, 27]. Besides, according to Moguillansky and Simari [28], an ontology model is not only formal and machine-understandable, but also available for knowledge sharing. Therefore, the ontology methodology is considered as a suitable method to model green construction evaluation indicators within BIM. An ontology can formally be specified using an ontology language. Because of the better expressive power, the OWL (Ontology Web Language) was recommended by the W3C (World Wide Web Consortium) as the ontology language [29]. The basic components of OWL are class, property, and instance. Class describes a set of instances which share common properties, while attribute connects instances with property values.

Data exploration helps us understand the investigated reality in a faster and better way. The data to be explored are domain knowledge bases with rules representation [30]. To best realize the power of ontology method in green construction evaluation and fit it in the task model, it is essential to construct a knowledge base with ontologies. As a technical basis, knowledge base is used to store complex structured and unstructured information that describes the target object in a computer system [31]. Furthermore, Liu and El-Gohary [32] suggested a way to extract the semantic features based on a bridge deterioration knowledge ontology. Warren et al. [33] suggested the advantage of knowledge base in facilitating information sharing, intelligent "queryability" of data based on ontologies, and high reliability due to the standardized expression. Priya et al. [34] adopted knowledge reasoning method based on rules and utilize reasoning engine Drools to enhance the expressivity and richness of knowledge. Moreover, knowledge reuse plays also an important part in effective utilization of target objects in knowledge base.

In summary, there have been quite a number of studies on green construction evaluation over the last decade. Some of them deal with evaluation methods for green construction performances and others are for key technologies in green construction. Still others are for ontologies of the green

construction knowledge. However, there seem to have limited studies specifically on the creation and utilization of BIM and ontologies to integrate the appropriate information for the purpose of green construction evaluation. Green construction evaluation is getting more and more complicated, and this is mainly due to the increased volume of the construction information and knowledge. This complexity and the need of reliable results claim for the utilization of existing tools, like BIM. The literature reviewed above identifies that BIM and evaluation methods are both necessary techniques that are used to facilitate the analysis and interpretation of green construction. Furthermore, evaluation indicator selection strategies offer limited integration of ontology and geometric data models. Related works lack a centralized knowledge database containing original data and solutions that can be used to determine problematic areas before finalizing optimization to green construction. Thus, developing an integrated evaluation system for green construction using existing experiences in ontology and BIM is key to effectively improve the sustainability of construction activities.

3. Methodology

The objective of this research is to establish an automatic green construction evaluation and optimization system. Hence, an ontology-based knowledge base from which the evaluation information of green construction could be inferred is proposed in consideration of four main steps: (1) five primary indicators and relevant attribute sets are defined based on previous studies and standards; (2) IFC expression is developed to describe the evaluation information and mapped to OWL as the data source; (3) combining BIM ontology and the evaluation indicator system of green construction, the framework of knowledge base is constructed; (4) the evaluation process is demonstrated using BIM knowledge base, and the results of the evaluation can be inferred from the collected data, as shown in Figure 1.

The proposed methodology, as the corresponding pseudocode shown in Algorithm 1, passes through the four steps to achieve the research objectives as follows. (1) After searching the existing standards and periodical articles concerning green construction evaluation, a green construction evaluation indicator system and the evaluation criteria are synthesized. (2) It further develops IFC extension which focuses on property sets P (p_1, p_2, ...) in order to express the indicators and attributes of green construction evaluation. Subsequently, the green construction evaluation indicator system is expressed as E (e_1, e_2, ...) by EXPRESS-G so that the relationships between entities can be graphically presented. Next, the IFC attributes of green construction evaluation are mapped into OWL language. The BIM model is used as the source data of green construction evaluation in the knowledge base. (3) BIM-shared ontology (BIMSO) and BIM Construction Ontology (BIMCO) are created. In parallel, Protégé Software is employed to simulate the green construction evaluation system. Since only formatted language could be understood and executed by computer, the model needs to be formatted by OWL. Combining BIM ontology and the evaluation model of green construction, the framework of knowledge base K is established in consideration of five aspects: BIM project, construction activities, green construction data, green construction evaluation, and optimization measures. (4) The proposed evaluation works by converting the knowledge of individual instance into Drools facts and converting SWRL (Semantic Web Rule Language) rules from the knowledge base, then running Drools inference based on rules, finally inferring new facts and updating the knowledge base. According to the calculation results, the unqualified indicators with scores lower than a limit t could be screened out by SPARQL inquiry. Afterwards, optimized measures could be inferred and the scheme of green construction could be modified. To demonstrate the evaluation process, a residential building is taken in this study as an example. Besides, based on the characters of knowledge reuse, the workflow to select the optimal scheme of green construction is suggested, which includes matching similar projects, modifying the green construction scheme, and updating the BIM database.

4. IFC Expression and Data Mapping

4.1. IFC Expression of the Evaluation Indicators. IFC is commonly adopted as the standard format for BIM data exchange and collaboration. This work develops a solution for the expression of the evaluation indicators of green construction, which could be used as the extended attribute sets of IFC entities. Because the extension is carried out based on the attribute set, considering beams, slabs, columns, and walls as entities in IFC standard, there is no need to define new entities and the original architecture of IFC standard remains unaffected. The process of IFC extension is shown in Figure 2. First, with reference to the characteristics of the evaluation indicator of green construction, corresponding entities and attributes in IFC standard are determined; second, the indicators are divided into attribute sets according to the properties of the evaluation; finally, the attributes and attribute sets are defined and the extension of IFC-based evaluation indicator of green construction is completed.

Over the last few decades, many management models have been adopted for the purpose of enhancing the performance of the construction projects. Some potential key performance indicators widely adopted can be used to evaluate and compare the performance of construction. With reference to previous studies by Nie et al. [35], Li et al. [17], and Zhang and He [18], there are five primary indicators, and their relevant attribute sets are defined in this work (as shown in Table 1).

The IFC4 standard has given definitions about generic attributes of beams, slabs, columns, and walls. Therefore, attributes and attribute sets mentioned above need to be specified. The specification of attributes includes attribute name, attribute type (IfcPropertySingleValue), and attribute value type (IfcReal). On the other hand, the attribute set

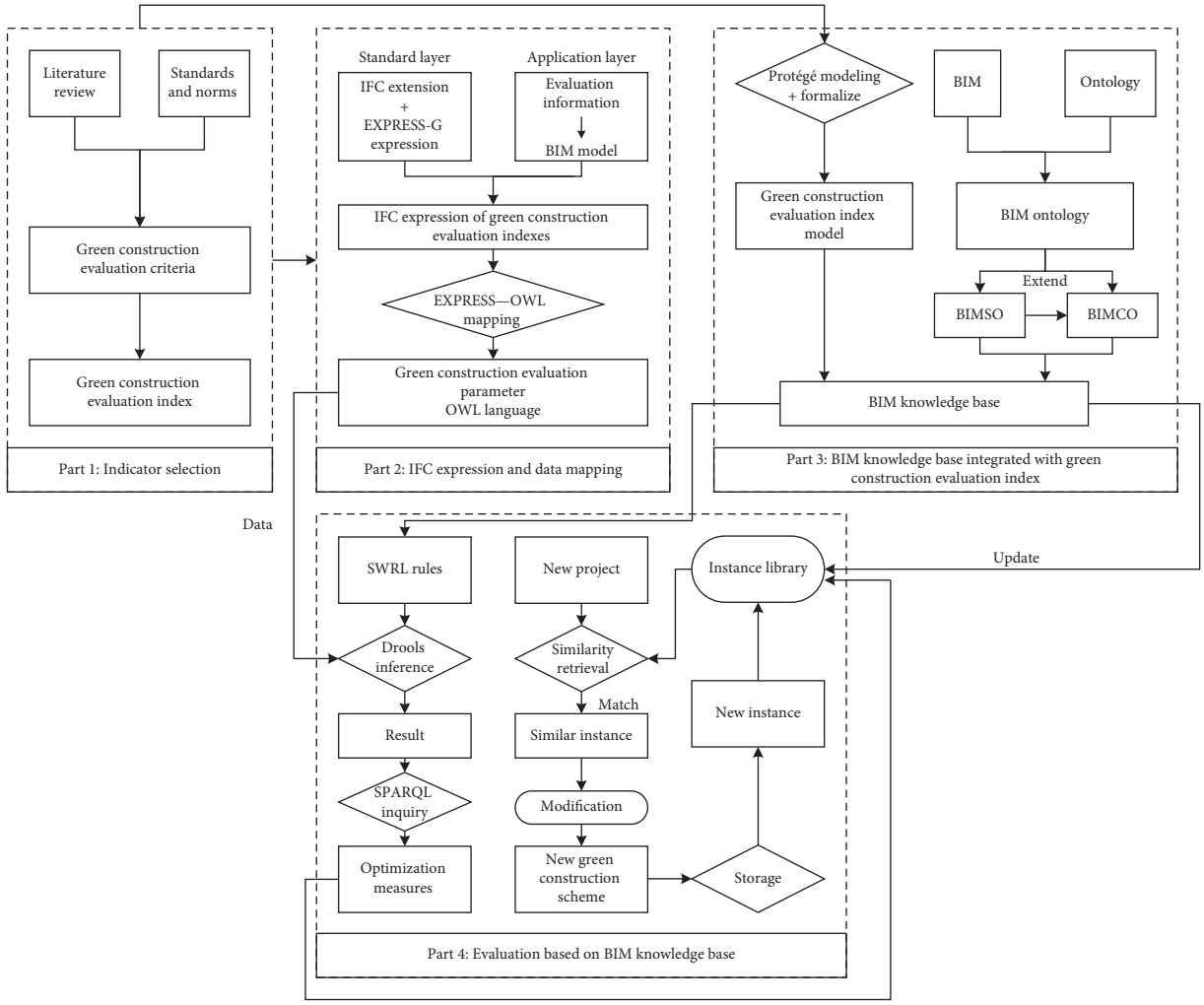

Figure 1: Overview of the implementation of proposed methodology.

Evaluation algorithm for green construction.
(1) **In:** Evaluation Indicator of green construction.
(2) **Out:** Evaluation scores and specific indicators needing improvements
(3) **Start**
//the first stage
(3) Synthesize the green construction evaluation indicators and criteria
//the second stage
(4) Develop Ifc-extended attributes P (p_1, p_2, ...) to represent the property sets.
(5) Develop Ontology-based parameter E (e_1, e_2, ...) to represent the evaluation indicators.
(6) Map (P/E, {p_1, p_2, ...}/{e_1, e_2, ...})
//the third stage
(7) Build the knowledge base $K \supseteq E$
//the fourth stage
(8) Generate the evaluation score of all indicators E_i based on values from K
(9) Retrieve specific indicator with $e_i < t$ which needs to be improved and optimized//t is the lower limit for the evaluation result.
(10) **End**

Algorithm 1: Pseudocode description of the proposed methodology.

definition includes set name, applicable entity, applicable type, and set description. As an example, the attribute set of construction preparation indicator is defined in Table 2.

4.2. Indicator Expression in EXPRESS-G. After the green construction evaluation indicator is extended into IFC, the IFC expression needs to be realized. The data modeling

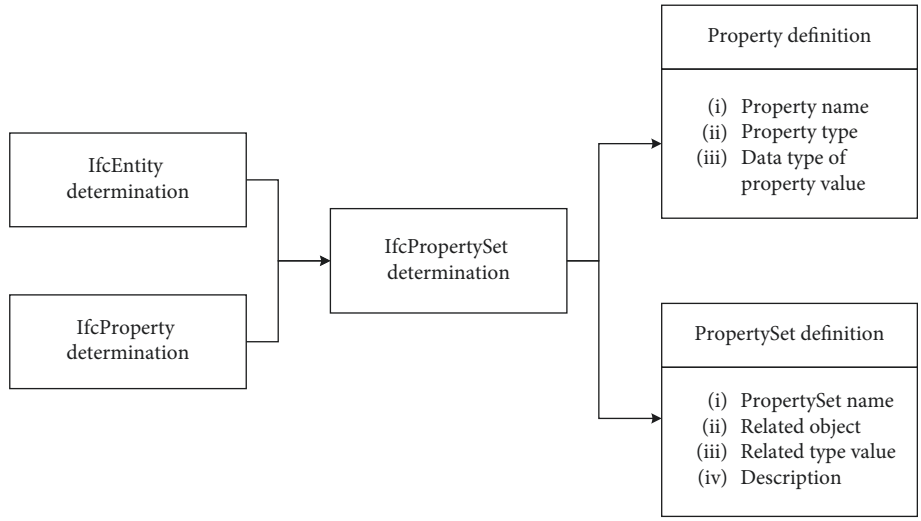

Figure 2: The process of IFC extension.

Table 1: Indicator attribute set.

Indicator	Attribute set
Construction Preparation	PSet_ Construction Preparation
Construction Site	PSet_ Construction Site
Ground and Foundation Engineering	PSet_ Ground and Foundation Engineering
Main Structure Engineering	PSet_ Main Structure Engineering
Decoration and Electromechanical Engineering	PSet_ Decoration and Electromechanical Engineering

Table 2: IFC construction preparation attribute set definition.

Attribute set name	PSet_ Construction preparation
Applicable entity	IfcEntity
Applicable type	Construction preparation
Set description	This property set describes indicators of construction preparation, aiming to conduct green construction evaluation

language of IFC schema is called EXPRESS, which is an international standard data modeling language for product data [22]. An EXPRESS data model can be described in two ways: the textual form of EXPRESS program and the tree-structured graphical notation called EXPRESS-G (a companion to the EXPRESS text, it is also called the graphical subset of the EXPRESS language). One of the advantages of EXPRESS-G is that the relationships between entities can be graphically presented in a more understandable manner. Therefore, EXPRESS-G notation is adopted as the method of expression in this work.

As shown in Figure 3, the EXPRESS-G diagram illustrates the IFC attributes with IfcRoot, IfcObjectDefinition, IfcObject, IfcProduct, IfcElement, IfcBuildingElement, IfcPropertySetDefinition, IfcPropertySet, and IfcProperty. The thick solid line represents the inheritance relationships between adjacent entities. The correlation between IfcPropertySet and IfcEntity is realized through IfcPropertySetDefinition. In this way, the status of IfcEntity can be represented by the evaluation indicator contained in IfcProperty. IfcProperty entity includes two subentities: IfcSimpleProperty and IfcComplexProperty. Moreover, IfcSimpleProperty consists of six subentities. The five attribute sets defined in this part are optional attribute sets of IfcBeam/Slab/Column/Wall (entities that inherits all the properties of IfcBuildingElement). The correlation between them is represented by dotted lines. All indicators are contained in the dotted box. The indicators can be displayed in the five attribute sets, and the relationships between them are represented by thin solid lines. The attribute value type of all the attributes is Real. "ABS" stands for abstract type. This study uses Revit to create specific BIM model in order to establish the correlation between the evaluation information of green construction and BIM model. The correlation process is comprised of four steps: ① setting up Revit family files, ② establishing the evaluation parameters of green construction and correlating them with family files, ③ loading family files into the project and inputting values of parameters, and ④ exporting IFC files.

4.3. Mapping IFC to the Evaluation Ontology. The evaluation information of green construction is stored in the BIM model in the form of IFC parameter. In this work, the IFC-based parameter is mapped to OWL and will be used as the data source of the evaluation indicators of green construction in BIM knowledge base.

4.3.1. EXPRESS—OWL Mapping Framework. By mapping the EXPRESS language of IFC standard to OWL, the information related to the BIM model and the ontology can be shared and integrated. The schema of IFC data conversion is illustrated in Figure 4. The conversion process obeys by the following principles: ① semantics described by EXPRESS before mapping is consistent with that described by OWL after mapping; ② if the definitions in IFC cannot be clarified with concepts or grammars in OWL, external grammar will

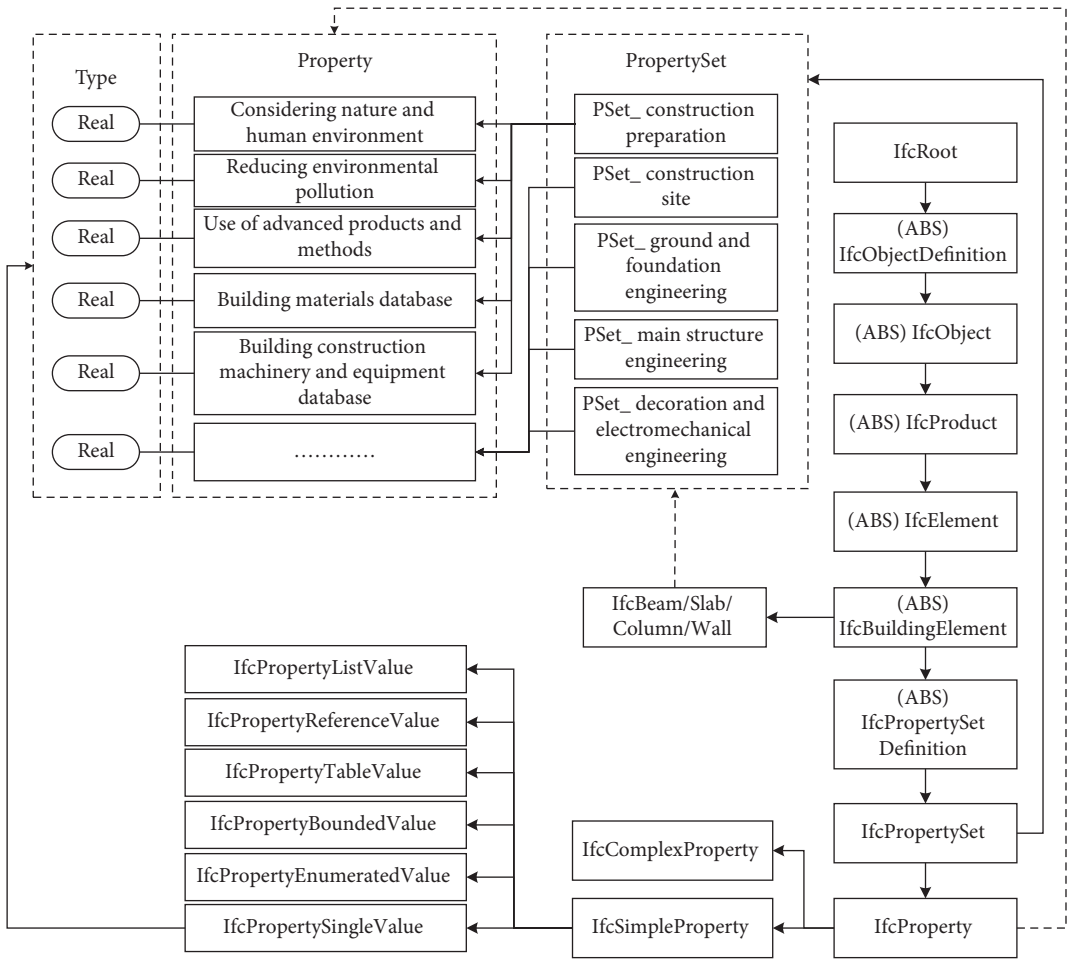

Figure 3: EXPRESS-G chart of the evaluation indicators on green construction.

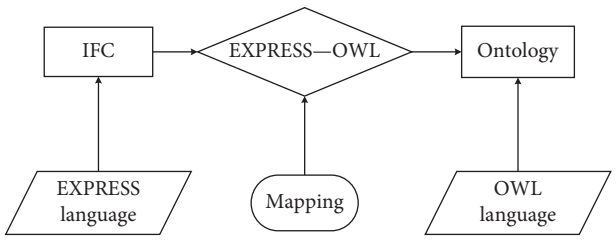

Figure 4: Diagram of IFC data mapping.

be adopted. Through the analysis of EXPRESS language based on the conversion mode between IFC and OWL, the EXPRESS-OWL mapping framework is developed, and therefore, the conversion of BIM data is realized (as shown in Table 3).

4.3.2. Mapping OWL to the Evaluation Indicator. The next step is to associate green construction evaluation information to the OWL parameter. Among all IFC-based parameters, "Dust control" is selected in this work as an example. Figure 5 shows the EXPRESS-OWL mapping of "Dust control," which is also applied to other parameters. The detailed illustration on the relationship between EXPRESS and OWL expression of "Dust control" is listed in Table 4. Through the mapping process, all indicators are converted into OWL format and the conversation of BIM data to OWL data is realized. The converted OWL data then will be used as the source data of green construction evaluation in the knowledge base.

5. BIM Knowledge Base Integrated with the Evaluation Indicators of Green Construction

5.1. BIM Ontology

5.1.1. BIM-Shared Ontology (BIMSO). A BIM model consists of numerous building elements, which are the basic composition units of the BIM model. Therefore, by specifying the basic attributes of every building elements, the model can be defined exactly. According to the basic attributes of building elements, a basic BIM-shared ontology is constructed in this work. The shared ontology can be applied to the construction field by supplementing corresponding attributes. The basic attributes in the form of the building elements, which are contained in the established BIM shared ontology (BIMSO), are identity, size, space, and material. The detailed BIM-shared ontology is illustrated in Figure 6. BIMSO:Building stands for building element; BIMSO:

Table 3: Mapping between EXPRESS language and OWL language.

			EXPRESS expression	OWL expression
Patterns and interface specifications			(i) Pattern (ii) User interface specifications (iii) Reference interface specifications	(i) Ontology (ii) rdf:about (iii) owl:import
Data type	Simple data types		Data type: (i) Boolean (ii) Integer (iii) String (iv) Real (v) Binary (vi) Number	owl: Datatypeproperty: (i) xsd:boolean (ii) xsd:integer (iii) xsd:string (iv) xsd:real (v) hexBinary/base64Binary (vi) Methods to customize axiom
	Aggregation types		LOGICAL ARRAY BAG SET LIST	Expressed by union in XML schema Expressed by user-defined data types in XML schema rdf:Lists
	Constructed types		ENUMERATION SELECT	owl:one of rdfs:subclasses owl:unionOf
	Defined data types		Defined data	Expressed by user-defined data types in XML schema
	Entity data types		Entity data	Add prefix information when defining entity properties
Entity type	Entity—classes		Entity + entity name	<owl:Class rdf:ID = "entity name">
	Entity—instances		Entity + instance name	<owl: individual = "instance name">
	Entity attribute	Explicit attribute	Mandatory	<owl:ObjectProperty rdf: ID = "EntityName_PropertyName"><owl: DatatypeProperty rdf: ID = "EntityName_PropertyName">
		Derive attribute	Optional Derive	OPT_ Specific owl:Class
		Inverse attribute	Inverse	ObjectInverseOf declaration of a property as inverse property InverseObjectProperties declaration of two properties as mutual inverse properties
	Local rules	Domain rule	Where	swrl:equal
		Unique rule	Unique	Expression key hasKey of axion hasKey
	Supertype&Subtype		Supertype&Subtype	rdfs:superClassOf rdfs:subClassOf

hasIdentity, BIMSO:hasSize, BIMSO:hasSpace, and BIMSO: hasMaterial stand for the four basic attributes that are contained in the building elements.

(i) Identity: it includes description, ID value, Manufacturer, etc.

(ii) Size: it includes length, height, thickness, volume, etc.

(iii) Space: it includes associated floor number and room position

(iv) Material: it includes qualitative properties of the materials like the grade and color of the cement and quantitative properties of the materials like density and compression strength.

(v) fc: ConstructionAndBuildingMaterials is designed based on the existing Free Class OWL ontology (FC) and represents the building material; qudt_schema: Unit is designed based on the existing QUDT ontology and stands for unit.

5.1.2. BIM Construction Ontology (BIMCO). By extending BIM shared ontology, the BIM construction ontology (BIMCO) can be constructed. BIMCO will be utilized as the foundation of the BIM knowledge base. The details of BIM construction ontology are shown in Figure 7. By supplying relevant information about green construction extension (BIMSO:hasGreenConstruction) into BIMSO:Building, BIMCO: Element is created and consists of two parts.

(1) Principles of Green Construction. According to the green construction specification, there are five principles: BIMCO: EnergyConservation, BIMCO:WaterConservation, BIMCO: LandConservation, BIMCO:MaterialConservation, and BIMCO: EnvironmentalProtection.

(2) First Level Indicators of Green Construction Evaluation (BIMCO:FirstIndicator). The first level of green construction evaluation information consists of five indicators which are extended into BIM model ontology: BIMCO:ConstructionPreparation, BIMCO:ConstructionSite, BIMCO:

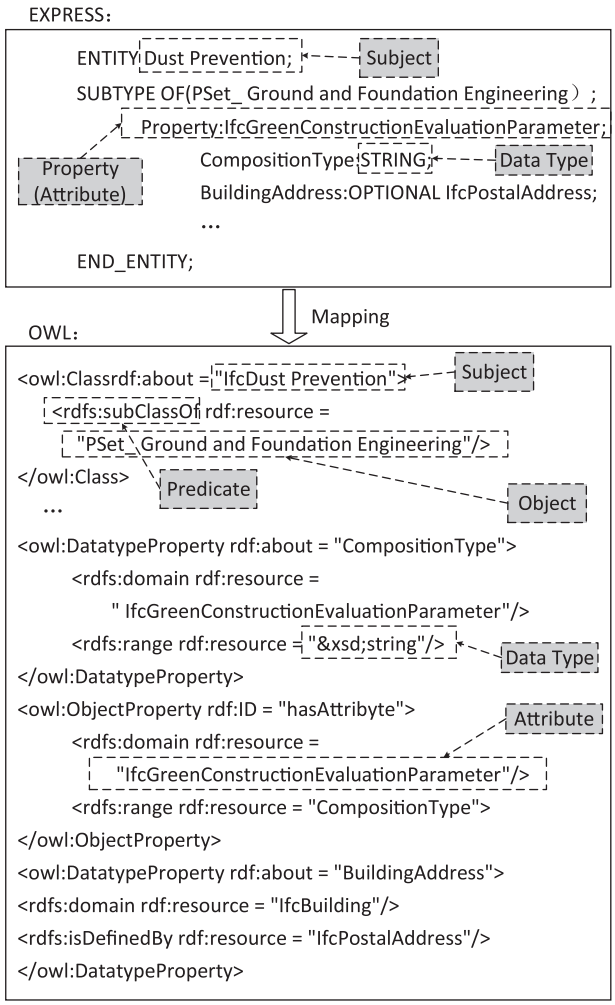

Figure 5: EXPRESS-OWL mapping of dust control parameter.

GroundAndFoundation, BIMCO:MainStructure, and BIMCO: DecorationAndElectromechanicalEngineering.

5.2. BIM Knowledge Base Framework. In this study, Protégé is applied to model the evaluation indicator system of green construction, which could support the integration of evaluation indicator system and BIM knowledge base. Protégé is always viewed as a professional tool especially in ontology modeling and knowledge acquiring based on Java environment. It is an open source software application and is widely used for ontology modeling in semantic network. Since only formatted language could be understood and executed by computers, after the evaluation indicator framework is constructed, its expression needs to be formatted. In this paper, OWL is used to formalize expressions, and classes need to be defined and declared. Their subordination relations are then determined before OWL code is programmed.

By combining BIM ontology and the evaluation indicator system of green construction, the framework of knowledge base is determined in consideration of five aspects: BIM project, construction activities, green construction data, green construction evaluation, and optimized measures. An instance of the framework is represented in Figure 8. As shown in this example, after the BIM project is created, the next step is to collect data from construction activities. The "construction activities" is divided into five first-level indicators: construction preparations, construction site, ground and foundation engineering, main structural engineering, and decoration and electromechanical installation engineering. "Construction activities" generates "green construction data," which is viewed as the second-level indicator. After collecting green construction data, the evaluation process is to be conducted, and optimized measures can be suggested. Finally, based on the evaluation indicator framework of green construction and the composition of the BIM model, the BIM knowledge base is established. BIM knowledge base mainly consists of the relationships between classes, object properties, data properties, and instance creation.

5.2.1. Relationship between Classes. Class is the basic element in the knowledge base. The five basic aspects, including BIM project, construction activities, green construction data, evaluation of green construction, and optimization measures, are defined by class as shown in Table 5.

5.2.2. Object Properties. To describe the nonhierarchical relationships between classes, numerous object properties could be defined in the knowledge base. "BIM project" includes "construction activities," and their relationships can be expressed by "hasConstruction;" "Construction activities" produces large amounts of "green construction data," and their relationships are represented by "produceInformation;" the property of "Evaluation of green construction" is conducted based on "green construction data," and this step is called "conductEvaluation;" "optimization measures" is developed according to "evaluation of green construction" and described based on "raiseOptimization."

Name, domain, range, and function properties are defined as the four object properties mentioned above (as shown in Table 6). The definition of domain is the origin of the attribute relations, and the definition of range is the ending of the attribute relations. In other words, domain and range are linked by attribute relationships. "Functional" means that the attribute could only connect one entity and "inverse functional" means that the inverse property of the attribute has the functional property. According to the analysis, all four attributes have inverse functional properties. Although there always have been several construction activities in one project, each specific construction activity belongs to only one project.

5.2.3. Data Properties. Data property represents the relationship between class and data, which is simpler than object property. Data is linked to class by data properties, and data properties exist depending on class. Data properties of five basic classes are analyzed, and the detailed results are listed in Table 7.

Table 4: EXPRESS-OWL mapping of dust control parameters.

EXPRESS expression	OWL expression
Dust prevention is an entity called dust prevention Relationship: SUBTYPE OF Property set that it belongs to: PSet_Ground and Foundation Engineering IfcGreenConstructionEvaluationParameter Property: IfcGreenConstructionEvaluationParameter Composition type: Data type STRING	Correspondence: OWL subject—owl:class rdf:about = "IfcDust Prevention" Correspondence: OWL predicate—rdfs:subClassOf Correspondence: OWL object—rdf:resource = "PSet_Ground and Foundation Engineering" Correspondence: OWL ObjectProperty, its domain is rdfs:domain rdf: resource = "IfcGreenConstructionEvaluationParameter" Correspondence: OWL DataTypeProperty, its domain is rdfs:range rdf: resource = "&xsd:string"

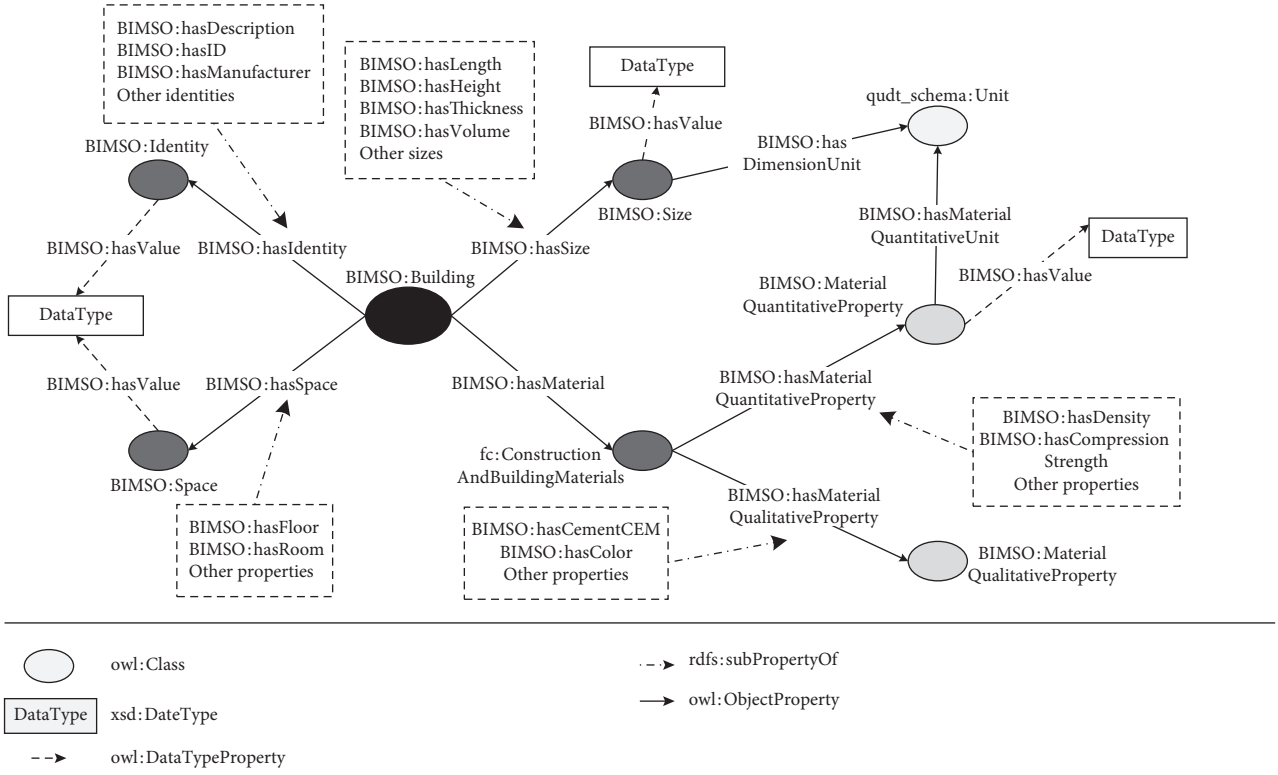

Figure 6: Concept of BIM ontology.

5.2.4. Instances Creation. After establishing classes and properties, the next step is to create instances according to classes. In comparison with the class which is an abstract concept, the instance represents the specific entity. The establishment of instances is of great significance for the application of the knowledge base. For example, a specific BIM project is an instance and the construction activities generated are corresponding specific instances. Considering the instance of "decoration and electromechanical installation" as an example, the environmental pollutant concentration indicator, which is one of the indicators of green construction information, is selected to help evaluate green construction and develop optimized measures. This whole process is named as "instances creation."

Through the establishment of instances, corresponding links are formed between BIM projects, construction activities, green construction data, evaluation of green construction, and optimized measures (as shown in Figure 9). Instances are added and linked to the former ones through the addition of object properties which point to another instance. The complete link of BIM knowledge base contains the following parts. "Residential Building BIM project" has the construction activity of "indoor decoration," which generates the "data of indoor pollutant concentration" as part of the green concentration data. With reference to the "data of indoor pollutant concentration," the evaluation of green construction is conducted and the result "indoor pollutant concentration is high" is obtained. To solve the detected problem, optimized measure "low-pollution materials should be used for decoration" is raised.

6. Evaluation Based on BIM Knowledge Base

To demonstrate the evaluation process, a BIM project of a residential building is taken in this work as an example, from which some indicators of green construction are collected

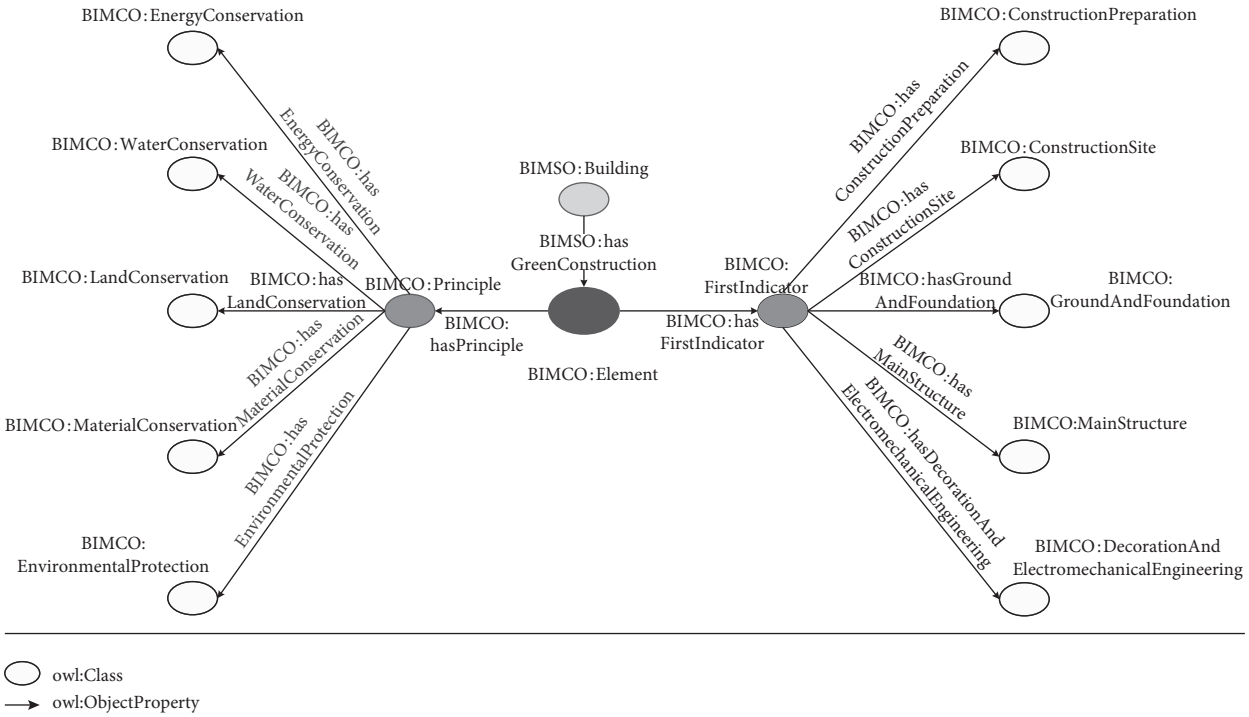

Figure 7: Concept of BIM construction ontology.

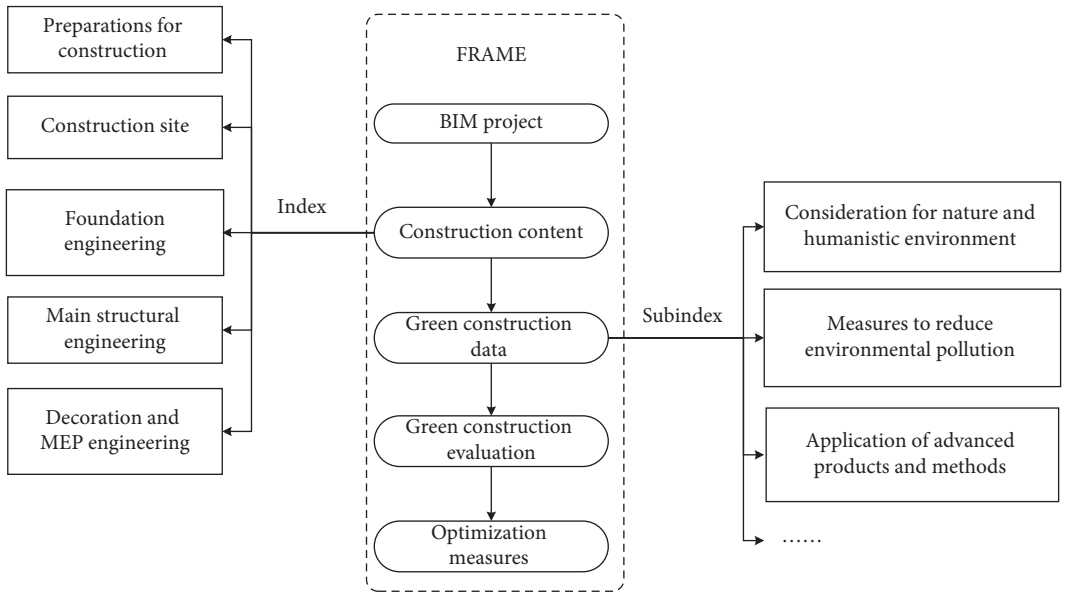

Figure 8: Framework of BIM knowledge base.

and the evaluation of green construction is conducted accordingly. Firstly, the standards for evaluation indicators are developed and described by SWRL before it is input BIM knowledge base; secondly, the values of green construction indicators are determined, which are derived from the extension of BIM model and have been converted to OWL language format; lastly, with the help of SWRL rule base, the evaluation results can be inferred from the collected data of the indicators.

(1) Establishment of property rules

According to the link diagram of BIM knowledge base, the relationships between BIM projects, construction activities, green construction data, evaluation of the green construction, and optimized measures are simulated as follows: BIM project and construction activities are connected by "hasConstruction" property; construction activities and green construction data are connected by "produceInformation" property;

Table 5: Definitions of basic classes.

Class name	Abbreviation in English	Description
BIM project	BIM	BIM model of the project
Construction activity	Construction	Construction activities of the project, mainly the first-grade indicators of the indicator system
Green construction data	Information	Relevant green construction data, mainly the second-grade indicators of the indicator system
Green construction evaluation	Evaluation	Green construction evaluation according to green construction indicator values
Optimization measure	Optimization	Optimization measures according to green construction evaluation result

Table 6: Definitions of object properties.

Property name	Domain	Range	Function characteristic
hasConstruction	BIM project	Construction activity	Inverse functional
produceInformation	Construction activity	Green construction data	Inverse functional
conductEvaluation	Green construction data	Green construction evaluation	Inverse functional
raiseOptimization	Green construction evaluation	Optimization measures	Inverse functional

Table 7: The definition of data properties.

	BIM project	Construction activity	Green construction data	Green construction evaluation	Optimization measure
Data property	(i) Project number (ii) Project name (iii) Project address (iv) Project description (v) Contract price (vi) Owner unit (vii) Design unit (viii) Construction unit (ix) Supervision unit (x) Starting date (xi) Construction period	(i) Serial number of construction activity (ii) Name of construction activity (iii) Construction phase (iv) Relevant project (v) Description of construction activity (vi) Builders (vii) Construction material (viii) Construction machinery (ix) Construction environment	(i) Relevant construction activity (ii) Relevant project (iii) Indicator name (iv) Green construction description (v) Constructor (vi) Construction material (vii) Construction machinery (viii) Construction environment	(i) Relevant construction activity (ii) Relevant project (iii) Indicator name (iv) Energy conservation (v) Water conservation (vi) Land conservation (vii) Material conservation (viii) Environmental protection (ix) Score (x) Evaluation result	(i) Relevant construction activity (ii) Relevant project (iii) Evaluation result (iv) Scores of indicators (v) Optimization measure
Value type	int or string	int or string	int or string	int or string	int or string
Function type	Functional	Functional	Functional	Functional	Functional

green construction data and evaluation of green construction are connected by "conductEvaluation" property; and evaluation of green construction and optimization measures are connected by "raiseOptimization" property, and the inference rules of property of the relationship between nodes are as follows:

Rule-A: assume that $X \in$ BIM project, $Y \in$ Construction, $Z \in$ green construction data, A $\in$ green construction evaluation, B $\in$ optimization measures, and X (hasConstruction) Y, Y (produceInformation) Z, Z (conductEvaluation) A, A (raiseOptimization) B; then, X (produceInformation) Z, X (conductEvaluation) A, X (raiseOptimization) B.

Rule-B: assume that $X \in$ BIM project, $Y \in$ Construction, $Z \in$ green construction evaluation, A $\in$ optimization measures, and X (produceInformation) Y, Y (conductEvaluation) Z, Z (raiseOptimization) A; then, X (conductEvaluation) Z, X (raiseOptimization) A.

Rule-C: assume that $X \in$ green construction data, $Y \in$ green construction evaluation, $Z \in$ optimization measures, and X (conductEvaluation) Y, Y (raiseOptimization) Z; then, X (raiseOptimization) Z.

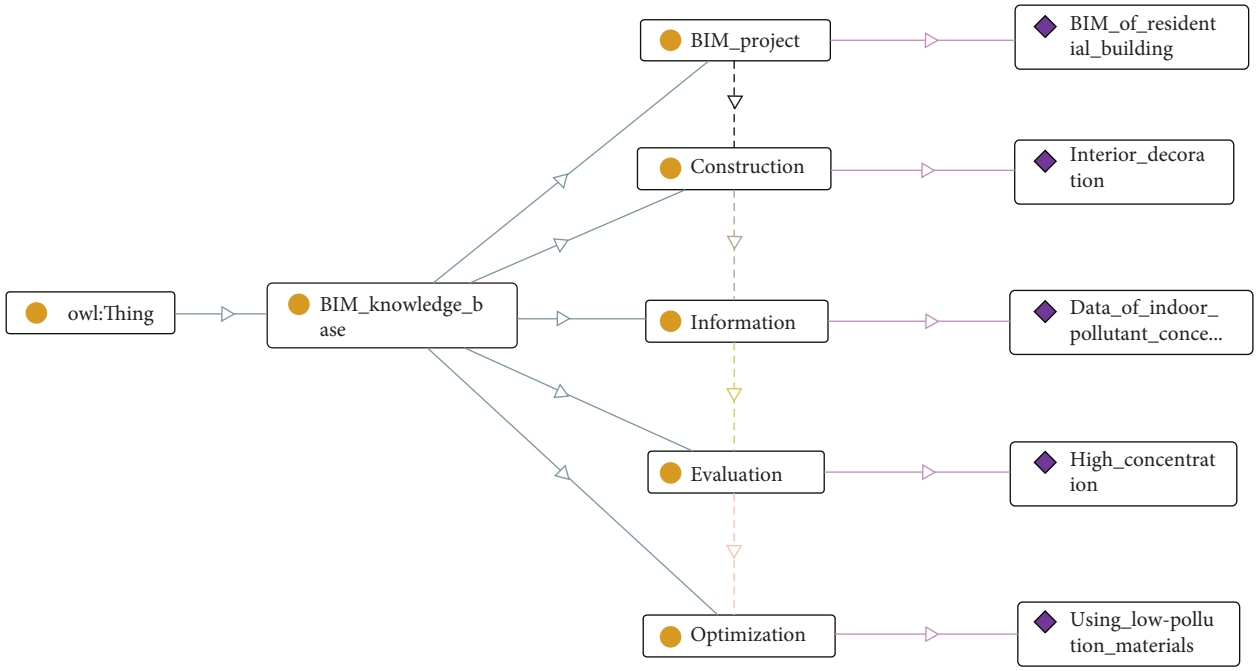

Figure 9: Link relationship of BIM knowledge base.

The rules above can be represented directly by Figure 10. The solid lines stand for the known relationships, while dotted lines stand for the implicit relationships inferred by SWRL rules.

According to the three rules mentioned above and taking indicator "dust control" as an instance, its expression in SWRL rule language is summarized as follows. First, Protégé system identifies the value of indicator "dust control" with a score 1.5, which confirms to Rule-1.1 ($1.3 < X \leq 1.5$) and infers the result conductEvaluation (?x, 1), i.e., the score is 1 point. The result of induction is shown in Figure 11. Then, optimized measures are derived from raiseOptimization.

(2) Establishment of Instance rules

With reference to four evaluation standards and norms for green construction, including Guidelines for Green Construction (2007), Evaluation standard for Green *Construction of Building (GB/T50640-2010)*, *Code for Green Construction of Building (GB/T50905-2014)*, and *Assessment Standard for Green Buildings (GB/T50378-2014)*, as well as specific standards *Emission Standard of Environmental Noise for Boundary of Construction Site (GB12523-2011)* and *Integrated Wastewater Discharge Standard (GB8978-1996)*, the evaluation indicator and scoring criteria of one specific residential building project is created in order to establish instance rules.

6.1. Green Construction Evaluation Based on Drools Inference. Based on the actual data of indicators collected and the evaluation criteria, the results of evaluation will be inferred in Drools. When Drools is provided with certain domain rules and data, it can process a variety of inference tasks. Through the conversion of the corresponding format, the knowledge presented in ontology form and rules expressed in SWRL could be transformed into facts and rules that can be understood and supported by Drools. Afterwards, the inference engine of Drools is able to infer issues in the field of domains and generate new facts. The inference engine of Drools has been integrated into software Protégé. It can transform ontology instances and SWRL rules into Drools facts and Drools rule in order to obtain the fact and rule basis. The inference is comprised of four steps: ① converting the knowledge of individual instance into Drools facts; ② converting SWRL rules to Drools rules; ③ running Drools inference based on facts and rules; ④ inferring new facts and updating the knowledge base with them. The inferring process of Drools based on BIM knowledge base is shown in Figure 12.

The indicator values in Table 8 are derived from the data of BIM model and have been converted into OWL language before stored in BIM knowledge base. Here, "dust control" is taken as a sample to conduct Drools inference.

Figure 13 shows the instance of "Dust control." The value of indicator 1.5 has been already stored in the knowledge base. Inference is then conducted upon the value of indicator. Rule-1.1, Rule-1.2, and Rule-1.3, SWRL rule language specifically written in previous section for dust control, are edited in SWRL Tab before the Drools inference. First OWL + SWRL -> Drools is run, in which system converts ontology knowledge (indicator value 1.5) and SWRL rules into knowledge and rules that Drools can understand and support. Then, Run Drools is executed for inference. The system identifies that the indicator value 1.5 is within the range of Rule-1.1 ($1.3 < X < 1.5$) and then

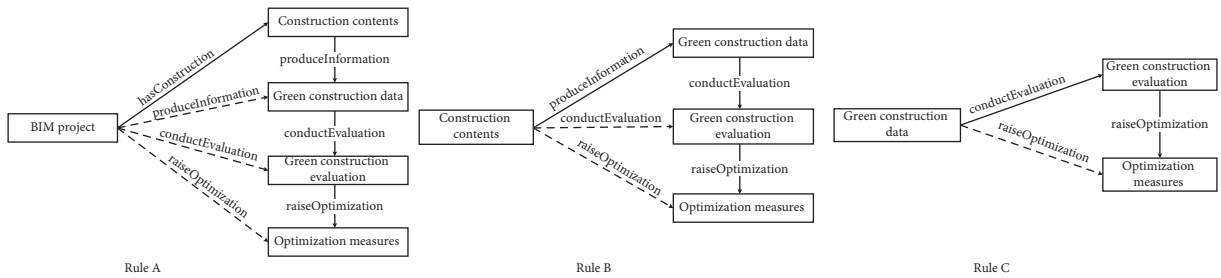

Figure 10: Illustration of SWRL rules.

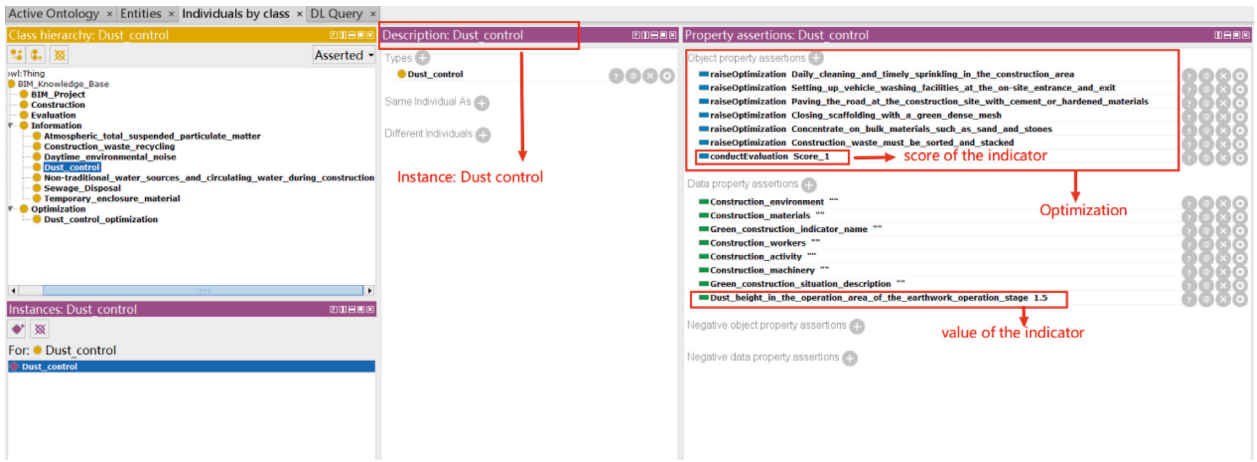

Figure 11: Induction instance of "dust control."

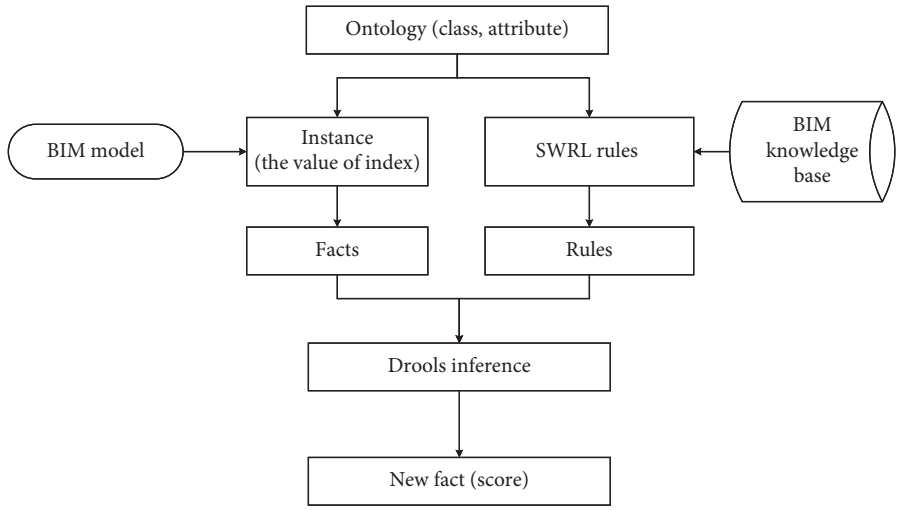

Figure 12: Flow chart of Drools inference.

indicates the result conductEvaluation (? X, 1), i.e., the score is 1.

In the same way, 16 indicators in SWRL rule language are listed and entered into the knowledge base. Drools inference is conducted upon 16 indicator values stored in BIM knowledge base, and the scores of evaluations are obtained as shown in Table 9.

6.2. SPARQL Inquiry-Integrated Green Construction Optimization. In view of the result, the specific indicators could be identified which do not conform to the requirements and also lead to the results of disqualification; then, optimized measures need to be put forward. In this paper, the evaluation of indicators is completed in BIM knowledge base, and a way to inquire is proposed. SPARQL

Table 8: Indicator results.

Number	Specific indicator content	Indicator values
1	Dust control: visual inspection of the fugitive dust height in the earthwork area (m)	1.5
2	Ambient noise at daytime (dB)	65
3	Suspended solid content in sewage water (mg/L)	300
4	Difference between monthly average total suspend particulate (TSP) on site and the city back ground value (mg/m^3)	0.065
5	Recycle and recovery ratio of construction wastes (%)	15
6	Reuse ratio of field temporary housing and retaining wall material (%)	40
7	Reuse ratio of unconventional water and recycled water (%)	45
8	Illumination should not exceed the percentage of the minimum illumination (%)	20
9	Equip ratio of water-saving devices in administrative area and living quarters on site (%)	80
10	Ratio of energy-saving lightings (%)	95
11	Ratio of reusable partition walls (%)	60
12	Ratio of prefabricated parts (%)	35
13	Ratio of premixed mortar to building mortar (%)	65
14	Ratio of ordinary rebar with higher grades than 400 MPa (%)	45
15	Lost rate of reinforcement field processing (%)	3
16	Usage of tool type combination formwork (%)	80

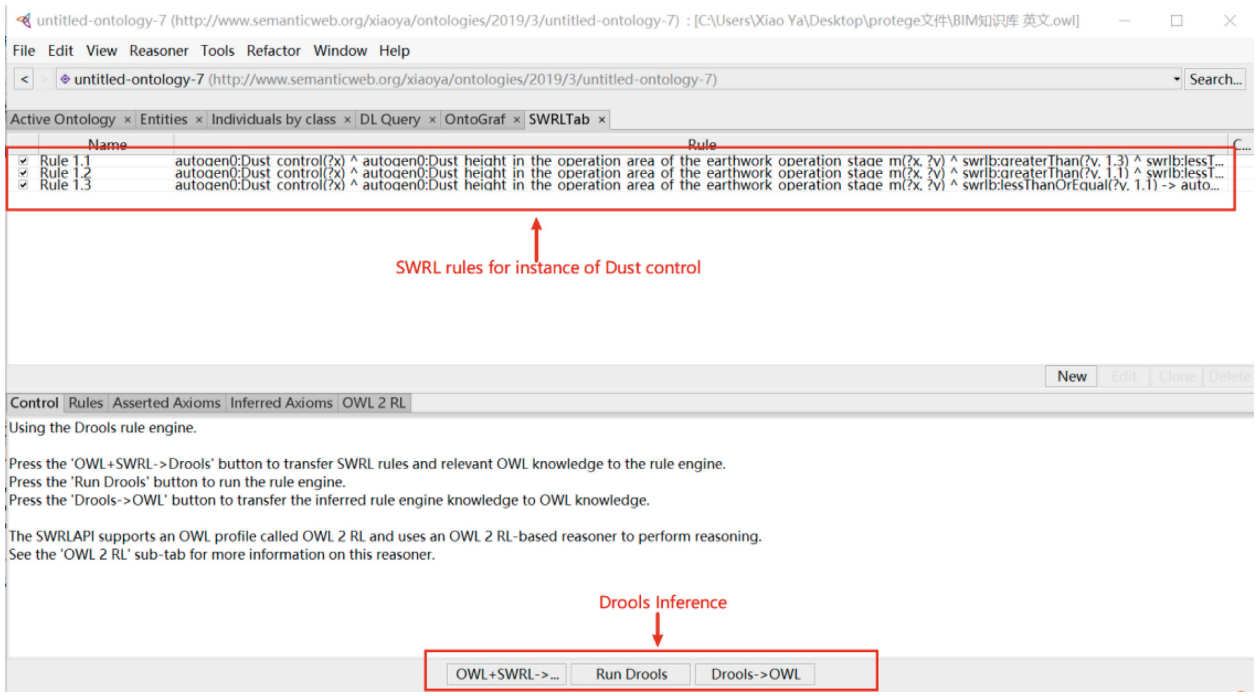

Figure 13: Induction instance of "dust control."

is chosen as the language to inquire BIM knowledge base. SPARQL, as the inquiry language for semantic network developed and recommended by W3C, could be used to retrieve the information in BIM knowledge base. Programming code is input into the editing block of SPARQL inquiry. SPARQL inquiry is a command inquiry tool from Protégé, which is used to search for information in the knowledge base. SPARQL inquiry coding is run and the indicators with scores less than 2 points are shown in the following Table 10.

Considering the 9 indicators with scores less than 2 points, with the help of knowledge inference, optimized

Table 9: Evaluation result.

Number	Specific indicator content	Indicator values	Scores
1	Dust control: visual inspection of the fugitive dust height in the earthwork area (m)	1.5	1
2	Ambient noise at daytime (dB)	65	1
3	Suspended solid content in sewage water (mg/L)	300	1
4	Difference between monthly average total suspend particulate (TSP) on site and the city back ground value (mg/m^3)	0.065	2
5	Recycle and recovery ratio of construction wastes (%)	15	0
6	Reuse ratio of field temporary housing and retaining wall material (%)	40	1
7	Reuse ratio of unconventional water and recycled water (%)	45	2
8	Illumination should not exceed the percentage of the minimum illumination (%)	20	1
9	Equip ratio of water-saving devices in administrative area and living quarters on site (%)	80	1
10	Ratio of energy-saving lightings (%)	95	3
11	Ratio of reusable partition walls (%)	60	2
12	Ratio of prefabricated parts (%)	35	2
13	Ratio of premixed mortar to building mortar (%)	65	1
14	Ratio of ordinary rebar with higher grades than 400 MPa (%)	45	1
15	Lost rate of reinforcement field processing (%)	3	2
16	Usage of tool type combination formwork (%)	80	2

Table 10: SPARQL query on indicators with scores less than 2 points.

Number	Specific indicator content	Indicator values	Scores
1	Dust control: visual inspection of the fugitive dust height in the earthwork area (m)	1.5	1
2	Ambient noise at daytime (dB)	65	1
3	Suspended solid content in sewage water (mg/L)	300	1
4	Recycle and recovery ratio of construction wastes (%)	15	0
5	Reuse ratio of field temporary housing and retaining wall material	40	1
6	Illumination should not exceed the percentage of the minimum illumination (%)	20	1
7	Equip ratio of water-saving devices in administrative area and living quarters on site (%)	80	1
8	Ratio of premixed mortar to building mortar (%)	65	1
9	Ratio of ordinary rebar with higher grades than 400 MPa (%)	45	1

measures for these indicators are given. Firstly, SWRL rule language for optimized measures is constructed. Based on the 16 indicators constructed in SWRL rule language above, SWRL rules corresponding to optimized measures of indicators are designed. The next step is the Drools inference. The indicator "Dust control" is taken as an instance and six optimized measures are proposed from raiseOptimization: ① vehicle rinsing facilities are to be established at the entrance and exit of construction site; ② roads on construction site are to be paved; ③ granular materials such as sand, gravel, and cement are to be stockpiled and covered; ④ construction area is to be cleaned and sprinkled regularly daily; ⑤ waste classification must be in place for construction waste; and ⑥ scaffolding must be enwrapped by green closely knitted safety net. The method is used to infer the other eight indicators and optimization measures are suggested. The optimized measures are listed in Table 11.

7. Limitation and Future Work

Two main limitations of this work are acknowledged. First, the proposed evaluation methodology only considers a selected evaluation indicator system defined by previous studies and related standards. A larger indicator system could better capture the needed attributes to evaluate green construction in practice. Further research is needed to study systematically the ontology for semantic interpretation of green construction indicators. It is necessary to explore the

Table 11: Optimization method.

NO.	Specific indicator content	Values	Scores	Optimized measures
1	Dust control: visual inspection of the fugitive dust height in the earthwork area (m)	1.5	1	(i) Establish vehicle rinsing facilities at the entrance and exit of construction site (ii) Pave the roads on construction site (iii) Stockpile and cover granular materials such as sand, gravel and cement (iv) Clean and sprinkle construction area regularly daily (v) Waste classification must be in place for construction waste (vi) Enwrap scaffolding with green closely knitted safety net
2	Ambient noise at daytime (dB)	65	1	(i) Reduce the noise of concrete vibrators, use low-frequency vibrators instead of high-frequency vibrators (ii) Isolate inevitable noise sources
3	Suspended solid content in sewage water (mg/L)	300	1	(iii) Equip effective sewage treatment facilities (iv) Build settling ponds, oil interceptors, and septic tanks
4	Recycle and recovery ratio of construction wastes (%)	15	0	(v) Improve the recovery and reutilization of construction wastes
5	Reuse ratio of field temporary housing and retaining wall material (%)	40	1	(vi) Improve the reutilization of temporary housing and retaining wall material
6	Illumination should not exceed the percentage of the minimum illumination (%)	20	1	(vii) Properly reduce the number of lightings
7	Equip ratio of water-saving devices in administrative area and living quarters on site (%)	80	1	(viii) Increase the equip ratio of water-saving devices
8	Ratio of premixed mortar to building mortar (%)	65	1	(ix) Increase the ratio of premixed mortar
9	Ratio of ordinary rebar with higher grades than 400 MPa (%)	45	1	(x) Increase the use of ordinary rebar with higher grade than 400 Mpa

various types of green construction information and identify which types of data can be extracted in a BIM-based quantitative way and which would require subjective evaluation and verification. Even for the type of subjective evaluation on green construction, the proposed approach in this study could be useful in acting as a possible way to construct the knowledge base of subjective opinions, and ensure the alignment with the concept representations of the green construction information. Second, the process of the proposed evaluation approach is not totally automatic, which would require some level of human involvement. It is essential to achieve high performance in extracting green construction information and generating corresponding IFC attributes to support the functional requirements in evaluation tools. In future work, in order to study possible ways for further performance improvement, further research could be conducted to explore different methods for integrating BIM software and evaluation tools.

8. Conclusion

BIM-based construction management has begun to expand [36]. Since the number of practices that use BIM-based information management has significantly increased, the construction industry has augmented its use of BIM model and knowledge base during construction projects. However, although the BIM tool may supply geometric attributes extraction, it cannot provide directly and automatically any information on the evaluation items on green construction. Theoretically, the information needed for managing green construction can be automatically obtained from BIM. Practically, however, the information that can be obtained from BIM will remain very limited unless BIM contains full information and knowledge. Therefore, although BIM tools are used for construction simulation, the corresponding optimization measures on green construction cannot be linked to BIM model directly.

In this paper, it is demonstrated that in BIM knowledge base, through the construction of SWRL rule language of indicators and the Drools inference, the scores of indicators could be obtained. By analyzing the scores, green construction could be evaluated. According to the results of the evaluation, unqualified indicators could be screened out by SPARQL inquiry. Afterwards, corresponding optimized measures could be inferred and the scheme of green construction could be modified. In comparison to existing evaluation methods' efforts in the green construction domain, this work contributes to the body of knowledge in two main ways. First, the proposed method integrates the evaluation indicators of green construction with IFC expression. The integration allows for extracting evaluation information directly from BIM models, which avoids both

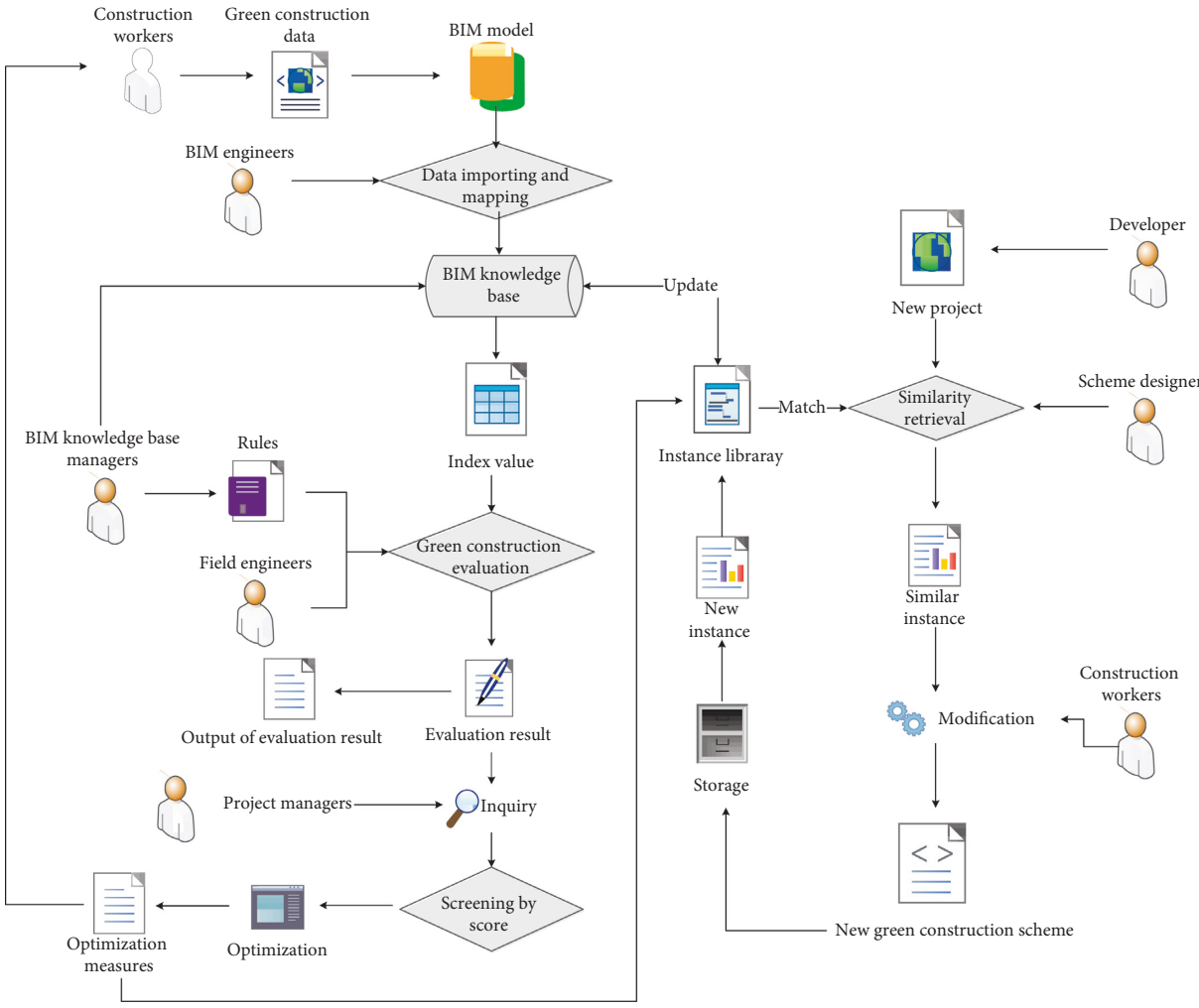

Figure 14: Flow chart of BIM knowledge base application.

errors and computational effort resulting from processing large amounts of construction data. Second, this work proposes to use the ontology for green construction to build a conceptual knowledge base for the evaluation information and proposes a SPARQL inquiry-integrated evaluation method. The experimental results show that the use of the proposed approach was effective in designing optimized measures in green construction.

Knowledge base can facilitate knowledge sharing. Therefore, BIM knowledge base for the evaluation of green construction could realize the sharing, maintenance, and acquisition of knowledge among different participants of the project and improve the management of green construction. Through the analysis of the BIM knowledge base, the workflow of the system is determined (as shown in Figure 14). First, construction site personnel collect relevant green construction data from the site and input into BIM model. Second, the BIM engineer maps and transforms the input data into BIM knowledge base to derive the value of the evaluation indicator of green construction. Then, managers of BIM knowledge base establish the rules of evaluation. Afterwards, site engineers can utilize BIM knowledge base to evaluate green construction in order to obtain and output results. Next, project managers inquire the results of evaluation, screen scores, optimize green construction, put forward optimization measures, and deliver these measures to constructors as feedback. In the meantime, project and its optimization measure plan are saved in BIM knowledge base as an instance. When the contractor plans for a new project and need to determine green construction scheme, engineers can conduct a similarity retrieval of project cases from the base of project cases in BIM knowledge base to find the matching case and make improvements to suit the new one. The new project and its scheme of green construction will also be stored as a new instance in the base of project cases, which will be regularly updated and maintained by managers.

Data Availability

The data used to support the findings of this study are available from the corresponding author upon request.

Conflicts of Interest

The authors declare that they have no conflicts of interest.

Acknowledgments

The authors' special thanks go to all survey participants and reviewers of the paper and appreciation to the National Science Council of P. R. C. (NSFC-71071482 and 71841025) and National Key R&D Program of China (2016YFC02001-06) for the financial support.

References

[1] A. R. Pearce and Y. H. Ahn, *Sustainable Buildings and Infrastructure: Paths to the Future*, Routledge, Abingdon, UK, 2018.

[2] P. O. Akadiri, E. A. Chinyio, and P. O. Olomolaiye, "Design of a sustainable building: a conceptual framework for implementing sustainability in the building sector," *Buildings*, vol. 2, no. 2, pp. 126–152, 2012.

[3] Q. Shi, J. Zuo, R. Huang, J., and S. Huang, "Identifying the critical factors for green construction—an empirical study in China," *Habitat International*, vol. 40, pp. 1–8, 2013.

[4] S. S. M. Isa, N. M. Salleh, W. N. W. Ismail, Z. Z. Abidin, and N. Md. Zain, "Performance measurement of industrialised building system (IBS) towards achieving green construction and sustainability in construction project in Malaysia," in *Regional Conference on Science, Technology and Social Sciences (RCSTSS 2016)*, N. Yacob, N. Mohd Noor, N. Mohd Yunus, R. Lob Yussof, and S. Zakaria, Eds., Springer, Singapore, 2008.

[5] A. Kamarul, A. Zuhairi, M. Ghani, C. O. Egbu, and M. Arif, "Collaboration initiative on green construction and sustainability through industrialized buildings systems (IBS) in the Malaysian construction industry," *International Journal of Sustainable Construction Engineering & Technology*, vol. 1, no. 1, pp. 119–127, 2010.

[6] V. Bokalders and M. Block, *The Whole Building Handbook: How to Design Healthy, Efficient, and Sustainable Buildings*, Earthscan, London, UK, 2010.

[7] L. Klotz, M. Horman, D. Riley, and J. Bechtel, "Process transparency for sustainable building delivery," *International Journal of Sustainable Engineering*, vol. 2, no. 4, pp. 298–307, 2009.

[8] S. Sayce, L. Ellison, and P. Parnell, "Understanding investment drivers for UK sustainable property," *Building Research & Information*, vol. 35, no. 6, pp. 629–643, 2007.

[9] Y. Li, W. Yu, B. Li, and R. Yao, "A multidimensional model for green building assessment: a case study of a highest-rated project in Chongqing," *Energy and Buildings*, vol. 125, pp. 231–243, 2016.

[10] S. Yao and M. T. Birgonul, "Preventing claims in green construction projects through investigating the components of contractual and legal risks," *Journal of Cleaner Production*, vol. 139, pp. 1078–1084, 2016.

[11] M. A. Zanni, R. Soetanto, and K. Ruikar, "Exploring the potential of BIM-integrated sustainability assessment in AEC," in *Proceedings of the Sustainable Building and Construction Conference (SB13)*, Coventry, UK, July 2013.

[12] K. Munir and M. Sheraz Anjum, "The use of ontologies for effective knowledge modelling and information retrieval," *Applied Computing and Informatics*, vol. 14, no. 2, pp. 116–126, 2018.

[13] A. Meštrović and A. Calì, "An ontology-based approach to information retrieval," in *Semantic Keyword-Based Search on Structured Data Sources. IKC 2016. Lecture Notes in Computer Science*, A. Calì, D. Gorgan, and M. Ugarte, Eds., vol. 10151, Springer, Cham, Switzerland, 2016.

[14] F. Ramli, S. A. Noah, and T. B. Kurniawan, "Ontology-based information retrieval for historical documents," in *Proceedings of the Third International Conference on Information Retrieval & Knowledge Management*, IEEE, Bandar Hilir, Malaysia, August 2017.

[15] A. Mazen, M. K. Mahmood, and H. Maqbool, "Automated ontology generation framework powered by linked biomedical ontologies for disease-drug domain," *Computer Methods and Programs in Biomedicine*, vol. 165, pp. 117–128, 2018.

[16] Y. Liu, X. Yu, and Y. C. Zhang, "Information management and green construction evaluation," in *Proceedings fo the 2017 6th International Conference on Energy and Environmental Protection (ICEEP 2017)*, Atlantis Press, Zhuhai, China, June 2017.

[17] J. Li, X. N. Zhang, and Z. Bao, "Green construction evaluation of water conservancy and hydropower project based on fuzzy matter element," *Water Resources and Power*, vol. 35, no. 3, pp. 158–162, 2017.

[18] J. B. Zhang and R. He, "Research and application of green construction evaluation model for building engineering," *Construction Technology*, vol. 46, no. 01, pp. 119–123, 2017.

[19] T. J. Gu and Y. Li, "An empirical study on intrinsic modeling and evaluation support of quality conformity evaluation system," *Operations Research and Management Science*, vol. 26, no. 12, pp. 135–141, 2017.

[20] W. Passornpakorn and S. Kamolphiwong, "Ontology based framework for interactive self-assessment of e-health applications," *IEICE Transactions on Information and Systems*, vol. E99.D, no. 1, pp. 2–9, 2016.

[21] P. Pauwels and W. Terkaj, "EXPRESS to OWL for construction industry: towards a recommendable and usable ifcOWL ontology towards a recommendable and usable ifcOWL ontology," *Automation in Construction*, vol. 63, pp. 100–133, 2016.

[22] J. Yang, J. X. Cao, and H. L. Gao, "Ontology-based knowledge base model for telecommunication fraud analysis," *Computer Engineering and Design*, vol. 38, no. 6, pp. 1418–1423, 2017.

[23] S. Maltese, L. C. Tagliabue, F. R. Cecconi, D. Pasini, M. Manfren, and A. L. C. Ciribini, "Sustainability assessment through green BIM for environmental, social and economic efficiency," *Procedia Engineering*, vol. 180, pp. 520–530, 2017.

[24] K. Kim, H. Kim, W. Kim, C., J. Kim, and J. Yu, "Integration of ifc objects and facility management work information using Semantic Web," *Automation in Construction*, vol. 87, pp. 173–187, 2018.

[25] W. Terkaj and A. Š& ka, "Ontology-based representation of IFC EXPRESS rules: an enhancement of the ifcOWL ontology," *Automation in Construction*, vol. 57, pp. 188–201, 2015.

[26] P. Zhou and N. El-Gohary, "Ontology-based automated information extraction from building energy conservation codes," *Automation in Construction*, vol. 74, pp. 103–117, 2017.

[27] J. Zhang and T. E. El-Diraby, "Social semantic approach to support communication in AEC," *Journal of Computing in Civil Engineering*, vol. 26, no. 1, pp. 90–104, 2012.

[28] M. O. Moguillansky and G. R. Simari, "A generalized abstract argumentation framework for inconsistency-tolerant ontology reasoning," *Expert Systems with Applications*, vol. 64, pp. 141–168, 2016.

[29] R. H. Sudath, S. Rolf, and A. O. Mehmet, "OWL 2 learn profile: an ontology sublanguage for the learning domain," *SpringerPlus*, vol. 5, no. 1, pp. 291–315, 2016.

[30] N. B. Agnieszka and W. D. Alicja, "Exploration of rule-based knowledge bases: a knowledge engineer'," *Information Sciences*, vol. 485, pp. 301–318, 2019.

[31] E.-S. Shaker and E. Mohammed, "A fuzzy ontology modeling for case base knowledge in diabetes mellitus domain," *Engineering Science and Technology, an International Journal*, vol. 20, no. 3, pp. 1025–1040, 2017.

[32] K. Liu and N. El-Gohary, "Ontology-based sequence labelling for automated information extraction for supporting bridge data analytics," *Procedia Engineering*, vol. 145, pp. 504–510, 2016.

[33] J. R. Warren, D. George, N. Goran, R. Noel, S. Robert, and W. Jerry, "The BioHub knowledge base: ontology and repository for sustainable biosourcing," *Journal of Biomedical Semantics*, vol. 7, no. 1, p. 30, 2016.

[34] S. Priya, Y. Guo, M. Spear, and J. Heflin, "Partitioning OWL knowledge bases for parallel reasoning," in *Proceedings of the IEEE International Conference on Semantic Computing*, IEEE, Newport Beach, CA, USA, June 2014.

[35] M. Nie, Y. Li, X. Wanng et al., "Assessment of hazards in the construction of mountainous expressway: MLES approach," in *Proceedings of the International Conference of Chinese Transportation Professionals*, Beijing, China, August 2010.

[36] S. K. Lee, K. R. Kim, and J. H. Yu, "BIM and ontology-based approach for building cost estimation," *Automation in Construction*, vol. 41, pp. 96–105, 2014.

Hindawi
Advances in Civil Engineering
Volume 2019, Article ID 9391857, 12 pages
https://doi.org/10.1155/2019/9391857

Research Article

A Comparative Life Cycle Assessment (LCA) of Warm Mix Asphalt (WMA) and Hot Mix Asphalt (HMA) Pavement: A Case Study in China

Hui Ma,[1,2] Zhigang Zhang,[1] Xia Zhao,[3] and Shuang Wu[4]

[1]*Key Laboratory of New Technology for Construction of Cities in Mountain Area (Chongqing University), Ministry of Education, Chongqing 400045, China*
[2]*Jiangsu Expressway Engineering Maintenance Technology Co. Ltd., Nanjing 211106, China*
[3]*School of Foreign Language and Cultures, Chongqing University, Chongqing 400045, China*
[4]*School of Transportation Engineering, Southeast University, Nanjing 210096, China*

Correspondence should be addressed to Zhigang Zhang; zhangzg@cqu.edu.cn

Received 22 May 2019; Revised 17 July 2019; Accepted 14 August 2019; Published 9 September 2019

Guest Editor: Endong Wang

Generally, the warm mix asphalt (WMA) technology can reduce the mixing and paving temperature effectively as compared with that of hot mix asphalt (HMA), which is considered more environment-friendly. In this study, the environmental impacts and resource consumptions of WMA and HMA pavements were analyzed comparatively using the life cycle assessment (LCA) method. A LCA model of pavement was built; meanwhile, the relevant life cycle inventory (LCI) of WMA and HMA pavements was also collected and analyzed. The midpoint impact categories including Global Warming Potential (GWP), Chinese Abiotic Depletion Potential (CADP), and Particulate Matter Formation (PMF) were assessed for five cases. The assessment results showed that the resource consumptions of both WMA and HMA pavements in entire life were almost at the same level, while the environmental impacts of WMA pavement related to greenhouse gases and $PM_{2.5}$ emissions were significantly less than that of HMA pavement, except for the case where the long-term performance of WMA pavement is much worse than that of HMA pavement. In final, it could be concluded that WMA pavement is more environment-friendly compared with HMA pavement although they have the same-level resource consumptions.

1. Introduction

Nowadays, transport is vital for the well-functioning of economic activities and a key to ensuring social well-being and cohesion of populations. Transport ensures everyday mobility of people and is crucial to the production and distribution of goods. Transport infrastructure refers to the framework that supports our transport system and is a fundamental precondition for transport systems. However, the construction and maintenance of transportation infrastructures has become and will continue to be a significant contributor to the consumption of raw materials and greenhouse gases emissions worldwide. In America, more than 350 million tons of raw materials were consumed each year in highway construction and maintenance [1]. A third of total CO_2 emissions were contributed by the transportation industry in Denmark, of which 95% comes from the construction and operations of transportation infrastructures [2]. In China, the highway industry contributed about 290 million tons of CO_2 emissions in 2004, and the predicted emission is expected to reach 1.1 billion tons in 2030 [3].

In recent years, the mileage of highway has been reached 108,000 kilometers in China. Asphalt pavement is the dominating pavement form in expressway due to the following advantages: smooth surface, comfortable driving, low noise, simple construction, and rapid open-to-traffic. Nevertheless, due to the high manufacturing temperature (150~190°C) of typical hot mix asphalt (HMA) mixtures, the energy consumptions (fuel oil and electricity usage, etc.) and

gases emissions (CO_2 and other pollutants) are quite high during the construction process. In order to construct environment-friendly pavements, the warm mix asphalt (WMA) mixture, which has the relatively lower manufacturing temperature of 100~140°C and has similar mechanical properties to that of HMA mixture, has drawn much attention in the past decade [4–6].

WMA mixture has a lower viscosity and remains in good workability at a relatively lower temperature by adding viscosity-reducing agents (e.g., Sasobit and Evotherm) or incorporating water (e.g., Asphalt-min and Double Barrel Green) during the mixing process [7, 8]. Among them, chemical additives including a combination of emulsification agents, surfactants, polymers, and other additives were normally used to improve coating, mixture workability, compaction, and adhesion performances of asphalt. A series of studies have been conducted to compare the environmental impacts between HMA and WMA mixtures [9–11], which showed that WMA had the advantages of lower energy consumption, fewer emissions, and better working condition during mixing and paving process. However, the long-term performances of WMA pavement are not very clear, and water damage is easier to occur in WMA pavement than that in HMA pavement. Furthermore, the energy consumptions and environmental impacts of the upstream supply chains (e.g., the production of additive agents and transportation) and downstream processes (e.g., operation and maintenance) have not been considered in previous studies. Therefore, a more systematic and complete comparative assessment between WMA and HMA is necessary to be studied.

Life cycle assessment (LCA) is a useful method to assess the environmental impacts of a product system throughout its entire life cycle, including extracting and processing of raw materials, manufacturing, transportation, utilization, maintenance, recycling, and final disposal during end-of-life stage [12–15]. In the mid-1990s, Häkkinen first introduced the concept of LCA into pavement engineering by comparing the environmental impacts of portland cement concrete (PCC) and stone mastic asphalt (SMA) pavements in Finland [16]. They concluded that the CO_2 emission of PCC pavement is 40%~60% more than that of SMA pavement; however, the nonrenewable energy consumption of SMA pavement is twice more than that of PCC pavement due to the high feedstock energy of asphalt. Following their pioneering research, a series of studies associated with LCA on pavement engineering was conducted. For example, Yu built an LCA model to evaluate the environmental impacts of pavement, and concluded that the portland cement concrete (PCC) pavement had a smaller environmental burden as compared with that of HMA [17]. Horvath evaluated the environmental impacts of HMA and continuously reinforced concrete pavement (CRCP) pavements in America using economic input-output life cycle assessment model [18]. Nevertheless, most of the researchers (e.g., Wilfred [19], Berthiaume and Bouchard [20], Nisbet et al. [21], and Stripple [22]) just focused on the comparison between traditional HMA pavement and PCC pavement due to limited data availability for the other pavement forms. Due to the relatively new technique of WMA for pavement construction, to date, the LCA study of WMA pavement was still rarely conducted. Tatari et al. assessed the environmental impacts of different types of WMA pavement and constructed a comparison between the WMA pavement and the traditional HMA pavement based on a hybrid LCA model. The results demonstrated that it should not be the only phase to evaluate the amount of atmospheric emission of asphalt pavements, although the mixing phase is important [23]. Rosario et al. assessed the environmental impacts of HMA and zeolite-based WMA with reclaimed asphalt pavement (RAP) material. It concluded that during the entire life cycle, the impacts of zeolite-based WMA pavements were almost equal to the impacts of HMA pavements with the same RAP content [24].

In this study, it emphasizes on the comparative assessment associated with environmental impacts between WMA and HMA pavements using LCA method. Firstly, the LCA models of these two pavements were built and the research scope was identified, including the production of asphalt, aggregates and chemical additives, asphalt mixture manufacturing and transportation, pavement construction and operation, maintenance, and dismantling at the end of life. Furthermore, the inventory data including raw materials/energy consumptions and environmental emissions of WMA and HMA pavements in all stages were collected and analyzed. Finally, five cases were assumed for long-term performances of WMA pavement to comparatively analyze the environmental impacts for these two pavements.

2. LCA Method and Model of Pavement

2.1. Goal and Scope Definition. According to ISO standards [25, 26], generally, LCA incorporates four phases: goal and scope definition, life cycle inventory (LCI), life cycle impact assessment (LCIA), and life cycle interpretation. The goal and scope definitions of LCA determine the guidelines to be followed during the rest of the assessment. The goal decides the model type and evaluation index of LCA. This study aimed to evaluate the environmental impacts and resource consumptions of WMA and HMA pavements during their entire life cycle, which is expected to facilitate more informed decision as environment-sensitive pavement construction comes with the uncertainty of newly constructed WMA pavement. Whenever possible, local data from Chinese practice will be adopted. In the situation of the unavailable data, complementary data from elsewhere, such as European Bitumen Association (EBA) and US Environmental Protection Agency (EPA), will be adopted to complete the study.

The scope of LCA has a direct impact on the collection of inventory data. Generally, the life cycle of road pavements included six major stages: pavement design, raw materials' production, transportation, construction, use, maintenance, and final disposal at the end of life [27]. The environmental impacts in the pavement design stage are mainly involving the print of blueprints and transportation of designers, which could be negligible compared with the other stages. Additionally, the environmental impacts in the use stage of pavement are mainly including the fossil fuel combustion of the vehicle, which is assumed to be the same for both WMA

and HMA pavements. Therefore, the stages of pavement design and use were not included in this study. The main differences between environmental impacts and resource consumptions between WMA and HMA pavements are from asphalt mixture production, and this process will be analyzed separately. Based on the above descriptions, the scope of the pavement LCA model in this study consisted of the following stages: raw materials' production and transportation, asphalt mixture production and transportation, pavement construction and maintenance, and disposal at the end of life, as shown in Figure 1.

The life cycle of WMA and HMA pavements in this study started from the stage of raw materials' production. The raw materials mainly included aggregates (sand, mineral powder, and macadam), asphalt binders (petroleum asphalt and modified asphalt), and warm-mixing agents. The resource consumptions at this stage mainly include heavy oil, diesel oil, gasoline, and electricity, which are consumed by the operation of relative machines used to produce and process raw materials, while the environmental impacts mainly come from mineral extraction, asphalt refinement, production of warm-mixing agents, and transportation of these raw materials to the asphalt-mixing plant.

As the raw materials were transported to the asphalt-mixing plant, the aggregates will be dried and screened; meanwhile, the asphalt would be heated. Then, the asphalt mixture was produced and transported to the construction site of pavement. The main resource consumptions are fuel and electricity used by machinery in the processes of drying and screening, heating and mixing, and transportation. The environmental impacts in this stage are mainly caused by the burning of fossil fuels.

The stage of pavement construction comprises the following processes: site cleaning and preparation, foundation compaction, construction of subbase and base layers, asphalt-mixture paving, levelling, and rolling. As the difference of environmental impacts between WMA and HMA pavement construction lies in the process of asphalt-mixture paving, only this process was assessed in this stage. The main resource consumption is fossil fuel used by paving machinery. The gas emissions in this stage are mainly from the burning of fossil fuels and the hot/warm asphalt mixture.

After a certain period of service, the pavement needs to be maintained due to its deterioration with the combination of environmental impacts and repeatable vehicle loading. In this study, for simplification, it was assumed that only medium repair with overlay will be adopted. The environmental impacts in this stage are mainly involving the demolition of damaged asphalt layers, cleaning the substrate, and paving a new layer of asphalt mixture.

At the end of service life, the pavement materials need to be properly disposed of. There are a number of options for end-of-life treatment, such as abandonment (together with pavement), landfill, or recycling. In this study, the recycling option was selected due to its high popularity. The resource consumptions and pollution emissions are mainly from the burning of fossil fuel by the equipment during demolition, transport, and landfill.

2.2. Functional Unit. The functional unit was defined as a quantitative benchmark unit that should represent the function of the analyzed system. For a more accurate comparison, the same function unit for different road pavement systems is used in this paper. Herein, the function unit for road pavement LCA is defined based on the geometry, performances, and service life of the pavement. For the case study presented later, the section of road pavement with 6 lanes concerned has a length of 1 km and a width of 33 m. The entire service life of this road is assumed to be 15 years, which is the designed life of asphalt pavement. The average daily traffic volume is 20,000, of which 8% are heavy vehicles. The total thickness of the asphalt layer is 18 cm as the pavement structure consists of three layers from top to bottom, which is 4 cm stone mastic asphalt (SMA-13), 6 cm asphalt concrete (AC-20), and 8 cm AC-25, respectively, as shown in Figure 2. The compositions of asphalt mixture are listed in Table 1. Evotherm DAT manufactured by MeadWestvaco Co. Ltd. was used as the warm-mixing agent at dosage of 5% to asphalt by weight [28].

In the stage of asphalt-mixture production, the initial temperature of the raw materials is assumed as 25°C, and the mixing temperature of HMA and WMA mixtures is 180°C and 140°C, respectively. All asphalt mixtures are transported from the asphalt plant to the construction site with an assumed average distance of 10 km. In the stage of end of life, the demolished pavement materials were recycled.

The pavement condition index (PCI) deterioration model was used to determine the moment of maintenance conduction in this study [29]. The PCI can be calculated using

$$\mathrm{PCI} = \mathrm{PCI}_0 \left\{ 1 - \exp\left[-\left(\frac{\alpha^{\beta}}{y} \right) \right] \right\}, \quad (1)$$

where PCI_0 is the initial pavement condition index, y is the age of road, and α and β are the service life index and geometric shape index, respectively.

In this study, the maintenance will be conducted when the PCI reduces to 70, after which the PCI will be upgraded to a level equivalent to that of before five years ago, as shown in Figure 3. The maintenance area is half of the total area specified in the functional unit.

For WMA pavement, there were five assumed maintenance scenarios to account for the uncertainty of its long-term performance: (1) the PCI of WMA pavement deteriorated slower than that of HMA pavement by 20%, and the maintenance area was 20% less than HMA; (2) the PCI of WMA pavement deteriorated 10% slower than that of HMA pavement, and the maintenance area was 10% less than HMA; (3) the WMA pavement has the same maintenance condition with HMA pavement; (4) the PCI of WMA pavement deteriorated 10% faster than that of HMA pavement, and the maintenance area was 10% larger than HMA pavement; and (5) the PCI of WMA pavement deteriorated 20% faster than that of HMA pavement, and the maintenance area was 20% larger than HMA pavement.

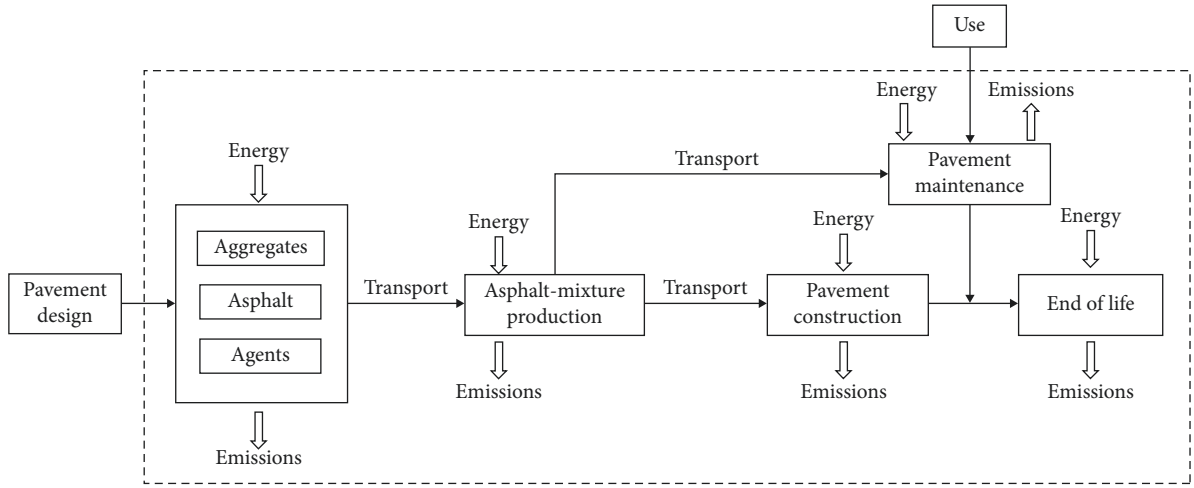

Figure 1: The scope of pavement LCA model in this study.

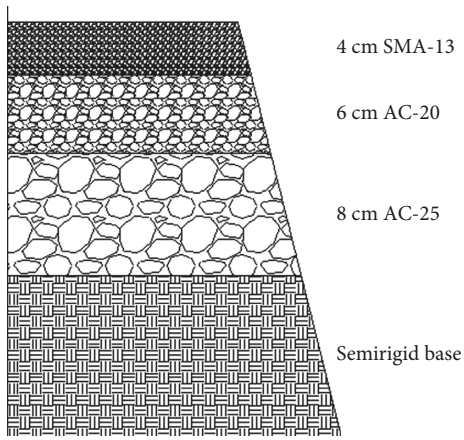

Figure 2: The pavement structure of asphalt pavement.

2.3. Life Cycle Inventory (LCI) Analysis

2.3.1. Raw Materials. The raw materials of asphalt mixture mainly include natural aggregates (sand, mineral powder, gravel, and stone chips), asphalt (petroleum asphalt and modified asphalt), and warm-mixing agents. The LCI of natural aggregates was from the Chinese Life Cycle Database (CLCD), which covers a large amount of LCI data for basic industry products in China, averaged over different scales of manufacturing and degree of technical sophistication. The LCI of asphalt comes from European Bitumen Association (EBA) because the CLCD lacks the environmental impact data for asphalt production, and the source of crude oil and refining process in China are the same as those in Europe. The Evotherm warm-mixing technology was used most widely in China for WMA mixture production, and hence, the LCI data were also from the Ecoinvent database from Europe.

2.3.2. Asphalt-Mixture Production. The energy consumptions during the production of asphalt mixture mainly involve fuel and electricity consumptions. The fuel is consumed for asphalt heating and aggregate drying, while the construction machinery consumes the electricity. During this process, the aggregates drying and heating are likely to bring out plenty of dust, while the burning of fossil fuel leads to CO_2 emission. Moreover, the asphalt heating during mixing releases a lot of harmful gases.

For the hot mixture asphalt (HMA), the energy consumptions are calculated using Chinese Highway Engineering Budget Quota and Machinery Quota (JTG/T B-06-02-2007) (JTG/T B-06-03-2007) (in short: Quota method). The number of machine team when producing every 1000 m^3 HMA was surveyed from the Budget Quota, whereas the energy consumptions of machinery in unit machine team were surveyed from Machinery Quota. Then, the energy consumptions can be calculated through the product of these two sets of data. The energy consumptions of producing 1000 m^3 coarse-graded asphalt (CGA) mixture are listed in Table 2. The pollutant emissions during the production of HMA were calculated based on the emission factors, including CO, CO_2, NO_X, SO_2, and $PM_{2.5}$ emissions, from the US Environmental Protection Agency (EPA) [30]. There are 0.2 kg CO emission, 18.5 kg CO_2 emission, 0.06 kg NO_X emission, 0.044 kg SO_2 emission, and 2.25 kg $PM_{2.5}$ emission, during the production of every one ton of HMA mixture. Based on the above descriptions, the LCI of mixing every 1000 m^3 HMA is calculated and listed in Table 3.

For warm mix asphalt mixture, the energy consumptions were calculated using the thermodynamic equilibrium:

$$M \cdot q \cdot \lambda \cdot \eta = \sum_i c_i m_i \cdot (T_f - T_i) + c_w m_w \cdot (T_w - T_i) + L_w m_w, \quad (2)$$

where M is the weight of fuel (kg), q is the calorific value of fuel (J/kg), λ is combustion efficiency, η is the heat exchange rate of equipment, n is the total number of aggregate type, c_i is the specific heat capacity of the i-th aggregate (J·kg^{-1}°C), m_i is the weight of i-th aggregate (kg), T_f the final temperature of aggregate after heating (°C), T_i is the initial temperature of aggregate (°C), c_w is the specific heat capacity of water (4190 J·kg^{-1}°C), m_w is the weight of water (kg), T_w is the boiling point of water, 100°C, and L_w is the latent heat of vaporization (2256 kJ/kg).

Table 1: Composition of 1000 m^3 asphalt mixtures.

Asphalt mixture	SBS-modified bitumen (t)	#70 asphalt (t)	Fiber stabilizer (t)	Sand (m^3)	Mineral powder (m^3)	Stone chip (m^3)	Gravel (m^3)
SMA-13	144.32	—	7.34	119.38	246.74	126.56	1111.35
AC-20	—	122.54	—	471.22	128.40	261.18	723.22
AC-25	—	113.47	—	389.79	117.72	226.75	854.79

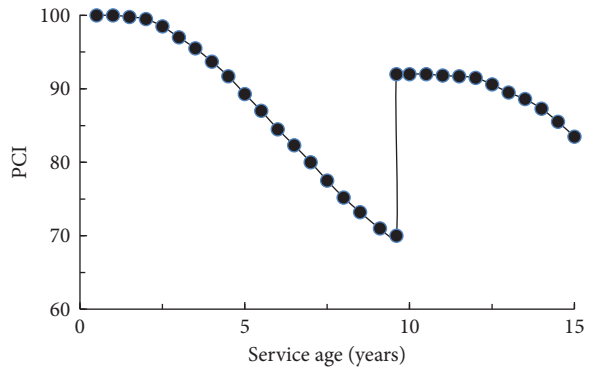

Figure 3: The change of PCI with age (maintenance event occurs at 10 years).

Table 2: Energy consumptions of producing 1000 m^3 coarse-graded asphalt (CGA) mixture.

Equipment	Machine team	Energy consumption per machine team			Total energy consumption		
		Heavy oil (kg)	Electricity (kWh)	Diesel oil (kg)	Heavy oil (kg)	Electricity (kWh)	Diesel oil (kg)
Mixer (320 t/h)	1.35	9574.4	5917.61	—	12925.44	7988.77	—
Loader (3 m^3)	2.53	—	—	115.15	—	—	291.33

Table 3: The LCIs of mixing every 1000 m^3 HMA and WMA mixtures.

Type of consumption/emission	Amount	
	HMA	WMA
Heavy fuel oil (kg)	12955.44	9900.55
Electricity (kWh)	7988.77	6105.02
Diesel (kg)	291.33	222.63
CO_2 (kg)	45510	18204
NO_X (kg)	147.6	40.44
SO_2 (kg)	108.24	26.84
$PM_{2.5}$ (kg)	10.33	5.38

As listed in Table 3, the calculation results indicate that the total resource consumptions during the production of WMA are 23.6% less than that of HMA. Qing et al. measured the actual resource consumptions during HMA and WMA mixing in asphalt-mixing plant [31]. Their results indicate that the energy consumption of WMA mixing is 22.1% less than that of HMA. Therefore, the thermodynamic equilibrium equation can be used reliably to predict the energy consumptions during the production of WMA in this study. Furthermore, their results indicate that compared with HMA, WMA emissions reduce significantly by 60%, 72.6%, 75.2%, and 47.9%, respectively, for CO_2, NO_X, SO_2, and $PM_{2.5}$. The LCI of mixing 1000 m^3 WMA is also listed in Table 3.

2.3.3. Transportation. The mixed asphalt mixture is transported by dumper truck from the asphalt-mixing plant to the construction site and poured into paving machinery. In this study, the carrying capacity of a dumper truck is assumed as 15 tons. The environmental impacts in this stage are from the burning of fuel by the vehicles. The energy consumptions also can be calculated using the Chinese Quotas mentioned before. 542.44 kg of diesel oil will be consumed when transporting 1000 m^3 asphalt mixture for 1 km distance. The gaseous emissions are calculated based on the emission factors, including CO_2, NO_X, CO, $PM_{2.5}$, N_2O, and NH_3, from the European Environment Agency (EEA) [32]. It produces 3140 g CO_2 emission, 33.4 g NO_X, emission, 7.58 g CO emission, 0.94 g $PM_{2.5}$ emission, 0.051 g N_2O emission, and 0.013 NH_3 emission as every 1 kg diesel oil was burnt during the running of equipment.

2.3.4. Construction. During the pavement construction stage, it comprises different processes, whereas this study just focused on the asphalt-mixture paving process. The energy consumptions in this stage come from the fuel consumed by the paver and roller compaction machinery, which are calculated through the Quota method. The diesel oil consumptions of constructing 100 m^2 stone mastic asphalt (SMA), medium-sized particle asphalt (MSPA), and coarse-graded asphalt (CGA) concrete pavement are 445.75 kg, 280.02 kg, and 279.71 kg, respectively. The gaseous emissions data are referenced from GB 20891-2007 and listed in Table 4.

Table 4: Gaseous emissions of constructing 100 m^2 asphalt concrete pavement.

Pavement type	Gases emissions				
	CO_2 (kg)	NO_X (g)	CO (g)	PM (g)	HC (g)
SMA	2817.11	89.25	60.95	3.57	14.87
MSPA	1793.62	70.62	47.29	2.76	11.68
CGA	1779.43	69.47	46.89	2.74	11.58

2.3.5. Maintenance. The maintenance was conducted periodically throughout the entire service life of the pavement. In this study, only the overlay technology was chosen to maintain the distressed pavement. The energy consumptions were calculated using the Quota method. Due to the similarity of the necessary processes for both new construction and maintenance (only asphalt-mixture paving process considered in new construction, whereas the rest is considered the same for both HMA and WMA pavements), the pollution emissions of maintenance can be calculated similarly (Refer to Section 2.3.2 to 2.3.4). The energy consumptions and pollution emissions of 1000 m^2 overlay with 4 cm thickness are listed in Table 5.

2.3.6. End of Life. As mentioned previously, the environmental impacts were mainly from the use of fuel by demolition, transport, and landfill equipment at the end-of-life stage. The energy consumptions and pollution emissions can be calculated using the Quota method and emission factors from the European Environment Agency (EEA), respectively.

2.4. Impact Assessment and Sensitivity/Uncertainty Analysis

2.4.1. Impact Assessment. The impact assessments of WMA and HMA pavements were conducted using LCA-based software. These impacts were assessed in accordance with two sets of impact categories, which are midpoint impact categories and endpoint impact categories, respectively. The endpoint impact categories include damage to human health, damage to ecosystem diversity, and damage to resource availability. They may be affected by environmental conditions in different regions, such as atmosphere, water, soil, and ecological system. Due to a lack of such data in China, the endpoint impact categories were not assessed in this study.

Three midpoint impact categories, which are Global Warming Potential (GWP), Chinese Abiotic Depletion Potential-fossil fuel (CADP), and Particulate Matter Formation (PMF), were selected in this study to assess environment impacts and resource consumptions. GWP contains the impact factors of CO_2, CH_4, CO, and N_2O, which are characterized as CO_2 and expressed as GWP/kg. CADP is an exclusive midpoint impact category in China, which was obtained based on Abiotic Depletion Potential (ADP) of China applying CML method. The impact factors of CADP include coal, petroleum, and natural gas, of which the characteristic factor of CADP is coal, and expressed as CADP/kg. The impact factors of PMF contains of PM_{10} and $PM_{2.5}$. The characteristic factor is $PM_{2.5}$, which is expressed as PMF/kg.

Table 5: The energy consumptions and pollution emissions of 1000 m^2 overlay.

Energy consumptions (kg)		Pollution emissions (kg)	
Heavy oil	583.44	CO_2	2340.63
Electricity	393.94	SO_2	4.73
Diesel oil	144.09	NO_X	13.41
Gasoline	1.03	CO	26.44
—	—	PM	257.57

2.4.2. Sensitivity and Uncertainty Analyses. The sensitivity analysis is used to quantitatively analyze the influence of inputs on the outputs for a mathematical model, which can be calculated using equation (3). Based on the analysis of sensitivity, the most effective improvements to reduce the environmental impacts can be obtained, i.e., identifying the most sensitive inputs for any particular output (an indicator of interest):

$$S_m = \frac{(\Delta O_m / O_m)}{(\Delta I_n / I_n)}, \tag{3}$$

where S_m is sensitivity, O_m is the first m result index value of LCA, and I_n is the first n LCI data.

The credibility of LCA results is influenced by uncertainty during the LCA processes. The uncertainty of LCA consists of original data uncertainty and algorithm uncertainty. The original data uncertainty can be assessed in terms of data source reliability, sample integrity, technical, time, and geographical representativeness. In this study, original data uncertainty was obtained from the Ecoinvent database [33] and calculated using the following equation:

$$U_r = \sqrt{\sum_{1}^{5} U_i}, \tag{4}$$

where U_r is the original data uncertainty and U_i is the original data uncertainty in the first term.

The algorithm uncertainty depends on the rationality of the algorithm. The uncertainties of algorithms: directly acquire algorithm, total algorithm, balancing algorithm, experience algorithm, and theory algorithm are 0, 0, 0.025, 0.05, and 0.1, respectively [34]. Based on the above descriptions, the uncertainty of LCA results can be calculated using the following equation:

$$U = \sqrt{U_r^2 + U_a^2}, \tag{5}$$

where U is the overall uncertainty of LCA results, U_r is the original data uncertainty, and U_a is the algorithm uncertainty.

2.5. LCA-Based Tool. A commercial LCA-based software was used in this study to calculate the environmental impacts and resource consumptions of the WMA and HMA

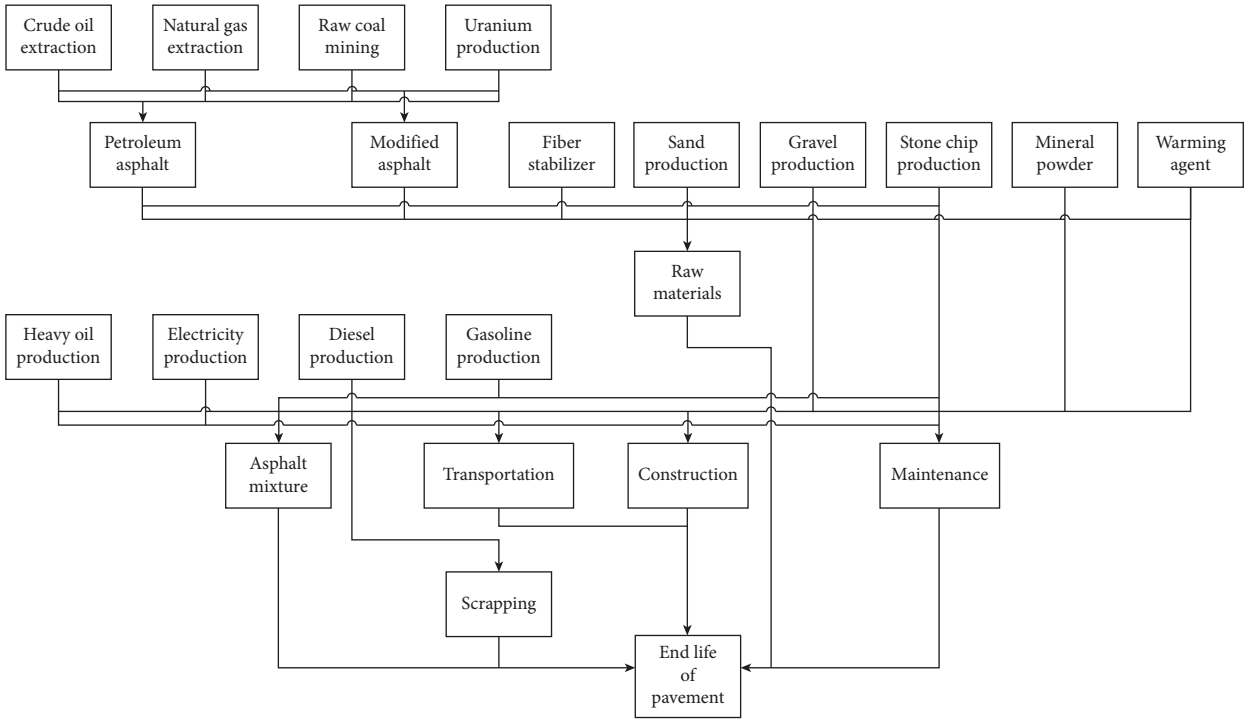

Figure 4: The LCA modeling process of WMA and HMA pavements in LCA-based software.

pavements. This software contains the key features of international popular LCA-based software, including data collection records and automatic generation of LCA reports. The inventory data can be obtained from Chinese life cycle database (CLCD), European life cycle database (ELCD), and Ecoinvent database, which are incorporated within this software. It also allows users to add new data and calculations to the database. The LCA modeling process of WMA and HMA pavements using this software is shown in Figure 4. In addition, the Microsoft Excel spreadsheet was also used to prepare the LCI data and helps the process of calculating environmental impacts of both pavements.

3. Assessment Results and Discussion

3.1. Impact Assessment

3.1.1. Impact Category of GWP. Figure 5 presents the GWP of HMA and WMA pavements for five cases. As can be seen, besides the case 5, which assumed WMA performance is much worse than HMA, WMA pavement exhibits pronounced reduction of total GWP when compared with HMA pavement. This is mainly caused by less fuel burning and CO_2 emission due to the lower mixing temperature of WMA, as indicated by a 46.7% GWP reduction of WMA over HMA when asphalt-mixture production is considered separately. On the other hand, the GWP of WMA pavement for raw materials' production is only 2.8% more than that of HMA pavement due to the addition of the warm-mixing agent. In case 5, although the long-term performance of WMA pavement is much inferior to that of HMA pavement, the GWP of WMA pavement is still comparable to that of HMA pavement. For case 5, the evident increase of GWP impacts in WMA pavement is attributed to the increased GWP value at the maintenance stage, of which the GWP value of WMA pavement is 2.13 times higher than that of HMA pavement due to the relatively higher maintenance times and area of WMA pavement as compared with HMA pavement.

3.1.2. Impact Category of CADP. Figure 6 shows the CADP of HMA and WMA pavements. As can be seen from Figure 6, the stage of raw materials' production has the highest contribution to the CADP in the entire life cycle. Although, in the cases 1 to 3, the CADP of WMA pavement is above 20% less than HMA pavement in the stages of asphalt-mixture production and maintenance, the adoption of warm-mixing agent in WMA pavement increases the CADP in the stage of asphalt-mixture production. Therefore, the total resource consumption of WMA pavement is slightly less than HMA pavement. However, in case 5, the CADP of WMA pavements is 14.3% more than that of HMA pavements because maintenances were conducted twice in the entire life cycle of WMA pavement.

3.1.3. Impact Category of PMF. Figure 7 illustrates the PMF of WMA and HMA pavements. As can be seen from Figure 7, although the PMF of WMA pavement for raw materials is slightly higher than that of HMA pavement due to warm-mixing agent production, WMA pavement has an obvious lower PMF compared with HMA pavement in cases 1 to 4. The reduction (about 47.4%) of PMF of the WMA pavement is mainly contributed from the stages of asphalt-mixture production due to the lower mixing temperature. The $PM_{2.5}$ emission reduces evidently with the lower mixing temperature. In case 5, there is no obvious difference of the PMF between WMA and HMA pavements

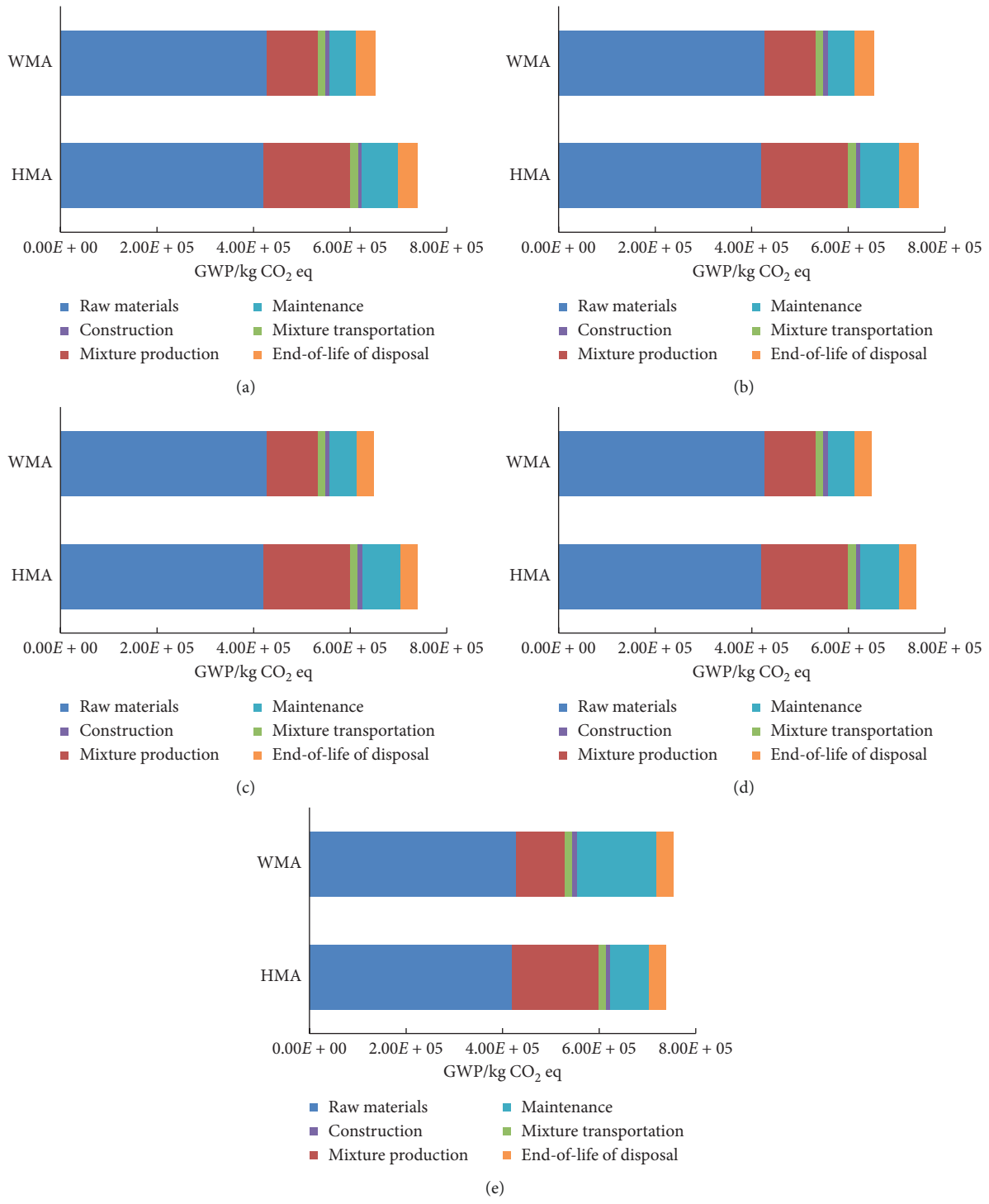

Figure 5: The GWP impacts of HMA and WMA pavements for five cases: (a) case 1; (b) case 2; (c) case 3; (d) case 4; and (e) case 5.

because maintenances were conducted twice on WMA pavement during the entire life cycle.

Based on the above discussions, constructing WMA pavement has almost no advantage of saving resources. Nevertheless, the WMA pavement has an obvious effect to reduce the greenhouse gases and $PM_{2.5}$ emissions. Therefore, popularizing WMA pavement is beneficial to the construction of environment-friendly society.

3.2. Results Assessments

3.2.1. Sensitivity Assessments. In this section, the sensitivity of impact category factors GWP, CADP, and PMF (relative change of factor induced by the change of unit process/inventory) was calculated. The pairs of unit process/factor that have sensitivity value larger than 10% are listed in Table 6. As can be seen from Table 6, the production of raw materials

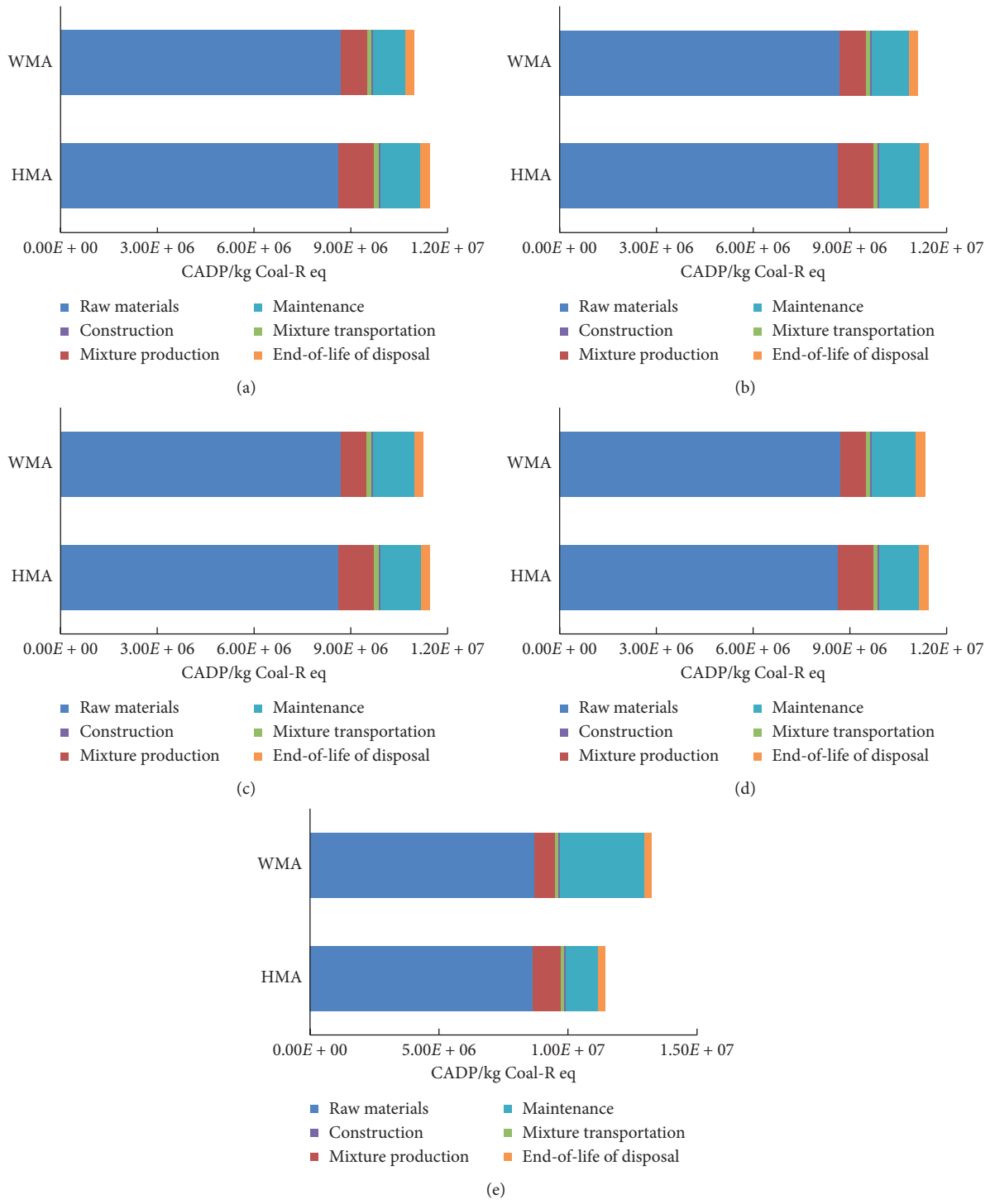

Figure 6: The CADP impacts of HMA and WMA pavements for five cases: (a) case 1; (b) case 2; (c) case 3; (d) case 4; and (e) case 5.

including petroleum asphalt and raw petroleum has the highest sensitivity for indexes GWP, CADP, and PMF. It suggests that improving the technology of raw materials' production, especially raw petroleum and asphalt production, is the most effective way to decrease the impact on the environment and the reduction of resource consumption. For WMA pavement, these unit processes and inventories have higher sensitivity as compared with HMA pavement, except asphalt-mixture production. It indicates that improving the technology of these unit processes, such as asphalt production and petroleum extraction, can be more effective to reduce GWP, CADP, and PMF for WMA pavement.

3.2.2. Uncertainty Assessments. In this study, an uncertainty assessment was also conducted to determine the

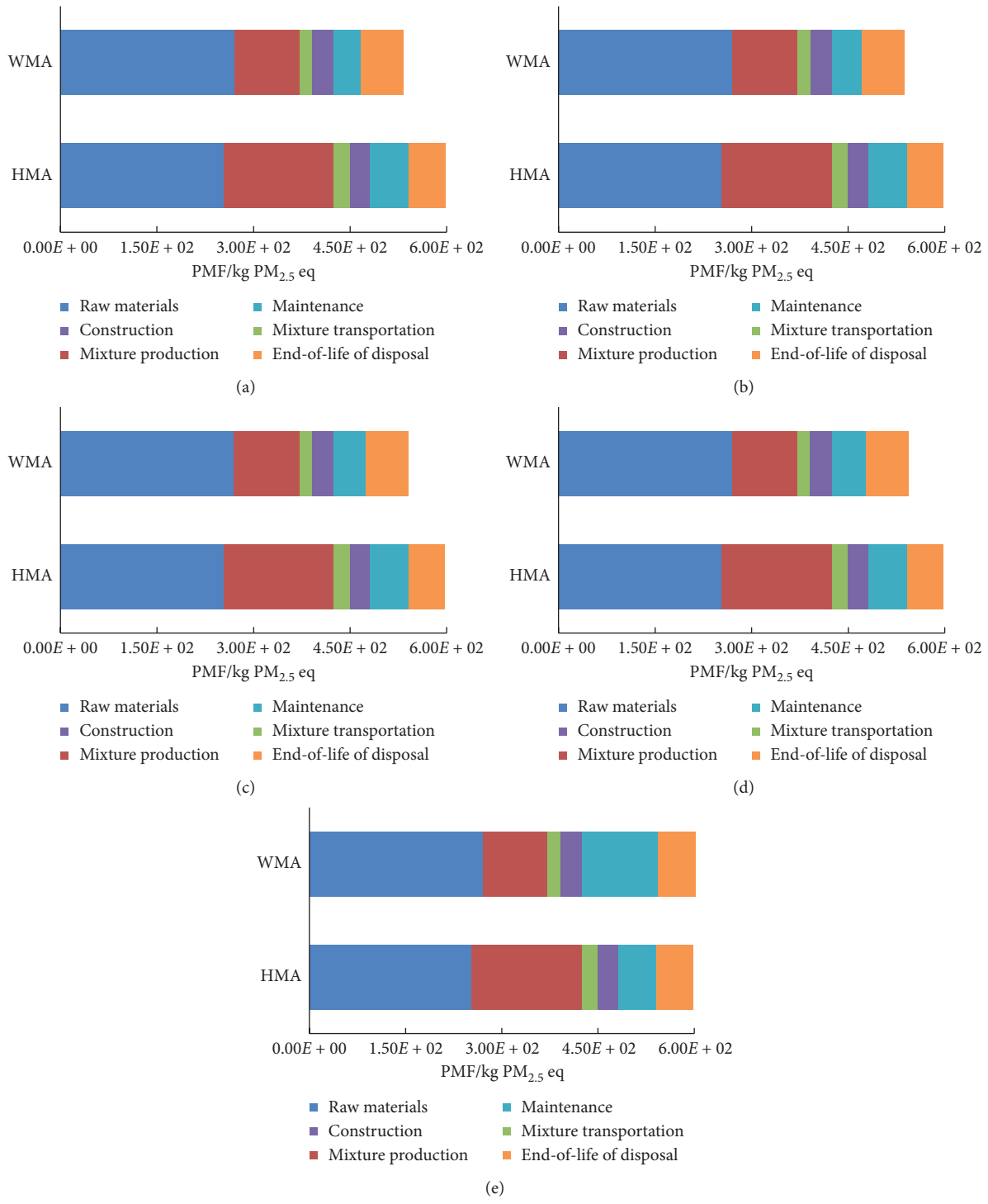

Figure 7: The PMF impacts of HMA and WMA pavements for five cases: (a) case 1; (b) case 2; (c) case 3; (d) case 4; and (e) case 5.

uncertainties of process inventories in the LCA results. The process inventories with sensitivity over 10% include asphalt pavement-raw materials, raw materials' production-petroleum asphalt, raw materials production-modified asphalt, asphalt pavement-asphalt mixture production, and asphalt pavement-maintenance, of which the uncertainty of these process inventories is 5.59, 11.46, 11.46, 10.00, and 10.31, respectively. Due to the LCI data of asphalt collected from different databases, the productions of petroleum asphalt and modified asphalt have higher uncertainty than other unit process inventories. Therefore, to improve the accuracy of results in an LCA project, the database should be settled or collect the data from the field directly. In addition, the uncertainties of all processes are smaller than 15%. It indicates that the results in this study are relatively credible.

Table 6: The sensitivity of GWP, CADP, and PMF with the corresponding unit process.

Unit process-inventory	GWP		CADP		PMF	
	HMA	WMA	HMA	WMA	HMA	WMA
Asphalt pavement-raw materials	56.56	65.70	74.88	77.04	41.28	50.10
Raw materials' production-petroleum asphalt	36.50	41.22	50.57	51.27	20.95	23.93
Petroleum asphalt production-raw petroleum	35.23	39.79	59.45	60.28	12.51	14.29
Asphalt pavement-asphalt-mixture production	24.88	14.72	—	—	28.37	17.03
Asphalt-mixture production-CO_2 emission	18.18	—	—	—	—	—
Raw materials' production-modified asphalt	15.75	17.79	19.42	19.68	11.18	12.78
Modified asphalt production-raw petroleum	11.33	12.80	19.13	19.39	—	—
Asphalt pavement-maintenance	10.75	10.76	11.30	11.32	—	—
Asphalt pavement-end of life	—	—	—	—	11.31	12.92

4. Conclusions

In this study, a comparative comprehensive life cycle assessment (LCA) was conducted for WMA and HMA pavements. The LCA of the pavement model was established, which includes the stages of raw materials' production, asphalt-mixture production and transportation, maintenance, and disposal at the end of life. The inventories of every unit process were collected and analyzed. Since the long-term performance of WMA pavement has not been well understood, five maintenance scenarios were assumed to assess the environmental impacts of WMA and HMA pavements. The specific conclusions can be drawn as follows:

(1) The results suggest that, assuming comparable long-term performances with that of HMA pavement, WMA pavement produces less CO_2 and $PM_{2.5}$ emissions during their entire life cycle, which indicates that WMA pavement is friendlier for environment.

(2) The assessment reveals that the difference in Chinese Abiotic Depletion Potential (CADP) between WMA and HMA pavements could be negligible, which indicated that WMA pavement technique consumes almost the same resource as that of HMA pavement during the entire service life.

(3) The sensitivity assessment results indicated that improving the technology in raw material production is the most effective way to reduce the environmental impacts for both WMA and HMA pavements.

Data Availability

In this paper, all the data used to support the findings of this study are available from the corresponding author upon request.

Conflicts of Interest

The authors declare that they have no conflicts of interest.

Acknowledgments

The authors would like to graciously thank the National Natural Science Foundation of China (Grant no. 51708061), 111 Project of China (Grant no. B18062), Science and Technology Research Program of Chongqing Municipal Education Commission (Grant no. KJQN201800126), State Education Ministry and Fundamental Research Funds for the Central Universities (no. 2019CDJSK04XK23), and the Fundamental and Frontier Research Project of Chongqing (no. cstc2018jcyjAX0535) for the financial support of this work.

References

[1] N. J. Santero, *Pavements and the Environment: A Life Cycle Assessment Approach*, University of California Berkeley, Berkeley, CA, USA, 2009.

[2] S. Bjarne and C. D. Jeppe, "CO_2 emission reduction by exploitation of rolling resistance modelling of pavements," *Procedia-Social and Behavioral Sciences*, vol. 48, pp. 311–320, 2012.

[3] C. Shang, Z. Zhang, and X. Li, "Research on energy consumption and emission of life cycle of expressway," *Journal of Highway and Transportation Research and Development*, vol. 27, no. 08, pp. 149–154, 2010, in Chinese.

[4] J. Gong, Y. Liu, Q. Wang et al., "Performance evaluation of warm mix asphalt additive modified epoxy asphalt rubbers," *Construction and Building Materials*, vol. 204, pp. 288–295, 2019.

[5] M. Sol-Sánchez, F. Moreno-Navarro, and M. Rubio-Gámez, "Study of surfactant additives for the manufacture of warm mix asphalt: from laboratory design to asphalt plant manufacture," *Applied Sciences*, vol. 7, no. 7, p. 745, 2017.

[6] S. Wu, W. Zhang, S. Shen, X. Li, B. Muhunthan, and L. N. Mohammad, "Field-aged asphalt binder performance evaluation for Evotherm warm mix asphalt: comparisons with hot mix asphalt," *Construction and Building Materials*, vol. 156, pp. 574–583, 2017.

[7] J. Liu, K. Yan, and J. Liu, "Rheological properties of warm mix asphalt binders and warm mix asphalt binders containing polyphosphoric acid," *International Journal of Pavement Research and Technology*, vol. 11, no. 5, pp. 481–487, 2018.

[8] M. C. Rubio, G. Martínez, L. Baena, and F. Moreno, "Warm mix asphalt: an overview," *Journal of Cleaner Production*, vol. 24, pp. 76–84, 2012.

[9] J. W. Button, C. Estakhri, and A. Wimsatt, *A Synthesis of Warm Mix Asphalt*, Texas Transportation Institute, College Station, TX, USA, 2007.

[10] L. Moretti, V. Mandrone, A. D'Andrea, and S. Caro, "Comparative "from cradle to gate" life cycle assessments of hot mix asphalt (HMA) materials," *Sustainability*, vol. 9, no. 3, p. 400, 2017.

[11] A. Woszuk and W. Franus, "A review of the application of zeolite materials in warm mix asphalt technologies," *Applied Sciences*, vol. 7, no. 3, p. 293, 2017.

[12] G. A. Keoleian, A. Kendall, J. E. Dettling et al., "Life cycle modeling of concrete bridge design: comparison of engineered cementitious composite link slabs and conventional steel expansion joints," *Journal of Infrastructure Systems*, vol. 11, no. 1, pp. 51–60, 2005.

[13] J. P. C. Araújo, J. R. M. Oliveira, and H. M. R. D. Silva, "The importance of the use phase on the LCA of environmentally friendly solutions for asphalt road pavements," *Transportation Research Part D: Transport and Environment*, vol. 32, pp. 97–110, 2014.

[14] SETAC, *Guidelines for Life-Cycle Assessment: A "Code of Practice"*, SETAC Publications, Pensacola, FL, USA, 1993.

[15] China Standards Press, *GB/T. 24040-2008 Environmental Management-Life Cycle Assessment-Principle and Framework*, China Standards Press, Beijing, China, 2008, in Chinese.

[16] T. Häkkinen and K. Mäkelä, *Environmental Adaption of Concrete: Environmental Impact of Concrete and Asphalt Pavements*, VTT Tiedotteita, Stockholm, Sweden, 1996.

[17] B. Yu and Q. Lu, "Life cycle assessment of pavement: methodology and case study," *Transportation Research Part D: Transport and Environment*, vol. 17, no. 5, pp. 380–388, 2012.

[18] A. Horvath and C. Hendrickson, "Comparison of environmental implications of asphalt and steel-reinforced concrete pavements," *Transportation Research Record: Journal of the Transportation Research Board*, vol. 1626, no. 1, pp. 105–113, 1998.

[19] H. R. Wilfred, *Environmental Value Engineering Assessment of Concrete and Asphalt Pavement*, Portland Cement Association, Skokie, IL, USA, 1999.

[20] R. Berthiaume and C. Bouchard, "Exergy analysis of the environmental impact of paving material manufacture," *Transactions of the Canadian Society for Mechanical Engineering*, vol. 23, no. 1B, pp. 187–196, 1999.

[21] M. Nisbet, M. L. Marceau, and M. G. VanGeem, *Environmental Life Cycle Inventory of Portland Cement Concrete and Asphalt Concrete Pavements*, Portland Cement Association, Skokie, IL, USA, 2001.

[22] H. Stripple, *Life Cycle Assessment of Road: A Pilot Study for Inventory Analysis*, Swedish National Road Administration, Stockholm, Sweden, 2001.

[23] O. Tatari, M. Nazzal, and M. Kucukvar, "Comparative sustainability assessment of warm-mix asphalts: a thermodynamic based hybrid life cycle analysis," *Resources, Conservation and Recycling*, vol. 58, pp. 18–24, 2012.

[24] V. Rosario, M. Enrique, and M. Germán, "Life cycle assessment of hot mix asphalt and zeolite-based warm mix asphalt with reclaimed asphalt pavement," *Resources, Conservation and Recycling*, vol. 74, no. 3, pp. 101–114, 2013.

[25] ISO, *ISO 14040: 2006—Environmental Management, Life Cycle Assessment, Principles and Framework*, International Organization for Standardization, Geneva, Switzerland, 2006.

[26] ISO, *ISO 14044: 2006—Environmental Management, Life Cycle Assessment, Requirements and Guidelines*, International Organization for Standardization, Geneva, Switzerland, 2006.

[27] N. Santero, E. Masanet, and A. Horvath, *Life Cycle Assessment of Pavements: A Critical Review of Existing Literature and Research*, Portland Cement Association, Skokie, IL, USA, 2010.

[28] Z. Zhang, L. Liu, and W. Tang, "Research of performance of Evotherm warm-mix asphalt," *Journal of Building Material*, vol. 12, no. 4, pp. 438–441, 2009, in Chinese.

[29] L. Sun, *The Theory of Asphalt Pavement Structure*, China Communications Press, Beijing, China, 2005, in Chinese.

[30] http://www.epa.gov/ttn/chief/ap42/ch11/bgdocs/b11s01.pdf, 2004.

[31] Y. Qing, S. Huang, J. Xu, and F. Li, "Test and analysis of energy saving and emission reduction of warm mixed asphalt," *Journal of Highway and Transportation Research and Development*, vol. 26, no. 8, pp. 33–37, 2009, in Chinese.

[32] European Environment Agency, *EMEP/EEA Air Pollutant Emission Inventory Guidebook 2013*, European Environment Agency, Copenhagen, Denmark, 2013.

[33] B. P. Weidema, C. Bauer, R. Hischier et al., "Overview and methodology. Data quality guideline for the ecoinvent database version 3," Ecoinvent Report No. 1, The Ecoinvent Centre, St. Gallen, Switzerland, 2011.

[34] N. Wang, H. Wang, C. Fan, C. Zhou, P. Hou, and J. Yang, "LCA data quality assessment and control based on uncertainty and sensitivity analysis," *Acta Scientiae Circumstantiae*, vol. 32, no. 6, pp. 1529–1536, 2012, in Chinese.

Hindawi
Advances in Civil Engineering
Volume 2019, Article ID 7094653, 18 pages
https://doi.org/10.1155/2019/7094653

Review Article

A Holistic Review of Public-Private Partnership Literature Published between 2008 and 2018

Liang Ma,[1] Junning Li,[1] Ruoyu Jin,[2] and Yongjian Ke[3]

[1]*School of Management, Shanghai University, Shanghai 200444, China*
[2]*Built Environment and Civil Engineering, University of Brighton, Brighton BN2 6NF, UK*
[3]*School of Built Environment, University of Technology Sydney, Ultimo, NSW, Australia*

Correspondence should be addressed to Ruoyu Jin; r.jin@brighton.ac.uk

Received 16 May 2019; Accepted 19 August 2019; Published 5 September 2019

Guest Editor: Jingfeng Yuan

Adopting a holistic approach in the review of the public-private partnership (PPP) literature published since 2008 by incorporating scientometric analysis and further systematic analysis, this study aims to provide the big picture of the state-of-the-art research in PPP by addressing major issues and suggesting research trends in PPP. Following a three-step research methodology, this study started from a bibliometric analysis with science mapping to provide the state-of-the-art information on PPP research keywords, scholars, journal articles, institutions, and countries. A further systematic review was also conducted to identify future research directions of PPP in project management. The review of the existing literature in PPP revealed that there had been insufficient systematic approach in summarizing the research topics and proposing new research trends in PPP-related project management. It was further indicated that sustainability and innovation in PPP could be further studied, such as integrating building information modeling with PPP. Factors related to barriers in PPP implementation would continue growing. Future research directions in PPP were also proposed following the systematic review, for example, comparative studies of PPP practice between developing and developed countries. The current study provides a comprehensive approach by integrating bibliometric analysis, science mapping, and qualitative analysis in the latest PPP research. It reveals the contemporary research themes in PPP and provides directions for near-future directions of PPP research in project management.

1. Introduction

Public-private partnership (PPP) refers to the procurement approach where the project is executed with a broader span of contractual relationships between the public and private sectors to provide an asset and/or a service [1]. It is a procurement model to deliver public infrastructure and/or service crossing various sectors including transportation, water treatment, energy, environment, health, and education [2–5]. PPP is believed to provide benefits to the public sector, private sector, and consumers by involving the participation of the government and the private financing initiatives [4]. However, conflicting opinions exist considering the negotiation efficiency, service quality, and accountability within PPPs [6]. PPP-based research has aroused wide interests in recent decades [6, 7]. Both developing and developed countries have actively been inviting private sectors to be involved in constructing infrastructure projects [8, 9].

Although PPP is still at the initial stages in meeting infrastructure development needs for many developing countries [10], new scenarios, findings, and designs have been proposed, adopted, or explored in the PPP field [11]. Case studies of PPP projects have widely been adopted crossing industries leading to new topics and paved the way forward for PPP research [6], including developing PPP-related frameworks [12], project financing [13], critical success factors (CSFs) [14], concession-related issues [15], and risk allocation and management [16]. Despite of these multiple PPP studies conducted, there has been insufficient attention on outlining the framework and development trends of PPP research [6]. Although certain effort has been paid to explore the research trends in PPP through content

analysis of renowned construction journals, such as studies conducted by Al-Sharif and Kaka [17] and Ke et al. [18], Song et al. [6] argued that these studies had relied on subjective judgements which might be unreliable due to the possible misinterpretations and misunderstanding on the part of the researchers.

Literature review is an expedient approach to gain in-depth understanding of a research field [19]. Existing review-based studies in PPP focused on either a certain industry or a wider scope crossing industries. The reviews of Ke et al. [18] and Tang et al. [7] on PPP projects focused on the construction industry. Similarly, Wang et al.'s [20] review of the PPP literature was restricted to the field of public administration. de Castro e Silva Neto et al. [21] started applying bibliometric analysis into the review of PPP studies crossing multiple project sectors such as transportation, health, and energy. But the study of de Castro e Silva Neto et al. [21] was a statistical summary of the existing literature without a deeper analysis (e.g., research trends in PPP). Song et al. [6] adopted the scientometric analysis of PPP-related research in a wide scope covering subjects of engineering, business and economics, and public administration. Researchers in this study believe that these review-based studies can be extended with a more comprehensive coverage, such as research methodology applied in existing PPP studies, the major research focus areas in the last ten years, and the expectations of research directions for the future work. So far limited reviews have linked PPP within the context of project management across multiple industries or sectors with a holistic approach by combining bibliometric analysis, science mapping, and further qualitative analysis.

Continuing from these previous review-based studies in PPP, this study contributes to the body of knowledge by (1) starting from a bibliometric analysis and science mapping of the existing literature since 2008 focusing on PPP in project management, (2) adopting a systematic review of the selected literature sample to summarize and analyze research methods, countries/regions where the PPP studies were performed, project sectors, and key issues within PPP, and (3) analyzing mainstream research topics and recommending future PPP research directions. This study integrates bibliometric analysis, science mapping, quantitative measurements of productive scholars, institutions, countries in PPP research, and systematic review in a holistic approach.

2. Methodology

This study adopted a bibliometric analysis of the PPP-based literature followed by the science mapping defined by Tijssen and van Raan [22] and Cobo et al. [23]. A bibliometric analysis examines the bibliographical material from an objective and quantitative perspective which is useful to organize information in a specific field [24, 25]. A bibliometric analysis, by using keywords, allows the analysis of details in main topics within a domain and relationships at the microlevel [26]. Compared to other literature review techniques, bibliometrics provides more objective and reliable analyses [27]. Science mapping describes and diagnoses research policy purposes and processes immense reservoirs of bibliometric data [22]. It displays the structural and dynamic aspects of a scientific research [23, 28] and represents spatially how disciplines, fields, and individual articles or authors relate to one another [29]. Following several existing studies adopting a comprehensive review workflow [30–32], the overall research steps in this review-based study of PPP are described in Figure 1, which consists of bibliometric analysis through literature search, science mapping, and follow-up systematic review.

2.1. Bibliometric Analysis. Keyword search was performed in *Scopus*, which was identified by Aghaei Chadegani et al. [33] as the literature source with a wider coverage of journals and more recent publications compared to other search engines such as *Web of Science*. Scopus has also been recommended by other studies [19, 34] and [35] within the project management field as the literature source. The literature search was set initially by inputting keywords in *Scopus* denoted below:

TITLE-ABS-KEY ("*public-private partnership*" OR "*public-private partnerships*" OR "*public private partnership*" OR "*public private partnerships*" OR "*Public/private Partnerships*").

The scope of the search was limited to those published in recent ten years (i.e., from 2008 to 2018), and only journal articles published in English were included in the first-round search. Sources from conference proceedings were excluded. As suggested in [36], conference papers have been published in large number but little has been gained by including them, given the extra amount of complexity added to the analyses. According to Figure 1, after obtaining all journal articles through keyword search, the second-round refinement of the literature was performed to remove articles that did not fall into the project management field. Project management, as defined by multiple studies [37–40], generally involves the monitoring and control of project performance in terms of cost, time, quality, and risks. Following the second-round refinement, a third-round checking was performed to further remove articles which did not focus on PPP-related research themes. In other words, although PPP or relevant terms were mentioned in the article, they were not the focus of the study in project management.

2.2. Science Mapping. The text mining software tool, *VOSViewer* [41], was adopted to generate the bibliometric map of PPP. In recent years, *VOSViewer* has been applied in scientometric analysis in the field of project management, such as building information modeling [34], building control [42], and offsite construction [35]. The scientometric review method can also be applied in other research topics [43]. As recommended by Hosseini et al. [35] and Park and Nagy [42], *VOSViewer* was utilized in this research to (1) import the literature source from *Scopus* to *VOSViewer*, (2) compute the frequency and co-occurrence of keywords, (3) extract the citation relationship among articles, authors, publication sources, and institutions, and (4) cluster and visualize keywords, publication sources, and institutions by co-occurrences.

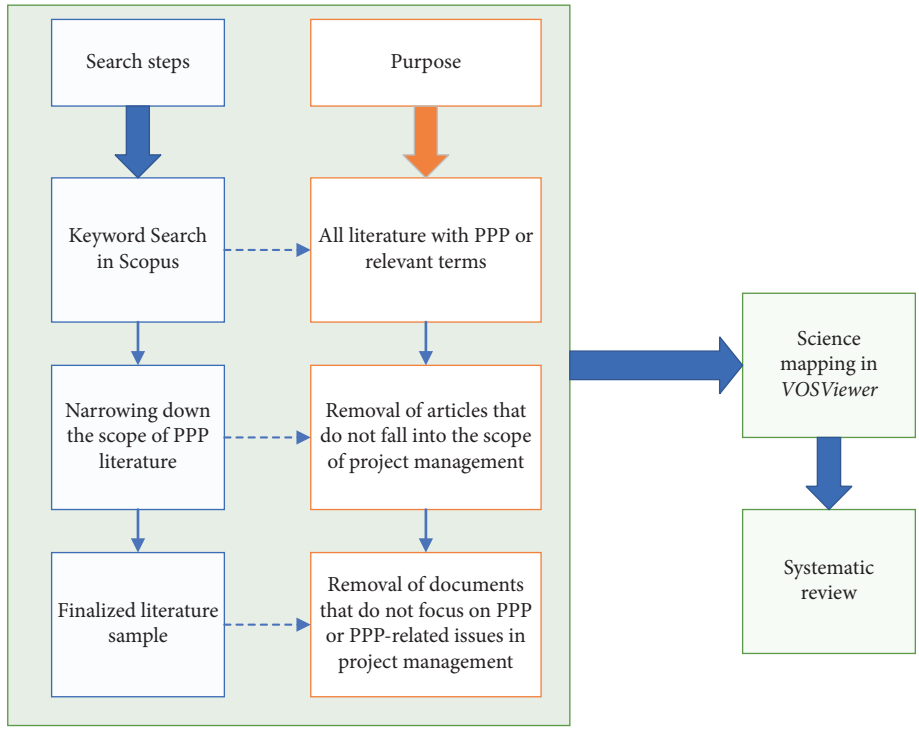

Figure 1: The description of research steps in PPP literature review.

2.3. Systematic Review. Following the bibliometric analysis and science mapping, the systematic review was performed to summarize the current research focus areas in PPP-related project management and to provide suggestions for near-future research trends in PPP themes. Following the suggestions of Tang et al. [7] and de Castro e Silva Neto et al. [21], this study categorized and summarized key issues (e.g., contract performance, financing, and concession) within the refined PPP literature aiming to generate new insights into state-of-the-art research focuses. Besides, project sectors [21] and regions/countries of PPP studies [6] were also categorized and summarized together with methodologies adopted in the literature sample.

3. Results and Discussion

By performing the literature search in *Scopus*, originally 2,340 journal articles published from 2008 to 2018 were found. The majority of the literature in this sample was published from 2008 to 2018 and was hence considered a ten-year span. Reading through the abstract of these selected journal articles, those with PPP in the abstract or keywords but falling out of the scope of project management were excluded to narrow down the search scope. For example, Vasmant's [44] study in the biomedical field, though with PPP-relevant terminology in the abstract and keyword list, did not fall into the category of PPP in project management. Also, those with PPP in the abstract or keyword list but not focusing on PPP-related study were also further excluded. For example, Whyte and Lobo's [45] study focused on the application digital technology in a PPP type of infrastructure project. Although PPP was mentioned in the abstract, it was not the focus of the research. Therefore, journal articles such as Whyte and Lobo [45] was removed from the reference list. Ultimately, totally 1,209 journal articles were selected as the literature sample for this research.

3.1. An Overview of the PPP Literature Sample. The numbers of journal articles published from 2008 to 2018 in the literature sample are summarized in Figure 2.

It can be seen in Figure 2 that generally the number of yearly number of articles has slowly been increasing from 2008 to 2017, with a significant increase in 2018 to reach 353 articles. It could be inferred that the academic research of PPP themes in project management has been remaining or even becoming more popular in recent years. The sources of these articles are visualized in Figure 3 and further described in Table 1.

Setting the minimum number of articles and minimum citations of a source to be 10 and 10, respectively in *VOSViewer*, totally 14 sources met the requirements and visualized in Figure 3. It should be noticed that there is not really a standardized quantification for the threshold values of article number and citations [46]. However, following the scientometric analysis guide in other project management related studies (e.g., Oraee et al.) [34, 35, 46] and considering the context of this PPP literature sample, the minimum number of articles and citations were determined. Similar threshold values for keywords, coauthorship, articles, institutions, and countries in PPP-related research could also be determined in the consistent approach following these prior studies. A larger font size in Figure 3 indicates more articles published in the given source. The connection lines

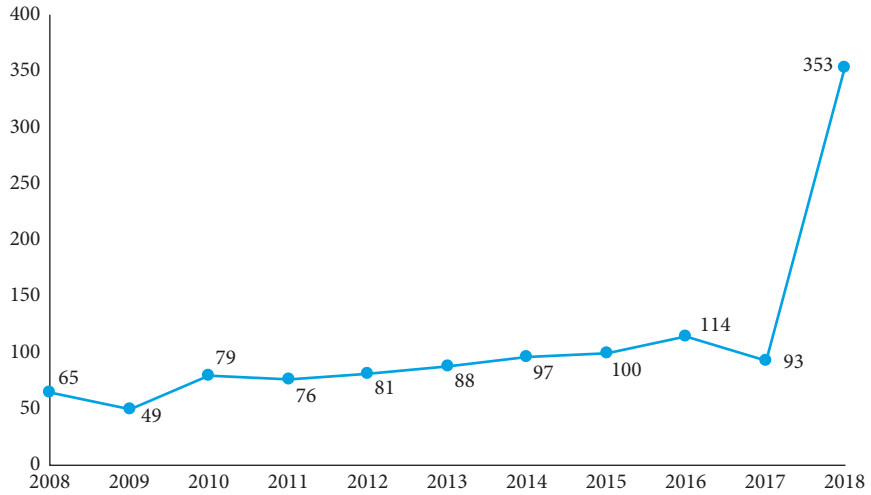

Figure 2: Number of journal articles published from 2008 to 2018.

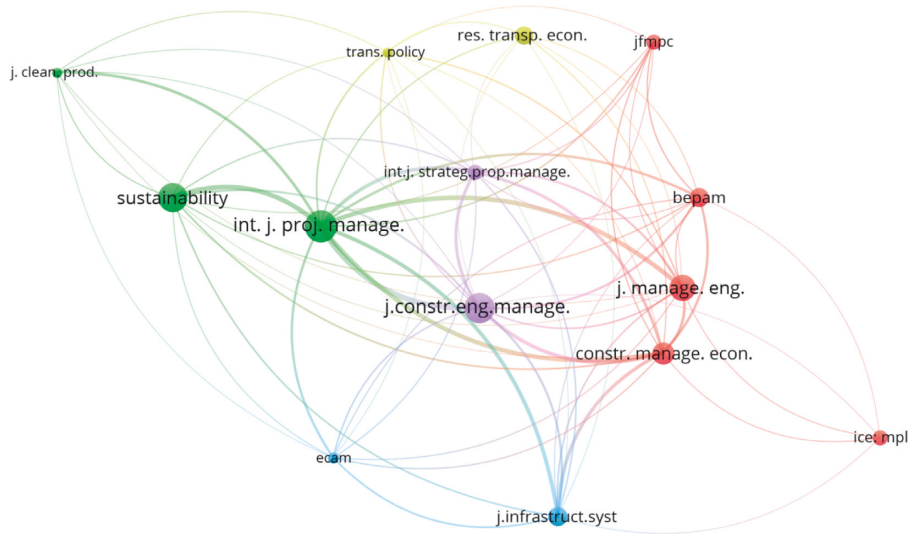

Figure 3: Mapping of sources of journal articles within this research. Note: Journal names are presented in Figure 2 using acronyms or abbreviation. The full name of journals can be found in Table 1.

indicate the citation between the pair of given sources. For example, it can be found in Figure 3 that *International Journal of Project Management* (i.e., *Int. J. Proj. Manage.*) has a strong cocitation with *Journal of Construction Engineering and Management* (i.e., *J. Constr. Eng. Manage.*) in the PPP area. Detailed number of articles, link strength, and citations are listed in Table 1.

Based on the link strength, number of articles published, number of citations, and average citation per article listed in Table 1, the most influential sources in the PPP field would be *International Journal of Project Management*, followed by *Construction Management and Economics*, *Journal of Construction Engineering and Management*, and *Journal of Management in Engineering*. Other journals indicating the project sectors, including *Journal of Infrastructure Systems* and *Research in Transportation Economics*, although not with high total link strength, are also the main sources of the PPP literature considering the number of articles published in these two journals. Among the infrastructure sector, transportation is one of the main sectors that PPP research has focused on. Besides *Research in Transportation Economics* which contributes to 21 articles in this literature sample, other PPP-related research were found in the transportation sector in sources such as *Transportation Research Part A: Policy and Practice*, *Transportation Research Part D: Transport and Environment*, and *Transportation Journal*.

3.2. Science Mapping. Continuing using *VOSViewer* as the science mapping tool, the following sientometric analysis was performed in terms of research keywords in the selected PPP literature sample, coauthorship, highly cited journal articles in PPP, and highly productive research organizations and countries in the field of PPP.

3.2.1. Co-Occurrence of Keywords. Keywords represent the core contents of existing studies and describe the areas

Table 1: Analysis of sources in PPP.

Source	Acronym or abbreviation in Figure 3	Total link strength	Number of articles	Total citations	Average citations
Built Environment Project and Asset Management	BEPAM	66	22	85	3.9
Construction Management and Economics	Constr. Manage. Econ.	188	27	522	19.3
Engineering, Construction and Architectural Management	ECAM	46	11	119	10.8
Proceedings of Institution of Civil Engineers: Management, Procurement and Law	ICE: MPL	7	17	32	1.9
International Journal of Project Management	Int. J. Proj. Manage.	366	45	887	19.7
International Journal of Strategic Property Management	Int. J. Strateg. Prop. Manage.	112	17	127	7.5
Journal of Cleaner Production	J. Clean. Prod.	33	10	37	3.7
Journal of Management in Engineering	J. Manage. Eng.	113	33	365	11.1
Journal of Construction Engineering and Management	J. Constr. Eng. Manage.	193	41	723	17.6
Journal of Infrastructure Systems	J. Infrastruct. Syst	107	23	182	7.9
Journal of Financial Management of Property and Construction	JFMPC	26	17	103	6.1
Research in Transportation Economics	Res. Transp. Econ.	15	21	136	6.5
Sustainability (Switzerland)	Sustainability	99	39	66	1.7
Transport Policy	Trans. Policy	29	10	90	9.0

Total link strength corresponds to Figure 3 and indicates the interrelatedness between the given journal and other peer journals.

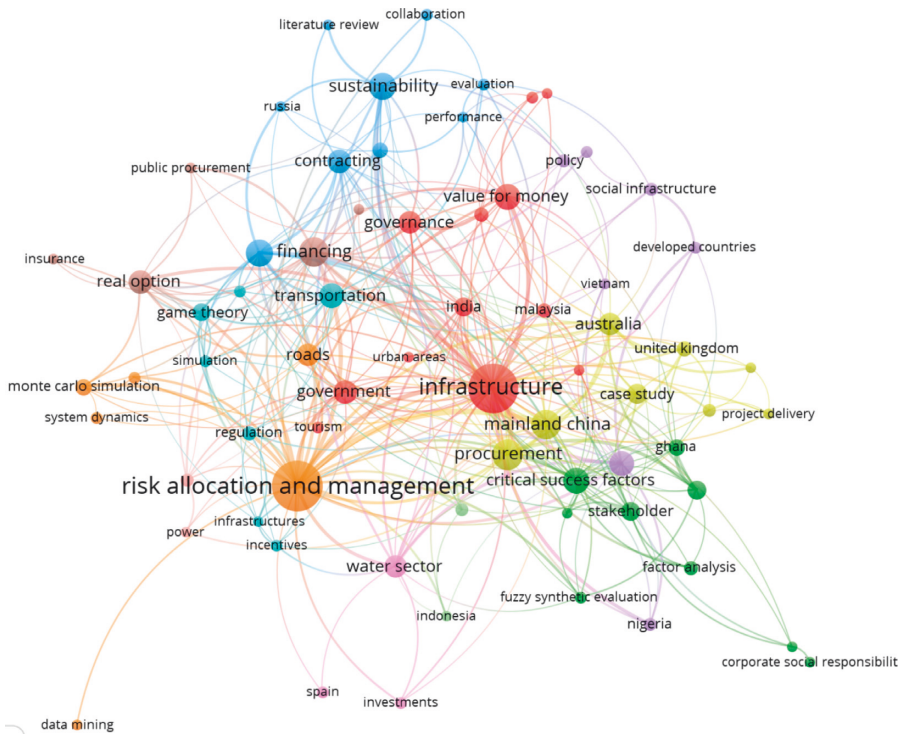

Figure 4: Co-occurrence of keywords.

researched within the boundaries of a domain [47]. According to van Eck and Waltman [48], a network of keywords provides the picture of knowledge in terms of patterns, relationships, and intellectual organization of research topics. From totally 2,669 keywords extracted through the literature database, with the minimum number of occurrences set at 5 using Author Keywords, and by removing some generic keywords (e.g., "PPP," "public-private partnerships," and "project,"), originally 99 keywords were generated. By further merging keywords with

Table 2: Summaries of most frequently studied keywords in PPP.

Studied keywords	Total link strength	Frequency	Average year published	Average citations
Risk Allocation and Management (RAM)	88	132	2013	12
Infrastructure	88	124	2014	11
Procurement	36	47	2013	13
Mainland China	34	43	2014	20
Financing	30	42	2013	9
Concession	26	37	2014	6
Sustainability	23	37	2016	3
Critical Success Factors	20	32	2015	13
Value for Money	20	32	2013	9
Developing Countries	25	30	2015	4
Transportation	18	29	2015	5
Government	19	27	2015	5
Real Option	19	27	2014	11
Contracting	15	26	2015	4
Australia	25	25	2013	11
Roads	17	24	2014	10
Water Sector	21	24	2012	7
Governance	13	23	2015	4
Case Study	11	18	2015	9
India	14	17	2014	6
Hong Kong	15	16	2013	15
Stakeholder	12	16	2015	10
Game Theory	9	14	2016	3
Monte Carlo Simulation	9	13	2016	5
Ghana	7	12	2017	3
Innovation	6	11	2015	6

consistent semantic meanings (e.g., "case study" and "case studies") and categorizing keywords (e.g., "risk analysis," "risk management," and "risk assessment" were all categorized into "risk allocation and management"), finally 72 keywords were generated. This corresponding network was created using VOSViewer in Figure 4.

The following can be indicated from the node size and connection lines: (1) Risk allocation and management (RAM) is one of the most frequently studied research topics in PPP projects. Other key research topics in PPP involve procurement, critical success factors (CSF), financing, concession, regulation, contracting, value for money (VFM), and governance. (2) Infrastructure, including roads and water, is the sector that PPP research has frequently focused on. (3) Some widely applied research methods used in PPP-based project management include case study, simulation, data mining, game theory, and fuzzy synthetic evaluation. (4) Besides developed countries (e.g., U.K., Australia, and Spain), PPP has also widely been studied in developing countries such as China, India, Ghana, Malaysia, and Nigeria. (5) The project participants (e.g., government and stakeholder) in both public and private sectors were also one key issue studied. (6) Sustainability and innovation were another two frequently studied issues in PPP research. A more quantitative analysis of these main keywords is summarized in Table 2.

It should be noticed that only part of the most frequently studied keywords from the total sample of 72 are listed in Table 2. Most keywords appear in the literature from 2011 to 2014, indicating that most of them have been in the research community before 2014. Only a few other keywords including "game theory," "Monte Carlo simulation," and "data mining" appear, coming to the research community more recently with the average publication year in 2015. The correlation analysis among total link strength, frequency, and average citation of the totally 72 keywords revealed that the total link strength is highly correlated to the frequency of the keyword, with a Pearson correlation coefficient at 0.991. However, the average citation of a keyword is not affected by its frequency of being studied in the literature, with a Pearson correlation coefficient at 0.214 and corresponding p value at 0.071 between the average citation and the frequency. This weak relationship between frequency and average citation can be proved in the example of RAM, which has the highest frequency of being studied in the literature. Nevertheless, keywords that receive highest average citations is "Mainland China," followed by Hong Kong, CSF, and "procurement." It can be inferred that research topics related to CSF and procurement tend to have higher impact on the academic community of PPP, although RAM tends to be the most popular research topic.

3.2.2. Coauthorship Analysis. Awareness of the existing scientific collaboration networks in a research field enhances the access to funds, specialties, and expertise, improves productivity, and helps researchers reduce isolation [35]. The science mapping in *VOSViewer* was also used to identify the most productive scholars and the research collaboration among them. With totally 2,396 *authors* extracted from the literature sample and 3 *articles* and 30 *citations* set as the minimum criteria, totally 72 authors were found meeting the threshold. The coauthorship analysis is visualized in Figure 5.

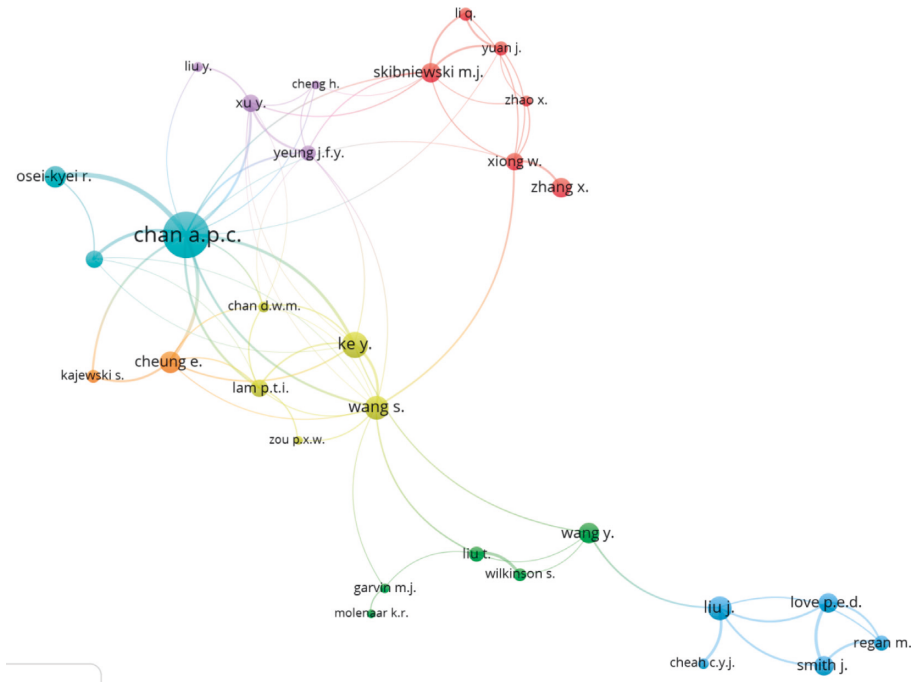

Figure 5: Coauthorship analysis.

It can be indicated from the clusters represented by different colors of nodes, node sizes, and connection lines among scholars shown in Figure 5 that Chan A. P. C., as the most productive author in PPP, has strong collaboration with Ameyaw E. E. and Oseu-Kyer R. Chan A. P. C. has also collaboration with the research network consisting of Ke Y., Wang S., Zou P. X. W., and Lam P. T. I. The other three PPP-based research networks tend to work more closely within their own groups. These three research groups are: (1) network consisting of Love P. E. D., Liu, J., Regan M., Smith J., and Cheah, C. Y. J.; (2) network comprised of Xu Y., Yeung J. F. Y., and Cheng H.; and (3) collaboration among Skiniewski M. J., Yuan J., and Li Q. More detailed description of these main active scholars in PPP field is provided in Table 3.

Totally 30 productive authors are listed in Table 3. Their average publication years of articles range from 2011 to 2017. Scholars such as Zou P. X. W., Cheng H., and Cheung E. have more of their PPP articles published in earlier years around 2011. In comparison, some scholars are more recently active researchers in the PPP field. For example, Osei-Kyei R. and Ameyaw E. E. have their work published more recently in 2017 and 2016, respectively. The four major parameters of scholars' PPP research outputs, namely, total link strength, number of articles published, total citations in the academic community, and average citation per article, are analyzed of their internal correlations. Table 4 summarizes the correlation analysis results.

It is found from Table 4 that average citation per article is not related to the total link strength or number of articles published by a scholar. However, it has significant correlation with the total citations. For example, Chan D. W. M., although having only published five articles, has the highest average citation at 58.0 and also high total citations at 290. An author who has published more articles will have also a higher impact on the research community measured by total link strength (e.g., Chan A. P. C.).

3.2.3. Citation of Articles. Published PPP-related articles were also mapped based on the citation numbers received. With the minimum number of citations of an article set at 30, totally 64 meet the threshold. These articles receiving most citations are visualized in Figure 6.

It can be found from Figure 6 that these most influential PPP articles in recent ten years were published from 2008 to 2012. Many of these published studies were led by active scholars included in Figure 5 and Table 3, such as Ke Y., Chan A. P. C., Yuan J., and Xu Y. These top 15 articles receiving the highest citations are listed in Table 5.

The number of links listed in Table 5 indicated the interrelatedness of the article to others in the selected sample of highly cited articles. An article with more links indicates that it is more highly cited or citing other articles in the sample. However, it differs from the number of citation in that the latter shows the overall impact of the article to the whole research community. These two parameters are not correlated. For example, the article published by Chan et al. [50] received one of the highest citations in PPP field, although it is with only one link among these articles in the network shown in Figure 6. In contrast, the article published by Jin and Doloi [53] was cited by only 75 times, but it has eight links with other articles shown in Figure 6, indicating its higher degree of interrelatedness with the rest of the articles.

3.2.4. Institutions Productive in PPP Research. Adopting VOSViewer, institutions were analyzed of their

Table 3: List of active scholars in PPP research.

Author	Total link strength	Number of articles	Total citations	Average publication year	Average citation
Ameyaw E. E.	8	10	59	2016	5.9
Chan A. P. C.	52	57	1069	2014	18.8
Chan D. W. M.	5	5	290	2010	58.0
Cheah C. Y. J.	5	5	43	2015	8.6
Cheng H.	2	3	36	2011	12.0
Cheung E.	14	15	490	2011	32.7
Garvin M. J.	2	4	55	2014	13.8
Kajewski S.	6	6	109	2010	18.2
Ke Y.	16	20	688	2012	34.4
Lam P. T. I.	9	10	367	2012	36.7
Li Q.	6	6	149	2012	24.8
Liu J.	14	17	131	2016	7.7
Liu T.	8	8	52	2015	6.5
Liu Y.	2	4	30	2017	7.5
Love P. E. D.	12	12	104	2015	8.7
Molenaar K. R.	1	3	44	2016	14.7
Osei-Kyei R.	15	15	63	2017	4.2
Regan M.	8	8	110	2014	13.8
Skibniewski M. J.	10	13	193	2014	14.8
Smith J.	13	13	133	2015	10.2
Wang S.	15	17	474	2013	27.9
Wang Y.	4	14	44	2016	3.1
Wilkinson S.	6	6	52	2014	8.7
Xiong W.	9	10	31	2016	3.1
Xu Y.	10	10	202	2013	20.2
Yeung J. F. Y.	8	8	254	2012	31.8
Yuan J.	7	7	129	2014	18.4
Zhang X.	3	13	127	2014	9.8
Zhao X.	2	5	70	2017	14.0
Zou P. X. W.	2	3	57	2011	19.0

Table 4: The Pearson correlation analysis among parameters related to authors' impact on PPP research community.

Correlation analysis	Total link strength	Number of articles	Total citations	Average citation
Total link strength		$r = 0.965$; $p = 0.000$	$r = 0.835$; $p = 0.000$	$r = 0.093$; $p = 0.626$
Number of articles			$r = 0.830$; $p = 0.000$	$r = 0.034$; $p = 0.857$
Total citations				$r = 0.522$; $p = 0.003$

r is the Pearson correlation between the selected pair of authors' parameters, and a corresponding p value lower than 0.05 would indicate a significant relationship between the pair of parameters.

contributions to the research outputs of PPP. By setting the minimum number of articles at 3 and minimum citations at 30 as threshold values to screen the totally 2,182 institutions, 14 of them were identified as most research active organizations in PPP.

Figure 7 conveys the information that Hong Kong-based universities, including Hong Kong Polytechnic University (HK Poly U), Hong Kong University of Science and Technology, and Hong Kong Baptist University, are active in PPP research. These three universities have developed their research collaboration with peer institutions in the mainland of China. For example, HK Poly U has displayed strong collaboration with Tsinghua University, Zhejiang Sci-Tech University, and Southeast University in China. The closer geographic distance could be one factor driving the collaboration for these universities among Taiwan, Hong Kong, and mainland of China (i.e., HK Poly U, National Taiwan University, and Tsinghua University China). In comparison, Australian universities, including Bond University, Queensland University of Technology, and Curtin University, seem more closely collaborating among themselves by forming their own cluster, although they have developed certain collaboration with peer institutions from other continents, including University of Maryland, Southeast University China, and HK Poly U.

3.2.5. Countries or Regions Active in PPP Research. Similar to the study of institutions productive in PPP research, countries that have been active in PPP research were also analyzed. Setting the minimum number of articles published at 5, minimum citations received at 30, totally 32 out of 96 countries met the threshold. These countries where most PPP researchers were based are visualized in Figure 8.

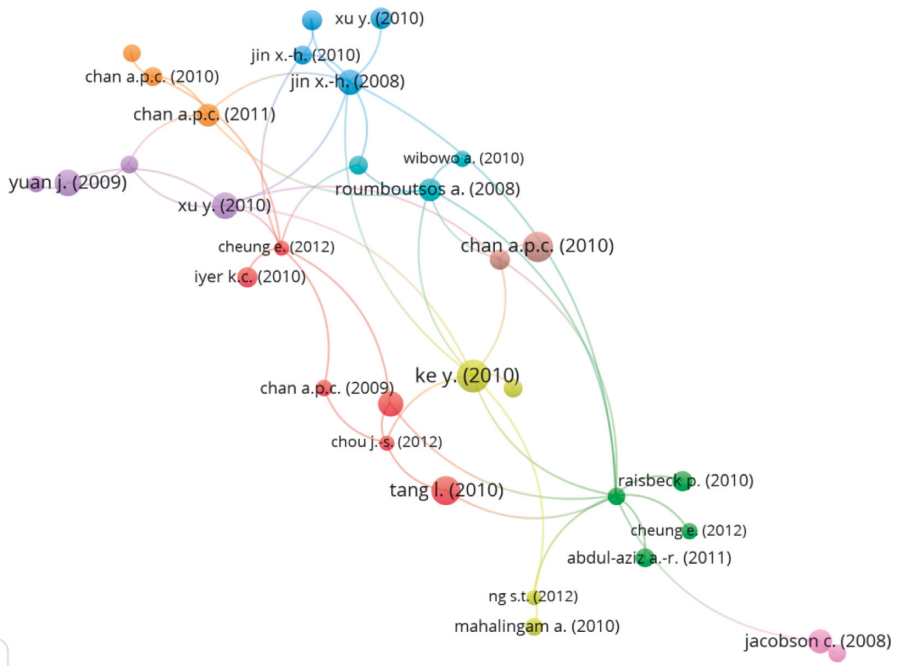

Figure 6: Science mapping of PPP articles.

Table 5: List of PPP articles with high citations.

Article	Title	Number of links	Number of citations
Ke et al. [49]	Preferred risk allocation in China's public–private partnership (PPP) projects	8	116
Chan et al. [50]	Critical success factors for PPPs in infrastructure developments: Chinese perspective	1	105
Tang et al. [7]	A review of studies on public–private partnership projects in the construction industry	2	93
Yuan et al. [51]	Selection of performance objectives and key performance indicators in public–private partnership projects to achieve value for money	3	82
Xu et al. [52]	Developing a risk assessment model for PPP projects in China—a fuzzy synthetic evaluation approach	6	80
Jin and Doloi [53]	Interpreting risk allocation mechanism in public–private partnership projects: An empirical study in a transaction cost economics perspective	8	75
Ke et al. [18]	Research trends of public-private partnership in construction journals	3	74
Jacobson and Choi [54]	Success factors: public works and public-private partnerships	2	70
Roumboutsos a Anagnostopoulos [57]	Public–private partnership projects in Greece: risk ranking and preferred risk allocation	6	61
Chan et al. [16]	Empirical study of risk assessment and allocation of public-private partnership projects in China	4	60
Xu et al. [51]	Developing a fuzzy risk allocation model for PPP projects in China	1	55
Iyer and Sagheer [57]	Hierarchical structuring of PPP risks using interpretative structural modeling	1	54
Jin and Zhang [58]	Modeling optimal risk allocation in PPP projects using artificial neural networks	2	53
Hwang et al. [59]	Public-private partnership projects in Singapore: factors, critical risks and preferred risk allocation from the perspective of contractors	5	51
Raisbeck et al. [60]	Comparative performance of PPPs and traditional procurement in Australia	1	49

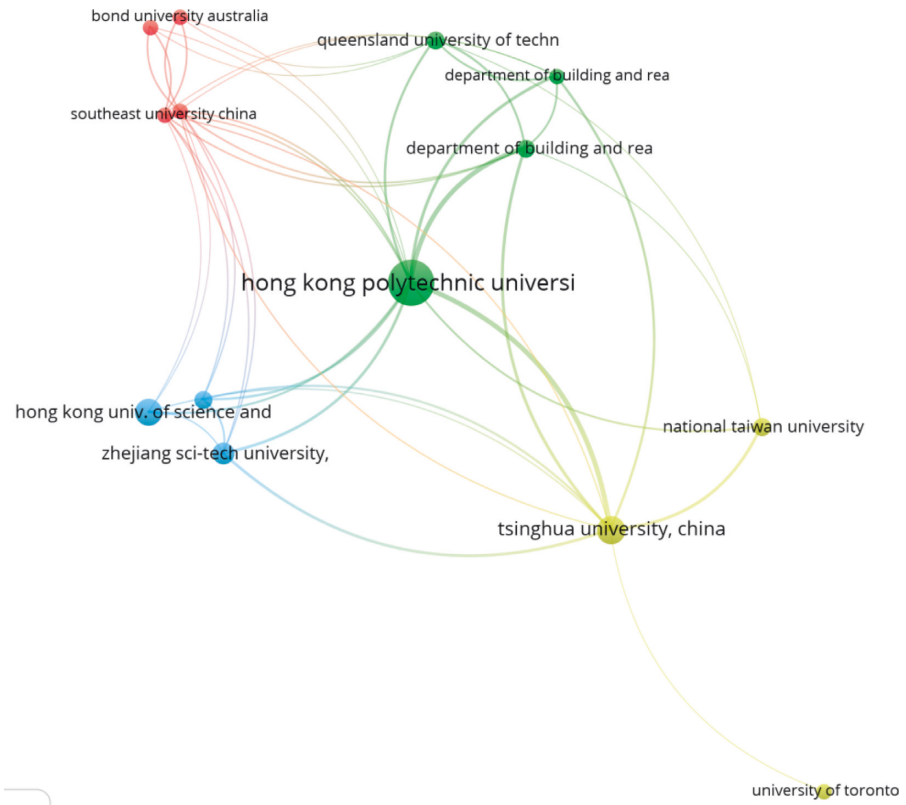

Figure 7: Mapping of organizations active in PPP research.

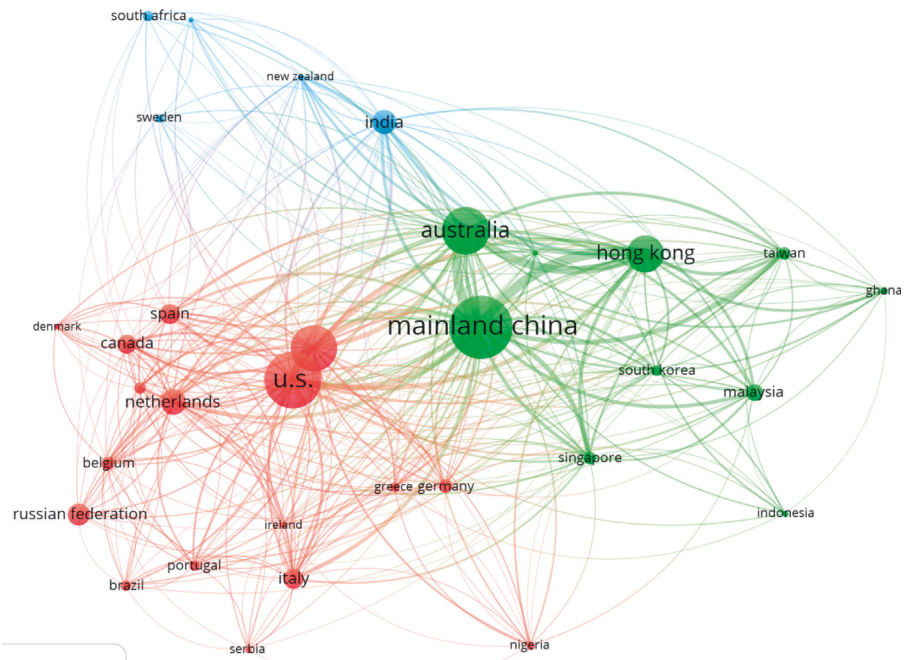

Figure 8: Mapping of countries/regions where PPP researchers were located.

It can be inferred from Figure 8 that PPP researchers have widely distributed crossing developing and developed countries. Developed countries including U.K., U.S., and Australia have largely contributed to the PPP research field. Researchers from developing countries, as indicated by both Figures 4 and 8, have also been active in PPP research, such as China, India, Malaysia, and Ghana. These quantitative measurements of countries where PPP researchers are located are summarized in Table 6.

Table 6 shows that China is the country that is most productive in PPP research in terms of total link strength, number of PPP journal articles published, and total citations.

Table 6: Countries or regions where PPP researchers are based.

Country/region	Total link strength	Number of articles	Number of citations	Average publication year	Average citation
Mainland China	1740	180	1428	2016	7.9
U.S.	683	159	958	2015	6.0
Australia	1211	126	1077	2015	8.5
UK	591	125	895	2014	7.2
Hong Kong	1250	93	1289	2014	13.9
Netherlands	276	61	676	2014	11.1
India	218	57	305	2015	5.4
Russian Federation	58	51	56	2016	1.1
Italy	247	47	269	2015	5.7
Spain	161	45	197	2015	4.4
Canada	138	44	255	2015	5.8
Malaysia	216	37	158	2015	4.3
Germany	97	30	186	2013	6.2
Belgium	121	27	122	2016	4.5
Singapore	320	26	347	2013	13.3
Taiwan	274	26	151	2015	5.8
France	107	25	286	2014	11.4
South Korea	120	23	123	2016	5.3
Brazil	55	22	96	2015	4.4
Portugal	109	22	171	2014	7.8

Not all 32 countries are listed in Table 6 but the top 20 countries with most PPP articles published are listed.

Table 7: Pearson correlation analysis among parameters related to countries/regions' impacts on PPP research.

Correlation analysis	Total link strength	Number of articles	Number of citations	Average citation
Total link strength		$r = 0.871$; $p = 0.000$	$r = 0.947$; $p = 0.000$	$r = 0.324$; $p = 0.070$
Number of articles			$r = 0.920$; $p = 0.000$	$r = 0.101$; $p = 0.582$
Number of citations				$r = 0.404$; $p = 0.022$

With China as the exception, developed countries or regions are mainstream contributors to PPP research. As can be seen in Table 6, U.S., U.K., Australia, Hong Kong, and Netherlands are also highly productive in PPP studies. The average publication year of articles generally range from 2011 to 2014 among the 32 countries, with the exception that Russia and Belgium are with articles published around 2015. It is inferred that these two countries have more recently become active in PPP research. A correlation analysis among the four parameters (i.e., total link strength, number of articles published, total citations, and average citations) is performed and summarized in Table 7.

Table 7 demonstrates that these four parameters are generally significantly correlated to each other, except that the number of articles published from a country is not correlated to the average citation per article. Overall, a country's impact to the global PPP research community can be measured by either total link strength, number of published journal articles, total citations, or average citation.

3.3. Systematic Review. Based on the analysis from science mapping, systematic review was performed to the literature sample in terms of the research methodology, project sectors, studied regions/countries, and qualitative analysis of key issues within PPP. It should be noticed that studied region/countries differ from science mapping shown in Figure 8, where the countries refer to where the authors of the published literature were based. The studied countries or regions in this section refer to whether the PPP-related study was performed in the context of a certain country or region. An example explaining the difference could be the study of Osei-Kyei and Chan [61]; while the researchers were located in Hong Kong, the studied country included Ghana.

3.3.1. Summary of Research Methods. The 1,209 articles were summarized of their research methods. As indicated by Figure 4, case studies and other modeling methods (e.g., fuzzy synthetic evaluation) were widely been applied in PPP studies. These main research methods listed in Table 8 include case studies, research modeling and framework, questionnaire survey, interview, literature review, and others.

Other methods listed in Table 8 refer to those without specified methods or generally with qualitative analysis. For example, in the study of Brthen and Odeck [62], an overview of various toll road projects was provided followed by discussions on socioeconomic efficiency via public funding. Similar qualitative analysis can be found in PPP studies including Sohail and Maslyukivska [63], Tang and Lo [64], Mahalingam et al. [65], Petersen [66], and Deshpande and Rokade [67]. It can be found from Table 8 that case studies and modeling are the mainstream research methods implemented in PPP research, followed by questionnaire-based survey and interview to PPP-related professionals.

Table 8: Summary of research methodologies in the literature sample.

Research method	Number of articles	Percentage
Case study	375	29.0
Modeling or framework/model development	398	31.0
Questionnaire survey	113	8.7
Interview	105	8.1
Review	54	4.2
Others	248	19.0

The total percentage may be summed up to be over 100%, as some studies may adopt more than one method. The case that the summed percentage may be higher than 100% also applies to Tables 9 and 10 where the project sectors and key issues in PPP are summarized respectively.

Table 9: Summary of project sectors in the PPP literature.

Project sectors	Number of articles	Percentage
Transportation	162	13.4
Water	62	5.1
Healthcare	63	5.2
Other construction projects	42	3.5
Public housing	27	2.2
Education	27	2.2
Agriculture	31	2.6
Energy	36	3.0
Waste recycling	15	1.2
Information and communication technology	11	1.0
Preventation/postdisaster projects	6	0.5
Tourism	17	1.4
Physical culture and sport	5	0.4
Apparel and textile industry	1	0.1
Prison	3	0.2
Unspecified	700	58.0

Other construction projects include museum and building construction.

Case studies have been chosen as the research methodology due to the exploratory nature of the research, the limited amount of similar previous research, and the intent to develop knowledge on a contemporary phenomenon [68, 69]. Modeling approach has also widely been applied in PPP-involved projects to achieve optimized project performance by considering uncertainties and risks during the project delivery process. Examples of modelling approach in PPP projects include Carbonara and Pellegrino [70] where Monte Carlo simulation was employed, Osei-Kyei and Chan [61] who adopted fuzzy synthetic evaluation method, and Roumboutsos et al. [71] who applied the game theoretic model. Previous studies had also focused on establishing, developing, and testing frameworks for PPP projects, such as Shrestha et al.'s [72] work to build the framework to examine risk allocation for PPP water projects in China. Questionnaire survey, interviews, and review are not unique in PPP research but commonly adopted methods in the field of project management.

3.3.2. Project Sectors. Project sectors targeted in the PPP literature sample are summarized in Table 9.

Consistent to the statistical summary performed by de Castro e Silva Neto et al. [21], the majority of PPP studies did not specify the project sectors. As indicated from the science mapping presented in Figure 4, infrastructure was one of the most frequently studied keywords in the PPP literature. Among the infrastructure projects, transportation was the sector that was most widely studied according to this study and that of de Castro e Silva Neto et al. [21]. Consistently between these two studies, PPP projects were found applied in multiple sectors including health, education, housing, energy, agriculture, and communication. However, unlike the study of de Castro e Silva Neto et al. [21], who found that the health sector was the second most widely studied sector in PPP, this research identified the water sector as the second most frequently studied sector followed by the health sector. This difference could be due to the years and types of the literature selected. This study only chose journal articles published within the recent ten years, and de Castro e Silva Neto et al. [21] used the literature including both journal articles and conference papers published from 1990 to 2014. It seems that journal articles have been focusing more on infrastructure project sectors, including transportation and water and waste management.

3.3.3. Studied Regions/Countries. The countries or regions where PPP studies were conducted were also summarized. Around 40% of the selected studies did not specify countries. For the remaining studies falling into the context of certain countries or regions, the frequencies of countries targeted in the literature sample are presented in Figure 9.

It is shown in Figure 9 that China is the country that has been studied most frequently from the selected literature.

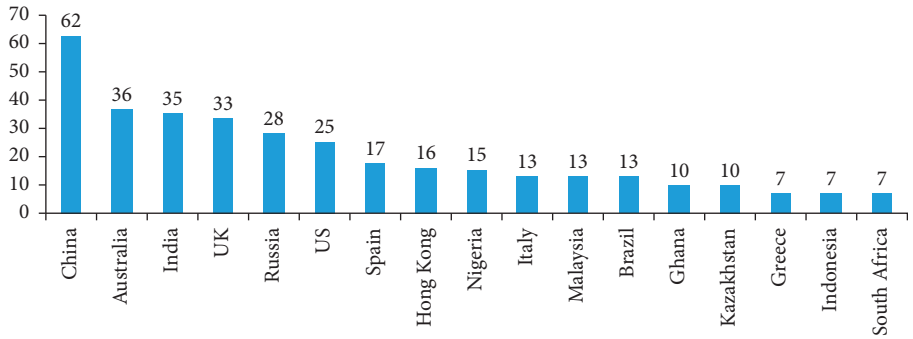

Figure 9: Frequencies of countries that have been studied in the literature sample.

Table 10: Summary of key issues in the literature sample.

Key issues	References	Number of articles	Percentage
Project governance (PG)	Guarini and Battisti [75]; Opara and Elloumi [76]	303	22.7
Risk allocation and management (RAM)	[77, 78]	166	12.4
Critical success factors (CSF)	[79, 80]	120	9.0
Performance evaluation (PE)	[81, 82]	114	8.7
PPP models and applications (PMA)	[83, 84]	188	14.1
Economics and financing (EF)	[85, 86]	91	6.8
Contract management (CM)	[87, 88]	82	6.1
Procurement management (PM)	[89, 90]	45	3.4
Legislation and legal issues (LLI)	[91, 92]	40	3.0
Hindering PPP factors (HPF)	[93, 94]	34	2.5
Innovation in PPP (IP)	[95, 96]	46	3.4
Value for money (VFM)	[97, 98]	26	2.0
Concession-related models, pricing, and periods (CMPP)	[99, 100]	18	1.3
Others	[101, 102]	62	4.6

Figure 8 and Table 6 show that China was the country where scholars had published most PPP-related articles, and Figure 9 further infers that China is also the country that has received the highest attention on PPP research. This could be due to fact indicated by Zhang et al. [73] and Yang et al. [74] that PPP has been gaining wide implementation and aroused a wide attention from Chinese industry, government, and academia in the last decade.

3.3.4. Qualitative Analysis of Key Issues. Following the studies of Tang et al. [7] and de Castro e Silva Neto et al. [21], as well as key research topics mapped in Figure 4 and Table 2, key issues that have been studied in the literature sample are listed in Table 10.

Each key issue in Table 10 is accompanied with examples of studies from the literature sample. Other key issues studied in the PPP literature include sustainability [103], general summary of PPP project experience [104], overview of PPP research trends [18], application conditions of PPP [105], comparative analysis of PPP [106], and public involvement [107]. Table 10 conveys the information that project governance and risk-related topics have been the most frequently studied issues in the last ten years. Other key issues which were also predicted by Tang et al. [7] that would receive wide concern in PPP research include financing and costs, CSF, risk allocation and management (RAM), concession-related issues (e.g., concession period), contract management (CM), development of PPP models, and applications. Taking RAM, for example, which is always an active research topic for PPP projects [7], most studies of RAM paid attention to which and to what extent of the risks should be allocated to the relevant stakeholders, i.e., government or private side, and few studies focused on designing or carrying out a realistic risk sharing strategy or reasonable risk sharing ratio between the two parties [73].

4. Discussion on the Findings

Based on the three research steps illustrated in Figure 1, this review-based study adopted a bibliometric analysis of journal articles published within the last ten years in the PPP field. Science mapping was applied to explore the research keywords, influential researchers, articles, journal sources, institutions, and countries that had been with high impacts in PPP. The further systematic review of the literature sample provided the statistical summary of the studied countries or regions, research methods, project sectors, and key issues from the selected PPP literature sample.

PPP-based studies in project management have been undergoing a steady increase in the last few years. These few journals, including *International Journal of Project Management*, *Construction Management and Economics*, *Journal of Construction Engineering and Management*, and *Journal of*

Management in Engineering, play major roles in PPP research, based on their total link strength, number of articles published in PPP, and citations in the academic community. Research keywords within the PPP literature could be categorized into key issues (e.g., governance), countries (e.g., China), research method (e.g., case study), and project sectors (e.g., transportation). Sustainability and innovation had also been concerned in PPP research. As a sustainable concept, BIM (i.e., building information modeling) was perceived to have significant correlations with PPP projects [108]. Love et al. [109] and Ren and Li [110] proposed utilizing BIM as the digital approach to assist the decision-making in VFM within PPP projects. It is indicated that although most PPP studies have focused on the managerial aspects of project management, sustainability and innovation integrated with PPP could be emerging research topics for the future PPP study.

The science mapping of PPP articles, scholars, institutions, and countries indicated that China had generated the most outputs in PPP, in terms of the number of articles published, citations, and total link strength. It was found that these parameters to quantify the impact of a country or an individual scholar on PPP research was generally significantly correlated to each other, meaning that either the total link strength, number of publications, or citation numbers can be used to measure the contribution of the individual scholar, institution, or the country. Chan A. P. C. and his affiliation (i.e., Hong Kong Polytechnic University) are the most productive scholar and institution, respectively, in PPP field during the recent ten years. It is inferred that through the research collaboration with Chan A. P. C., Ameway E. E. and Osei-Kyei R. become rising researchers in more recent years. It can be further indicated that collaboration among scholars and institutions could drive the movement of PPP research in joint efforts.

Although developed countries, such as U.K., U.S., and Australia, have been contributing to more of the existing PPP studies, it is expected that more PPP studies will be carried out in developing countries (e.g., China, India, Ghana, Indonesia, and Nigeria). Some comparative studies between developed countries/regions and their developing counterparts (e.g., [111]) can be expected for the future study in PPP, as political, legislation, and cultural aspects within certain developing countries (e.g., China) would affect the implementation of PPP. When adopting PPP in project management, public and private sectors should consider the regional or the country's context.

Though recently published PPP studies indicated a certain degree of variety within key issues identified in Table 10, a review of these key issues showed that governance, risk management, and CSF represented the most widely studied topics in PPP, these under-represented issues (e.g., hindering factors) could be continued in the future. Hindering factors that cause difficulties or barriers (e.g., uncertainty in decision-making) in PPP implementation would be the ongoing research direction by applying various research methods, such as questionnaire survey and modeling.

5. Conclusions

The bibliometric analysis and systematic review of PPP journal articles published revealed that PPP is still steadily growing in the recent ten years. Visualized science mapping and quantitative measurement using parameters (e.g., number of citations) provided the information of popular research keywords, productive PPP scholars, articles with high impacts, and institutions and countries contributing to the PPP research community. The visualized mapping was extended by a follow-up systematic review, based on the summaries of research methods, project sectors, countries that PPP studies focused on, and key issues within PPP research. Major findings from this holistic review-based study can be summarized below:

(1) The most frequently adopted research keywords from the recent ten years' PPP literature could be categorized as key issues (e.g., governance), countries (e.g., Australia), research methods (e.g., case study), industry sectors (e.g., water), and others (e.g., sustainability and innovation).

(2) Sustainability and innovation, such as PPP linked to BIM, could be one of the future research topics.

(3) Hindering factors focusing on barriers and challenges encountered in PPP implementation would be an increasingly studied key issue in PPP research.

(4) Although these more traditional key issues, such as risk management and concession, remain continuing research topics in PPP, a variety of key issues in PPP research can be expected, involving some new emerging topics, for example, the comparative study of PPP adoption between developing and developed countries.

(5) China would be the country where more PPP research are carried out in the near future. Collaboration will continue between China-based researchers and their international peers in PPP.

(6) Case study and modeling/framework are main research methods in PPP research, followed by the traditional questionnaire survey and interview. Qualitative analysis is also being widely applied in PPP studies.

(7) Transportation and water treatment are the two main infrastructure sectors with highest numbers of PPP studies. Linked to sustainability, it could be expected that energy and environment-related projects including waste recycling and diversion projects could receive more attention in PPP research.

Besides the major findings, this study also contributes to the existing knowledge in PPP by providing the following suggestions for future research:

(1) Technological innovation and integration with PPP projects

(2) Modeling or framework established to address hindering factors affecting PPP implementation under certain cultural or legislation context

(3) Studies tailoring the experience from developed countries to their developing counterparts

(4) Integrating multiple key issues in PPP, for example, how would legislation and legal issues affect the procurement, which would lead to performance evaluation

Conflicts of Interest

The authors declare that they have no conflicts of interest regarding the publication of this paper.

Acknowledgments

This study was supported by the Major Project of Shanghai Municipal People's Government Decision-Making Research (Grant number: 2017-A-046) and Shanghai Pujiang Program (Grant number: 16PJ1432400). The authors would also like to acknowledge the Writing Retreat Fund provided by University of Brighton, UK.

References

[1] L. Tang, Q. Shen, M. Skitmore, and E. W. L. Cheng, "Ranked critical factors in PPP briefings," *Journal of Management in Engineering*, vol. 29, no. 2, pp. 164–171, 2013.

[2] R. Widdus, "Public-private partnerships for health: their main targets, their diversity, and their future directions," *Bulletin of the World Health Organization*, vol. 79, no. 8, pp. 713–720, 2001.

[3] N. F. D. Cruz and R. C. Marques, "Delivering local infrastructure through PPPs: evidence from the school sector," *Journal of Construction Engineering and Management*, vol. 138, no. 12, pp. 1433–1443, 2012.

[4] J. Yuan, M. Guang, X. Wang, Q. Li, and M. J. Skibniewski, "Quantitative SWOT analysis of public housing delivery by public-private partnerships in China based on the perspective of the public sector," *Journal of Management in Engineering*, vol. 28, no. 4, pp. 407–420, 2012.

[5] J. Song, D. Song, X. Zhang, and Y. Sun, "Risk identification for PPP waste-to-energy incineration projects in China," *Energy Policy*, vol. 61, pp. 953–962, 2013.

[6] J. Song, H. Zhang, and W. Dong, "A review of emerging trends in global PPP research: analysis and visualization," *Scientometrics*, vol. 107, no. 3, pp. 1111–1147, 2016.

[7] L. Tang, Q. Shen, and E. W. L. Cheng, "A review of studies on public-private partnership projects in the construction industry," *International Journal of Project Management*, vol. 28, no. 7, pp. 683–694, 2010.

[8] H. P. Tserng, J. S. Russell, C.-W. Hsu, and C. Lin, "Analyzing the role of national PPP units in promoting PPPs: using new institutional economics and a case study," *Journal of Construction Engineering and Management*, vol. 138, no. 2, pp. 242–249, 2012.

[9] A. P. C. Chan, R. Osei-Kyei, Y. Hu, and Y. Le, "A fuzzy model for assessing the risk exposure of procuring infrastructure mega-projects through public-private partnership: the case of Hong Kong-Zhuhai-Macao bridge," *Frontiers of Engineering Management*, vol. 5, no. 1, pp. 64–77, 2018.

[10] A. P. Gurgun and A. Touran, ""Public–private partnership experience in the international arena: case of Turkey," *Journal of Management in Engineering*, vol. 30, no. 6, Article ID 04014029, 2014.

[11] B. Li, A. Akintoye, P. J. Edwards, and C. Hardcastle, "Critical success factors for PPP/PFI projects in the UK construction industry," *Construction Management and Economics*, vol. 23, no. 5, pp. 459–471, 2005.

[12] J. Liu, P. Love, B. Carey, J. Smith, and M. Regan, "Ex-ante evaluation of public–private partnerships: macroeconomic analysis," *Journal of Infrastructure Systems*, vol. 21, no. 2, article 04014038, 2015.

[13] L. Tang and G. Q. Shen, "Finance-related critical success factors for the briefing of PPP projects inconstruction," in *Proceedings of the International Conference on Construction and Real Estate Management*, pp. 427–437, Karlsruhe, Germany, October 2013.

[14] M. Soomro and X. Q. Zhang, "Evaluation of the functions of public sector partners in transportation public–private partnerships failures," *Journal of Management in Engineering*, vol. 32, no. 1, article 04015027, 2015.

[15] X. Zhang, "Criteria for selecting the private-sector partner in public-private partnerships," *Journal of Construction Engineering and Management*, vol. 131, no. 6, pp. 631–644, 2005.

[16] A. P. C. Chan, J. F. Y. Yeung, C. C. P. Yu, S. Q. Wang, and Y. Ke, "Empirical study of risk assessment and allocation of public-private partnership projects in China," *Journal of Management in Engineering*, vol. 27, no. 3, pp. 136–148, 2011.

[17] F. Al-Sharif and A. Kaka, "PFI/PPP topic coverage in construction journals," in *Proceedings of the 20th Annual ARCOM Conference*, pp. 711–719, Edinburgh, UK, September 2004.

[18] Y. Ke, S. Wang, A. P. Chan, and E. Cheung, "Research trend of public-private partnership in construction journals," *Journal of Construction Engineering and Management*, vol. 135, no. 10, pp. 1076–1086, 2009.

[19] Q. He, G. Wang, L. Luo, Q. Shi, J. Xie, and X. Meng, "Mapping the managerial areas of building information modeling (BIM) using scientometric analysis," *International Journal of Project Management*, vol. 35, no. 4, pp. 670–685, 2017.

[20] H. Wang, W. Xiong, G. Wu, and D. Zhu, "Public-private partnership in public administration discipline: a literature review," *Public Management Review*, vol. 20, no. 2, pp. 293–316, 2018.

[21] D. de Castro e Silva Neto, C. O. Cruz, F. Rodrigues, and P. Silva, "Bibliometric analysis of PPP and PFI literature: overview of 25 years of research," *Journal of Construction Engineering and Management*, vol. 142, no. 10, Article ID 06016002, 2016.

[22] R. J. W. Tijssen and A. F. J. van Raan, "Mapping changes in science and technology," *Evaluation Review*, vol. 18, no. 1, pp. 98–115, 1994.

[23] M. J. Cobo, A. G. López-Herrera, E. Herrera-Viedma, and F. Herrera, "An approach for detecting, quantifying, and visualizing the evolution of a research field: a practical application to the fuzzy sets theory field," *Journal of Informetrics*, vol. 5, no. 1, pp. 146–166, 2011.

[24] J. M. Merigó, A. M. Gil-Lafuente, and R. R. Yager, "An overview of fuzzy research with bibliometric indicators," *Applied Soft Computing*, vol. 27, pp. 420–433, 2015.

[25] G. Albort-Morant and D. Ribeiro-Soriano, "A bibliometric analysis of international impact of business incubators," *Journal of Business Research*, vol. 69, no. 5, pp. 1775–1779, 2016.

[26] G. Chen and L. Xiao, "Selecting publication keywords for domain analysis in bibliometrics: a comparison of three

methods," *Journal of Informetrics*, vol. 10, no. 1, pp. 212–223, 2016.

[27] M. Aria and C. Cuccurullo, "Bibliometrix: an R-tool for comprehensive science mapping analysis," *Journal of Informetrics*, vol. 11, no. 4, pp. 959–975, 2017.

[28] M. J. Cobo, A. G. López-Herrera, E. Herrera-Viedma, and F. Herrera, "Science mapping software tools: review, analysis, and cooperative study among tools," *Journal of the American Society for Information Science and Technology*, vol. 62, no. 7, pp. 1382–1402, 2011.

[29] H. Small, "Visualizing science by citation mapping," *Journal of the American Society for Information Science*, vol. 50, no. 9, pp. 799–813, 1999.

[30] Y. Xu, J. Zeng, W. Chen, R. Jin, B. Li, and Z. Pan, "A holistic review of cement composites reinforced with graphene oxide," *Construction and Building Materials*, vol. 171, pp. 291–302, 2018.

[31] W. Chen, R. Jin, Y. Xu et al., "Adopting recycled aggregates as sustainable construction materials: a review of the scientific literature," *Construction and Building Materials*, vol. 218, pp. 483–496, 2019.

[32] R. Jin, H. Yuan, and Q. Chen, "Science mapping approach to assisting the review of construction and demolition waste management research published between 2009 and 2018," *Resources, Conservation and Recycling*, vol. 140, pp. 175–188, 2019.

[33] A. Aghaei Chadegani, H. Salehi, M. M. Md Yunus et al., "A comparison between two main academic literature collections: web of science and scopus databases," *Asian Social Science*, vol. 9, no. 5, pp. 18–26, 2013.

[34] M. Oraee, M. R. Hosseini, E. Papadonikolaki, R. Palliyaguru, and M. Arashpour, "Collaboration in BIM-based construction networks: a bibliometric-qualitative literature review," *International Journal of Project Management*, vol. 35, no. 7, pp. 1288–1301, 2017.

[35] M. R. Hosseini, I. Martek, E. K. Zavadskas, A. A. Aibinu, M. Arashpour, and N. Chileshe, "Critical evaluation of off-site construction research: a scientometric analysis," *Automation in Construction*, vol. 87, pp. 235–247, 2018.

[36] L. Butler and M. S. Visser, "Extending citation analysis to non-source items," *Scientometrics*, vol. 66, no. 2, pp. 327–343, 2006.

[37] A. Abdi, S. Taghipour, and H. Khamooshi, "A model to control environmental performance of project execution process based on greenhouse gas emissions using earned value management," *International Journal of Project Management*, vol. 36, no. 3, pp. 397–413, 2018.

[38] Y. Li, Y. Lu, J. E. Taylor, and Y. Han, "Bibliographic and comparative analyses to explore emerging classic texts in megaproject management," *International Journal of Project Management*, vol. 36, no. 2, pp. 342–361, 2018.

[39] P. Sirisomboonsuk, V. C. Gu, R. Q. Cao, and J. R. Burns, "Relationships between project governance and information technology governance and their impact on project performance," *International Journal of Project Management*, vol. 36, no. 2, pp. 287–300, 2018.

[40] F. Zuo and K. Zhang, "Selection of risk response actions with consideration of secondary risks," *International Journal of Project Management*, vol. 36, no. 2, pp. 241–254, 2018.

[41] N. J. van Eck and L. Waltman, "Software survey: VOS viewer, a computer program for bibliometric mapping," *Scientometrics*, vol. 84, no. 2, pp. 523–538, 2010.

[42] J. Y. Park and Z. Nagy, "Comprehensive analysis of the relationship between thermal comfort and building control research—a data-driven literature review," *Renewable and Sustainable Energy Reviews*, vol. 82, pp. 2664–2679, 2018.

[43] X. Zhao, "A scientometric review of global BIM research: analysis and visualization," *Automation in Construction*, vol. 80, pp. 37–47, 2017.

[44] D. Vasmant, "Les pôles de compétitivité biomédicaux français: une opportunité pour la recherche partenariale public-privé en santé," *Bulletin de l'Académie Nationale de Médecine*, vol. 193, no. 9, pp. 2035–2044, 2009.

[45] J. Whyte and S. Lobo, "Coordination and control in project-based work: digital objects and infrastructures for delivery," *Construction Management and Economics*, vol. 28, no. 6, pp. 557–567, 2010.

[46] R. Jin, S. Gao, A. Cheshmehzangi, and E. Aboagye-Nimo, "A holistic review of off-site construction literature published between 2008 and 2018," *Journal of Cleaner Production*, vol. 202, pp. 1202–1219, 2018.

[47] H.-N. Su and P.-C. Lee, "Mapping knowledge structure by keyword co-occurrence: a first look at journal papers in technology foresight," *Scientometrics*, vol. 85, no. 1, pp. 65–79, 2010.

[48] N. J. van Eck and L. Waltman, "Visualizing bibliometric networks," in *Measuring Scholarly Impact*, Y. Ding, R. Rousseau, and D. Wolfram, Eds., pp. 285–320, Springer, Cham, Switerzland, 2014.

[49] Y. Ke, S. Wang, A. P. C. Chan, and P. T. I. Lam, "Preferred risk allocation in China's public-private partnership (PPP) projects," *International Journal of Project Management*, vol. 28, no. 5, pp. 482–492, 2010.

[50] A. P. C. Chan, P. T. I. Lam, D. W. M. Chan, E. Cheung, and Y. Ke, "Critical success factors for PPPs in infrastructure developments: Chinese perspective," *Journal of Construction Engineering and Management*, vol. 136, no. 5, pp. 484–494, 2010.

[51] J. Yuan, A. Y. Zeng, M. J. Skibniewski, and Q. Li, "Selection of performance objectives and key performance indicators in public-private partnership projects to achieve value for money," *Construction Management and Economics*, vol. 27, no. 3, pp. 253–270, 2009.

[52] Y. Xu, J. F. Y. Yeung, A. P. C. Chan, D. W. M. Chan, S. Q. Wang, and Y. Ke, "Developing a risk assessment model for PPP projects in China—a fuzzy synthetic evaluation approach," *Automation in Construction*, vol. 19, no. 7, pp. 929–943, 2010.

[53] X. H. Jin and H. Doloi, "Interpreting risk allocation mechanism in public-private partnership projects: an empirical study in a transaction cost economics perspective," *Construction Management and Economics*, vol. 26, no. 7, pp. 707–721, 2008.

[54] C. Jacobson and S. Ok Choi, "Success factors: public works and public-private partnerships," *International Journal of Public Sector Management*, vol. 21, no. 6, pp. 637–657, 2008.

[55] A. Roumboutsos and K. P. Anagnostopoulos, "Public-private partnership projects in Greece: risk ranking and preferred risk allocation," *Construction Management and Economics*, vol. 26, no. 7, pp. 751–763, 2008.

[56] Y. Xu, A. P. C. Chan, and J. F. Y. Yeung, "Developing a fuzzy risk allocation model for PPP projects in China," *Journal of Construction Engineering and Management*, vol. 136, no. 8, pp. 894–903, 2010.

[57] K. C. Iyer and M. Sagheer, "Hierarchical structuring of PPP risks using interpretative structural modeling," *Journal of Construction Engineering and Management*, vol. 136, no. 2, pp. 151–159, 2010.

[58] X.-H. Jin and G. Zhang, "Modelling optimal risk allocation in PPP projects using artificial neural networks," *International Journal of Project Management*, vol. 29, no. 5, pp. 591–603, 2011.

[59] B.-G. Hwang, X. Zhao, and M. J. S. Gay, "Public private partnership projects in Singapore: factors, critical risks and preferred risk allocation from the perspective of contractors," *International Journal of Project Management*, vol. 31, no. 3, pp. 424–433, 2013.

[60] P. Raisbeck, C. Duffield, and M. Xu, "Comparative performance of PPPs and traditional procurement in Australia," *Construction Management and Economics*, vol. 28, no. 4, pp. 345–359, 2010.

[61] R. Osei-Kyei and A. P. C. Chan, "Risk assessment in public-private partnership infrastructure projects," *Construction Innovation*, vol. 17, no. 2, pp. 204–223, 2017.

[62] S. Brthen and J. Odeck, "Road funding in Norway: experiences and perspectives," *International Journal of Sustainable Transportation*, vol. 3, no. 5-6, pp. 373–388, 2009.

[63] M. Sohail and O. Maslyukivska, "Learning from water sector reforms in Europe and Asia," *Proceedings of the Institution of Civil Engineers—Management, Procurement and Law*, vol. 162, no. 3, pp. 107–116, 2009.

[64] S. Tang and H. K. Lo, "Assessment of public private partnership models for mass rail transit-an influence diagram approach," *Public Transport*, vol. 2, no. 1-2, pp. 111–134, 2010.

[65] A. Mahalingam, G. A. Devkar, and S. N. Kalidindi, "A comparative analysis of public- private partnership (PPP) coordination agencies in India," *Public Works Management & Policy*, vol. 16, no. 4, pp. 341–372, 2011.

[66] O. H. Petersen, "Multi-level governance of public-private partnerships, an analysis of the Irish case," *Halduskultuur–Administrative Culture*, vol. 12, no. 2, pp. 162–188, 2011.

[67] P. Deshpande and S. Rokade, "Prioritization and assessment of critical risks of public private partnership highway projects in India using analytical hierarchical process," *International Journal of Civil Engineering and Technology*, vol. 8, no. 6, pp. 605–620, 2017.

[68] R. K. Yin, *Case Study Research: Design and Methods*, Sage, Los Angeles, CA, USA, 5th edition, 2014.

[69] J. Kivilä, M. Martinsuo, and L. Vuorinen, "Sustainable project management through project control in infrastructure projects," *International Journal of Project Management*, vol. 35, no. 6, pp. 1167–1183, 2017.

[70] N. Carbonara and R. Pellegrino, "Public-private partnerships for energy efficiency projects: a win-win model to choose the energy performance contracting structure," *Journal of Cleaner Production*, vol. 170, pp. 1064–1075, 2018.

[71] A. Roumboutsos, A. Suárez Alemán, and R. Ågren, "Construction firms in public-private partnerships: a place to grow," *Construction Management and Economics*, vol. 35, no. 10, pp. 627–640, 2017.

[72] A. Shrestha, A. A. Aibinu, T. K. Chan, and C. Chen, "Risk allocation in public private partnerships in China's water projects: a principal agent approach," in *Water Resources Management VII*, vol. 171, pp. 85–96, WIT Press, Southampton, UK, 2013.

[73] S. Zhang, A. P. C. Chan, Y. Feng, H. Duan, and Y. Ke, "Critical review on PPP research—a search from the Chinese and international journals," *International Journal of Project Management*, vol. 34, no. 4, pp. 597–612, 2016.

[74] T. Yang, R. Long, and W. Li, "Suggestion on tax policy for promoting the PPP projects of charging infrastructure in China," *Journal of Cleaner Production*, vol. 174, pp. 133–138, 2018.

[75] M. R. Guarini and F. Battisti, "A model to assess the feasibility of public-private partnership for social housing," *Buildings*, vol. 7, no. 2, p. 44, 2017.

[76] M. Opara and F. Elloumi, "The emergence of public-private partnerships (P3s) in Alberta: lessons from the Anthony Henday highway," *Canadian Public Administration*, vol. 60, no. 2, pp. 268–288, 2017.

[77] A. Shrestha, T. K. Chan, A. A. Aibinu, C. Chen, and I. Martek, "Risks in PPP water projects in China: perspective of local governments," *Journal of Construction Engineering and Management*, vol. 143, no. 7, Article ID 05017006, 2017.

[78] X. Y. Cai and G. G. Zhou, "The real option value analysis of income adjustment during operating period in the toll road public private partnership projects," *Journal of Transportation Systems Engineering and Information Technology*, vol. 17, no. 3, pp. 7–11, 2017.

[79] K. Curtain and J. Betts, "Busting some of the public private partnership myths from a government perspective," *Australian Journal of Public Administration*, vol. 76, no. 3, pp. 283–287, 2017.

[80] D. Danau and A. Vinella, "From fixed to state-dependent duration in public-private partnerships," *Journal of Economics & Management Strategy*, vol. 26, no. 3, pp. 636–660, 2017.

[81] Z. Chen, N. Daito, and J. L. Gifford, "Socioeconomic impacts of transportation public-private partnerships: a dynamic CGE assessment," *Transport Policy*, vol. 58, pp. 80–87, 2017.

[82] M. Regan, J. Smith, and P. E. D. Love, "Financing of public private partnerships: transactional evidence from Australian toll roads," *Case Studies on Transport Policy*, vol. 5, no. 2, pp. 267–278, 2017.

[83] S. K. Enloe, L. A. Schulte, and J. C. Tyndall, "Public-private partnerships working beyond scale challenges toward water quality improvements from private lands," *Environmental Management*, vol. 60, no. 4, pp. 574–587, 2017.

[84] M. Himmel and M. Siemiatycki, "Infrastructure public-private partnerships as drivers of innovation? Lessons from Ontario, Canada," *Environment and Planning C: Politics and Space*, vol. 35, no. 5, pp. 746–764, 2017.

[85] B. Guo, W. Yang, and H. Zhang, "Government compensation on rental indemnificatory housing in public private partnerships," *Boletin Tecnico/Technical Bulletin*, vol. 55, no. 9, pp. 476–485, 2017.

[86] Z. Muhammad and F. Johar, "A conceptual framework for evaluating the success of public-private partnership (PPP) projects," *Advanced Science Letters*, vol. 23, no. 9, pp. 9130–9134, 2017.

[87] E. I. Antillon, K. R. Molenaar, and A. Javernick-Will, "Evaluating the effect of contract timing on lifecycle-design innovation in public-private partnerships: comparative case study of highway projects," *Journal of Construction Engineering and Management*, vol. 143, no. 4, Article ID 05016023, 2017.

[88] H. Ç. Demirel, W. Leendertse, L. Volker, and M. Hertogh, "Flexibility in PPP contracts—dealing with potential change in the pre-contract phase of a construction project," *Construction Management and Economics*, vol. 35, no. 4, pp. 196–206, 2017.

[89] N. Agarchand and B. Laishram, "Sustainable infrastructure development challenges through PPP procurement process," *International Journal of Managing Projects in Business*, vol. 10, no. 3, pp. 642–662, 2017.

[90] E. Reeves and D. Palcic, "Getting back on track: the expanded use of PPPs in Ireland since the global financial crisis," *Policy Studies*, vol. 38, no. 4, pp. 339–355, 2017.

[91] B. Rakic, T. Milenkovic-Kerkovic, and T. Radjenovic, "Infrastructure development through public-private partnership," *Actual Problems of Economics*, vol. 152, no. 2, pp. 94–105, 2014.

[92] C. Mukhopadhyay, "A nested framework for transparency in public private partnerships: case studies in highway development projects in India," *Progress in Planning*, vol. 107, pp. 1–36, 2016.

[93] J. Cao and M. Yang, "The dynamic allocation strategy of profits from PPP projects," *Agro Food Industry Hi-Tech*, vol. 28, no. 1, pp. 3362–3365, 2017.

[94] S. S. Cutrim, J. A. M. Tristão, and V. T. V. Tristão, "Application of the Delphi method to identify and evaluate the factors restricting the realization of public-private partnerships (PPP)," *Revista Espacios*, vol. 38, no. 22, p. 29, 2017.

[95] E. Dmitrieva and M. Guseva, "Justification of approach to classification of innovations in public-private partnership," *Economic Annals-XXI*, vol. 163, no. 1-2, pp. 64–70, 2017.

[96] T. Tkacheva and L. Afanasjeva, "Public-private partnership as an encouragement tool of innovative development," *Istrazivanja I Projektovanja Za Privredu*, vol. 15, no. 3, pp. 242–246, 2017.

[97] M. H. Sobhiyah, M. R. Bemanian, and Y. K. Kashtiban, "Increasing VFM in PPP power station projects—case study: rudeshur gas turbine power station," *International Journal of Project Management*, vol. 27, no. 5, pp. 512–521, 2009.

[98] D. Juričić and S. Marenjak, "Value for money evidence in croatian PPP projects," *Ekonomski Pregled*, vol. 67, no. 6, pp. 581–604, 2016.

[99] P. T. Nguyen and V. Likhitruangsilp, "Identification risk factors affecting concession period length for public-private partnership infrastructure projects," *International Journal of Civil Engineering and Technology*, vol. 8, no. 6, pp. 342–348, 2017.

[100] S. K. Sundararajan and C. L. Tseng, "Managing project performance risks under uncertainty, using a dynamic capital structure approach in infrastructure project financing," *Journal of Construction Engineering and Management*, vol. 143, no. 8, article 04017046, 2017.

[101] X. Wu, R. Schuyler House, and R. Peri, "Public-private partnerships (PPPs) in water and sanitation in India: lessons from China," *Water Policy*, vol. 18, no. 1, pp. 153–176, 2016.

[102] G. Aerts, M. Dooms, and E. Haezendonck, "Knowledge transfers and project-based learning in large scale infrastructure development projects: an exploratory and comparative ex-post analysis," *International Journal of Project Management*, vol. 35, no. 3, pp. 224–240, 2017.

[103] S. Kyvelou, N. Marava, and G. Kokkoni, "Perspectives of local public-private partnerships towards urban sustainability in Greece," *International Journal of Sustainable Development*, vol. 14, no. 1-2, pp. 95–111, 2011.

[104] G. U. Atmo, C. Duffield, L. Zhang, and D. I. Wilson, "Comparative performance of PPPs and traditional procurement projects in Indonesia," *International Journal of Public Sector Management*, vol. 30, no. 2, pp. 118–136, 2017.

[105] S. V. Khusainova, F. A. Ruslanovna, and K. S. Damirovna, "Public-private partnership as the basis of interaction between the state and business," *International Business Management*, vol. 9, no. 5, pp. 909–916, 2015.

[106] L. V. Semenova, N. A. Zaitseva, A. A. Larionova, A. A. Gorbacheva, and E. V. Ivanova, "International experience of implementation projects of public-private partnership in tourism," *Man in India*, vol. 97, no. 14, pp. 317–327, 2017.

[107] K. Feng, W. Xiong, S. Wang, C. Wu, and Y. Xue, "Optimizing an equity capital structure model for public-private partnership projects involved with public funds," *Journal of Construction Engineering and Management*, vol. 143, no. 9, Article ID 04017067, 2017.

[108] L. Ma, Y. Le, H. Li, R. Jin, P. Piroozfar, and M. Liu, "Regional comparisons of contemporary construction industry sustainable concepts in the Chinese context," *Sustainability*, vol. 10, no. 11, p. 3831, 2018.

[109] P. E. D. Love, J. Liu, J. Matthews, C.-P. Sing, and J. Smith, "Future proofing PPPs: life-cycle performance measurement and building information modelling," *Automation in Construction*, vol. 56, pp. 26–35, 2015.

[110] G. Ren and H. Li, "BIM based value for money assessment in public-rivate partnership" in *Proceedings of the 18th IFIPWG 5.5 Working Conference on Virtual Enterprises, PRO-VE 2017,* H. Afsarmanesh, L. M. Camarinha-atos, and R. Fornasiero, Eds., vol. 56, pp. 51–62, Springer New York LLC, Vicenza, Italy, September 2017.

[111] R. Osei-Kyei and A. P. C. Chan, "Developing a project success index for public-private partnership projects in developing countries," *Journal of Infrastructure Systems*, vol. 23, no. 4, Article ID 04017028, 2017.

Hindawi
Advances in Civil Engineering
Volume 2019, Article ID 2818219, 8 pages
https://doi.org/10.1155/2019/2818219

Research Article

A Study on the Improvement of Structural Performance by Glass Fiber-Reinforced Polyurea (GFRPU) Reinforcement

Jun-Hyeok Song,[1] Eun-Taik Lee,[2] and Hee-Chang Eun [1]

[1]*Department of Architectural Engineering, Kangwon National University, Chuncheon, Republic of Korea*
[2]*Department of Architectural Engineering, Chung-Ang University, Seoul, Republic of Korea*

Correspondence should be addressed to Hee-Chang Eun; heechang@kangwon.ac.kr

Received 14 May 2019; Revised 14 July 2019; Accepted 18 July 2019; Published 19 August 2019

Guest Editor: Xiaodong Zhang

Polyurea has a high tensile strength, elongation, and the capability to absorb the energy generated by dynamic and impulsive blast loading. Glass fibers are a reinforcement material for repairing and retrofitting the concrete members. The polyurea provides ductility, and the fibers provide improved stiffness and strength to the composite system. Glass-fiber reinforced polyurea (GFRPU) is a composite of polyurea and fibers and is applied as a reinforcement through a simple spraying method. GFRPU coating has a simple construction, and unlike existing strengthening methods such as fiber-reinforced polymer (FRP) or a steel plate, it prevents a debonding from the concrete surface. Seven beams of one externally nonreinforced concrete beam and six concrete beams with and without a reinforcing bar are tested using the thickness of the spray and the number of coating faces. The applicability of GFRPU was investigated through the experiments, and the test results indicate that the GFRPU strengthening method is feasible for enhancing the load-carrying capacity and flexural ductility.

1. Introduction

The structural performance of a reinforced concrete structure can deteriorate owing to an unexpected change in the external load or environment during the service period. Aged and deteriorated members, such as those at the end of their service life or undergoing steel corrosion or concrete spalling, should be repaired to enhance their strength and durability. The structural performance needs to be recovered for continuous and safe occupancy. The building structures need to implement effective and economical repair and strengthening methods.

The structural performance can be recovered using retrofitting techniques corresponding to the increased loading requirements, change in use, and structural deterioration. Structural strengthening techniques contain a section enlargement, reinforced jacketing, externally bonded steel elements, or FRPs, among other factors.

Numerous studies have attempted to introduce repair and retrofitting methods, such as a steel plate or FRP reinforcement method, to enhance the deteriorated strength and ductility. Steel plates have been utilized in the strengthening of concrete beams owing to their economic and ductile characteristics. Barnes et al. [1] compared experimentally the plate attachment methods of adhesive bonding and bolting to external surfaces of concrete beams. Ying et al. [2] introduced a simplified anchoring system using a shear bolt-plate applied directly onto the reinforced concrete beams for strengthening with steel plates. Thamrin and Sari [3] conducted an experimental study on the flexural capacity of strengthened reinforced concrete beams using a web-bonded steel plate. They observed that web-bonded steel plates increase the stiffness of the beam and the flexural capacity and avoid a debonding of the steel plates. Aykac et al. [4] presented the experimental results related with the beam ductility and the anchorage of the plate to the beam. Ozbek et al. [5] identified an increase in strength by the bonding of steel plates to the beams and maintained the ductility despite the increase in strength.

FRPs have been effectively utilized in structural engineering as internal and external reinforcements. FRPs are

made up of high-tensile-strength fibers embedded in an epoxy matrix. An explicit bonding for a sufficient adhesive ability between the FRPs and concrete structures is required for transferring the stress along them. FRPs with a high tensile strength and low weight have failed through a concrete cover separation and interfacial debonding.

Gideon and Alagusundaramoorthy [6] studied the flexural behavior and failure mode of prototype reinforced concrete (RC) beams of a high shear span ratio externally bonded with CFRP laminates. Li et al. [7] found that the shear capacity of the strengthened beam varies strongly depending on the strengthened area. Alferjani et al. [8] observed that an epoxy resin is favored in terms of strengthening and an end anchorage is needed to eliminate the debonding failure. FRP-strengthened beams have resulted in enhanced ultimate load carrying and stiffness and exhibit failure modes of the debonding at the ends of the beams without end anchorages and a rupture of the FRP in the beams with an end anchorage [9–16].

One of the weaknesses of an FRP composite is a poor fire performance, leading to an interface debonding between the FRP composites and concrete substrates. There have been many attempts to investigate FRP debonding and intermediate crack bonding. Oehlers et al. [17] presented a single mechanism based on intermediate crack debonding mechanics for explaining the structural behavior of FRP RC beams. Yang et al. [18] proved the prevention of plate-end and midspan debonding using an epoxy adhesive to bond a prefabricated CFRP grid-reinforced engineered cementitious composite (ECC) plate.

An elastomer is a class of polymetric materials. Polyurea as an elastomer is an excellent water-proofing material with many mechanical characteristics, such as a high tensile strength, ductility, and high rate of expansion and contraction. It has the capability of flexural and shear reinforcement for structural members rather than blast or impact mitigation [19]. The reinforcing fibers can be utilized for obtaining more load-carrying capacity. The polyurea coating plays a role in improving the ductility and toughness, and fibers need to be added for more load-bearing capacity. Marawan et al. [20] observed an increase in the flexural and shear capacities of small- and large-scale beams strengthened using a sprayed polyurea system depending on the polyurea thickness. Parniani and Toutanji [19] investigated the behavior of concrete beams strengthened using a polyurea coating system. They found that the polyurea coating system increases the flexural capacity and ductility of RC beams. Tarigan et al. [21] compared the flexural strength of reinforced concrete beams using steel plates, CFRP, and GFRP. Gangarao and Vijay [15] compared the flexural strength of reinforced concrete beams strengthened with carbon fiber wraps and bonded steel plates.

Glass fiber is divided into two types of chopped and milled glass fibers. The milled glass fibers are created by cutting E-glass fibers into shorter pieces. E-glass fibers have an excellent electrical insulation property and can be processed into various shapes and are mainly applied in the reinforcement of plastics. This is effective in improving not only the strength but also the surface condition and dimensional stability. They are also used as a reinforcement and filler medium in a plastic composite, adhesives, and coatings used to enhance the mechanical properties, increase the modulus, improve the dimensional stability, and minimize the distortion under elevated temperatures. Chopped glass fibers are longer fibers used to increase the tensile and compressive properties of any resin and building materials including concrete.

GFRPU is a composite using a strengthened elastic polyurea material and milled glass fibers. The GFRPU coating systems can yield a multihazard retrofitted material suitable for aging structures and can be used in repair and retrofit applications for strengthening the structural capacity, improving the seismic performance and mitigating the blast and impact damage. Greene and Myers [22] investigated the flexural and shear reinforcement capabilities of the systems provided by externally applied discrete fiber-reinforced polyurea (DFRP) coating systems. A DFRP system is a composite system used to simultaneously spray the polyurea and chopped glass fibers into a spray pattern. They found measurable strengthening in both flexural and shear capacities and substantial gains in ductility. In addition, they mentioned that an increased fiber length significantly reduces the ductility. Carey and Myers [23] also considered the addition of discrete chopped fibers into the polyurea for greater strength and developed a fiber characterization of the polyurea system.

In the existing fiber-reinforced polymer sheet (FRPS) methods, the FRF and polyurea are separately constructed on the members. In this study, milled glass fibers are utilized as reinforcing fibers, and the strengthening is completed by simply spraying the GFRPU without the process to bond the fiber on the members. This study was planned for evaluating the strengthening effect of the GFRPU, and the validity was investigated in the concrete beam test. A GFRPU coating is applied by spraying the premixed polyurea and glass fibers. Seven beams, namely, one externally nonreinforced concrete beam and six concrete beams with and without a reinforcing bar, are tested based on the spraying thickness and number of spraying faces. The superiority and applicability of the GFRPU for strengthening concrete members are illustrated in the experiments, and the test results indicate that the GFRPU may enhance the load-carrying capacity and flexural ductility.

2. Experiment

2.1. GFRPU. GFRPU is a composite manufactured using the polyurea made of a prepolymer and a hardener and milled glass fibers with a length of 300 μm. After stirring the prepolymer and fibers and premixing the prepolymer and hardener, the GFRPU is pushed through a hose using a high-pressure spray gun. Table 1 shows the chemical constituents of the polyurea utilized in this experiment.

The GFRPU spraying proceeds as follows. First, the primer is painted onto the surface of the concrete member, as shown in Figure 1(a), after the laitance, foreign substances, and pollutants are removed to improve the bonding performance. After curing for 24 h, the prepolymer and milled glass fibers are mixed and stirred, as shown in

Table 1: Chemical constituents of polyurea.

	Chemicals	Content (%)
Prepolymer	α-(2-Aminomethylethyl)-ω-(2-aminomethylethoxy) poly[oxy(methyl-1,2-ethanediyl)]	60~70
	ar,ar-Diethyl-ar-methylbenzenediamine	20~30
	Poly[oxy(methyl-1,2-ethanediyl)], α, α', α''-1,2,3-propanetriyltris[ω-(2-aminomethyl-ethoxy)-	1~10
	Titanium dioxide	1~2.7
	1,4-Benzenedicarboxylic acid, bis (2-ethylhexyl) ester	1~10
	etc.	1~10
Hardener	Polyurethane resin	90~100
	4-Methyl-1,3-dioxolan-2-one	1~10

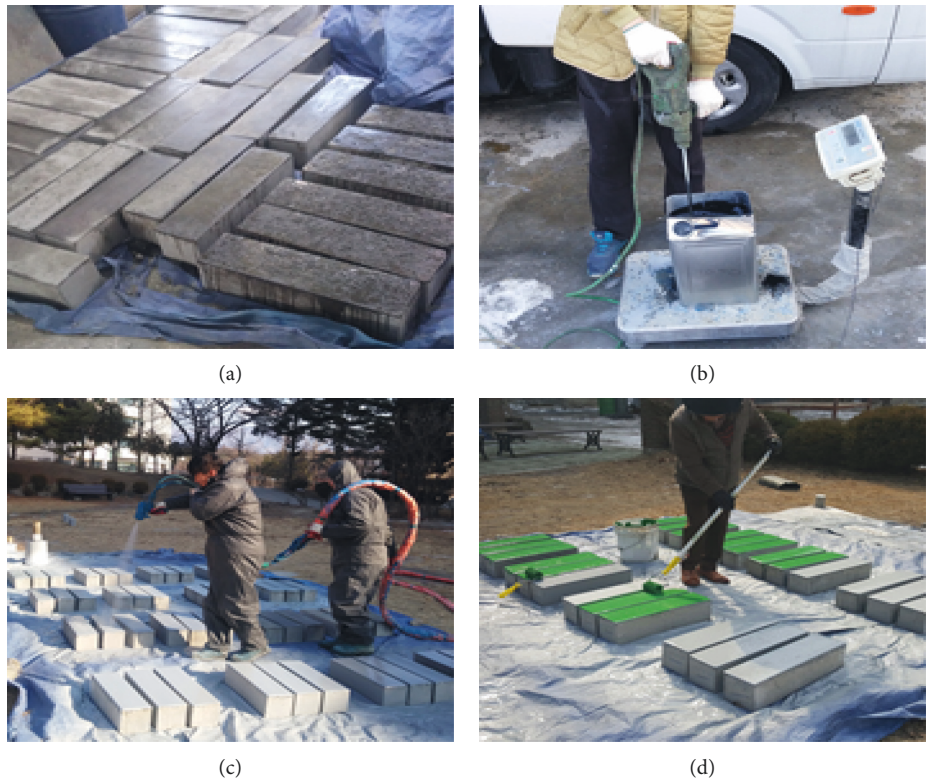

Figure 1: GFRPU coating operation of (a) primer painting; (b) mixing of prepolymer and fibers; (c) GFRPU spraying; (d) primer painting.

Figure 1(b), and the premixed prepolymer and glass fibers are sprayed out onto the member surface through the hose along with the hardener, as shown in Figure 1(c). After the GFRPU is sprayed, the coating is finished with a primer painting, as shown in Figure 1(d). The GFRPU coating is completely bonded to the member without an anchorage.

2.2. Specimens. Seven concrete beams, one without an external reinforcement as a control, three without reinforcing bars, and three fully reinforced concrete beams were prepared for testing. The six specimens other than the control beam were strengthened using polyurea or GFRPU. Previous experiments have indicated that the optimum weight ratio of milled glass fibers of 300 μm in length for enhancing the load-carrying capacity and flexural ductility is within the range of 5%–7%. The flexural ductility of the test beams is estimated based on the area under the load-deflection curve prior to failure. The test parameters include the coating thickness and number of spraying faces under a constant weight-to-content ratio of 5%. Coating thicknesses of 3 and 5 mm, and the spraying of one or three faces, as shown in Figure 2, are applied for testing. The specimens are classified using the sign shown in Figure 3. In the figure, the letters U and R denote the concrete beams without and with a reinforcing bar, respectively. The numbers 3 and 5 indicate the coating thickness, and P is the spraying using polyurea only. The last numbers 1 and 3 represent the number of faces sprayed.

The four-week compressive strength of concrete after concrete casting was shown to be 43.07 MPa. AD10 reinforcing bar with a yield strength of 493 MPa is utilized. The test beams are strengthened using polyurea or GFRPU applied three days in advance. The polyurea and GFRPU act

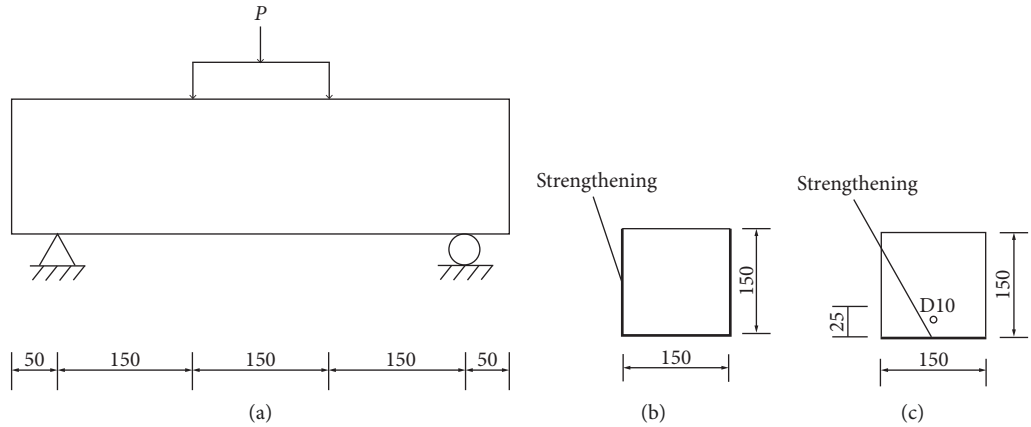

Figure 2: (a) Experiment of coated beam (unit: mm) of specimen under two-point loading, (b) strengthening at three faces without reinforcing bar, and (c) strengthening at a single face with reinforcing bar.

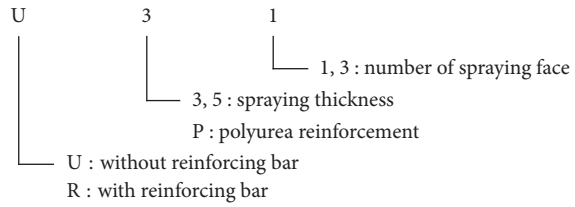

Figure 3: Specimen sign.

as a lateral reinforcement and lead to an enhanced strength and ductility.

2.3. Experimental Results. Steel forms of 150 mm × 150 mm × 550 mm for testing the flexural strength of concrete were prepared, the concrete was casted into the required forms, and the concrete was cured after demolding during three days. The loading of the specimen was applied at two points, as shown in Figure 4, and pure bending occurred in the midspan region. Based on the experiment results, the mechanical performance such as the load-carrying capacity and flexural ductility of test beams was compared.

The initial crack began at the bottom face of the midspan section because of the low tensile strength of the concrete. The failure modes of the U-series specimens are shown in Figure 5. The U-series specimens strengthened by polyurea or GFRPU exhibit an abrupt reduction in the load-resisting capacity during the moment of occurrence of the initial cracking. Diagonal-tension cracking cannot be observed, and the concrete beams retain sufficient shear-resisting capacity. The load after the initial cracking gradually increases, and it is carried by the polyurea or GFRPU on the tension side without the development of diagonal cracks. The specimens with a three-faced reinforcement retain more load-carrying capacity than those of a one-face reinforcement owing to a confinement through the reinforcement.

The GFRPU exhibits a similar mechanical behavior as the tensile reinforcing bar. The increase in tension-resisting region and capacity leads to an enhanced peak load-carrying capacity. The specimens reaching the second peak load carry the tension force through the polyurea or GFRPU. The

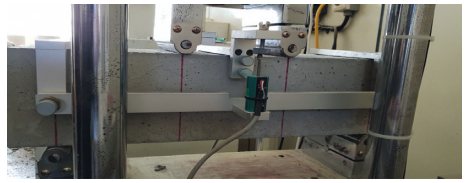

Figure 4: Setting of the specimen in UTM.

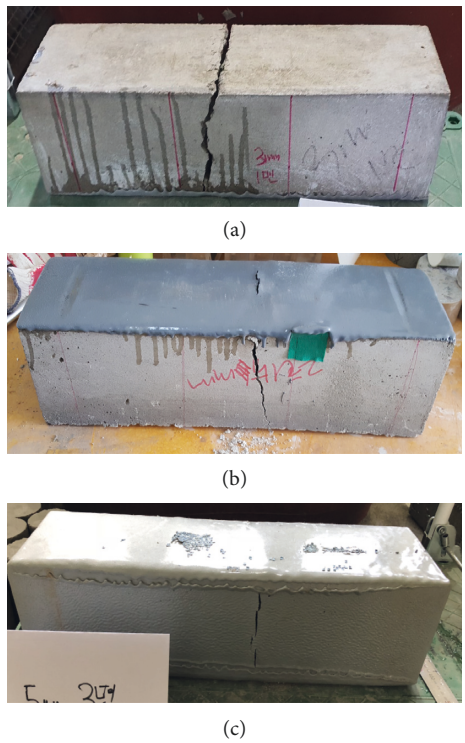

(a)

(b)

(c)

Figure 5: Failure modes of U-series specimens of (a) U31, (b) U51, and (c) U53.

development of diagonal cracks can rarely be observed by the naked eye. The additional cracks and their widths are gradually propagated within the neighborhood of the midspan region with an increase in load. The polyurea or

GFRPU controls the development without peeling from the concrete surface. Eventually, the strengthened specimens exhibit flexural failure modes.

The R-series specimens also represent a similar mechanical behavior as the U-series. The specimens ultimately fail through a flexure because they retain a sufficient concrete-carrying shear strength. The R51 specimen shown in Figure 6(c) exhibits a failure mode by the diagonal-tension cracking through the additional loading after testing.

Tables 2 and 3 summarize the experiment results. The flexural ductility is estimated by the area under the load-deflection curve prior to failure. In addition, the ratio is calculated by dividing the ductility of the coated beams through the ductility of the control beams U31 and RP of the U- and R-series specimens, respectively. The peak load-carrying capacity ratio is determined as the peak load-carrying capacity of the strengthened concrete beams with respect to the control beams. After the occurrence of cracks, the beam exhibits an additional load and sufficient ductility and reaches the second peak load-resistance capacity. The concrete beam without any reinforcement abruptly fails at the bisection at the peak load of 29.17 kN corresponding to the flexural tension strength of 3.89 MPa. It was demonstrated that the flexural tension strength of the U-series specimens from the GFRPU reinforcement is enhanced 1.45–1.47 times as much as the unreinforced concrete beam. It was observed that the load-carrying capacity is more sensitive to the number of coating faces than the coating thickness. The load-carrying capacity and flexural ductility must be improved through a lateral confinement of the beams such as lateral reinforcing bars. This concept can be expanded to a seismic-reinforced design because of the enhanced load-carrying capacity as well as the improved flexural ductility.

The R-series specimens exhibit a flexural failure mode by flexural cracks in the pure bending region. The flexural strength of the GFRPU-reinforced concrete beams corresponds to 1.19-and 1.25-times that of the control beam without the GFRPU reinforcement. The increase in flexural strength among the RP, R33, and R51 specimens shown in Table 3 corresponds to the flexural strengthening effect. The shear failure mode of the specimens can rarely be observed. In addition, the specimens resist the shear force by the concrete and GFRPU. The concrete-carrying shear strength is specified by $1/6\sqrt{f'_c}b\ d$ in the Korean structural design code, which is calculated as 42.6 kN. Thus, it can be predicted that the GFRPU carries at least a shear strength of 34.57 and 31.05 kN at specimens R33 and R51, respectively, under the premise of a flexural failure.

The analytical flexural capacity of the GFRPU-reinforced beam shown in Table 3 is derived as follows. Considering the flexural strength of the beam reinforced using a tensile reinforcing bar and GFRPU in Figure 7 and neglecting the tensile strength of concrete, the following equilibrium requirement should be satisfied:

$$C = T_s + T_p, \tag{1a}$$

$$0.85 f'_c ab = A_s f_y + A_p f_p. \tag{1b}$$

(a)

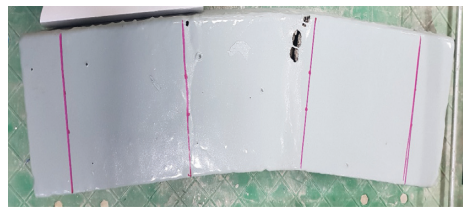

(b)

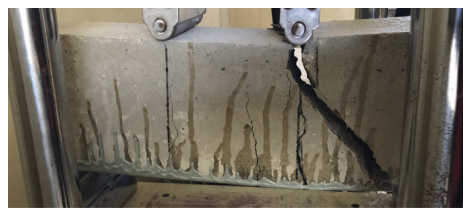

(c)

Figure 6: Failure modes of R-series specimens of (a) RP, (b) R33, and (c) R51.

The area of the GFRPU in tension is calculated using

$$A_p = 2(h - c)t_p + bt_p. \tag{2}$$

Substituting equation (2) into equation (1b) and using $a = \beta_1 c$, c can be calculated. Here, β_1 denotes the ratio between the height of the equivalent rectangular concrete compression stress block and neutral depth. The centroid of the GFRPU-carrying tensile force is calculated using

$$d_p = \frac{(h - c)^2 t_p + (b/2)t_p^2}{A_p}, \tag{3}$$

where d_p is the distance from the tension face to the centroid of the coating cross-section below the neutral axis (mm).

Taking the moment at the centroid of the reinforcing bar, the nominal flexural strength can be derived by

$$M_n = 0.85 f'_c ab\left(d - \frac{a}{2}\right) - A_p f_p\left(d_p - s\right), \tag{4}$$

where s is the distance from the centroid of the reinforcing bar to the extreme tension fiber (mm) and d is the distance from extreme compression fiber to the centroid of the reinforcing bar (mm).

If the mechanical properties of the GFRPU are given, the nominal flexural strength of the specimens can be calculated, as listed in Table 3. It can be seen that the analytical flexural strength properly predicts the actual experiment results.

Figure 8(a) shows the load-deflection curves of the U-series specimens. The load-resistance capacity is abruptly reduced at the same time as the occurrence of concrete cracks on the tension face despite the GFRPU reinforcement.

Table 2: Summary of test results (without reinforcing bar).

Specimen	Load-carrying capacity		Flexural tensile strength ratio	Flexural ductility	
	Peak (kN)	Ratio		Ductility (kN · mm)	Ratio
U	29.17	—	1		
U31	43.01	1	1.47	248.7	1
U51	42.37	0.99	1.45	249.35	1.00
U53	45.94	1.07	1.57	474.37	1.91

Table 3: Summary of test results (with reinforcing bar).

Specimen	Load-carrying capacity (exp.)		Load-carrying capacity (anal.)		Flexural ductility	
	Peak (kN)	Ratio	Peak (kN)	Anal./exp.	Ductility (kN · mm)	Ratio
RP	61.65	1	69.8	1.13	298.2	1
R33	77.17	1.25	80.8	1.05	1,085.7	3.64
R51	73.65	1.19	76.6	1.04	999.6	3.35

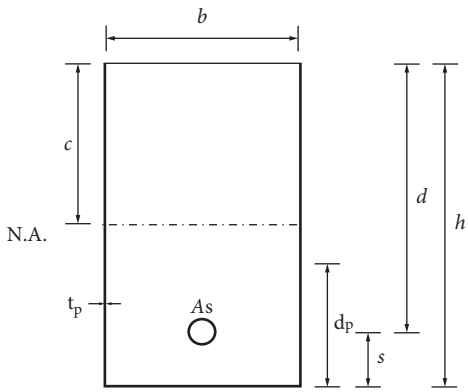

Figure 7: GFRPU-reinforced concrete beam.

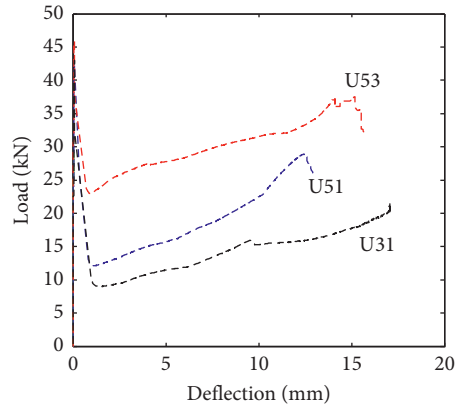

(a)

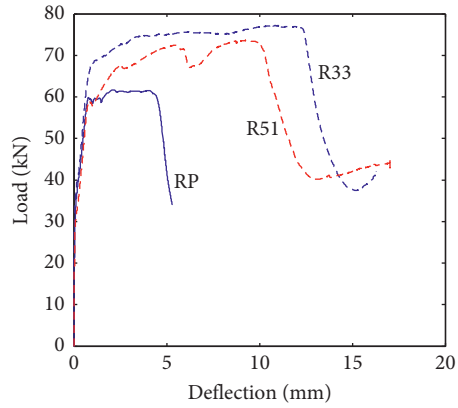

(b)

Figure 8: Load-deflection curves of (a) U-series and (b) R-series.

The deteriorated load at the moment a concrete crack occurs is carried by the GFRPU, and its resistance capacity is enhanced when the spraying thickness and the number of coating faces are increased. After this stage, the load-carrying capacity and the flexural ductility are retained to a certain degree and the specimens ultimately fail through a flexure. It can be observed that the load-carrying capacity is sensitive to the coating thickness and the number of spraying faces because they are related to the flexural tension force.

Figure 8(b) shows the load-deflection curves of the R-series specimens. It can be observed that the strengthening by the GFRPU leads to an enhanced load-carrying capacity as well as an improved flexural ductility. In addition, they are more sensitive to the number of coating faces than the coating thickness in that the side-reinforcement of the beam section provides a greater flexure-resisting capacity.

Figure 9 shows the peak load and ductility ratios according to the specimen. It can be seen that the peak load and flexural ductility of specimen U31 are 7% and 90% higher than those of specimen U53, respectively. In addition, the peak load of specimens R33 and D51 is 25% and 19% higher than that of specimen RP, respectively. Their ductility is 3.64 and 3.35 times as much as that of specimen RP. It can be seen that the GFRPU is effective in strengthening the flexural strength and improving the ductility and can also be utilized in strengthening the shear strength.

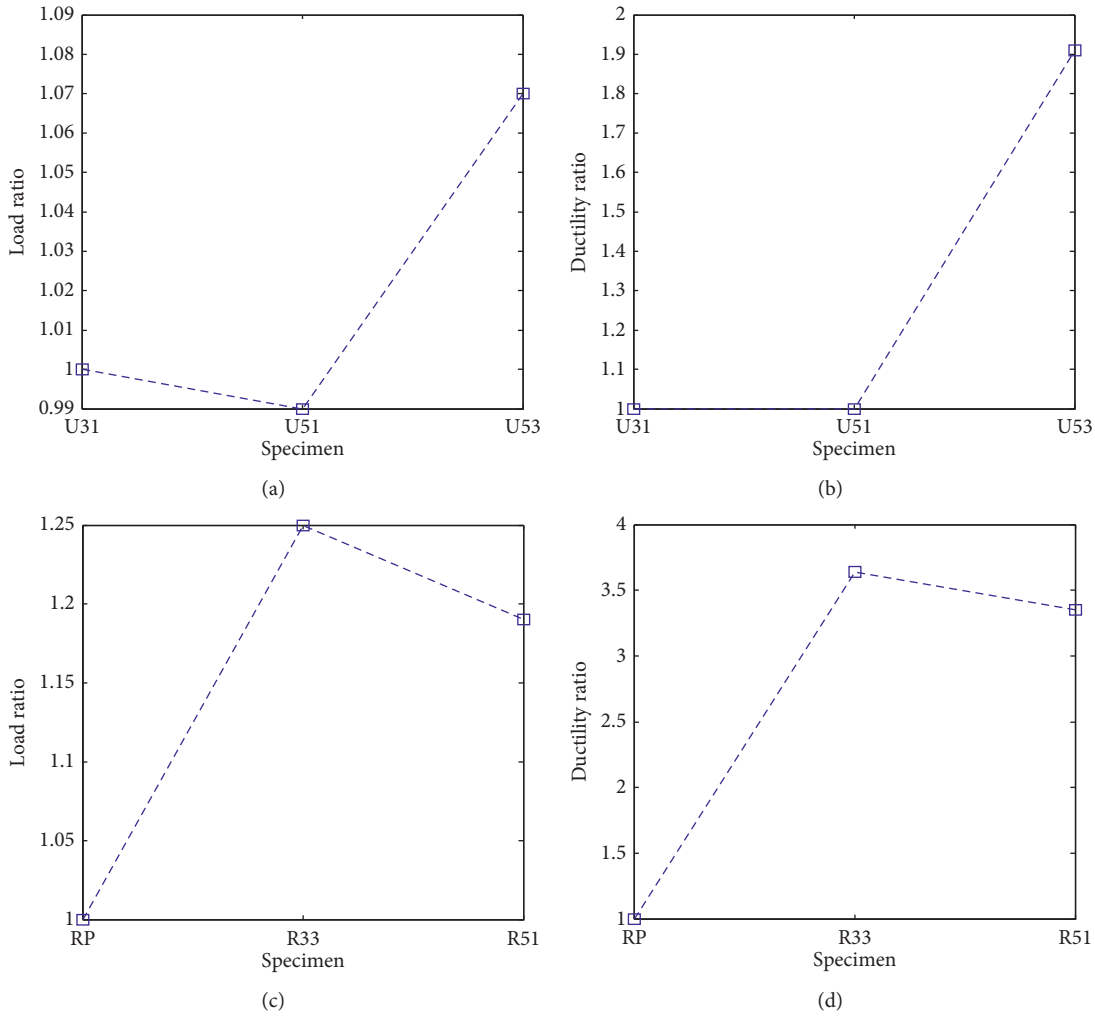

Figure 9: Peak load ratio of (a) U-series and (c) R-series; ductility ratio of (b) U-series and (d) R-series.

3. Conclusions

The structural performance of the GFRPU composite of polyurea and glass fibers was evaluated in this study. The GFRPU reinforcement can prevent an abrupt concrete spalling and failure by debonding. In addition, it is simply completed through a spraying method. The GFRPU reinforcement leads to an enhanced load-carrying capacity as well as an improved flexural ductility. Assuming the use of GFRPU as a tensile reinforcing bar, the analyzed flexural strength can properly predict the strength found experimentally. The experimental results on the flexural strength are more sensitive to the number of spraying faces than the spraying thickness because the side-reinforcement provides a greater flexure-resisting capacity. In addition, it has been estimated from the analytical results that the GFRPU reinforcement retains the shear-resistance capacity.

Data Availability

The data used to support the findings of this study are available from the corresponding author upon request.

Conflicts of Interest

The authors declare that there are no conflicts of interest regarding the publication of this paper.

Acknowledgments

This study was supported by the 2018 Research Grant (PoINT) from Kangwon National University.

References

[1] R. A. Barnes, P. S. Baglin, G. C. Mays, and N. K. Subedi, "External steel plate systems for the shear strengthening of reinforced concrete beams," *Engineering Structures*, vol. 23, no. 9, pp. 1162–1176, 2001.

[2] H. Ying, P. Huawei, Q. Xueyou et al., "Performance of reinforced concrete beams retrofitted by a direct-shear anchorage retrofitting system," *Procedia Engineering*, vol. 210, pp. 132–140, 2017.

[3] R. Thamrin and R. P. Sari, "Flexural capacity of strengthened reinforced concrete beams with web bonded steel plates," *Procedia Engineering*, vol. 171, pp. 1129–1136, 2017.

[4] S. Aykac, I. Kalkan, B. Aykac, S. Karahan, and S. Kayar, "Strengthening and repair of reinforced concrete beams using external steel plates," *Journal of Structural Engineering*, vol. 139, no. 6, pp. 929–939, 2013.

[5] E. Ozbek, M. Bocek, and S. Aycak, "Strengthening of RC beams with solid steel plates," *Athens Journal of Technology & Engineering*, vol. 3, no. 4, pp. 291–298, 2016.

[6] D. S. A. Gideon and P. Alagusundaramoorthy, "Flexural retrofit of RC beams using CFRP laminates," *Materials Science and Engineering*, vol. 431, no. 7, article 072006, 2018.

[7] A. Li, C. Diagana, and Y. Delmas, "Shear strengthening effect by bonded composite fabrics on RC beams," *Composites Part B: Engineering*, vol. 33, no. 3, pp. 225–239, 2002.

[8] M. B. S. Alferjani, A. A. B. A. Samad, B. S. Elrawaff, N. B. Mohamad, and M. H. B. Ahmad, "Shear strengthening of reinforced concrete beams using carbon fiber reinforced polymer laminate: a review," *American Journal of Civil Engineering*, vol. 2, no. 1, pp. 1–7, 2014.

[9] T. B. Carlos, J. P. C. Rodrigues, R. C. A. de Lima, and D. Dhima, "Experimental analysis on flexural behaviour of RC beams strengthened with CFRP laminates and under fire conditions," *Composite Structures*, vol. 189, no. 1, pp. 516–528, 2018.

[10] S. F. Brena, R. M. Bramblett, S. L. Wood, and M. E. Kreger, "Increasing flexural capacity of reinforced concrete beams using carbon fiber-reinforced polymer composites," *ACI Structural Journal*, vol. 100, no. 1, pp. 36–46, 2003.

[11] S. F. Brena and B. M. Macri, "Effect of carbon-fiber-reinforced polymer laminate configuration on the behavior of strengthened reinforced concrete beams," *Journal of Composites for Construction*, vol. 8, no. 3, pp. 1090–0268, 2004.

[12] P. J. Fanning and O. Kelly, "Ultimate response of RC beams strengthened with CFRP plates," *Journal of Composites for Construction*, vol. 5, no. 2, pp. 1090–0268, 2001.

[13] P. Alagusundaramoothy, I. E. Harik, and C. C. Choo, "Flexural behavior of R/C beams strengthened with carbon fiber reinforced polymer sheets or fabric," *Journal of Composites for Construction*, vol. 7, no. 4, pp. 292–301, 2003.

[14] F. Ceroni, "Experimental performances of RC beams strengthened with FRP materials," *Construction and Building Materials*, vol. 24, no. 9, pp. 1547–1559, 2010.

[15] H. V. S. Gangarao and P. V. Vijay, "Bending behavior of concrete beams wrapped with carbon fabric," *Journal of Structural Engineering*, vol. 124, no. 1, pp. 0733–9445, 1998.

[16] G. Spadea, F. Bencardino, and R. N. Swamy, "Structural behavior of composite RC beams with externally bonded CFRP," *Journal of Composites for Construction*, vol. 2, no. 3, pp. 1090–0268, 1998.

[17] D. J. Oehlers, M. S. Mohame Ali, M. Haskett, W. Lucas, R. Muhamad, and P. Visintin, "FRP-reinforced concrete beams: unified approach based on IC theory," *Journal of Composites for Construction*, vol. 15, no. 3, pp. 293–303, 2010.

[18] X. Yang, W.-Y. Gao, J.-G. Dai, Z.-D. Lu, and K.-Q. Yu, "Flexural strengthening of RC beams with CFRP grid-reinforced ECC matrix," *Composite Structures*, vol. 189, pp. 9–26, 2018.

[19] S. Parniani and H. Toutanji, "Monotonic and fatigue performance of RC beams strengthened with a polyurea coating system," *Construction and Building Materials*, vol. 101, no. 1, pp. 22–29, 2015.

[20] A. E. Marawan, A. S. Debaiky, and N. N. Khalil, "Shear and flexural behavior of R.C. beams strengthened with polyurea spray," *International Journal of Advance Research in Science and Engineering*, vol. 4, no. 11, pp. 12–26, 2015.

[21] J. Tarigan, F. M. Patra, and T. Sitorus, "Flexural strength using steel plate, carbon fiber reinforced polymer (CFRP) and glass fiber reinforced polymer (GFRP) on reinforced concrete beam in building technology," *Earth and Environmental Science*, vol. 126, no. 1, article 012025, 2018.

[22] C. Greene and J. J. Myers, *Flexural and Shear Reinforcement of Reinforced Concrete Beams Using Fiber Reinforced Polyurea Coatings*, Missouri University of Science and Technology, Rolla, MO, USA, 2012, https://www.northeastern.edu/alert/assets/HSD_p1.pdf.

[23] N. L. Carey and J. J. Myers, "Elastomeric systems with discrete fiber for infrastructure repair and rehabilitation," in *Proceedings of the Structural Faults and Repair*, Edinburgh, UK, 2010.

Hindawi
Advances in Civil Engineering
Volume 2019, Article ID 3240812, 10 pages
https://doi.org/10.1155/2019/3240812

Research Article

A Novel Experiment to Study the Roll Motion Characteristics of a Sailing Ship in a Landslide-Generated Wave in the Three Gorges Reservoir

Peiyin Yuan,[1,2] **Pingyi Wang**,[1] **and Yu Zhao**[1,3]

[1]*College of River and Ocean Engineering, Chongqing Jiaotong University, Chongqing 400074, China*
[2]*College of Shipping and Naval Architecture, Chongqing Jiaotong University, Chongqing 400074, China*
[3]*College of Architecture and Urban Planning, Chongqing Jiaotong University, Chongqing 400074, China*

Correspondence should be addressed to Peiyin Yuan; yuan_pei_yin@163.com

Received 24 April 2019; Revised 15 May 2019; Accepted 21 May 2019; Published 2 July 2019

Guest Editor: Endong Wang

Strong earthquakes, heavy rains, changes in reservoir water levels, and other external factors destabilize large rock masses causing them to fall into the water at high speed, thereby destroying the original ecological balance in the region. These occurrences cause fluctuations in water levels and form landslide-induced waves, which behave similar to tsunamis upon reaching the shore, a dam structure, or ships. The impact invariably threatens residents' lives and properties in the upper and lower reaches of the reservoir area. In the current study, we conducted orthogonal experiments of landslide-induced impulse waves to assess their related hazards. To explore the effects of a landslide-generated wave on the roll characteristics of a ship, experimental model tests were performed using different speed vessels, landslide bodies, and navigation positions. Accordingly, a reasonable optimization strategy was proposed to provide technical support for ship navigation safety in regions of landslide-generated waves.

1. Introduction

External factors such as earthquakes, heavy rain, and changes in reservoir water levels can cause rapid and violent sliding of slope rock and soil masses [1]. Numerous landslide bodies interact with water to excite waves, which have an inestimable direct impact on rivers, lakes, and passing vessels (i.e., ship)—even when a ship is suspended or prohibited from navigation. Other effects include damage to hydraulic structures in the reservoir, causing dams to burst; destruction of downstream farmland, houses, railways, and roads; and threatening the safety of life and property of urban residents [2, 3].

Recent research efforts investigating landslide-generated waves have been productive. The formation, propagation, and run-up of landslide-generated waves have been studied through simple physical experiments [1, 4–6], analytical formulae [7, 8], scale-model physical experiments [9–11], and numerical simulations [12–16]. Furthermore, wave types, water body geometry effects, block model parameters, and wave kinematics have been systematically studied by Heller and others [17–21].

Extensive research has been conducted on the behavior of ships using theoretical analysis [22–26], the method of simulation [27–30], the strip theory [31], the novel technique [32], physical experiments [33, 34], and comparative analysis of numerical and experimental results [35].

Based on the literature review, little work has been reported on the motion characteristics of sailing ships in relation to impulse waves. The current study is based on the Three Gorges Reservoir region. We focused on the interaction between the landslide-generated wave and ship, investigated the propagation characteristics of the landslide-generated wave, and explored the effect of a landslide impulse wave on the roll characteristics of a ship, which can provide reasonable speed and position references for navigation of ships with the results of a model test.

2. Model Experiment Design

Before the test, all rock-soil was placed above water. The defining characteristic of a landslide into water was the rock-soil mass being completely submerged after deposition during the test, which was accounted for during our experimental design. Experimental landslide blocks were made of concrete, with 2300–2400 kg/m^3 density, similar to that of a rock-soil mass. The ratio of these dimensional geometric parameters was determined based on the geometric parameter ratio of landslides in the Three Gorges Reservoir. The limiting criteria for scale models of impulse waves generated by subaerial landslides including solid, air, and water are discussed based on the literature review and detailed two-dimensional experimentation. Scale effects were primarily attributed to impact crater formation, in addition to air entrainment and detrainment. The reasonable Froude similitude was conducted, including intermediate-water wave spectrum, before the experiment was performed.

Five experiments were performed for each group: the first experiment was to determine the initial impulse wave's position and to affix the wave gauges, the second experiment was to determine the position of the container ship and to improve measurement accuracy, and the others were to acquire the initial wave's height and the ship's motion values regarding the roll and pitch. Subsequently, average data values were calculated and were considered to be the group's experimental result values.

2.1. Sliding Body Experiment Design. In the model test, the landslide rock was generalized into a rectangular parallelepiped shape, with a 1 m set length. This was combined with aspect ratio statistics of the landslide body in the reservoir area by controlling sliding body volume using different aspect ratios. This allowed us to investigate different impulse wave characteristics produced by the same volume at varying sliding body aspect ratios. The sliding blocks were generated according to the actual landslide situation, composed of different granular sizes (Figure 1). A net was placed above the slope in the model test process to ensure that the landslides reach the specified angle and prevent landslides sliding prior to the model test. Net properties were adjusted to keep the friction angle at 40 degrees.

2.2. Slip Angle Design. According to numerous statistics on the sliding surface gradient of landslides in a reservoir area, the landslide sliding surface slope was distributed between 20° and 60°, with an average of 40°. At the same time, considering the test's operability factor and energy conversion efficiency, a 40° inclination angle was chosen for the sliding surface during this test. Water-level collectors were used to detect water-level changes in the channel river. Seven water-level collectors were placed at designated spots. Pressure sensors were installed on water-level collectors, and pressure values were captured and converted into water-level values.

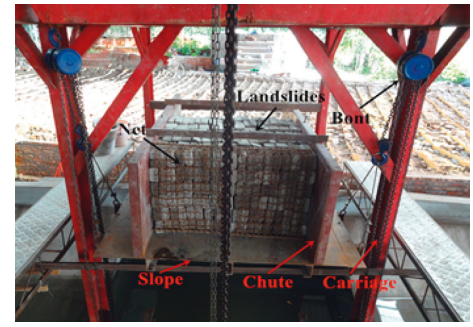

Figure 1: Arrangement of sliding blocks.

2.3. River Channel Model Design. The reservoir's geometry scale was 1 : 70. During the Three Gorges Reservoir operation, three water levels of 145, 155, and 175 m were mainly present. Considering the reservoir's actual water level and the river's water depth, according to the geometric scale model, water depths were 0.74, 0.88, and 1.16 m. In this paper, a 0.74 m water depth was selected as the research subject. The river model width was 8 m, and the ship's navigation position distance was 0.5 m from the navigation center line. The distance between monitoring points 1 and 3 was 8.94 m from the landslide entry point, and the landslide point distance was 3.3 m. Monitoring point 1 was located at the straight end of the river, monitoring point 2 at the landslide section, and monitoring point 3 at the bend of the river. Figure 2 shows the river channel model layout, and Figure 3 shows the river channel model.

2.4. Ship Model Design. The ship model—designed to the scale of 1 : 70—was based on the Froude similarity [6]. The 3500 T container ship was selected as the model type for this study. During the model test, (1) the ship's drive was controlled by a servo motor; (2) its speed was accurately controlled at 0.3, 0.5, and 0.7 m/s; (3) the ship was fully loaded; (4) its draught was controlled by adding various types of weights; and (5) the ship's motion amplitude and roll acceleration were independently designed and developed. Parameters of the ship model are listed in Table 1. Disk ratio is the ratio of the average height to the critical length of a rudder.

Figure 4 shows photographs of the ship's plan and experimental models.

3. Experimental Verification

3.1. Experimental Verification of Landslide-Generated Wave. In order to verify the correctness of the model test, the experimental model was similar to Heinrich's model [36]—known in the field for its high accuracy and representativeness—with the same model test parameters. The landslide body size was 0.5 m × 0.5 m. Slope angle was 45 degrees, water depth was 0.4 m, and the landslide body slid under gravity. Our experimental results concurred with Heinrich's results, as shown in Figure 5. Our experimental results have increasing phase at the beginning while Heinrich's do not. This is due to two main reasons. One reason is that landslide

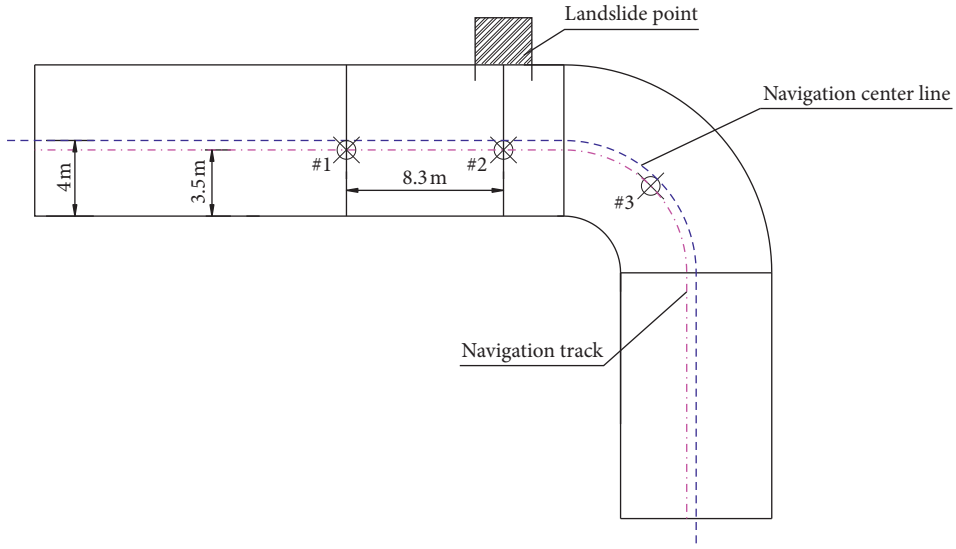

Figure 2: Layout of the river channel model.

Figure 3: River channel model.

Table 1: Primary parameters of the ship.

Parameter	Real ship	Ship model
Length (m)	94.5	1.350
Beam (m)	15.1	0.216
Moulded depth (m)	9.0	0.129
Draught (m)	5.6	0.08
C_b	0.7	0.7
C_p	0.69	0.69
Displacement (t/g)	3500 t	10,150 g
Area of rudder (m^2/cm^2)	14.3	2.9
Rudder height (m/cm)	4.1	5.9
Aspect ratio of the propeller	1.72	1.72
Number of blades, Z	4	4
Propeller diameter (m/cm)	3.1	4.4
Screw pitch (m/cm)	2.6	3.7
Disk ratio of rudder	0.67	0.67

body slides into the channel, the wave peak of the landslide-generated wave is steep, and it has a large amount of splashing liquid; hence, it is hard to monitor the water level. The other reason is that the number of water-level collectors is closely arranged, which can accurately monitor the change in the water level. These data show that the experimental model can be accurately applied to the case of landslide-generated waves.

3.2. Free Attenuation Test. Roll decay tests in calm water were performed, which mainly verified the ship's loading conditions. Damping present in a ship's roll motion is assessed via a free decay experiment. In the absence of waves, the ship is given initial roll amplitude and then released. By processing the resulting decaying oscillatory trace, it is possible to estimate quantitatively the degree of damping, even when this is nonlinear. The ship's freedom degree in the vertical plane exhibits the recovery characteristic. The ship model deviates from the position of equilibrium under external loading. When the external force disappears, the ship returns to its original position, depending on its own recovery characteristic. In a free roll decay test, the model is heeled in calm water to an initial heel angle and released. The model starts to perform free decaying oscillations at a frequency depending on the amplitude. Subsequently, the accuracy of the model test can be verified. The roll motion's decay curve is shown in Figure 6. The test results demonstrate that the ship's decay meets loading condition requirements, and the experimental data were used to tune the ship's hydrodynamic inertia properties, the natural roll period, the roll damping, and the inertia.

4. Study of Landslide-Generated Wave Propagation Characteristics

Experimental observation of the landslide-generated wave during the initial wave formation revealed that the landslide body interacts nonlinearly with the water body—the landslide body completely enters the water and the water surface rises rapidly. Once the energy is fully exchanged, two types of waves are generated: the oscillating wave, which is the reciprocating movement of the induced water quality point around its original position, and the passing wave, which

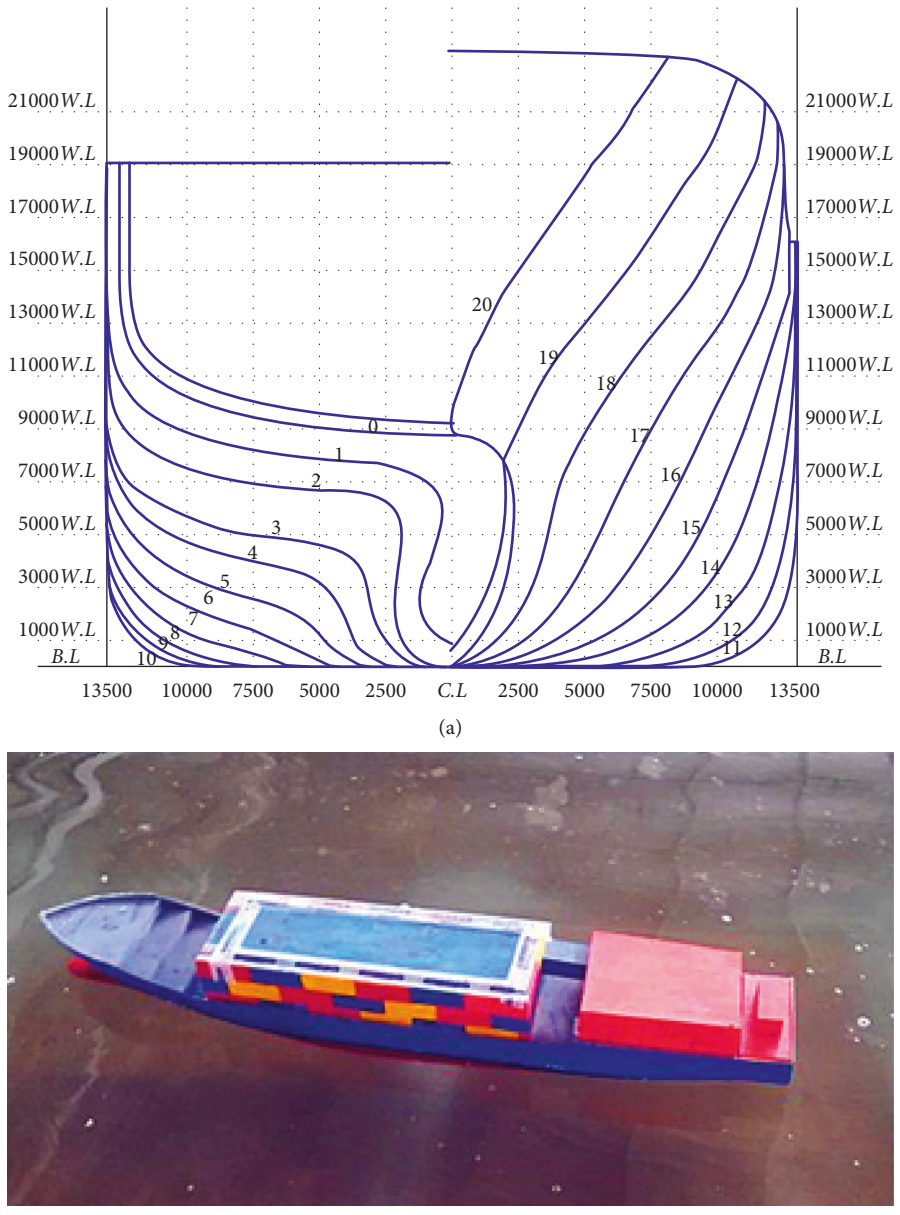

Figure 4: (a) Plan of the ship model; (b) experimental model.

originates from the forward movement of the landslide body, causing the water quality point to move forward and generate a ridge height and hence spreading the water particles in different directions.

4.1. Landslide-Generated Wave Condition Design for Rock Mass. There were 45 cases in the physical model test. The volume of the landslide, navigational position of the ship, and speed of the ship were single-factor variables. The specific working conditions are listed in Table 2.

4.2. Study on the Height of the Landslide's First Wave. Impulse waves are formed by a rapid or impulsive transfer of momentum from a mass flow to a water body. The wave generator is the landslide, which may be considered as a moving object disturbing the water. Not all landslide energy is transferred onto the water body. In the experiments, frictional losses are due to the bed friction between the landslide and the slope. Therefore, part of the landslide energy is taken out of the system or lost in the slide's internal deformation. Water displacement resulting in an uplift or hump at the free surface forms the potential energy.

In this work, we studied different height trends of the first wave generated by the landslide caused by the same volume at different width-thickness ratios. The first wave height-monitoring point of the landslide body was located at 1.5 m from the water inlet point of the landslide body. Flow separation on the rockslide shoulder, due to fast slide

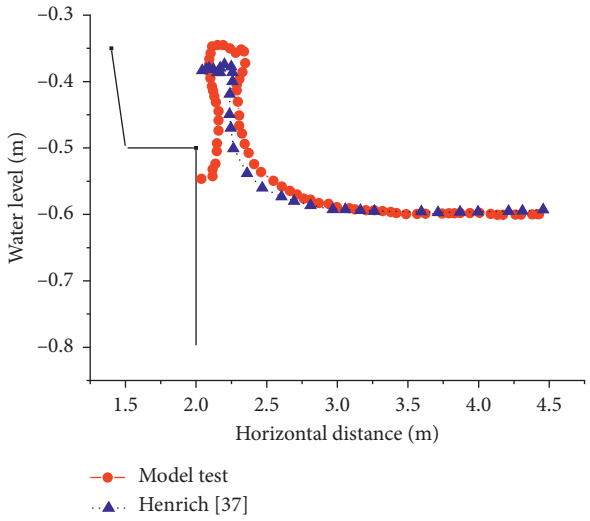

Figure 5: Comparison between Heinrich's [36] and the experimental free surface at 0.6 s.

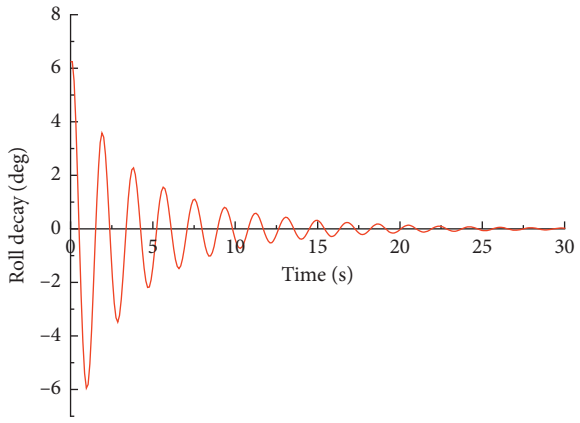

Figure 6: Roll motion decay curve.

Table 2: Table of cases.

Case	Entry angle (°)	Depth (m)	Speed (m/s)	Location	Volume
Case 1	40	0.74	0.3	1	1 × 1.5 × 0.2
Case 2	40	0.74	0.3	2	1 × 1.5 × 0.2
Case 3	40	0.74	0.3	3	1 × 1.5 × 0.2
Case 4	40	0.74	0.5	2	1 × 1.5 × 0.2
Case 5	40	0.74	0.7	2	1 × 1.5 × 0.2
Case 6	40	0.74	0.3	2	1 × 0.5 × 0.6

penetration into the water body, creates a large air cavity on the back of the slide.

Figure 7 shows that before the landslide body enters the water, the water level of each monitoring point in the river channel is zero, which was in a static state. The landslide body slides along the trough section and acts on the water body, causing fluctuations in water particles. Water particles were implicated on each other, causing water-level changes at the monitoring point. Changes in water-level values of the initial surge indicate that the initial wave of the rock landslide is random, and its shape is asymmetrical. The

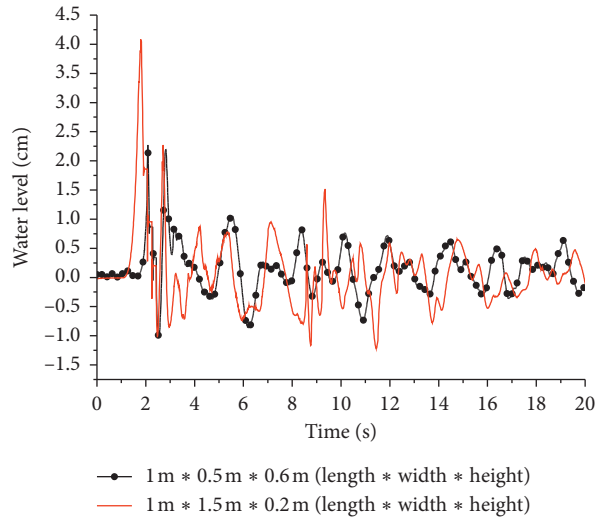

Figure 7: First landslide-generated wave height at different width-to-thickness ratios.

initial height under working case 2 was twice that of the initial height under working case 1. Case 1 produced the peak value earlier than the working case 2. The maximum wave crest amplitude was 4.082 cm, and the maximum wave trough was 1.212 cm. According to the scale ratio conversion, the actual wave crest height of the landslide-generated wave was 2.86 m and the actual wave trough height was 0.85 m. Furthermore, working conditions 1 and 2 were affected by river topography, propagation distance, and river channel bending shape after maximum peak and trough occurrence. The monitoring point's wave energy and water-level value gradually decreased. The landslide body with the same landslide volume and different aspect ratios produced different characteristics of the landslide-generated wave. A larger width-to-thickness ratio resulted in a higher first wave of the landslide-generated wave, a larger wave energy, and a bigger impact on the hydraulic structure. Increase in the time and attenuation of the wave led to a gradual decrease in the landslide-generated wave's asymmetry, and the water surface became calm.

5. Impact of Landslide and Surge on the Motion Characteristics of a Sailing Ship

Ship stability prediction during the early stages of design was very important from the perspective of a vessel's safety. Of the six ship motions, the roll motion is a critical factor in ship capsizing. This section focuses on the roll motion characteristics of a ship in various cases.

5.1. Interaction between the Ship and Landslide-Generated Wave. Landslide-generated waves were classified into weakly nonlinear oscillatory and nonlinear transition. These classifications were based on the landslide Froude number and thickness at impact. It was found that nonlinear oscillation appeared at the Froude number = 1.6 and nonlinear transition appeared at the Froude number = 2.9. In this paper, we studied the interaction between the ship and

landslide-induced wave. The main stages are shown in Figure 8.

The whole process can be subdivided into three main stages: (a) The formation of a landslide-generated wave: all the landslide bodies submerge in the model test, which reflects real-world situations. (b) The propagation of the landslide-generated wave: the crater collapses outward, resulting in the secondary wave. (c) Interaction between the ship and landslide-generated wave: a relative motion between a ship and fluid is a common occurrence.

5.2. Effect of Ship's Roll Performance at Different Locations. This section mainly studies the effect of ship's roll performance on monitoring point 1, monitoring point 2, and monitoring point 3 in the region of landslide-generated wave, making the comparative analysis of ship's roll and roll angular velocity at different locations.

Roll motion is a major response of a ship in waves, which can be determined by analyzing various kinds of moments acting on the ship: virtual and actual mass moments of inertia, the roll damping moment, the restoring moment, wave excitation, and other moments caused by other modes of ship motion.

In this study, the ship sailed straight along the scheduled route at 0.3 m/s. The three tests followed the landslide at No. 1, No. 2, and No. 3 positions of focusing on the ship's roll. The landslide volume was 1 m × 1.5 m × 0.2 m. Our focus was to study the variation law in the ship's roll angle and roll angular velocity.

According to the model test, the model ship in a landslide-generated wave moved with forward speed. As shown in Figure 9, in the three test condition locations, the ship's roll motion amplitude variation was within a reasonable range. The ship passed position No. 1, and the landslide body entered the water and exchanged energy with the water body. The ship's navigation direction was opposite to the wave propagation direction, and the landslide body entered the water. After 7 s, the landslide-generated wave propagated to the navigation position and interacted with the ship, causing a large roll motion with 5.4° maximum amplitude. The ship passed through position No. 3, and the landslide occurred. The ship's sailing direction was similar to the wave's propagation direction, i.e., in a state of landslide spur chasing the sailing ship. After the landslide body interacted with the water body for 10 s, the landslide-generated wave propagated to the ship's navigation position, interacted with it, and acted on its tail, causing a smaller roll motion amplitude. The ship passed through position No. 2, which is close to the landslide point. After a landslide occurred for 3 s, the ship's roll motion amplitude changed significantly. After passing through position No. 1, No. 2, and No. 3, the ship encountered a landslide-generated wave at different moments. The ship relies on its own restoring torque and slowly reaches equilibrium.

Figure 10 shows three cases of the physical test as the ship passes via position No. 1, No. 2, and No. 3. The amplitude of change in the ship's roll angular velocity at position No. 1 was the largest, followed by that of navigation position No. 2, whereas navigation position No. 3 was the smallest. The maximum wave amplitude was 35.37 deg/s at position No. 1. The moment of the initial change in the roll angular velocity was the same as that for the initial change in the roll angle, which occurred at the moment of interaction between the landslide-generated wave and ship. When the ship is sailing, higher roll angle speed causes worse comfort and less stable loading cargo. From this Figure 10, it can be observed that the ship's roll motion was affected at low-frequency wave excitation. When the ship is sailing, sudden landslides occur, and the position of the landslide site is critical to the ship's safety. When the landslide point is in front of the ship, the speed of the ship should be controlled to increase the distance between the ship and landslide point. When the landslide point is located in the opposite direction of the ship's navigation, it should increase the speed of the ship to subjoin the distance between the ship and landslide point. This reduces the landslide's impact and surge on the sailing ship, improves the ship's navigation safety, enhances passenger comfort, and stabilizes the loading cargo.

5.3. Effect of Ship's Rolling Characteristics at Different Navigation Speeds. A landslide occurred when the ship passed through landslide location No. 2. The landslide volume was 1 m × 1.5 m × 0.2 m, and the ship sailed in a straight line at 0.3, 0.5, and 0.7 m/s, respectively, guided by the variation law of the ship's roll angle and roll angle speed.

As shown in Figure 11, ships passing position No. 2 at different speeds experienced the same volume of landslides, but their roll motion amplitudes were different, with the largest reaching 15° at a speed of 0.3 m/s. The landslide body position under the three cases was similar to the ship's navigation position. It can be noted here that the slight increase of drag in the high-speed range was due to the nonlinear lifting effect. Owing to the ships' different sailing speeds, the landslide-generated wave and time of the ship's action were slightly different. The roll motion curves of the ship under the three working conditions first increased nonlinearly, and then the nonlinearity was reduced. This is related to the ship sailing at different forward speeds, generated travelling waves, and landslide-generated wave. As time proceeded, the ship gradually returned to the short-range fluctuation state by relying on its own recovery torque. When the ship moved at 0.3 m/s, the roll amplitude was large, which is cause for concern.

The experimental data were combined with the ship's construction—optimizing keel size and increasing ship damping were considered in the landslide-generated wave region. Changing the external load's influence on the hull pressure distribution and water depth in the ballast tank prevented water movement from hitting the top of the antirolling tank when the ship's roll motion amplitude became larger, which also reduced the antishake effects of the system.

Figure 12 indicates that a ship passing track line position No. 2 at 0.3, 0.5, and 0.7 m/s had different time-history curves of ship's roll angular velocity. The roll speed corresponding to the forward speed of 0.3 m/s was most affected

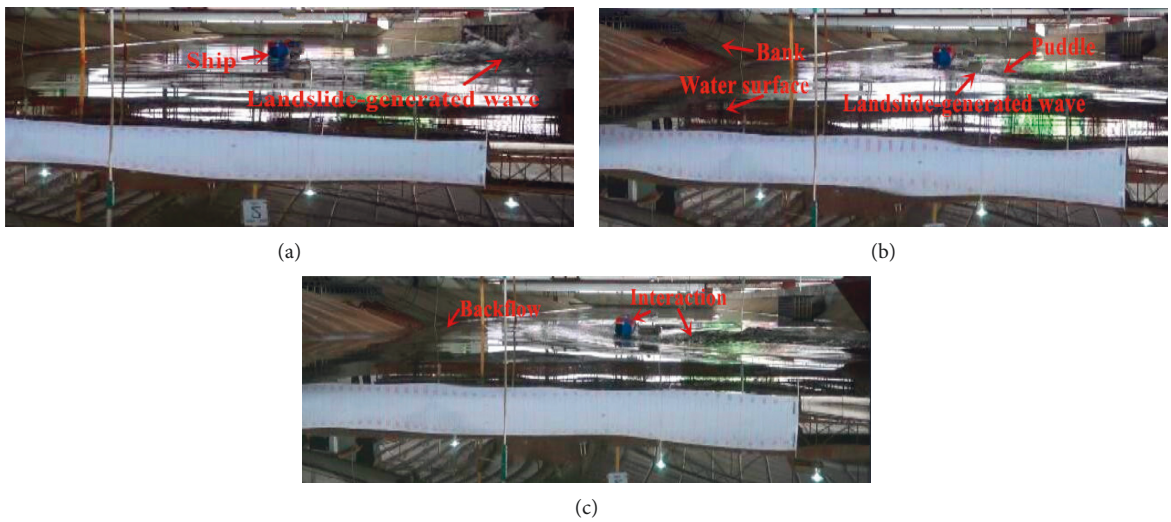

Figure 8: Main stages of interaction between a ship and a landslide-generated wave. (a) The formation of a landslide-generated wave; (b) the propagation of a landslide-generated wave; (c) the interaction between a ship and a landslide-generated wave.

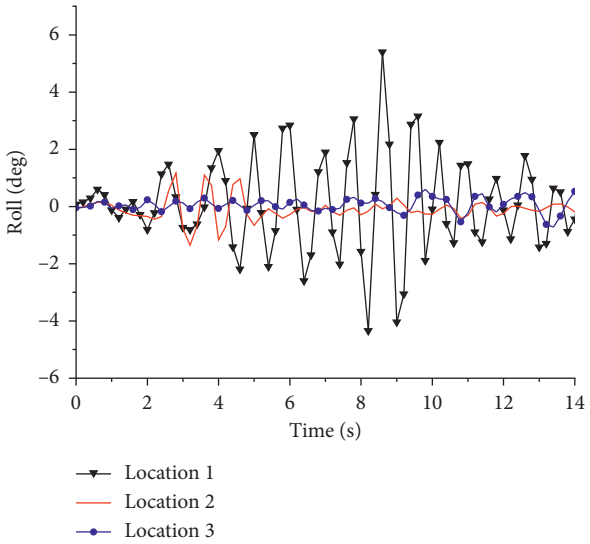

Figure 9: Ship's roll-time curve at different navigation positions.

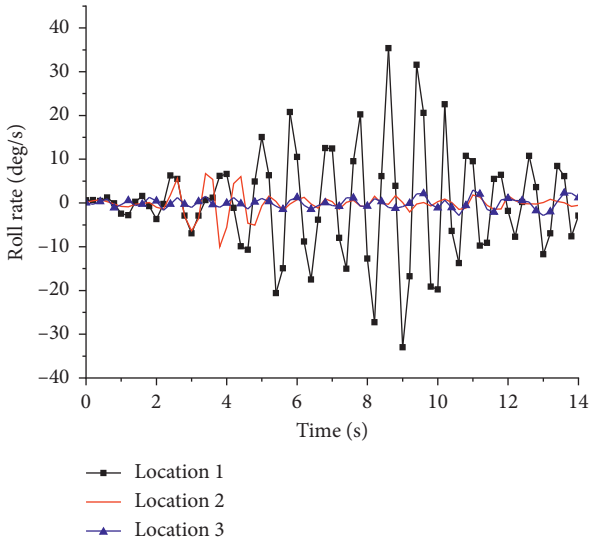

Figure 10: Time-history curve of the ship's roll angular velocity at different navigation positions.

by the landslide-generated wave. The maximum value reached 95°/s. Concurrently, when the ship's sailing speed was slow, the impulse load of the landslide-generated wave acted on the hull, the roll angular velocity curve of the hull first changed, and the roll angular velocity curve of the ship began to change at 0.8 s. Under the landslide's influence, the roll angle reached its maximum value in 3 s, showing a very strong transient nature. Furthermore, the action process was accompanied by a high roll angle velocity, which adversely affected passenger comfort and the loaded cargo's stability.

5.4. Influence of the Rolling Characteristics of a Ship at Different Ratios. The landslide occurred when the ship passed through location No. 2. The landslide body dimensions were 1 m × 1.5 m × 0.2 m and 1 m × 0.5 m × 0.6 m, and the ship sailed at a fixed speed of 0.3 m/s in a straight line, with emphasis on the ship's roll angle and variation in its angular velocity.

Figure 13 demonstrates that when the landslide body entered the water at a high speed, it was accompanied by a high-pressure peak. However, when a landslide body with the same volume and different ratios entered the water, the impact load size was different. A large difference in roll was also observed. Wave height contributes significantly to roll movement; when the landslide-generated wave propagates in the channel, the roll motion is dramatically reduced. The width-thickness ratio under working condition 6 was small; hence, the ship's roll motion peak appeared earlier. The load between the landslide and water body was small, and the amplitude of the roll motion was small. The aspect ratio under working condition 3 was large, and the peak of the

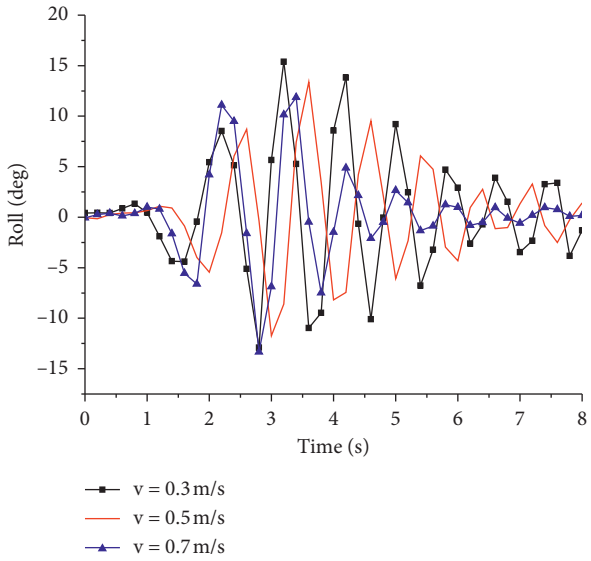

Figure 11: Ship's roll time-history curve for different speeds.

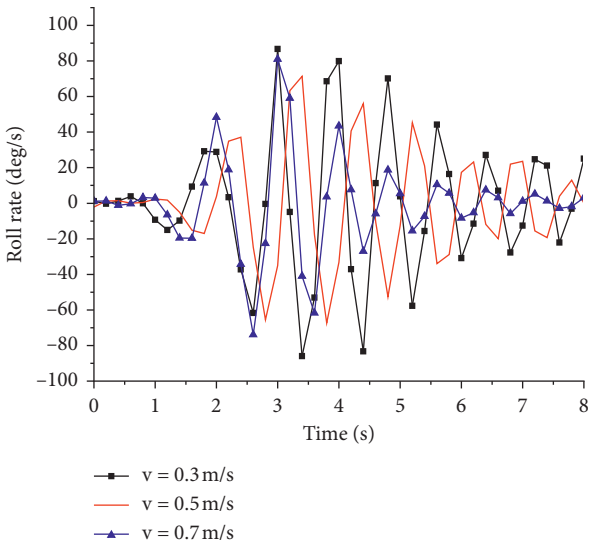

Figure 12: Ship's roll angular velocity time-history curve at different ship speeds.

ship's roll motion had a certain delay. Furthermore, the roll motion's amplitude was large, reaching 15°, which was close to the ultimate roll angle of the navigation in the reservoir area. A larger aspect ratio with the same landslide body amount has a larger impact on the ship's roll characteristics, leading to worse ship navigation safety. In actual disaster prevention projects, to reduce the effect of a landslide-generated wave on the hydraulic structures, the width-to-thickness ratio of the smaller rock mass is reduced and treated in stages to prevent large-scale mountain landslides.

Figure 14 shows that the fixed speed of the ship was 0.3 m/s straight ahead, and landslides with different ratios occurred through landslide No. 2. The landslide bodies with the same volume and different aspect ratios had different effects on the ship's roll angular velocity, and the asymmetry of the landslide-generated wave led to angular velocity

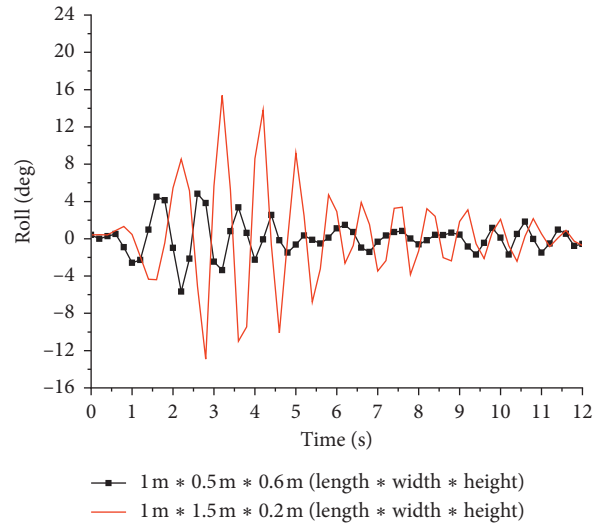

Figure 13: Roll time-history curve with different landslides.

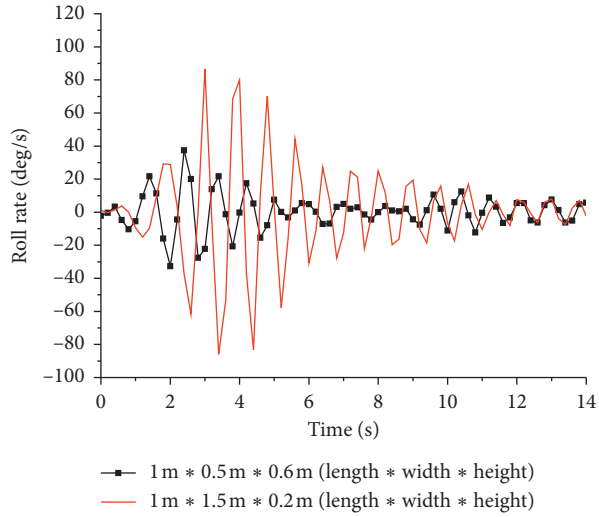

Figure 14: Ship's roll angular velocity time-history curve for different landslides.

asymmetry of the ship. The landslide body with a significant thickness had a major effect on the ship's roll angular velocity. The maximum value was 90°/s. From this Figure 14, the motions of both roll movement and roll angular velocity were in good agreement with the landslide-generated wave. A landslide body of relatively less thickness had little influence on the ship's roll angular velocity. Two types of landslide bodies enter the water to produce a landslide-generated wave. The action process of the landslides is consistent with the ship. The roll angular velocity of the ship increases instantaneously in a short period. After some time, the landslide-generated wave energy is attenuated. The ship relies on its own restoring force to reduce the roll angle and roll angular speeds, allowing it to reach a relatively stable state.

5.5. Influence of Ship's Rolling Characteristics at Stationary and Travelling States. When the ship is stationary or sailing

at 0.6 m/s through the waters of a landslide section, landslides occur (Figure 15). These landslides present adverse effects on stationary and sailing ships. Landslide impacts on ships sailing at 0.6 m/s are divided into two stages: The first stage occurs within 1–5 s. When the landslide body enters the water, the impact generates a landslide wave and the liquid splashes significantly, accompanied by the waves on the deck. As the ship has been sailing straight, the landslide-generated wave acts on the middle and rear parts of the ship. Thus, a large amplitude of swaying motion is easily produced, and the motion amplitude change rate is steep. The second stage occurs at 11–18 s, caused by the landslide-generated wave. The direction is transmitted, finally reaching the end of the river, thereby impacting the bank slope, forming reflection, reflow, and superimposing the impact of the synthetic wave on the sailing ship. The first stage's maximum roll motion amplitude was 10°. The maximum roll motion of the second-stage ship was 9°. When the ship encounters a landslide during the actual navigation process, it should focus on controlling the navigation speed and water field instability to prevent the landslide-generated wave from causing a "secondary damage" to the ship. The ship is stationary in the waters of the landslide section, and the landslide body generates a landslide-generated wave after entering the water. The ship's roll motion amplitude appeared at 1–14 s, showing a single peak state, with the landslide's wave energy gradually decreasing along the landslide. The ship relies on its own recovery torque and recovery damping. The amplitude of the roll motion gradually decreased, and eventually stabilized. The ship was stationary in the sluice waters. It is necessary to focus on the landslide starting moment and prevent the landslide. The impact of the first wave on the ship, reasonable and effective disaster prevention, and mitigation procedures should be considered.

6. Discussion and Conclusions

In this paper, we discussed the design of a landslide surge model in rivers based on a physical test model. We mainly focused on the influence of the pulse surge generated by landslides, having the same volume but different aspect ratios, on a ship's rolling characteristics. We further studied the effects of the same landslide on the ship's rolling characteristics at different cruising speeds. The rolling characteristics of the landslide-generated wave were examined before the ship reached different positions. The main conclusions are as follows:

(1) After the diffraction and superimposition of the reflected waves, a large wave momentum implies a greater influence on the hydraulic structure. For the same 0.6 m^3 volume of landslide bodies, a larger width-to-thickness ratio implies a greater height of the first landslide wave, the width-to-thickness ratio is 1 : 9; the maximum value ratio is about 1 : 2, and maximum value is 2.86 m.

(2) When the ship sails and sudden landslides occur, the position of the landslide site is critical to the ship's safety. When ship's navigation direction was opposite to the wave propagation direction, the frequency of ship motion is more violent, the maximum value is 5.4 deg, and the maximum roll angular velocity is 35.37 deg/s.

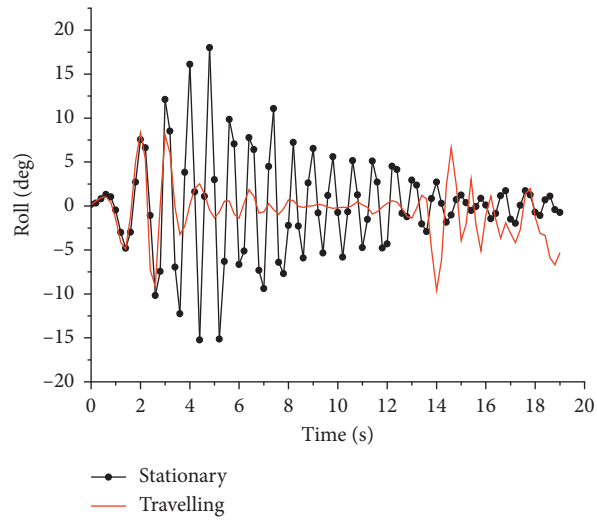

Figure 15: Ship's roll time-history curve.

(3) During a voyage, a ship suddenly encounters a landslide-generated wave. The impulse surge generated by the same volume of landslides has different effects on the ships at different voyage speeds. The maximum roll angle and roll angular velocity are 15.39 deg and 86.72 deg/s, respectively, at a speed of 0.3 m/s. In order to increase passenger comfort and cargo-loading safety, the sailors should take the initiative to reduce the ship's speed by reducing the acceleration itself.

(4) The roll motion characteristic curve of stationary and travelling ships is totally different. A travelling ship generates waves, which lead to other overlapping complicated waves; thus, the period of wave and roll motion appears twice. The first roll motion curve of travelling ships has two large crests: the first peak value is 8.34 deg and the second peak value is 6.62 deg; both are in the reasonable portion. While the other has one large crest, the maximum value is 18.02 deg.

Data Availability

The data in figures and tables used to support the findings of this study are included herein.

Conflicts of Interest

The authors declare that they have no conflicts of interest.

Acknowledgments

This study was financially supported by the National Natural Science Foundation (51479015) and the Social Science and Technology Innovation Program for People's Livelihood

in Chongqing (cstc2018jscx-msybx0233, cstc2017shms-zdyfX0026, cstc2018jszx-cyzdX0019, cstc2018jszx-zdyfxmX0013, and cstc2017jcyjBX0070).

References

[1] H. M. Fritz, W. H. Hager, and H.-E. Minor, "Landslide generated impulse waves," *Experiments in Fluids*, vol. 35, no. 6, pp. 505–519, 2003.

[2] B. Ataie-Ashtiani and A. Nik-Khah, "Impulsive waves caused by subaerial landslides," *Environmental Fluid Mechanics*, vol. 8, no. 3, pp. 263–280, 2008.

[3] S. Yavari-Ramshe and B. Ataie-Ashtiani, "A rigorous finite volume model to simulate subaerial and submarine landslide-generated waves," *Landslides*, vol. 14, no. 1, pp. 203–221, 2017.

[4] H. M. Fritz, W. H. Hager, and H.-E. Minor, "Landslide generated impulse waves. 2. Hydrodynamic impact craters," *Experiments in Fluids*, vol. 35, no. 6, pp. 520–532, 2003.

[5] F. Evers, *Spatial Propagation of Landslide Generated Impulse Waves*, Ph.D. thesis, ETH Zurich, Zurich Switzerland, 2017.

[6] V. Heller, W. H. Hager, and H.-E. Minor, "Scale effects in subaerial landslide generated impulse waves," *Experiments in Fluids*, vol. 44, no. 5, pp. 691–703, 2008.

[7] E. Noda, "Water waves generated by landslide," *J. Water Port. Coast Ocean Div. Am. Soc. Civ. Eng.*, vol. 96, pp. 835–855, 1970.

[8] J. Kamphuis, "Impulse waves generated by landslides," in *Proceedings of the 12th Coastal Engineering Conference*, pp. 575–588, Washington, DC, USA, 1970.

[9] D. Muller, "Impulse waves generated by an artificially induced rockfall in a Swiss lake," in *Proceedings of the 25th IAHR Congress*, vol. 4, pp. 209–216, Tokyo, Japan, August-September 1993.

[10] K. Yin, "Physical model experiments of landslide-induced surge in three Gorges reservoir," *Earth Science*, vol. 37, pp. 1067–1074, 2012.

[11] M. Risio and P. Sammarco, "Analytical modeling of landslide-generated impulse waves," *Journal of Waterway, Port, Coastal, and Ocean Engineering*, vol. 134, no. 1, pp. 53–60, 2008.

[12] C. F. Waythomas and P. Watts, "Numerical simulation of tsunami generation by underwater landslides," *Journal of Waterway, Port, Coastal, and Ocean Engineering*, vol. 124, pp. 127–137, 1998.

[13] S. M. Abadie, J. C. Harris, S. T. Grilli, and R. Fabre, "Numerical modeling of tsunami waves generated by the flank collapse of the Cumbre Vieja Volcano (La Palma, Canary Islands): tsunami source and near field effects," *Journal of Geophysical Research: Oceans*, vol. 117, no. 5, 2012.

[14] V. Heller, W. H. Hager, and H. Minor, *Landslide Generated Impulse Waves in Reservoirs—Basics and Computation*, Versuchsanstalt fur Wasserbau, Zurich, Switzerland, 2009.

[15] H. Tan, G. Ruffini, V. Heller, and S. Chen, "A numerical landslide-tsunami hazard assessment technique applied on hypothetical scenarios at Es Vedrà, offshore Ibiza," *Journal of Marine Science and Engineering*, vol. 6, no. 4, pp. 1–22, 2018.

[16] G. Ma, F. Shi, and J. T. Kirby, "Shock-capturing non-hydrostatic model for fully dispersive surface wave processes," *Ocean Model*, vol. 43, pp. 22–35, 2013.

[17] V. Heller and W. H. Hager, "Wave types of landslide generated impulse waves," *Ocean Engineering*, vol. 38, no. 4, pp. 630–640, 2011.

[18] V. Heller and J. Spinneken, "Improved landslide-tsunami prediction: effects of block model parameters and slide model," *Journal of Geophysical Research: Oceans*, vol. 118, no. 3, pp. 1489–1507, 2013.

[19] V. Heller and J. Spinneken, "On the effect of the water body geometry on landslide-tsunamis: physical insight from laboratory tests and 2D to 3D wave parameter transformation," *Coastal Engineering*, vol. 104, pp. 113–134, 2015.

[20] V. Heller, M. Bruggemann, J. Spinneken, and B. D. Rogers, "Composite modelling of subaerial landslide-tsunamis in different water body geometries and novel insight into slide and wave kinematics," *Coastal Engineering*, vol. 109, pp. 20–41, 2016.

[21] L. Nie, Z. Gao, G. Zhu, and Z. Pan, "Study on dynamic responses of duct-water coupled components for aqueduct with seismic isulation," *Journal of Hydroelectric Engineering*, vol. 30, no. 6, pp. 62–66, 2011.

[22] J. L. Cercos-Pita, G. Bulian, L. Pérez-Rojas, and A. Francescutto, "Coupled simulation of nonlinear ship motions and a free surface tank," *Ocean Engineering*, vol. 120, pp. 281–288, 2016.

[23] K. J. Spyrou and I. G. Tigkas, "Nonlinear surge dynamics of a ship in astern seas: "continuation analysis" of periodic states with hydrodynamic memory," *Journal of Ship Research*, vol. 55, pp. 19–28, 2011.

[24] G. C. Soares and N. Fonseca, "Abnormal wave-induced load effects in ship structures," *Journal of Ship Research*, vol. 52, pp. 30–44, 2008.

[25] Y. Kim, B. W. Nam, D. W. Kim, and Y. S. Kim, "Study on coupling effects of ship motion and sloshing," *Ocean Engineering*, vol. 34, no. 16, pp. 2176–2187, 2007.

[26] O. Faltinsen and R. Zhao, "Numerical predictions of ship motions at high forward speed," *Philosophical Transactions of the Royal Society of London. Series A: Physical and Engineering Sciences*, vol. 334, pp. 241–252, 1991.

[27] S. K. Das and S. N. Das, "Note on sway, roll and yaw motions of a ship with forward speed: analytical study," *Acta Mechanica*, vol. 186, no. 1–4, pp. 221–227, 2006.

[28] S. K. Das and S. N. Das, "Modelling and analysis of coupled nonlinear oscillations of a floating body in two degrees of freedom," *Acta Mechanica*, vol. 181, no. 1-2, pp. 31–42, 2006.

[29] M. Soylemez, "Motion response simulation of a twin-hulled semi-submersible," *Ocean Engineering*, vol. 25, pp. 359–383, 1998.

[30] K. Mctaggart, "Lateral ship motions and sea loads in waves including appendage and viscous forces," *International Shipbuilding Progress*, vol. 47, pp. 141–160, 2000.

[31] H. Hatecke, "The impulse response fitting and ship motions," *Ship Technology Research*, vol. 62, no. 2, pp. 97–106, 2015.

[32] S. Murashige and K. Aihara, "Experimental study on chaotic motion of a flooded ship in waves," *Proceedings of the Royal Society of London. Series A: Mathematical, Physical and Engineering Sciences*, vol. 454, no. 1978, pp. 2537–2553, 1998.

[33] R. Pethiyagoda, T. J. Moroney, G. J. Macfarlane, J. R. Binns, and S. W. McCue, "Time-frequency analysis of ship wave patterns in shallow water: modelling and experiments," *Ocean Engineering*, vol. 158, pp. 123–131, 2018.

[34] S. Sigmund and O. el Moctar, "Numerical and experimental investigation of added resistance of different ship types in short and long waves," *Ocean Engineering*, vol. 147, pp. 51–67, 2018.

[35] N. Fonseca and C. Guedes Soares, "Comparison of numerical and experimental results of nonlinear wave-induced vertical ship motions and loads," *Journal of Marine Science and Technology*, vol. 6, no. 4, pp. 193–204, 2002.

[36] P. Heinrich, "Nonlinear water waves generated by submarine and aerial landslides," *Journal of Waterway, Port, Coastal, and Ocean Engineering*, vol. 118, pp. 223–238, 1992.

Hindawi
Advances in Civil Engineering
Volume 2019, Article ID 6134803, 16 pages
https://doi.org/10.1155/2019/6134803

Review Article

A Review of Multicriteria Assessment Techniques Applied to Sustainable Infrastructure Design

Ignacio J. Navarro,[1] Víctor Yepes ,[2] and José V. Martí[2]

[1]*Dept. of Construction Engineering, Universitat Politècnica de València, 46022 Valencia, Spain*
[2]*Institute of Concrete Science and Technology (ICITECH), Universitat Politècnica de València, 46022 Valencia, Spain*

Correspondence should be addressed to Víctor Yepes; vyepesp@cst.upv.es

Received 10 April 2019; Revised 20 May 2019; Accepted 29 May 2019; Published 17 June 2019

Guest Editor: Endong Wang

Given the great impacts associated with the construction and maintenance of infrastructures in both the environmental, the economic and the social dimensions, a sustainable approach to their design appears essential to ease the fulfilment of the Sustainable Development Goals set by the United Nations. Multicriteria decision-making methods are usually applied to address the complex and often conflicting criteria that characterise sustainability. The present study aims to review the current state of the art regarding the application of such techniques in the sustainability assessment of infrastructures, analysing as well the sustainability impacts and criteria included in the assessments. The Analytic Hierarchy Process is the most frequently used weighting technique. Simple Additive Weighting has turned out to be the most applied decision-making method to assess the weighted criteria. Although a life cycle assessment approach is recurrently used to evaluate sustainability, standardised concepts, such as cost discounting, or presentation of the assumed functional unit or system boundaries, as required by ISO 14040, are still only marginally used. Additionally, a need for further research in the inclusion of fuzziness in the handling of linguistic variables is identified.

1. Introduction

Sustainable development was first defined in 1987 by the Brundtland Commission as a way to meet the present needs of the society without compromising the ability of future generations to meet their own needs. Sustainable actions and decisions shall therefore be based on the simultaneous consideration of their economic, environmental, and social consequences over time. Sustainable design of products, as an application of the sustainability concept in the industry, takes particular relevance when considering the construction sector. In recent times, construction industry has become one of the main environmental stressors of our society, since it is responsible for 30% of global energy consumption, 40% of raw material extraction, and 30% of greenhouse gas emissions [1]. In particular, only the production of cement for concrete contributes around 8% of global annual CO_2 emissions [2]. On the other hand, investments in public capital, such as infrastructures, promote the economic wellbeing and social development of countries, since they contribute to the territorial structuring of regions and to the adequate provision of services. For example, about 20 per cent of World Bank loans in recent years have been allocated to transport infrastructure [3].

So, given the relevant implications of infrastructure design, and considering that most infrastructures are designed to serve a significant group of people over a long, intergenerational period of time, the assessment of the different dimensions of sustainability related to the infrastructure design has been in the spotlight of many researchers in recent times. Studies have been conducted on cost optimisation of infrastructure design [4, 5] and maintenance [6, 7]. Attention has also been paid to the environmental impacts derived along the life cycle of structures, from bridges [8–10] to buildings [11], as well as those derived from particular construction processes, such as concrete production [12]. Social impacts related to the use of different building materials [13] for building construction [14] and for road infrastructure projects [15] have also been assessed in recent years. However, the current state of science lacks an objective and universal methodology to properly

assess the sustainability of a particular infrastructure design. Thus, although standardised tools exist to assess the different life cycle impacts of products, there is no consensus on how to cope with the simultaneous consideration of the three pillars that define sustainability, nor on what particular criteria should be considered in the decision-making process of sustainable infrastructure design [16].

To deal with the assessment of the conflicting dimensions of sustainability in a multistakeholder and long-term context like infrastructure design, the use of multicriteria decision-making (MCDM) techniques has revealed itself as the most suitable approach compared to other methods commonly used in infrastructure design, such as single- or multiobjective optimisation. MCDM techniques allow the decision maker to assess complex problems involving multiple and divergent criteria on the basis of the subjective judgements of a panel of experts or of stakeholders affected by the decision. Therefore, this paper is devoted to analysing the current trends regarding the application of MCDM techniques to the sustainability assessment of infrastructure design, paying special attention to the particular criteria considered in these assessments.

The rest of the paper is structured as follows. Section 2 presents the research methodology, exposing the research questions to be answered by means of this manuscript, as well as describing the data acquisition strategy followed in the review. Section 3 presents the results obtained. In particular, Section 3.1 provides a general overview of the gathered data; Section 3.2 presents the indicators selected to characterise each of the three dimensions of sustainability, as well as the methods considered to assess such impacts. Section 3.3 presents a brief review on how qualitative data are treated in the analysed manuscripts; Section 3.4 investigates the normalisation techniques found in the reviewed literature; Section 3.5 describes the weighting techniques used; Section 3.6 presents the methods used in the analysed studies to aggregate the weighted indicators; Section 3.7 offers an overview of the aspects object of sensitivity analyses in sustainability MCDM assessments; Section 3.8 presents how the subjectivity of the experts' judgements is handled throughout the whole decision-making process. Finally, Section 4 provides the conclusions of the present literature review.

2. Materials and Methods

2.1. Research Question. The present study formulates two research questions, namely, how MCDM methods have been applied for the sustainability assessment of infrastructures in recent times, and what particular impact criteria and indicators have been considered in these evaluations as representative for the sustainability of an infrastructure design.

2.2. Data Sampling Strategy. The data collection process performed in the present literature review consists of two stages, as shown in Figure 1. The objective of the first stage is to create a preliminary set of contributions to serve as a basis for the construction of a final set through an appropriate filtering and expanding process in a second stage.

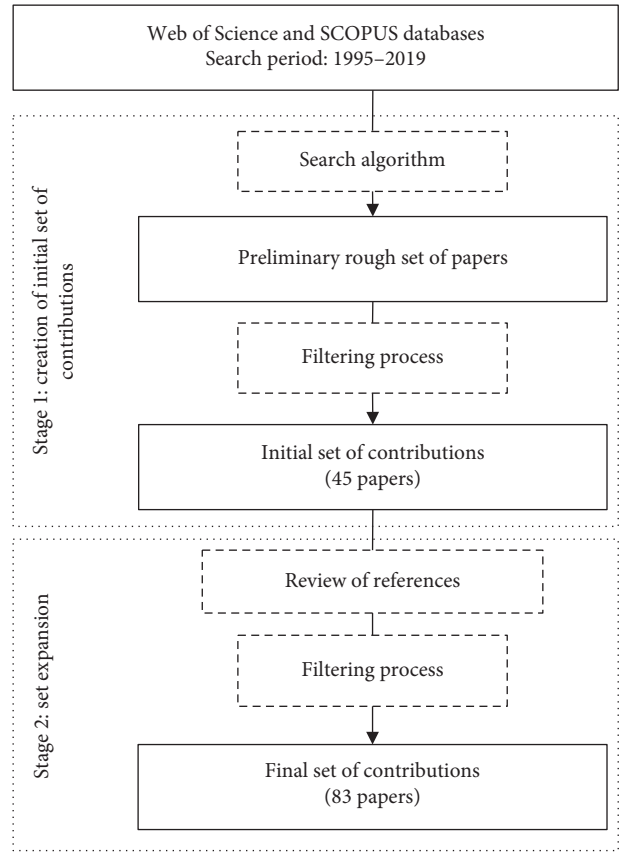

Figure 1: Systematic literature review.

The search is carried out through the scientific bibliographic databases SCOPUS and Web of Science. The search period is established from 1995 to 2019, since there is no evidence of relevant contributions before that date. The search algorithm used to identify the articles conforming the preliminary set consists of a combination of the terms "Multi-criteria decision making," "MCDM," and "Sustainability" along with other civil engineering-related terms, such as "Construction" or "Infrastructure," by means of the Boolean operators "AND" and "OR."

To filter the obtained results, some exclusion criteria have been followed to build the first set of papers. First, only original, peer-reviewed scientific articles and conference proceedings are included. Secondly, those manuscripts that do not clearly identify either the MCDM technique used or the sustainability criteria considered are excluded. Third, articles are required to consider at least two of the three dimensions of sustainability in the assessment through an appropriate selection of decision criteria. Finally, it should be taken into account that only articles written in English are considered in this study. This structured filtering process resulted in an initial set of 45 papers.

Once the initial set of contributions is generated, the references included in the selected manuscripts are then reviewed and analysed. The set is then expanded by applying the filtering process exposed above to the articles referenced in the papers included in the first set, which results in a final and expanded set of manuscripts. This sampling technique

has been used previously in other literature review works [17, 18]. The expanded final set has resulted here in 83 contributions.

3. Results and Discussion

3.1. General Overview of the Retrieved Data. Although in 2007 there was a first rebound in the number of publications regarding sustainability assessment of infrastructures, the number of contributions increases drastically in 2015 (Figure 2). Over 50% of the publications applying MCDM techniques to sustainable infrastructure design were made between 2015 and the present. This increase is explained by the fact that it was in 2015 when the General Assembly of the United Nations established the Sustainable Development Goals for the first time. Among the 17 Goals set, some of them are related to sustainable economic growth, decent work, resilient and sustainable infrastructures, and climate action. This would explain the great efforts made by the scientific community since 2015 to contribute to providing tools that allow the sustainable design of infrastructures. After reviewing the gathered data, 6 different main applications of MCDM techniques were identified:

(i) *Buildings.* 38.6% of the analysed contributions (32 papers) are devoted to assess the sustainability of different aspects related to the design of buildings. While some authors have focused on the design assessment of particular elements of the building structure, such as slabs [19, 20], columns [21], and beams [22], others pay attention to the sustainable design of building envelopes [23–31]. Pons and Aguado [32], Akadiri et al. [33], Motuziene et al. [34], Samani et al. [35], and Nassar et al. [36] also compare the sustainability of the application of different construction materials to buildings. Research is also conducted on the development of indicators suitable to measure the sustainability of buildings [37–41]. Particular attention is paid to the sustainable design of industrial buildings [42–45]. Formisano and Mazzolani [46], and Terracciano et al. [47] evaluate the sustainability of different alternatives for energetic retrofitting of buildings in locations with high seismicity. Finally, other purposes are covered, such as restoration alternatives for derelict buildings [48, 49], or optimal building location [50].

(ii) *Bridges.* 15.7% of the reviewed manuscripts (13 papers) deal with the sustainability assessment of bridges. Most of them focus either on the sustainability of bridge deck designs [51–57] or on the selection of optimal maintenance strategies [58–60]. Attention is also paid to the sustainability of different strengthening or repair schemes [61, 62] and to the selection of the most sustainable construction method [63].

(iii) *Energy Infrastructure.* 14.5% of the papers (12 articles in total) deal with the sustainability of different topics related to energy infrastructure, such as the selection of the most sustainable energy production system [64–70], the selection of the optimal location of energy production plants [71, 72], and the sustainability performance evaluation of different designs of wind turbines and towers [73–75].

(iv) *Hydraulic Infrastructure.* 13.3% of the publications handle with the sustainability of different hydraulic infrastructures, such as dams [76–78], urban drainage [79–81], sewerage systems [82], and water supply systems [83–86].

(v) *Transport Infrastructure.* 7.2% of the manuscripts deal with the sustainability of different elements and topics related to transport systems, such as the sustainable design of road pavements [87–90], the selection of the optimal road location [91], or the development of assessment tools for the evaluation of transport projects [92].

(vi) *Others.* The remaining papers reviewed (10.7%) cover a variety of aspects related to sustainable infrastructure design, such as the assessment of tunnel projects [93, 94], ports [95], location of demolition waste facilities [96], the selection of coating materials for construction [97], and the development of assessment tools for the evaluation of construction projects in general terms [98–101].

3.2. Impact Assessment and Selection of Indicators. As sustainability life cycle assessments are based on the life cycle impacts derived from the different activities considered in the analysis, it is essential to define in the early stages of the decision process not only which impacts (criteria) are going to be considered in the analysis, but also how those impacts are going to be assessed. Of the analysed publications, 74.7% (62 papers) base their assessments on the impacts derived from at least two different stages of the life cycle of the infrastructure under study. To evaluate the life cycle impacts and establish coherent impact categories, an objective methodology has been standardised in the environmental field [102, 103] to allow a rigorous assessment of different alternatives. Although such an ISO standard does not yet exist for the economic field, life cycle costing shows a highly mature state of development [104]. However, the evaluation of the social dimension of sustainability is still under development. It was first in 2009 when an attempt was made to establish an objective methodology to identify and evaluate social impacts through the "Guidelines for social life cycle assessment of products" [105], which relies on the ISO standardised methodology for environmental impact assessments. Notwithstanding the above, only 4 out of the 83 reviewed papers (4.8%) follow the ISO methodology, explicitly defining an adequate functional unit and the system boundaries assumed in the assessment [20, 34, 35, 70]. Although not strictly following the ISO methodology, other authors do explicitly define the functional unit and system boundaries [30, 82, 87, 93, 94].

3.2.1. Economic Criteria. Out of the 83 reviewed manuscripts, only 7 do not consider economic criteria in their sustainability assessments. Among the rest, three main

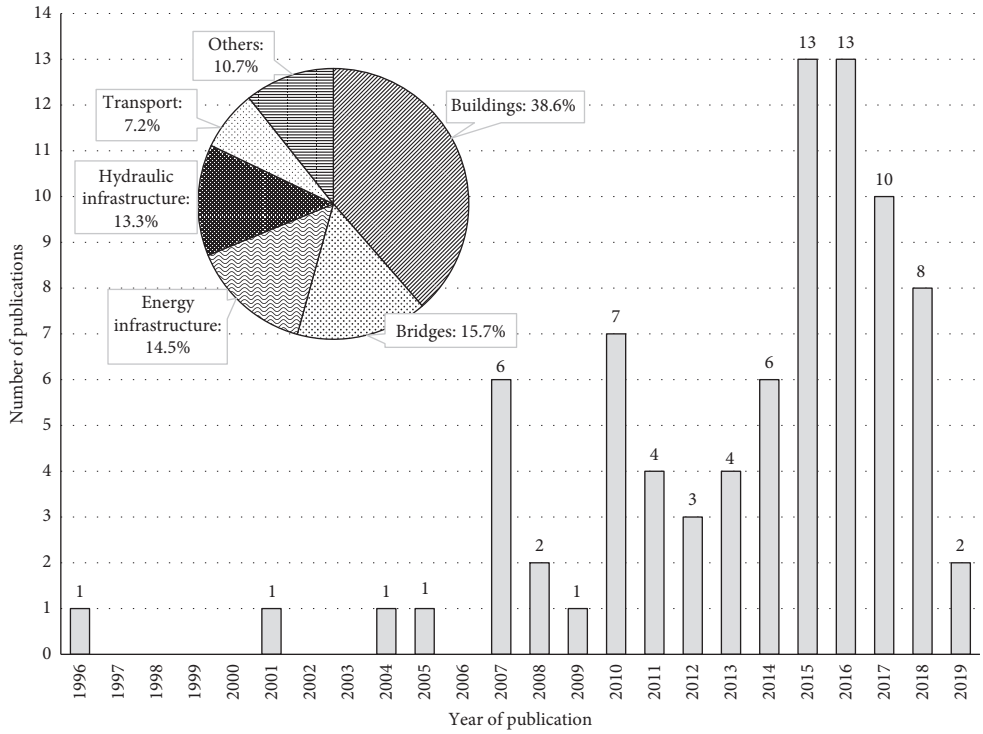

Figure 2: Distribution of contributions per year (1996–2019).

economic impacts have been identified, namely, the construction or implementation costs, the costs derived from maintenance and operation of the infrastructure, and the costs resulting from the end of life stage. Table 1 presents the main economic indicators considered in the reviewed studies. 94.7% of the reviewed papers that take into account the economic dimension of sustainability assume the costs derived from the installation of the infrastructure relevant in the assessment. Only 13.3% of the reviewed papers consider the direct costs associated with the disposal of the infrastructure in their assessments and 63.9% the costs of the maintenance and operation life cycle stage.

It shall be noted that, among the reviewed papers, only 5 explicitly present the assumed discount rates that allow to transform future costs into present currency values. In the field of building design, Mosalam et al. [22] consider a discount rate of 3%, Jalei et al. [25] assume a discount rate of 5%, and Perini and Rosasco [24] evaluate three different economic scenarios, with discount rates that range from 4.5% to 5.5%. Torres-Machí et al. [89], when assessing the sustainability of road pavement treatments, assume a discount rate of 5%. Klein and Whalley [68] evaluate a cost discounting range that varies from 3% up to 10%.

3.2.2. Environmental Criteria. Regarding the environmental dimension of sustainability, seven main impact categories have been found to be recurrent in the reviewed studies, namely, emission of pollutants, energy consumption, resources depletion, waste generation, land use, eutrophication, and ozone layer depletion. Table 2 presents the main environmental indicators considered in the reviewed studies for the evaluation of the mentioned criteria.

The emission of pollutants as an indicator of the environmental impact of an infrastructure is the most used criterion within the reviewed papers. It considers the emissions derived from the production of construction materials and construction works, but also from the externalities associated with the construction of infrastructure and its maintenance, such as traffic congestion [61]. While some authors explicitly focus on particular air pollutants, such as carbon dioxide [24, 27, 30, 57, 93], SO_2 or NO_x [64, 70], or general greenhouse gases [31, 73], attention is also paid to pollutants emitted to water [79–81] when dealing with urban water systems.

46.3% of the articles include energy consumptions as an additional measure of the environmental impact of an infrastructure. The majority of articles consider the energy needed to produce the construction materials and to construct the particular infrastructure under assessment [31, 34, 75], while certain authors also consider the energy savings resulting from building envelope designs [24].

The depletion of natural resources is accepted as one of the main consequences of unsustainable construction practices. 32 studies account for the consumption of natural resources into construction materials in their sustainability assessments. Some authors take into consideration the positive environmental impact of using recycled materials [25, 28, 88] or using potentially reusable ones [26, 33, 36, 90].

Given that the construction industry is considered one of the greatest producers of wastes in a global scale [106], efforts have been made to account their harmful impact in environmental assessments. 25.3% of the analysed manuscripts take into consideration the generation of waste resulting from the industrial processes involved in the production of

Table 1: Main economic criteria and indicators.

Economic criteria	Indicator	Assessment	References
Installation costs	€/output unit	Quantitative	[19–41, 43–50, 52–58, 61–72, 74, 75, 79–91, 93, 94, 96–99, 101]
Maintenance and operation costs	€/output unit	Quantitative	[20–22, 24–28, 30–34, 36–39, 41, 43, 45, 52–55, 58–61, 64, 66–69, 74, 75, 79–82, 84, 86–90, 92–98, 101]
Disposal costs	€/output unit	Quantitative	[24–26, 30, 31, 36, 43, 53, 74, 75, 88]

Table 2: Main environmental criteria and indicators.

Environmental criteria	Indicator	Assessment	References
Emission of pollutants	kg CO_2/output unit	Quantitative	[19–21, 26–28, 30, 32, 34–36, 56, 64, 65, 67, 68, 70, 72, 74, 75, 82, 87–90, 92–94]
	kg SO_2/output unit	Quantitative	[20, 35, 64, 67, 68, 70, 72, 92]
	kg NOx/output unit	Quantitative	[20, 35, 64, 65, 67, 68, 70, 72, 92]
	€/kg pollutant removed	Quantitative	[24]
	Costs of medical care needs due to pollution (€)	Quantitative	[61]
	Oxygen, nitrogen, and phosphates emitted to water	Quantitative	[80]
	Assessment by experts through point scale	Qualitative	[23, 25, 29, 31, 33, 38, 39, 41, 43, 45, 52, 54, 55, 58–60, 62, 63, 66, 69, 71, 73, 78, 81, 83, 85, 91, 95, 97, 98, 100, 101]
Energy consumption	MJ (MWh)/output unit	Quantitative	[19, 20, 26–28, 30, 32, 34–36, 72, 74, 75, 82, 87, 88, 90, 93, 94]
	€/year/output unit	Quantitative	[24]
	Tonnes of oil equivalent (TOE)	Quantitative	[99]
	Assessment by experts through point scale	Qualitative	[25, 29, 31, 33, 38–40, 42, 45, 73, 95, 101]
Raw material consumption	Consumption/output unit	Quantitative	[19–21, 26–28, 35, 68, 72, 74, 75, 87, 88, 90, 93, 94]
	Assessment by experts through point scale	Qualitative	[25, 31, 33, 38–40, 42, 43, 45, 82, 96, 98]
Waste generation	kg/output unit	Quantitative	[26, 32, 35, 72, 87]
	Assessment by experts through point scale	Qualitative	[29, 31, 33, 38, 39, 42, 43, 45, 95, 96, 98, 100]
Land use	m^2/output unit		[68]
	Assessment by experts through point scale	Qualitative	[24, 28, 29, 38, 39, 42, 45, 51, 55, 66, 69, 71, 73, 77, 78, 91, 96, 98]
	Aquatic ecotoxicity, salinity, biological indices	Quantitative	[70, 79, 80]
Eutrophication	kg phosphate/output unit	Quantitative	[35, 36, 70, 72, 90]
	Assessment by experts through point scale	Qualitative	[42, 77, 78, 98]
Ozone depletion	kg CFC (Chlorofluorocarbons)/ output unit	Quantitative	[34–36, 70, 72, 90]
	Assessment by experts through point scale	Qualitative	[33, 42]

construction materials or from the demolition works. Consideration is given to both solid wastes from construction materials [22, 26] and water wastes [86].

Land use is an environmental concept that implies both land occupation and transformation of land. Land use derived from the construction of infrastructures results in damage to ecosystems and loss of biodiversity. From the 83 reviewed articles, 25 (30.1%) take land use into account as an indicator of the environmental damage derived from infrastructures. The effects of land use have been accounted for as local ecosystem disturbances [96], destruction of wildlife habitats [45, 91], proximity to migratory paths [71], and effects on biodiversity [28, 70]. Given the particular scope of their study, Perini and Rosasco [24] consider the creation of habitats.

Eutrophication is the consequence of the emission of particular pollutants, mainly phosphate, derived from human activities to water, promoting an uncontrolled growth of algae that shall compromise the survival of other water species. This environmental impact has been considered by nine articles (10.8% of total).

Ozone layer is essential for life, as it hinders harmful solar ultraviolet radiation. Ozone layer depletion because of the emission of substances containing chlorine and bromine atoms has been accounted in eight studies as an additional indicator capable of measuring the environmental damage derived from infrastructures and their associated activities.

3.2.3. Social Criteria. Regarding the social dimension of sustainability, the criteria assessed in the studies reviewed shall be grouped into eight main categories, namely, social wellbeing, aesthetics, job creation, development of local economies, externalities, innovation, culture, and health. Table 3 presents the main social indicators considered in the reviewed studies for the evaluation of the mentioned criteria.

Table 3: Main social criteria and indicators.

Social criteria	Indicator	Assessment	References
Social wellbeing	Increase of income of local population (€/year)	Quantitative	[48, 49]
	Assessment by experts through point scale	Qualitative	[25, 28, 29, 31, 36, 39–41, 45, 66, 69, 71, 73, 77, 78, 81, 88, 91, 98, 101]
	Habitability increase (m^2)	Quantitative	[21]
	Comfort (hours/year)	Quantitative	[30]
Aesthetics	Assessment by experts through point scale	Qualitative	[23–25, 27, 31, 33, 38, 40, 42, 43, 51, 52, 54, 55, 58, 62, 63, 67, 71, 75, 77, 81, 88, 96–98]
Job creation	Hours of work/output unit	Quantitative	[64, 65, 68, 70, 87]
	Gross value added/hour worked	Quantitative	[99]
	Unemployment rate	Quantitative	[96]
	Employment increase (%)	Quantitative	[48, 49]
	Assessment by experts through point scale	Qualitative	[45, 66, 69, 73, 77]
Development of local economies	GDP increase (€)	Quantitative	[48, 49, 99]
	Land value degradation (€/m^2)	Quantitative	[96]
	Assessment by experts through point scale	Qualitative	[31, 33, 45, 67, 71, 73, 77, 78, 98]
Externalities	Noise pollution (dB)	Quantitative	[19, 90, 92–94, 96]
	Traffic congestion (travel time)	Quantitative	[90]
	Vehicle operating costs (€), user delay costs (€)	Quantitative	[53]
	Assessment by experts through point scale	Qualitative	[29, 31, 39, 42, 45, 51, 54, 59, 60, 63, 100]
Innovation	Assessment by experts through point scale	Qualitative	[38–40, 45, 75, 98]
Culture	Assessment by experts through point scale	Qualitative	[29, 31, 38, 45, 62, 71, 77, 98]
Health and safety	Injuries/output unit	Quantitative	[65, 67, 87]
	Fatalities/output unit	Quantitative	[68]
	Particulate matter (PM) concentration (PM2.5/PM10)	Quantitative	[36, 90]
	Safety costs (€)	Quantitative	[53]
	Assessment by experts through point scale	Qualitative	[19, 21, 29, 31–33, 39, 42, 43, 45, 58–60, 75, 77, 82, 85, 88, 91, 93, 94, 97, 98, 100, 101]

The impact of an infrastructure on the social wellbeing is included in 34 manuscripts (41% of total) and combines aspects such as public acceptance [31, 50, 66, 69, 70, 101], social welfare and income increase [48, 71, 73, 81], accessibility [78, 79, 86], or leisure [76]. Assessments focused on building and road pavement design also account for the comfort of the users [26, 27, 30, 45, 88, 92].

Aesthetics has also been identified as a main indicator for social sustainability, which is closely related to social acceptance of the project. The aesthetic, which has been assessed in 26 articles, includes not only the aesthetical perception of the infrastructure itself, but also its integration with the urban [43, 50] or rural environment [48, 49].

Direct and indirect working opportunities derived from the construction and maintenance of an infrastructure have been considered in 16 studies (19.3% of total), which is closely related to an increase of the social welfare. Although the methodological sheets for social life cycle assessments developed by UNEP/SETAC [107] give preference not to the generated employment in general, but to that generated for the local communities, it is common practice in social life cycle assessments to use the generated employment in general terms as an indicator of social sustainability [104, 108].

16 studies take into consideration the effects of an infrastructure on the local development of a region, resulting from both the construction and maintenance activities, as well as from the serviceability provided by the infrastructure. Aspects such as the increase of the Gross Domestic Product [49, 99], the increase in tourism [77, 78] or the regional economic benefits derived from the use of local materials and resources [26, 33, 70, 98] have been included in this social impact category.

Externalities derived from infrastructure construction and, mainly, from infrastructure maintenance have been considered in 33.7% of the reviewed studies. Effects such as traffic disruption [54, 60, 62, 63, 90] or the increase in vehicle operating costs due to detours [53, 59, 61] are found to be social indicators recurrently used when assessing the sustainability of bridge infrastructure. Other externalities frequently assessed are noise or dust pollution derived from construction works [22, 45].

The inclusion of innovative concepts in the infrastructure design is also accounted for as a social indicator, as it seeks to ensure the progress and technological development of the society. 9 articles have taken such aspect into account. The evaluation of this impact is based either on a binary indicator, which scores 1 if the design includes patented materials or solutions [22, 74, 75] or relies on the knowledge of the chosen panel of experts [37, 40].

13.3% of the reviewed manuscripts include culture as a measure of social sustainability, paying special attention to the respect for the cultural heritage of a region [29, 31, 37, 38, 45, 62], or for its traditional architecture [26]. Given the difficulties to quantitatively assess cultural indicators [107], most authors rely on the knowledge of the chosen panel of experts for the evaluation of cultural impacts [45, 71, 77].

Health and safety include both the practices of construction and industry companies to protect the lives of their workers, but also the risk of accidents for users of an infrastructure. The impact of the activities associated with the construction and maintenance of an infrastructure on the safety of the involved workers, as well as the risks to the health of the users of the infrastructures, has been considered in 42 articles (50.6% of total).

3.3. Treatment of Qualitative Data. Once the indicators are selected that properly characterise the problem and condition the decision, the following step in a multicriteria decision-making problem consists in transforming them into quantitative values. While the numerical assessment of quantitative variables is straightforward, handling with qualitative criteria requires a certain preprocessing so as to transform such values into numerical ones. When dealing with qualitative criteria, such as aesthetics or comfort, many studies require the experts to evaluate such variables by assigning them scores on different scales ranging from 0 to 1, or from 0 to 10 in the most of the reviewed cases [28, 50, 52, 81, 101].

In other cases, experts are required to evaluate qualitative criteria by choosing one of the different answer options provided by the decision maker in a closed form, which are then directly related to specific numerical values. This approach is often preferred when dealing with complex problems, where experts find it easier to reflect their judgements in linguistic terms rather than in the form of precise numbers. For example, Gumus et al. [73] base the evaluation of each of the criteria assumed for the assessment of wind power plants on the mentioned translation of linguistic variables into numerical values. De la Fuente et al. [82] require experts to evaluate linguistically different functional and social aspects related to sewerage systems, such as surface degradation, risk of accidents, and the affection of pollutants and construction time on the wellbeing of the population. The use of linguistic variables has been used by [93, 94] when assessing the risks derived from handling and installing precast tunnel segments. Heravi et al. [45] also use a similar approach when handling the attitudes of experts towards different types of risks when establishing their judgements. Similar approaches have been conducted in other studies [34, 40, 54, 66, 67, 100]. Samani et al. [35] use the PROMETHEE usual preference function to transform linguistic variables into numerical values.

Kripka et al. [57] use the AHP method based on Saaty's fundamental scale to determine a normalised score for each of the qualitative criteria considered in the sustainability assessment, namely, architectural value and security sensation. Other studies also base the scoring of qualitative data on such approach, such as [55, 60, 62].

3.4. Normalisation of the Indicators. When dealing with indicators that are measured in different units, and prior to proceed to their aggregation into a final score, indicator values shall be normalised into dimensionless, comparable values. The most basic normalisation technique used is the so-called linear normalisation and consists in dividing the indicator value x_{ij} of a particular alternative i associated with criterion j by the sum of the indicator values related to the complete set of alternatives:

$$\overline{x}_{ij} = \frac{x_{ij}}{\sum_i x_{ij}}. \tag{1}$$

Such approach is followed by the vast majority of studies reviewed [25, 29, 30, 34, 38–41, 47, 48, 52, 70, 89, 95]. When the decision-making problem involves the simultaneous consideration of both criteria with maximising and minimising optimal values, indicators are then normalised on the basis of the preferable optimum for each of them:

$$\begin{aligned} \overline{x}_{ij} &= \frac{x_{ij}}{\max_i \{x_{ij}\}}, \quad \text{where } \max_i \{x_{ij}\} \text{ is preferred,} \\ \overline{x}_{ij} &= \frac{\min_i \{x_{ij}\}}{x_{ij}}, \quad \text{where } \min_i \{x_{ij}\} \text{ is preferred.} \end{aligned} \tag{2}$$

Such approach is followed by [23, 28, 51, 101]. This normalisation technique based on the preferred optimum of each criterion has been extended into the so-called Weitendorf's linear normalisation, so as to take into consideration their distance to the worst value [68, 77, 85]:

$$\begin{aligned} \overline{x}_{ij} &= \frac{x_{ij} - x_{\min}}{x_{\max} - x_{\min}}, \quad \text{for maximising optima,} \\ \overline{x}_{ij} &= \frac{x_{\max} - x_{ij}}{x_{\max} - x_{\min}}, \quad \text{for minimising optima.} \end{aligned} \tag{3}$$

Other studies, such as [31, 36, 73, 81, 86, 87], normalise the values of the decision variables by using a vector normalisation technique, where each element x_{ij} of the decision matrix is normalised by dividing it by its norm:

$$\overline{x}_{ij} = \frac{x_{ij}}{\sqrt{\sum_i x_{ij}^2}}. \tag{4}$$

Particular value functions have been also used to normalise the indicator values into dimensionless values. So, studies based on the Simple Additive Weighting technique called MIVES [19, 21, 26, 32, 42–44, 50, 67, 74, 75, 82, 88, 92–94, 100] use exponential value functions defined as:

$$\overline{x}_{ij} = \left[1 - e^{-K_i\left(\left(x_{ij} - x_{\text{opt}}\right)/c_i\right)^{P_i}}\right] \cdot \left[1 - e^{-K_i\left(\left(x_{\text{opt}} - x_{ij}\right)/c_i\right)^{P_i}}\right], \tag{5}$$

where x_{opt} is the least preferable value of the indicator under evaluation, P_i is a shape factor that makes the value function be concave, linear, convex, or S-shaped, C_i is the curve's inflexion point, and K_i tends towards x_{ij} at the inflexion point.

The aggregation technique PROMETHEE also bases the normalisation step on the construction of preference functions. Vincke and Brans [109] proposed six basic types of preference functions. Depending on the nature of the criteria

to be assessed, different value functions shall be used. For example, Balali et al. [54] combine the use of V-shaped preference functions and linear preference functions. Samani et al. [35] use the usual preference function for qualitative criteria and the V-shaped function for the quantitative ones. Other preference functions such as exponential functions [53, 69, 76] are also used. One of the main advantages of using such exponential functions is that they are continuously defined and consequently easier to use when compared to the other discrete, stepped preference functions.

Finally, it shall be highlighted that the normalisation of indicator values only makes sense when the involved indicators are measured in different units. Thus, those studies based on the qualitative criteria assessment of experts, who set scores for each criterion based on their expertise [60, 62, 78], do not require such normalisation step prior to their aggregation.

3.5. Weighting Techniques. Weighting the criteria is an essential step in a decision-making process, as it will condition the results of an assessment. Figure 3 shows the weighting methods identified among the reviewed publications, as well as the number of times that each one has been applied. By far, the Analytic Hierarchy Process (AHP) is the most used method to determine the weights of the criteria considered in a decision-making process, used by 65.1% of the authors. This widely used method allows to transform, through a systematic procedure, the pairwise judgements emitted by a single or a group of decision makers into a relevance score, which will be used in the later assessment of the impacts. No particular relationship has been identified between the use of this weighting technique and either the year of publication or the type of infrastructure assessed.

The direct allocation of weights has been identified as the second most used method (16 papers, 19.3% of the publications). By using this technique, the evaluator directly sets the score that represents the importance of each criterion on the decision-making problem. Shanon entropy methods are used to provide weightings less based on the subjectivity inherent in the previously mentioned techniques by measuring the uncertainty associated with the provided judgements [23, 25, 54, 73, 87]. Similar results have been previously reported regarding the application frequency of AHP, direct allocation, and entropy methods in relation to the social sustainability of infrastructures [17].

At last, three other techniques have been marginally used, namely, the Best-Worst method (BWM) [41], the Quality Function Deployment (QFD) [40, 51], and the SWARA method [29] to assess the sustainability criteria weights. While the methodology related to the Best-Worst technique is close to the AHP, the Quality Function Deployment method has been used as a means to handle with complex and conflicting criteria, such as those describing sustainability, which can often be difficult to assess by decision makers. SWARA method is a so-called order relation technique based on the direct assignation of criteria relevance by a group of experts. It shall be noted that 4 contributions do not explicitly report the methodology used in the criteria weights assignation.

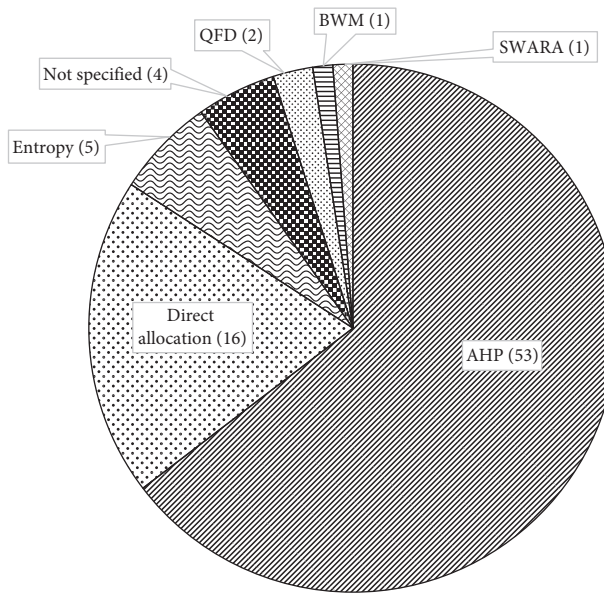

Figure 3: Weighting techniques applied within the reviewed papers.

3.6. Aggregation of Indicators. Once the relevance of each criterion is established, the next step in a decision-making process is to assess the obtained results. Figure 4 shows the frequency of use of the multicriteria assessment techniques applied in the reviewed contributions, as well as the specific infrastructure field in which they have been applied. The most frequently used technique is the Simple Additive Weighting (SAW) or direct aggregation of the criteria [110], which has been applied by 43 publications (51.8% of total). The popularity of this technique is based on its ease of application, as it consists in the simple addition of the normalised criteria scores weighted by their corresponding relevance factors obtained in a previous step. SAW is a compensatory technique that is revealed as a very intuitive tool for decision makers, based on an extremely simple and transparent calculation procedure. However, SAW is limited by the fact that it can only deal with maximising, positive defined criteria [111]. Minimising criteria should be properly converted to maximising ones before being used. Similar conversions should be applied to negative defined criteria. The results of the assessments using SAW technique depend therefore on the transformation applied [111].

Thus, to overcome such limitations when handling with more complex criteria, other MCDM methods are used. Among them, the most applied one is TOPSIS (Technique for Order Preference by Similarity to Ideal Solution), used by 15.7% (13 studies) of the reviewed papers. TOPSIS allows to rank different alternatives in a multicriteria context, considering the fact that the most preferred solution should have the shortest geometric

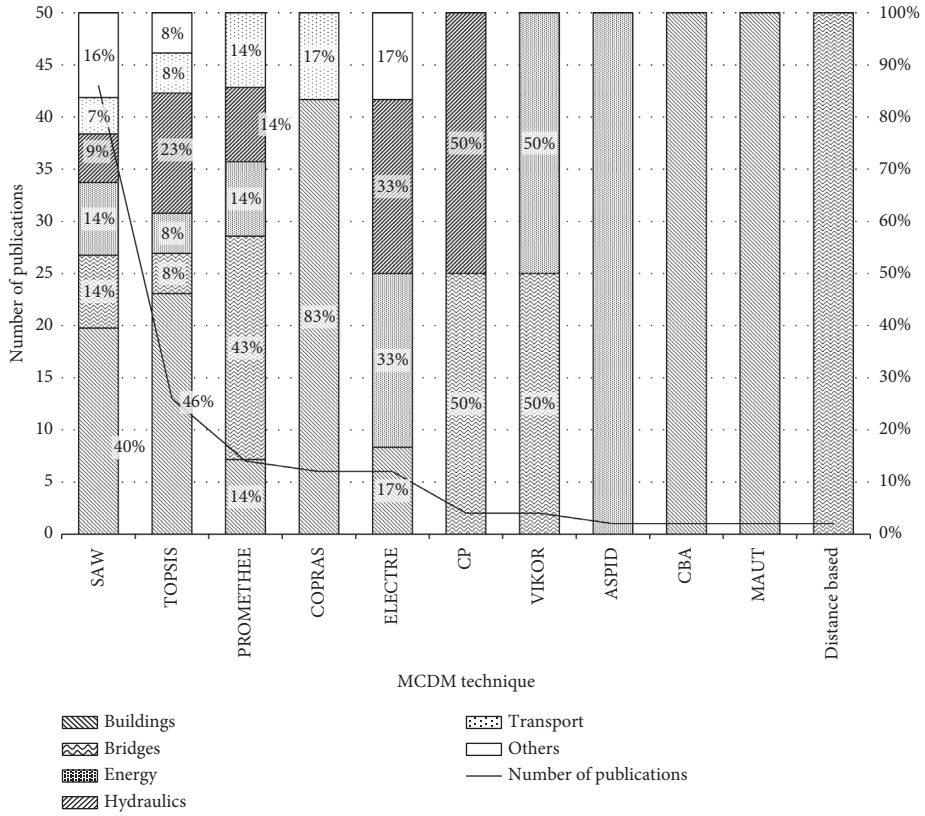

Figure 4: MCDM assessment techniques applied within the reviewed papers.

distance to the positive ideal solution and the longest distance to the less preferred solution [112]. TOPSIS is based on a simple, comprehensible concept that aims to represent the rationale of human decision processes [113]. Its high flexibility to accommodate to further extensions based on fuzzy sets or grey theory, for example, and its computational efficiency are additionally recognised advantages of this method [114]. Transparency along the decision-making process is revealed as an essential requirement when choosing an adequate MCDM method [115]. The traceability of the analysis, i.e., the ability to investigate into the different analysis steps to identify strengths and weaknesses of each alternative under evaluation, is considered as a main source to provide argumentation in a decision-making process. The transparency associated with TOPSIS is one of the main advantages of this technique [114].

PROMETHEE has been applied in 8.4% of the papers reviewed. This outranking method has suffered different modifications over the course of time, so as to overcome some of its initial limitations. PROMETHEE III, for example, does not even require the variables to be normalised and is applicable when information is missing [116]. However, PROMETHEE techniques are recognised to be very time consuming and not intuitive, making it often difficult to keep an overview over the problem when a significant number of criteria are involved [117]. In addition, in some cases, the ranking of alternatives can drastically change and even reverse when a new alternative is introduced [53], which is one of the main disadvantages of these techniques.

7.2% of the studies reviewed use ELECTRE in their assessments. ELECTRE is another outranking technique based on concordance analysis. This noncompensatory method is particularly useful when ordinal scales are used to measure criteria [86]. It has the ability to include vagueness and uncertainty in the assessments, but, as with PROMETHEE, outcomes can be hard to explain [111]. As the outcomes are provided as an ordinal ranking, ELECTRE does not allow the decision makers to identify the particular strengths and weaknesses of the assessed alternatives, or even determine how much better an alternative is over the rest [118]. One of the advantages of ELECTRE methods is that, in contrast to PROMETHEE techniques, they do not rely on the selection or construction of appropriate utility functions by the decision makers, which are not always straightforward and may condition the assessment results.

COPRAS has also turned out to be one of the most used techniques in sustainability assessment of infrastructures. As ELECTRE method, COPRAS has been applied in 7.2% of the papers reviewed. COPRAS is recognised to be simple to calculate and, in contrast with SAW, adequate when dealing with both maximising and minimising criteria values [119]. Other MCDM techniques, such as Cost-Benefit Analysis (CBA) [24], Compromise Programming (CP) [61, 84], Multiattribute Utility Theory (MAUT) [22], Analysis and Synthesis of Parameters under Information Deficiency (ASPID) [64], Distance-Based methods [56], and VIKOR

technique [57, 66], have been marginally applied to assess the sustainability of particular infrastructure designs. Although no systematic relationship is found between the MCDM method applied and the field of assessment or the weighting method used, it is interesting to note that five out of the six publications using COPRAS are focused on the sustainability evaluation of buildings.

It shall be noted that the proportions found in the present review regarding the use of MCDM techniques for the sustainability assessment of infrastructures have also been found in other fields of application. As an example, Kaya et al. [120] report that 44% of the studies dealing with the assessment of energy policies use SAW technique, 23% TOPSIS, 8% PROMETHEE, and 6% ELECTRE, results that are quite similar to the ones obtained in the present review. Likewise, Mardani et al. [121] focus on the use of MCDM techniques to solve management problems associated with construction, risk, and safety and report that 33% of the reviewed studies use SAW, 11% TOPSIS, 8% ELECTRE, and 6% PROMETHEE. Similar results are reported by other studies, dealing with application fields such as mining and mineral processing [122].

Besides SAW, TOPSIS is revealed as the most used method to assess MCDM problems in different fields, such as supplier selection [123], manufacturing and product recovery [124], supply chain management [125], or material selection in the automotive industry [126], just to cite some examples. After analysing the use of MCDM in other fields of application, it shall be concluded that the trends detected in the field of sustainability assessment of infrastructures are quite similar to those popular in other fields.

3.7. Sensitivity Analysis. An important step in MCDM problems is to perform sensitivity analyses on those aspects that might alter significantly the conclusions of the assessment, so as to ensure the consistency of the final decision. From the total of the reviewed studies, only 18 (21.7%) include a sensitivity analysis in their assessments.

The majority of them (13 out of 18 manuscripts) focus their attention on the results sensitivity against the chosen criteria weights. This evidences that the weighting is considered as a great source of uncertainty in MCDM problems, usually derived from the subjectivity inherent to weighting based on experts' judgements [127]. The nonprobabilistic uncertainty introduced in MCDM problems through experts' opinions is greater the more complex is the problem. So, when dealing with sustainability assessments, where criteria are often conflicting and usually of very different nature, decision makers might be unable to provide precise judgements and become overwhelmed by the problem to be assessed.

The usual way to proceed is to make one of the involved decision criteria predominant with respect to the rest and compare the results with the ones obtained after the conventional weighting [21, 28, 67, 77, 82, 93–95]. This allows the decision makers identify those criteria where the subjectivity is greater and is therefore more sensitive to experts' biases. Mosalam et al. [22] analyse different weighting scenarios where the weighting of one of the criteria is changed continuously, from 0% to 100%. By doing so, the decision maker is able to determine for which weights the results are more prone to change and check if the weights obtained in his/her analysis are close to such thresholds or not.

Ignatius et al. [40] and Heravi et al. [45] perform a sensitivity analysis on the power assigned to each of the involved experts in the decision-making problem. Several authors also focus on the sensitivity that the obtained results have on the parameters defining the aggregation techniques that they are using. So, Gervásio and Da Silva [53] evaluate the sensitivity of the results on the PROMETHEE preference function used to normalise the indicator values. In addition, a second sensitivity analysis is also conducted on the criteria weights. Similarly, Martin et al. [79] conduct a sensitivity analysis not only on the criteria weights, but on the selected indifference, preference, and veto thresholds assumed when using the ELECTRE method.

3.8. Dealing with the Experts' Subjectivity. MCDM problems have a highly subjective component, since they are generally based on the cognitive capacity of the decision makers, who are usually required to provide the relevance of each criterion and even to assign performance values to the selected criteria indicators, as derived from the results shown in the present literature review. However, during the application of the described steps inherent in a decision-making process, it is common practice to handle with so-called crisp or bivalued data. This is proved by 72.3% of the analysed manuscripts (60 papers), as shown in Figure 5. Such crisp approach to MCDM problems presumes the information provided by the judgements emitted by the decision makers to be absolutely precise and certain and has been therefore subject to strong criticism for not being able to reflect the vague and qualitative nature of human thinking [128]. So, when dealing with complex problems such as sustainability assessments, with criteria that are usually conflicting and only difficultly to be compared, neglecting the fuzziness of human thinking may lead to erroneous conclusions [128]. So as to deal with the mentioned nonprobabilistic uncertainties associated with human thinking, efforts have been made by several authors to apply different mathematical approaches to deal with the information resulting from the judgements of the decision makers. So, since 2007, 17 manuscripts (20.5% of total) have been found to apply the fuzzy sets theory [129] in the MCDM process for the sustainability assessment of infrastructures combined with a variety of weighting and MCDM techniques (AHP, TOPSIS, VIKOR, SAW, PROMETHEE, ELECTRE, and COPRAS). As an alternative, grey numbers have been recently applied by Heravi et al. [45] in the assessment of the sustainability of industrial buildings.

The fuzzy theory was further developed by Atanassov [130] into the intuitionistic fuzzy sets theory, which has been used in sustainability MCDM assessments of infrastructures only since 2013 [63, 69, 73, 87]. At present, the intuitionistic approach has been further generalised into the neutrosophic sets

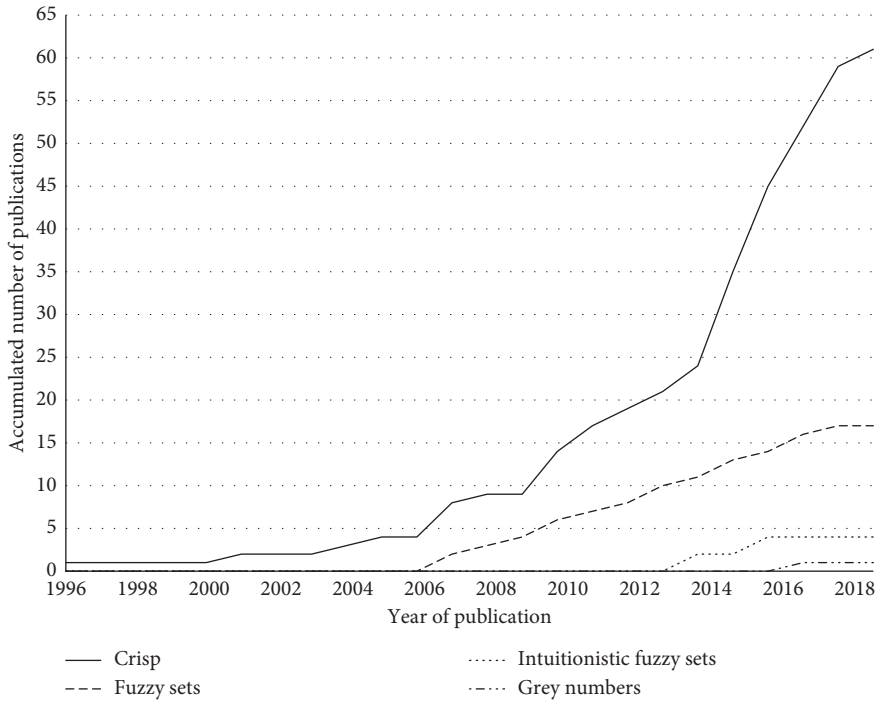

Figure 5: Handling of linguistic variables within the reviewed papers.

approach, developed by Smarandache in 1999 [131]. No application of the neutrosophic approach has yet been found to be applied in MCDM related to the infrastructure assessment.

4. Conclusions

This study presents a systematic literature review on the sustainability assessment of infrastructure projects and designs developed by means of MCDM techniques. Given the complex characterisation of sustainability, MCDM is revealed as a useful tool to integrate decision criteria related to the different dimensions of sustainability, namely, economy, environment, and society. MCDM has gained relevance to evaluate sustainability mainly since 2015, when the Sustainable Development Goals were set by the United Nations. In particular, MCDM has been found to be mainly applied for the assessment of buildings (38.6%), bridges (15.7%), energy infrastructure (14.5%), hydraulic infrastructure (13.3%), and transport infrastructure (7.2%). In view of the results, more efforts should be put in the sustainability analysis of infrastructures where long-lasting, intergenerational service lives are required, such as bridges or dams. In those cases, where the required service life frequently exceeds 100 years, and where the magnitude of the impacts is not negligible given the dimensions of the infrastructures and their material and maintenance demands, evaluating the sustainability throughout their life cycle acquires an essential relevance.

AHP is revealed as the most used weighting technique to identify the relevance of the decision criteria, being applied in 65.1% of the analysed studies. Regarding the assessment technique used to evaluate the final sustainability scores of the design alternatives under consideration, SAW has resulted to be by far the preferred option, used by 51.8% of the authors. This technique, despite its undoubted advantages, such as its ease of use, is limited by the fact that it can only deal with positive defined, maximising criteria. Given the complex relations between sustainability criteria, and their often conflicting nature, other techniques have been used by the scientific community, being TOPSIS the most applied (15.7% of the contributions).

Regarding the mathematical handling of the linguistic variables involved in MCDM process, where the main variables to derive the criteria weights are usually the judgements and opinion of experts, it has been found that the vast majority of manuscripts assume a crisp approach. It is first since 2007 when authors have started to implement the fuzziness of human judgements into the decision-making process. Although fuzzy sets theory, and to some extent even intuitionistic fuzzy sets theory, have been applied in the sustainability assessment of infrastructures, the recently developed and more generalised neutrosophic sets have not been used to date for such purpose.

Regarding the criteria considered in the assessments, it shall be said that 74.7% base their definition on the framework of the life cycle of the infrastructure, which is in good accordance with the temporal dimension of sustainability. However, although recognised standards exist that provide guidelines for coherent and robust life cycle analyses, it has been found that only 4.8% of the publications base their studies on such standards, properly defining basic concepts such as the functional unit or the system boundaries assumed in the evaluation. It shall also be noted that none of the studies base the definition of the social criteria and indicators on the "Guidelines for social life cycle assessment of products,"

which provides, at present, the most recognised methodology to perform social life cycle assessments. With regard to life cycle costing, only 6.1% of the authors take into consideration the discounting of costs related to time.

In view of the obtained review results, further research is required to integrate the existing life cycle impact assessment methodologies (economic, environmental, and social) into the multicriteria sustainability assessment of infrastructures, so as to provide robust and integral assessment tools based on a universal, systematic, and transparent methodology. In addition, further efforts should be made to consider the fuzziness of experts' judgements in future assessment models.

Conflicts of Interest

The authors declare that there are no conflicts of interest regarding the publication of this paper.

Acknowledgments

The authors acknowledge the financial support of the Spanish Ministry of Economy and Competitiveness, along with FEDER funding (Project no. BIA2017-85098-R).

References

[1] J.-H. Choi, "Strategy for reducing carbon dioxide emissions from maintenance and rehabilitation of highway pavement," *Journal of Cleaner Production*, vol. 209, pp. 88–100, 2019.

[2] J. Olivier, G. Janssens-Maenhout, M. Muntean, and J. Peters, "Trends in global CO2 emissions: 2016 report," PBL Netherlands Environmental Assessment Agency, The Hague, Netherlands, 2016.

[3] A. P. Kyriacou, L. Muinelo-Gallo, and O. Roca-Sagalés, "The efficiency of transport infrastructure investment and the role of government quality: an empirical analysis," *Transport Policy*, vol. 74, pp. 93–102, 2019.

[4] T. García-Segura, V. Yepes, J. V. Alcalá, and J. Alcalá, "Optimization of concrete I-beams using a new hybrid glowworm swarm algorithm," *Latin American Journal of Solids and Structures*, vol. 11, no. 7, pp. 1190–1205, 2014.

[5] V. Yepes, J. V. Martí, T. García-Segura, and F. González-Vidosa, "Heuristics in optimal detailed design of precast road bridges," *Archives of Civil and Mechanical Engineering*, vol. 17, no. 4, pp. 738–749, 2017.

[6] D. M. Frangopol, "Life-cycle performance, management, and optimisation of structural systems under uncertainty: accomplishments and challenges1," *Structure and Infrastructure Engineering*, vol. 7, no. 6, pp. 389–413, 2011.

[7] M. Safi, H. Sundquist, and R. Karoumi, "Cost-efficient procurement of bridge infrastructures by incorporating life-cycle cost analysis with bridge management systems," *Journal of Bridge Engineering*, vol. 20, no. 6, 2015.

[8] I. J. Navarro, V. Yepes, J. V. González-Vidosa, and F. González-Vidosa, "Life cycle impact assessment of corrosion preventive designs applied to prestressed concrete bridge decks," *Journal of Cleaner Production*, vol. 196, pp. 698–713, 2018.

[9] Y.-R. Zhang, W.-J. Wu, and Y.-F. Wang, "Bridge life cycle assessment with data uncertainty," *International Journal of Life Cycle Assessment*, vol. 21, no. 4, pp. 569–576, 2016.

[10] T. García-Segura, V. Penadés-Plà, and V. Yepes, "Sustainable bridge design by metamodel-assisted multi-objective optimization and decision-making under uncertainty," *Journal of Cleaner Production*, vol. 202, pp. 904–915, 2018.

[11] P. Van den Heede and N. De Belie, "A service life based global warming potential for high-volume fly ash concrete exposed to carbonation," *Construction and Building Materials*, vol. 55, pp. 183–193, 2014.

[12] A. M. Braga, J. D. Silvestre, and J. de Brito, "Compared environmental and economic impact from cradle to gate of concrete with natural and recycled coarse aggregates," *Journal of Cleaner Production*, vol. 162, pp. 529–543, 2017.

[13] M. U. Hossain, C. S. Poon, Y. H. Dong, I. M. C. Lo, and J. C. P. Cheng, "Development of social sustainability assessment method and a comparative case study on assessing recycled construction materials," *International Journal of Life Cycle Assessment*, vol. 23, no. 8, pp. 1654–1674, 2018.

[14] Y. H. Dong and S. T. Ng, "A social life cycle assessment model for building construction in Hong Kong," *International Journal of Life Cycle Assessment*, vol. 20, no. 8, pp. 1166–1180, 2015.

[15] L. A. Sierra, V. Yepes, T. García-Segura, and E. Pellicer, "Bayesian network method for decision-making about the social sustainability of infrastructure projects," *Journal of Cleaner Production*, vol. 176, pp. 521–534, 2018.

[16] L. Montalbán-Domingo, T. García-Segura, M. A. Sanz, and E. Pellicer, "Social sustainability criteria in public-work procurement: an international perspective," *Journal of Cleaner Production*, vol. 198, pp. 1355–1371, 2018.

[17] I. Zamarrón-Mieza, V. Yepes, and J. M. Moreno-Jiménez, "A systematic review of application of multi-criteria decision analysis for aging-dam management," *Journal of Cleaner Production*, vol. 147, pp. 217–230, 2017.

[18] L. A. Sierra, V. Yepes, and E. Pellicer, "A review of multi-criteria assessment of the social sustainability of infrastructures," *Journal of Cleaner Production*, vol. 187, pp. 496–513, 2018.

[19] A. Blanco, A. De la Fuente, and A. Aguado, "Sustainability analysis of steel fibre reinforced concrete slabs," in *Proceedings of the 2nd International Conference on Concrete Sustainability*, Madrid, Spain, June 2016.

[20] B. Reza, R. Sadiq, and K. Hewage, "Sustainability assessment of flooring systems in the city of Tehran: an AHP-based life cycle analysis," *Construction and Building Materials*, vol. 25, no. 4, pp. 2053–2066, 2011.

[21] O. Pons and A. De la Fuente, "Integrated sustainability assessment method applied to structural concrete columns," *Construction and Building Materials*, vol. 49, pp. 882–893, 2013.

[22] K. M. Mosalam, U. Alibrandi, H. Lee, and J. Armengou, "Performance-based engineering and multi-criteria decision analysis for sustainable and resilient building design," *Structural Safety*, vol. 74, pp. 1–13, 2018.

[23] J. Saparauskas, E. K. Zavadskas, and Z. Turskis, "Evaluation of alternative building designs according to the three criteria of optimality," in *Proceedings of the 10nd International Conference on Modern Building, structures and Techniques*, Vilnius, Lithuania, May 2010.

[24] K. Perini and P. Rosasco, "Cost-benefit analysis for green façades and living wall systems," *Building and Environment*, vol. 70, pp. 110–121, 2013.

[25] F. Jalaei, A. Jrade, and M. Nassiri, "Integrating decision support system (DSS) and building information modeling (BIM) to optimize the selection of sustainable building components," *Journal of Information Technology in Construction*, vol. 20, pp. 399–420, 2015.

[26] G. Gilani, A. Blanco, and A. d. l. Fuente, "A new sustainability assessment approach based on stakeholder's satisfaction for building façades," *Energy Procedia*, vol. 115, pp. 50–58, 2017.

[27] Z. Moussavi, A. Akbarnezhad, J. Ferre, and J. Xiao, "Multicriteria selection of façade systems based on sustainability criteria," *Building and Environment*, vol. 121, pp. 67–78, 2017.

[28] S. Guzmán-Sánchez, D. Jato-Espino, I. Lombillo, and J. M. Diaz-Sarachaga, "Assessment of the contributions of different flat roof types to achieving sustainable development," *Building and Environment*, vol. 141, pp. 182–192, 2018.

[29] S. Hashemkhani, M. Pourhossein, M. Yazdani, and E. K. Zavadskas, "Evaluating construction projects of hotels based on environmental sustainability with MCDM framework," *Alexandria Engineering Journal*, vol. 57, no. 1, pp. 357–365, 2018.

[30] A. Invidiata, M. Lavagna, and E. Ghisi, "Selecting design strategies using multi-criteria decision making to improve the sustainability of buildings," *Building and Environment*, vol. 139, pp. 58–68, 2018.

[31] M. Kamali, K. Hewage, and A. S. Milani, "Life cycle sustainability performance assessment framework for residential modular buildings: aggregated sustainability indices," *Building and Environment*, vol. 138, pp. 21–41, 2018.

[32] O. Pons and A. Aguado, "Integrated value model for sustainable assessment applied to technologies used to build schools in Catalonia, Spain," *Building and Environment*, vol. 53, pp. 49–58, 2012.

[33] P. O. Akidari, P. O. Olomolaiye, and E. A. Chintio, "Multicriteria evaluation model for the selection of sustainable materials for building projects," *Automation in Construction*, vol. 30, pp. 113–125, 2013.

[34] V. Motuziene, A. Rogoza, V. Lapinskiene, and T. Vilutiene, "Construction solutions for energy efficient single-family house based on its life cycle multi-criteria analysis: a case study," *Journal of Cleaner production*, vol. 112, pp. 532–541, 2016.

[35] P. Samani, A. Mendes, V. Leal, J. Miranda Guedes, and N. Correia, "A sustainability assessment of advanced materials for novel housing solutions," *Building and Environment*, vol. 92, pp. 182–191, 2015.

[36] F. A. Nassar, R. Ruparathna, G. Chhipi-Shrestha, H. Haider, K. Hewage, and R. Sadiq, "Sustainability assessment framework for low rise commercial buildings: life cycle impact index-based approach," *Clean Technologies and Environmental Policy*, vol. 18, no. 8, pp. 2579–25910, 2016.

[37] H. Alwaer and D. Clements-Croome, "Key performance indicators (KPIs) and priority setting in using the multi-attribute approach for assessing sustainable intelligent buildings," *Building and Environment*, vol. 45, no. 4, pp. 799–807, 2010.

[38] J. Yu, B. Dang, D. Clements-Croome, and S. Xu, "Sustainability assessment indicators and methodology for intelligent buildings," *Advanced Materials Research*, vol. 368–373, pp. 3829–3832, 2012.

[39] R. Drejeris and A. Kavolynas, "Multi-criteria evaluation of building sustainability behavior," *Procedia-Social and Behavioral Sciences*, vol. 110, pp. 502–511, 2014.

[40] J. Ignatius, A. Rahman, M. Yazdani, J. Šaparauskas, and S. H. Haron, "An integrated fuzzy ANP-QFD approach for green building assessment," *Journal of Civil Engineering and Management*, vol. 22, no. 4, pp. 551–563, 2016.

[41] H. Mahdiraji, S. Arzaghi, G. Stauskis, and E. K. Zavadskas, "A hybrid fuzzy BWM-COPRAS method for analyzing key factors of sustainable architecture," *Sustainability*, vol. 10, no. 5, 1626 pages, 2018.

[42] J. Lombera and I. Aprea, "A system approach to the environmental analysis of industrial buildings," *Building and Environment*, vol. 45, no. 3, pp. 673–683, 2010.

[43] J. Cuadrado, M. Zubizarreta, E. Rojí, and H. García, "Sustainability-related decision making in industrial buildings: an AHP analysis," *Mathematical Problems in Engineering*, vol. 2015, Article ID 157129, 13 pages, 2015.

[44] J. Cuadrado, M. Zubizarreta, E. Rojí, M. Larrauri, and I. Álvarez, "Sustainability assessment methodology for industrial buildings: three case studies," *Civil Engineering and Environmental Systems*, vol. 33, no. 2, pp. 106–124, 2016.

[45] G. Heravi, M. Fathi, and S. Faeghi, "Multi-criteria group decision-making method for optimal selection of sustainable industrial building options focused on petrochemical projects," *Journal of Cleaner Production*, vol. 142, pp. 2999–3013, 2017.

[46] A. Formisano and F. M. Mazzolani, "On the selection by MCDM methods of the optimal system for seismic retrofitting and vertical addition of existing buildings," *Computers and Structures*, vol. 159, pp. 1–13, 2015.

[47] G. Terracciano, G. Di Lorenzo, A. Formisano, and R. Landolfo, "Cold-formed thin-walled steel structures as vertical addition and energetic retrofitting systems of existing masonry buildings," *European Journal of Environmental and Civil Engineering*, vol. 19, no. 7, 2015.

[48] E. K. Zavadskas and J. Antucheviciene, "Multiple criteria evaluation of rural building's regeneration alternatives," *Building and Environment*, vol. 42, no. 1, pp. 436–451, 2007.

[49] E. K. Zavadskas and J. Antucheviciene, "Evaluation of buildings' redevelopment alternatives with an emphasis on the multipartite sustainability," *Journal of Strategic Property Management*, vol. 8, no. 2, pp. 121–128, 2010.

[50] S. Hosseini, A. De la Fuente, and O. Pons, "Multicriteria decision-making method for sustainable site location of post-disaster temporary housing in urban areas," *Journal of Construction Engineering and Management*, vol. 142, no. 9, 2016.

[51] H. Malekly, S. Meysam Mousavi, and H. Hashemi, "A fuzzy integrated methodology for evaluating conceptual bridge design," *Expert Systems with Applications*, vol. 37, no. 7, pp. 4910–4920, 2010.

[52] A. Farkas, "Multi-criteria comparison of bridge design," *Acta Polytechnica Hungarica*, vol. 8, no. 1, pp. 173–191, 2011.

[53] H. Gervásio and L. Simões da Silva, "A probabilistic decision-making approach for the sustainable assessment of infrastructures," *Expert Systems with Applications*, vol. 39, no. 8, pp. 7121–7131, 2012.

[54] V. Balali, A. Mottaghi, O. Shoghli, and M. Golabchi, "Selection of appropriate material, construction technique, and structural system of bridges by use of multicriteria decision-making method," *Transportation Research Record: Journal of the Transportation Research Board*, vol. 2431, no. 1, pp. 79–87, 2014.

[55] P. Jakiel and D. Fabianowski, "FAHP model used for assessment of highway RC bridge structural and technological arrangements," *Expert Systems with Applications*, vol. 42, no. 8, pp. 4054–4061, 2015.

[56] V. Yepes, T. García-Segura, and J. M. Moreno-Jiménez, "A cognitive approach for the multi-objective optimization of

RC structural problems," *Archives of Civil and Mechanical Engineering*, vol. 15, no. 4, pp. 1024–1036, 2015.

[57] M. Kripka, V. Yepes, and C. J. Milani, "Selection of sustainable short-span bridge design in Brazil," *Sustainability*, vol. 11, no. 5, p. 1307, 2019.

[58] Y.-M. Wang, J. Liu, and T. M. S. Elhag, "An integrated AHP-DEA methodology for bridge risk assessment," *Computers and Industrial Engineering*, vol. 54, no. 3, pp. 513–525, 2008.

[59] S. Dabous and S. Alkass, "Decision support method for multi-criteria selection of bridge rehabilitation strategy," *Construction Management and Economics*, vol. 26, pp. 883–893, 2008.

[60] M. Rashidi, B. Samali, and P. Sharafi, "A new model for bridge management: Part B: decision support system for remediation planning," *Australian Journal of Civil Engineering*, vol. 14, no. 1, pp. 46–53, 2016.

[61] M. Mikawi, "A methodology for the evaluation of the use of advanced composites in structural civil engineering applications," *Composites Part B: Engineering*, vol. 27, pp. 203–215, 1996.

[62] M. Rashidi, M. Ghodrat, B. Samali, B. Kendall, and C. Zhang, "Remedial modelling of steel bridges through application of Analytical Hierarchy Process (AHP)," *Applied Sciences*, vol. 7, no. 2, p. 168, 2017.

[63] T.-Y. Chen, "The extended linear assignment method for multiple criteria decision analysis based on interval-valued intuitionistic fuzzy sets," *Applied Mathematical Modelling*, vol. 38, no. 7-8, pp. 2101–2117, 2014.

[64] F. Begic and N. H. Afgan, "Sustainability assessment tool for the decision making in selection of energy system—Bosnian case," *Energy*, vol. 32, no. 10, pp. 1979–1985, 2007.

[65] M. Jovanovic, N. Afgan, P. Radovanovic, and V. Stevanovic, "Sustainable development of the Belgrade energy system," *Energy*, vol. 34, no. 5, pp. 532–539, 2009.

[66] T. Kaya and C. Kahraman, "Multicriteria renewable energy planning using an integrated fuzzy VIKOR & AHP methodology: the case of Istanbul," *Energy*, vol. 35, no. 6, pp. 2517–2527, 2010.

[67] J. Barros, M. Coira, M. López, and A. Gochi, "Assessing the global sustainability of different electricity generation systems," *Energy*, vol. 89, pp. 473–489, 2015.

[68] S. J. W. Klein and S. Whalley, "Comparing the sustainability of U.S. electricity options through multi-criteria decision analysis," *Energy Policy*, vol. 79, pp. 127–149, 2015.

[69] M. Montajabiha, "An extended PROMETHE II multi-criteria group decision making technique based on intuitionistic fuzzy logic for sustainable energy planning," *Group Decision and Negotiation*, vol. 25, no. 2, pp. 221–244, 2016.

[70] S. Väisänen, M. Mikkilä, J. Havukainen, L. Sokka, M. Luoranen, and M. Horttanainen, "Using a multi-method approach for decision-making about a sustainable local distributed energy system: a case study from Finland," *Journal of Cleaner Production*, vol. 137, pp. 1330–1338, 2016.

[71] A. Fetanat and E. Khorasaninejad, "A novel hybrid MCDM approach for offshore wind farm site selection: a case study of Iran," *Ocean and Coastal Management*, vol. 109, pp. 17–28, 2015.

[72] S. Medina-González, A. Espuña, and L. Puigjaner, "An efficient uncertainty representation for the design of sustainable energy generation systems," *Chemical Engineering Research and Design*, vol. 131, pp. 144–159, 2018.

[73] S. Gumus, M. Kucukvar, and O. Tatari, "Intuitionistic fuzzy multi-criteria decision making framework based on life cycle environmental, economic and social impacts: the case of U.S. wind energy," *Sustainable Production and Consumption*, vol. 8, pp. 78–92, 2016.

[74] A. De la Fuente, J. Armengou, O. Pons, and A. Aguado, "Multi-criteria decision-making model for assessing the sustainability index of wind-turbine support systems: application to a new precast concrete alternative," *Journal of Civil Engineering and Management*, vol. 23, no. 2, 2017.

[75] O. Pons, A. De la Fuente, J. Armengou, and A. Aguado, "Towards the sustainability in the design of wind towers," *Energy Procedia*, vol. 115, pp. 41–49, 2017.

[76] A. Gento, "Selection of a dam in the river basin of river Duero by promethee method," in *Proceedings of the International Conference on Modelling and Simulation*, pp. 341–347, Orlando, FL, USA, May 2004.

[77] A. Afshar, M. A. Mariño, M. Saadatpour, and A. Afshar, "Fuzzy TOPSIS multi-criteria decision analysis applied to Karun reservoirs system," *Water Resources Management*, vol. 25, no. 2, pp. 545–563, 2011.

[78] X. Sun, P. Ning, X. Tang et al., "Environmental risk assessment system for phosphogypsum tailing dams," *The Scientific World Journal*, vol. 2013, Article ID 680798, 13 pages, 2013.

[79] C. Martin, Y. Ruperd, and M. Legret, "Urban stormwater drainage management: the development of a multicriteria decision aid approach for best management practices," *European Journal of Operational Research*, vol. 181, no. 1, pp. 338–349, 2007.

[80] X. Dong, S. Zeng, J. Chen, and D. Zhao, "An integrated assessment method of urban drainage system: a case study in Shenzhen City, China," *Frontiers of Environmental Science and Engineering in China*, vol. 2, no. 2, pp. 150–156, 2008.

[81] Y. Tahmasebi and F. Yazdandoost, "An integrated framework to evaluate resilient-sustainable urban drainage management plans using a combined-adaptive MCDM technique," *Water Resources Management*, vol. 32, no. 8, pp. 2817–2835, 2018.

[82] A. De la Fuente, O. Pons, A. Josa, and A. Aguado, "Multi-criteria decision making in the sustainability assessment of sewerage pipe systems," *Journal of Cleaner Production*, vol. 112, pp. 4762–4770, 2016.

[83] J. Jaber and M. Mohsen, "Evaluation of non-conventional water resources supply in Jordan," *Desalination*, vol. 136, no. 1–3, pp. 83–92, 2001.

[84] A. Abrishamchi, A. Ebrahimian, M. Tajrishi, and M. A. Mariño, "Case study: application of multicriteria decision making to urban water supply," *Journal of Water Resources Planning and Management*, vol. 131, no. 4, pp. 326–335, 2005.

[85] U. Pascal, Q. Xie, and L. Xu, "A fuzzy TOPSIS model framework for ranking sustainable water supply alternatives," *Water Resources Management*, vol. 31, pp. 2579–2593, 2017.

[86] G. Chhipi-Shrestha, K. Hewage, and R. Sadiq, "Selecting sustainability indicators for small to medium sized urban water systems using fuzzy-ELECTRE," *Water Environment Research*, vol. 89, no. 3, pp. 238–249, 2017.

[87] M. Kucukvar, S. Gumus, G. Egilmez, and O. Tatari, "Ranking the sustainability performance of pavements: an intuitionistic fuzzy decision making method," *Automation in Construction*, vol. 40, pp. 33–43, 2014.

[88] D. Jato-Espino, J. Rodriguez-Hernandez, V. C. Andrés-Valeri, and F. Ballester-Muñoz, "A fuzzy stochastic multi-

criteria model for the selection of urban pervious pavements," *Expert Systems with Applications*, vol. 41, no. 15, pp. 6807–6817, 2014.

[89] C. Torres-Machí, A. Chamorro, E. Pellicer, V. Yepes, and C. Videla, "Sustainable pavement management," *Transportation Research Record: Journal of the Transportation Research Board*, vol. 2523, no. 1, pp. 56–63, 2015.

[90] J. Santos, S. Bressi, V. Cerezo, and D. Lo Presti, "SUP&R DSS: SUP&R DSS: a sustainability-based decision support system for road pavements," *Journal of Cleaner Production*, vol. 206, pp. 524–540, 2019.

[91] S. Hashemkhani, N. Rezaeiniya, E. Zavadskas, and Z. Turskis, "Forest roads locating based on AHP and on COPRAS-G methods: an empirical study based on Iran," *Economics and Management*, vol. 4, pp. 6–20, 2011.

[92] U. Oses, E. Rojí, J. Cuadrado, and M. Larrauri, "Multiple-criteriadecision-making tool for local governments to evaluate the global and local sustainability of transportation systems in urban areas: case study," *Journal of Urban Planning and Development*, vol. 144, no. 1, 2017.

[93] A. De la Fuente, A. Blanco, S. Cavalaro, and A. Aguado, "Sustainability assessment of precast concrete segments for TBM tunnels," in *Proceedings of the 2nd International Conference on Concrete Sustainability*, Madrid, Spain, June 2016.

[94] A. De la Fuente, A. Blanco, J. Armengou, and A. Aguado, "Sustainability based-approach to determine the concrete type and reinforcement configuration of TBM tunnels linings. Case study: extension line to Barcelona Airport T1," *Tunnelling and Underground Space Technology*, vol. 61, pp. 179–188, 2017.

[95] N. Asgari, A. Hassani, D. Jones, and H. H. Nguye, "Sustainability ranking of the UK major ports: methodology and case study," *Transportation Research Part E: Logistics and Transportation Review*, vol. 78, pp. 19–39, 2015.

[96] G. Banias, C. Achillas, C. Vlachokostas, N. Moussiopoulos, and S. Tarsenis, "Assessing multiple criteria for the optimal location of a construction and demolition waste management facility," *Building and Environment*, vol. 45, no. 10, pp. 2317–2326, 2010.

[97] M. Rochikashvili and J. C. Bongaerts, "Multi-criteriadecision-making for sustainable wall paints and coatings using Analytic Hierarchy Process," *Energy Procedia*, vol. 96, pp. 923–933, 2016.

[98] O. Ugwu and T. Haupt, "Key performance indicators and assessment methods for infrastructure sustainability—a South African construction industry perspective," *Building and Environment*, vol. 42, no. 2, pp. 665–680, 2007.

[99] J. Saparauskas, "The main aspects of sustainability evaluation in construction," in *Proceedings of the 9th International Conference on Modern Building Materials, Structures and Techniques*, Vilnius, Lithuania, May 2007.

[100] J. P. Reyes, J. T. San-José, J. Cuadrado, and R. Sancibrian, "Health & Safety criteria for determining the sustainable value of construction projects," *Safety Science*, vol. 62, pp. 221–232, 2014.

[101] N. Dobrovolskiiene and R. Tamosiuniene, "An index to measure sustainability of a business project in construction industry: Lithuanian case," *Sustainability*, vol. 8, no. 1, 2016.

[102] ISO, *Environmental Management:—Life Cycle Assessment—Principles and Framework*, International Standards Organization, Geneva, Switzerland, 2006.

[103] ISO, *Environmental Management—Life Cycle Assessment—Requirements and Guidelines*, International Standards Organization, Geneva, Switzerland, 2006.

[104] D. Hunkeler, K. Lichtenvort, G. Rebitzer et al., *Environmental Life Cycle Costing*, SETAC Publications, Brussels, Belgium, 2008.

[105] UNEP/SETAC, "Guidelines for social life cycle assessment of products," in *Proceedings of the Paris SETAC Life Cycle Initiative United Nations Environment Programme*, Paris, France, January 2009.

[106] M. Marzourk and S. Azab, "Environmental and economic impact assessment of construction and demolition waste disposal using system dynamics," *Resources, Conservation and Recycling*, vol. 82, pp. 41–49, 2014.

[107] UNEP/SETAC, *The Methodological Sheets for Subcategories in Social Life Cycle Assessment (S-LCA)*, UNEP-SETACLife-Cycle Initiative, Paris, France, 2013.

[108] I. J. Navarro, V. Yepes, and J. V. Martí, "Social life cycle assessment of concrete bridge decks exposed to aggressive environments," *Environmental Impact Assessment Review*, vol. 72, pp. 50–63, 2018.

[109] P. Vincke and J. Brans, "A preference ranking organization method. The PROMETHEE method for MCDM," *Management Science*, vol. 31, pp. 647–656, 1985.

[110] Y. B. Shin, S. Lee, S. G. Chun, and D. Chung, "A critical review of popular multi-criteria decision making methodologies," *Issues in Information Systems*, vol. 14, no. 1, pp. 358–365, 2013.

[111] M. Velasquez and P. T. Hester, "An analysis of multi-criteria decision making methods," *International Journal of Operations Research*, vol. 10, no. 2, pp. 56–66, 2013.

[112] V. Penadés-Plà, T. García-Segura, J. V. Martí, and V. Yepes, "A review of multi-criteria decision-making methods applied to the sustainable bridge design," *Sustainability*, vol. 8, no. 12, p. 1295, 2016.

[113] E. Roszkowska, "Multi-criteria decision making models by applying the TOPSIS method to crisp and interval data," *Multiple Criteria Decision Making*, vol. 6, 2011.

[114] C. C. Hung and L. H. Chen, "A fuzzy TOPSIS decision making model with Entropy weight under intuitionistic fuzzy environment," in *Proceedings of the International Multi-Conference of Engineers and Computer Scientists IMECS*, Hong Kong, Japan, March 2009.

[115] P. Goodwin and G. Wright, *Decision Analysis for Management Judgment*, John Wiley & Sons, Chichester, UK, 2000.

[116] A. Pires, N. B. Chang, and G. Martinho, "An AHP-based fuzzy interval TOPSIS assessment for sustainable expansion of the solid waste management system in Setúbal Peninsula, Portugal," *Resources, Conservation and Recycling*, vol. 56, pp. 7–21, 2011.

[117] G. Kabir, R. Sadiq, and S. Tesfamariam, "A review of multi-criteria decision-making methods for infrastructure management," *Structure and Infrastructure Engineering*, vol. 10, no. 9, pp. 1176–1210, 2014.

[118] M. E. Ahmine, J. Pailles, and N. Perry, "Comparison of different multiple-criteria decision analysis methods in the context of conceptual design: application to the development of a solar collector structure," in *Proceedings of Joint Conference on Mechanical, Design Engineering & Advanced Manufacturing*, Toulouse, France, June 2014.

[119] V. Podvezko, "The comparative analysis of MCDA methods SAW and COPRAS," *Engineering Economics*, vol. 22, no. 2, 2011.

[120] İ. Kaya, M. Çolak, and F. Terzi, "Use of MCDM techniques for energy policy and decision-making problems: a review," *International Journal of Energy Research*, vol. 42, no. 7, pp. 2344–2372, 2018.

[121] A. Mardani, A. Jusoh, K. Nor, Z. Khalifah, N. Zakwan, and A. Valipour, "Multiple criteria decision-making techniques and their applications—a review of the literature from 2000 to 2014," *Economic Research*, vol. 28, 2015.

[122] F. Sitorus, J. J. Cilliers, and P. R. Brito-Parada, "Multi-criteria decision making for the choice problem in mining and mineral processing: applications and trends," *Expert Systems with Applications*, vol. 121, pp. 393–417, 2019.

[123] K. Renganath and M. Suresh, "Supplier selection using fuzzy MCDM techniques: a literature review," in *Proceedings of the IEEE International Conference on Computational Intelligence and Computing Research (ICCIC)*, Chennai, India, December 2016.

[124] M. A. Ilgin, S. M. Gupta, and O. Battaïa, "Use of MCDM techniques in environmentally conscious manufacturing and product recovery: state of the art," *Journal of Manufacturing Systems*, vol. 37, pp. 746–758, 2015.

[125] S. A. Khan, A. Chaabane, and F. T. Dweiri, "Multi-criteriadecision-making methods application in supply chain management: a systematic literature review," in *Multi-Criteria Methods and Techniques Applied to Supply Chain Management*, IntechOpen, London, UK, 2018.

[126] M. Noryani, S. M. Sapuan, M. T. Mastura et al., "Multi-criteriadecision-making tools for material selection of natural fibre composites: a review," *Journal of Mechanical Engineering and Sciences*, vol. 12, no. 1, pp. 3330–3353, 2018.

[127] L. Scholten, N. Schuwirth, P. Reichert, and J. Lienert, "Tackling uncertainty in multi-criteria decision analysis—an application to water supply infrastructure planning," *European Journal of Operational Research*, vol. 242, no. 1, pp. 243–260, 2015.

[128] N. Radwan, M. Senousy, and A. Riad, "Neutrosophic AHP Multi-Criteria Decision Making method applied on the selection of learning management system," *International Journal of Advancements in Computing Technology*, vol. 8, no. 5, pp. 95–105, 2016.

[129] L. A. Zadeh, "Fuzzy sets," *Information and Control*, vol. 8, no. 3, pp. 338–353, 1965.

[130] K. Atanassov, "Intuitionistic fuzzy sets," *Fuzzy Sets and Systems*, vol. 20, no. 1, pp. 87–96, 1986.

[131] F. Smarandache, *A Unifying Field in Logics, Neutrosophy: Neutrosophic Probability, Set and Logic*, American Research Press, Rehoboth, NM, USA, 1999.

Hindawi
Advances in Civil Engineering
Volume 2019, Article ID 7168703, 9 pages
https://doi.org/10.1155/2019/7168703

Research Article

Optimization of the Mixture Design of Low-CO_2 High-Strength Concrete Containing Silica Fume

Seung-Jun Kwon [1] **and Xiao-Yong Wang** [2]

[1]*Department of Civil and Environmental Engineering, Hannam University, Daejeon-Si, Republic of Korea*
[2]*Department of Architectural Engineering, Kangwon National University, Chuncheon-Si, Republic of Korea*

Correspondence should be addressed to Xiao-Yong Wang; wxbrave@kangwon.ac.kr

Received 15 March 2019; Accepted 23 May 2019; Published 11 June 2019

Guest Editor: Endong Wang

As abundant CO_2 is released by high-strength concrete due to its high binder content, the reduction of CO_2 emissions has become increasingly important. This study proposed a general procedure to optimize the mixture design of low-CO_2 high-strength concrete containing silica fume. First, the equations for evaluating strength and slump were regressed based on available experimental results. CO_2 emissions were calculated based on the concrete mixtures and the unit CO_2 emissions of the concrete components. By using the genetic algorithm, the concrete mixtures with the lowest CO_2 emissions were determined by considering various constraints. Second, the cost of concrete was calculated based on the concrete mixtures and the unit cost of the concrete components. Similarly, the concrete mixtures with the lowest cost were determined based on the genetic algorithm. We found that, in some cases, the mixtures with the lowest CO_2 emissions were different from those with the lowest cost. Third, through adding the constraint equation of cost, Pareto optimal mixtures with relatively lower CO_2 emissions and lower cost were determined. In summary, the proposed technique is valuable for designing high-strength concrete considering both CO_2 emissions and cost.

1. Introduction

High-strength concrete is increasingly used in the modern construction industry. Many advantages can be achieved by using high-strength concrete such as reducing the quantity of sections needed in structural elements, increasing the occupancy rate of buildings, and extending the service life of the building [1]. However, high-strength concrete generally has a lower water-to-binder ratio than normal strength concrete. As abundant binder is used and lots of CO_2 is released when producing high-strength concrete, the reduction of CO_2 emissions has become more and more important [2].

Fundamental studies have been conducted regarding the evaluation of CO_2 emissions of high-strength concrete. Larsen et al. [3] found that ultra-high-performance concrete could offer increased benefits over traditional concrete design. Voo and Foster [4] and Yu et al. [5] proposed that using slag in producing ultra-high-performance concrete could reduce CO_2 emissions and embodied energy and save total life cycle cost. Park et al. [6] assessed the life cycle CO_2 emissions of concrete with different strength levels and found that life cycle CO_2 increased linearly as the compressive strength increased. Kim et al. [7] proposed a method for evaluating CO_2 emissions from the production process of concrete and found that the application of high-strength concrete and the standardization of the mixing process could reduce CO_2 emissions in the construction stage. Latawiec et al. [8] proposed an index for concrete desirability where the effects of compressive strength, durability, CO_2 emissions, and cost on concrete desirability were considered.

On the other hand, some methods have been proposed for the material design of low-CO_2 or low-cost concrete. Based on neural networks and the genetic algorithm, Yeh [9] proposed software for designing concrete mixtures with the

lowest possible cost. Mosaberpanah and Eren [10] proposed a full factorial method to maximize the strength and minimize the carbon dioxide emissions. The effects of cement content, silica fume content, fiber content, water-to-binder ratio, and superplasticizer are considered for determining strength and CO_2 emissions. Yang et al. [11] proposed an approach for designing low-CO_2 concrete containing various supplementary cementitious materials such as fly ash, slag, and silica fume. Tapali et al. [12] proposed an iteration approach to design concrete with a low environmental cost, considering strength and service life. Khan et al. [13] designed low-cost high-strength self-compacting concrete using a response surface methodology. The optimal combinations of cement, water-to-binder ratio, fine aggregate, fly ash, and superplasticizer were determined using a desirability function. Ji et al. [14] combined neural networks and a harmony search algorithm to find the optimal design of reactive powder concrete with the lowest cost. Although many studies [9–14] have been carried out on the design of low-CO_2 or low-cost concrete, some questions need to be further clarified: first, what are the differences between the mixture designs of low-CO_2 concrete and low-cost concrete? Second, how can we design concrete with both low CO_2 emissions and low cost? Third, how can we create a general design procedure of low-CO_2 concrete for different countries whose design codes may be different?

In this study, we proposed a general procedure to optimize the mixture design of low-CO_2 high-strength concrete containing silica fume. By using the genetic algorithm, concrete mixtures with the lowest CO_2 emissions and lowest cost were individually determined. We found that, for some cases, the mixtures with the lowest CO_2 emissions were different from those with the lowest cost. Furthermore, through adding the constraint equation of cost, Pareto optimal mixtures with relatively lower CO_2 emissions and lower cost were determined.

The innovations of this study are summarized as follows: first, we propose a general method for designing low-CO_2 concrete; second, we consider the difference between low-CO_2 concrete and low-cost concrete; third, we propose a Pareto optimal method to determine mixtures with lower CO_2 and lower cost.

2. Optimization Design of Concrete Mix Proportions

To optimize the mixing proportions of high-strength concrete containing silica fume, the object function and constraint conditions need to be established. In this study, the CO_2 emissions were placed as the object function. The constraint conditions were the desired concrete strength, workability, component contents, component ratios, and absolute volume [9].

2.1. Object Function. The total CO_2 emissions of silica fume-blended concrete include CO_2 emissions from the concrete materials and transport and from the mixing of the concrete [15]. The total CO_2 emissions can be calculated from the following equation [15]:

$$CO_{2-e} = CO_{2-eM} + CO_{2-eT} + CO_{2-eP} \quad (1)$$

where CO_{2-e}, CO_{2-eM}, CO_{2-eT}, and CO_{2-eP} represent the total CO_2 emissions, CO_2 emissions from concrete materials, CO_2 emissions from transport, and CO_2 emissions from the mixing operation of concrete, respectively. CO_{2-eM} can be calculated according to the concrete mixture and unit CO_2 emissions of the concrete components as follows:

$$\begin{aligned} CO_{2-eM} = {} & CO_{2-C} * C + CO_{2-SF} * SF + CO_{2-W} * W \\ & + CO_{2-CA} * CA + CO_{2-S} * S + CO_{2-SP} * SP \end{aligned} \quad (2)$$

where CO_{2-C}, CO_{2-SF}, CO_{2-W}, CO_{2-CA}, CO_{2-S}, and CO_{2-SP} are the unit CO_2 emissions of cement, silica fume, water, coarse aggregate, sand, and superplasticizer, respectively, and C, SF, W, CA, S, and SP are the masses of cement, silica fume, water, coarse aggregate, sand, and superplasticizer in the concrete mixtures, respectively. Table 1 shows the CO_2 emissions of the concrete components [11]. In this study, the object function was placed as CO_{2-eM}.

2.2. Constraint Conditions. The object function (the minimum CO_2 emission, CO_{2-eM}) is exposed to various constraints, for example, concrete strength, workability, component contents, component ratios, and absolute volume [9].

The strength constraint means that the design strength should be higher than the required strength. The formula for the strength constraint is shown as follows [9]:

$$f_c(t) \geq f_{cr}(t), \quad t = 3, 7, 28, \ldots, \text{days}, \quad (3)$$

where $f_c(t)$ is the concrete strength at age t and $f_{cr}(t)$ is the required strength at age t.

The workability constraint of fresh concrete is shown in the following equation [9]:

$$\text{Slump} \geq \text{Slump}^r, \quad (4)$$

where Slump^r is the required slump of concrete.

The range of component contents is shown as follows:

$$\text{lower} \leq \text{component} \leq \text{upper}, \quad (5)$$

where the components are the cement, silica fume, binder, water, fine aggregate, coarse aggregate, and superplasticizer. Table 2 shows the lower and upper limits of the contents of concrete components [16].

The component ratio constraint is shown as follows:

$$R_l \leq R_i \leq R_u, \quad (6)$$

where R_i is the component ratio (for example, the water-to-binder ratio, water-to-cement ratio, sand ratio, silica fume-to-binder ratio, and superplasticizer-to-binder ratio). R_l and R_u are the lower and upper limits of the component ratio, respectively. Table 3 shows the component ratio constraints [16]. Because the aim of this study is to design silica fume-blended concrete with high strength, the range of binder

Table 1: Unit CO_2 emissions of the concrete components [11].

Cement (kg/kg)	Silica fume (kg/kg)	Water (kg/kg)	Fine aggregate (kg/kg)	Coarse aggregate (kg/kg)	Superplasticizer (kg/kg)
0.931	1.05	0.000196	0.0026	0.0075	0.25

Table 2: Constraints of the contents of concrete components.

	Cement (kg/m^3)	Silica fume (kg/m^3)	Binder (cement + silica fume) (kg/m^3)	Water (kg/m^3)	Fine aggregate (kg/m^3)	Coarse aggregate (kg/m^3)
Lower limit	450	25	574	140	500	700
Upper limit	710	210	833	165	900	1050

Table 3: Constraints of the ratios of concrete components.

	Water-to-binder ratio	Water-to-cement ratio	Sand ratio	Silica fume-to-binder ratio	Superplasticizer-to-binder ratio
Lower limit	0.18	0.211	0.35	0.05	0.0188
Upper limit	0.27	0.317	0.39	0.25	0.0469

content is higher and the range of water-to-binder ratio is lower than those of ordinary strength concrete [9].

The absolute volume constraint is shown as follows:

$$\frac{W}{\rho_W} + \frac{C}{\rho_C} + \frac{SF}{\rho_{SF}} + \frac{S}{\rho_S} + \frac{CA}{\rho_{CA}} + \frac{SP}{\rho_{SP}} + V_{air} = 1, \quad (7)$$

where ρ_W, ρ_C, ρ_{SF}, ρ_S, ρ_{CA}, and ρ_{SP} are the densities of water, cement, silica fume, sand, coarse aggregate, and superplasticizer, respectively, and V_{air} is the volume of air in the concrete. The densities of water, cement, silica fume, sand, coarse aggregate, and superplasticizer are 1000, 3150, 2260, 2610, 2700, and 1220 kg/m^3, respectively. Equation (7) implies that the sum of each concrete component should equal 1 m^3 [9].

2.3. Property Evaluation of the Silica Fume-Blended Concrete. Lim et al. [16] conducted experimental studies on the strength and slump of silica fume-blended high-strength concrete where a total of 77 mixing proportions of concrete were studied. The effects of the water-to-binder ratio, water content, sand ratio, silica fume replacement ratio, and superplasticizer content on the mechanical workability of concrete were considered [16]. The compressive strength of high-strength concrete at 28 days ranged from 90 to 120 MPa. The slump of concrete ranged between 180 and 235 mm. The upper and lower limits of contents of concrete components are shown in Table 2. The upper and lower limits of the ratios of concrete components are shown in Table 3. Based on the experimental results of compressive strength [16], the strength of concrete at 28 days can be regressed as a function of the water-to-binder ratio, water content, sand ratio, and silica fume replacement ratio. The regression equation of compressive strength is shown as follows:

$$f_c = -182.90\frac{W}{C+SF} - 0.51 * W + 117.15\frac{S}{S+CA} + 49.49\frac{SF}{C+SF} + 170.17. \quad (8)$$

First, equation (8) shows that as the water content and water-to-binder ratio increases, concrete strength decreases. This is due to the increase in the porosity of the concrete. Next, as the sand ratio increases, the strength of the concrete increases. This is because when compared with coarse aggregate, the range of the interfacial transition zone of fine aggregate is not obvious [17]. Third, as the silica fume replacement ratio increases, the concrete strength increases. This is because the pozzolanic reaction of silica fume can produce secondary calcium silicate hydrate and improve the concrete strength. The correlation index between the experimental results and the regression results of compressive strength was 0.954. The high correlation index proves the validity of equation (8).

Based on the experimental results of slump [16], the slump of concrete can be regressed as a function of the water-to-binder ratio, water content, sand ratio, silica fume replacement ratio, and superplasticizer content. The regression equation of slump is shown as follows:

$$\text{slump} = 209.27 * \frac{W}{C+SF} + 1.33 * W - 325.10\frac{S}{S+CA} - 69.28 * \frac{SF}{C+SF} + 1.28 * SP + 63.30. \quad (9)$$

As shown in this equation, as the water content, superplasticizer content, and water-to-binder ratio increase, the concrete slump increases. As the sand ratio and silica fume replacement ratio increase, the concrete slump decreases.

Based on the mixtures of concrete, the superplasticizer content is determined as a function of the water-to-binder ratio and the silica fume replacement ratio [16]. The regression equation of superplasticizer content is shown as follows:

$$SP = 47.34 - 142.46\frac{W}{C+SF} + 28.77\frac{SF}{C+SF}. \quad (10)$$

As shown in this equation, as the water-to-binder ratio decreases or the silica fume replacement ratio increases, the superplasticizer content increases [18].

Summarily, within this section, we determined the object function and constraints of the concrete mixing proportions. The object function was the minimum CO_2 emissions, CO_{2-eM}. The constraints included various mechanical and constructability performance measures, for example, the compressive strength, workability of fresh concrete, component contents, component ratios, and absolute volume of the concrete mixture. Once the object's function and constraints are solved, concrete mixtures that meet various performance requirements can be acquired.

On the other hand, it should be noticed that the equations for evaluating strength, slump, and superplasticizer content are obtained from materials mixed by Lim et al. [16]. For other countries, because the compositions of binders and the varieties of superplasticizer may be different from Lim et al. [16], the calculation equations of strength, slump, and superplasticizer may also be different from those proposed in this study.

The technique for solving the object's function with constraints is the genetic algorithm. The genetic algorithm is an adaptive global optimization probability search algorithm that simulates the genetic and evolutionary processes of living things in the natural environment [19]. The process of the genetic algorithm is summarized as follows: Step 1: generate the initial population; Step 2: calculate the fitness; Step 3: select cross mutation operations, and compute fitness function; Step 4: check convergence criteria; and Step 5: repeat Step 3 until the convergence criteria are met.

In this study, we used the MATLAB global optimization toolbox for solving objective optimization with constraints [19]. The object function and constraints equation can be set in the MATLAB global optimization toolbox. According to the genetic algorithm, the optimal mixture which has the minimum CO_2 emission and can meet various constraints can be found.

3. Illustrative Examples

3.1. Design of Low-CO_2 High-Strength Concrete. In this section, examples are shown for the mixture design of low-CO_2 high-strength concrete with different strength levels such as 95, 100, 105, 110, and 115 MPa. The required slump was assumed to be 180 mm. The air content was assumed to be 2%. The object function of the genetic algorithm was the minimum CO_2 emission.

The strength of concrete can be evaluated using equation (8), the slump of concrete can be evaluated using equation (9), and CO_2 emissions can be evaluated using the unit CO_2 emission (Table 1) and concrete mixtures. The constraints included the range of the concrete components, range of the component ratios, and absolute volume. Based on the genetic algorithm that considers the various constraints, the mixtures were calculated and are shown in Table 4. The strengths of Mix1, Mix2, Mix3, Mix4, and Mix5 were 95, 100, 105, 110, and 115 MPa, respectively. The following results were obtained based on the contents of Table 4. First, as the required strength of concrete increased, the silica fume contents in the mixtures also increased. This shows the significance of silica fume in producing high-strength concrete. Second, the water contents for concrete with higher strengths, such as Mix3 (105 MPa), Mix4 (110 MPa), and Mix5 (115 MPa), were equal to the lower limit of water (Table 2). This means that a lower water content is helpful for producing high-strength concrete.

The performances of Mixes 1–5 are shown in Table 5. The following results were obtained based on the contents of Table 5. First, as the compressive strength of concrete increased from 95 MPa to 115 MPa, the water-to-binder ratio decreased from 0.26 to 0.23 and the silica fume replacement ratio increased from 0.05 to 0.25. This means that a lower water-to-binder ratio and a higher silica fume replacement ratio can improve the strength of concrete. Second, the sand ratio for each mixture was equal to the upper limit of the sand ratio (Table 3). This is because the concrete strength increases as the sand ratio increases (equation (8)). Third, the slumps for each mixture were all higher than the required slump of 180 mm. As the strength of the concrete increased, the superplasticizer content also increased. Fourth, as shown in Figure 1(a), as the strength of concrete increased, the CO_2 emissions also increased. Furthermore, based on the unit cost of concrete components (Table 6 [9]) and concrete mixtures, the cost for each mixture was calculated and they are shown in Figure 1(b). As the strength of concrete increased, the cost for each mixture also increased.

3.2. Design of Low-Cost High-Strength Concrete. In Section 3.1, the objective function of the genetic optimization was set as the minimum CO_2 emissions. However, in the concrete industry, concrete producers and construction companies are interested not only in CO_2 emissions but also in the cost of concrete. Like CO_2 emissions, the cost of concrete can also be calculated from the contents and unit prices of the concrete components (Table 6 [9]).

Based on similar methods in Section 3.1, the concrete mixture with the lowest price, considering various constraint equations, can be determined. The mixtures were calculated and are shown in Table 7. The strengths of Mix6, Mix7, Mix8, Mix9, and Mix10 were 95, 100, 105, 110, and 115 MPa, respectively. The following results were obtained based on the contents of Tables 7 and 8. First, for concrete with strengths of 95 and 100 MPa, the mixtures of the lowest cost were the same as that of the lowest CO_2 emissions (Mix1 was the same as Mix6 and Mix2 was the same as Mix7). For the concrete with strengths of 95 MPa and 100 MPa, the silica fume replacement ratio was 0.05, which equaled the lower limit of the silica fume replacement ratio (Table 3). Second, for concrete with strengths of 105, 110, and 115 MPa, the silica fume replacement ratio of the lowest cost mixtures (Mix8, Mix9, and Mix10) was lower than that of the lowest CO_2 emission mixtures (Mix3, Mix4, and Mix5). For example, the compressive strengths of Mix3 and Mix8 were both 105 MPa, but the silica fume replacement ratio of Mix8 was lower than that of Mix3. This is because the unit price of silica fume is much higher than that of cement (the unit price

Table 4: Mixtures of low-CO_2 high-strength concrete.

Low-CO_2 concrete	Cement (kg/m^3)	Silica fume (kg/m^3)	Water (kg/m^3)	Fine aggregate (kg/m^3)	Coarse aggregate (kg/m^3)	Superplasticizer (kg/m^3)
Mix1-95 MPa	545.30	28.70	149.62	659.81	1032.01	11.65
Mix2-100 MPa	545.30	28.70	143.55	664.83	1039.86	13.15
Mix3-105 MPa	521.27	52.73	140.00	663.62	1037.97	15.24
Mix4-110 MPa	463.29	110.71	140.00	653.61	1022.32	18.14
Mix5-115 MPa	452.54	150.85	140.00	635.86	994.56	21.48

Table 5: Performance of low-CO_2 high-strength concrete.

Low-CO_2 concrete	f_c (MPa)	Slump (mm)	CO_2 emission (kg/m^3)	Cost (NT dollar/m^3)	Water/binder	Silica fume/binder	Sand ratio	Sp/binder
Mix1-95 MPa	95.00	202.79	550.21	2271.93	0.26	0.05	0.39	0.02
Mix2-100 MPa	100.00	194.40	550.65	2312.92	0.25	0.05	0.39	0.02
Mix3-105 MPa	105.00	188.14	554.02	2580.69	0.24	0.09	0.39	0.03
Mix4-110 MPa	110.00	184.89	561.50	3169.04	0.24	0.19	0.39	0.03
Mix5-115 MPa	115.00	182.74	594.22	3668.59	0.23	0.25	0.39	0.04

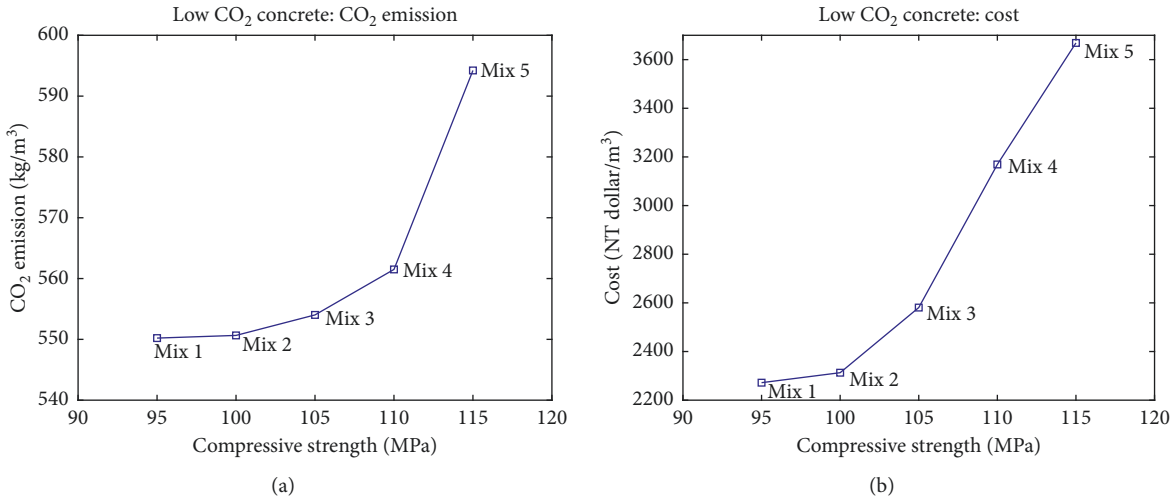

Figure 1: (a) CO_2 emissions of low-CO_2 concrete. (b) Cost of low-CO_2 concrete.

Table 6: Unit cost of the concrete components [9].

Cement (NT dollar/kg)	Silica fume (NT dollar/kg)	Water (NT dollar/kg)	Fine aggregate (NT dollar/kg)	Coarse aggregate (NT dollar/kg)	Superplasticizer (NT dollar/kg)
2.25	11.25	0.01	0.28	0.236	25.1

Table 7: Mixtures of low-cost high-strength concrete.

Low-cost concrete	Cement (kg/m^3)	Silica fume (kg/m^3)	Water (kg/m^3)	Fine aggregate (kg/m^3)	Coarse aggregate (kg/m^3)	Superplasticizer (kg/m^3)
Mix6-95 MPa	545.30	28.70	149.62	659.81	1032.01	11.65
Mix7-100 MPa	545.30	28.70	143.55	664.83	1039.86	13.15
Mix8-105 MPa	571.86	30.10	140.00	656.99	1027.60	15.65
Mix9-110 MPa	648.03	34.11	140.00	626.71	980.23	19.54
Mix10-115 MPa	663.51	71.13	140.00	601.65	941.05	22.98

Table 8: Performance of low-cost high-strength concrete.

Low-cost concrete	f_c (MPa)	Slump (mm)	Cost (NT dollar/m^3)	CO_2 emission (kg/m^3)	Water/binder	Silica fume/binder	Sand ratio	Sp/binder
Mix6-95 MPa	95.00	202.79	2271.93	550.21	0.26	0.05	0.39	0.02
Mix7-100 MPa	100.00	194.40	2312.92	550.65	0.25	0.05	0.39	0.02
Mix8-105 MPa	105.00	189.20	2445.90	577.36	0.23	0.05	0.39	0.03
Mix9-110 MPa	110.00	188.50	2740.48	653.02	0.21	0.05	0.39	0.03
Mix10-115 MPa	115.00	186.61	3261.80	706.80	0.19	0.10	0.39	0.03

of silica fume is five times that of cement (Table 6)). When the object function is the lowest price, the content of silica fume will be as low as possible. Third, for concrete with strengths of 105 MPa, 110 MPa, and 115 MPa, the water-to-binder ratio of the lowest cost mixtures (Mix8, Mix9, and Mix10) was lower than that of the lowest CO_2 emission mixtures (Mix3, Mix4, and Mix5). This means that a lower water-to-binder ratio can compensate for the impairment of strength due to the lower silica fume content. Fourth, the slumps for each mixture were all higher than the required slump of 180 mm. As the strength of concrete increased, the superplasticizer content also increased. Fifth, as shown in Figure 2(a), as the strength of concrete increased, the cost of concrete also increased. As shown in Figure 2(b), as the strength of concrete increased, the CO_2 emissions for each mixture also increased.

3.3. Pareto Optimal Mixtures for Lower CO_2 Emissions and Lower Cost. As shown in Sections 3.1 and 3.2, for concrete with higher strengths such as 105, 110, and 115 MPa, the mixtures with the lowest cost were different from those with the lowest CO_2 emissions. Although the aims of the lowest CO_2 emissions and lowest price cannot be achieved simultaneously, some compromises can be made between low CO_2 emissions and low price. In other words, we can design concrete with relatively lower CO_2 emissions at a relatively lower price. To design concrete with both lower cost and lower CO_2 emissions, we set an additional constraint regarding the cost of concrete. For example, when the required strength of concrete is given as 110 MPa (the strengths of Mix4 and Mix9 were both 110 MPa), the constraint equation of cost can be set as follows:

$$\text{COST} = (2800, 2900, 3000, 3100). \quad (11)$$

The values of cost (2800, 2900, 3000, and 3100) were between the cost of Mix4 and Mix9 (the cost of Mix4 and Mix9 was 3169.04 and 2740.48, respectively).

The design requirements can be summarized as follows: the object function was the lowest CO_2 emission; the cost of each mixture was equal to 2800 or 2900 or 3000 or 3100, respectively; the design value of compressive strength was 110 MPa; the design value of the slump was 180 mm; and the air content was 2%. In this section, the additional equality constraint was the cost of concrete (equation (11)), while in Section 3.1, there was no constraint for cost.

Based on the genetic algorithm, the mixtures were calculated and named as Mix11, Mix12, Mix13, and Mix14, respectively (shown in Table 9). The performances of Mix11 to Mix14 are shown in Table 10. The following results were obtained based on the contents of Table 10. First, the compressive strengths of Mix11, Mix12, Mix13, and Mix14 were the same, i.e., 110 MPa, and the slumps of Mix11, Mix12, Mix13, and Mix14 were higher than the required slump of 180 mm. Second, the cost of Mix11, Mix12, Mix13, and Mix14 was 2800, 2900, 3000, and 3100, respectively, and the CO_2 emissions of Mix11, Mix12, Mix13, and Mix14 were 640.46, 619.25, 597.92, and 576.43, respectively. The cost and CO_2 emissions of Mix11, Mix12, Mix13, and Mix14 were generally between Mix4 and Mix9. In other words, Mix11, Mix12, Mix13, and Mix14 had both lower cost and lower CO_2 emissions. Figure 3(a) shows the CO_2 emissions versus the concrete cost. As CO_2 emissions increased, concrete cost decreased.

The Pareto optimality is an ideal state of resource allocation. Given an inherent group of people and assignable resources, if there is a change from one state of assignment to another, at least one person's situation becomes better without making anyone's situation worse; this is the Pareto improved state. Pareto's optimal state is the idea that it is impossible to have more Pareto's improved state; in other words, it is impossible to improve the situation of some people without damaging anyone else [20]. Figure 3(b) shows an illustration of the Pareto optimal solutions [21, 22]. The x-axis and y-axis represent that of function f2 and performance f1, correspondingly. Point A and point B are a pair of points on the Pareto optimal solutions graph. At point A, the value of f1 is greater, while at point B, the value of f2 is greater.

Based on the comparison between Figures 3(a) and 3(b), we found that Mix11, Mix12, Mix13, and Mix14 were the Pareto optimal solutions for designing lower CO_2 emissions and lower concrete cost.

3.4. Generalization of the Proposed Method. In this study, the calculation equations of strength and slump were obtained based on the regression of experimental results in [16]. For different design specifications, the calculation equations of strength and slump may be different from those used in this study [23–25]. In addition, the unit CO_2 emission, unit price, constraints of component range, and component ratio used in this study cannot cover all cases presented in different countries and regions [26]. In Sections 3.1–3.3, the air content of concrete is assumed as 2%. The additional mixture designs are performed for different-strength concrete with 1% air content. The analysis results show that when air content changes from 2% to 1%, the contents of cement, silica fume, water, and sand ratio of optimized mixtures do

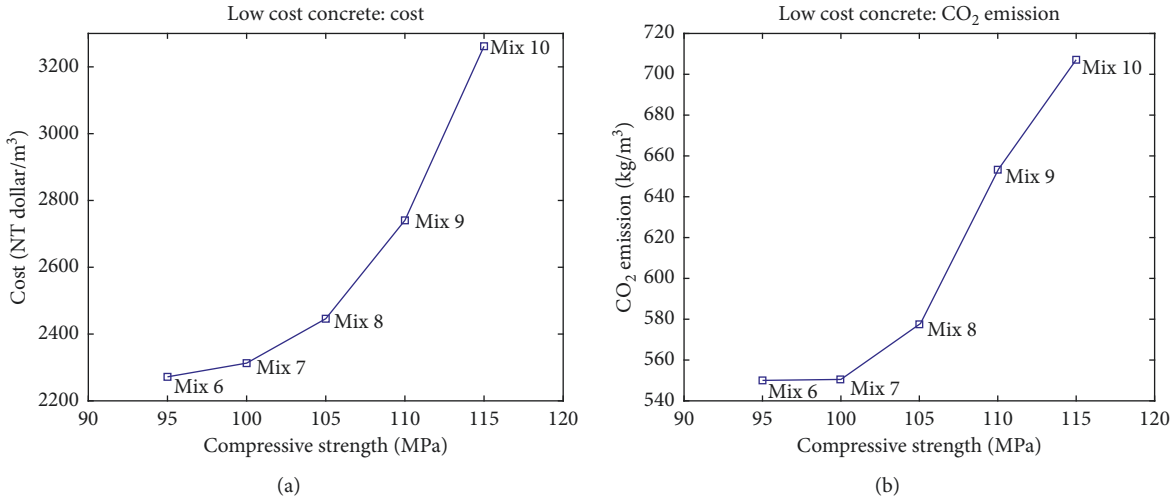

Figure 2: (a) Cost of low-cost concrete. (b) CO_2 emissions of low-cost concrete.

Table 9: Mixtures of 110 MPa concrete with lower CO_2 emissions and lower cost.

Low-CO_2 and cost concrete	Cement (kg/m^3)	Silica fume (kg/m^3)	Water (kg/m^3)	Fine aggregate (kg/m^3)	Coarse aggregate (kg/m^3)	Superplasticizer (kg/m^3)
Mix11-110 MPa	622.65	44.63	140.00	630.38	985.98	19.38
Mix12-110 MPa	579.84	62.38	140.00	636.59	995.69	19.08
Mix13-110 MPa	536.78	80.24	140.00	642.86	1005.50	18.76
Mix14-110 MPa	493.42	98.22	140.00	649.20	1015.41	18.41

Table 10: Performance of 110 MPa concrete with lower CO_2 emissions and lower cost.

Low-CO_2 and cost concrete	Cost (NT dollar/m^3)	CO_2 emissions (kg/m^3)	f_c (MPa)	Slump (mm)	Water/binder	Silica fume/binder	Sand ratio	Sp/binder
Mix11-110 MPa	2800.00	640.46	110.00	188.07	0.21	0.07	0.39	0.03
Mix12-110 MPa	2900.00	619.25	110.00	187.31	0.22	0.10	0.39	0.03
Mix13-110 MPa	3000.00	597.92	110.00	186.48	0.23	0.13	0.39	0.03
Mix14-110 MPa	3100.00	576.43	110.00	185.57	0.24	0.17	0.39	0.03

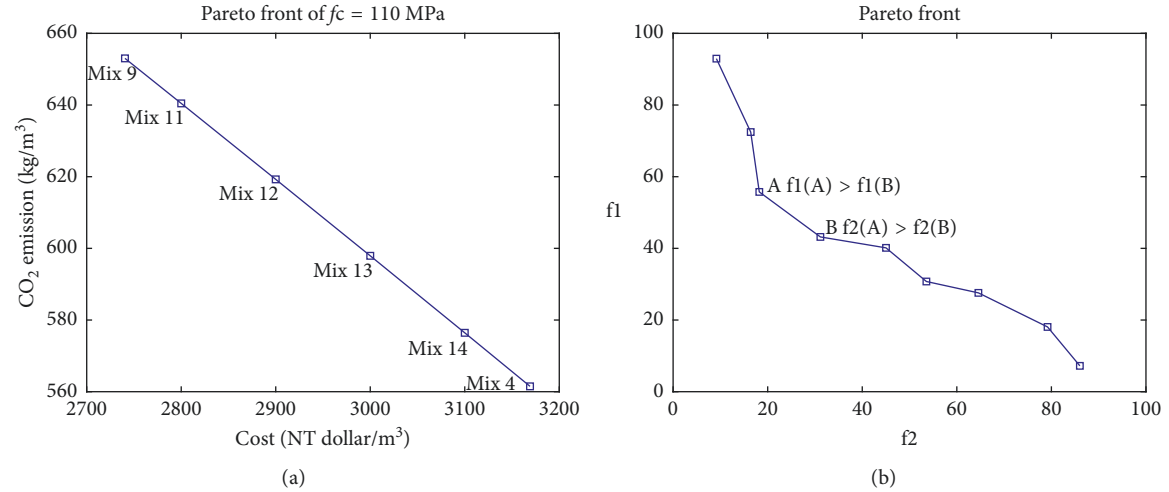

Figure 3: (a) Mixtures for 110 MPa concrete with lower CO_2 emissions and lower cost. (b) Illustration of the Pareto optimal solution.

not change, while the contents of fine aggregate and coarse aggregate increase.

To adapt the proposed design method, other researchers can use their own equations to replace the corresponding equations such as the equations for strength, slump, and various constraints. Although the calculation equations may be different, the basic calculation procedure is very similar. Hence, to some extent the proposed method can be regarded as a general method for the design of low-CO_2 high-strength concrete. On the other hand, as this study focused on the mixture design of high-strength concrete, durability aspects such as carbonation or chloride ingress were not considered. These durability aspects can be considered as additional inequality constraints of the concrete mixture [27].

4. Conclusions

This study proposed a general procedure to optimize the mixture design of low-CO_2 high-strength concrete containing silica fume.

First, CO_2 emissions were calculated based on the concrete mixtures and the unit CO_2 emissions of the concrete components. By using the genetic algorithm, concrete mixtures with the lowest CO_2 emissions were determined considering the various constraints. Similarly, concrete mixtures with the lowest cost were determined based on the genetic algorithm. We found that for concrete with design strengths higher than 105 MPa, the mixtures with the lowest CO_2 emissions were different from those with the lowest cost. As the strength of concrete increased, the CO_2 emissions and cost of concrete also increased.

Second, for concrete with design strength higher than 105 MPa, the objects of the lowest CO_2 emissions and lowest cost cannot be achieved simultaneously. By adding a constraint equation of cost, Pareto optimal mixtures were determined. The Pareto optimal mixtures had relatively lower CO_2 emissions and lower cost. Regarding the Pareto optimal mixtures, as CO_2 emissions increased, the concrete cost decreased. The cost and CO_2 emissions of the Pareto optimal mixtures were between the lowest cost mixture and lowest CO_2 emissions mixture.

In conclusion, the proposed technique is valuable for designing high-strength concrete that considers both CO_2 emissions and cost. To adapt the proposed design method, other researchers can use their own equations to replace the corresponding equations in this study.

Data Availability

The data used to support the findings of this study are available from the corresponding author upon request.

Conflicts of Interest

The authors declare that they have no conflicts of interest.

Acknowledgments

This research was supported by the Basic Science Research Program through the National Research Foundation of Korea (NRF) funded by the Ministry of Science, ICT & Future Planning (No. 2015R1A5A1037548), and a NRF grant (NRF-2017R1C1B1010076).

References

[1] V. G. Papadakis, "Effect of supplementary cementing materials on concrete resistance against carbonation and chloride ingress," *Cement and Concrete Research*, vol. 30, no. 2, pp. 291–299, 2000.

[2] P. K. Mehta, "Reducing the environmental impact of concrete," *Concrete International*, vol. 23, pp. 61–66, 2001.

[3] I. L. Larsen, I. G. Aasbakken, R. O. Born, K. Vertes, and R. T. Thorstensen, "Determining the environmental benefits of ultra high performance concrete as a bridge construction material," *IOP Conference Series: Materials Science and Engineering*, vol. 245, article 052096, 2017.

[4] Y. L. Voo and S. J. Foster, "Characteristics of ultra-high performance "ductile" concrete and its impact on sustainable construction," *IES Journal Part A: Civil & Structural Engineering*, vol. 3, no. 3, pp. 168–187, 2010.

[5] R. Yu, P. Spiesz, and H. J. H. Brouwers, "Development of an eco-friendly ultra-high performance concrete (UHPC) with efficient cement and mineral admixtures uses," *Cement and Concrete Composites*, vol. 55, pp. 383–394, 2015.

[6] J. Park, S. Tae, and T. Kim, "Life cycle CO_2 assessment of concrete by compressive strength on construction site in Korea," *Renewable and Sustainable Energy Reviews*, vol. 16, no. 5, pp. 2940–2946, 2012.

[7] T. Kim, C. Chae, G. Kim, and H. Jang, "Analysis of CO_2 emission characteristics of concrete used at construction sites," *Sustainability*, vol. 8, no. 4, pp. 348–362, 2016.

[8] R. Latawiec, P. Woyciechowski, and K. J. Kowalski, "Sustainable concrete performance—CO_2-emission," *Environments*, vol. 5, no. 2, pp. 27–41, 2018.

[9] I.-C. Yeh, "Computer-aided design for optimum concrete mixtures," *Cement and Concrete Composites*, vol. 29, no. 3, pp. 193–202, 2007.

[10] M. A. Mosaberpanah and O. Eren, "CO_2-full factorial optimization of an ultra-high performance concrete mix design," *European Journal of Environmental and Civil Engineering*, vol. 22, no. 4, pp. 450–463, 2018.

[11] K. H. Yang, S. H. Tae, and D. U. Choi, "Mixture proportioning approach for low-CO_2 concrete using supplementary cementitious materials," *ACI Materials Journal*, vol. 113, no. 4, pp. 533–542, 2016.

[12] J. G. Tapali, S. Demis, and V. G. Papadakis, "Sustainable concrete mix design for a target strength and service life," *Computers and Concrete*, vol. 12, no. 6, pp. 755–774, 2013.

[13] A. Khan, J. Do, and D. Kim, "Cost effective optimal mix proportioning of high strength self compacting concrete using response surface methodology," *Computers and Concrete*, vol. 17, no. 5, pp. 629–638, 2016.

[14] T. Ji, Y. Yang, M. Y. Fu, B. C. Chen, and H. C. Wu, "Optimum design of reactive powder concrete mixture proportion based on artificial neural and harmony search algorithm," *ACI Materials Journal*, vol. 114, no. 1, pp. 41–47, 2017.

[15] H.-S. Lee and X.-Y. Wang, "Evaluation of the carbon dioxide uptake of slag-blended concrete structures, considering the effect of carbonation," *Sustainability*, vol. 8, no. 4, pp. 312–330, 2016.

[16] C.-H. Lim, Y.-S. Yoon, and J.-H. Kim, "Genetic algorithm in mix proportioning of high-performance concrete," *Cement and Concrete Research*, vol. 34, no. 3, pp. 409–420, 2004.

[17] Z. Wu, C. Shi, K. H. Khayat, and S. Wan, "Effects of different nanomaterials on hardening and performance of ultra-high strength concrete (UHSC)," *Cement and Concrete Composites*, vol. 70, pp. 24–34, 2016.

[18] C. Shi, D. Wang, L. Wu, and Z. Wu, "The hydration and microstructure of ultra high-strength concrete with cement-silica fume-slag binder," *Cement and Concrete Composites*, vol. 61, pp. 44–52, 2015.

[19] "Mathworks," 2018, http://www.mathworks.com.

[20] T. Noguchi, I. Maruyama, and M. Kanematsu, "Performance based design system for concrete mixture with multi-optimizing genetic algorithm," in *Proceedings of the 11th International Congress on the Chemistry of Cement (ICCC)*, Durban, South Africa, May 2003.

[21] M. A. DeRousseau, J. R. Kasprzyk, and W. V. Srubar III, "Computational design optimization of concrete mixtures: a review," *Cement and Concrete Research*, vol. 109, pp. 42–53, 2018.

[22] V. Yepes, J. V. Martí, T. García-Segura, and F. González-Vidosa, "Heuristics in optimal detailed design of precast road bridges," *Archives of Civil and Mechanical Engineering*, vol. 17, no. 4, pp. 738–749, 2017.

[23] A. Behnood, V. Behnood, M. M. Gharehveran, and K. E. Alyamac, "Prediction of the compressive strength of normal and high-performance concretes using M5P model tree algorithm," *Construction and Building Materials*, vol. 142, pp. 199–207, 2017.

[24] Z. H. Duan, S. C. Kou, and C. S. Poon, "Prediction of compressive strength of recycled aggregate concrete using artificial neural networks," *Construction and Building Materials*, vol. 40, pp. 1200–1206, 2013.

[25] V. Mechtcherine and S. Shyshko, "Simulating the behaviour of fresh concrete with the distinct element method—deriving model parameters related to the yield stress," *Cement and Concrete Composites*, vol. 55, pp. 81–90, 2015.

[26] J.-S. Chou, C.-F. Tsai, A.-D. Pham, and Y.-H. Lu, "Machine learning in concrete strength simulations: multi-nation data analytics," *Construction and Building Materials*, vol. 73, pp. 771–780, 2014.

[27] X. Y. Wang and Y. Luan, "Modeling of hydration, strength development, and optimum combinations of cement-slag-limestone ternary concrete," *International Journal of Concrete Structures and Materials*, vol. 12, no. 1, pp. 1–13, 2018.

Hindawi
Advances in Civil Engineering
Volume 2019, Article ID 7907234, 15 pages
https://doi.org/10.1155/2019/7907234

Research Article

Identifying Factors Affecting the Sustainability of Water Environment Treatment Public-Private Partnership Projects

Huimin Li[1,2], **Qing Xia**[1,3], **Shiping Wen**[4], **Lunyan Wang**[1,5] and **Lelin Lv**[1,3]

[1]*School of Water Resources, North China University of Water Resources and Electric Power, Zhengzhou 450046, China*
[2]*Henan Key Laboratory of Water Environment Simulation and Treatment, Zhengzhou 450045, China*
[3]*Collaborative Innovation Center of Water Resources Efficient Utilization and Protection Engineering, Zhengzhou 450045, China*
[4]*School of Economics and Management, Tongji University, Shanghai 200092, China*
[5]*Academician Workstation of Water Environment Governance and Ecological Restoration, Henan Province, Zhengzhou 450002, China*

Correspondence should be addressed to Shiping Wen; pp66dd@126.com

Received 18 February 2019; Accepted 9 April 2019; Published 2 May 2019

Guest Editor: Endong Wang

Sustainability has recently been acknowledged as a crucial issue in infrastructure projects. Developing a model to evaluate project sustainability according to sustainability indicators plays a major role in promoting the sustainable development of water environment treatment public-private partnership (PPP) projects. Traditional sustainability assessments are mostly based on the triple bottom line (economic, social, and environmental) and lack a more integrated indicator system. To connect the research gap, this paper identifies 27 factors that affect the sustainability of water environment treatment PPP projects from five dimensions: economy, society, resources and environment, engineering, and project management using exploratory factor analysis. The fitting degree between the model and original data is verified by confirmatory factor analysis. The results showed that the fitting was successful. This paper makes two contributions: first, it provides a comprehensive sustainability evaluation indicator system from five aspects, laying a foundation for the evaluation of project sustainability. Second, this study defines a methodology to evaluate and rank factors, identifies the indicators that show the most significant impact on project sustainability in the five dimensions, which provide a reliable reference for the public and private sector to take appropriate measures to improve the sustainability level of water environment treatment public-private partnership projects.

1. Introduction

With the rapid development of economy and society, the problem of water environment pollution in China increases significantly. The government has been fully responsible for the investment and management of environmental treatment in the past decades, not only leading to notable financial pressure but also challenging the government's management ability. Water environment treatment projects involve social infrastructure projects, such as sewage treatment, ecological restoration, and landscape greening; such projects require professional knowledge, and thus, guaranteeing efficiency while completely depending on the government presents difficulty [1]. Introducing public-private partnership (PPP) into water environment treatment has gradually become critical. On the one hand, it can alleviate the burden of public financial shortage and ensure the timely provision of needed infrastructure [2]. On the other hand, a private sector with valuable business opportunities can use innovative technologies and advanced management skills to improve governance efficiency and enhance the effect of water environment treatment [3, 4]. In recent years, the government has exerted considerable effort to promote the comprehensive improvement of the water environment and conducted numerous water environment treatment PPP projects, as shown in Figure 1.

Since the concept of "sustainable development" was defined in the Brundtland Report in 1987, it has gradually been accepted by organizations and governments worldwide [5]. Sustainable development is defined as development that meets the needs of the present without compromising the ability of future generations to meet their own needs. PPP is

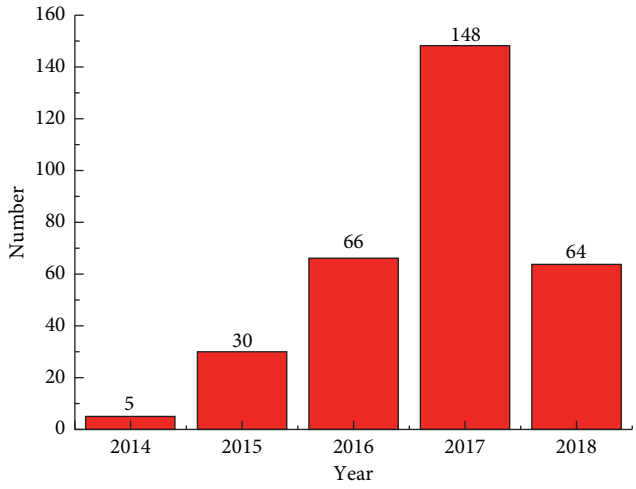

Figure 1: The number of water environment treatment PPP projects undertaken in the past five years. *Note.* The data of this paper are from the PPP center project management database of the Ministry of Finance, and the statistical time is as of October 11, 2018.

sometimes mentioned as a potential method for achieving sustainability goals [6]. Given the financial pressures faced by the government and the increased efficiency provided by the private sector, PPP has become one of the preferred ways for the government to develop infrastructure. However, as the participation of the private sector in PPP projects is profit-driven, it is easy to pay too much attention to the economic target of whether the project is profitable, while ignoring the impact of the project on the environment and society. Second, the private sector emphasizes short-term financial returns on investment, but the sustainability performance of projects can only be achieved from a long-term perspective. Thus, the concept of sustainable development needs to be included in infrastructure projects delivered through PPP; otherwise, the projects would fail [7]. The sustainability of PPP projects should consider two aspects. First, PPP infrastructure projects should be consistent with the level of regional economic development, which means not only meeting the long-term and effective demand of the public but also promoting the sustainable development of society, economy, environment, and resources. Second, the development of the project itself should be sustainable, including aspects such as the durability of the project itself, life-cycle cost, and energy consumption. Therefore, in order to achieve sustainability and promote the healthy development of PPP projects, it is necessary to evaluate their sustainability.

Infrastructure projects have major effects on implementing the principles of sustainable development. Therefore, researchers investigated infrastructure project sustainability from different perspectives. Timmermans and Beroggi [8] studied the sustainability assessment of infrastructure from several aspects, including economic sustainability, social sustainability, technological safety, attractiveness for living, and attractiveness for businesses. Sahely et al. [9] developed a framework that focuses on key interactions and feedback mechanisms between infrastructure and surrounding environmental, economic, and social systems for the sustainability assessment of urban infrastructure systems. Shen et al. [10] introduced key assessment indicators (KAIs) for assessing the sustainability performance of an infrastructure project from three dimensions embodied in sustainable development principles (i.e., economic, environmental, and social). Most research started from the sustainable triple bottom line, economic, social, and environmental aspects and lacked more comprehensive assessment indicators, which constitute an obstacle to effectively assessing the sustainability of infrastructure projects. For example, projects may succeed or fail in terms of how they reach their goals and how they are managed [11]. Achievement of project goals requires efficient project control [12]. Previous studies focused on the environmental aspects of sustainability in project deliverables while giving less attention to sustainable project management during project delivery [13]. Armanios [14] believed that if we are to possess a more complete and holistic view of sustainability, engineering sustainability needs to be considered and discussed more. At present, few investigations are available on the sustainability of PPP infrastructure projects. Hueskes et al. [7] showed that sustainability considerations currently play only a limited role and that social dimensions of sustainability are largely neglected in PPP infrastructure projects.

To connect these gaps, we aim to consider more comprehensive sustainability aspects into the water environment treatment PPP projects. This paper aims to identify the sustainability indicators (economy, society, resources and environment, engineering, and project management) in water environment treatment PPP projects according to previous studies. This paper also ascertains how such factors are identified and measured. Finally, this paper also aims to determine a methodology for evaluating and ranking critical factors of water environment treatment PPP projects. This study constructs a theoretical research framework for sustainability evaluation of water environment treatment public-private partnership projects in a comprehensive and multidimensional way. Moreover, this paper identifies the indicators that show the most significant impact on project sustainability, which provide a useful reference for the public and private sector to take appropriate measures to improve the sustainability level of water environment treatment public-private partnership projects.

The remainder of the paper is organized as follows. Section 2 reviews the sustainability literature on infrastructure projects, PPP, and water management. Section 3 preliminarily constructs the PPP project sustainability evaluation index system from five aspects: economy, society, resources and environment, engineering, and project management sustainability. Section 4 introduces the research methodology. Section 5 presents the data analysis, including exploratory factor analysis, confirmatory factor analysis, and calculation of indicator weights. Section 6 discusses the factors influencing water environment treatment PPP projects. Finally, Section 7 describes the conclusions, practical implications, limitations, and future work of this study.

2. Literature Review

2.1. Sustainability of Infrastructure Projects. Sustainability is commonly understood through its three components, which

are often referred to as the triple bottom line. In infrastructure projects, the sustainability of deliverables and delivery processes are both crucial as they can have remarkable social and environmental impacts [13].

Infrastructure is the foundation of social and economic development, hence resulting in the heavy infrastructure investment in developing countries. From 1970 to 2005, more than 30% of the World Bank's investment served to implement various types of infrastructure in developing countries [10]. In general, infrastructure projects provide a natural monopoly, externality, and indirect benefits. Therefore, evaluating their sustainability is necessary [15].

Researchers conducted sustainable research on infrastructure projects from different perspectives. Shen et al. [16] suggested that to achieve better sustainability, interests, powers, and responsibilities should be divided among the project parties within the concession term of the infrastructure project. Dasgupta and Tam [17] synthesized the sustainability indicators of civil infrastructure projects by using a multiobjective decision approach to facilitate the choice of practical alternatives for better sustainability performance. Ugwu et al. [18] used the weighted-sum model technique in multicriteria decision analysis (MCDA) and the additive utility model in the analytical hierarchical process (AHP) to develop a multicriterion decision-making model for sustainability appraisal in infrastructure projects. Timmermans and Beroggi [8] argued that economic sustainability, social sustainability, technological safety, attractiveness for living, and attractiveness for businesses should be considered when assessing infrastructure project sustainability. Shen et al. [10] believed that project sustainability assessment indicators in previous studies were fragmental and that a complete assessment system was lacking. Therefore, they introduced KAIs for assessing the sustainability performance of an infrastructure project according to the triple bottom line. Kivilä et al. [13] argued that less attention has been directed at sustainable project management during project delivery and indicated that sustainable project management is implemented using not only indicators but also a holistic control package, in which control mechanisms are used differently for various sustainability dimensions. Internal project control is complemented with sustainable project governance, which links the project to external stakeholders and regulations. Amiril et al. [19] explored the relationship between sustainability factors and the performance of transportation infrastructure projects and identified the sustainability factors involved in environmental, economic, social, engineering/resource utilization, and project administration issues. Their findings will promote the implementation of sustainability strategies and provide theoretical support and reference for the study of the sustainability of water environment treatment projects.

In summary, sustainability has received wide attention in infrastructure projects. Previous studies examined the sustainability of infrastructure from the triple bottom line principle. Recently, several researchers have begun to study the sustainability of infrastructure from other aspects, e.g., project management sustainability and engineering sustainability. For an infrastructure project, not only its impact on the outside environment (economic, social, and environmental) but also the sustainability of the engineering itself and project management should be paid attention to. Engineering sustainability is the foundation for water environment treatment PPP projects. Project management sustainability is the core meaning to guarantee and promote the sustainable development of economy, society and environment.

2.2. Sustainability of PPP Projects. PPP is a procurement approach where the public and private sectors join forces to deliver a public service or facility. In this arrangement, normally, the public and private sectors will contribute their expertise and resources to the project and share the involved risks [20, 21]. PPP is widely used in infrastructure construction and public services because of its effective financing capacity, which can help mitigate the risk of local government debt [22].

With the global application of PPP, more related studies have been conducted, such as those on PPP risk management [23], key success factors [24], governance [7], and sustainable development [7, 25, 26].

PPP has been adopted as the preferred route for the development of infrastructure projects by both developing and developed countries. However, Koppenjan and Enserink [27] argued that private sector involvement in infrastructure leads not necessarily to sustainable development as the private sector is primarily concerned with short-term financial returns on investment, and the sustainability performance of projects can only be achieved from a long-term perspective. Ye and Deng [28] proposed four partnership characteristics, including maintaining the consistency of objectives, long-term cooperation, equal coordination, and benefit-risk sharing, among the three stakeholders, namely, the government sector, the private sector, and the public sector; moreover, the authors developed a method to realize the sustainability of PPP infrastructure projects. Shen et al. [25] believed in the differing expectations of the public and private sectors; allocation of investment between these stakeholders poses a significant impact on the sustainable performance of projects. The sustainability performance-based evaluation model (SPbEM) was developed to assess the level of sustainability performance of PPP projects. Patil et al. [21] proposed the sustainability evaluation principle of PPP projects based on stakeholder participation and empowerment, institutional capacity, efficient project implementation, socioecological compatibility, resource utilization efficiency and maintenance, value for money, quality of life, affordability, and compensation. Hueskes et al. [7] observed that the social dimensions of sustainability were largely neglected due to the difficulties encountered in formulating measurable social sustainability criteria. However, a "strong" sustainability perspective is inherently incompatible with the contractual PPP project structure, thus requiring measurable and enforceable performance indicators. Such incompatibility is a major challenge for the sustainability evaluation for PPP projects.

There are many studies on sustainability in the field of infrastructure, but few focused on the PPP domain, as PPP projects different from traditional investment models, involve many stakeholders, and include complex management structures. Moreover, given its profit-driven nature, the private sector only pays attention to short-term economic benefits and ignores the long-term impact on the economy, society, and environment, thus preventing the realization of sustainable development goals. Therefore, studying the sustainability of PPP projects is valuable.

2.3. Sustainability of Water Management. An increasing number of developing countries are faced with water shortages, for reasons that include the scarcity of natural water resources, population growth, high standards of living, and lack of well-developed supply infrastructure. Water sustainability is essential for humans to live in a healthy manner while maintaining the natural environment [29]. Water also plays a fundamental role in the security of food and energy and in economic growth and poverty reduction. Water shortages, if not met in a timely and sustainable manner, will inevitably result in serious adverse effects on socioeconomic and commercial development [30]. Moreover, for the past 60 years, rapid economic development and urban population growth have outpaced environmental infrastructure in urban cities around the world. Cities lack sewer networks. Uncontained raw sewer flows into water bodies, ultimately contaminating the environment. Similarly, sewage pollution threatens human health and wildlife in different regions around the world. This increase in environmental pollution underscores the need for effective environmental resource management [31].

A number of researchers have investigated water sustainability. Elnaboulsi [31] believed that sustainable development of public wastewater utilities can be achieved by promoting full-cost pricing and considering external costs from wastewater services. Reduction in drinking water consumption, also through the reuse and recycling of unconventional sources of water, has been identified as one of the goals of sustainable development. Therefore, Zanni et al. [32] evaluated and compared the environmental impacts attributable to the use of water supply sources (such as rainwater harvesting and graywater recycling), which present alternatives to the traditional one, through the combined use of life-cycle assessment and a hydrological model. Pellicer-Martínez and Martínez-Paz [33] proposed the use of water footprint indicator to assess environmental sustainability in water resource management at the river basin level. Nuong et al. [34] used the AHP approach to evaluate the social sustainability of Hanoi's groundwater resources from three aspects: quantity, quality, and management of water.

In summary, most studies on water sustainability focus on one aspect: economy, society, or environment. Furthermore, many investigations were conducted on the sustainability of water resources but few on water pollution and water environment treatment. A healthy water environment is the premise and foundation for the sustainable development of cities and towns. It is an important factor to ensuring the harmonious development of human and nature, human and society, and the city, economy, and environment, aside from being an objective requirement for the healthy development of China's urbanization. At present, water environment treatment PPP projects have become an important part of China's public infrastructure construction projects. Therefore, it is necessary for the government to evaluate the sustainability of water environment treatment PPP projects from comprehensive dimensions.

A review of the current literature indicates that sustainability has been widely researched in infrastructure projects and water resources, but little research has been done on PPP projects, water pollution, and water environment treatment. Furthermore, most research started from the sustainable triple bottom line and lacked more comprehensive assessment indicators. To connect these gaps, this paper provides a comprehensive sustainability evaluation indicator system of water environment treatment PPP projects from the economic, social, resource and environment, engineering, and project management aspects through structural equation modeling (SEM). This approach will further lead researchers to identify factors that affect the sustainability of other industry sector PPP projects.

3. Establishment of Sustainability Evaluation Indicator System of Water Environment Treatment PPP Projects

In practice, sustainability is represented in assessment processes through the use of certain sustainability indicators, where indicators should provide a simplified but still sufficient interpretation of sustainability. The development of sustainability indicators has emerged as a field of study in its own right, albeit one has been described as rather confusing and nonconsensual [35].

Most researchers have proposed various methods and evaluation index systems to assess the sustainability of infrastructure projects from the perspective of the sustainable triple bottom line. In this paper, we will construct a sustainability evaluation indicator system of the water environmental treatment PPP project from the five aspects of economic, social, resource and environment, engineering, and project management (Figure 2).

3.1. Economic Sustainability. Economic sustainability not only means that PPP projects should bring long-term, stable, and reasonable investment returns to the project itself [36] but also the impact on the local economy and development. Long-term in this description means that the private sector should effectively integrate the construction stage with the operation and maintenance stage to reduce the life-cycle cost and avoid the situation wherein contractors only consider short-term construction profits and ignore long-term operation and maintenance efficiency. Stability requires local governments to possess the capability and credit to continue paying. A common problem is that the projects implemented by the current local government leader are not

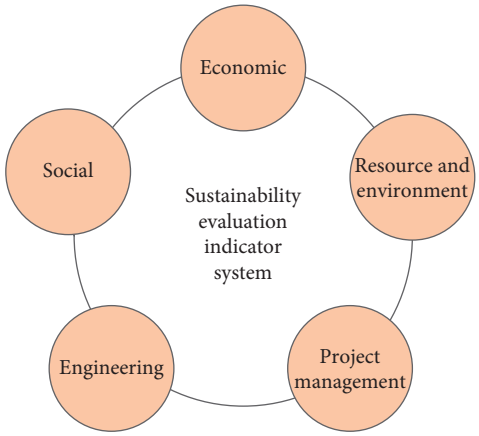

Figure 2: The sustainability evaluation indicator system of water environmental treatment PPP projects.

recognized by the next leader, thereby causing the government to break the contract. Reasonable means that, on the one hand, the profit rate of the project should be able to attract the private sector, and on the other hand, the project should not generate excessive profits. Balancing the relationship between the social and economic aspects of PPP projects is necessary. Besides the economic sustainability of the project itself, a water environmental treatment PPP project would also increase the land value around the project and promote local economic development.

3.2. Social Sustainability. Among the three main pillars of the sustainability concept (including environmental, social, and economic pillars) [37], the social criterion has specifically received less consideration than the economic and environmental criteria [38], because this concept is typically difficult to define and quantify. No specific definition of social sustainability exists. Thus, each study defines the concept according to its own specific viewpoints. In this paper, social sustainability refers to providing the public with satisfactory goods and services through measures that enhance the social development potential of the project area, provide employment opportunities for local people, and improve the quality of life.

3.3. Resource and Environment Sustainability. Resource and environmental sustainability mean giving a better world to the future generation and protecting ecological balance and natural systems from destruction [39]. People require extensive infrastructure to sustain their lives. During infrastructure construction, operation, and maintenance, environmental problems will arise, and they can be attributed to the consumption of nonrenewable resources and the decrease in biological diversity [40]. Therefore, adopting green building technology and using renewable energy during infrastructure construction are necessary to achieve energy conservation, emission reduction, and environmental protection. In addition, for water environment treatment projects, the sustainability of resources and the environment can be improved by reducing pollutant discharge, improving sewage treatment rate, and comprehensive utilization of water resources.

3.4. Engineering Sustainability. The definition of PPP project sustainability implies that PPP infrastructure projects should not only promote the sustainable development of society, economy, resources, and environment but also require the sustainable development of the project itself, specifically, its durability (i.e., engineering quality), operation, and maintenance capability and the sustainability of the technology itself.

Various governments around the world have spent considerably more money on new infrastructure and less on infrastructure maintenance. For example, reports of gas pipe leak or explosion, bridge collapse, or supply water pollution are common in China. Such accidents are caused by the insufficient maintenance of infrastructure. Poorly maintained infrastructure projects have led to various social and environmental problems. Therefore, to achieve healthy project development, the operation and maintenance capacity of projects should be improved, and attention on the sustainability of the engineering should be strengthened.

3.5. Project Management Sustainability. Project management sustainability refers to ensuring profitable, fair, transparent, safe, ethical, and environmentally friendly project delivery, which aims at a project deliverable that is socially and environmentally acceptable throughout its life cycle [41].

Carvalho [42] indicated the importance of soft skills, such as those related to communication and stakeholder management, in project management. Scott-Young and Samson [43] also pointed out that personnel management factors contribute more to the success of a project than technical factors. For water environment treatment PPP projects, professional technicians and managers are needed. Moreover, such projects involve a long operation, a wide range, and numerous stakeholders. Thus, the organization structure should change with different concessionary stages. Furthermore, a stable project organization structure and effective communication are needed in the operation period to ensure the continuous and healthy operation of the project.

In summary, this paper uses literature review and expert interviews to identify the sustainability evaluation indicators of water environment treatment PPP projects from five aspects: economic, social, resource and environment, engineering, and project management. Table 1 shows the specific indicators.

4. Research Method

4.1. Questionnaire Survey. This research was conducted using a combination of structured interviews with industry professionals, a review of sustainability literature, and questionnaire-based survey for indicator validation. The survey was conducted over a two-month period from 1 August 2018 to 1 October 2018. A total of 200 questionnaires

Table 1: Sustainable development indicators.

Dimension	Codes	Indicator	Sources
Economic sustainability (Eco)	Eco1	Internal return ratio (IRR)	[10, 44]
	Eco2	Land value-added benefit around the project	[10, 39, 45] expert interviews
	Eco3	Life-cycle cost	[10, 18, 39, 46–48]
	Eco4	Sustainable cash flow	[10, 45]
	Eco5	Effects on local economy and development	[10, 45, 49]
	Eco6	Fiscal pressures of government	[50, 51] expert interviews
Social sustainability (Soc)	Soc1	Public satisfaction	[13, 46–48, 52] expert interviews
	Soc2	Provision of employment opportunities	[10, 39, 45, 53]
	Soc3	Potential impact on social development	[10, 45, 54]
	Soc4	Trust between public and government	[55, 56]
	Soc5	Provision of ancillary infrastructure to local area	[10, 45, 47, 48]
	Soc6	Improvement of the cognition level of the public regarding sustainable development	[45, 57, 58]
Resource and environment sustainability (Res)	Res1	Effect on water quality	[10, 45]
	Res2	Reduction of pollutant discharge	[59, 60] expert interviews
	Res3	Energy efficiency (e.g., reduction of energy consumption and use of renewable energy resources)	[10, 18, 45, 61]
	Res4	Biodiversity protection	[10, 39, 46]
	Res5	Protection for landscape and historical sites	[10, 39, 46, 61]
	Res6	Sewage treatment rate	[62, 63] expert interviews
	Res7	Comprehensive utilization of water resources	[46, 64]
	Res8	Use of innovative materials	[10, 18, 39, 46, 61, 65]
Engineering sustainability (Eng)	Eng1	Completeness of supporting facilities for the project	[66] expert interviews
	Eng2	Renewal of project facilities	[9, 13]
	Eng3	Construction quality	[61]
	Eng4	Control of pollution sources	[59, 60]
	Eng5	Adoption of advanced engineering technology	[9, 44]
	Eng6	Project quality during operation	[52]
	Eng7	Sustainability of the technology itself	[52, 67] expert interviews
	Eng8	Capabilities of operation and maintenance	[9, 64]
	Eng9	Utilization of construction waste	[9, 39, 46–48, 61]
	Eng10	Waste recycling and reuse	[39, 46, 57]
Project management sustainability (Pro)	Pro1	Organization structure	[25, 47]
	Pro2	Continual improvement of the operation management system	[52, 67]
	Pro3	Competence and skills of the project team	[47, 68]
	Pro4	Contractual arrangements	[13, 25, 44, 61]
	Pro5	Establishment of the PPP contract renegotiation mechanism	[25] expert interviews
	Pro6	(Good) relationship with stakeholders	[47]

were distributed to experts and scholars in the fields of water environment treatment, PPP, project management, and sustainable development, as well as to employees participating in water environment treatment PPP projects. The questionnaire comprised three parts. The first section includes the questionnaire description, which introduces the purpose and content of the survey. The second section involves the basic personal information of the respondents, including the type of organization, the number of projects involved, and work experience. The third section focuses on assessing the importance of the proposed indicators affecting project sustainability, including the aspects of economy, society, resources and environment, engineering, and project management. This section asked respondents to rank each indicator from 1 to 5 to determine their importance in assessing project sustainability. This ranking translates as follows on the Likert scale: 1 = negligible, 2 = unimportant, 3 = average, 4 = important, and 5 = most important.

To validate the questionnaire prior to the survey, a pilot study was also conducted; it involved 30 respondents with more than three PPP projects on water environment treatment. Although minor changes were made in the sentence structure of the final questionnaire, the overall findings of the pilot study indicated the reliability and validity of the questionnaire used for data collection.

4.2. Data Collection. A total of 124 valid questionnaires were collected, with a response rate of approximately 62%. Most respondents (39.5%) came from research institutions, 17.7%

from investment companies, and 11.3% from government agency. Furthermore, according to the number of PPP projects involved in water environmental treatment, most respondents (65.3%) have participated in 1-2 specific projects, followed by those with 3–5 projects (19.4%) and more than 6 projects (10.5%). Overall, 95.2% of respondents have participated in related projects. In terms of work experience, most respondents (63.7%) reported 3–5 years of work experience, 16.9% claimed 6–10 years, 4.0% declared 11–15 years, and only 15.3% professed less than 2 years of work experience. To sum up, the respondents possessed certain work experience, ensuring the effectiveness of the survey results. Table 2 summarizes the demographic information of the respondents.

Table 2: The demographic information of the respondents.

Demographic categories	Category	Frequency	Percentage
Type of organization	Research institution	49	39.5
	Design company	7	5.6
	Construction organization	10	8.1
	Investment company	22	17.7
	Government agency	14	11.3
	Consultancy	12	9.7
	Others	10	8.1
Number of projects involved	0	6	4.8
	1-2	81	65.3
	3–5	24	19.4
	≥6	13	10.5
Work experience	≤2	19	15.3
	3–5	79	63.7
	6–10	21	16.9
	11–15	5	4.0

4.3. Analytical Strategies. The emergence and development of SEM have been regarded an important statistical development in social sciences in recent decades, and this multivariate analysis method has been widely applied in theoretical explorations and empirical validations in various disciplines [69, 70]. Compared with other statistical tools, such as factor analysis and multivariate regression, SEM performs the factor analysis and path analysis simultaneously [71]. Structural equation models include measurement models and structural models. Factor analysis is the analysis method corresponding to the measurement model, and that corresponding to the structural model is path analysis. Regarding the discussion of the sample size during SEM analysis, although the sample size of most studies is more than 200, Lomax [72] and Loehlin [73] believe that in SEM analysis, if the sample size is not more than 200, there should be at least 100. The number of samples is 124 in this paper, greater than 100, which can be analyzed by SEM.

In this paper, factor analysis was used to analyze the collected data. In the process, two-stage procedures recommended by Anderson and Gerbing [74] were followed. In the first stage, exploratory factor analysis was used to define the correlation between variables in samples and a provided set of factors. EFA helps to develop factors for a measurement model through identification of data patterns, determination of the relationship among patterns, and data reduction. Then, the fitting degree of the model and original data was measured by confirmatory factor analysis.

5. Data Analysis and Results

5.1. Common-Method Variance Bias Test. In order to determine the possible presence of common-method variance bias among variables, this study employs Harman [75] one-factor test. We observed the guidelines and approach of Podsakoff et al. [76] for conducting Harman one-factor test. For this purpose, all items of the measurement scale were entered into a principal component analysis with varimax rotation, so that any signs of single factor could be identified from factor analysis. The results extracted five different factors from 36 items of measurement constructs and rotation converged in 7 iterations. On the base of these results, it is determined that this study do not have any problem of common-method variance bias.

5.2. Nonresponse Bias Test. Beuckelaer and Wagner [77] believe that researchers risk losing statistical power in their findings when using small sample survey research, so it is necessary to "test for the possibility of nonresponse bias, and reflect on reasons as to why the sample is so small." This study employs extrapolation method, for testing nonresponse bias. Extrapolation method is most commonly used technique which involves comparison of early and late respondents for possible difference in demographics and mean values of other key constructs [78]. For this purpose, an independent sample t-test was performed for comparing the responses of first 50 and last 50 questionnaires. Findings of the independent sample t-test revealed that there was no significant 0.05 level difference in the mean values of both groups (i.e., first 50 respondents vs. last 50 respondents). Thus, on the base of the findings of the independent sample t-test, it was concluded that there was no substantial difference in the responses of both groups; hence, nonresponse bias is not a problem for this study.

5.3. Exploratory Factor Analysis (EFA). Before factor analysis, Kaiser–Meyer–Olkin (KMO) sample measure and the Bartlett sphere test were first performed to verify whether the indicators were suitable for factor analysis. The test results are shown in Table 3. The results of the KMO measure of sample adequacy and Bartlett's test of sphericity of the entire variables considered in the investigation revealed a KMO value of 0.865, which is >0.7 and is satisfactory. The value of Bartlett's test of sphericity is 0.000, which is <0.05 and is significant at the 95.0% confidence level, indicating that the results were satisfactory for further analysis.

IBM SPSS Statistics 22.0 [79] was used to perform EFA on the sample data. To reduce the multicollinearity between the indicators and delete factors with minimal influence, EFA was utilized to reduce the dimensions. In this paper,

Table 3: Test values of KMO and Bartlett.

KMO	Bartlett's test of sphericity		
	χ^2	*df*	Significant level
0.865	1631.411	351	0.000

principal component extraction and orthogonal rotation with Kaiser standardization were adopted to extract eigenvalues greater than 1. Table 4 shows the rotated component matrix which converged in seven iterations. Bold values denote loading for items, which are above the recommended value of 0.5. The overall Cronbach's alpha (α) of the questionnaire is 0.942; Cronbach's alpha values for each dimension are shown in Table 5. Cronbach's alpha for each factor exceeds the recommended 0.70 level, thereby indicating sufficient reliability [80]. The factors identified for each dimension are described as follows.

Factors affecting economic sustainability include internal return ratio (IRR) (Eco1), land value-added benefit around the project (Eco2), life-cycle cost (Eco3), sustainable cash flow (Eco4), and fiscal pressures of government (Eco6).

Factors affecting social sustainability include public satisfaction (Sco1), provision of employment opportunities (Sco2), and the potential impact on social development (Soc3).

Factors affecting social sustainability comprise effect on water quality (Res1), reduction of pollutant discharge (Res2), energy efficiency (e.g., reduction of energy consumption and use of renewable energy resources) (Res3), protection for landscape and historical sites (Res5), sewage treatment rate (Res6), comprehensive utilization of water resources (Res7), and use of innovative materials (Res8).

Factors affecting resource and environment sustainability include the completeness of supporting facilities for the project (Eng1), renewal of project facilities (Eng2), construction quality (Eng3), control of pollution sources (Eng4), adoption of advanced engineering technology (Eng5), sustainability of the technology itself (Eng7), capabilities of operation and maintenance (Eng8), utilization of construction waste (Eng9), and waste recycling and reuse (Eng10).

Factors affecting resource and environment sustainability include organization structure (Pro1), continual improvement of the operation management system (Pro2), and competence and skills of the project team (Pro3).

5.4. Confirmatory Factor Analysis (CFA). CFA was performed using IBM AMOS version 22.0 [79] to test the validity of the measurement model. The measurement model met Bollen's criteria [81]; that is, each latent variable should feature at least two indicators, and each observed variable is determined by one latent variable. Calculation revealed that the initial model cannot fully meet the criteria of goodness-of-fit (GOF) model. Specifically, the goodness-of-fit index (GFI) was equal to 0.765, which is less than the recommended level of 0.9, the adjusted goodness-of-fit index (AGFI) was equal to 0.718, which is less than the recommended level of 0.8, and root mean square error of approximation (RMSEA) was equal to 0.077, which is less than the recommended level of 0.05. Thus, the model needs to be modified.

Table 4: Measures of the rotated component matrix.

Item	Component				
	1	2	3	4	5
Eco1	0.006	−0.066	**0.668**	0.243	0.200
Eco2	−0.005	0.299	**0.570**	−0.097	0.127
Eco3	0.170	0.236	**0.693**	−0.019	0.088
Eco4	0.180	−0.012	**0.758**	0.042	−0.005
Eco5	0.071	0.039	0.385	0.266	−0.138
Eco6	0.093	0.072	**0.575**	0.370	−0.245
Soc1	0.201	0.504	0.026	0.235	**0.569**
Soc2	0.034	0.266	0.050	0.218	**0.670**
Soc3	0.274	−0.014	0.355	0.003	**0.589**
Soc4	0.228	0.046	0.090	0.209	0.473
Soc5	0.162	0.038	0.218	0.048	0.481
Soc6	0.157	0.049	0.375	0.178	0.371
Res1	0.245	**0.719**	−0.008	0.187	0.240
Res2	0.273	**0.761**	0.218	−0.026	0.135
Res3	0.388	**0.577**	0.088	0.283	0.103
Res4	0.459	0.373	0.346	0.092	−0.002
Res5	0.132	**0.554**	0.125	0.239	0.073
Res6	0.357	**0.571**	−0.039	0.123	0.209
Res7	0.312	**0.568**	0.245	0.250	−0.369
Res8	0.168	**0.755**	0.092	0.184	−0.023
Eng1	**0.667**	0.293	0.147	0.107	0.200
Eng2	**0.655**	0.245	0.134	0.219	0.159
Eng3	**0.649**	0.184	0.170	0.272	−0.111
Eng4	**0.551**	0.085	0.259	0.391	0.088
Eng5	**0.542**	0.082	0.062	0.330	0.264
Eng6	0.403	0.096	0.367	0.067	0.309
Eng7	**0.720**	0.183	0.067	0.283	−0.141
Eng8	**0.724**	0.221	0.119	−0.069	0.178
Eng9	**0.781**	0.162	−0.033	−0.090	0.062
Eng10	**0.694**	0.235	0.047	0.108	0.010
Pro1	0.230	0.197	0.168	**0.762**	0.206
Pro2	0.158	0.368	0.089	**0.633**	−0.053
Pro3	0.175	0.267	−0.004	**0.736**	0.225
Pro4	0.129	0.178	0.059	0.401	0.212
Pro5	0.251	0.019	0.017	0.354	0.278
Pro6	−0.027	0.311	−1.122	0.467	0.103

After improving the initial model according to the suggestions of GOF measures and modification indices (MI)—adding covariance error paths among variables or latent factors—the model showed a good fit, and all GOF measures satisfied the recommended levels. For example, the values for GFI were higher than 0.9, and those for AGFI were greater than 0.8, thereby indicating the acceptable fit between the measurement model and raw data. The RMSEA value of 0.046, which is less than 0.5, implies that the modified model is acceptable at a certain confidence level. Additionally, all the relative indexes of IFI, TLI, and CFI were above 0.9, thus providing strong evidence for the acceptable fit between the measurement model and data [82, 83]. In summary, the GOF measures of the modified model demonstrated a successful fit between the measurement model and raw data (Table 6). Figure 3 shows the modified measurement model with standardized coefficients and factor loadings. Table 7 presents the standardized

Table 5: Cronbach's alpha.

	Economic sustainability	Social sustainability	Resource and environment sustainability	Engineering sustainability	Project management sustainability
Cronbach's alpha	0.704	0.764	0.854	0.885	0.839

regression weights and covariance estimates for the modified measurement model with the corresponding standard effort of estimates and p values. All the standardized path coefficients for regression weights and covariance are highly positive and are significant at the 0.001 level (Table 7), implying that all the regression weights and covariance are significant.

5.5. Weights for Indicators. The weight of an indicator reflects its importance in the whole indicator system. This importance can be demonstrated by measuring the path coefficient values in the model. A higher path coefficient indicates the greater effect of the observed variable on the potential variable, because its factor has the highest level of characteristics [84]. Due to the different influences of each variable, the indicator weight of project sustainability can be obtained according to the value of the path coefficient. For example, q_{Eco1}, the weight of indicator Eco1 of the economic dimension, can be calculated by the following equation:

$$q_{Eco1} = \frac{W_{Eco1}}{W_{Eco1} + W_{Eco2} + W_{Eco3} + W_{Eco4} + W_{Eco6}}. \quad (1)$$

where W_{Eco1} refers to the path coefficient value of Eco1 in the measurement model.

The weights of other indicators can be obtained similarly.

Figure 3 shows that sustainable cash flow features the highest path coefficient of the economic variable, thereby indicating that this variable presents the most significant influence on economic sustainability. Therefore, the weight of this variable would also be the highest. Consequently, the path coefficient is applied to equation (1) to calculate the weight and rank each indicator. Table 8 shows the final sustainability evaluation indicator system of water environmental treatment PPP projects and the corresponding weight and ranking.

6. Discussion

Through the study of factors affecting the sustainability of water environment treatment PPP projects, 27 factors were identified. These factors were extracted in five categories, namely, economic sustainability, social sustainability, resource and environment sustainability, engineering sustainability, and project management sustainability. Combined with the indicator weight and ranking calculated in Section 5.3, the indicators of each dimension can be discussed as follows.

The economic sustainability dimension includes five indicators. The indicator "sustainable cash flow" is ranked as the most important indicator. If the project lacks cash flow, the financial resources needed in construction and operation cannot be guaranteed, and such condition is not conducive to the continuous operation of the project. Other indicators include "life-cycle cost," "internal return ratio (IRR)," "land value-added benefit around the project," and "fiscal pressures of government." To achieve economic sustainability in water environment treatment public-private partnership projects, we should shift their emphasis from first costs to life-cycle costs, where price of materials should account for costs such as emission, pollution, and waste [85]. IRR is one of the important indicators for evaluating the benefits of investment projects. A higher IRR indicates stronger project profitability. The private sector aims to achieve maximum IRR, but the public sector cannot accept higher IRR. Thus, the IRR should be at a reasonable level. Furthermore, treatment of water pollution areas can increase the value of lands around the project and promote regional economic development [1]. In China, the Ministry of Finance stipulates that the total expenditure of PPP projects per year cannot exceed 10% of the general public's budget. For the government, balancing the relationship between short-term and long-term development and formulating a long-term plan for fiscal expenditure is necessary. In addition, before the private sectors decide to invest in PPP projects, they need to consider the government's financial payment capacity. If the payment risk of the government is relatively high, the project may not achieve economic sustainability.

The social sustainability dimension includes three indicators. The indicator "public satisfaction" is ranked the most important in this group. The public represents an important stakeholder who is the most direct beneficiary and perceiver of water environment treatment PPP projects and whose satisfaction should be considered a crucial part of a performance evaluation system to achieve social sustainability development [86]. Other indicators in the social dimension include "provision of employment opportunities" and "potential impact on social development." These indicators exhibit a significant influence on promoting social sustainability because in project implementation, they can

Table 6: GOF measures of the modified measurement model.

Index name	GOF measures	Refined	Recommended levels	Evaluation
Absolute fit index	χ^2/df	1.383	1–3	Acceptable
	RMSEA	0.046	<0.05	Acceptable
	RMR	0.039	<0.05	Acceptable
	GFI	0.915	>0.90	Acceptable
	AGFI	0.867	>0.80	Acceptable
Incremental fit index	NFI	0.766	>0.70	Acceptable
	IFI	0.922	>0.90	Acceptable
	TLI	0.906	>0.90	Acceptable
	CFI	0.919	>0.90	Acceptable
Parsimonious fit measure	PNFI	0.655	>0.5	Acceptable
	PGNI	0.647	>0.5	Acceptable
	PCFI	0.786	>0.5	Acceptable

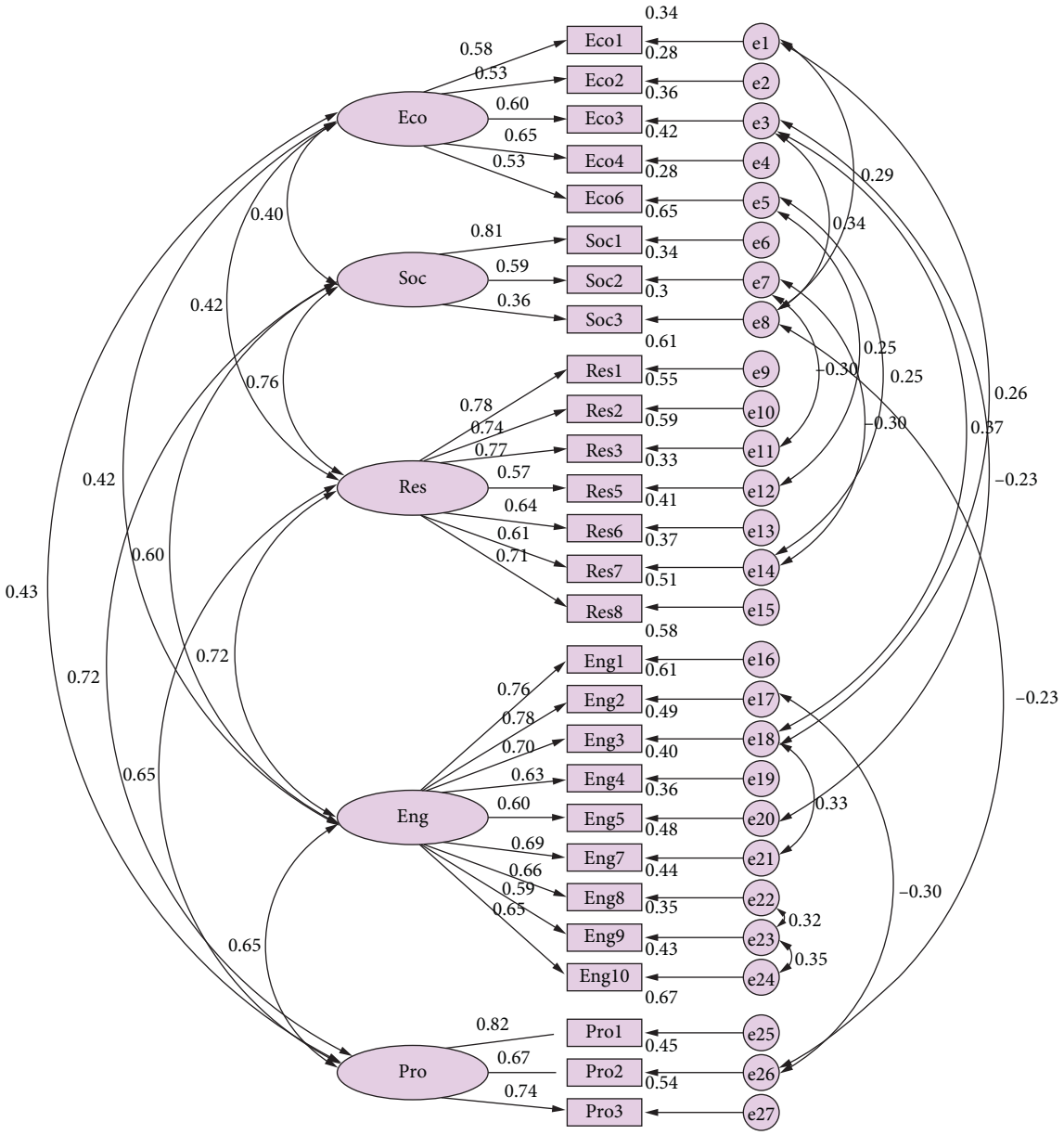

Figure 3: The modified measurement model with standardized path coefficients and factor loadings.

provide employment opportunities for vulnerable groups in society (such as those with low education, laid-off workers, and farmers) to fulfill food and clothing needs. Such a project can also improve people's living environment and promote the development of local tourism.

The resource and environment sustainability dimension includes seven indicators. The indicators of "effect on water quality" and "energy efficiency" rank first and second, respectively. For water environment treatment PPP projects, the most direct performance of the treatment is water quality, which is also the key to the sustainability of the whole project. People require extensive infrastructure for sustaining their lives. These facilities cause environmental problems during their construction, operation, and maintenance. They also consume substantial energy and natural resource. Therefore, the indicator of energy efficiency is crucial for project sustainability, because measures, such as reducing energy consumption and using renewable energy, can reduce greenhouse gas emissions, improve air quality, and build environment-friendly projects. Other indicators in the resource and environmental dimension include "reduction of pollutant discharge," "use of innovative materials," "sewage treatment rate," "comprehensive utilization of water resources," and "protection for landscape and historical sites."

The engineering sustainability dimension includes nine indicators, namely, "Completeness of supporting facilities for the project," "Renewal of project facilities," "Construction quality," "Control of pollution sources," "Adoption of advanced engineering technology," "Sustainability of the technology itself," "Capabilities of operation and maintenance," "Utilization of construction waste," and "Waste

Table 7: The standardized regression weights and covariance estimates of the modified measurement model.

			Estimate	S.E.	C.R.	p
Eco1	<---	Eco	0.585			
Eco2	<---	Eco	0.526	0.208	4.396	***
Eco3	<---	Eco	0.602	0.229	4.690	***
Eco4	<---	Eco	0.646	0.206	4.993	***
Eco6	<---	Eco	0.527	0.224	4.498	***
Soc1	<---	Soc	0.805			
Soc2	<---	Soc	0.587	0.112	5.719	***
Soc3	<---	Soc	0.356	0.111	3.727	***
Res1	<---	Res	0.782			
Res2	<---	Res	0.741	0.105	8.565	***
Res3	<---	Res	0.768	0.123	8.899	***
Res5	<---	Res	0.573	0.107	6.465	***
Res6	<---	Res	0.640	0.122	7.224	***
Res7	<---	Res	0.608	0.090	6.894	***
Res8	<---	Res	0.715	0.099	8.203	***
Eng1	<---	Eng	0.764			
Eng2	<---	Eng	0.782	0.103	8.843	***
Eng3	<---	Eng	0.700	0.108	7.976	***
Eng4	<---	Eng	0.634	0.107	6.976	***
Eng5	<---	Eng	0.604	0.124	6.691	***
Eng7	<---	Eng	0.692	0.116	7.657	***
Eng8	<---	Eng	0.660	0.110	7.291	***
Eng9	<---	Eng	0.591	0.115	6.441	***
Eng10	<---	Eng	0.652	0.115	7.198	***
Pro1	<---	Pro	0.820			
Pro2	<---	Pro	0.671	0.115	7.275	***
Pro3	<---	Pro	0.738	0.124	8.015	***

***The standardized regression weights and the covariance are significantly different from 0 at the 0.001 level (two-tailed).

Table 8: Weight of the indicators.

Dimension	Indicators	Indicators weights	Rank
Economic	Internal return ratio (IRR)	0.203	3
	Land value-added benefit around the project	0.182	5
	Life-cycle cost	0.209	2
	Sustainable cash flow	0.224	1
	Fiscal pressures of government	0.183	4
Social	Public satisfaction	0.461	1
	Provision of employment opportunities	0.336	2
	Potential impact on social development	0.204	3
Resource and environment	Effect on water quality	0.162	1
	Reduction of pollutant discharge	0.154	3
	Energy efficiency (e.g., reduction of energy consumption and use of renewable energy resources)	0.159	2
	Protection for landscape and historical sites	0.119	7
	Sewage treatment rate	0.133	5
	Comprehensive utilization of water resources	0.126	6
	Use of innovation materials	0.148	4
Engineering	Completeness of supporting facilities for the project	0.126	2
	Renewal of project facilities	0.129	1
	Construction quality	0.115	3
	Control of pollution sources	0.104	7
	Adoption of advanced engineering technology	0.099	8
	Sustainability of the technology itself	0.114	4
	Capabilities of operation and maintenance	0.109	5
	Utilization of construction waste	0.097	9
	Waste recycling and reuse	0.107	6
Project management	Organization structure	0.368	1
	Continual improvement of the operation management system	0.301	3
	Competence and skills of the project team	0.331	2

recycling and reuse." Among them, "renewal of project facilities" is ranked as the most important indicator. Project facilities are easy to maintain and replace which will reduce operating costs and improve management efficiency. Therefore, the appropriate project facility renewal capability can extend service time and effectively improve operational efficiency to enhance the sustainability of a project [13]. For water environment treatment PPP projects, supporting facilities play an important role in maintaining daily construction and smooth operation. Project quality is the premise and guarantee of engineering sustainability. Corrosion of reinforcing steel in reinforced concrete structures has caused deterioration and damage that require repairs and maintenance to extend their service life [87, 88]. In China, accidents such as bridge collapse or supply water pollution caused by the insufficient maintenance of infrastructure are common and have led to various social and environmental problems [10]. Therefore, the operational and maintenance capacity also play an important role in ensuring engineering sustainability. A sustainable water environment treatment PPP project not only requires that the treatment technology itself be sustainable but must also preclude damage to the natural environment. For example, in the early stage of water restoration, micro-nano aeration technology can increase dissolved oxygen in the water and provide a suitable living environment for submerged plants, emergent plants, and beneficial microorganisms. Furthermore, the complex microbial community can restore the self-purification (assimilative) capacity of water bodies through its own functional activities of digestion, decomposing, and metabolism. During construction, the project itself would also generate various construction wastes. For example, waste concrete can be crushed and sieved to fabricate recycled aggregates, which can then be produced into recycled concrete or recycled permeable concrete and finally be used in the project to realize construction waste recycling.

The project management sustainability dimension includes three indicators. The indicator "organization structure" is ranked as the most important in this group. The organization structure of a project can affect resource availability and project execution, which bears significance

to sustainable project management. Water environment treatment PPP projects involve a long operation, a wide range, and numerous stakeholders. Thus, the organization structure should change with different concessionary stages. Furthermore, a stable project organization structure and effective communication are needed to ensure a continuous and healthy project operation. Human resource management factors contribute more to project sustainability than technical factors [43]. Project sustainability is limited in the early stage of management, because the concept of sustainable development has not been widely accepted. Therefore, all positive measures should be considered to improve the quality of project management personnel through various forms of learning and training. Furthermore, application of the PDCA cycle theory in the construction of a project management system can improve the scientific management level and work efficiency, reduce the project management cost, and promote the sustainable and healthy development of a project.

7. Conclusions and Implications

7.1. Conclusions. With the rapid development of economy and society, the problem of water environment pollution in China increases in severity. National attention to water pollution has resulted in a growing number of water environment treatment PPP projects, which should be evaluated in relation to sustainability for the healthy development of the projects. The idea of integrating sustainability into infrastructure projects has received widespread attention. Identifying factors that affect water environmental treatment PPP projects sustainability is an important issue that can lead to more sustainable infrastructures. Past research on sustainability evaluation of water environmental treatment PPP projects is relatively limited and based on the triple bottom line of economy, society, and environment, thereby lacking a more comprehensive evaluation index system. This paper connects these gaps by exploring the factors affecting project sustainability from five aspects: economy, society, resources and environment, engineering, and project management.

To ascertain the factors that influence the sustainability of water environment treatment PPP projects, a sustainability evaluation indicator system was initially constructed. A questionnaire survey was used to collect the opinions regarding the importance of sustainability indicators of projects. EFA was performed using SPSS to extract potential factors in the five dimensions mentioned, achieving a total of 27 influencing factors. Then, fitting degree analysis of the sample data and the model constructed by AMOS 22.0 was performed. The results showed that the modified model and original data were successfully fitted. Finally, index weight was calculated by path coefficient in the measuring model to ascertain the most important index in the different dimensions of project sustainability. The most important indicators in the five dimensions include economy (sustainable cash flow), society (public satisfaction), resources and environment (effect on water quality), engineering (renewal of project facilities), and project management (structure of management organization).

Traditional evaluation indexes come directly from literatures, and the quantity of literatures will affect the construction of the evaluation index system; so, it has certain randomness and uncertainty. On the basis of literature collection, the index system constructed in this paper considered the experience and knowledge of experts, screened the index through SPSS exploratory factor analysis, and carried out fitting degree analysis on the model constructed by AMOS to ensure the reliability of the index system.

7.2. Practical Implications. This study applied SEM method to provide a new perspective on the identification factors, affecting the sustainability for water environment treatment public-private partnership projects. The indicators have the most significant impact on project sustainability in the five dimensions, which provide a useful reference for the public and private sector to take appropriate measures to improve the sustainability level of water environment treatment public-private partnership projects. The research results provide a good reference for the public sector to conduct a new sustainability project decision-making, issue a sustainability regulation rule, and review a sustainability design plan. The private sector can easily find a solution to develop a sustainability water environment treatment project from all the perspective of economy, society, resources and environment, engineering, and project management. In summary, this research can be seen as a step up to have a holistic viewpoint in assessments of the sustainability of PPP projects focused on water environment treatment. The adopted approach and the results can be a stimulus for further studies to consider the effects of economic, social, resource and environment, engineering and project management dimensions on each other. The research method adopted in this paper has been applied in the procurement, decision-making, and operation management of water environment treatment PPP project in Xuchang City, China.

7.3. Limitations and Future Work. This paper provides two contributions: first, it identifies the sustainability indicators from five aspects in water environment treatment PPP projects. Second, this paper describes a methodology for evaluating and ranking factors and assesses the indicators featuring the most significant impact on project sustainability. This paper also has some limitations. Firstly, since sustainable development is a dynamic process which passes in time and depends on numerous parameters, there is no coincident conception of sustainability, and the indicators were not unambiguously qualified. There are differences between different types of PPP projects in different regions, so it is inappropriate to establish a universal indicator system. The index system established in this paper can provide a new comprehensive perspective for the sustainability evaluation of water environment treatment PPP projects, while it cannot be directly applied to other types of PPP projects. Therefore, in future studies, it is necessary to

explore the sustainability evaluation index system and methods, and balance the completeness, adaptability, and the simplicity of operation of sustainable coverage, so that the system can be applied to other PPP projects. In addition, in the questionnaire survey process, the evaluation results of the importance of indicators largely depend on the experience of experts, which is highly subjective. Finally, the number of samples used in the survey is small, and increasing the sample size can result in achievements of more credible findings.

Data Availability

The data used to support the findings of this study are available from the corresponding author upon request.

Conflicts of Interest

The authors declare that there are no conflicts of interest regarding the publication of this paper.

Acknowledgments

This study was supported by the National Key R&D Program of China (no. 2018YFC0406905), MOE (Ministry of Education in China) Project of Humanities and Social Sciences (no. 19YJC630078), National Natural Science Foundation of China (#Project no. 71302191), the Foundation for Distinguished Young Talents in Higher Education of Henan (Humanities and Social Sciences) (no. 2017-cxrc-023), Training Program for Young Backbone Teachers in Institutions of Higher Learning of Henan (no. 2018GGJS080), and the 10th graduate student innovation project of North China University of Water Resources and Electric Power (no. YK2018-04).

References

[1] X. An, H. Li, L. Wang, Z. Wang, J. Ding, and Y. Cao, "Compensation mechanism for urban water environment treatment PPP project in China," *Journal of Cleaner Production*, vol. 201, pp. 246–253, 2018.

[2] Y. Ke, "Is public-private partnership a panacea for infrastructure development? The case of Beijing National Stadium," *International Journal of Construction Management*, vol. 14, no. 2, pp. 90–100, 2014.

[3] B.-G. Hwang, X. Zhao, and M. J. S. Gay, "Public private partnership projects in Singapore: factors, critical risks and preferred risk allocation from the perspective of contractors," *International Journal of Project Management*, vol. 31, no. 3, pp. 424–433, 2013.

[4] L. Tang, Q. Shen, and E. W. L. Cheng, "A review of studies on public-private partnership projects in the construction industry," *International Journal of Project Management*, vol. 28, no. 7, pp. 683–694, 2010.

[5] E. G. Satolo and A. T. Simon, "Critical analysis of assessment methodologies for intraorganizational sustainability," *Management of Environmental Quality: An International Journal*, vol. 26, no. 2, pp. 214–232, 2015.

[6] S. Lenferink, T. Tillema, and J. Arts, "Towards sustainable infrastructure development through integrated contracts: experiences with inclusiveness in Dutch infrastructure projects," *International Journal of Project Management*, vol. 31, no. 4, pp. 615–627, 2013.

[7] M. Hueskes, K. Verhoest, and T. Block, "Governing public–private partnerships for sustainability: an analysis of procurement and governance practices of PPP infrastructure projects," *International Journal of Project Management*, vol. 35, no. 6, pp. 1184–1195, 2017.

[8] J. S. Timmermans and G. E. G. Beroggi, "Conflict resolution in sustainable infrastructure management," *Safety Science*, vol. 35, no. 1–3, pp. 175–192, 2000.

[9] H. R. Sahely, C. A. Kennedy, and B. J. Adams, "Developing sustainability criteria for urban infrastructure systems," *Canadian Journal of Civil Engineering*, vol. 32, no. 1, pp. 72–85, 2005.

[10] L. Shen, Y. Wu, and X. Zhang, "Key assessment indicators for the sustainability of infrastructure projects," *Journal of Construction Engineering and Management*, vol. 137, no. 6, pp. 441–451, 2011.

[11] M. Martinsuo and P. Lehtonen, "Role of single-project management in achieving portfolio management efficiency," *International Journal of Project Management*, vol. 25, no. 1, pp. 56–65, 2007.

[12] A. Nieminen and M. Lehtonen, "Organisational control in programme teams: an empirical study in change programme context," *International Journal of Project Management*, vol. 26, no. 1, pp. 63–72, 2008.

[13] J. Kivilä, M. Martinsuo, and L. Vuorinen, "Sustainable project management through project control in infrastructure projects," *International Journal of Project Management*, vol. 35, no. 6, pp. 1167–1183, 2017.

[14] D. E. Armanios, "Sustainable development as a community of practice: insights from rural water projects in Egypt," *Sustainable Development*, vol. 20, no. 1, pp. 42–57, 2012.

[15] L. Gan, L. Shen, and H. Fu, "Study of infrastructure project evaluation factors based on sustainable development," *China Civil Engineering Journal*, vol. 42, no. 11, pp. 133–138, 2009.

[16] L. Shen, H. Li, and Q. M. Li, "Alternative concession model for build operate transfer contract projects," *Journal of Construction Engineering and Management*, vol. 131, pp. 211–220, 2002.

[17] S. Dasgupta and E. K. L. Tam, "Indicators and framework for assessing sustainable infrastructure," *Canadian Journal of Civil Engineering*, vol. 32, no. 1, pp. 30–44, 2005.

[18] O. O. Ugwu, M. M. Kumaraswamy, A. Wong, and S. T. Ng, "Sustainability appraisal in infrastructure projects (SUSAIP)," *Automation in Construction*, vol. 15, no. 2, pp. 239–251, 2006.

[19] A. Amiril, A. H. Nawawi, R. Takim, and S. N. F. A. Latif, "Transportation infrastructure project sustainability factors and performance," *Procedia-Social and Behavioral Sciences*, vol. 153, pp. 90–98, 2014.

[20] E. Cheung, A. P. C. Chan, P. T. I. Lam, D. W. M. Chan, and Y. Ke, "A comparative study of critical success factors for public private partnerships (PPP) between Mainland China and the Hong Kong Special Administrative Region," *Facilities*, vol. 30, no. 13-14, pp. 647–666, 2012.

[21] N. A. Patil, D. Tharun, and B. Laishram, "Infrastructure development through PPPs in India: criteria for sustainability assessment," *Journal of Environmental Planning and Management*, vol. 59, no. 4, 2016.

[22] A. P. C. Chan, P. T. I. Lam, Y. Wen et al., "Cross-sectional analysis of critical risk factors for PPP water projects in China," *Journal of Infrastructure Systems*, vol. 21, no. 1, p. 10, 2015.

[23] Y. Ke, S. Wang, and A. P. C. Chan, "Risk management practice in China's public-private partnership projects," *Journal of*

Civil Engineering and Management, vol. 18, no. 5, pp. 675–684, 2012.

[24] R. Osei-Kyei and A. P. C. Chan, "Review of studies on the critical success factors for public-private partnership (PPP) projects from 1990 to 2013," *International Journal of Project Management*, vol. 33, no. 6, pp. 1335–1346, 2015.

[25] L. Shen, V. W. Y. Tam, L. Gan et al., "Improving sustainability performance for public-private-partnership (PPP) projects," *Sustainability*, vol. 8, no. 3, p. 15, 2016.

[26] N. A. Patil and B. Laishram, "Public–private partnerships from sustainability perspective-a critical analysis of the Indian case," *International Journal of Construction Management*, vol. 16, no. 2, pp. 161–174, 2016.

[27] J. F. M. Koppenjan and B. Enserink, "Public–private partnerships in urban infrastructures: reconciling private sector participation and sustainability," *Public Administration Review*, vol. 69, pp. 284–296, 2010.

[28] X. Ye and Y. Deng, "Research on the approach to realize sustainability of PPP infrastructure project from the perspective of partnership," *Proceedings of Science and Technology Management Research*, vol. 34, no. 12, pp. 189–193, 2014.

[29] A. M. Al-Damkhi, S. A. Abdul-Wahab, and A. S. Al-Nafisi, "On the need to reconsider water management in Kuwait," *Clean Technologies and Environmental Policy*, vol. 11, no. 4, pp. 379–384, 2009.

[30] J. Almedeij, "The future sustainability of water supply in Kuwait," *Water International*, vol. 32, pp. 604–617, 2007.

[31] J. C. Elnaboulsi, "An efficient pollution control instrument: the case of urban wastewater pollution," *Environmental Modeling & Assessment*, vol. 16, no. 4, pp. 343–358, 2011.

[32] S. Zanni, S. S. Cipolla, E. D. Fusco et al., "Modeling for sustainability: life cycle assessment application to evaluate environmental performance of water recycling solutions at the dwelling level," *Sustainable Production and Consumption*, vol. 17, pp. 47–61, 2019.

[33] F. Pellicer-Martínez and J. M. Martínez-Paz, "The water footprint as an indicator of environmental sustainability in water use at the river basin level," *Science of the Total Environment*, vol. 571, pp. 561–574, 2016.

[34] B. Nuong, A. Kawamura, H. Amaguchi et al., "Social sustainability assessment of groundwater resources: a case study of Hanoi, Vietnam," *Ecological Indicators*, vol. 93, pp. 1034–1042, 2018.

[35] T. Ramos and S. M. Pires, *Sustainability Assessment: The Role of Indicators*, Springer, Berlin, Germany, 2013.

[36] W. Xiong and D. Zhu, "Theory and practice of sustainability–oriented public private partnership," *Journal of Tongji University*, vol. 28, pp. 78–84, 2017.

[37] D. K. Chatterjee, "Review symposium: our common future: the world commission on environment and development," *Australian Geographer*, vol. 20, pp. 195–201, 1989.

[38] V. Mani, A. Gunasekaran, T. Papadopoulos, B. Hazen, and R. Dubey, "Supply chain social sustainability for developing nations: evidence from India," *Resources, Conservation and Recycling*, vol. 111, pp. 42–52, 2016.

[39] M. Yılmaz and A. Bakış, "Sustainability in construction sector," *Procedia-Social and Behavioral Sciences*, vol. 195, pp. 2253–2262, 2015.

[40] S. Vyas, S. Ahmed, and A. Parashar, "BEE (bureau of energy efficiency) and green buildings," *Berichte Der Deutschen Chemischen Gesellschaft*, vol. 58, pp. 23–32, 2014.

[41] R. P. J. Schipper and A. J. G. Silvius, "Sustainability in project management: a literature review and impact analysis," *Social Business*, vol. 4, no. 1, pp. 63–96, 2014.

[42] M. M. Carvalho, "An investigation of the role of communication in IT projects," *International Journal of Operations and Production Management*, vol. 34, no. 1, pp. 36–64, 2014.

[43] C. Scott-Young and D. Samson, "Project success and project team management: evidence from capital projects in the process industries," *Journal of Operations Management*, vol. 26, no. 6, pp. 749–766, 2008.

[44] L.-y. Shen, V. W. Y. Tam, L. Tam, and Y.-b. Ji, "Project feasibility study: the key to successful implementation of sustainable and socially responsible construction management practice," *Journal of Cleaner Production*, vol. 18, no. 3, pp. 254–259, 2010.

[45] L.-Y. Shen, J. L. Hao, V. W.-Y. Tam, and H. Yao, "A checklist for assessing sustainability performance of construction projects," *Journal of Civil Engineering and Management*, vol. 13, no. 4, pp. 273–281, 2007.

[46] G. Fernández-Sánchez and F. Rodríguez-López, "A methodology to identify sustainability indicators in construction project management-application to infrastructure projects in Spain," *Ecological Indicators*, vol. 10, no. 6, pp. 1193–1201, 2010.

[47] R. K. Mavi and C. Standing, "Critical success factors of sustainable project management in construction: a fuzzy DEMATEL-ANP approach," *Journal of Cleaner Production*, vol. 194, pp. 751–765, 2018.

[48] G. Heravi, M. Fathi, and S. Faeghi, "Evaluation of sustainability indicators of industrial buildings focused on petrochemical projects," *Journal of Cleaner Production*, vol. 109, pp. 92–107, 2015.

[49] H. Alwaer, M. Sibley, and J. Lewis, "Factors and priorities for assessing sustainability of regional shopping centres in the UK," *Architectural Science Review*, vol. 51, no. 4, pp. 391–402, 2008.

[50] C. S. Ko, E. Y. Shon, and J. E. Jeong, "A comparative analysis on implementation methods of road PPP project∗-a case study of incheon international airport expressway project," *Seoul Studies*, vol. 18, pp. 41–51, 2017.

[51] Y. Wang and Z. J. Zhao, "Motivations, obstacles, and resources," *Public Performance & Management Review*, vol. 37, no. 4, pp. 679–704, 2014.

[52] J. P. Walters and A. N. Javernick-Will, "Long-term functionality of rural water services in developing countries: a system dynamics approach to understanding the dynamic interaction of factors," *Environmental Science & Technology*, vol. 49, no. 8, pp. 5035–5043, 2015.

[53] V. Klevas, D. Streimikiene, and A. Kleviene, "Sustainability assessment of the energy projects implementation in regional scale," *Renewable and Sustainable Energy Reviews*, vol. 13, no. 1, pp. 155–166, 2009.

[54] H. Alwaer, M. Sibley, and J. Lewis, "Different stakeholder perceptions of sustainability assessment," *Architectural Science Review*, vol. 51, no. 1, pp. 48–59, 2008.

[55] F. Boschetti, C. Cvitanovic, A. Fleming, and E. Fulton, "A call for empirically based guidelines for building trust among stakeholders in environmental sustainability projects," *Sustainability Science*, vol. 11, no. 5, pp. 855–859, 2016.

[56] S. G. Moon, S. Y. Jeong, and Y. Choi, "Moderating effects of trust on environmentally significant behavior in Korea," *Sustainability*, vol. 9, p. 19, 2017.

[57] P. Bynum, R. R. A. Issa, and S. Olbina, "Building information modeling in support of sustainable design and construction," *Journal of Construction Engineering and Management*, vol. 139, no. 1, pp. 24–34, 2013.

[58] L. B. Robichaud and V. S. Anantatmula, "Greening project management practices for sustainable construction," *Journal of Management in Engineering*, vol. 27, no. 1, pp. 48–57, 2011.

[59] C.-P. Tung, T.-C. Lee, W.-T. Liao, and Y.-J. Chen, "Climate change impact assessment for sustainable water quality management," *Terrestrial, Atmospheric and Oceanic Sciences*, vol. 23, no. 5, pp. 565–576, 2012.

[60] S. Yu and H. Lu, "Integrated watershed management through multi-level and stepwise optimization for allocation of total load of water pollutants at large scales," *Environmental Earth Sciences*, vol. 77, no. 10, p. 13, 2018.

[61] O. O. Ugwu and T. C. Haupt, "Key performance indicators and assessment methods for infrastructure sustainability-a South African construction industry perspective," *Building and Environment*, vol. 42, no. 2, pp. 665–680, 2007.

[62] M. Lundin and G. M. Morrison, "A life cycle assessment based procedure for development of environmental sustainability indicators for urban water systems," *Urban Water*, vol. 4, no. 2, pp. 145–152, 2002.

[63] X. Wang, J. Liu, N.-Q. Ren, H.-Q. Yu, D.-J. Lee, and X. Guo, "Assessment of multiple sustainability demands for wastewater treatment alternatives: a refined evaluation scheme and case study," *Environmental Science & Technology*, vol. 46, no. 10, pp. 5542–5549, 2012.

[64] A. J. Balkema, H. A. Preisig, R. Otterpohl, and F. J. D. Lambert, "Indicators for the sustainability assessment of wastewater treatment systems," *Urban Water*, vol. 4, no. 2, pp. 153–161, 2002.

[65] M. A. Brown and B. K. Sovacool, "Developing an 'energy sustainability index' to evaluate energy policy," *Interdisciplinary Science Reviews*, vol. 32, no. 4, pp. 335–349, 2007.

[66] J. Davis, H. Lukacs, M. Jeuland et al., "Sustaining the benefits of rural water supply investments: experience from Cochabamba and Chuquisaca, Bolivia," *Water Resources Research*, vol. 44, no. 12, 2008.

[67] D. Whittington, J. Davis, L. Prokopy et al., "How well is the demand-driven, community management model for rural water supply systems doing?," *SSRN Electronic Journal*, vol. 11, no. 2208, pp. 696–718, 2008.

[68] G. Cserháti and L. Szabó, "The relationship between success criteria and success factors in organisational event projects," *International Journal of Project Management*, vol. 32, no. 4, pp. 613–624, 2014.

[69] R. B. Kline, "Principles and practice of structural equation modeling," *Journal of the American Statistical Association*, vol. 101, 2011.

[70] F. D. F. Larcker, "Structural equation models with unobservable variables and measurement error: algebra and statistics," *Journal of Marketing Research*, vol. 18, pp. 39–50, 1981.

[71] B. Xiong, M. Skitmore, B. Xia, M. A. Masrom, K. Ye, and A. Bridge, "Examining the influence of participant performance factors on contractor satisfaction: a structural equation model," *International Journal of Project Management*, vol. 32, no. 3, pp. 482–491, 2014.

[72] R. Lomax, "Covariance structure analysis: extensions and development," *Advance in Social Science Methodology*, vol. 1, pp. 171–204, 1989.

[73] J. C. Loehlin, *Latent Variable Model: An Introduction to Factor, Path, and Structural Analysis*, CRC Press, Boca Raton, FL, USA, 1992.

[74] J. C. Anderson and D. W. Gerbing, "Structural equation modeling in practice: a review and recommended two-step approach," *Psychological Bulletin*, vol. 103, no. 3, pp. 411–423, 1988.

[75] H. H. Harman, *Modern Factor Analysis*, University of Chicago Press, Chicago, IL, USA, 1976.

[76] P. M. Podsakoff, S. B. Mackenzie, J.-Y. Lee, and N. P. Podsakoff, "Common method biases in behavioral research: a critical review of the literature and recommended remedies," *Journal of Applied Psychology*, vol. 88, no. 5, pp. 879–903, 2003.

[77] A. D. Beuckelaer and S. M. Wagner, "Small sample surveys: increasing rigor in supply chain management research," *International Journal of Physical Distribution and Logistics Management*, vol. 42, no. 7, pp. 615–639, 2012.

[78] J. S. Armstrong and T. S. Overton, "Estimating nonresponse bias in mail surveys," *Journal of Marketing Research*, vol. 14, no. 3, pp. 396–402, 1977.

[79] N. Blunch, "Introduction to structural equation modelling: using SPSS and AMOS," *British Journal of Psychology*, vol. 34, no. 3, pp. 211–213, 2019.

[80] J. Guan and N. Ma, "Structural equation model with PLS path modeling for an integrated system of publicly funded basic research," *Scientometrics*, vol. 81, no. 3, pp. 683–698, 2009.

[81] R. L. Matsueda, "Structural equations with latent Variables.Kenneth A. Bollen," *American Journal of Sociology*, vol. 96, no. 6, pp. 1553–1555, 1991.

[82] D. L. Jackson, J. A. Gillaspy, and R. Purc-Stephenson, "Reporting practices in confirmatory factor analysis: an overview and some recommendations," *Psychological Methods*, vol. 14, no. 1, pp. 6–23, 2009.

[83] J. Meng, B. Xue, B. Liu, and N. Fang, "Relationships between top managers' leadership and infrastructure sustainability," *Engineering, Construction and Architectural Management*, vol. 22, no. 6, pp. 692–714, 2015.

[84] L. Jiao, L. Shen, C. Shuai et al., "A novel approach for assessing the performance of sustainable urbanization based on structural equation modeling: a China case study," *Sustainability*, vol. 8, no. 9, p. 910, 2016.

[85] C. J. Kibert, *Sustainable Construction: Green Building Design and Delivery*, Wiley, Chichester, UK, Chichester, UK, 4th edition, 2016.

[86] W. Xiong, J.-F. Yuan, Q. Li, and M. J. Skibniewski, "Performance objective-based dynamic adjustment model to balance the stakeholders' satisfaction in PPP projects," *Journal of Civil Engineering and Management*, vol. 21, no. 5, pp. 539–547, 2015.

[87] Z. C. Gao, A. K. Patnaika, and R. Liang, "VIKOR method for ranking concrete bridge repair projects with target-based criteria," in *Proceedings of Corrosion Risk Management Conference*, pp. 175–192, Houston, TX, USA, 2016.

[88] Z. Gao and J. Li, "Fuzzy analytic hierarchy process evaluation method in assessing corrosion damage of reinforced concrete bridges," *Civil Engineering Journal*, vol. 4, no. 4, pp. 843–856, 2018.